19TH INTERNATIONAL COSMIC RAY CONFERENCE

LA JOLLA, USA AUGUST 11-23, 1985

CONFERENCE PROGRAM SESSIONS VOL. 8

19TH INTERNATIONAL COSMIC RAY CONFERENCE

LA JOLLA, USA AUGUST 11-23, 1985

CONFERENCE PAPERS

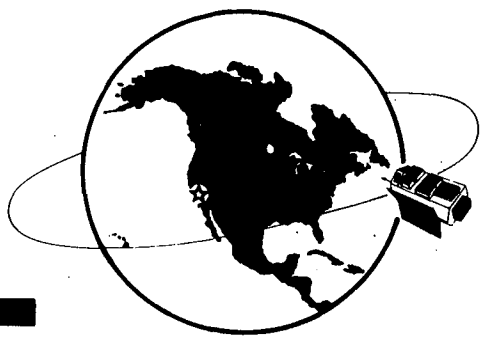

HE

SESSIONS
VOL. 8

NASA Conference Publication 2376

Published by
Scientific and Technical Information Branch
National Aeronautics and Space Administration
Washington, D.C. 20546

August 1985

For sale by the National Technical Information Service, Springfield, VA 22151

PREFACE

The 19th International Cosmic Ray Conference, under the auspices of the Cosmic Ray Commission of the International Union of Pure and Applied Physics, is being held on the campus of the University of California, San Diego, on 11 through 23 August 1985. In keeping with the tradition begun in 1971 by the Australian organizers of the 12th ICRC, the Proceedings of this conference are appearing in two sets of volumes. The first set, consisting of volumes 1 through 8, is being distributed to all participants at the beginning of the conference. This set contains the contributed papers. The second set, distributed after the conference, contains invited, rapporteur, and highlight papers. The papers are reproduced here exactly as they were received from the authors, without refereeing.

For the 19th ICRC, the scientific program was organized according to three major divisions-- OG (cosmic rays and gamma rays of Galactic Origin), SH (Solar and Heliosphere), and HE (High Energy). Technical papers are included in each of the three divisions.

This conference depended on funds from several agencies of the United States government, including major financial support from the National Aeronautics and Space Administration and support from the National Science Foundation, the Department of Energy, and the Air Force Geophysics Laboratory. Important financial support also came from the Center for Astrophysics and Space Sciences of the University of California, San Diego, from the California Space Institute of the University of California, from the Department of Physics and Astronomy of the University of Maryland, College park, from the International Union for Pure and Applied Physics, and from several corporate sponsors who will be acknowledged by name in the post-conference volumes.

We appreciate the confidence placed in the conference organizers by the Cosmic Ray Commission, and acknowledge with thanks the role of the Commission members in setting up the rules for the conference and in advising the organizers during its planning.

We are grateful to all of the members of the various organizing committees listed at the front of this volume. The three Program Committees went to great effort to organize a coherent scientific program and to schedule four parallel sessions with a minimum of conflicts. The Local Organizing Committee has worked long and hard to ensure efficient and hospitable accommodations for all the participants, both in the scientific sessions and outside them. The Publications Committee not only took great pains to assemble these volumes but also maintained an orderly data base of papers and authors which was extremely helpful to the program committees. The General Organizing Committee made important contributions of ideas and efforts to make the conference possible; this committee included international representation from all of North America, thus the departure from the traditional name of National Organizing Committee. And the entire effort was coordinated by the dedicated members of the Steering Committee.

Martin H. Israel, Chairman
General Organizing Committee

August, 1985

LETTER FROM THE EDITORS

This conference marks a departure from previous conferences in this series in that the publication of the Conference Papers was carried out an entire continent away from the activities of Local Organising Committee. This posed some problems but, to the considerable surprise of the Publications Committee members, the one that was expected to be the most trouble turned out not to be significant. The overwhelming majority of those submitting papers and abstracts sent them to the correct address, not to La Jolla as was feared. We wish to thank our many authors for their alertness and commend them for handling a complicated situation so well.

There are eight volumes to be distributed to the conference participants in addition to the Conference Program and Author Index: three volumes for OG, two for SH and three for HE. the detailed makeup of these volumes is described in the prefaces written by the Scientific Program chairmen for their respective volumes. Out of some 1100 abstracts that were accepted by the Scientific Program Committees for inclusion in the conference some 929 papers were finally received in time for inclusion in the Conference Papers. This represents a response of approximately 84 percent, a modest improvement. Even if one excludes the 42 one page papers that should be considered as "confirming abstracts", even though there was no such formal category, the response was somewhat higher than that of recent years. We attribute this to the carrot of a later deadline than before coupled with the stick of there being no printing of post deadline contributed papers. We believe that this decision of the General Organising Committee was a wise one. Of course invited, rapporteur, and highlight talks will be printed in volumes to be distributed to the participants after the conference as usual.

The Publications Committee had much generous help in performing its duties: from Goddard Space Flight Center we had the help of B. Glasser, L. Harris, E. Schronce, N. Smith, J. Esposito and T. Smith. From the Naval Research Laboratory we were helped by T. Mazzotta, and at the University of Maryland M. L. Snidow and J. Mucha gave much needed assistance. Special thanks are due to Caryl Short, the lone staff member of the Publications Committee. She maintained the computer data base, organized the abstracts as they arrived, and kept track of the papers themselves to see that the finally arrived in the right place at the right time. Without her help the job would have been far more difficult than it was.

PUBLICATIONS COMMITTEE August, 1985

Frank C. Jones, Chm.
Jim Adams
Glen M. Mason

HE SESSIONS
VOLUME VIII

19th INTERNATIONAL COSMIC RAY CONFERENCE
LA JOLLA, USA
AUGUST 11–23, 1985

INTERNATIONAL UNION OF PURE AND APPLIED PHYSICS
MEMBERS OF THE COMMISSION ON COSMIC RAYS OF IUPAP

A.E. Chudakov, Chm.
F.B. McDonald
G.C. Castagnoli
P.H. Fowler
D. Hovestadt
J. Kota
T.O. Montmerle
H. Moraal
J.R. Prescot
B.V. Sreekantan
K. Suga
J. Wdowczyk

STEERING COMMITTEE

F. McDonald, Chm.
G. Burbage
M. Forman
T. Gaisser
M. Israel
F. Jones
R. Lingenfelter
R. Mewaldt
L. Peterson

GENERAL ORGANIZING COMMITTEE

M. Israel, Chm.
M. Bercovitch
P. Freier
R. Gall
R. Jokipii
L. Jones
V. Jones
S. Krimigis
J. Kurfess
J. Lockwood
P. Meyer
B. Price
R. Ramaty
F. Reines
M. Shapiro
M. Shea
J. Simpson
E. Stone
D. Venkatesan
J. Waddington
S. White

PROGRAM COMMITTEES

OG SESSIONS
R. Mewaldt, Chm.
G. Cassiday
C. Fichtel
A. Harding
J. Matteson
D. Muller
W. Webber

SH SESSIONS
M. Forman, Chm.
H. Hudson
G. Mason
B. McKibben
M. Pomerantz

HE SESSIONS
T. Gaisser, Chm.
K. Lande
J. Linsley
E. Loh
G. Yodh

PUBLICATIONS
F. Jones, Chm.
J. Adams
G. Mason

LOCAL ORGANIZING COMMITTEE

L. Peterson,Chm.
G. Burbidge
R. Lingenfelter
R. Rothschild
J. Arnold
W. Baity
A. Buffington
M. Burbidge
W. Fillius
R. Gall
R. Gould
H. Hudson
J. Linsley
K. Marti
G. Masek
J. Matteson
C. McIlwain
R. Mewaldt
O. Piccioni
M. Thiemens
W. Thompson
H. Ticho
R. White

Sponsored by
National Aeronautics and Space Administration
National Science Foundation
Department of Energy
Center for Astrophysics and Space Science, University of California, San Diego
California Space Institute, University of California
Department of Physics and Astronomy, University of Maryland, College Park

Preface to HE Volumes

Papers contributed to the XIX International Cosmic Ray Conference were arranged into three major divisions: Origin and Galactic phenomena (OG), Solar and Heliospheric (SH), and High Energy (HE). The HE sessions at this conference comprise all the subjects formerly included in the muon and neutrino sessions (MN) and the extensive air shower sections (EA) as well as those on high energy interactions, new particle searches and emulsion chamber results, which were previously classified in HE. In addition, technical papers have not been classified separately, but have been inserted in appropriate subject sections. All the papers now classified as HE are contained in volumes 6, 7 and 8.

Volume 6 includes sessions HE1 (cross sections and interactions of particles and nuclei at high energy) and HE3 (emulsion chamber results). Extensive air shower papers (HE4) are in volume 7. Papers on muons and neutrinos (HE5), searches for new particles and processes (HE6) and some on new techniques (HE7) are in volume 8.

Altogether some 380 abstracts were received for the HE sections. These were divided into the 25 groups listed in the tables of contents of the HE volumes. (These groups correspond only approximately to the 26 contributed paper sessions at the conference.)

Four rapporteurs were selected to cover the subjects of the HE sessions:

L.W. Jones	High Energy Interactions and New Particle Searches (HE1 & HE6);
M. Shibata	Emulsion Chamber Observations and Interpretation (HE3);
R.W. Clay	Extensive Air Showers (HE4);
K. Sivaprasad	Muons and Neutrinos (HE5).

The written versions of the rapporteur talks are contained in the post-conference volume together with highlight and invited papers.

The work of arranging the HE program was shared by a committee consisting of

T.K. Gaisser (Bartol), Chairman
K. Lande (Pennsylvania)
E.C. Loh (Utah)
J. Linsley (New Mexico)
G.B. Yodh (Maryland)

This conference is the 19th in a series. Previous conferences in this series were held at:

Cracow, Poland	–	1947
Como, Italy	–	1949
Bagneres–de–Bigorre, France	–	1953
Guanjuato, Mexico	–	1955
Varenna, Italy	–	1957
Moscow, USSR	–	1959
Kyoto, Japan	–	1961
Jaipur, India	–	1963
London, UK	–	1965
Calgary, Canada	–	1967
Budapest, Hungary	–	1969
Hobart, Australia	–	1971
Denver, USA	–	1973
Munchen, FRG	–	1975
Plovdiv, Bulgaria	–	1977
Kyoto, Japan	–	1979
Paris, France	–	1981
Bangalore, India	–	1983

HE 5.1
UNDERGROUND MUONS

VOLUME 8

HE 5.2
MUONS

HE 5.3
NEUTRINOS

VOLUME 8

HE 5.4
MUONS

HE 6.1
MAGNETIC MONOPOLES

VOLUME 8

HE 6.2
NUCLEON DECAY AND NEW PARTICLE SEARCHES

HE 7.1
ACOUSTIC AND THERMAL DETECTION TECHNIQUES

VOLUME 8

PRELIMINARY RESULTS ON UNDERGROUND MUON BUNDLES OBSERVED IN THE "FREJUS" PROTON-DECAY DETECTOR

Aachen - Orsay - Palaiseau - Saclay - Wuppertal Collaboration

Presented by B. DEGRANGE, LPNHE, Ecole Polytechnique
91128 - PALAISEAU (FRANCE)

1. Introduction. The proton-decay detector installed in the "Modane Underground laboratory" (4400 mwe) [1] in the Fréjus tunnel (French Alps) has recorded 80 880 single muon and 2 322 multi-muon events between March'84 and March'85 (6425 hours of active time). During this period, a part of this modular detector was running, while new modules were being mounted, so that the detector size has continuously increased. The final detector has been completed in May'85.

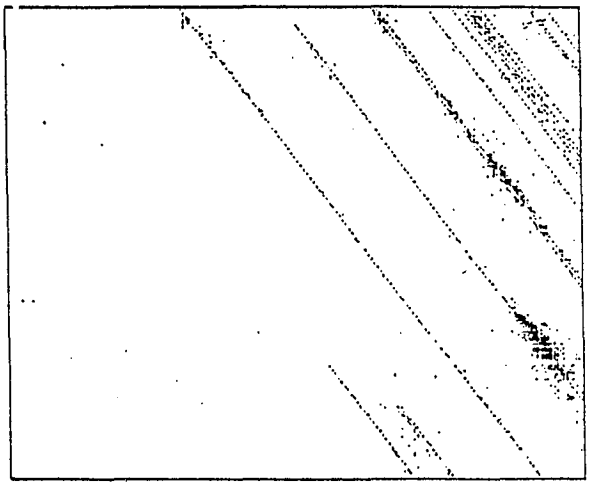

Figure 1

The experimental set-up is described in another paper presented at this Conference [2]. We just recall here the features which are relevant for underground muon studies. The final size of the apparatus is 6x6x13 m^3 corresponding to an apparent detection area averaged over all muon directions of 96m^2. This surface is reduced to 60m^2 for the data presented here which were taken with a part of the modules. The "Fréjus" detector thus combines a rather large detection area with a high spatial resolution (flash-tube size 5x5 mm^2). Both qualities are needed in order to be sensitive to high muon multiplicities at the depth of 4400 mwe, which reflect, at least partially, the composition of primary cosmic rays in the range 10^5 - 10^8 GeV. The importance of the spatial resolution is illustrated in figure 1, showing a bundle of 15 muons observed in the Fréjus detector.

2. Results Figure 2 shows the observed multiplicity distribution. For those bundles including 3 muons or more, the following characteristic distances have been calculated:

- the smallest distance between muons;
- the average distance of all muons pairs;
- the radius of the smallest circle surrounding all muon impacts in the plane perpendicular to the shower direction.

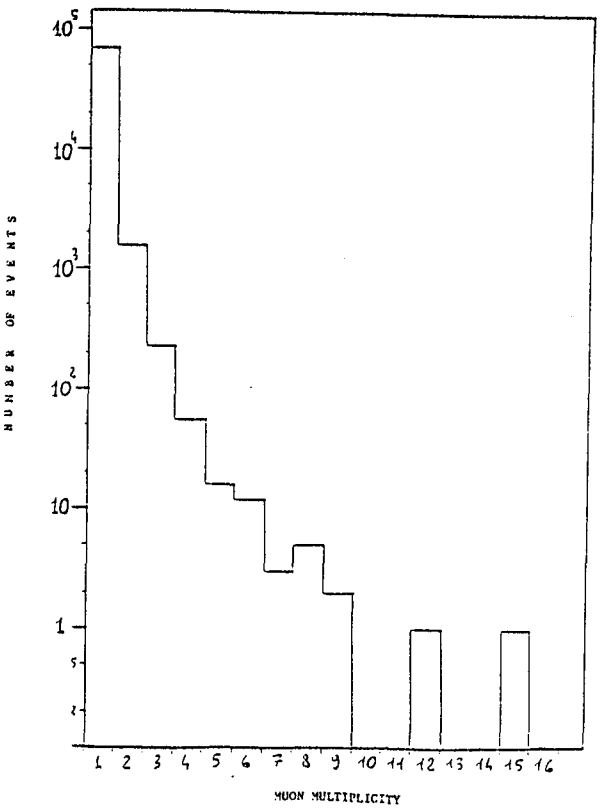

Figure 2

The following table displays the average values of the preceding distances obtained in the present data sample. The average distance between muons in di-muon events is also shown.

Average smallest distance ($N_\mu \geq 3$)	1.30 ± 0.06 M
Average distance ($N_\mu \geq 3$)	2.75 ± 0.07 M
Average circle radius ($N_\mu \geq 3$)	2.08 ± 0.06 M
Average distance muons in di-muon events	2.78 ± 0.05 M

3. Interpretation

These experimental data can only be interpreted by means of Monte-Carlo calculations simulating extensive air showers producing muons with energies greater than several TeV. The comparison with the data presented here is however not straightforward since the size of the detector has been regularly increased. The following analysis is very preliminary.

A Monte-Carlo simulation was developed and calibrated using ISR and collider data [3]. Violations of KNO scaling for multiplicity distributions as well as violations of Feynman scaling for rapidity and transverse momentum distributions were taken into account. The K/π ratio was assumed to increase linearly with charged multiplicity. The muons were propagated in the Fréjus rock (average density 2.75)

simulating all kinds of energy losses (ionisation, pair production, bremsstrahlung and nuclear collisions), then the detector acceptance was taken into account. The calculations show that the contribution of heavy nuclei essentially comes from primaries with energies greater than 10^6 GeV. In order to compare with protons or light nuclei in the same energy range, it is convenient to consider events with at least 4 muons. As a matter of fact, events with a lower multiplicity are dominated by primaries in the range 10^4-10^6 GeV, and a normalization to such events would lead to additionnal uncertainties in the ratio of primary fluxes at different energies.

If N is the number of detected muons, the ratio

$$\rho = \frac{\text{Number of events with } N_\mu \geq 7}{\text{Number of events with } 4 \leq N_\mu \leq 6}$$

is very sensitive to primary composition, ranging from several percent for proton primaries, up to 30% - 50% (depending upon the spectral index) for iron nuclei. Our experimental result

$$\rho_{exp} = (14 \pm 4)\%$$

is consistent with the value expected from the so-called "low energy" composition [4], on the basis of our Monte-Carlo program. Similarly, the characteristic distances displayed in Table 1 are accounted for with this composition.

References

1. A. Rousset, P. Delcros, M. Levy and J.M. Demorieux (Fev. 1983), in "Travaux" p. 9
2. AOPSW Collaboration, Contribution to this Conference.
3. W. Thome et al. (1977) Nucl. Phys. B 129, 365
   G. Arnison et al. (1982) Phys. Lett. 118 B, 167
   K. Alpgard etal. (1983) Phys. Lett. 121B, 209
   G. Arnison et al. (1983) Phys. Lett. 123B, 108.
4. J.W.Elbert, T.K. Gaisser and T. Stanev, (1983) Phys. Rev. D27, 1448.

Muon and Neutrino Results from KGF Experiment at a depth of 7000 hg/cm^2

M.R. Krishnaswamy, M.G.K. Menon, N.K. Mondal*,
V.S. Narasimham and B.V. Sreekantan
Tata Institute of Fundamental Research, Bombay - 400005, India

Y. Hayashi, N. Ito and S. Kawakami
Osaka City University, Osaka, Japan

S. Miyake
Institute for Cosmic Ray Research, University of Tokyo, Tokyo, Japan

1. Introduction

The KGF nucleon decay experiment at a depth of 7000 hg/cm^2 has provided valuable data on muons and neutrinos. The detector comprising of 34 crossed layers of proportional counters (cross section 10 x 10 cm^2; lengths 4m and 6m) sandwiched between 1.2cm thick iron plates can record tracks of charged particles to an accuracy of 1° for tracks that traverse the whole of the detector. A special two-fold coincidence system enables the detector to record charged particles that enter at very large zenith angles.

In a live time of 3.6 years about 2600 events have been recorded. These events include atmospheric muons, neutrino induced muons from rock, stopping muons, showers and events which have their production vertex inside the detector. In this paper we present the results on atmospheric muons and neutrino events.

2. Results on atmospheric muons

The angular distribution of muons in the zenith angular interval 0°-55° agrees very well with expectations based on the assumption that atmospheric muons are produced through decays of π's and K's. This part of the angular distribution has been used to study possible direct (prompt) production of muons in high energy ($E_\mu \sim 15$-500 TeV) collisions. We compare the observed ratio of I_{TOTAL}/I_{DECAY} with theoretical predictions for different values of the parameter $x = \mu_{DIRECT}/\pi$ in hadron collisions. From this we set a conservative upper limit of 10^{-3} for the ratio of prompt muons to pions in hadron collisions leading to muons of energy 15-500 TeV.

* On leave of absence at Argonne National Laboratory, USA.

3. Results on neutrino induced events

The zenith angular distribution of muons with $\theta > 55^{o}$ has been compared with calculations which assume that the cross sections found at accelerators for neutrino interactions at low energies can be extrapolated to high energies. The agreement between the observed and predicted results is good within statistics.

Further, we have recorded 40 events that have vertex inside the detector. These have been analysed mainly from the point of view of their contribution to the background for nucleon decay events. In this analysis, by using the rate of neutrino induced muons from rock and events inside the detector we establish that the assumed neutrino energy spectrum is a correct one.

Out of these 40 events with vertex inside the detector 19 events are fully confined within the volume of the detector. These special events comprise of 9 single prong and 10 multiprong events. A detailed calculation using the above mentioned neutrino spectrum was done to predict the visible energy spectrum of these fully confined events. The agreement between prediction and observation is good. But it is to be pointed out that track configuration, total energy content and momentum balance of four of these confined events is such that they are unlikely to be neutrino induced events and indeed are consistent with nucleon decay.

4. Acknowledgements

we are indebted to Messers B. Satyanarayana, R.P. Mittal, S.D. Kalmani, K.S. Anand, P.S. Murthy, T. Ravindran and J.D. Kulkarni for their technical help during the experiment. We are grateful to the officers and other staff of Bharat Gold Mines Ltd., for their kind cooperation. The Ministry of Education, Japan is thanked for financial assistance.

6

RELEVANCE OF MULTIPLE MUONS DETECTED UNDERGROUND TO THE MASS COMPOSITION OF PRIMARY COSMIC RAYS

Szabelski, J., Wdowczyk, J.,
Institute of Nuclear Science, Lodz, Poland.
Wolfendale, A.W.,
Physics Department, University of Durham, Durham, U.K.

ABSTRACT

Calculations have been made of the expected frequencies of multiple muons in the Soudan underground proton decay detector. It is concluded that the flux of heavy nuclei ($z > 10$) in the range 10^{15} - 10^{16}eV/nucleus is at most 25% of the total particle flux in the same range.

1. Introduction. The installation of a number of large detectors underground designed to search for proton decay has led to renewed interest in the multiple muons which are recorded. Some 15 years ago we (Adcock et al., 1969, 1971) made detailed calculations of the expected number of such multiple muons for the situation of the experiment of Keuffel and co-workers in Utah. Here, we update the calculations in the light of new knowledge about the nature of high energy collisions and apply them to the condition of the Soudan I experiment (Bartlet et al., 1985, *in press*).

The objective is the same as before: to endeavour to elucidate the problem of the mass composition of cosmic ray primaries above 10^{14}eV.

2. The Model. The early calculations used the CKP model. Here we use our model (Wdowczyk and Wolfendale, 1984) which fits the $p\bar{p}$ collider results, extrapolated to higher energies. The main features, summarised briefly, are:

(i) a multiplicity coefficient, α, which increases slowly with energy reaching 0.25 at $\sim 10^{14}$eV and being constant above.
(ii) inelasticities for pion production such that the total is energy independent but $K_{\pi}^{\pm}$ falls as $(E_o/205)^{-0.061}$, *with E_o in GeV.*
(iii) the inclusion of kaons and baryons.
(iv) multiplicity fluctuations according to the KNO formulism.

The shape of the spectra of all secondaries is the same and is as given in our 1984 paper.

3. Results for the mean numbers of muons, mean radii. As an example, we give typical values for muons of energy above 500 GeV (roughly appropriate to Soudan I) produced in vertical showers generated by primary protons. For primary energies of 10^4, 10^5, 10^6, 10^7 GeV the mean number and mean lateral radius (in brackets, metres) are, respectively; 0.4(7.2), 3.3(5.7), 19(4.9) and 120(4.4). An interesting result is the ratio of number of kaons from kaons to the number from pions; the ratios as a function of E_o (values as above) are, 0.55, 0.95, 1.20 and 1.42. The dependence of mean muon number on threshold energy can be considered for the important primary energy $E_o = 10^6$GeV. the means are, for muon threshold energies of 500, 1000, 2000 and 3000 GeV: 19, 8.5, 2.3 and 1.2.

4. Estimated rates for the Soudan experiment and Conclusions. Estimation of the expected rates involves calculations for a variety of zenith angles with an adopted primary spectrum and mass composition, allowance for magnetic deflection and scattering of the muons and the important problem of the finite area of the detector. We find that magnetic deflection and scattering correspond to an increase of mean muon radius by approximately 10%.

The adopted trial primary spectrum is that of Gawin et al. (1985); an important parameter here is the ratio of the flux of H and Fe nuclei to the total number of nuclei; the ratios are, at 10^{14}, 10^{15} and 10^{16}eV/nucleus: 29%, 34%, 22% (and falling very rapidly above 10^{16}eV/nucleus).

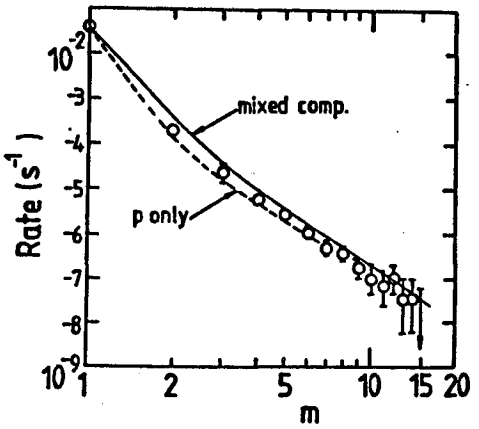

Fig. 1. Observed and predicted frequencies of muons (multiplicity m) in the Soudan experiment. The analysis favours a very small fraction of heavy nuclei.

The corresponding total integral intensities are 1.6×10^{-8}, 4.7×10^{-10} and 3.2×10^{-12} $cm^{-2}s^{-1}sr^{-1}$.

Figure 1 shows a comparison between the Soudan observations and our predictions. It will be noted that there is good agreement for the number of singles but the predictions are somewhat in excess at higher multiplicities. Insofar as the contribution from heavy nuclei is relatively higher for $m > 1$ the most likely interpretation is that the intensity of heavy nuclei is somewhat less than we have assumed. Surprisingly, perhaps, the energy range of primary heavy nuclei contributing to $2 < m < 15$ is not large: 2.10^{15}eV = 3.10^{16}eV per nucleus. A reduction of heavy nucleus flux by about a factor 2 would give a more reasonable fit; at 6.10^{15}eV per nucleus the ratio of heavy nuclei ($z > 10$) to total would then be $\sim$ 12% only.

Confining attention to the ratio of heavy nuclei to total particles in the 10^{15}-10^{16}eV/nucleus region, we have shown that

25% can be regarded as an extreme upper limit.

References

1. Adcock, C. et al., (1969), J.Phys.A, 2, 574; (1971), J.Phys.A. 4, 276.
2. Gawin, J. et al. (1985), in the press.
3. Wdowczyk, J., and Wolfendale, A.W. (1984), J.Phys.G. 19, 257.

HE 5.1-5

MULTIMUONS EVENTS AND PRIMARY COMPOSITION

B.S. Acharya
NASA/GSFC, Greenbelt, MD 20771, USA

and

J.N. Capdevielle
Laboratoire de Physique Théorique, Université de Bordeaux I
Rue du Solarium, 33170 GRADIGNAN, FRANCE

1. Introduction

Nucleon decay detectors at large depths offers now a total area larger than 1000 m^2 to registrate muons of energy exceeding 1 TeV. Near complete high energy muon families are detected in those arrays and we have started an extensive 3D Monte-Carlo simulation in view to understand the spatial distribution of those events and the possible link with elementary act or primary composition.

As pion or kaon parents have a very small decay probability at so high energy, multimuon phenomena occurs at high altitude where the atmospheric density is small after the most energetic collisions.

2. Monte-Carlo modelling and target diagramms

For a first attempt, we described the multiple production of secondary hadrons by the scale breaking model (1). The energy of secondaries are generated from the SBM fit of the invariant cross section

$$E \frac{d^3\sigma}{dp^3} = f\left(x\left(\frac{s}{s_o}\right)^{\alpha/2}, p_t\right)\left(\frac{s}{s_o}\right)^{\alpha/2}$$

The average multiplicity obtained is comparable to the fit of Thome, slightly more important than in usual scaling model. At energy exceeding the collider possibility, i.e., more than 155 TeV, we assumed

$$n_s \sim \left(\frac{s}{s_o}\right)^{\alpha/2}$$

with $\alpha/2 = 0.13$, taking into account different reviews on $\bar{p}$-p data (2)(3).

An important violation (especially for multimuon production) of KNO scaling has been incorporated in the calculation, as shown in fig. 1, where the fluctuations of multiplicity $\Psi(z)$ are quite larger than usually assumed in Slattery's distribution.

Transverse momenta are generated following

$$\frac{dN}{dp_t} = \left(p_t/p_o\right)^{1.5} \exp\left(-p_t/p_o\right)$$

where $< p_t> = 2.5\ p_o$ and $< p_t> = 0.0151\ \mathrm{Ln}\ E + 0.24$.

15% of the pions are treated like kaons and charged pions are

submitted to probability charge exchange with probability 1/3. The zenith angle of emission is calculated for each secondary following its longitudinal and transverse momenta. A rotation matrix provides the director cosines of outgoing particles versus those of the incoming hadron.

More recently, we have described the multiple production by a multicluster independent model, in better agreement with short range order correlations, especially adapted to nucleon-air collision, presented in the papers 4.1-9, 10. For nucleus primaries, we have used superposition models, or, as in p-air nucleus collisions, assumed a rise of central rapidity density correlated with the number of "participating nucleons" following the rules edicted by Faessler (4).

Pions and kaons decays, with the subsequent deviations are also treated by the Monte-Carlo method like 2-body decays, with respect to individual lifetime and masses. Earth magnetic field is also taken into account with some approximations for near vertical muons (5). A 3D Monte-Carlo method incorporating muon bremstrahlung, pair production, nuclear interaction, ionisation and multiple Coulomb scattering (6) is used finally to propagate the muons at large depths in the rock.

For each muon family, we have obtained the coordinates, the director cosines and the energy of the muons recorded at depths 1800, 4200, 5000 mwe corresponding approximately to the levels of Soudan, Momestake or Frejus, and Mont-Blanc installations, respectively.

3. Topological aspects of multimuons

The average number of muons $\bar{n}_\mu$ versus primary energy are plotted on fig. 2. At very high energy, heavy nuclei would become more efficient to produce multimuons however. This must be weighted according to their abundance.

It is shown on fig. 3, how events with large separation $\bar{r}_{ij}$ and large n_μ would be more likely generated by heavy nuclei. (The plot contains 50 events generated by iron of 5.10^6 GeV and nucleons of 10^7 GeV, assumed to have the same frequency). The separation $\bar{r}_{ij}$ of a multimuon is taken as

$$\bar{r}_{ij} = \frac{1}{n_\mu} \Sigma \left((x_i - x_j)^2 + (y_i - y_j)^2\right)^{1/2}$$

The aspect of individual target diagramms (fig. 4) suggests reduction of the average radius, as well as separation when primary energy is rising (respectively 1.8 and 3.5 m for vertical protons of 10^7 GeV).

4. Discussion

Pseudo-random target diagramms suggest that multimuons initiated by nucleons would have stronger concentration in the delimited area. A criterium to recognize nucleon primary could be proposed such as $n_\mu/2$ contained in a circle of radius $r_{ij}/3$. On the opposite events with large $\bar{r}_{ij}$ and large n_μ would have to be associated to heavies. A more accurate procedure will be deduced from a larger statistics of simulation.

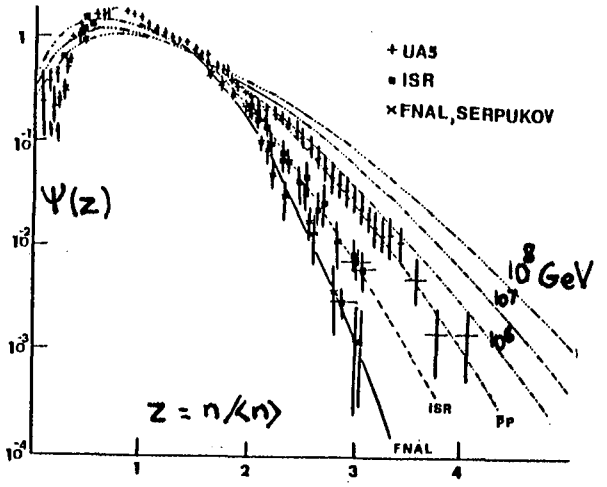

Fig. 1 : Fluctuations assumed for multiplicity.

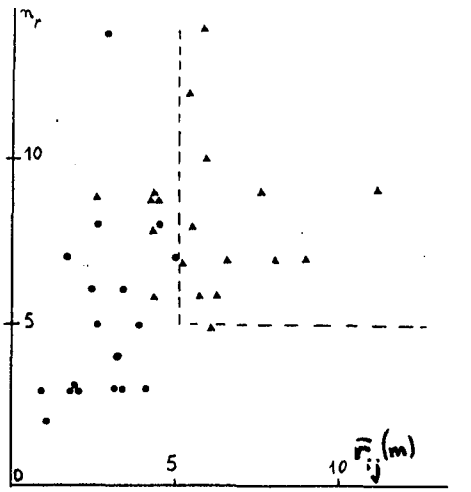

Fig. 3 : $\bar{r}_{ij}$ versus n_μ for protons and nuclei.
• proton primaries 10^7 GeV
▲ iron primaries 5.10^6 GeV

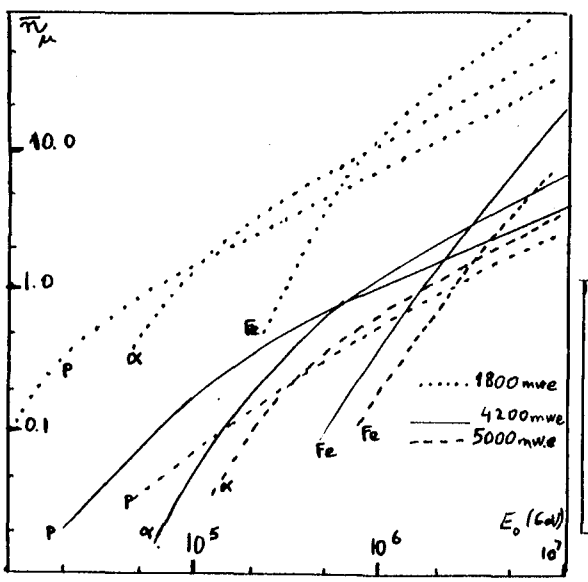

Fig. 2 : $\bar{n}_\mu = f(E)$

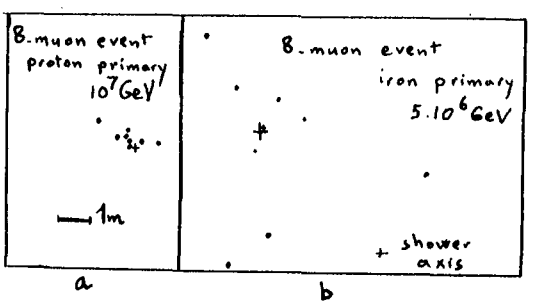

Fig. 4 : Individual target diagramms with $\bar{n}_\mu = 8$.
a. vertical proton 10^7 GeV
b. vertical iron 5.10^6 GeV.

Comparison of the intensity obtained assuming the JACEE spectrum is in tolerable agreement up to 5 muons, with Soudan, Homestake and Nusex results (7) ; more interesting will be the comparison for $n_\mu > 5$ which will give information in the decade 10^6-10^7 GeV, depending together on primary spectrum intensity behaviour and composition. Energy calibration by an EAS surface array could be promising, for instance, a multimuon event would be associated to a surface muon size (> 1 GeV) of 6.10^4 muons instead of 2.10^4 according to a primary iron at nucleon of 5.10^6 GeV.

The introduction of the multicluster independent model doesn't modify very much the profile of multimuons events, when compared to SBM. According to the high energy threshold, the modification of the plateau of rapidity in central region for nucleon-nucleus and nucleus-nucleus collision have no appreciable effects, those muons being produced by secondaries of high rapidity.

The multimuon radius is enlarged with zenith angle, but always reduced with primary energy, becoming lower than 2 meters for an incoming proton of 10^7 GeV (θ = 22°5) at 4200 mwe (the threshold corresponding to 3 TeV).

References

1. Wdowczyk, J. and Wolfendale, H., 1984, J.Phys. G10, 257.
2. Rushbrooke, J.G., 1984, CERN preprint EP 84/34.
3. Yamdagni, N., 1982, Proc. Workshop on hign energy interaction, Philadelphia, 36.
4. Faessler, M.A., 1984, CERN preprint, EP 84/165.
5. Gaisser, T.K. and Stanev, T., 1982, Proc. Workshop high energy interaction, Philadelphia, 295.
6. Capdevielle, J.N., et al., 1985, J.Phys. G11, 565.
7. Acharya, B.S. and Capdevielle, J.N., 1985, proposed to Journ. of Phys. G.

THE SPECTRUM OF COSMIC RAY MUONS OBTAINED WITH 100-TON SCINTILLATION DETECTOR UNDERGROUND AND THE ANALYSIS OF RECENT EXPERIMENTAL RESULTS

F.F.Khalchukov, E.V.Korolkova, V.A.Kudryavtsev, A.S.Malgin, O.G.Ryazhskaya, G.T.Zatsepin

Institute for Nuclear Research, the USSR Academy of Sciences, 60th October Anniversary prospect,7a, Mosoow 117312, USSR

ABSTRACT

The vertical muon spectrum up to 15 TeV obtained with the underground installation is presented. Recent experimental data dealing with horizontal and vertical cosmic ray muon spectra are analyzed and discussed.

1. Results. The 100-ton scintillation detector /1/ has been used to obtain the final results on cosmic ray muon spectrum up to 15 TeV. The spectrum is measured at the depth of 570 m.w.e. in the salt mine.It has been determined by detecting the energy releases of electromagnetic cascades.

About 70% of cascade energy (for the energy range 0.1 ÷ 6 TeV) are detected by the installation. The electromagnetic cascades were obtained after the separation of nuclear cascades from electromagnetic ones by different number of neutrons in them.

A total of 16235 electromagnetic cascade events was obtained during 13188 hours of installation operation. The range of observed energy releases, ε, extends from 0.07 to 4 TeV. It corresponds to the muon energies at the depth, E_μ, from 0.26 to 10 TeV and the muon energies at sea level, E_{μ_0}, from 0.6 to 15 TeV.

The power index of π - and K-meson spectrum has been determined as follows. We used the muon spectrum at sea level in the form as presented in /2/ with various values of $\gamma_{\pi,K}$. To calculate the muon spectrum at our depth we have applied the solution of kinetic equation for the muons passing through the material, the fluctuations being taken into account /3/.The spectrum of energy releases was obtained analytically and by Monte Carlo simulation. For both cases salt-scintillator transition effect was allowed for. The cascade curves for the various scintillator thicknesses were obtained in /4/. The nonuniformity of light collection and its fluctuations in the detector were taken into account in Monte Carlo simulation. The calculations had shown the energy releases detected to be a little greater than the energy releases without light collection fluctuations. Analitical and Monte Carlo spectra are of the same shape, the latter being 15 % higher in absolute intensity. Taking into account the surface topology, the index of calculated spectra is somewhat increased ($\Delta\gamma \approx 0.05$).

To compare the experimental data with the calculations the χ^2 -test has been used. The best fit is obtained for $\gamma_{\pi,K} = 2.75 \pm 0.08$, however $\gamma_{\pi,K} = 2.65$ for $E_{\mu_o} < 1$ TeV and $\gamma_{\pi,K} = 2.85$ for $E_{\mu_o} > 1$ TeV don't contradict our results.

2. Discussion. The cosmic ray muon spectra in energy range 0.3 ÷ 20 TeV were measured in the experiments with magnetic spectrometers (DEIS/5/, MUTRON /6/, MARS /7,8/, Kiel /9,10/, Nottingham /22/), X-ray emulsion chambers /11,12/, ionization calorimeters /13-16/ and depth-intensity curve method /17,18/. The spectral index of muon parents, $\gamma_{\pi,K}$, obtained with magnetic spectrometer DEIS and MUTRON (horisontal direction of incident muons) is 2.71 ÷ 2.74 for $E_{\mu_o} > 0.3$ TeV. The depth-intensity curve gives $\gamma_{\pi,K} = 2.60 \div 2.75$, $\gamma_{\pi,K}$ following the X-ray chamber experiments being 2.75 ÷ 2.85. The data of ionization calorimeters/13-15/ agree with cascade spectrum index $\gamma_{cascade} = 2.1 \div 2.3$. To explain these results some speculations have been proposed: the existence of an hypothetic particle /19/, an anomalous interaction of muons with heavy atoms ($A \geq 100$) or with polycrystals /20/. Even the authors of these works believe the cascade spectrum flatness not to refer to the muon spectrum. Fig.1 shows the vertical muon spectra at sea level presented in various papers. The full points are derived from our energy release spectrum. The horizontal spectra of MUTRON and DEIS were reconstructed to the vertical direction using the approximate formulae from /6/. Use was made of approximate formulae from /2/ with $\gamma_{\pi,K} = 2.65$ for $E_{\mu_o} < 0.3$ TeV and $\gamma_{\pi,K} = 2.75$ for $E_{\mu_o} > 0.3$ TeV to draw the solid curve in Fig.1. One can see the bulk of data for $E_{\mu_o} > 0.3$ TeV doesn't contradict $\gamma_{\pi,K} = 2.75$, the range of small energies being well described by $\gamma_{\pi,K} = 2.65$. The spectrum of muon parents seems to be approximated by the power law with index varying from 2.65 to 2.75. The cause of this variation is difficult to determine unambiguously.

The errors of primary spectrum measurements are too great to compare $\gamma_{\pi,K}$ with γ_p of primary spectrum. To illustrate, the JACEE collaboration gives $\gamma_p = 2.81 \pm 0.13$ for $E_p = (1 \div 100)$TeV /21/. The $\gamma_p \sim 2.65$ up to 1000 TeV follows from the EAS experiments /23-26/. The discrepancy between this value and $\gamma_{\pi,K}$ from muon spectrum may be interpreted as the weak violation of scaling in the fragmentation region.But as there are some experiments giving the γ_p for $E_p > 1$ TeV more greater

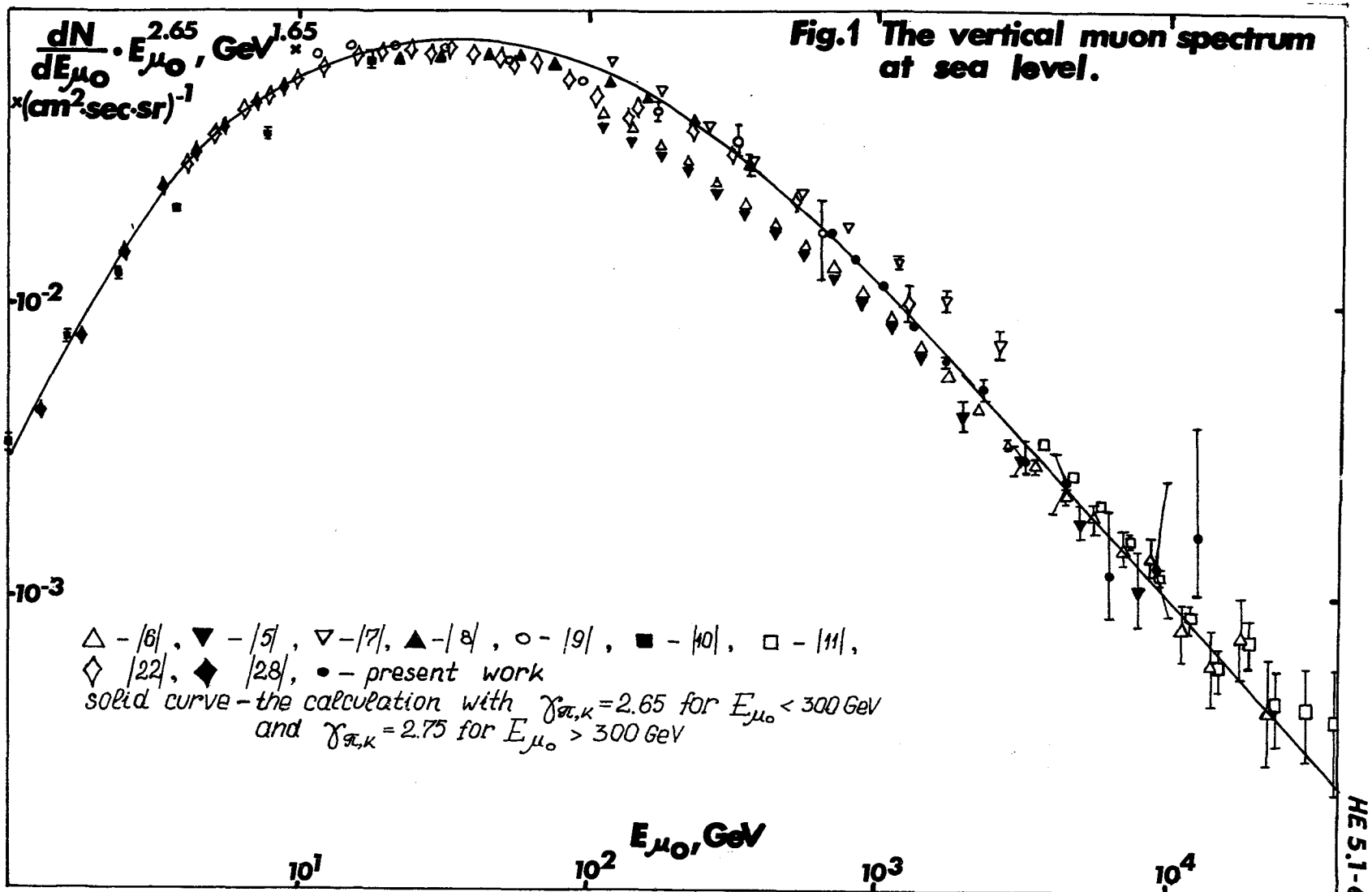

Fig.1 The vertical muon spectrum at sea level.

HE 5.1-6

than 2.65 /21,27/ as we can not exclude the steepening of primary spectrum.

Thus the existence of small steepening of π- and K--meson spectra can be explained by either the steepening of primary spectrum or the scaling violation, or both the former and the latter.

References

1. R.I.Enikeev et al. Proc.16th ICRC, Kyoto, 10,214(1979)
   R.I.Enikeev et al. Proc.17th ICRC, Paris,10, 329 (1981)
2. L.A.Kuzmichev , L.V.Volkova, G.T.Zatsepin. Sov.J.Nucl. Physics, 29,1252(1979)
3. V.I.Gurentsov, E.D.Mikhalchi, G.T.Zatsepin. Sov.J.Nucl. Phys., 5,101(1976)
4. T.A.Chuykova . Proc.18th ICRC, Bangalore,5,316 (1983)
5. O.C.Allkofer et al. Proc.17th ICRC, Paris, 10,321(1981)
6. S.Matsuno et al. Phys.Rev.D29,1(1984)
7. M.G.Thompson et al. Prpc. 15th ICRC, Plovdiv,6,21(1977)
8. C.A.Ayre et al. J.Phys.G.,1, 584(1975)
9. O.C.Allkofer et al. Phys.Lett.,36B,425(1971)
10. O.C.Allkofer et al. Nuovo Cim.Lett.,12,107(1975)
11. M.A.Ivanova et al. Proc.19th ICRC, La Jolla (1985)
12. M.Ichiju et al. Proc.17th ICRC, Paris, 7,27(1981)
13. Yu.N.Bazhutov et al. Proc.17th ICRC, 7,59(1981)
14. A.D.Erlykin et al. Proc.13 ICRC, Denver,3,1803(1973)
15. V.A.Aglamazov et al.Proc.17th ICRC, Paris,7, 63(1981)
16. K.Mitsui et al.J.Phys.G., 9, 573(1983)
17. M.R.Krishnaswamy et al. Proc.15th ICRC, Plovdiv, 5,85 (1977)
18. L.Bergamasco et al. Nuovo Cimento,6C,569(1983)
19. Yu.N.Bazhutov et al. Izv.AN SSSR, ser.phys.,46,2425 (1981)
20. A.P.Chubenko et al. Proc.17th ICRC, Paris,7,98(1981)
21. I.C.Gregory et al.Phys.Rev.Lett.,51,1010(1983)
22. B.C.Rastin. J.Phys.G., 10,1609(1984)
23. I.N.Kirov et al. Proc.17th ICRC, Paris,2,109(1981)
24. B.S.Acharya et al.Proc.17th ICRC, Paris,9,162(1981)
25. T.Hara et al.Proc.18th ICRC, Bangalore, 9,198(1983)
26. G.B.Khristiansen et al. Proc.18th ICRC, Bangalore,9, 195 (1983)
27. V.G.Abulova et al. Proc.18th ICRC, Bangalore, 9 , 179 (1983).
28. A.I.Barbouti, B.C.Rastin. J.Phys.G., 9, 573 (1983)

A Large Area Cosmic Muon Detector located at Ōhya stone mine

N. Nii
Dep. of Physics, Ashikaga Kogyo Univ., Ashikaga, Tochigi
K. Mizutzni
Dep. of Physics, Saitama Univ., Urawa, Saitama
T.Aoki, T.Kitamura, K.Mitsui, S.Matsuno, Y.Muraki, Y.Ohashi,A.Okada
Inst. for Cosmic Rays, Univ. of Tokyo, Tanashi, Tokyo, 188
Y. Kamiya, I. Nakmura, S. Shibata
Dep. of Physics, Nagoya Univ., Chikusa, Nagoya
H. Kojima
Dep. of Physics., Nagoya Medical College, Toyoake, Aichi
S. Higashi, T. Takahashi,H. Umeda,T. Sato,N. Hiraoka,T.Suwada
S. Chang, H. Kujirai
Dep. of Phys., Osaka City Univ., Sumiyoshi, Osaka
S. Minorikawa
Dep. of Phys., Kinki Univ., Higashi-Osaka, Osaka
K. Kobayakawa, H. Inazawa
Dep. of Phys., Fac. of Art.,Kobe Univ., Kobe
K. Mizushima
Dep. of Physics, Kobe Womans College, Kobe
H. Shibata
Dep. of Phys., Okayama Univ., Okayama

1. The Experimental Aims of Ōhya project

The experimental aims of Ōhya project[1] are

(1) Search for the ultra high-energy gamma-rays,
(2) Search for the GUT monopole created at Big Bang,
(3) Search for the muon bundle,
(4) Determination of the chemical composition of the primary cosmic rays between 10^{15}eV and 10^{18}eV.

For such a sake, a large number of muon chambers will be installed at the shallow underground near Nikko (∿100 Km north of Tokyo, situated at Ōhya-town, Utsunomiya-city). At the surface of the mine, a very fast 100 channel scintillation counters will be equipped in order to measure the direction of air showers. These air shower array will be operated at the same time , together with the underground muon chamber.

Surface is almost flat and the underground room is distributed in the area 2 Km X 3 Km. The depth of the underground room distributes from a few meters to ∿100 m. We can select any place according to the experimental purposes. The temperature is fixed in 2-9 C° in a year. The experimental equipment will be arranged to be easily removed by the purpose of the experiments. We use a large number of muon chambers as a"cosmic"accelerator. The schematic view of Ōhya project is given in Fig. 1.

2. the Detector Characteristics

The angular resolution of the surface telescope has been measured with use of real air shower events (the trigger rate was 0.6/min). We have got the angular resolution in the determination of the air shower direction as to be 0.5°(Fig.2).[2] The time jittering of the phtomultipliers(R329) and the electronics are 1 ns and 250 ps respectively. A combination of the good resolution air shower telescope with the large number of muon chamber underground will be powerful probe to the universe especially search for the UHE gamma-ray point source[3].

The muon chamber is made of the pillared iron pipe with a dimension 10 cm X 10 cm X 10 m(length) (Fig. 3). The energy resolution of the counter is given in Fig. 4 as a function of distance. In case of the observation of the magnetic - monopole created at the Big Bang, the internal gas of the counter is exchanged to the mixed gas of 90%He + 10%CH_4 . The proto-type experiment to use the Drell-mechanism has been published in Ref. 4.

As a powerful device to determine the primary composition between 10^{15}eV to 10^{16}eV, a 100 m^2 solid iron Mutron magnet will be used in the underground. The magnet has a thickness of 1 m and the maximum detectable momentum of 3.5 TeV/c when we use the drift chamber with the position resolution of 0.5 mm. The wire of the drift chamber will be spanned with the accuracy of 0.3 mm. The both corner of the wire will be measured by the optical telescope. Typical height of the underground is 10 m but it is easy to find the place with the height of 20 m.

3. the Budget and Size

We present the scale of the detector and the budget in Table I. The detector will be operated after three years later of the approval by the Ministry of Education.

Table I

Station	Number	Total area	Budget
air shower scintillator	100 (1 m^2)	150x150 m^2	6,500 man Yen = 260K$
muon chamber	5760 (1 m^2)	5760 m^2	20,160 man Yen = 800K$
muon chamber	2250 (0.2 m^2)	450 m^2	7,800 man Yen = 310K$
read-out			10,380 man Yen = 415K$
drift cahmber	3360	2000 m^2	10,720 man Yen = 430K$
Mutron removal		100 m^2	3,840 man Yen = 150K$
Total Sum			59,400 man Yen = 2365K$

References

1) Proceed. 18th ICRC, 7(1983),58.
2) This conference Proceed. OG 9.4-3(1985).
3) Proceed. 17th ICRC, 7(1983), 54.
4) Phys. Rev. Lett., 52 (1984), 1373.

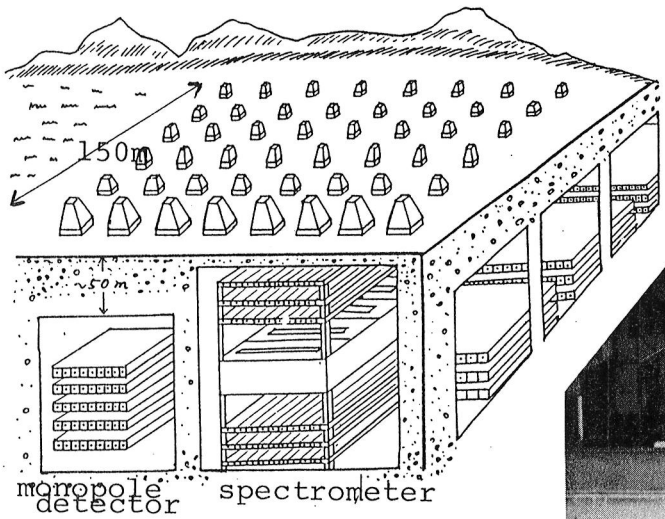

Fig. 1 Schematic View of Ōhya project

Fig. 3

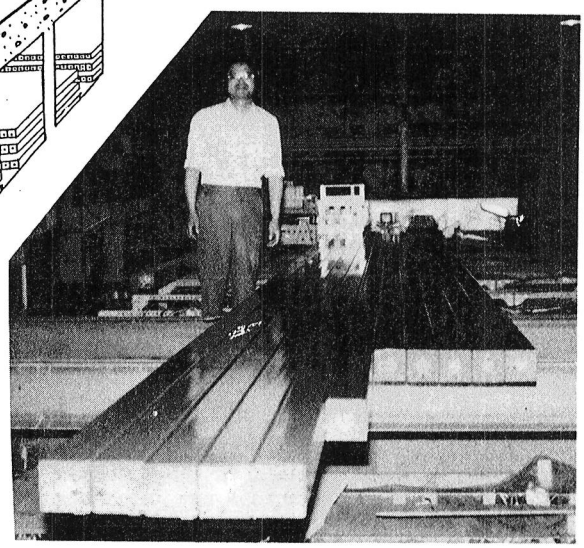

Photo of 10 m muon chambers

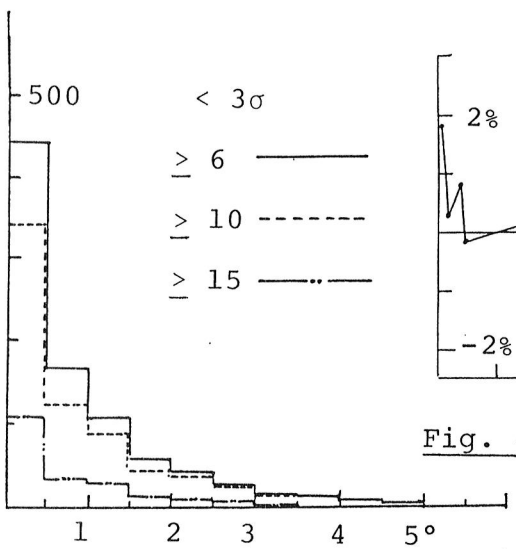

Fig. 2 Angular resolution

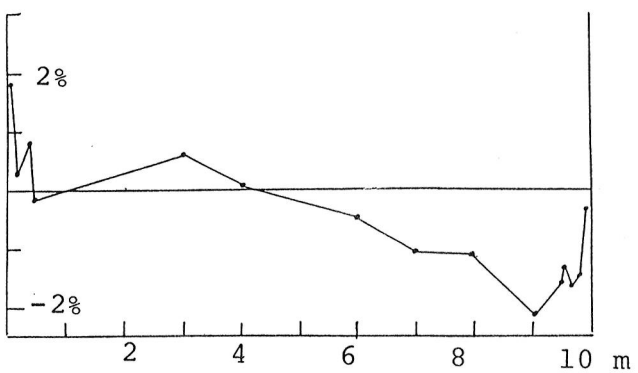

Fig. 4 Position dependency of chamber resolution

A NEW WORLD SURVEY EXPRESSION FOR COSMIC RAY VERTICAL INTENSITY VS. DEPTH IN STANDARD ROCK

Marshall Crouch
Case Western Reserve University, Cleveland, OH 44106, USA

ABSTRACT

The cosmic ray data on vertical intensity versus depth below 10^5 g cm^{-2} is fitted to a 5-parameter empirical formula to give an analytical expression for interpretation of muon fluxes in underground measurements. This expression updates earlier published results and complements the more precise curves obtained by numerical integration or Monte Carlo techniques in which the fit is made to an energy spectrum at the top of the atmosphere. The expression is valid in the transitional region where neutrino induced muons begin to be important, as well as at great depths where this component becomes dominant.

1. Introduction. A "World Survey" curve of cosmic ray intensity vs. depth underground was published by Cassiday, Keuffel and Thompson[1] in 1973. This was a largely empirical curve based on 14 data points. Miyake[2] has published a semi-empirical curve for the Kolar Gold Fields (KGF) data which is more physically meaningful. An improved world survey analysis carried out at Utah[3] was based on 22 data points. However the analysis was made by finding the best fit to the pion intensity and spectral index, with a numerical integration to give the underground muon intensity. As a result no analytic expression giving muon intensity vs. depth was determined. Similarly an extensive 1983 Monte Carlo analysis by Takahashi et al.[4] does not yield an analytical expression.

In the present work a direct fit of an empirical relation is made in order to give a convenient tool for analysis of underground measurements and planning of experiments. 31 data points are analyzed, including extensive 1978 data from South Africa[5] at great depths. Since data are relatively abundant, measurements made in horizontal tunnels or drifts under mountainous terrain are not included, because of inherent uncertainties in depth determination. An additional parameter is added to the fitting function to include the contribution of neutrino induced muons.

2. The World Survey Data. Table I lists the measurements on which the analysis is based. Depths are corrected to equivalent depth in standard rock. Measurements actually made at large zenith angle are corrected for the earth's curvature.

TABLE I.

h Depth in Standard Rock hg/cm^2	I_v Vertical Intensity (particles/cm^2 ster sec)	Error	Reference
1068	1.03 E-06	5.07 E-08	7
1500	3.90 E-07	1.46 E-08	8
1535	3.40 E-07	1.51 E-08	9
1574	3.31 E-07	1.17 E-08	10
1840	1.91 E-07	7.71 E-09	8
1853	2.00 E-07	1.36 E-08	11
1853	1.77 E-07	9.52 E-09	12
2235	9.70 E-08	6.11 E-09	7
3534	1.15 E-08	8.01 E-10	9
3562	1.42 E-08	1.53 E-09	12
4312	4.63 E-09	6.23 E-10	11
4508	3.24 E-09	4.04 E-10	12
6808	1.92 E-10	4.97 E-11	12
7486	1.10 E-10	2.15 E-11	13
8742	1.87 E-11	3.05 E-12	14
9141	1.13 E-11	6.30 E-12	5
9358	1.36 E-11	3.60 E-12	5
9660	4.59 E-12	1.30 E-12	5
10060	3.77 E-12	8.90 E-13	5
10580	2.56 E-12	5.90 E-13	5
11250	9.07 E-13	2.90 E-13	5
12100	6.84 E-13	2.00 E-13	5
13210	3.48 E-13	1.20 E-13	5
14660	2.57 E-13	8.90 E-14	5
16610	2.34 E-13	7.70 E-14	5
19320	1.67 E-13	6.00 E-14	5
23300	2.81 E-13	7.20 E-14	5
29620	2.15 E-13	5.90 E-14	5
41050	1.87 E-13	5.20 E-14	5
67440	1.88 E-13	4.90 E-14	5
182700	2.61 E-13	5.40 E-14	5

3. The Fitting Procedure. The fitting function used is

$$I_v(h) = \exp(A_1 + A_2\, h) + \exp(A_3 + A_4\, h) + A_5$$

This is the function used by the Utah group with the constant parameter A_5, the neutrino term, added.

The least squares fit was made using an algorithm due to Marquardt[6]. The program was developed independently, but good agreement was found with the Utah results when the same analysis was used with their input data. Table II gives the values obtained for the five parameters.

TABLE II

A_1	-11.24 ± 0.18
A_2	$-.00264 \pm .00014$
A_3	$-13.98 \pm .14$
A_4	$-.001227 \pm .000021$
A_5	$(2.18 \pm .21) \times 10^{-13}$

I_v is in g^{-1} cm^2 sr^{-1}. h is in hg cm^{-2} (1 hg = 100 g. Therefore a 1 meter thick absorber represents 1 hg cm^{-2}, and, of course, 1 Meter Water Equivalent). The accompanying figure shows the 31 data points together with the fitted function described above.

For those not familiar with the subject, the intensity at a vertical depth h at an arbitrary zenith angle θ is given to a very good approximation by

$$I(h,\theta) = I_v(h/\cos\theta, \theta)/\cos\theta$$

That is, the intensity is that corresponding to a depth equal to the slant thickness of earth above the detector, with a "sec θ enhancement factor" due to the increased decay probability for pions traversing the atmosphere at large zenith angles. In the competition between decay and capture processes, obliquely traveling pions spend more time in regions of low atmospheric density.

References.

1. G.L. Cassiday, J.W. Keuffel, and J.A. Thompson, Phys. Rev. D7, 2022 (1973).
2. S. Miyake, Rapporteur Paper on Muons and Neutrinos, Proceedings of the 13th International Cosmic Ray Conference, Vol. 5, p. 3638, Denver (1973).
3. G.W. Carlson, Ph.D. Thesis, University of Utah, 1972. Some of the analysis for the curve of intensity vs. depth was contributed by D.E. Groom.
4. N. Takahashi, H. Kujirai, A. Adachi, N. Ogita, and A. Misaki, Proceedings of the Dumand Project Workshop, Institute for Cosmic Ray Research, University of Tokyo, 11 November 1983.
5. M.F. Crouch, P.B. Landecker, J.F. Lathrop, F. Reines, W.G. Sandie, H.W. Sobel, H. Coxell and J.P.F. Sellschop, Phys. Rev. D18, 2238 (1978).
6. P.R. Bevington, Data Reduction and Error Analysis for the Physical Sciences, McGraw-Hill (1969).
7. C.T. Stockel, J. Phys. A. 2, 639 (1969).
8. L.M. Bollinger, Cornell Univ. Thesis (1951, Unpublished); Phys. Rev. 79, 207A (1950) (Abstract, no Results); Results given in Barrett et al. (Ref. 10).

9. M.R. Krishnaswamy, M.G.K. Menon, V.S. Narasimham, S. Kawakami, S. Miyake, and A. Mizohata, Acta Phys. Acad. Sci. Hungariae 29, Suppl. 4, 221 (1970).
10. P.H. Barrett, L.M. Bollinger, G. Coconi, Y. Eisenberg, and K. Greisen, Rev. Mod. Phys. 24, 133 (1952).
11. C.V. Achar, V.S. Narasimham, P.V. Ramana Murthy, Nuovo Cimento 32, 1505 (1964).
12. S. Miyake, V.S. Narasimham, and P.V. Ramanamurthy, Nuovo Cimento 35, 969 (1965).
13. M.R. Krishnaswamy, M.G.K. Menon, V.S. Narasimham, H. Hinotani, N. Ito, S. Miyake, J.L. Osborne, A.J. Parsons, and A.W. Wolfendale, Proc. Roy. Soc. Lond. A 323, 511 (1971).
14. B.S. Meyer, J.P.F. Sellschop, M.F. Crouch, W.R. Kropp, H.W. Sobel, H.S. Gurr, J. Lathrop, and F. Reines, Phys. Rev. D1, 2229 (1970).

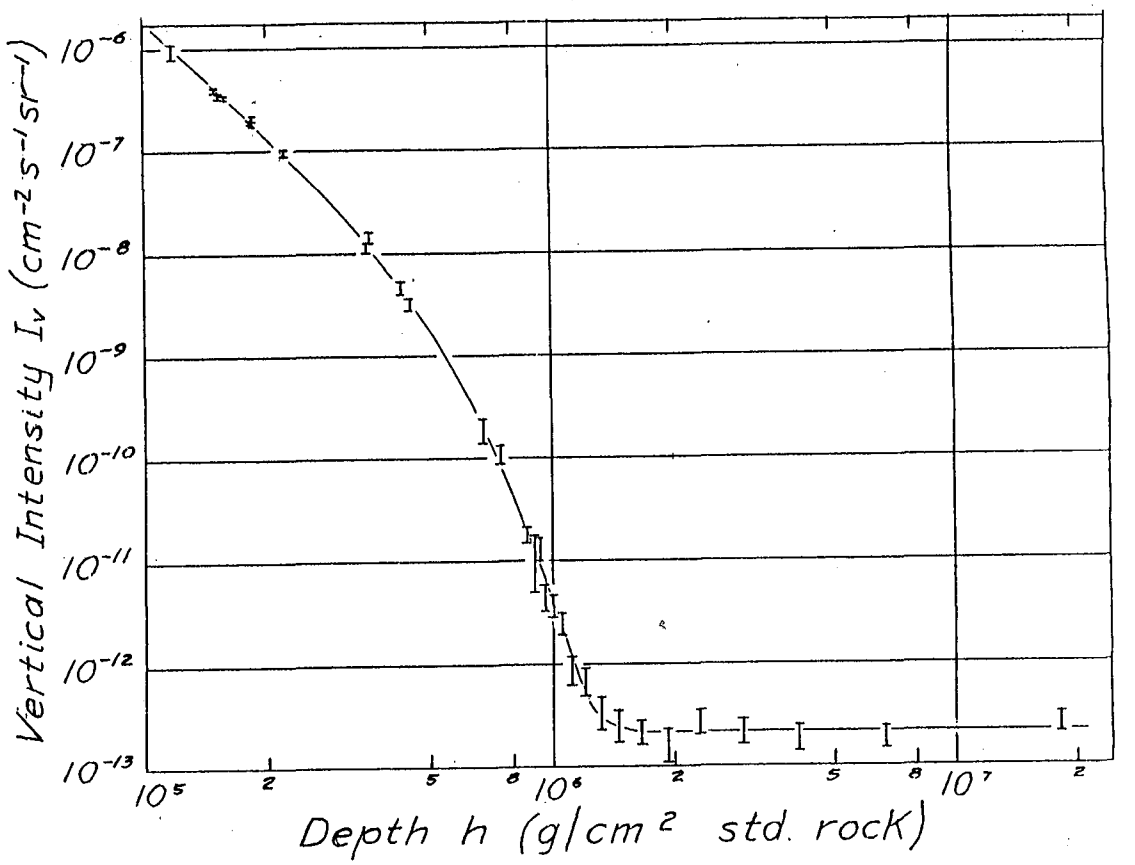

MUON GROUPS AND PRIMARY COMPOSITION AT 10^{13}-10^{15} EV

E.V.Budko,A.E.Chudakov,V.A.Dogujaev,A.R.Mihelev,
V.A.Padey,V.A.Petkov,P.S.Striganov,O.V.Suvorova,
A.V.Voevodsky

Institute for Nuclear Research,the USSR Academy
of Sciences,Moscow

ABSTRACT

The data on muon groups observed at Baksan underground scintillation telescope is analysed.In this analysis we compare the experimental data with calculations, based on a superposition model in order to obtain the effective atomic number of primary cosmic rays in the energy range 10^{13}-10^{15}ev.

1.Introduction. Our general approach to the problem was presented in Kyoto (1),and the first experimental data from Baksan in (2).The first attempt to analyse Baksan multiplicity spectrum in terms of primary composition was made in Bangalore (3).Now we have to correct one of conclusions made in (3) concerning effective atomic number.The change came for two reasons:1)now a smaller zenith angle interval was accepted $0^\circ \leq \theta < 30^\circ$, corrections for individual events inside this interval were made.This affected the obtained decoherence curve,making it 20% narrower,2)the second reason is the choice of more reliable function $N_\mu = F(E_0)$ which represents the mean number of muons from primary nucleon of energy E_0.

2.Experiment. The observed multiplicity or muon number spectrum is shown in fig. 1.It is practically the same as in (3) the difference $m^{-3.4}$ or $m^{-3.3}$ being not significant.All the difference with (3) is in calculated curves.The experimental decoherence curve is shown in fig.2.It deviates slightly from pure exponential one with parameter (12 ± 1) m.The decoherence curve is used to choose the parameters of assumed lateral distribution functions (LDF) in such a way as to fit the experimental curve, $D(R).F_1(r) \div F_4(r)$:examples of tried LDF.

Then the important function $\Delta(R)$ (see below) does not depend much on the choice of the type of LDF.

3.Calculations of expected muon number spectra for a given primary atomic number A. To do this following assumption have been made:

1.the muon group from A is a superposition of A independent groups from constituent nucleons,
2.LDF does not depend on A and energy per nucleon E_0,
3.fluctuations of the muon numbers are pure Poissonian,
4.the power law energy spectrum of primaries of a given A,
5.the mean number of muons of energy $E_\mu \geq E_{th}$ from primary nucleon of energy E_0 was taken as $f(E_0) = 0.355 (E_0^{0.47} - 0.55)^{2.55}$

for E_{th}=0.22 Tev, E_0 in Tev on the basis of numerous Monte-Carlo simulations of cascades in atmosphere (5,6).

The problem is presented by a system of equations:

$$N = A * f(E_0) \qquad /1/$$

$$N' = N * \Delta(R) \qquad /2/$$

$$P(E_0)dE_0 \sim E_0^{-\gamma-1} dE_0 \qquad /3/$$

$$J_A(m) = \int_0^\infty e^{-N'} \frac{(N')^m}{m!} \varphi_A(N') dN' \qquad /4/$$

$$I_A(m) = J_A(m) \Big/ \sum_{m=1}^{\infty} m * J_A(m) \qquad /5/$$

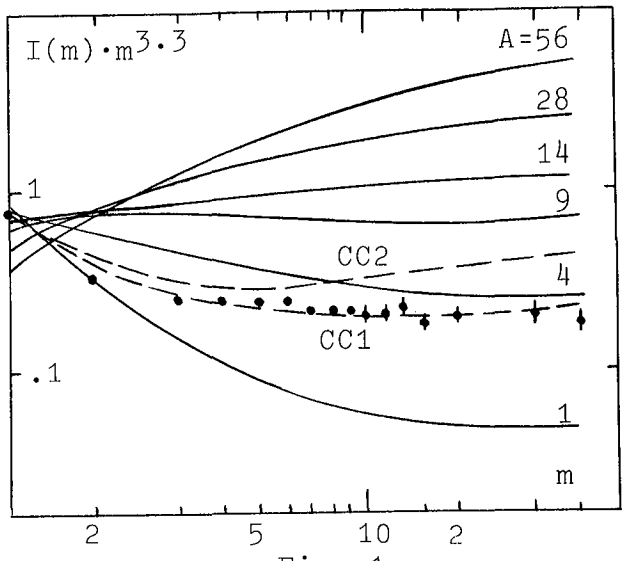

Fig. 1

Here: N is the mean number of muons $E_\mu > E_{th}$ from nucleus A with total energy $A \cdot E_0$; $\Delta(R)$ is the fraction of N which is expected to be inside detecting area when the core of group is at the distance R from telescope centre ($\Delta(R)$ is calculated using assumed LDF); $\varphi_A(N')$ is distribution of N' (expected numbers inside area), which is obtained by solving eqs./1-3/; $J_A(m)$ is the intensity of multiplicities m for a given A; $I_A(m)$ the same, but normalized to the total muon flux through detecting area. The resulting from these calculations $I_A(m)$ are shown in fig. 1 for several A and mixed composition. Obviously, these results depend on γ=1.7 (which is in agreement with experiment) and on functions $f(E_0)$ and $\Delta(R)$.

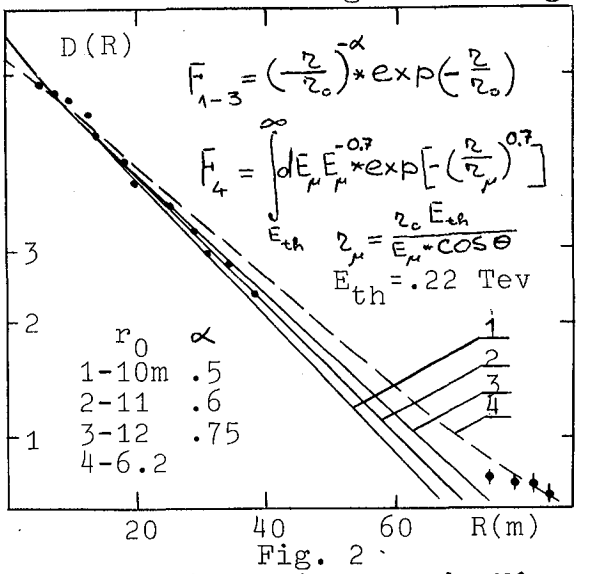

Fig. 2

4. Discussion. To demonstrate the sensitivity of A_{eff} to assumed functions $f(E_0)$ and $\Delta(R)$ let us use "N_0-approximation", introduced in (1), valid for $m \gg 1$; which consists of following:

1. at large N $f(E_0) \sim E_0^{\delta}$, then $\varphi_1(N') \approx C * (N')^{-\gamma/\delta-1}$ at large N',

2. suppose this power law distribution is valid for $N' > N_0'$ and is cut to zero for $N' < N_0'$; determine N_0' by

$$\int_0^{N_0'} \varphi_1(N') N' dN' = \int_{N_0'}^{\infty} C * N' * (N')^{-\gamma/\delta-1}$$

so providing the correct total number of muons.

In a similar way we determine N_0 which corresponds to the

case $\Delta(R)=1$. Fig.3 shows the original $f(E_0)$ (5) - the dependence of number of muons N, $E\mu > 220$ Gev on the primary nucleon energy E_0 and its power law version in "N_0-approximation". The total number of muons after integrating over primary spectrum should be the same for both versions. Substituting the functions $f(E_0)$ and $\varphi_A(N')$ in /1/ and /4/ by power law versions using the mentioned procedure we obtain a simple solution of eqs. /1-5/:

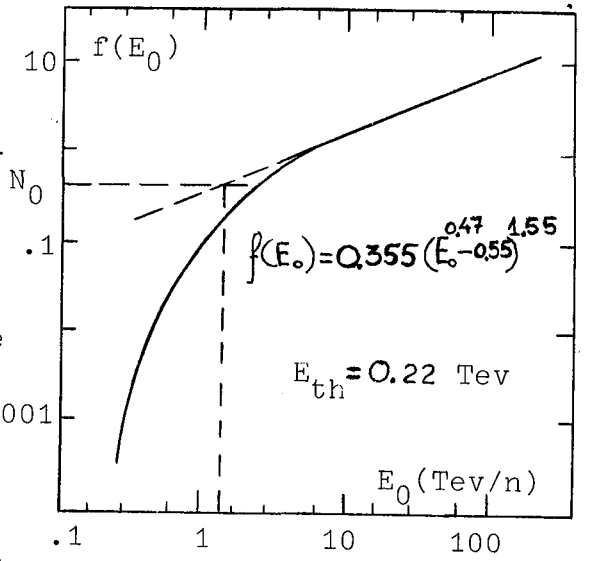

Fig. 3

$$I_A(m)=\frac{\gamma-\delta}{\delta}(N_0')^{\frac{\gamma-\delta}{\delta}}\int_{N_0'}^{\infty}e^{-N'}\frac{(N')^{m-\frac{\gamma}{\delta}-1}}{m!}dN' \qquad /6/$$

where $N_0'=N_0\cdot A\cdot\Delta_{eff}$, $\Delta_{eff}=\left[\frac{1}{S}\int_0^{\infty}2\pi R\,dR\,(\Delta(R))^{\gamma/\delta}\right]^{\frac{\delta}{\gamma-\delta}}$ - is the "effective fraction" of total number of muons in the group expected in detection area. For $m\gg N_0'$ and $m\gg 1$

$$I_A(m)=\frac{\gamma-\delta}{\delta}*(N_0*A*\Delta_{eff})^{\frac{\gamma-\delta}{\delta}}*m^{-\frac{\gamma}{\delta}-1}*\lambda(m) \qquad /7/$$

where $\lambda(m)\to 1$ if $m\to\infty$. When γ and δ are fixed the results depends only on the product $N_0\cdot A\cdot\Delta_{eff}$. The eq. /7/ describes the asymptotic behavior of expression /5/ shown as solid curves on fig.1. By definition the effective atomic number for a mixed composition is:

$$A_{eff}=\left[\frac{\sum_{i=1}^{6}\rho_i A_i^{\gamma/\delta}}{\sum_{i=1}^{6}\rho_i A_i}\right]^{\frac{\delta}{\gamma-\delta}} \qquad /8/$$

which we can evaluate comparing /7/ with experimental data. For $\gamma=1.7$, $\delta=0.73$, $N_0=0.43\pm0.12$, $\Delta_{eff}=0.15\pm0.02$ (of them only N_0 is model dependent (5,6)) the new value of A_{eff} is $A_{eff}=3.9\pm1.5$ (using experimental value of I(m) at m=10).

Table 1

	A	1	4	9	14	28	56
ρ (Gev/n)	ρ_i	.939	.055	.0009	.0035	.0011	.0003
CC1	γ_i	1.7	1.7	1.7	1.7	1.7	1.7
CC2	γ_i	1.7	1.7	1.7	1.7	1.6	1.6

Table 1 shows two suggested examples of chemical composition, ρ_i -fraction of nuclei A_i with a given energy per nucleon (at 1 Gev/n). Number spectra for these two cases calculated using eqs. /1-5/ shown in fig.1 by dashed lines. A good fit to

experimental data is provided by CC1 which corresponds to the case of a constant chemical composition (a standard one) in all energy range from 1 Gev/n.The A_{eff} for CC1 according to /8/ is A_{eff}=4.8,which is about 20% bigger than obtained using "N_0-approximation" at m=10;this is because $f(E_0)$ did not reach asymptotic behavior at m=10 for heavy primaries.Different multiplicities m represent different primary energies but also different selection of A.Table 2 shows,assuming CC1 and eqs./1-5/,relative contributions of different A,also their mean energy,to different m,q is relative contribution.

Table 2

	m =	1	2	3	5	10	30	
A=1	E =	6.1	25	86	240	520	2500	
	q =	.83	.64	.47	.32	.22	.16	
A=4	E =	20	44	94	170	340	1600	E in
	q =	.14	.26	.33	.33	.26	.2	Tev/nucleus
A=14	E =	53	78	106	160	250	1050	
	q =	.02	.07	.13	.2	.23	.2	
A=56	E =	170	200	210	220	245	730	
	q =	.005	.03	.07	.15	.3	.44	

4.Conclusions. The Baksan muon number spectrum at $E_\mu > E_{th}$ = =220 Gev is well explained suggesting a constant chemical composition (the same as at 1Gev/n) till~20 Tev/n.

The integral exponent of the heavy primaries power law spectrum should be $\gamma = 1.7 \pm 0.1$ till 10^{15} ev/nucleus.

References

1. A.E.Chudakov et al. Proc. of 16 ICRC,v.10,p.188,1979.
2. A.E.Chudakov et al. Proc. of 16 ICRC,v.10,p.175,1979.
3. V.N.Bakatanov et al. Proc. of 18 ICRC,v.7,p.51,1983.
4. A.E.Chudakov et al. Proc. of 16 ICRC,v.10,p.192,1979.
5. A.D.Erlykin Private communication.
6. J.W.Elbert and P.Summers Phys. Dep. University of Utah, UUHEP 83/20,1983.

PRIMARY CHEMICAL COMPOSITION FROM SIMULTANEOUS RECORDING OF MUONS INDUCED CASCADES AND ACCOMPANYING MUON GROUP UNDERGROUND

V.N.Bakatanov,S.N.Boziev,A.E.Chudakov,Yu.F.Novosel'tsev,M.V.Novosel'tseva,Yu.F.Sten'kin,
A.V.Voevodsky
Institute for Nuclear Research,the USSR Academy of Sciences,Moscow

ABSTRACT

A new method to estimate the mean atomic number of primary cosmic rays in energy range 10^3-10^5 Gev/nucleon is suggested.The Baksan underground scintillation telescope data are used for this analysis.The results of 7500 h run of this experiment are presented.

Introduction. The big area and calorimetric properties of Baksan underground scintillation telescope (1-3) allows a simultaneous measurement of cascade energy and the multiplicity of accompanying muons.Assuming superposition model one can calculate the energy E_0 of primary nucleon,responsible for a given cascade,more strictly-distribution of these energies. Suppose we know the muon multiplicity at the given depth as a function of primary nucleon energy,namely $N_0=f(E_0)$.The experimental value is expected as $N=f(E_0)\cdot\bar{A}$,where $\bar{A}$ is the mean primary atomic number.Comparing experimental data (N) with the theory ($f(E_0)$) we obtain $\bar{A}=N/f(E_0)$.

The energy distribution of primary nucleons,responsible for cascade energy E_c. This was calculated in several steps:

1. The muon energy spectrum at our depth was taken in a form

$$P(E_{\mu 0})dE_{\mu 0}=(220+E_{\mu 0})^{-3.7}dE_{\mu 0},E_{\mu 0} \text{ in Gev.}$$

2.The muon energy distribution,responsible for E_c:

$P_1(E_{\mu 0},E_c)dE_{\mu 0}=P(E_{\mu 0})\cdot W_\mu(E_{\mu 0},E_c)dE_{\mu 0}$,where $W_\mu(E_{\mu 0},E_c)$-probability of energy transfer E_c by muon with energy $E_{\mu 0}$ taking into account bremstrahlung,"knock-on" electrons,photonuclear

and the e^+e^- production (4-7).

3. Taking into account muon energy losses to our depth x obtain muon production spectrum:

$$P_2(E_\mu,E_c)dE_\mu=0.7\cdot P_1(0.7\cdot(E_\mu-220),E_c)dE_\mu,\quad 0.7=\exp(-b\cdot x).$$

4. Transform from muon to pion spectrum:

$$P_3(E_\pi,E_c)dE_\pi=dE_\pi\int_{nE_\pi}^{E_\pi}\left(\frac{\gamma+1}{1-n^{\gamma+1}}+\frac{\gamma+2}{1-n^{\gamma+2}}\cdot\frac{E_\mu}{B(\theta)}\right)\frac{E_\mu^{\gamma+1}\cdot P_2(E_\mu,E_c)dE_\mu}{E_\pi^{\gamma+2}\cdot(1+E_\pi/B(\theta))},$$

$n=(m_\mu/m_\pi)^2$, $B(\theta)=110/\cos\theta$, θ-zenith angle, $\gamma=1.7$-integral exponent of primary spectrum.

5. The nucleons energy distribution:

$$P_4(E_0,E_c)dE_0=\frac{dE_0}{E_0^{\gamma+2}}\cdot\int P_3(E_\pi,E_c)\cdot W_\pi(E_0,E_\pi)dE_\pi,$$ where $W_\pi(E_0,E_\pi)$- is the inclusive production function taken from (8).

Fig.1 shows the results of this calculations for several cascade energies E_c. The mean values of the variables involved are also shown in the table in Tev.

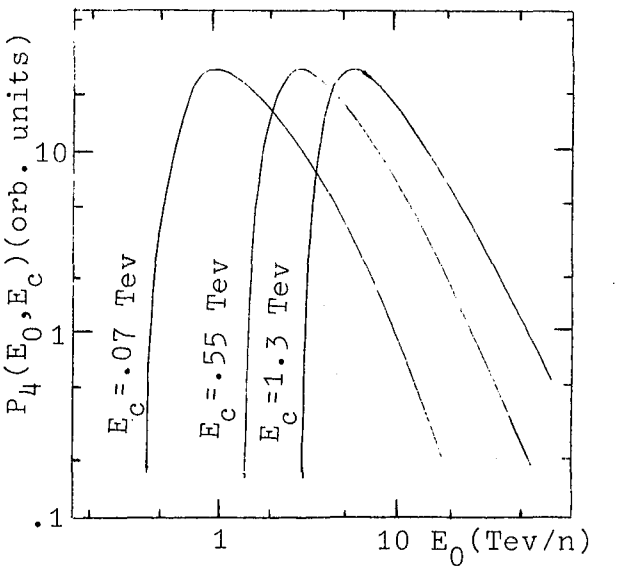

Fig.1

The multiplicity of accompanying muons. Two corrections should be made to experimentally observed number of accompanying muons m, which is only a fraction of the total number N. The correction factors $\bar{\Delta}$ and $\bar{k}$ have following meanings: $\bar{\Delta}$-mean ratio of muons inside telescope area to the total number N ($\bar{\Delta}<1$ due to the finite size of telescope): $\bar{k}$-mean ratio of muons, lost in the cascade core, to the total number N. Both correction factors depend on the cascade energy E_c and muon distribution function. The latter was taken in the form:

$$F(r,E_\mu,\theta)=E_\mu^{-0.7}\cdot\exp(-(r/r_\mu)^{0.7});\quad r_\mu=\frac{220\cdot r_0}{E_\mu\cdot\cos\theta},\ r_0=6.2\ \text{m},$$

$\cos\theta = 0.82$, which gives a good fit to the decoherence curve and stopping muon data. As one can see from the table calculations show an increase of $\bar{\Delta}$ as the E_c increases due to "attraction" of cores of muon group.

Table

E_c	from	.05	.10	.21	.44	.74	1.18	1.47	2.94	6.62
	to	.10	.21	.44	.74	1.18	1.47	2.94	6.62	-
$\bar{E}_c$	(Tev)	.07	.14	.29	.55	.90	1.30	1.91	3.38	8.21
$\bar{E}_{\mu 0}$		.43	.54	.79	1.25	1.89	2.60	3.73	7.26	14.9
$\bar{E}_{\mu}$		.84	1.0	1.36	2.0	2.94	3.97	5.60	10.7	21.7
$\bar{E}_{\pi}$		1.17	1.27	1.75	2.56	3.72	5.04	7.17	14.0	28.8
$\bar{E}_0$		4.19	5.44	7.90	12.6	18.9	25.8	36.6	67.7	126
$\bar{m}$		.58	.89	1.17	1.81	2.25	2.63	3.38	6.20	9.67
$\bar{\Delta}$		.21	.23	.25	.28	.30	.31	.32	.32	.33
$\bar{k}$		.03	.04	.07	.08	.09	.10	.11	.13	.16
$\bar{N}$		3.3	4.8	6.3	9.1	10.9	12.6	16.4	32.8	57.9

The correction was made as $\bar{N}=\bar{m}/(\bar{\Delta}-\bar{k})$. Note that muon, responsible for cascade, is not included in this formula also in experimental values in the table.

Conclusions. The comparison of obtained multiplicities N as a function of E_0 with the expected $f(E_0)$ (10-11) is shown in the fig.2.

Curves 1;2;3 correspond to $\bar{A}=1;3.5;4.5$. By definition mean atomic number in our case is

$$\bar{A} = \sum \beta_i \cdot A_i^2 / \sum \beta_i \cdot A_i ,$$

$\bar{A}=3.5$ correponds to the composition: $\beta_1=.939$, $\beta_4=.055$, $\beta_9=.0009$, $\beta_{14}=.0035$, $\beta_{28}=.0011$, $\beta_{56}=.0036$, which fits well both direct experimental data at 1 Gev/nucleon and Baksan gene-

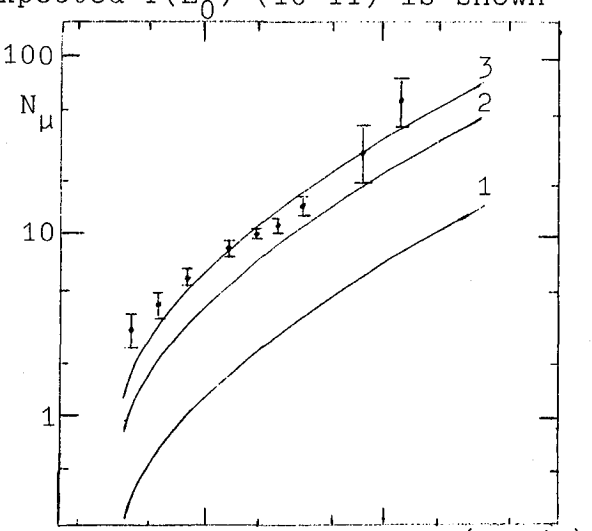

Fig.2

ral multiplicity spectrum.The data of this experiment is better fit by $\bar{A}=4.5$,but the difference is not significant on the basis of a possible systematic error.The conclusion is that in the range $1\text{-}10^5$ Gev/nucleon there is no visible change of the mean atomic number.

References

1. A.E.Chudakov et al. Proc. of 16 ICRC,v.10,p.188,1979.
2. A.E.Chudakov et al. Proc. of 16 ICRC,v.10,p.175,1979.
3. Yu.M.Andreyev et al. Proc of 17 ICRC,v.7,p.67,1981.
4. E.V.Bugaev et al. The cosmic ray muons and neutrino,Moscow, Nauka,p.15,1970.
5. S.Hayakava The cosmic ray physics,Moscow,Mir,v.2,p.511, 1970.
6. E.V.Bugaev et al. Cosmic ray muons and neutrino,Moscow, Nauka,p.23,1970.
7. L.B.Bezrukov and E.V.Bugaev Proc of 17 ICRC ,v.7,x.90,1981.
8. A.M.Hillas Proc. of 16 ICRC,v.6,p.13,1979.
9. E.V.Budko et al. Proc of 19 ICRC,HE 5.1-12
10. I.W.Elbert and P.Summers Preprint UUHEP,83/20,University of Utah.
11. A.D.Erlykin Private communication.

ON MUON ENERGY SPECTRUM IN MUON GROUPS UNDERGROUND

V.N.Bakatanov,A.E.Chudakov,Yu.F.Novosel'tsev,
M.V.Novosel'tseva,Yu.V.Sten'kin

Institute for Nuclear Research,the USSR Academy of Sciences,Moscow

ABSTRACT

A method is described which was used to measure muon energy spectrum characteristics in muon groups underground using μ-e decays recording.The Baksan Telescope's experimental data on μ-e decays intensity in muon groups of various multiplicities are analysed.The experimental data indicating very flat spectrum does not however represent the total spectrum in muon groups.Obviously the muon energy spectrum depends strongly on a distance from the group axis.The "core attraction" effect makes a significant distortion,making the spectrum flatter.After taking this into account and making corrections for this effect the integral total spectrum index in groups has a very small dependence on muon multiplicity and agrees well with expected one: $\beta=\beta_{expected}=1.75$.

1.Introduction. It has been shown (1) that μ-e decays method can be used to measure an effective exponent of muon energy spectrum in muon groups underground,which is expected (2) to be much flatter than the total muon flux spectrum*). Unfortunately,such measurements are affected by so called "core attraction" effect,which preferably selects the central part of the muon group making the spectrum of recorded muos flatter,as compared with the spectrum in the group as a whole.This effect depends on the ratio of detecting area size to the muon group dimension,on the form of lateral distribution function and on muon multiplicity spectrum.To make the corrections for "core attraction" effect we have to use the above mentioned parameters which we take from (1) and (7).Because the exponent of multiplicity spectrum is not a constant at small multiplicities,we have to do the analysis for different multiplicities separately.

For the total muon flux the relations between experimentally observed quantities R_{at} and R_{loc} and muon energy spectrum underground are well established and understood (3,4,5). By definition,R_{at} is the ratio of stopping to throughgoing muon fluxes normalized to 100 g/sm² target.R_{loc} is defined in similar way,but for cases when muon from atmosphere does

*) First experimental evidence of this has been presented in (5).

not stop and μ-e decays come from pions originated in muon induced hadronic cascade.

$$R_{at} = 100a \cdot \frac{dJ(0)/d\mathcal{E}_\mu}{J(>0)} \quad /1/; \qquad R_{at} = 100 \frac{a}{\mathcal{E}_0} \cdot \gamma \quad /1'/$$

$$R_{loc} = c \cdot \langle \mathcal{E}_\mu^{0.75} \rangle \quad /2/; \qquad R_{loc} = c \cdot \mathcal{E}_0^{0.75} (\gamma - 0.7)^{-0.8} \quad /2'/$$

$$dJ(\mathcal{E}_\mu)/d\mathcal{E}_\mu \simeq (\mathcal{E}_0 + \mathcal{E}_\mu)^{-\gamma-1} \quad /3/$$

The eqs. /1-2/ give these relations in general way. Here, $\mathcal{E}_\mu$ is muon energy underground, $a = 2.34 \cdot 10^{-3}$ Gev·sm²/g is mean ionization energy losses at our depth, $c = 2 \cdot 10^{-5}$ Gev$^{-.75}$ (adjusted by experiment). The eqs. /1'/ and /2'/ are valid if the spectrum underground is expressed by eq. /3/, $\mathcal{E}_0$ is a specific energy equal to 210 Gev for our depth. Eq. /3/ corresponds to purely power law muon spectrum $\sim E_\mu^{-\gamma-1}$, on the surface. Nevertheless, if the spectrum is not strictly a power law eqs. /1'/ and /2'/ can be used to determine the effective exponent γ near the depth energy threshold. But, in the case of muon groups such a procedure would be erroneous because of distortion due to "core attraction".

2. Experiment. In this experiment the μ-e decays were recorded in the second horizontal 200 m² and 40 tons scintillation layer of Baksan Telescope (4). Other 7 layers were used to determine the number of parallel muon trajectories (m) and to distinguich between "atmospheric" and "locally produced" events. The latter procedure is made with high confidence (~99%) for low multiplicities, but becomes difficult for m>30. The selection of m > 1 events was made by the off-line computer. All necessary data associated with these events were printed and analysed visually together with 10-beam oscilloscope slides of decay's electrons pulses. The only trigger used in the experiment was a delayed pulse in the mentioned scintillator layer with rate ≈30 h^{-1}. Data accumulated during 200 h of observation were included in the analysis. A flux of muons throughgoing the target layer in groups has been measured in a special short run with the same conditions and data processing but without requirement of μ-e decay.

3. Calculation of R_{at} and R_{loc} in muon groups. To do this the assumptions as in (1,2,7) and a number of consecutive integrations have to be made:

$$\varphi(N)dN \quad /4/; \qquad N' = N \cdot \Delta(R) \quad /5/; \qquad \Delta(R) = \iint_S F(z)\,dS \Big/ \int_0^\infty 2\pi z F(z)\,dz \quad /6/$$

$$F'(E_\mu, z) = E_\mu^{1-\beta} \cdot e^{-\left(\frac{z}{z_0} \cdot \frac{E_\mu}{E_t}\right)^{0.7}} \quad /7/; \qquad F(z) = \int_{E_t}^\infty F'(E_\mu, z)\,dE_\mu \quad /8/$$

$$G_m(R)dR = 2\pi R\,dR \int_0^\infty \frac{dN'}{\Delta(R)} \cdot \varphi\left(\frac{N'}{\Delta(R)}\right) \cdot e^{-N'} \frac{(N')^m}{m!} \quad /9/$$

$$Q_m(E_\mu) = m \int_0^\infty dR\, G_m(R) \cdot \Psi(R, E_\mu) \qquad /10/$$

$$\Psi(R, E_\mu) = \iint_S F'(E_\mu, z)\, dS' \Big/ \int_{E_t}^\infty dE_\mu \iint_S F'(E_\mu, z)\, dS' \qquad /11/$$

$$E_\mu = \varepsilon_\mu \cdot e^{\beta x} + \frac{a}{b}\left(e^{\beta x} - 1\right) \qquad /12/$$

Here in /4/:N is the mean number of muons at a given depth from definite primary, $\varphi(N)dN$ is a distribution of N assuming standard energy spectrum and chemical composition of primaries.

In /5/: $\Delta(R)$ is a fraction of N which happened to be inside detecting area,R is a distance between centre of area and muon group core.

In /6/ : $\Delta(R)$ is calculated using lateral distribution function F(r),where r is a distance between area element dS and core position.

Eq./7/represents the assumed lateral-energy distribution of muons,E_μ is muon energy at the surface,ß is integral exponent of power law muon spectrum there,E_t is the minimal energy to penetrate to a given depth.For our depth r_0=6.2 m if ß=1.75.Eq. /8/ represents muon lateral distribution.

In /9/:$G_m(R)$ is distribution of impact parameter R for a given multiplicity m.Poisson fluctuations of m for a given N' are assumed.Fig.1 shows these normalized distributions for several m.Curve ($m \geqslant 1$) represents the case without core attraction: $G_{\geqslant 1}(R) \sim 2\pi \cdot R \cdot \Delta(R)$.One can see that for $m > 3$ the distortion of distribution of R becomes standard,for m=1 the distortion is small,but of the opposite sign.

In /10/:by integrating $F'(E_\mu, r)$ over detecting area S, r being the distance between dS and the group core,then integrating over R we get the muon energy spectrum inside the detecting area for a given recorded multiplicity m.

Eq. /11/ represents the normalized muon energy spectrum at a given R.Eq. /12/ is relation between muon energy underground (ε_μ) and on the surface (E_μ).

Next steps are as follows:using /12/ transform /10/ into spectrum underground;put this spectrum into eqs./1-2/ and obtain the expected quantities R_{at} and R_{loc} for assumed ß;select ß which fits the experimental values of R_{at} and R_{loc}.So, for each m we obtain two values of ß: $ß_1$ related to R_{at},and $ß_2$ related to R_{loc}.If all the procedure is reliable and the surface muon spectrum follows power law,then $ß_1$and $ß_2$ should coincide.

4.Results. All the data are presented in Table. Denoted as $ß_1^*$ and $ß_2^*$ indices are exponents obtained without taking into account the "core attraction" effect, but simply using eqs. /1*/ and /2*/. It is seen, that corrected exponents ß are bigger than noncorrected ß*. On the other hand, one can see

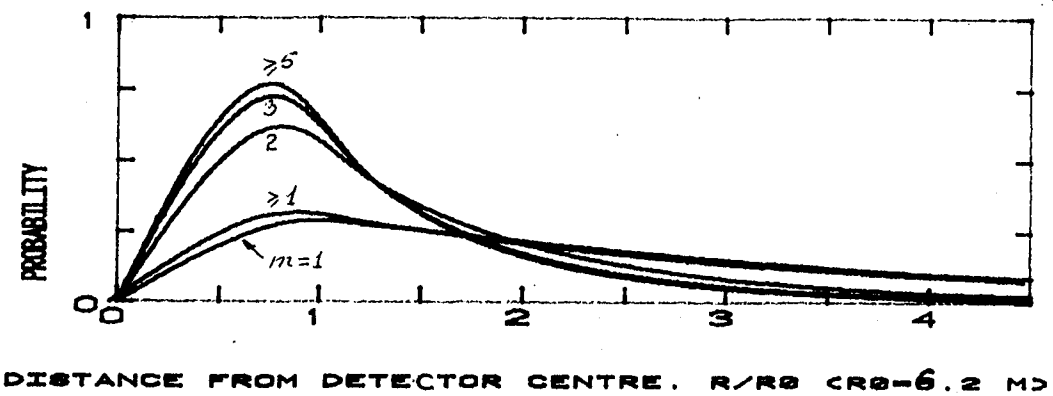

Fig.1. Distribution of impact parameter R for various multiplicities.

that β_1 and β_2 are closer to each other than β_1^* and β_2^* which indicates a good fit to the power law spectrum, what can be expected. Deviations from this for m=11÷30 has probably statistical origin, for m=2 it could be expected because of primary nucleon energy for m=2 is not big enough (7).

Taking all events with $m \geqslant 3$ and using both β_1 and β_2 we obtain the integral spectral index of muons in groups as $\beta = 1.67 \pm 0.11$ for $E_\mu \geqslant 200$ Gev. This result is in agreement with EAS data (6).

Table

m	2	3+4	5÷10	11÷30	≥1	≥2	≥3
$R_{at} \times 10^3$	1.18 ±.16	1.29 ±.26	1.15 ±.33	0.66 ±.29	2.31 ±.06	1.17 ±.09	1.16 ±.17
$R_{loc} \times 10^3$	0.87 ±.12	1.27 ±.23	1.75 ±.38	1.68 ±.47	0.75 ±.03	1.27 ±.08	1.76 ±.20
β_1^*	1.07 ±.15	1.17 ±.24	1.05 ±.30	0.60 ±.26	2.10 ±.08	1.06 ±.08	1.05 ±.15
β_2^*	2.08 ±.25	1.56 ±.20	1.27 ±.16	1.31 ±.23	2.36 ±.08	1.56 ±.06	1.27 ±.08
β_1	1.55 ±.14	1.83 ±.27	1.73 ±.35	1.18 ±.41	2.10 ±.08	1.54 ±.17	1.71 ±.25
β_2	2.32 ±.21	1.90 ±.16	1.67 ±.12	1.73 ±.18	2.36 ±.08	1.88 ±.06	1.66 ±.13

References

1.Bakatanov V.N. et al.Proc. 18 ICRC,Bangalore,11,453,(1983)
2.Chudakov A.E. Proc.16 ICRC,Kyoto, 10, 192, (1979)
3.Alexeyev E.N. et al. Proc. 13 ICRC,Denver,3,1936,(1973)
4.Bakatanov V.N. et al. Proc. 16 ICRC,Kyoto,10,179,(1979)
5.Bakatanov V.N. et al. Proc. 16 ICRC,Kyoto,10,175,(1979)
6.Atrashkevich V.B. et al.Proc.18 ICRC,Bangalore,11,229,(1983)
7.Budko E.V. et al. This conference, HE 5.1-12

ENERGY SPECTRUM OF CASCADES GENERATED BY MUONS IN BAKSAN UNDERGROUND SCINTILLATION TELESCOPE

V.N.Bakatanov, A.E.Chudakov, Yu.F.Novosel'tsev, M.V.Novosel'tseva, V.M.Achkasov, A.M.Semenov, Yu.V.Sten'kin

Institute for Nuclear Research, the USSR Academy of Sciences, Moscow

ABSTRACT

Spectrum of cascades generated by cosmic ray muons underground is presented. The mean zenith angle of the muon arrival is $\bar{\theta}=35°$, the depth $\sim 1000 hg/cm^2$. In cascades energy range >700 Gev the measured spectrum is in agreement with the sea-level integral muon spectrum index $\gamma=3.0$. Some decrease of this exponent has been found in the range >4000 Gev.

1. Introduction. General description of the Baksan Underground Telescope is given in ref. (1). The experiment (2) using the Telescope as a calorimeter to study muon induced electromagnetic and hadronic cascades is in progress now. New experimental data are available and analysed here.

2. Experimental details. The 4 scintillation layers structure, the large total thickness (~25 radiation lengths) and big area (>200 m^2) (1,2) enable to record muon-nucleus interactions with energy transfer up to ~20 Tev. The 4 scintillation layers are separated by 0.8 m or 144 g/cm^2 of absorber (low radioactive minerals mostly olivine, with $\bar{Z}\approx 14$ and $\bar{A}\approx 27$ placed on 8 mm iron sheet being used for support. The layer of 23.4 g/cm^2 of liquid scintillator is formed by 400 (or 576 for top layer) individual detectors, 30x70x70 cm^3 each. There is 2.5 m air gap between scintillators and iron sheet at the ceiling. Total thickness corresponding to one layer is 8.2 radiation lengths and a distance between the layers is 3.6 m.

Energy release is measured by logarithmic charge-to-time converters in every detector. The converters thresholds were adjusted to 500 Mev (10 r.p. - relativistic particles), using a pulsed X-ray sourse. These thresholds and converters slopes (22% per 1 step or 10 μs) were examined by ON-LINE computer monitor program permanently. Special low-level trigger ($\geqslant 7$ r.p. in any scintillator layer) is used for this purpose. Counting rate of each detector with 500 Mev threshold is only 0.3 h^{-1}. We use weekly the accumulated monitor information to check every detector and to repair or adjust it if required. The main trigger is produced in a case, when the energy release in any horizontal scintillator layer is $\geqslant 50$ r.p. (2.5 Gev). By this trigger all available information, associated with the event will be recorded on the magnetic tape and the 10-beam oscilloscope screen will be photographed. The oscillosco-

pe is used to visualize each scintillator layer's pulse for π-μ-e decays recording. Further data processing is carried out by OFF-LINE computer selecting events of given energy. Only cascade with axes crossing no less than 3 norizontal layers have been included in the analysis. Mean zenith angle due to such a selection equals to $\bar{\theta}=35°$.

3. Results. Data accumulated during a 11640^h run of the experiment are shown in fig.1. Solid curves represent calculated cascade size spectra obtainedin following assumptions:

i) all kinds of μ-A interactions can be expressed in analitical form as in ref.(3);

ii) muon see-level spectrum is purely power law and underground at our depth it has a form:

$$dN(E_\mu)/dE_\mu \sim (200+E_\mu)^{-\gamma-1}, \qquad E_\mu \text{ in Gev}$$

and $\gamma=2.8$ or $\gamma=3.0$.

To obtain the total cascade energy from visible one (released in scintillators) cascade curves (4,5) for homogeneous matter were used assuming uniform cascades production and observed angular distribution of the cascade axes.

These cascades curves have been corrected for transition effect, geometrical configuration and a loss because of 10 r.p.(500 Mev) energy threshold by Monte-Carlo cascade simulations. The correction factor ($\sim$20%) does not depend on cascade energy. The correction for the loss due to finite detectors energy thresholds, though small, was made individually for each event using low energy 0.25 r.p. integral discriminators installed in each detector. Monte-Carlo simulation showed that the mean energy release in the interval 0.25r.p. $<E<$ 10r.p. is 1.6r.p.. Finally, we have the transition factor from visible energy, released in scintillator, to the mean total energy. For electron-photon cascade and hadronic cascade these factors are slightly different, correspondingly 8.6 and 9.7, but practically do not depend on cascade energy for $E_c > 700$Gev.

4. Conclutions. Some excess of the experimental relative to calculated cascades spectrum can be seen in fig.1 in the energy range >4000 Gev. But, this is not statistically well established being less than 2σ effect. Note that the spectrum is presented in integral form, so the points are not statistically independent. Actually the point at $\sim$8000 Gev(6 events) is responsible for all excess. At lower energy in the range 1$\div$4 Tev the best fit is obtained for integral muon spectrum at the surface as E_μ^{-3}. This exponent $\gamma=3$ deviates from the most popular exponent $\gamma=2.8$ (6). One can hope that future experiments will clarify the situation and probably explain the small differenses, which traditionally are arising in different experiments dealing with muon induced cascades and muon spectra.

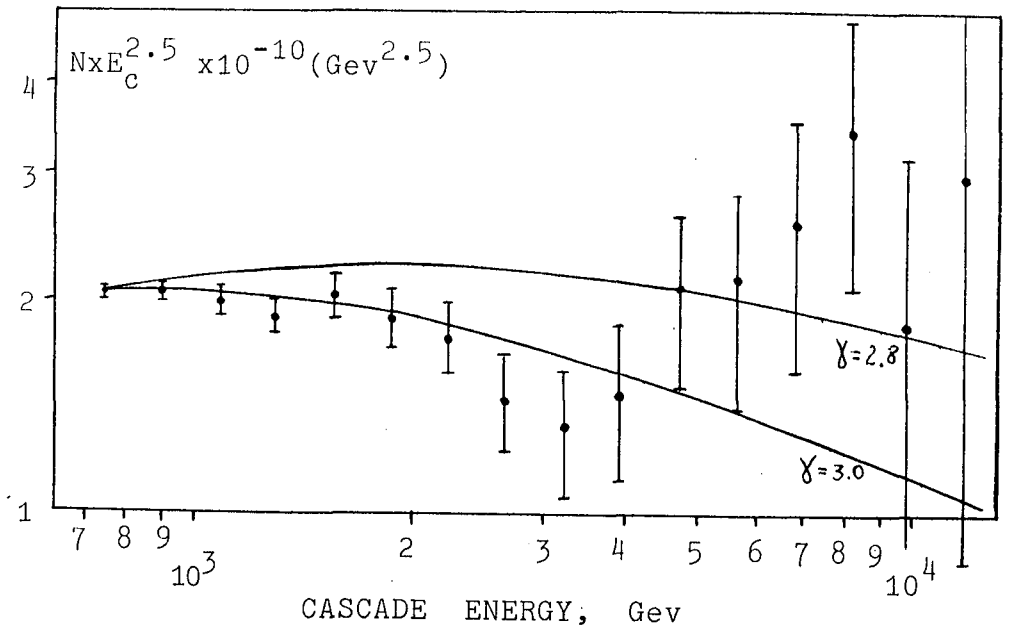

Fig.1. Cascades size spectrum.

References

1.Alexeyev E.N. et al.Proc. 16 ICRC, 10,276,(1979)
2.Andreyev Yu.M. et al.Proc. 17 ICRC, 7,67,(1981)
3.Bugaev E.V. et al.Cosmicheskie muony i neytrino.Nauka, Moskva, 1970.
4.Klimakov A.P. et al.Elementarnye chasticy.MIPhI,Moskva,1967
5.Dem'yanov A.I. et al.Yaderno-kaskadny process v plotnom veschestwe.Nauka, Moskva, 1977.
6.Elbert J.W. 18 ICRC, Rapporteur paper, 12,495, 1983.

HE 5.1-16

UNDERWATER MEASUREMENTS OF MUON INTENSITY

V.M.Fedorov, V.P.Pustovetov, Yu.A.Trubkin, A.V.Kirilenkov

P.N.Lebedev Physical Institute
117333, Moscow
USSR

ABSTRACT

Previous results of the experiment on underwater measuremens of muon intensity at depths down to 5 km are reported.

1. Introduction. Experimental measurements of cosmic ray muon intensity deep underwater aimed at determining a muon absorption curve are of considerable interest, as they allow to reproduce independently the muon energy spectrum at sea level. The comparison of the muon absorption curve in sea water with that in rock makes it possible to determine muon energy losses caused by nuclear interactions. The data available on muon absorption in water and that in rock are not equivalent. Underground measurements are numerous and have been carried out down to the depth of $\sim$ 15km w.e., whereas underwater muon intensity have been measured twice /1,2/ and only down to $\sim$ 3km deep.

2. Apparatus and Operation. To carry out muon intensity measurements in sea water at depths of 2 to 7km, a three-unit Cerenkov detector was developed to register Cerenkov light flashes of muons in the surrounding sea water. A detailed description of the Cerenkov unit and the results of its operation test have been given elsewhere /3/. In our case all the unit photomultipliers were connected into one electrical group, pulses inside the group being summarized. Unit signals were put to the three-fold coincidence scheme with a resolving time of 50nsec. The coincidence signals were recorded within 15 minute time intervals. The general design of the detector made it possible to change relative position of the units which could be arranged either abreast on a horizontal plane or in an upright chain("string"). The detector was fully autonomous, electric power being fed from an accumulator. The device was exposed at chosen depths on a cable from the board of a drifting research vessel. The depth of the device exposition was maintained constant with an accuracy of $\simeq$ 1-3%.

In 1983 during the 37-th voyage of the Soviet r/v "Akademik Kurchatov" measurements were taken of global intensity. Three detector units were arranged abreast horizontally, with photocathodes directed upwards. The measurements were carried out in the Caribbean sea (19°N; 76°W) and in the Atlantic Ocean within the DUMAND zone (22°N; 37°W). The results of the measurements are given in Table 1.

Underwater measurements of muon intensity were also carried out during the 40-th voyage in 1984, the detector units being arranged in an upright chain("string") with spacing of 3 m. When all the units photocathodes were directed upwards, mostly vertical muon fluxes were registered. The other way, when the photocathdes of the upper unit ewre directed downwards, a lateral flux was registered, i.e. particles move at the angle of more than $\simeq 60^{\circ}$ to the zenith. The studies were carried out within "DUMAND" zone in Canary Hollow. The results of the measurements are given

in Table 1.

Table 1

Flux measured	Depth, km	Exposition time, min	Registration threshold	Number of events
Global	2.0	150	≃ 1e	709*
	3.0	585		622
	2.0	150		744*
	2.0	135	≃ 1.5e	441*
	4.0	1200		288
	2.0	135		470*
	3.0	180	≃ 2e	75*
	5.0	1305		86
Vertical	2.0	330	≃ 1e	1304
	3.0	480		417
	5.0	1920		168
Lateral	1.5	345	≃1e	291
	2.0	765		177
	2.5	960		69
	3.0	540		16
	3.5	300		5

* - Normalization measurements

3. Results and Discussion. To obtain correct quantative results with the given detector, it necessary to consider background events which imitate muon registration. Since a three-fold coinsidence scheme is used to separate useful events, there may be events caused by appropriate combination of various background components. The Cerenkov light caused by sea water radioactiviyt is mainly due to the decay of K^{40}. The activity of K^{40} in sea water was determined from potassium salinity relation and was equal to $\sim 1.14.10^{4} m^{-3} s^{-1}$(ß-decay) and $\sim 1.34.10^{3} m^{-3} s^{-1}$(e-capture). The calculation of an average number of photons generated in one act of K^{40} decay is performed in /4/. The average photon numbers as fractions of the number of photons generated by a muon per 1cm path in water are equal to $9.7.10^{-2}$ at ß-decay, and to 0.141 at e-capture (in the first Compton scattering), and to 0.034 (in the second Compton scattering). Bioluminescence in deep sea water is a less studied background source. The latter depends strongly on various factors, such as exposition place, depth, excitation nature, etc. For a series of the measurements taken, the estimation of the background value can be obtained from the data registered at the depth of 3.5km by the detector, with the upper unit being directed downwards. In this case the expected muon number is much less then the detected number of events which can be taken for an averall background for the particular deepwater muon detector at the place where the measurements are carried out. The value of such a background is of the order of one event per an hour of the device operation.

The values of vertical cosmic muon intensity at large depth underwater were obtained on the basis of global muon flux data treatment and by taking

traditional cosmic muon angular distribution into consideration. These are:

$$I_o(H=2925^{+45}_{-65}\ \text{m}) = (3.1\pm0.5).10^{-8}\ \text{cm}^{-2}\text{s}^{-1}\text{sr}^{-1}\ ;$$

$$I_o(H=4025^{+22}_{-26}\ \text{m}) = (5.9^{+2.0}_{-2.5}).10^{-9}\ \text{cm}^{-2}\text{s}^{-1}\text{sr}^{-1}\ ;$$

$$I_o(H=5020^{+140}_{-200}\ \text{m}) = (4.1^{+1.6}_{-2.0}).10^{-9}\ \text{cm}^{-2}\text{s}^{-1}\text{sr}^{-1}\ .$$

The total of experimental data on muon absorption in sea water /1,2,5/ was treated with the help of the least square method and fitted by empirical expression:

$$I_o(H) = A\,H^{-\alpha}(H + H_o)^{-1}\,(1 - \exp(-\gamma H))\,\exp(-\beta H)$$

where: H - depth, hg.cm^{-2} , $I_o(H)$ - vertical intensity, cm^{-2}s^{-1}sr^{-1}, values of free parameters are equal

$$A = 3.73 \pm 0.06$$

$$\alpha = 1.130 \pm 0.004$$

$$\beta = (5.42 \pm 0.23).10^{-4}$$

$$H_o = 11.4 \pm 1.3$$

$$\gamma = (3.7 \pm 0.2).10^{-2}.$$

The data on cosmic muon intensity obtained at different depths in sea water and those obtained previously are presented in Fig.1. Here are also given estimated curves of muon absorption in water which were calculated on the basis of modern conception of muon generation/6/ and muon absorption/7/.

4. Conclusion. The experimental data are in a satisfactory agrrement with t the estimated ones within the limits of measurement errors. Hence the integral muon energy spectrum at sea level within the energy range 2-3.10^3 GeV is described by the mean value of index $\gamma_{\pi,K} = 1.65$ for particles - parents of muons.

References

1. Higashi S. et al.Nuovo Cimento(1966) v.43A, N2, p334
2. Davitaev L.N. et al. Proc.11-th ICRC(1969), Acta Phys.Hung.v.29,Suppl.4, p53
3. Davimus G.D. et al. Proc.17-th ICRC(1981) v.10, p380
4. Kirilenkov A.V. et al. Issledovanie muonov i neitrino v bolshikh vodnykh obyomakh,Alma-Ata(1983),p166.
5. Rogers I.W. et al. Proc.18-th ICRC, Bangalore(1983), v.7, p32
6. Volkova L.V. et al. Proc.15-th ICRC, Plovdiv(1977), v.6, p6
7. Bezrukov L.B. et al. Proc. 17-th ICRC,Paris(1981), v.7, p102

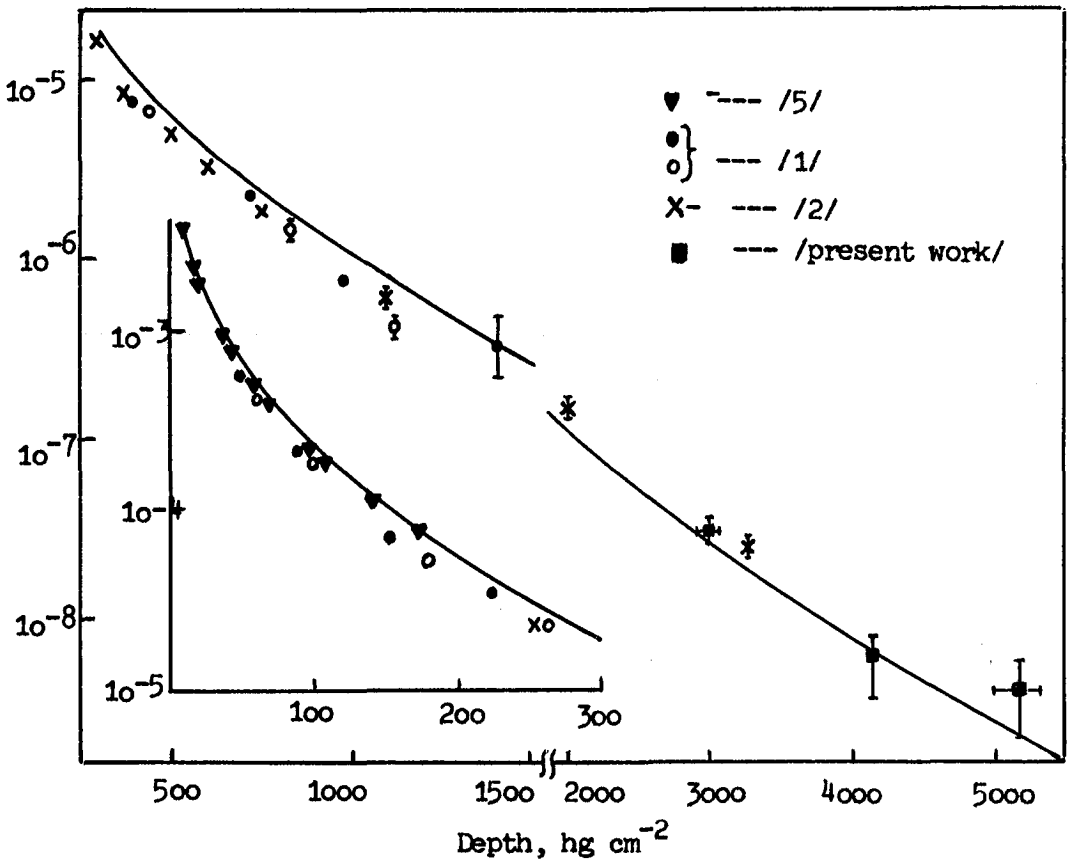

Fig.1. The total of experimental data on muon absorption in water as a function o fdepth.

Multiple Muons in MACRO

MACRO Collaboration (1)
presented by
R. Heinz
Indiana University

We show how an analysis of the multiple muon events in the Monopole Astrophysics and Cosmic Ray Observatory detector can be used to determine the cosmic ray composition. Particular emphasis is placed on the interesting primary cosmic ray energy region above 2000 TeV/nucleus.

An extensive study of muon production in cosmic ray showers has been done by Gaisser and Stanov (2). Results were used to parameterize the characteristics of muon penetration into the earth to the location of a detector.

The mean number of muons at a slant depth X is

$$\langle N_\mu \rangle = \frac{1}{E_\mu}(.0142)\left(\frac{E_p}{E_\mu}\right)^{.775}\left(1 - \frac{E_\mu}{E_p}\right)^{5.96}\sec\theta,$$

where E_p is the primary energy per nucleon, θ is the primary direction relative to the vertical, and

$$E_\mu(\text{TeV}) = .53(e^{.4X}-1)$$

is an effective muon threshold energy (so that $E_p > E_\mu$ is required). Each nucleon in a primary nucleus contributes this same average number of muons. The N_μ distribution is taken to be Poisson.

The lateral distribution of muons at the detector depth is

$$\frac{dN_\mu}{dR_\mu} \propto R_\mu e^{-2R_\mu/\langle R_\mu \rangle}, \text{ where}$$

$$\langle R_\mu \rangle = 3.13E_\mu^{-.46} + 13.2E_\mu^{-.31}\left(\frac{E_\mu}{E_p}\right)^{.62} .$$

Here R_μ is measured perpendicular to the shower core. The R_μ and N_μ distributions are uncorrelated.

These parameterizations yield predictions for the Kolar Gold Field experiment (3) which agree well with the data (4).

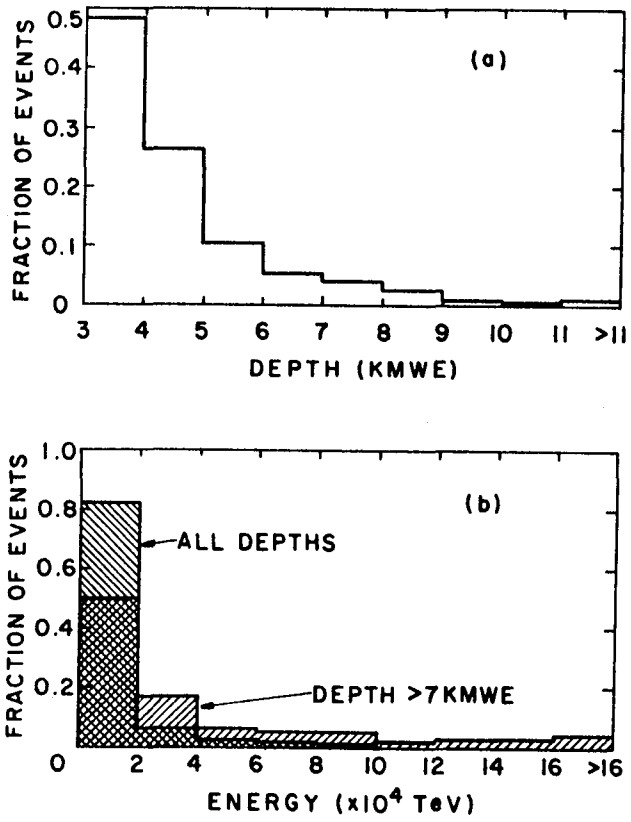

Fig. 1 a) Distribution of overburden (depth) that muons must penetrate to reach the detector. b) Distribution of primary cosmic ray energies (per nucleus) for all depths and for depths greater than 7 KMWE.

The MACRO detector is taken to be a horizontal rectangle 12m by 112m, and all muons striking this rectangle are assumed to be detected. (We are currently redesigning the apparatus so that it will have a significant size in the vertical direction; the present height is 5.7 m high).

Muons that reach the detector pass through a variable slant depth of material in the irregularly-shaped Gran Sasso Mountain. In Fig. 1a we show the slant depth distribution in units of KMWE. Because we measure muon directions with high resolution ($\sim .2^{o}$), we can select on the slant depth and thereby have a data sample with a distribution of primary energies that can be changed. For example, in Fig. 1b we show the distribution of primary energies (per nucleus) for all depths, and separately for depths that are greater than 7 KMWE. The percentage of events with primaries < 2000 TeV/nucleus is 31% for all events but only 8% for the restricted sample.

A major goal of MACRO is to determine the cosmic ray composition above the 2000 TeV "knee" in the energy distributions. We have studied four models for this high energy composition:

1. Fe — All primaries are iron nuclei.
2. Md — A mix of primaries is used with iron dominating at high energy.
3. LE — Primary composition at high energies is the same as at 50 GeV/nucleon.
4. p — All primaries are protons.

Models Md and LE are described in reference 3.

In Fig. 2 we show the detected muon multiplicity distributions for the four models (solid curves), all normalized to the single muon rate.

For a given nucleus energy, the proton has a much larger energy per nucleon than iron, so protons give many more single muon events; however, the iron nucleus produces many more muons so its multiple muon to single muon ratio is larger. However, lateral spreads (decoherence) from iron are larger, so a large detector like MACRO is needed to exploit this difference.

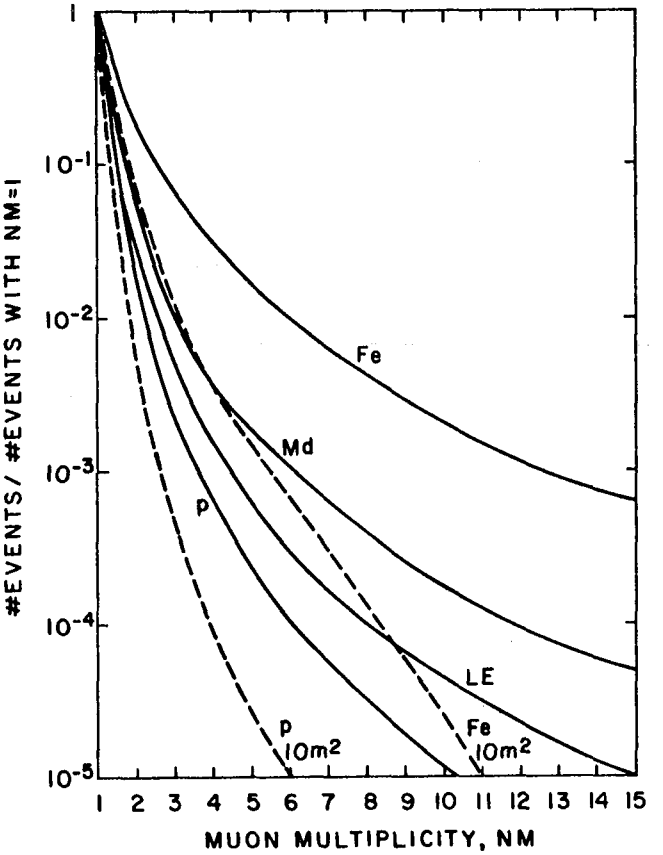

Fig. 2 Muon multiplicity distribution divided by single muon rate for various hypotheses. (See text.)

The dashed curves in Fig. 2 show how difficult it is for a small detector ($10m^2$ area) to measure high multiplicities. For 10 μ's, the Fe hypothesis yield is down two orders of magnitude. The absolute MACRO yields are about 500K/year for Fe and 13M/year for protons, including single muon events. Depending on composition, the number of events with NM > 5 will be 500 to 20,000!

One aspect of the muon decoherence which is particularly sensitive to primary composition is the maximum separation of a pair of muons in a multiple muon event. In Fig. 3 we show this distribution for the four composition hypotheses and for three different ranges of slant depth (and thus three different primary energy distributions).

Figures 2 and 3 both show that MACRO is sensitive to the cosmic ray primary composition at high energy.

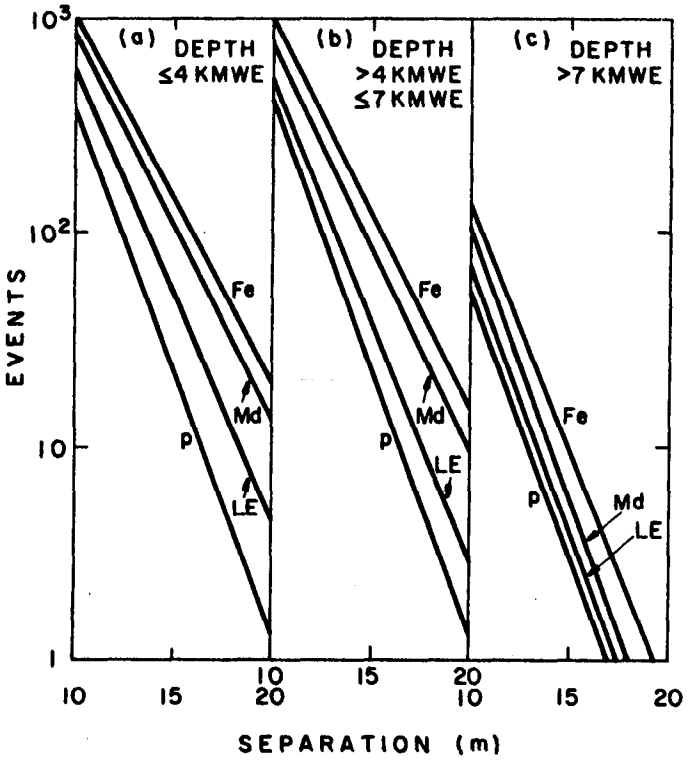

Fig. 3 Distribution of maximum two-muon separation in a multiple muon event for three ranges of overburden.

References

1. B. Barish, these proceedings.
2. T. Gaisser and T. Stanev, to be published in Nuclear Instruments and Methods.
3. G.B. Yodh, Todor Stanev and T.K. Gaisser, in Proceedings of ICOBAN 1984.
4. G. Yodh, T. Stanev, and T. Gaisser, 1984 ICOBAN, Park City, Utah.

THE NAGOYA COSMIC-RAY MUON SPECTROMETER III

I PRELIMINARY OBSERVATIONS

Kamiya,Y.,Shibata,S.,Iijima,K. and Iida,S.*
Nagoya University, Nagoya, Japan
Toyohashi University of Technology, Toyohashi, Japan

ABSTRACT

1.Introduction. There are some discrepancies among the data of absolute muon intensities at large zenith angles. Through the analysis of the data obtained in the previous measurement by Nagoya Cosmic Ray Spectrometer (II), we have found one of the sources of these discrepancies to be the ambiguity induced by the selection criteria with which "genuine" muons are distinguished from the backgrounds. To remove the ambiguity of this kind, it is necessary to know the amount of the backgrounds and their characteristics in detail.

At Paris conference, some features of the background events were reported from the observations by using this triggering system of Nagoya Cosmic Ray Spectrometer(III).

In this paper, the results of extended observations using track detector together with this system will be reported.

2.Experimental method. The trigger counter system consists of 1)outer trays(Sc1,Sc8 in Fig.1) placed at a distance of 5m from each other and 2)3 pairs of inner trays (Sc2,Sc5; Sc3,Sc6 and Sc4,Sc7 in Fig.1) placed on both sides of the magnet. The arrangement of them is shown Fig.1.

2 fold coincidence composed of outer trays determines the direction of incident particle with the time-of-flight method. At least one of the 3 pairs of inner trays has to be make a 2 fold coincidence.

If the delay time of T.O.F.method is set for 17nsec (corresponds to the distance 5m between outer trays), the events which satisfy conditions can be regarded as the horizontal muon passages.

The possible coincidences can be divided into 13 patterns of scintillator trays (No.1∼No.13 in Fig.2). In addition to these, the sum of 12 patterns (No.2∼No.13) is also given (No.14).

Counting rate of each pattern was measured at various delay times of

T.O.F. system and some examples of experimental results are shown in Fig.3. It is shown that backgrounds can be considered the mixture of local shower (low density) and air shower (high density).

3.Analysis. On the basis of these experimental results, following estimations for counting rates of shower trigger events are given.

The frequency of showers that incident at zenith angle Z with density of particle between Δ and $(\Delta+d\Delta)$ in solid angle $d\Omega$, $f(Z,\Delta)d\Delta d\Omega$, will be approximated as follows,

$$f(Z,\Delta)d\Delta d\Omega = f_0 \cos^N Z(\Delta+\Delta_0)^{-\gamma} d\Delta d\Omega.$$

where $f_0\cos^N Z$ and $(\Delta+\Delta_0)^{-\gamma}$ represent zenith angle distribution and density spectrum, respectively. If particle density is assumed to be uniform on a shower front, the coincidence rate can be expressed as a function of delay time, τ.

$$C(\tau)d\tau = 2f_0 \cdot 1/\tau m \cdot \{1-(\tau/\tau m)^2\}^{N/2} dt \int_0^{\pi/2} \cos^N\psi \cdot P \cdot d\psi d\Delta .$$

where P is a detection probability for each coincidence condition listed in Fig. 2. Using $C(\tau)$, practical counting rate of shower trigger events at each delay time can be expressed as follows,

$$F(\tau)d\tau = \frac{1}{\sqrt{2\pi}\sigma}\int_{-\infty}^{\infty} C(\tau') e^{-\frac{(\tau-\tau')^2}{2\sigma^2}} d\tau'.$$

where σ is the time resolution of detector including the fluctuation of shower front.

In above calculations, N, γ, Δ_0 and σ are included as parameters which describe the characteristics of shower. $F(\tau)$ is calculated for local shower ($F^L(\tau)$) and air shower ($F^A(\tau)$) respectively, and from these calculations counting rate $I^{cal}(\tau)$ which is comparable with experimental data can be expressed as follows,

$$I^{cal}(\tau) = \alpha_L \cdot F^L(\tau) + \alpha_A \cdot F^A(\tau)$$

where both of α_L and α_A are constants. From $I^{cal}(\tau)$ and experimental data $I^{exp}(\tau)$ around 0 nsec, chai-square value was calculated and 4 parameters for each of local shower and air shower were determined at chai- square minimum. α_L and α_A were also determined by the least square method between $I^{cal}(\tau)$ and $I^{exp}(\tau)$. The results are shown as follows.

	N	γ	$\Delta_0(m^2)$	σ(ns)	f_0 ($h^{-1}\cdot sr^{-1}\cdot m^{-2}$)
local shower	2	4.5	0.07	6.5	1.88×10^3
air shower	7	3.0	5.0	6.5	3.84×10^5

4.Conclusions. It is found that one of the sources of the discrepancies among the data of absolute muon intensities is to be the ambiguity induced by the selection criteria.

Some features of the background events which are considered to be the mixture of the showers, air shower and local shower, with different density spectra and diffrent zenith angle dependence, are obtained.

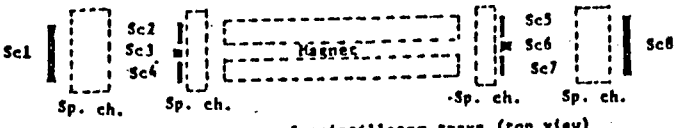

Fig.1, Arrangement of scintillator trays (top view)

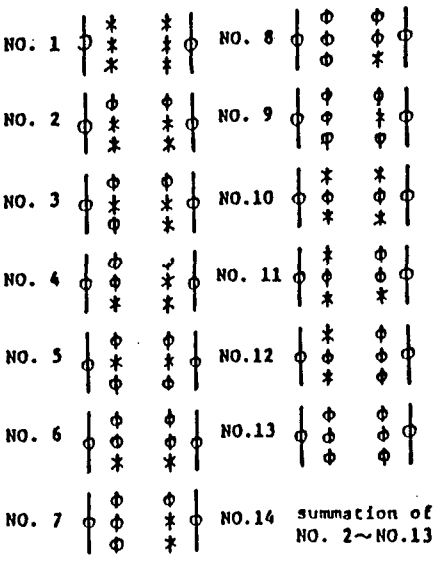

Fig.2,Patterns of coincidences

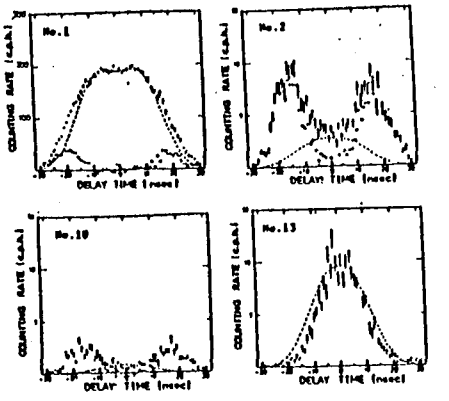

Fig.3, Counting rates of coincidences(examples)

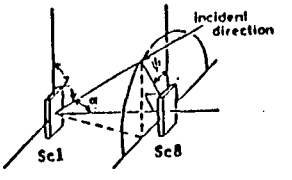

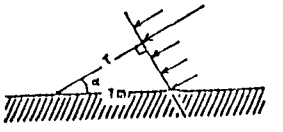

Fig.4

THE NAGOYA COSMIC-RAY MUON SPECTROMETER III

II TRACK DETECTOR

Shibata,S.,Iijima,K.,Kamiya,Y. and Iida,S.*
Nagoya University, Nagoya, Japan
* Toyohashi University of Technology, Toyohashi, Japan

ABSTRACT

Not only to obtain the precise locations of particles, but also to get some informations about the correspondences between segments of trajectories, we utilize the twelve wide gap spark chambers as the track detectors of the Nagoya cosmic-ray muon spectrometer (1).

The area of each chamber is 150 x 70 cm^2 and the width of a gap is 5 cm. The gas used is He at the atmospheric pressure. Each three pairs of them are placed on both sides of the deflection magnet. All images of sparks for each event are projected through the mirror system and recorded by two cameras stereoscopically.

The mean detection efficiency of each chamber is 95 ± 2 % and the spacial resolution (jitter and drift) obtained from the prototype-experiment (2) is 0.12 mm. Maximum detectable momentum of our spectrometer is estimated at about 10 TeV/c taking into account of these characteristics together with the effects of the energy loss and multiple Coulomb scattering of muons in the iron magnet (3).

All the chambers have already installed in the spectrometer and they worked well in test runs of full system. Now, we are operating this spectrometer to get the maximum detectable momentum experimentally with these track detection system.

References.

1. Kamiya,Y. et al., paper presented to this conference, HE 5.2-2.
2. Shibata,S. et al., 15th ICRC, plovdiv, 9, 56 (1977)
3. Kamiya,Y. et al., 17th ICRC, Paris, 9, 336 (1981)

HE 5.2-4

THE NAGOYA COSMIC-RAY MUON SPECTROMETER III

III AUTOMATIC FILM SCANNING EQUIPMENT

Shibata,S.,Kamiya,Y.,Iijima,K. and Iida,S.*

Nagoya University, Nagoya, Japan

* Toyohashi University of Technology, Toyohashi, Japan

ABSTRACT

In the regular operation of the Nagoya cosmic-ray muon spectrometer, about 2000 events per day will be recorded on the photographic film.

To derive the track locations from such a huge number of photographs with high accuracy in a short time, we have developed an automatic film scanning equipment. At Paris conference (1), we have reported the construction and characteristics of this equipment.

After that time, we have improved the film driving mechanism. Old mechanism is only used for the frame-to-frame advancement and the film is clamped on a table at every frame. For scanning of each frame, this table is driven by the pulsed stepping motor.

This modification makes the equipment suitable for the practical application to our measurments.

Reference.

1. Shibata,S. et al., 17th ICRC, Paris, 9, 376 (1981)

HE 5.2-5

THE NAGOYA COSMIC-RAY MUON SPECTROMETER III

IV TRACK RECONSTRUCTION METHOD

Shibata,S.,Kamiya,Y.,Iijima,K. and Iida,S.*

Nagoya University, Nagoya, Japan

* Toyohashi University of Technology, Toyohashi, Japan

ABSTRACT

For the measurements of the particle trajectories with the optical or visual detector system, it is one of the general problems to reconstruct the trajectories in real space from their recorded images.

In the Nagoya cosmic-ray muon spectrometer (1), muon tracks are detected by wide gap spark chambers and their images are recorded on the photographic film through an optical system of 10 mirrors and two cameras. For the spacial reconstruction, 42 parameters of the optical system such as the angles of mirrors should be known to determine the configulation of this system.

It will be almost impossible to measure these many parameters directly with usual technics. In order to solve this problem, we applied the inverse transformation method. In this method, all the optical parameters are determined from the locations of fiducial marks in real space and the locations of their images on the photographic film by the non-linear least square fitting.

reference.

1. Kamiya,Y. et al., paper presented to this conference, HE 5.2-2.

BACKGROUND LIGHT MEASUREMENTS AT THE DUMAND SITE

T.Aoki, T.Kitamura, S.Matsuno, K.Mitsui, Y.Ohashi and A.Okada
Institute for Cosmic Ray Research, University of Tokyo, Tanashi, Japan
D.R.Cady, J.G.Learned, D.O'Connor, M.McMurdo and R.Mitiguy
Hawaii DUMAND Center, University of Hawaii, Honolulu, USA
M.Webster
Department of Physics, Vanderbilt University, Nashville, USA
C.Wilson
Department of Physics, Purdue University, Lafayette, USA
P.Grieder
Institute of Physics, University of Bern, Switzerland

Ambient light intensities at the DUMAND site, west of the island of Hawaii were measured around the one photoelectron level. Throughout the water column between 1,500m and 4,700m, a substantial amount of stimulateable bioluminescence is observed with a ship suspended detector. But non-stimulated bioluminescence level is comparable, or less than, K^{40} background, when measured with a bottom tethered detector typical of a DUMAND optical module.

1.Introduction The deep ocean environment may be an excellent location for the study of high energy cosmic ray muons and neutrinos. Great depths provide a good shield against low energy cosmic ray muons, and the vast quantities of sea water can supply sufficient target material to detect interactions of very high energy neutrinos. A very large deep underwater muon and neutrino detector(DUMAND) has been proposed[1] and intensive feasibility studies have been performed. In the DUMAND project, very high energy muons and neutrinos are detected via the Cerenkov light emitted from secondary particles produced in their interactions within the sea water. However, even under deep ocean conditions there are some natural background light sources, Cerenkov light generated by radio isotopes and bioluminescent light by ocean inhabitants. We performed background light measurements by two different deployments, a ship suspended and a bottom tethered, and we have compared these two sets of data.

2.Apparatus and Experimental Procedures The instrument is self contained and powered by dry batteries. We used two 5" ϕ hemispherical photomultipliers(PMTs) mounted side by side in a glass housing of 17" ϕ. The space between PMTs and glass wall is filled with a transparent silicon jell to provide good optical contact. The high voltage power supplies and amplifiers for the PMTs are also mounted in the glass housing. The output signals from the PMTs are transmitted through cables to the data taking circuit contained in a separate metal housing.

The output signals from the PMTs are differentiated with time constant of 0.24 μsec and amplified with a gain of 100. The number of

pulses exceeding a preset discriminator level is counted by a 16bit counter. Signals coincident within 200ns from the two PMTs are also counted. The discriminator level and the gate time are automatically changed under control of a microprocessor following a program stored in the ROM. There are 23 sampling steps of the discriminator level ranging from 32mV to 800mV, which cover the signal region from one to ten photoelectrons. The gate time is selected for each threshold betweem 10ms and 10sec in order to smooth out statistical fluctuations.

Electronics including PMTs are activated by a timer. The number of signal counts together with channel number and gate time are stored in a microcassette recorder and these data are analyzed after recovery of the instrument.

Measurement were done on a cruise with University of Hawaii's research vessel Kana Keoki, August 24-26 1984 at the DUMAND site, 30km off Keahole point of the Big Island of Hawaii. First, the instrument was lowered down to 4,500m at a speed of 30m/min, suspended by a wire. After staying 45min at 4,500m, the instrument was wound up with a rate of 50m/min stopping every 1,000m. The data taking scheme was programed such that data were taken while stopping at the depths of 4,500 3,500, 2,500 and 1,500m. Next, the instrument was permitted to free fall to the sea floor of 4,800m depth. The sensor was mounted 100m above the mooring which included timed and acoustically triggerable releases. Flotation was attached to the instrument package and a buoy with radio beacons and strobe lights was attached 50m above. The data taking program was the same as for the first case except for the fact that measurements were repeated four times at the same depth.

3.Results In Fig.1 count rates versus time interval of observation are plotted. The data is for PMT No.1 at the threshold voltage of 320mV. Data points marked 1,2,3 and 4 are for the ship suspended case and each corresponds to count rates at the depth of 1,500, 2,500, 3,500 and 4,500m, respectively. Data with mark F is for the bottom tethered experiments. In Fig.1 we also plotted dark noise data, with mark C, measured in the laboratory at 3°C. From Fig.1 we can see clear differences in count rates depending upon the method of deployment. The ship suspended rates change with time very much except for case 1, where count rates are too high to be fully resolved. In contrast, the bottom tethered rates are comparatively stable and their absolute rates are about an order of magnitude lower than the ship suspended ones. The data for PMT No.2 shows almost the same behavior as PMT No.1.

Fig.2 shows the integral pulse height spectra observed by PMT No.1. Symbols 1,2,3,4,F and C are same as in Fig.1. The ship suspended data fluctuate very much and show a complicated behavior, whereas the bottom tethered spectrum is rather smooth. From Fig.2 we can see that the free fall count rate(F) converges to that of laboratory rate(C) in the highest channels. This result indicates that signals of F come from very weak sources.

Though the time variation of the bottom tethered rates are weak compared to the ship suspended case, we do observe some time spikes in the bottom tethered data. Such signals appear in both PMTs at the same time. Fig.3 shows examples of the time structure of the spike signals. It appears as if their time structure can be expressed by an exponen-

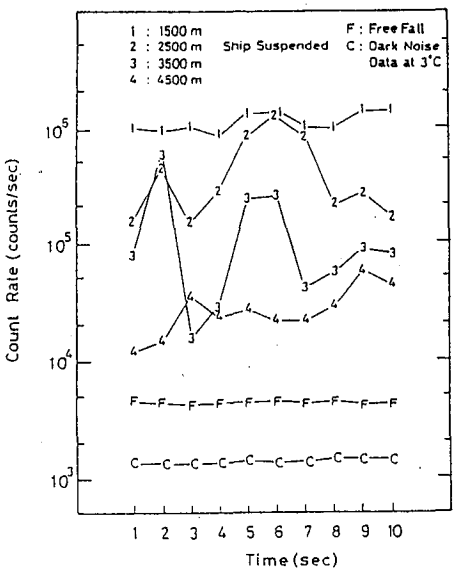

Fig. 1 Time Variation of Count Rate

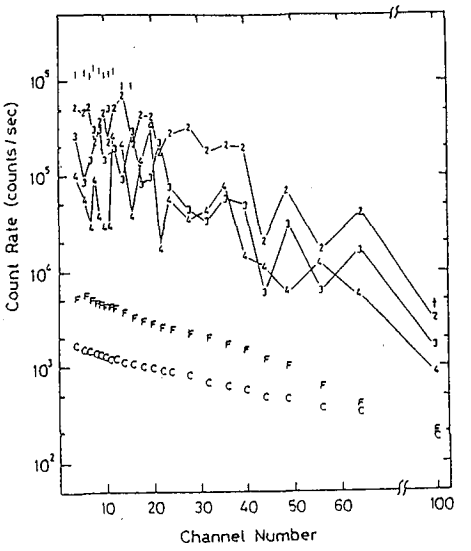

Fig. 2 Pulse Height Spectrum of Background

tial function with a time constant of 0.3 ~ 1.0sec. The observed frequencies and time structures seem to coincide with the expected signals in deep quiescent ocean basins.[2] In the case of the ship suspended method, the signal rates are too high for any time structure analysis with such a long time constant.

To estimate the absolute flux of the measured background light, we calibrated the detection power of our optical sensor[3]. Results of calibration show that the photon fluxes observed by the two PMTs No.1 and No.2 agree very well for all depths. Fig.4 shows the absolute light intensity versus depth. Because the count rates of the ship suspended case fluctuate largely, we plotted the median value in Fig. 4. The intensity curve can be expressed as a function of depth x as $I = 3.72 \times 10^5 \exp(-x(m)/877)$ quanta/cm^2· sec, which is quite similar to $I = 2.008 \times 10^5 \exp(-x(m)/960)$ quanta/cm^2· sec given by H.Bradner et al[4].

4.Discussions What is the origin of the differences in data sets for the two deployments? There are some reports[2),4)] on the observations of extensive stimulated bioluminescence in the deep ocean. The time dependence and depth dependence of our data also suggest it to be due to bioluminescence. It is

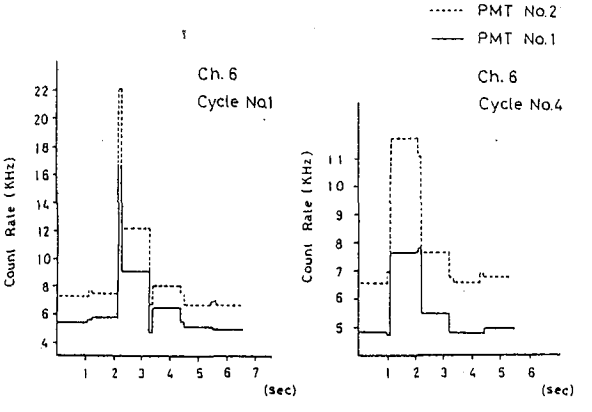

Fig. 3 Time Structure of Spike Signal

well known that luminous species easily respond to physical and chemical stimulation. For the case of the ship suspended runs, the environment of inhabitants can be agitated by the motion of the instrument. Under these circumstances it is quite natural that the light intensity due to bioluminescence changes greatly with time. Futher, it is known that the planktonic biomass y can be expressed by the equation $y = a_5 x \exp(-kx)$, where x is the depth[5]. Our data in the depth dependence of the light intensity shows a similar behavior, which suggests that the photon flux data may reflect the amounts of organisms in the environment.

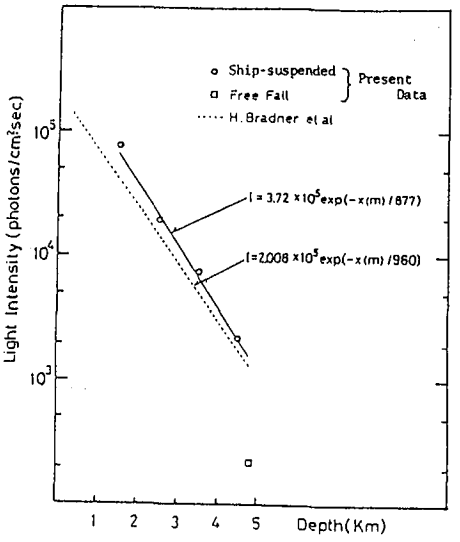

FIG. 4 Light Intensity Versus Depth

The mean value of the bottom tethered flux is 218^{+20}_{-60} cm^{-2} · sec^{-1}. For the bottom tethered case, the stimulation of luminous species is very weak. The cotribution of noticeable spike signals, which are considered to be due to such species, is only 6% of the total count rate. Several authors[6),7)] have calculated the photon flux due to Cerenkov light emitted by β-decay electrons from K^{40}. Their results scatter around 150 photons cm^{-2} · sec^{-1}. Considering the uncertainties of the energy loss process, light attenuation length and sensor detection efficiency assumed in the calculation, the expected value and our results are consistent with each other. Also, because Cerenkov light from individual K^{40} decays is quite feeble(typically 40 photons), this light will appear to the PMT as a single photon source[7)]. Our analysis of the pulse height spectra shows that the bottom tethered data does not contain large signals. From these results we conclude the main light source for the bottom tethered exposure is K^{40}.

In summation, we have found that the background at the DUMAND site is tolerable level for the DUMAND otical sensors.

References

1) Proposal To Construct A Deep-Ocean Laboratory For The Study Of High-Energy Neutrino Astrophysic, Cosmic Rays and Neutrino Interaction; DUMAND Nov.15,1982
2) J.R.Losse; Proc. 1980 DUMAND Signal Processing Workshop,9(1980)
3) T.Aoki et al; ICR-Report-124-85-5
4) H.Bradner et al; to be published in Nature
5) M.E.Vinogradov; "Vertical Distribution Of The Oceanic Zooplankton", (Wiener Bindery, Jerusalem 1970)
6) A.Roberts; DUMAND 1978 1 139(1978), J.G.Learned; DUMAND 1978 1 147 (1978)
7) B.D.Geelhood; Proc. 1982 Signal Processing Workshop,30(1982)

HE 5.2-8

MEASUREMENTS OF LIGHT BACKGROUND AT LARGE DEPTH IN THE OCEAN

Bannykh A.E., Beresnev V.I., Gaidash V.A., Gulkhandanyan O.M., Ivanov V.I., Markov M.A.,*Paka V.T., Shtranikh I.V., Surin N.M., Volkov A.N., Zheleznykh I.M.

Institute for Nuclear Research, the USSR Academy of Sciences, Moscow, USSR
*Institute of Oceanology of the USSR Academy of Sciences, Atlantic department, Kaliningrad, USSR

ABSTRACT

The mean intensity of Čerenkov emission from the products of K^{40} decay and bioluminescence was measured at depth to 5 km. The intensity of Ocean light background is founded to depend upon depth and at the 5 km level is equal on averaged to 300±60 quanta/cm^2s into spatial angle of 2π sterradian in transparency window. The amplitudes, duration and number of BL flashs were measured at various depth. The intensive flashs due to BL are shown to be observed rather seldom at depth over 4 km.

1.Introduction. Deep underwater Čerenkov detector of muons and neutrinos with the volume of 10^7-10^8 m^3 [1] can serve as a tool of investigation of the fundamental properties of microworld (neutrino microscope) as well as the structure and development of the Universe (neutrino telescope). Besides the problems of microworld and macrocosmos are closely connected with problems of Ocean Physics, sea-biology and deep underwater engineering. One of the main problem, required a preliminary solution, is an investigation of Ocean light background (LB) at large depths. The data on LB are essential for the choise of optimal parameters of registration system of short (10^{-8}s) light pulses due to Čerenkov emission of relativistic muons or electron-photon and hadron cascades from muons and neutrinos passed by a photodetector at a considerable distance. The main varieties of LB are: a)a background from radioactivity; b)a background from bioluminescence (BL).

LB from radioactivity in salt water arises from mainly at the expense of K^{40} decays. At the 25 m transparensy the flux of Čerenkov emission from β-electrons and Compton electrons into the spatial angle of 2π sterradians is 150 photon/cm^2s in the wave range 400-600 nm [2]. At better transparency background from K^{40} will be greater. Background from BL can be divided into two types [3]: i)quasi-isotropic background from spontaneous BL of organisms averaged over large volume of water; ii)pulse flashs of BL close by the device, exited by its movement. At present time the dependence of structure of background from BL versus depth has not been clear yet completely. To obtain the complete information about LB of Ocean it is necessary to carry out the detail investigation of its structure: mean intensity of background at a given

depth, as well as duration and amplitudes of light flashs at various depths.

2. Block diagram of measuring apparatus of weak light fluxes. For the purpose of detail investigation of the structure of LB of Ocean a complex of measuring apparatus was developed and tested during the 40th cruise of the scientific-research Ship "Academic Kurchatov". The block diagram of a submerged device is shown in Fig.1. The emission measuring apparatus is composed of the following blocks: 1 - a block of photodetectors (four PMT-130); 2-a block of amplifiers; 3 - a block of discriminators; 4 -a block of counters; 5-a summator 6-an electronic commutator and a code convertor; 7-a time interval measurement system; 8-a time pulse generator; 9-a block of pressure detector; 10-a block of data storage. The maximum intensity of light flashs registed by the measuring apparatus is equal to 10^6 pulse/s. The minimum duration of flash that can be measured is equal to 10^{-3}s. The maximum depth of submersion equals 6 km. The device works in an autonomous regime with recording the information on a compact-casset. Four PMT-130 are used as detectors of optical emission. The angle of aspect of each PMT is 120°. The construction of the advice allows to investigate Ocean optical emissions: a)in the regime of integral count of one electron pulses simultaneously with determined of duration and intensity of pulse flashs; b)in the regime of count of coinciding events from various PMT-s.

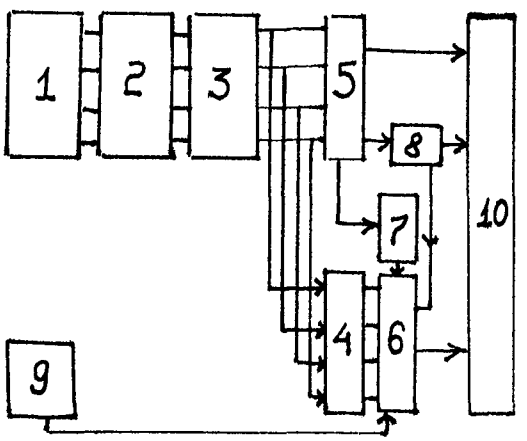

Fig.1. Block-diagram of submerged device.

3. Experimental results and discussion. The set of measurements of luminosity at various depths was taken in the central part of the Atlantic Ocean. Consider the results of the measurements made in the region 22°09'sl and 37°15'w.l. on the 7th of October, 1984. Detection of the light flux was made in the regime of one-electron pulses. The one-electron tresholdes were set up for two PMT, but for another two PMT the value of the thresholdes conforms to the amplitudes of two-electron pulses. Such experimental scheme allows to consider possible counting losses at the intensities more 10^6 pulse/s. The change of the mean intensity for a stay time at given depth of Ocean luminosity versus a device submersion depth is shown in Fig. 2a. The fluctuations of the mean intensity is seen to decrease considerably with depth. On submersion from 4 to 5km the mean intensity decreases 1,5-2 times. The dependence of the mean intensity versus time at the 5000 and 4000 m levels are shown in Fig. 2b and 2c respectively. Here averaging is made over storage time of 32512 pulses. The counding rate of one-electron pulses due to background from K^{40} calculated for

a given device at the 20 m transparency of water is shown by a dotted line. At the 5000 m level the mean intensity of Ocean luminosity changes slightly with time and twice exceeds the calculated background from K^{40}. At the 4000 m level the fluctuations of background intensity are far in excess the fluctuations of the background at the 5000 m depth. The mean intensity is approximately three times greater than the calculated one for K^{40}.

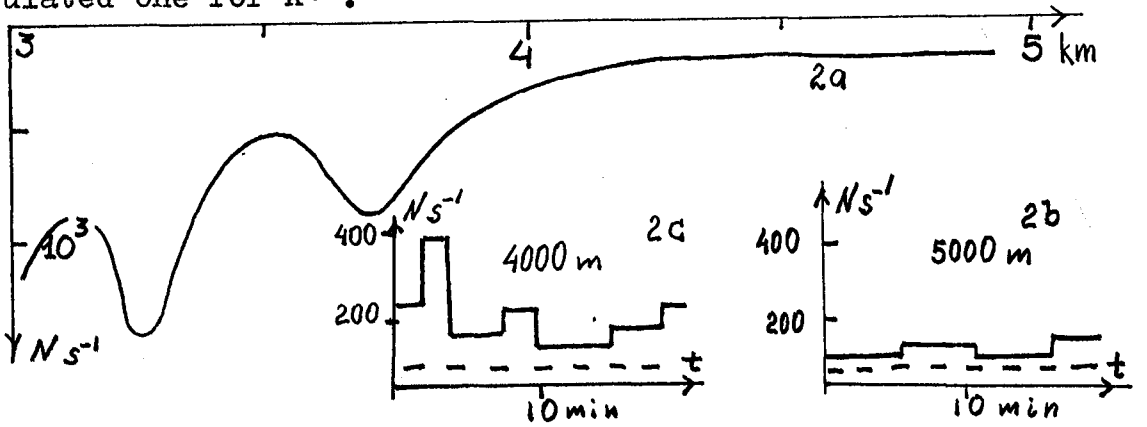

Fig. 2. 2a - a dependence of counting rate of one-electron pulses versus depth of submersion, averaged for stay time at given depth;
2b and 2c - a dependence of counting rate of one-electron pulses versus time at the 5000 m and 4000 m depths averaged for storage time of 32512 pulses.

The excerptions made at regular time intervals at the 5000 m and 4000 m levels with the time resolution of 10^{-3}s are shown in Fig.3. There are practically no intensive pulse flashs of small duration (10^{-2}-10^{-3}s) at the 5000 m depth. There is another situation for the 4000 m depth. Fig. 3b demonstrates the presence of the narrow (0,02-0,03 s) intensive pulse flashs repeated at unregular time intervals. One can suggest that the quasi-isotropic background at depths more 4000 m is caused mainly by Čerenkov emission from K^{40}(the calculated background for our device must be approximately 60 pulse/s at the 20 m transparensy) and from spontaneous BL of micro-

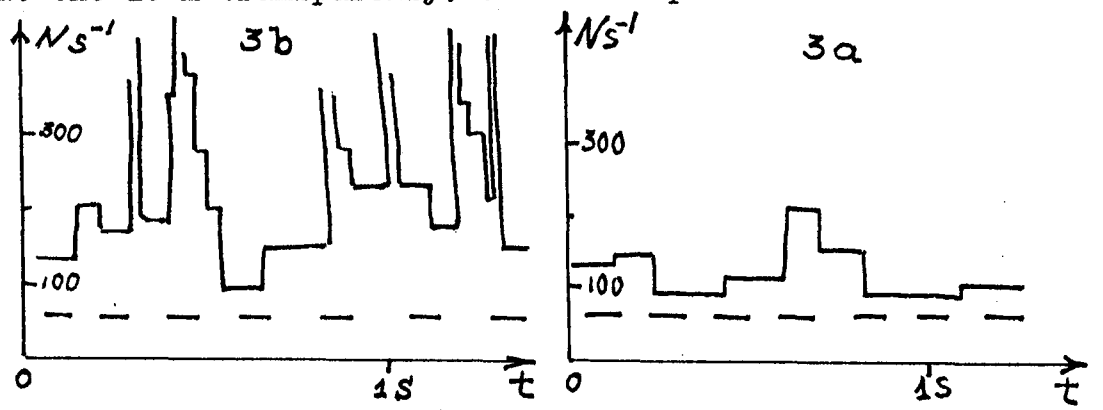

Fig. 3. A dependence of counting rate versus time. Time resolution is 10^{-3} s. 3a -5000 m, 3b-4000 m.

organisms averaged over a large volume of water (at the 4-5 km depth the background from spontaneous BL minus the background from K^{40} was 80-90 pulse/s). Small number of intensive pulse flashs at the 5000 m depth demonstrates small concentration of glowing micro-organisms at large depth.

4. Conclusion. Hense, the measurements of LB showed:

i) the intensity of LB at the depth of 5 km order is equal on average to 300±60 photon/cm^2s into the spatial angle of 2π sterradian and is characterized by comparatively high homogeneity (rather small number of short pulse flashs). At the 20 m transparency of salt water the background from K^{40} must be twice less and hense there is also spontaneous BL of microorganisms at large depths;

ii) at the 2-3 km depth mean intensity is greater than at the 4-5 km depth and is undergone by sharp fluctuations. These flashs can be connected with BL of microorganisms nearby an device exited by its movement;

iii) a comparatively low LB at the 5 km level makes these depths promising for employment of large optical detectors of DUMAND.

References

1. Markov, M.A., Proc. X Int.Conf.High-Energy Phys.(Rochester, 1960), p. 579.
Roberts, A., Stenger,V., Peterson, V., Learned, J., Proc. Int.Conf.Neutrino Phys. and Astrophys., 1981,v.2,p.240. ed. R. Cence, E. Ma,A. Roberts, Maui, Hawaii, 1981.
2. Roberts, A., Proc. DUMAND 1978 Summer Workshop, Vol. 1, p. 138, ed. A. Roberts, LaJolla, 1978.
3. Gitelzon, I.I., Shevyrnogov, A.P., Levin, L.A. et al. (1970), DAN USSR, v. 191, N 3.

HE 5.2-10

HYBRID TLC-PAIR METER FOR THE SPHINX PROJECT

Tomonori Wada
Okayama University, Japan
Isao Yamamoto and Nobusuke Takahashi
Okayama University of Science, Okayama Japan
Akeo Misaki
Saitama University, Urawa Japan

1. Introduction. The chief aims in THE SPHINX PROJECT are research of super lepton physics and new detector experiments. At the second phase of THE SPHINX PROJECT, we designed a hybrid TLC-PAIR METER for measuring vertical muon spectrum in the muon energy range 10 – 100 TeV, searching high energy neutrino sources ($E\nu$ > * TeV), searching high energy muon sources ($E\mu$ > 1 TeV) and measuring muon group ($E\mu$ > 1 TeV).

The principle of "PAIR METER" has been already proposed[1,2,3]. In this TLC-PAIR METER, electromagnetic shower induced by cosmic ray muons are detected by using TL (Thermoluminescence) sheets with position counters.

2. Designe of TLC-PAIR METER One cell of TLC-PAIR METER is shown in Fig. 1 and one unit is composed of 14 cells. The full-scale is composed of 18 units which is shown in Fig. 2. The cell TLC-P.M. consists of a) trigger and time measurement counters (scintillation counter, 3 layers), b) XY-position counters (Proportional chamber, 9 layers) and TL calorimeters (TL-sheets + 14 cm irons, 40 layers). An old type PAIR METER consisted of PRC calorimeter (proportional counters + 14 cm irons, 32 layers)[4].

The following table is the comparison one between a TLC and a PRC for 40 layers-PAIR METER.

Items	Prototype P R C	Hybrid-type T L C
Detector Height (m)	9.6	6.5
Detectable Efficiency	1.0	2.2
Number of Position Counters	41	9
Budget for counters and electronics (PRC-Amp. ADC, Discri, CAMAC System)	140 k$	60 k$

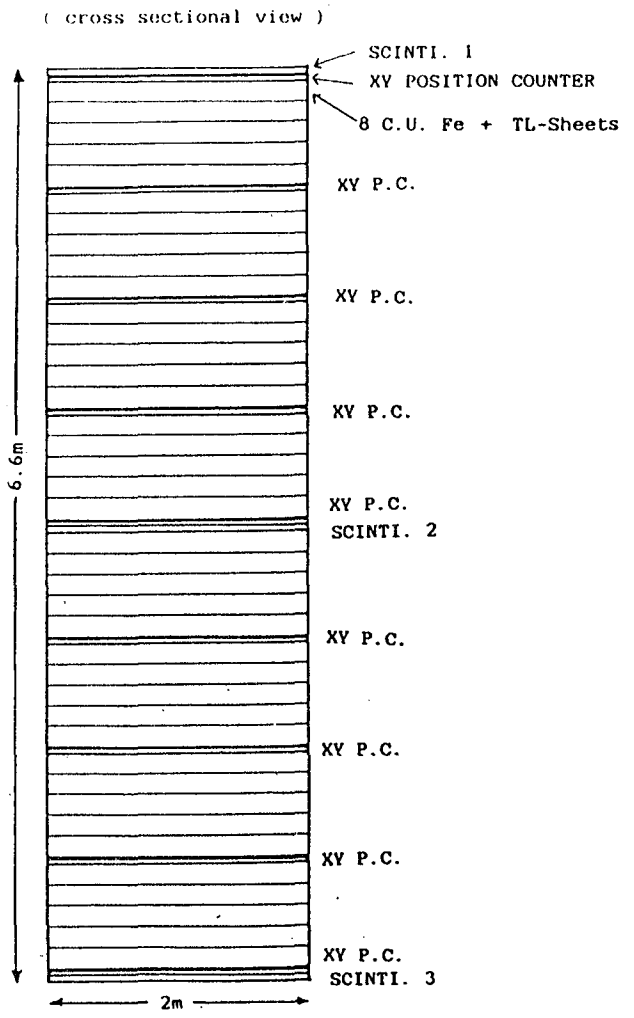

Fig. 1. One cell of TLC-PAIR METER. One cell size is 2 m x 2 m x 6.6 m. One unit of TLC-PAIR METER consists of 14 cells. TL-sheets which position counters indicate muon path are read out.

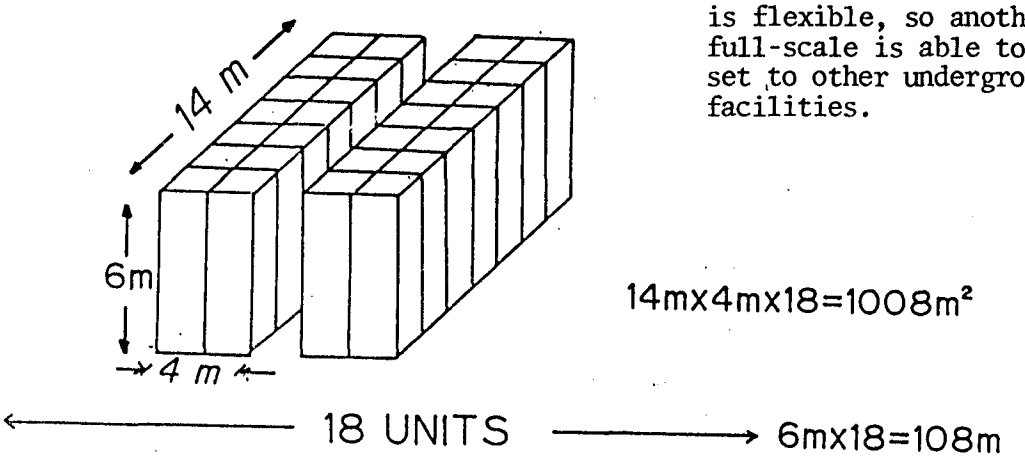

Fig. 2. The full-scale of TLC-PAIR METER. This scale is set to Gran Sasso Laboratory. A full-scale of TLC-PAIR METER is flexible, so another full-scale is able to be set to other underground facilities.

3. Simulations of TLC-PAIR METER For the PAIR METER, iron absorber is better than lead absorber and a thickness of one layer should have one nuclear mean free path, that is 14 cm; 8 C.U. The cell of PAIR METER shown in Fig. 1 has 40 layers, to attain little statistical fluctuation. Under these condition, various simulations have been performed. One of simulations is shown in Fig. 3. This figure shows that an incident muon energy ($E\mu$) relates to mean electron number ($\overline{Ne}$) of electromagnetic shower induced by a cosmic ray muon passing through 14 cm x 40 layers. By measuring $\overline{Ne}$ at PAIR METER, one can determine the $E\mu$ value with ± 30 %.

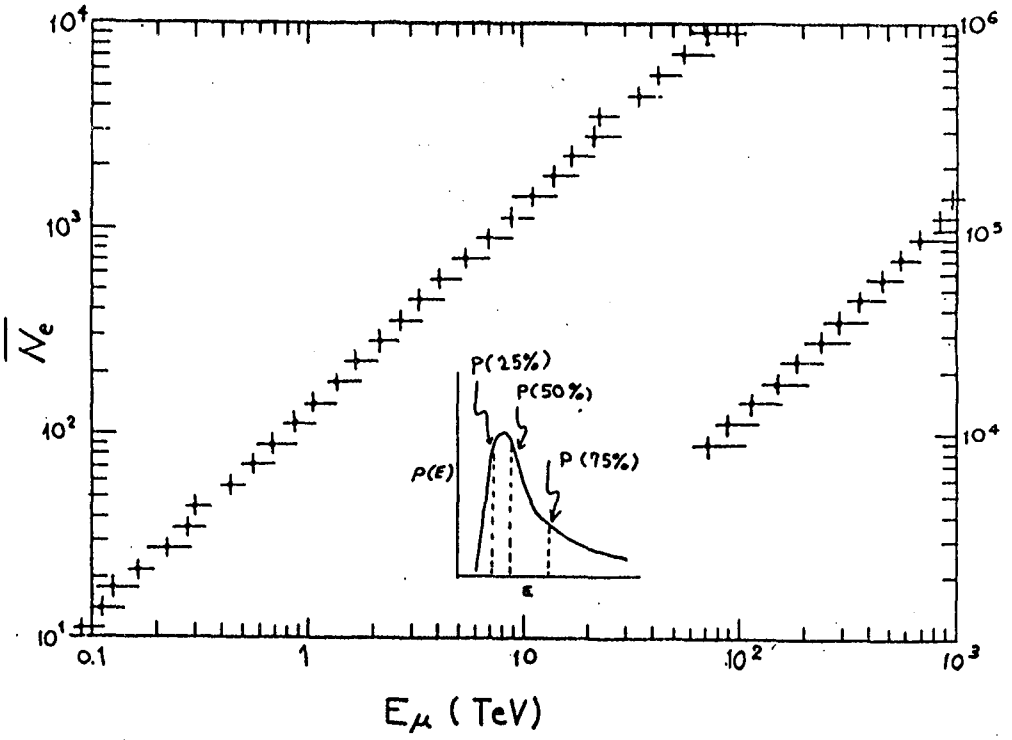

Fig. 3. Results of simulation to determine $E\mu$. In this case, vertical muon spectrum was used as $E\mu^{-2.7}$.

4. Detecting small shower In the 2nd phase of THE SPHINX PROJECT = a hybrid TLC-PAIR METER, the most important technique is to detect small electromagnetic showers induced by a high energy muon on a TL-sheet.

We tried to read out from a TL-sheet irradiated ^{90}Sr β-ray which is equivalent to electron number of 20 GeV shower and this sheet was already exposed by cosmic rays, background for one year at Mt.Norikura.

The " RAW DATA [f] " in Fig. 4 is a integrated frame picture. This irradiated sheet was read out by TL spatial distribution read out system[5]. The [f] corresponds to "Matrix" and each picture cell correspond to matrix

element. $[f_i]$ is an i-th frame picture, $\Sigma [f_i] = [f]$. $[S]$; S-matrix of standard Hadamard matrix, $[H]$.

$[S] \cdot [f_i] = [F_i]$; Hadamard transformed matrix,

$[F'_i]$: the treated matrix; when a matrix element has small value, that element reduces to zero.

$\Sigma [F'_i] = [F']$, $[S]^{-1} \cdot [F'] = [f']$

The matrix $[f']$ is a new frame picture applied Hadamard Transform Technique [HTT]. In Fig. 4, the frame picture $[f']$ after HTT is clearer than the $[f]$ for the shower position; the use of mutual-correlation at frame picture is effective to higher "Signal/Noise Ratio".

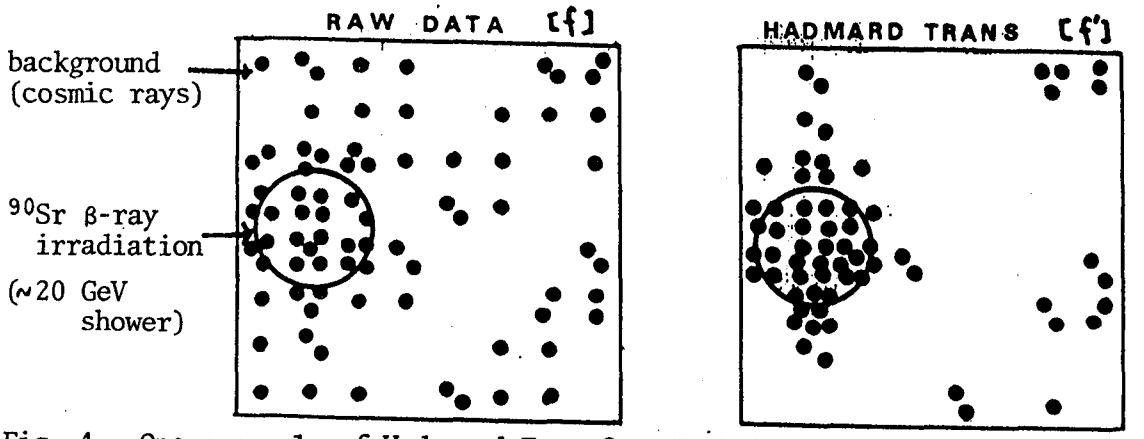

Fig. 4. One exsample of Hadamard Transform Technique.

5. Conclusions This TLC-PAIR METER proposal [Japan-Italy Colaboration] approved by the Gran Sasso International Committee. So, simulations are continued to attain more precise estimation-value and to select more suitable design. The HTT will be applied for frame pictures of real showers induced by muons.

References

1. Alekseyev, I.S. and Zatsepin, G.T. (1960), Proc. ICRC, Moscow, 1, 324.
2. Wada, T. and Kitamura, T. (1969), Prog. Theor. Phys. 41, 1587.
3. Moe, M.K. (1970), Nuovo Cimento, 66B, 90
4. Kokoulin, R.P. (1982), ICR-REPORT 103-82-6 and Yamamoto, I. and Wada, T. (1984), Uchusenkenkyu, 28-1, 162.
5. Yamamoto, I. et. al., (1985), This conference paper, HE 7.1-7.

PROPORTIONAL DRIFT TUBES FOR LARGE AREA MUON DETECTORS

C. Cho, S. Higashi, N. Hiraoka, A. Maruyama, T. Okusawa
T. Sato, T. Suwada, T. Takahashi and H. Umeda

Department of Physics, Osaka City University
Sugimoto, Sumiyoshi-ku, Osaka, Japan

ABSTRACT

A proportional drift chamber which consists of eight rectangular drift tubes with cross section of 10 cm x 5 cm, a sense wire of 100 μφ gold-plated tungsten wire and the length of 6 m, is constructed and tested using cosmic ray muons. Spatial resolution (rms) is between 0.5 and 1 mm over drift space of 50 mm, depending on incident angle and distance from sense wire.

1. INTRODUCTION

The large proportional drift chamber have been constructed for muon identification in the TOPAZ experiment at KEK to study e^+e^- interactions (1). A chamber contain eight rectangular drift tubes with cross section of 10 cm x 5 cm, length of 6 m and a sense wire for each cell (Fig. 1). Two adjacent planes of staggered tubes help to solve the left-right-ambiguity. The chamber with large area, very simple structure and good space resolution is also very useful to study muons in cosmic ray experiments, specially to measure the direction of muons for multiple muon study and spectrogragh. In this paper, we will describe the chamber design, and cosmic ray test on the three muon chambers aligned vertically, filled with mixture of Ar + 10% CH_4. Reconstructions of tracks of the cosmic ray in the chamber determine the drift distance from sense wire as a function of the electron's drift time,

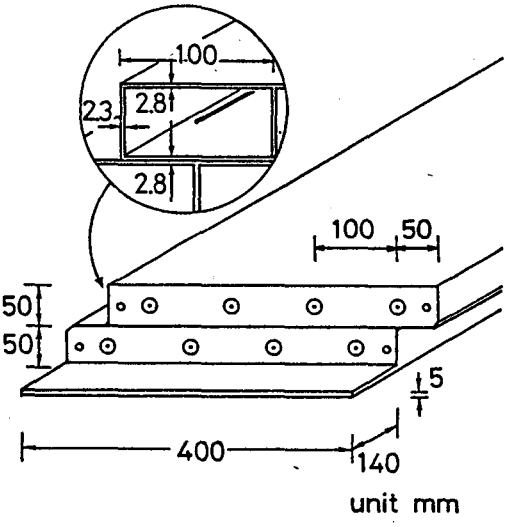

Fig. 1
Sketch of the proportional drift tube chamber.

the spatial resolution and the chamber efficiency.

2. CONSTRUCTION

A chamber consists of eight rectangular drift tubes with cross section of 10 cm x 5 cm and the length of 6 m. A chamber is made out of two four-cell structures which are extruded separately from 6063-T5 aluminium and welded together. The ends of the chamber are notched to allow serial gas flow between cells. Aluminium end caps are welded onto both ends of the four-cell structures to seal gas, which also used to support sense wires. Aluminium plates are welded onto both ends of the lower four-cell structure to mount the chamber on the apparatus. A maximum sagitta at the center of chamber is less than 3 mm, a maximum lateral twist about the wire axis less than 3° and a surface flatness for 400 mm wide less than 1.6 mm. The extrusion is cleaned with 10% sodium hydroxide to take off oil and nap on the aluminium surface. Each cell has a sense wire of gold-plated tungsten of 100 μm in diameter to get high electric field at the position far from the wire. The wire is soldered to copper pins in the center of Delrin plugs under the tension of 850 grams. Lids are attached to both ends to provide mechanical protection for the wire and electronics. Chambers can maintain a vacuum pressure of less than 0.1 Torr, which is the limit of the pump used.

High voltage and preamplifier/discriminator PC boards are mounted on the chamber. The wire is connected to the high voltage supply through a 10 Megohm register, and the preamplifier through a 500 pF coupling capacitor.

3. RESULTS

Fig. 2 shows a set-up of the chamber and read out system to measure the drift time as a function of a drift space,

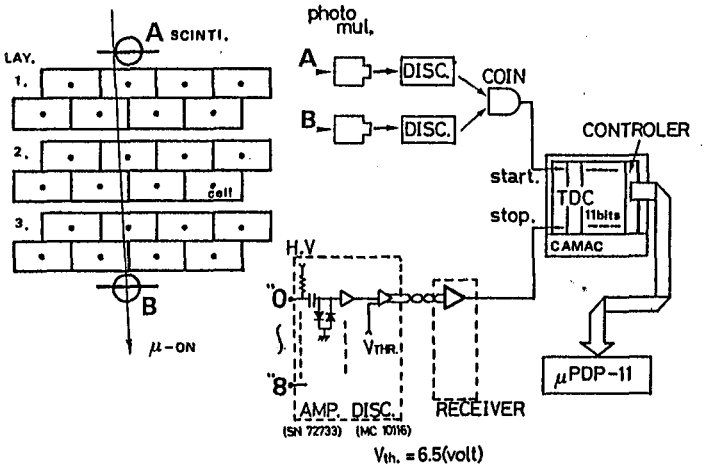

Fig. 2
Schematic view of the set-up for measuring the space resolution of the drift tubes with incident cosmic rays.

the spatial resolution and the detection efficiency. The set-up consists of three chambers and two scintillation counters with 10 cm width which are used to select cosmic ray muons and to generate start pulse for TDC. The drift times are digitized by 11 bit CAMAC TDC's with 2ns bins and read out to micro PDP-11. The data are taken for track angles 0°,28° and 45° with gas flow of 100 cc/min, high voltage of 3.1 KV and threshold of 500 μV. The analysis to get spatial resolution is as follows. Data on time, about $1x10^4$ events for a track angle are converted to drift distance from the wire using a time-distance relation which is assumed at first. Assuming the wire positions, the circular space contours are fitted with a straight line of a track using the method of least squares, which gives time new distance on the straight line. The mean of the

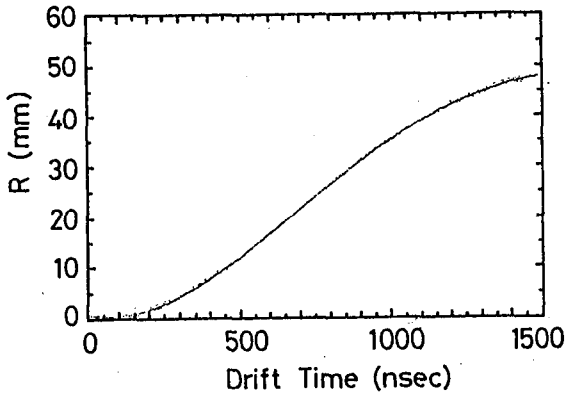

Fig. 3
Distance from the sense wire versus measured drift time for track angle 0°.

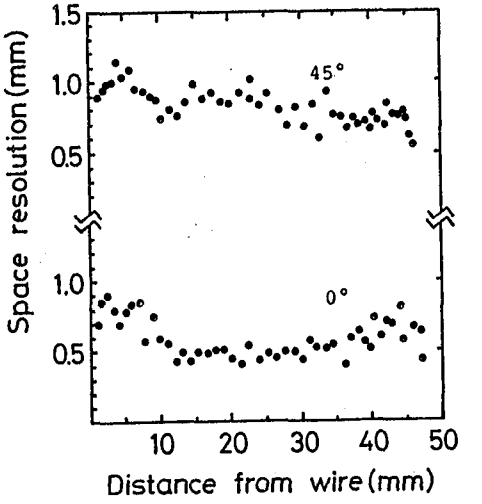

Fig. 4
Spatial resolution (rms) VS distance from wire for track angles 0°, 45°.

deviation from the straight line for each wire changes the wire position. By calculating the mean of the time-distance distribution, a empirical time-distance relation is obtained, which is used for next straight line fit. These calculations are continued until the width of the experimental time-distance distribution is minimized.

Fig. 3 shows a scatter plot of the drift time VS the distance of the track from the sense wire; time-distance distribution for track angle 0°. At larger track angles the

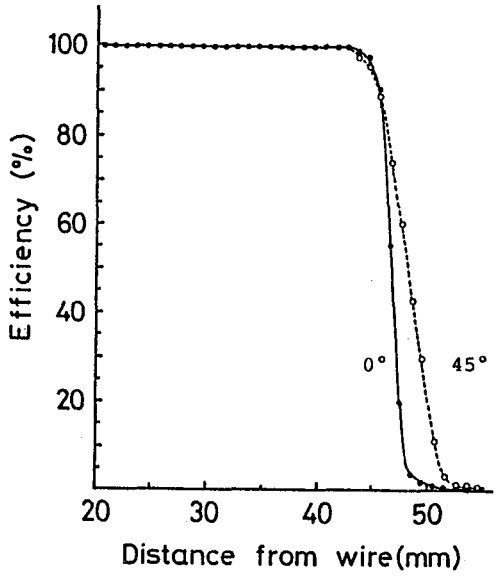

Fig. 5
Detection efficiencies for cosmic rays in the drift tubes for track angles 0°, 45°.

time-distance distribution is almost the same. Fig. 4 shows the spatial resolutions (rms) VS the distance at 0° and 45°, which are obtained from the time-distance distributions (Fig. 3). The resolution is 0.5 mm at the center and about 0.8 mm at near to and far away from the wire for track angle 0°, but gets worse at large track angle, ∿ 1 mm at 45°. Fig. 5 shoes the single wire efficiencies VS position distribution with a maximum collection time of 2 μs at 0° and 45°. The efficiency is greater than 99.97% within 43 mm but drops off rapidly near the ends.

4. CONCLUSION

Large area rectangular drift tube chamber with drift space of 5 cm are constructed and tested. The spatial resolution (rms) is better than 1 mm, and the efficiency for detecting the passage of a particle is greater than 99.9%. These characteristics are adequate for the purpose of a large muon detector in cosmic ray experiments.

REFERENCE

1. R. Hayano et al (1983) TRISTAN PROPOSAL, TRISTAN-EXP-002

ACKNOWLEDGEMENT

We wish to thank all members of TOPAZ-group, in particular, T. Kamae, S. Iwata and Y. Watanabe for there encouragement.

An Upper Limit of Muon Flux of Energies above 100 TeV Determined from Horizontal Air Showers Observed at Akeno

M.Nagano, H.Yoshii*, T.Hara, K.Kamata, S.Kawaguchi** and T.Kifune

Institute for Cosmic Ray Research, University of Tokyo, 3-2-1 Midoricho Tanashi, Tokyo, 188 Japan
* Faculty of General Education, Ehime University, Matsuyama, 790 Japan
** Faculty of General Education, Hirosaki University, Hirosaki, 036 Japan

Abstract Determination of muon energy spectrum above 100 TeV by observing the extensive air showers from the horizontal direction(HAS) has been continued at Akeno for four years. No definite muon originated shower of sizes above 10^5 and zenith angles above 60^o has been observed. The upper limit of HAS intensity is 5×10^{-12} m^{-2} s^{-1} sr^{-1} (90% confidence level) above 10^5. The value indicates that the upper limit of muon flux above 100 TeV is about 1.3×10^{-8} m^{-2} s^{-1} sr^{-1} and is in agreement with that expected from the primary spectrum with a "knee", assuming scaling in the fragmentation region and 40% protons in the primary beam. The critical energy at which muon flux from prompt processes(decay of charmed particle) take over that from the conventional process is higher than 100 TeV at horizontal direction.

1. Introduction

The determination of the muon spectrum above 50 TeV is interesting in relation to the proton spectrum in the primary beam and the production cross-section of prompt muons through leptonic decay of charmed mesons($D,\bar{D}$) or charmed baryon(Λ_c^+) in hadronic interaction. Predictions of the prompt muon spectrum are made by various authors[1]-[4]. An estimated crossover energy where the prompt muon flux take over the ordinary muon flux is different from authors, ranging from 75 to 1000 TeV at horizontal direction[5] and hence some models may be discriminated with the present experiment.

The extensive air showers(EAS) observed at large zenith angle are most probably initiated by bremsstrahlung gamma-ray of high energy muons produced at the early stage of the shower development and are called HAS. This experiment was stimulated by the observation of muon poor showers at around 55^o - 60^o[6] as a supporting evidence of the flattening of muon spectrum by Mikamo et al[7]. By adding the timing channels and the track detectors of muons, the discrimination of HAS from EAS is much improved in this experiment.

2. Experiment

At Akeno air shower array, 153 unshielded scintillation detectors of 1 m^2 (6 of them 2 m^2) and 9 shielded detectors of 25 m^2(muon stations) are distributed over an area of almost 1 km^2[8]. At the center two towers of 10m height are built and the two detectors are arranged in order not to trigger the vertical small showers. Around the tower, 25 detectors of 1/4 m^2 area and 29 of 1 m^2 are arranged for the size and age determination of small HAS. Out of all scintillation detectors, 86 are accommodated with timing circuits. 28 channels are in the central part and their timing resolution is 2.5 nsec each. Others are detectors of 120m spacing with 10 nsec resolution[9]. At two of nine muon stations, two more layers of 50 proportional counters each are arranged 25 cm apart from the adjacent

layers. Projected muon tracks obtained at two stations, in which proportional counters are arranged orthogonally to each other, are available to determine the zenith angle of muons.

The size and the arrival direction of the showers are determined by the least square fitting. For shower of size 10^5, the error in zenith angle determination is 3° at the zenith angle of 60° and 5° at 75° for small shower trigger. For large shower trigger that is about 8° above 10^6 at 60°. The zenith angles are also determined by measuring the muon tracks with three layer proportional counters. In case that the latter methods can be applied, zenith angle is determined within 3° above 60°. The error in size determination is less than 50% even for the flat shower of small size at 60°.

Observation time is 1.07×10^8 sec. The effective collection area is size and age dependent and is evaluated by the Monte Carlo simulation.

3 Results

In fig. 1 are plotted N_e versus N_μ relation for showers of zenith angles larger than 60°, which are selected by both timing and muon tracks. In case of muon poor showers, the arrival direction of some showers can not be determined by the muon tracks due to the lack of muons in three layer proportional counters. In such cases, the density map was used to check the arrival direction by comparing with that of artificial showers simulated with the determined electron size, core position and the arrival direction. The average N_e vs N_μ relations for showers of sec θ ranges 1.0 - 1.1 is drawn by a solid line for reference. The broken lines are upper and lower bounds of N_e vs N_μ relation for showers above 60° estimated from the data distribution and the triggering inefficiency. There are many showers of relatively low muon contents for showers of small size. These are mainly due to the underestimation of muon size, since the number of detectors of zero muons increases for small showers.

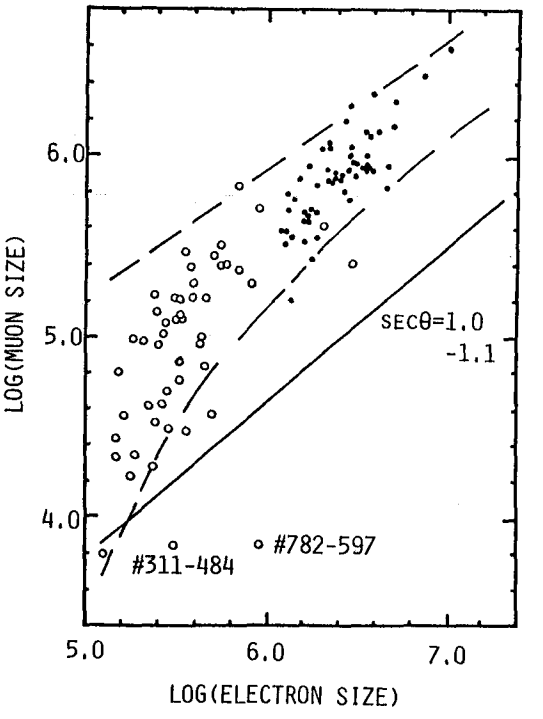

Fig. 1 Muon size vs. electron size for showers of zenith angles above 60°. Two events with event numbers are candidates of HAS.

There are two showers whose muon contents are about 1/10 th of lower bound of N_e vs N_μ relations. In table 1 are listed the properties of two candidates at zenith angles above 60°. These events are similar to the expected ones from HAS. However, there is no such candidate above 70° against more candidates below 60°. That is, the flux of this kind of

Table 1. Properties of two HAS candidates

Event No.	θ_{FT}	φ_{FT}	θ_μ	N_e	Age	N_μ	$(\frac{\rho_\mu}{\rho_e})$ at 32m
#311-484	68°	163°	$64^\circ \pm 3$	3.1×10^5	1.0	6.2×10^3	0.010 ± 0.008
#782-597	64°	296°	$63^\circ \pm 3$	9.6×10^5	0.65	7.5×10^3	0.004 ± 0.005

shower decreases with zenith angle and hence the zenith angle distribution is different from the expected one from conventional or prompt muons. Therefore, we can not conclude that these are showers initiated by high energy muons.

Assuming 1 event in each $\Delta \log N_e$ bin, the upper bound of the size spectrum of muon induced showers is evaluated. Since we have no definite HAS, the absolute value at 10^5 is determined by taking 2.3 events(C.L. 90%) above 10^5 after integrating $J(N_e)A(N_e)t\Omega\, dN_e$, where $A(N_e)$ is the size dependent effective area, and t and Ω are observed time and solid angle. The solid line with hatch in fig.2 shows the upper bound thus determined. The upper limit above 10^5 is 5×10^{-12} m^{-2} s^{-1} sr^{-1}.

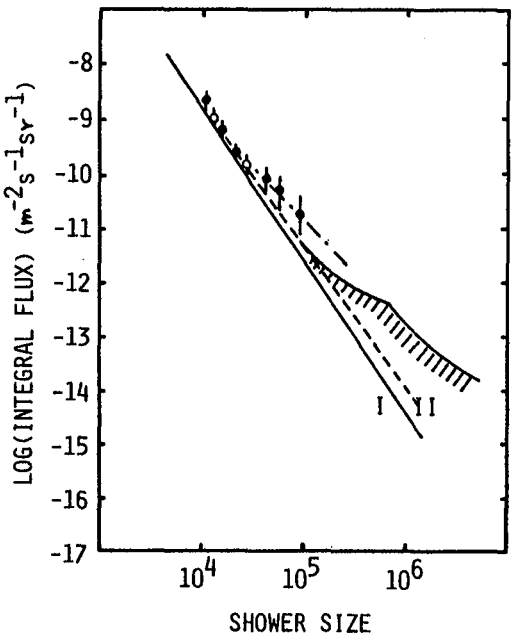

Fig. 2 Upper bound of HAS spectrum is shown by hatched area. Open circles are by Bohm and Nagano(10) and closed one by Mikamo et al(7). The expected HAS spectrum for two kinds of muon energy spctrum I and II are also shown.

4. Discussions

Though two events remained as candidates of muon induced showers among more than 500,000 triggered showers, they are not likely to be the showers initiated by muons from their zenith angle distributions. In fig.2, the previous results[7][10] are also plotted. The flattening of muon spectrum is not observed in this experiment. If their spectrum extends further to our size region, we should observe HAS above 70° more than 5 events during the observation time. The reason of the discrepancy of both experiments is not clear. The calculation of the effective area for each experiment was done by the same procedure. The acceptance times observation time for 10^5 of the present experiment is about three times larger than that of Mikamo et al[7].

The expected HAS spectrum from muon spectrum is evaluated and compared with the present upper limit of HAS spectrum. The muon spectra at 75° are calculated by Mitsui[11] with two kinds of nucleon spectrum. The spectrum I is extrapolation of proton spectrum measured by Ryan et al[12] plus nucleon spectrum from other nucleus with the same proportion of each component at 1 TeV. The spectrum II is assumed one that the composition does not change, but the total energy spectrum with knee is taken into account. The results are shown in fig. 3, where the flux is multiplied by E^2. The broken line is that from the spectrum II and solid one from I. In the same figure prompt muon spectra calculated by various authors; EGS model 1, 2, 3[2], C[3] and IKK model 1, 2[4] are also drawn.

The expected size spectra at 75° is derived by the Monte Carlo simulation by considering the bremsstrahlung process. The expected size spectra from I and II are drawn in fig.2 by a solid and a broken line, respectively. The upper bound at 10^5 is in agreement with the expected one from the primary spectrum with a "knee" and the so called "normal composition(40% protons)".

The present upper bound of HAS spectrum converted to muon energy spectrum is shown by shaded region in fig.3. The fluxes denoted by EGS model 1 and IKK model 2 are higher than our upper bound and hence may be

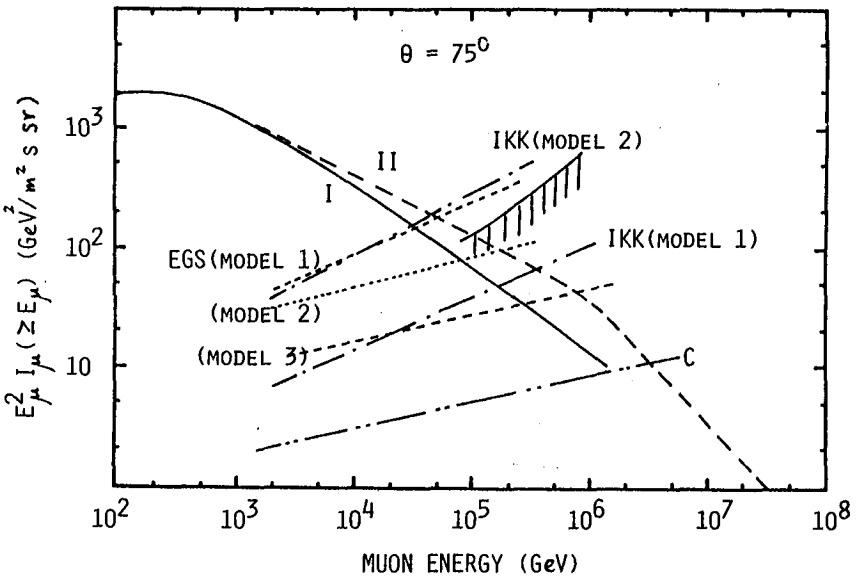

Fig. 3 Hatched region shows the upper bound of muon spectra estimated from the present upper bound of HAS spectrum. The muon energy spectra at $\theta=75^0$ calculated by Mitsui(11) with two different primary nucleon spectra I and II. The muon spectra from the prompt processes estimated by various authors are also shown.(2)(3)(4)

ruled out. The difference between models are mainly due to the differences of production cross-section of charmed particle and the fraction of energy delivered to charmed particle to incident energy. In case of EGS model 1, σ_{charm} (mb) = 0.36 ln(s/80 GeV^2). In model 2, this cross-section becomes constant(0.7mb) above s=4400 GeV^2. In two models denoted by IKK the diffractive production of D, $\bar{D}$ and Λ_c^+ are taken into account, whose contribution is about 40 times larger than their previous result with non-diffractive process[1]. This large difference is mainly due to the large transfer of energy to charmed particles in the diffractive process.

Acknowledgements

The authors wish to thank other members of Akeno air shower group for their help in constructing and maintaining the air shower array and in the analysis. They are also grateful to Dr. K. Mitsui for his calculation of muon spectrum. The data analysis and calculations were performed on FACOM M380 at the Computer Room of the Institute for Nuclear Study, University of Tokyo and on M-180 at the computor centers, Ehime University and Kyushu University.

References

(1) H.Inazawa and K.Kobayakawa: Prog. Theor. Phys. **69**(1983) 1195
(2) J.W.Elbert et al: Phys. Rev. **D27**(1983) 1448
(3) C.Castagnoli et al: Nuovo Cimento **82A**(1984) 78
(4) H.Inazawa et al: KU-85-03(Kobe University) (1985)
(5) J.W.Elbert: Rapporteur paper, Proc. 18th Int. Cosmic Ray Conference, Bangalore **12**(1983) 459
(6) N.Hayashida et al: Proc. 17th Int. Cosmic Ray Conference, Paris **7**(1981)1
(7) S.Mikamo et al : Lett. Nuovo Cimento **34**(1982) 237
(8) T.Hara et al : Proc 16th Int. Cosmic Ray Conference Kyoto **8**(1979) 135
(9) F.Ishikawa et al: Proc 17th Int. Cosmic Ray Conference Paris **8**(1981) 141
(10) E.Bohm and M.Nagano: J. Phys. A : Math. Nucl. Gen. **6**(1973) 1262
(11) K.Mitsui: private communication(1985)
(12) M.J.Ryan et al: Phys. Rev. Lett. **28**(1972) 985

COMMENTS ON THE MEASUREMENTS OF MULTIPLE MUON PHENOMENA

Sato,T., Takahashi,T. and Higashi,S.

Depertment of Physics, Osaka City University,

Osaka, Japan

Abstract

According to the Kiel group (1), the extensive air showers in the energy around 10^{15} eV include those initiated by astrophysical primary gamma-rays. In such observations, we need to have a precise measurement on the directions of primary particles. It is one of the methods to measure the directions of high-energy muons in air showers. We have investigated the accuracy in measuring the direction, by caluculating the cosmic-ray phenomena in the atomosphere at very high energy. The results caluculated by Monte Calro method suggest that one may determine the direction of primary cosmic-rays within errors of 10^{-3} rad in observing muons of above 100 GeV at sea level.

1. Introduction

On the observation of high-energy gamma-ray ($\sim 10^{15}$ eV) from point source such as Cyg-X3, it is very important to have a precise measurement on the direction of primary particles. When we observe the extensive air showers by using scintillation counters, the arrival direction of showers may be determined by measuring differences on the arrival time of incident particles into scintillation counters. However, the shower front having thickness of a few meters, it is difficult to make the errors in the detection of arrival direction less than 10^{-2} rad for the zenith angle.

On the other hand, high-energy muons in air showers are produced at the first stage of development of air showers, and the deviation of these direction from one of primary

particles depend on the transverse momentum ($\sim$ 400 MeV/c) of hadrons, which are parent of the muons in the first interaction. So, it is expected that these high-energy muons (above 100 GeV) may have much the same direction as primary particles have.

In this paper, the accuracy of the primary direction obtained by measuring the direction of muons at sea level have been investigated by Monte Calro method.

2. Method of simulation

Here the protons have been used as primary particles and energy region of primary particles are 10 $\sim$ 30 TeV. We have used the energy spectrum of primary cosmic-rays by Grigorov et al. , which have been measured as total particle spectrum (2). Our simulation have been made using the scaling model standing for the Feynman scaling in hadronic interaction (3). The interaction cross section of a hadron is assumed to increase as increasing of energy (4). The multiplicity distribution is assumed to obey the Koba-Nielsen-Olsen scaling low (5) (6). The transverse momentum of each secondary particle, p_t is sampled using the distribution of linear exponential form and the average value $\langle p_t \rangle$ set to 440 MeV/c. The effect of energy losses and of geomagnetic field have been taken into account.

3. Results of simulation and Discussion

The present simulation has been carried out on the high-energy muons initiated by primary cosmic-rays with vertical direction. The energy, the zenith angle, the position and the other properties of muons for each shower at sea level have been simulated (7). Fig. 1 shows the distribution of difference between the average arrival direction of muons and the direction of primary particle, $\Delta\theta$. In Fig. 1, a solid line , a dashed line and a dotted line shows the distribution taking 100 GeV, 200 GeV and 500 GeV as threshold energy of muons, respectively. The deviation of these

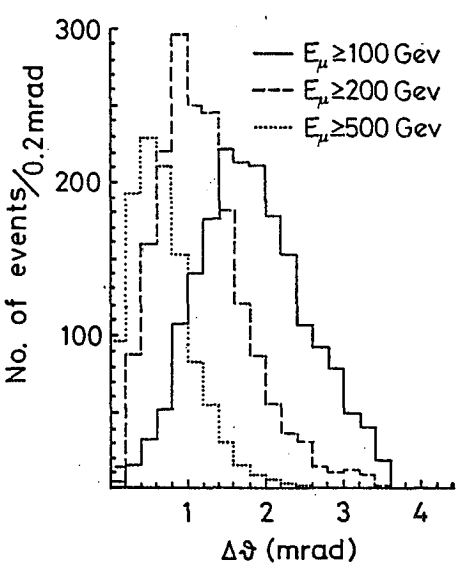

Fig.1 $\Delta\theta$-distribution.

distribution gives a accuracy of the measurement on the arrival direction, and the deviation for each threshold energy is decreasing as increasing of energy. Namely higher energy muons is detected, more precise observation on the arrival direction of primary particles is obtained, though number of muons detected is a few in higher threshold energy. In Fig. 2 the number of muons detected per shower for each threshold energy is shown. Though Kiel group had reported that the air shower started from gamma-ray primary is muon-rich , generally, such showers have a few muons. This method which use a few muons is very useful to determine the arrival direction of the showers started from gamma-rays.

For example, the extensive air showers around 10^{15} eV have $\sim$ 0.5 muons/m^2, which had energy above 100 GeV, in the core. Therefore, using the muon detector with the area of 100 m^2, we could observe $\sim$ 50 muons. Though the number of muons in the air shower started from gamma-rays are 1/20 of one in air shower started from proton, we can observe at least a few muons. Therefore, the arrival direction of the extensive air showers may be determined better than 2.0 mrad.

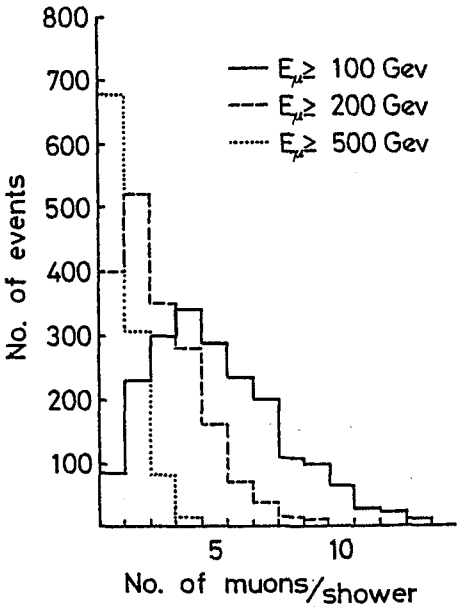

Fig.2 Number spectrum of muons.

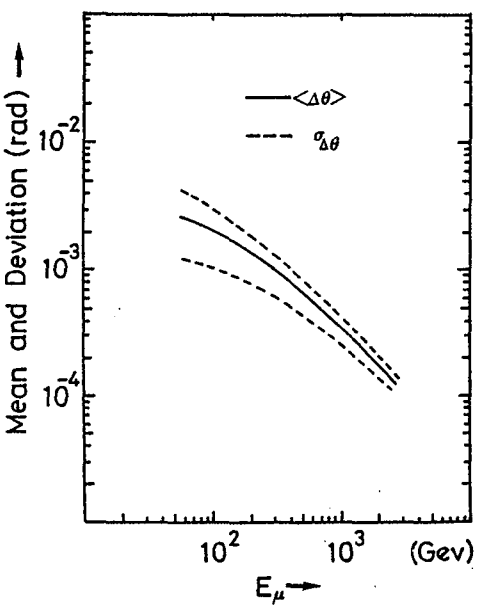

Fig.3 $<\Delta\theta>$ and $\sigma_{\Delta\theta}$ against threshold energies of muons.

4. Conclusion

The accuarcy in determining the arrival direction of extensive air showers by high-energy muons have been estimated by Monte Carlo simulation.

Fig. 3 shows the result of the simulation, where a solid line shows the means of difference between the direction determined by high-energy muons and the arrival direction of air showers against threshold energies of muons and a dashed line shows the dispersion of the differences. This simulation has not included the multiple Coulomb scatterring of charged particles in passing through the matter, which depend on total amount of matter above a muon detector. But the result in this paper may be help to attempt the experiments.

References

(1) Samorski, M. et al. , 18th ICRC, Bangalore, 1, 135, (1983).
(2) Grigorov, N. L. et al. , 12th ICRC, Hobart, 1971, 5, 1746, (1971).
(3) Feynman, R. P. , Phys. Rev. Lett. 23, 1451 (1969).
(4) Giacomelli, G. et al. , Phys. Rep. , 55, 1 (1980).
(5) Koba, Z. et al. , Nucl. Phys. , B40, 317 (1972).
(6) Slattery, P. , Phys. Rev. Lett. , 29, 1624 (1972).
(7) Mizutani, K. et al. , this Conference Paper, OG 5.2-9.

Acknowledgment

The authors would like to express their cordial thanks to T. Kitamura, Y. Muraki and K. Mizutani. FACOM M180IIAD and M380R of INS were used for present calculations.

ENERGY SPECTRUM OF CASCADE SHOWERS INDUCED BY COSMIC RAY MUONS IN THE RANGE FROM 50 GEV TO 5 TEV

Ashitkov V.D., Kirina T.M., Klimakov A.P.,
Kokoulin R.P., Petrukhin A.A., Yumatov V.I.

Moscow Physical Engineering Institute, Moscow 115409, USSR

Abstract. Results of a new measurement of the energy spectrum of cascade showers induced by electromagnetic interactions of high energy muons of horizontal cosmic ray flux in iron absorber are presented. The total observation time exceeded 22,000 hours. Both the energy spectrum and angular distributions of cascade showers are fairly described in terms of the usual muon generation processes (i.e. through π- and K-decays in the atmosphere) with a single power index of the parent meson spectrum over the muon energy range from 150 GeV to 5 TeV.

1. Introduction. Recent magnetic spectrometer measurements of cosmic ray muon spectrum at large zenith angles [1,2] agree well with each other and are successfully interpreted within the frames of the conventional muon generation processes with a value of the differential parent particle spectrum index of about 2.7 up to several TeV muon energies. A similar result was obtained earlier in the ionization calorimeter measurements of the spectrum of cascade showers initiated by muons [3] and was confirmed by the MUTRON calorimeter data published recently [4]. However, a number of experiments [5-8] give appreciably more rigid shower spectrum around 1 TeV, what is claimed to be caused either by some additional flux of muons (or some other penetrating particles) or by an anomalous muon interaction increasing with energy. On the other hand, in the experiments [9,10] the steepening spectrum of cascade showers was observed.

Here we present the first results of a new measurement of the cascade shower spectrum using an ionization calorimeter. Compared to our old data [3], the energy range has been extended to lower energies. The exposure time and hence statistics of high energy events have been doubled.

2. Experimental. A schematic diagram of the experimental arrangement is given in Fig.1. The arrangement consists of the six-layer calorimeter and G.M. counter hodoscope detectors. Two trigger modes have been used in the operation. The first one required the coincidence of any three layers of ionization chambers (ionization $\geqslant$ 80 cascade particles) together with the total energy deposition exceeding 60 GeV. The second trigger was organized to study the low energy part of the spectrum and included a coincidence of two hodoscope detectors and triggering of any pair of adjacent layers of the calorimeter with the above ionization thresh-

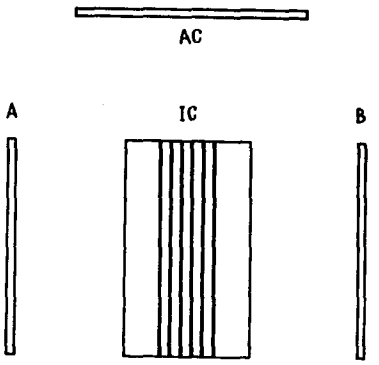

Fig.1

old. The cascade energy threshold in the latter case corresponded to approximately 20 GeV. A veto signal from an air shower shield was formed by a 4-fold coincidence in AC detector which consisted of 6 cells of 0.8 m^2 sensitive area each. A more detailed description of the experimental arrangement has been published in [11].

During five experimental runs in 1980 to 1984 with the total observation time of 8.0×10^7s of about 250000 events have been recorded and analysed. Only cascade showers initiated by muons crossing hodoscope detectors with zenith angles $\theta \geqslant 60^\circ$ have been selected to study the shower energy spectrum and angular distribution. Edge events and a small amount of nuclear showers (which are very different from electromagnetic ones in longitudinal development) have been rejected. The total number of reconstructed events equals to 8.2×10^4 for trajectories traversing both A and B hodoscope detectors with $\Lambda \geqslant 2$ triggered layers of the calorimeter, and 3.8×10^4 for three-layer events ($\Lambda \geqslant 3$) with at least one hodoscope detector (A or B) discharged. The maximum detected shower energy was about 16 TeV.

3. Data analysis and results. To derive cascade shower generation spectrum from the observed distributions the accurate account for experimental conditions (arrangement geometry, trigger and selection criteria, hodoscope and reconstruction efficiency, the difference between the real shower energy ε and its estimate $\tilde{\varepsilon}$, and so on) is necessary. We used the trial spectrum method to analyse our data. Calculations started from the expected (or "trial") spectrum of cascade shower generation in a unit target mass:

$$\mathcal{N}_0(\varepsilon,\theta) = \int_{E_{min}}^{\infty} \mathcal{N}_\mu(E,\theta)\, \sigma(E,\varepsilon)\, dE, \qquad (1)$$

where $\mathcal{N}_\mu(E,\theta)$ is the differential muon spectrum at the observation level (has been calculated after [12]), and $\sigma(E,\varepsilon)$ is the sum of the cross sections of electromagnetic muon interaction processes [13-15]. A Monte Carlo technique was used to calculate the response of the experimental arrangement - the matrix of the numbers of events $N_0(\Delta\tilde{\varepsilon},\Delta\theta)$ expected in the energy estimate interval $\Delta\tilde{\varepsilon}$ and zenith angle interval $\Delta\theta$. The experimental values of the differential cascade shower generation spectrum were then derived from a comparison of the observed $\tilde{N}(\Delta\tilde{\varepsilon},\Delta\theta)$ and calculated $N_0(\Delta\tilde{\varepsilon},\Delta\theta)$ matrices using the following relation:

$$\tilde{\mathcal{N}}(\varepsilon^*,\theta^*) \simeq \mathcal{N}_0(\varepsilon^*,\theta^*) \times \tilde{N}(\Delta\tilde{\varepsilon},\Delta\theta) / N_0(\Delta\tilde{\varepsilon},\Delta\theta). \qquad (2)$$

Here θ^* is the average zenith angle in the $\Delta\theta$ interval, and

ε^* is a logarithmically averaged value (i.e., $\varepsilon^* = \exp(\overline{\ln\varepsilon})$) of the cascade shower energy contributing to $\Delta\tilde{\varepsilon}$ interval. Such a choice of the reference energy minimizes the sensitivity of the derived spectrum to the slope of the trial one.

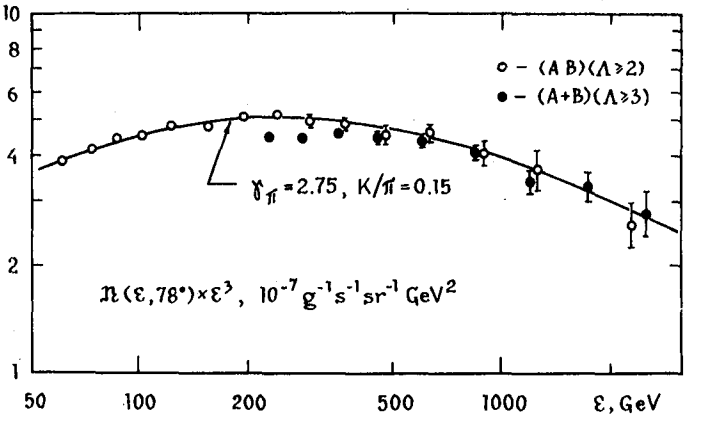

Fig.2

The experimental spectrum of cascade shower generation in iron is presented in Fig.2 for two selection criteria discussed in the previous section. Error bars indicated in the figure are statistical only. The systematic uncertainties may reach ≃15%. The best-fit value of the pion generation spectrum index is 2.75±0.02 in the shower energy interval 50 GeV ≤ ε ≤ 2 TeV for the events selected according to (AB)(Λ≥2) criterion, and 2.68±0.03 for (A+B)(Λ≥3) selection in the range 200 GeV ≤ ε ≤ 3 TeV. Effective muon energy range covered by this experiment is approximately from 150 GeV to 5 TeV.

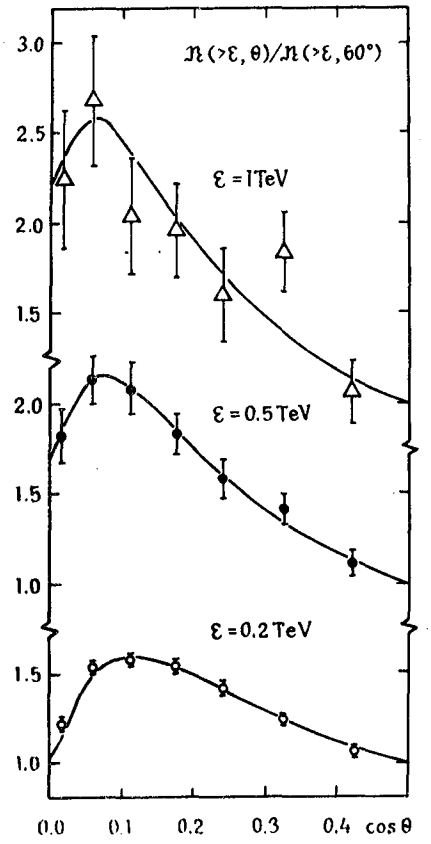

Fig.3

Angular distributions of cascade showers initiated by muons are given in Fig.3. The theoretical curves are calculated with γ_π = 2.70 and K/π = 0.15 and normalized to the experimental data. The agreement of the observed distributions with the theoretical prediction is excellent.

Cascade shower intesity above a certain energy ε_0 may be converted into absolute muon intensity above muon energy E_0. With an appropriate choice of the relation between ε_0 and E_0, the estimated muon intensity does not strongly depend on the spectrum model and relies mainly upon the electromagnetic interaction cross sections used in the conversion. Absolute muon intensities above 1 TeV at large zenith angles derived from the present experimental data are given in Fig.4 together with the recent magnetic spectrometer results. Errors quoted (except MUTRON point) are pure statistical. The

systematic uncertainty of our data is of about 15% and is related mainly to the absolute normalization of shower energy measurements.

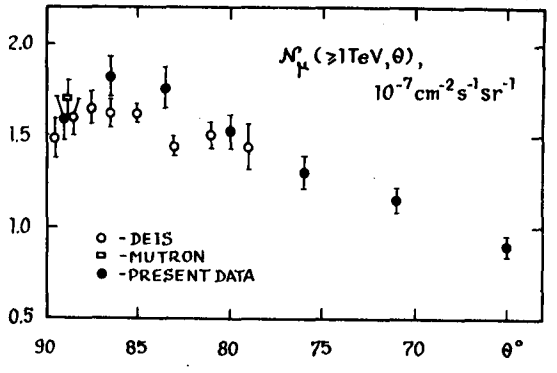

Fig.4

4. Conclusions. The energy spectrum of cascade showers initiated by cosmic ray muons and their angular distribution have been measured in a wide energy range with a good statistical accuracy. Both the spectrum and the angular distribution are fairly described by a conventional picture of muon generation in π- and K-decays with a single power index $\gamma_\pi = 2.68 - 2.75$ and K/π-ratio of 0.15 over the muon energy range from 150 GeV to 5 TeV. The absolute muon intensity at large zenith angles derived from the cascade shower intensity agrees with the recent magnetic spectrometer data and does not support the hypothesis of the additional muon interaction around 1 TeV muon energies.

References

1. O.C.Allkofer et al.Proc.17th ICRC, Paris, 10, 321 (1981)
2. S.Matsuno et al. Phys. Rev., D29, 1 (1984)
3. R.P.Kokoulin et al.Proc.13th ICRC, Denver, 3, 1797(1973)
4. K.Mitsui et al. Nuovo Cim., 73A, 209 (1983)
5. G.B.Khristiansen et al. Proc. 12th ICRC, Hobart, 6, 2122 (1971)
6. A.D.Erlykin et al.Proc.13th ICRC, Denver, 3, 1803 (1973)
7. Yu.N.Bazhutov et al. Proc.17th ICRC, Paris, 7, 59 (1981)
8. V.A.Aglamazov et al.Proc.17th ICRC, Paris, 7,63,76(1981)
9. M.A.Ivanova et al. Proc. 17th ICRC, Paris, 7, 23 (1981)
10. R.I.Enikeev et al.Proc.18th ICRC, Bangalore, 7, 36(1983)
11. V.D.Ashitkov et al. Izv.Akad.Nauk SSSR, Ser.Fiz.,45,1319 (1981)
12. L.V.Volkova. Preprint FIAN SSSR, No. 72, Moskva (1969)
13. H.J.Bhabha. Proc.Roy.Soc., A164, 257 (1938)
14. A.A.Petrukhin,V.V.Shestakov.Can.J.Phys., 46, S377 (1968)
15. R.P.Kokoulin,A.A.Petrukhin.Proc.11th ICRC, Budapest, 4, 277 (1970); Proc.12th ICRC, Hobart,6, 2436 (1971)

MEASUREMENT OF MUON INTENSITY BY CERENKOV METHOD

Liu Z.H., Li G.J., Bai G.Z.
Liu J.G., Geng Q.X., Ling J.
Chongqing Institute of Architecture and Engineering
Chongqing, People's Republic of China

1. Introduction.

Optical detection is one of the important techniques in studies and observations of air showers, muons and relevant phenomena. In order to measure the muon intensity in a proper energy range and to study some problems about cerenkov radiation of cosmic rays, a muon-telescope with cerenkov detector has been operated.

2. Experimental arrangement and method.

The telescope consists of two scintillation counters, one cerenkov detector and coincidence circuits. The cerenkov detector is installed in a closed cylindrical shell and is composed of bare photomultiplier, parabolic mirror with diameter 500 mm and focal distance 260 mm, pre-amplifier etc.

The hollow cylinder is assembled in sections and so that its height may be changed. Near by the telescope, another scintillator has been operated simultaneously to determine the influence of showers on the intensity.

Signals of cerenkov radition from photomultiplier are amplified and analysed by a multichannel analyser gated "on" by the telescope coincident output.

Since the number(n) of cerenkov photons emitted within a region of wavelengths λ_1 and λ_2 for a particle with $\beta \sim 1$ is given by:

$$n = 2\pi\alpha l\left(\frac{1}{\lambda_2} - \frac{1}{\lambda_1}\right) \sin^2\theta$$

the number of cerenkov photons emitted in a unit of path length can be calculated. In observations, the actual number

of photons reflected from the mirror and collected by the photomultiplier will depend on various factors. It can be compared with the value of theoretically expected.

3. Results and discussion.

The muon intensity measured is in agreement with the integral energy spectrum of cosmic ray muons. Details of data analysis will be presented as more observations are completed.

In order to get correct analysis to the experimental process, fluctuations and influence factors, it is better to operate the apparatus in various conditions, such as, varied height of the hollow cylinder, different placement of photomultiplier with different area of photocathode etc.

4. Acknowlegement

We are grateful to Mr G.F. Chen and Mr X.J. Zhan for help and discussions.

References.

(1) Gregry A.G. et al., 18th ICRC, Conference Papers, Vol.8, 145, 1983.

(2) Protheroe R.J., 18th ICRC, Conference Papers, Vol. 6, 240, 1983.

(3) Clay R.W. et al., 17th ICRC, Conference Papers, Vol.8, 130, 1981.

HE 5.2-16

ANALYTICAL CALCULATION OF MUON INTENSITIES UNDER DEEP SEA-WATER

Inazawa, H. and Kobayakawa, K.
The Graduate School of Science and Technology
and College of Liberal Arts, Kobe University
Nada, Kobe 657, JAPAN

1. Introduction. The study of the energy loss of high energy muons through different materials, such as rock and sea-water can cast light on characteristics of lepton interactions. There are less ambiguities for the values of atomic number (Z) and mass number (A) in sea-water than in rock. Muon intensities should be measured not only as fundamental data but also as back ground data for searching the fluxes of neutrino. The average rang-energy relation in sea-water is derived. The correction factors due to the range fluctuation is also computed. By applying these results, the intensities deep under sea are converted from a given muon energy spectra at sea-level. The spectra of conventional muons from π, K decays have $\sec\theta$ enhancement. On the other hand, the spectrum of prompt muons from charmed particles is almost isotropic. The effect of prompt muons is examined.

2. The energy loss of muon in sea-water. With respect to the Pacific Ocean near Hawaii, the salinity is taken as 34.5‰ and the density as 1.0275. Referring to (1, 2) we obtain the fundamental constants for this salinity as follows: $\langle Z\rangle = 7.471$, $\langle A\rangle = 14.873$, $\langle Z/A\rangle = 0.5525$ and $\langle Z^2/A\rangle = 3.779$ which differ a little bit from Varilov et al (3). The salinity and the inorganic composition of the sea-water over the apparatus is desirable to be directly measured.

The rate of muon energy loss is given by (4)

$$-dE/dt = k(E) + b(E)E \qquad (1)$$

and $$b(E) = b_p(E) + b_B(E) + B_N(E)\ , \qquad (2)$$

which are the terms from pair production, bremsstrahlung and nuclear interaction, respectively. In a good approximation, we have

$$B_N(E) = 5.043 + 0.1165\ \ln E(\mathrm{TeV}) \quad 10^{-7}/\mathrm{gcm}^{-2}, \qquad (3)$$

which corresponds to $\sigma(h\nu) = 125\mu b$ (5). The b_B term is corrected (6). The energy dependence of b is shown in Fig. 1, where those in standard rock (S.R.) and water are compared.

3. Average range-energy relation and correction factors. After integrating eq. (1) numerically, we get the average range D(E) corresponding to the muon energy E at sea-level. The E-D relation in sea-water is shown in Fig. 2, as well as in S.R. and water. One find $1\sim 2\%$ differences of D(E) in sea-water and in water near at E = 100 TeV. The corresponding zenith angles at DUMAND to ranges are added in Fig. 2. The vertical depth of DUMAND is taken as 4.8×10^5 g/cm^2 which muons with E = 3.1 TeV reach to.

The correction factor R is defined by $R = I_0(D)/I(D)$, where I and I_0 are intensities with and without the range fluctuations, respectively. The values of R depend on the exponent β of the integral energy spectrum at sea-level, i.e. $I(>E)\propto E^{-\beta}$. Following to the procedure in (4), the R values in sea-water are computed for $\beta = 2$ and 3. The R values with any β at a given depth D can be interpolated or extrapolated from the relation

$$\ln R(\beta) = -k_1\beta^{3/2} + k_2 \quad , \tag{4}$$

where k_1 and k_2 are constants determined from R(2) and R(3). Fig. 3 shows the dependence of R with D for β = 3, 2.7, 2.5.

4. Intensities deep under sea. The muon energy spectrum at sea-level can be converted by using the results obtained above. So the spectra are assumed as follows. The conventional spectrum at vertical direction is referred to Komori and Mitsui (7). This spectrum has almost constant β, i.e. 2.67, above E = 10 TeV. Since the conventional spectrum is enhanced by secθ, the enhance factors are estimated from those given by Maeda (8). These spectra are shown in Fig. 4 for both vertical and horizontal directions. The latter fits well with MUTRON data up to E = 25 TeV (9). The dashed curves in Fig. 4 shows prompt muon spectra which have no dependence of θ up to E = 1000 TeV (10). The maximum contribution (MAX.PROMPT) is estimated under the assumptions that the diffractive characters of the produced charmed particles are extremely stressed and the intrinsic charm distribution is very hard. The minimum contribution (MIN.PROMPT) is taken out of charm production only in non-diffractive processes. The maximum and minimum prompt spectra are well described by

$$I^p(>E) = 2.11\times10^{-9}\ E(\mathrm{TeV})^{-1.44}\ (\mathrm{cm^2\ s\ ster})^{-1}, \tag{5}$$

$$I^p(>E) = 7.36\times10^{-11}\ E(\mathrm{TeV})^{-1.49}\ (\mathrm{cm^2\ s\ ster})^{-1}, \tag{6}$$

respectively.

The intensity at a given vertical depth D can be obtained by the following procedure. The corresponding energy E to D is given by the average range energy relation. After β around E is determined from I(>E) in vertical direction, R with D and β is got from eq. (5). I(>E)/R is the vertical intensity at D. The resultant intensity is shown in Fig. 5 as a solid curve. When the energy spectrum includes the miximum prompt part, the intensities changes into a dashed curve. Old measurements of OCU group (11) and Vavilov et al. (3) are also plotted. The recent simulation (12) gives the almost same results with curves of the figure.

The same procedure is applied to the intensity at a slant depth. Here we consider a measurement at the vertical depth 4.8×10^5 g/cm^2 (DUMAND). Since the conventional energy spectrum is enhanced in an inclined direction with θ as shown in Fig. 4, we have a different R as well as I(>E) from vertical one, where E corresponds to the slant depth 4.8×10^5 secθ g/cm^2. The relative contribution of prompt muons, if any, to total intensity becomes the less as θ becomes the larger. The intensities vs slant depths (or zenith angles at DUMAND) are presented in Fig. 6. If the maximum prompt muons contribute, the intensity is about twice of that without prompt muons at θ = 70°.

5. Conclusions and discussions. The average range energy relation and the correction factors due to the range fluctuation have been computed in sea-water. From a given energy spectra at sea-level which are conventional (π. k decays) and prompt (charmed particles decays), the intensities in the vertical direction deep under sea have been obtained (Fig. 5). The angular dependence of intensities at DUMAND has been made clear (Fig. 6). It is concluded that measurements at larger zenith angle than 70° can reveal the contribution of prompt muons. The present calculations are useful for the measurement of muon neutrino

flux. Because this flux can be estimated from the deviation of the observed flux from the intensity described here.

References

1. Turekian, K.K., (1969), In Wedepohl, K.H. (ed.), Handbook of Geochemistry, Springer-Verlag, p309.
2. Horibe, S. (ed.), (1975), Inorganic Chemistry in Ocean, Oceanography Series 6, Tokyo Univ. Press, p58 (in Japanese).
3. Vavilov, Yu.N. et al, (1974), Sov. J. Nucl. Phys. 18, 434.
Davitaev, L.N. et al., (1969), 11th I.C.R.C., Budapest, 7, 53.
4. Kobayakawa, K., (1967), Nuovo Cimento, 47B, 156.
5. Kobayakawa, K., (1973), 13th I.C.R.C., Denver, 5, 3156,
6. Minorikawa, Y. et al., (1981), Nuovo Cimento, 4C, 471.
7. Komori, H. and Mitsui, K., (1982), J. Phys. G, 8, L197.
8. Maeda, K., (1973), Fortschr. Phys. 21, 113.
9. Matsuno, S. et al (1984), Phys. Rev. D, 29, 1.
10. Inazawa, H. et al., (1985), preprint KOBE 85-03 (to be submitted to J. of Phys. G)
11. Higashi, S. et al., (1966), Nuovo Cimento, 43A, 334.
12. Takahashi, N. et al., (1984), Uchusen Kenkyu (in Japanese), 28, 120.

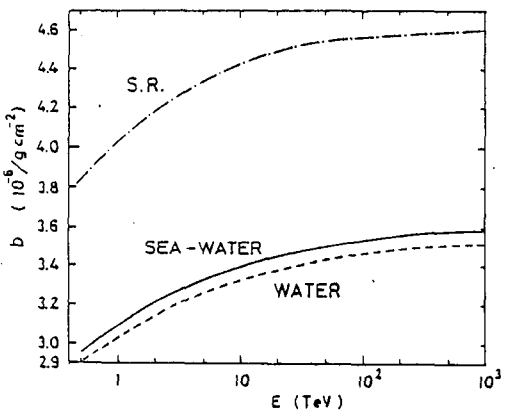

Fig.1 The energy dependence of b-term in sea-water, water and standard rock.

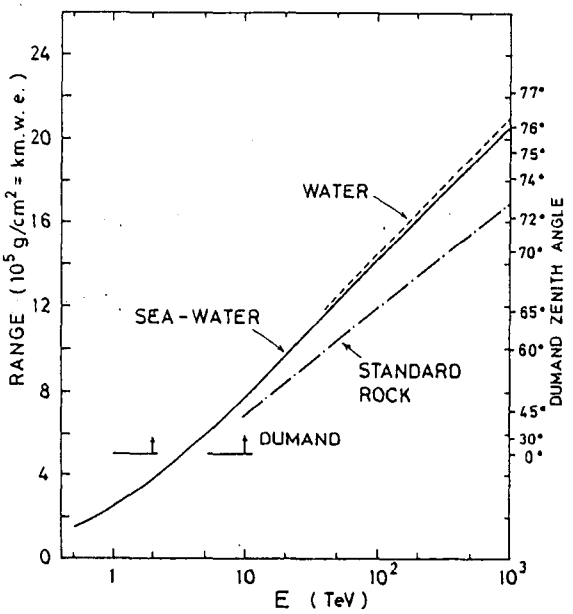

Fig.2 Average range energy relations in sea-water, water and standard rock. The zenith angles at DUMAND position (vertical depth 4.8×10^5 g/cm^2) are added.

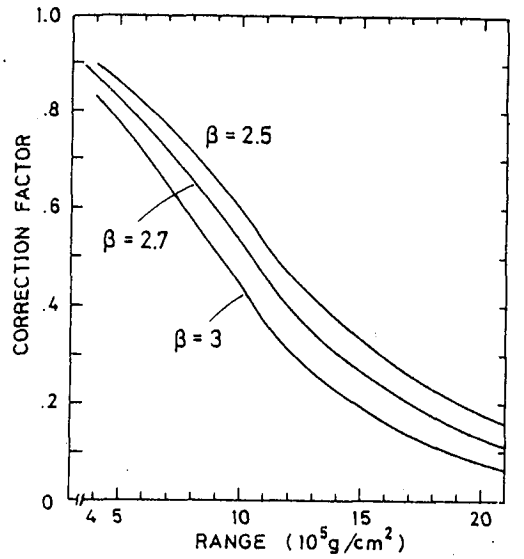

Fig.3 Correction factors in sea-water for β, the exponent of the integral energy spectrum of muons.

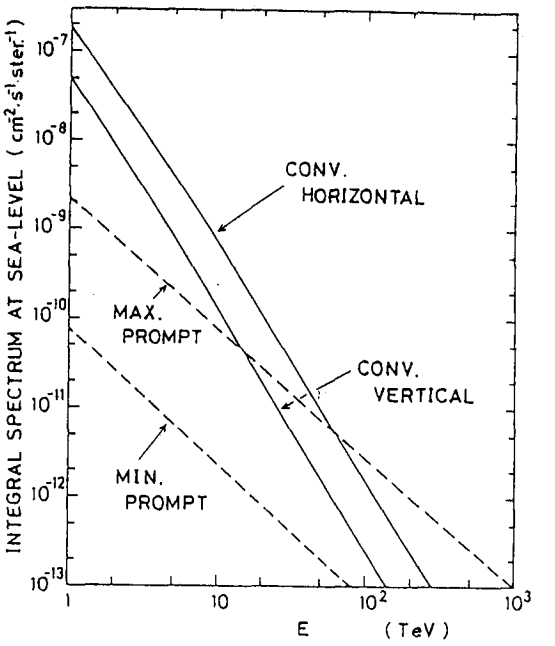

Fig.4 Adopted integral energy spectra of muons at sea-level: — conventional (π, k decays); - - - prompt (charmed particles decays).

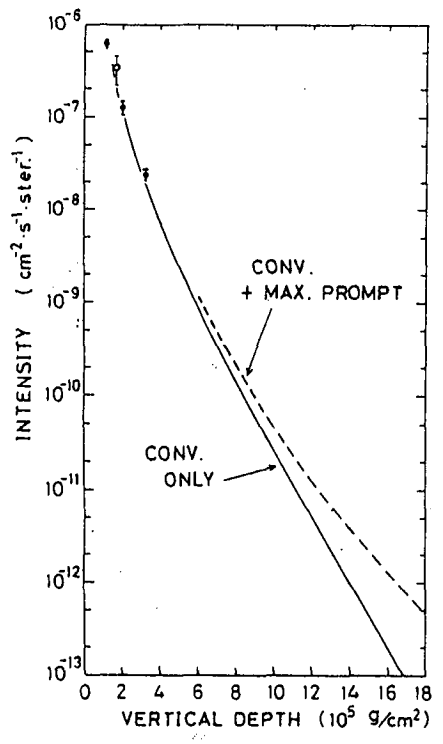

Fig.5 Intensity in the vertical direction at vertical depth under sea: — conventional only; - - - conventional plus maximum prompt; ○ OCU; ● Vavilov et al.

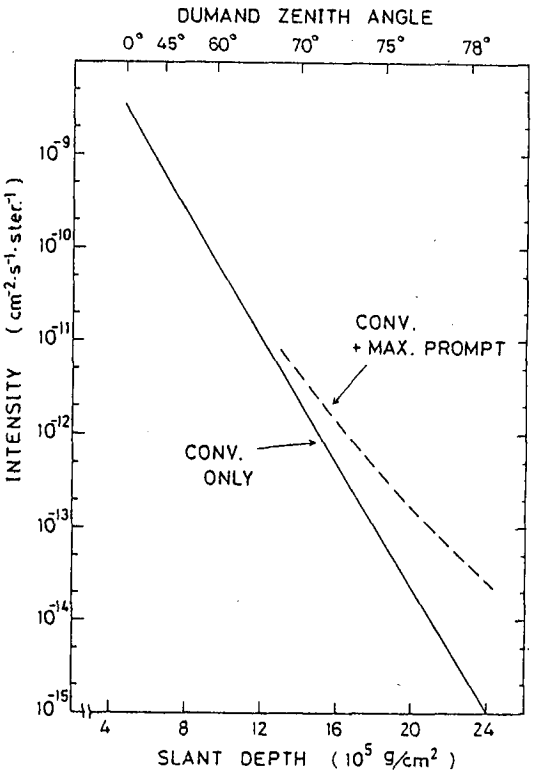

Fig.6 Intensity in the inclined directions at vertical depth 4.8×10^5 g/cm^2: — conventional only; - - - conventional plus maximum prompt.

HE 5-2-17

PHOTO NUCLEAR ENERGY LOSS TERM FOR MUON-NUCLEUS INTERACTIONS BASED ON ξ SCALING MODEL OF QCD

Rajkumar Roychoudhury
Electronics Unit
Indian Statistical Institute
Calcutta 700035, INDIA

1. Introduction. EMC collaboration experiments[1] discovered a significant deviation of the ratio of structure functions of iron and deuteron from unity (see Fig. 1).

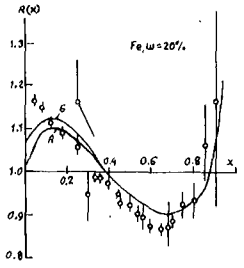

Fig.1: Ratio of the structure functions of iron and deuteron Data from the EMC.

This result was later verified by a SLAC group[2]. These results have established the fact that the quark parton distribution in nuclei are different from the corresponding distribution in the nucleous. In the present paper we examine whether these results have any effect on the calculation of photo nucleous energy loss term for muon-nucleus nuclear interaction. All the previous[3-7] calculations were based on the data of ep scattering in which the deviation discussed above was neglected. Though the EMC and SLAC data were restricted to rather large q^2 region it is expected that the deviation would persist even in the low q^2 domain[8]. The model used by us is a modified version of ξ scaling model of Georgi and Politzer[9]. For the ratio of iron and deuteron structure function we took a rather naive least square fit of the form $R(x) = a + bx$[9] and assume the formula to be valid for the whole q^2 region in the absence of any knowledge of $R(x)$ for small q^2.

2. ξ scaling model and Kinematics. If a massless quark carries a fraction ξ of the proton momentum and is kicked onto its mass shell by the collision, then

$$(\xi p + q)^2 = \xi^2 m_p^2 + 2\xi p\cdot q + q^2 = 0 \qquad (1)$$

from which we get

$$\xi = \frac{2x}{1 + (1 + 4x^2 m_p^2/q^2)^{1/2}} \qquad (2)$$

where x is the usual Bjorken scaling variable defined by $x = q^2/2m_p^2\nu$ being the energy transfer. Taking into account of scale breaking phenomena, nucleon structure function has been constructed after the scaling model of Georgi and Politzer[10] for large q^2 in the following way

$$\nu W_2 = \frac{a(1-\xi)^{3.5}}{\xi} \frac{x^2\,[1 + m_p\nu/(q^2 + \bar{a}^2)]}{(1 + 4m_p^2x^2/q^2)^{1.5}} \qquad (3)$$

For low q^2 ($< .1$ $(\text{Gev/c})^2$) the structure formation can be approximated by

$$\nu W_2 \simeq (aq^2 + bq^2/\nu) \qquad (4)$$

and we take

$$W_1 \simeq \nu W_2/2m_p x \tag{5}$$

A good fit[11] to the structure function for low and high q^2 values is obtained with a = ·655, $\bar{a}$ = ·3. The x dependance of the ratio R(x) $\nu W_2^{Fe} / \nu W_2^{D}$ is taken to be

$$R(x) \simeq 1·2 - ·5x \tag{6}$$

the energy loss term b_N is given by

$$b_N = \frac{N}{E} \int_{\nu_{min}}^{\nu_{max}} \int_{q^2_{min}}^{q^2_{max}} A^{n-1} \frac{d^2\sigma}{dq^2 d\nu} \, dq^2 d\nu \tag{7}$$

where q^2, E, ν are respectively the 4 dimensional momentum transfer squared, the muon energy and the energy transfer E - E'. N is the Avogadro number, A the atomic mass n mber and n is the power index describing the A dependance of the cross section and m_p is the proton mass. The limits of integrations are given by

$$\nu_{min} \simeq m_\pi , \quad \nu_{max} = E\left[1 - \frac{m_p}{2E}\left(1 + m_{\mu^2}/m_{p^2}\right)\right] \tag{8}$$

$$q^2_{min} = \frac{m_{\mu^2}\nu^2}{E(E-\nu)} , \quad q^2_{max} = 2 m_p \nu \tag{9}$$

m_π, m_μ being the pion and muon mass respectively. The double differential cross section for inelastic muon nucleus scattering is given by Drell and Walecka[12]

$$\frac{d^2\sigma}{dq^2 d\nu} = \frac{2\pi\alpha^2}{|\vec{p}|^2 q^4}\left[(q^2 - 2m_{\mu^2})W_1 + (2E(E-\nu) - q^2/2)W_2\right] \tag{10}$$

In principle b_N can be evaluated from (7) and (10) but the calculation is cumbersome and lengthy. However if we neglect terms of order 1/E then b_N can be expressed in a closed form.

$$b'_N = \frac{2\pi\alpha^2 A_{eff}}{A} N\bar{A}\left[1·45 \ln\left(m_{\mu^2} E + \bar{a}^2 m_p/2\right) + 8858\right] \tag{11}$$

where A for atmosphere is 14·75 and $A_{eff}/A \simeq$ ·8. the suffix 1 in b_N means that b_N has been calculated without taking into account of EMC effect. If we take into consideration of EMC effect and calculate b_N (call it b^2) then to the leading order

$$b^2_N \simeq 1·2\, b^1_N \tag{12}$$

3. Results and Discussions. Fig·2 shows the energy dependance of b_N found from the present calculation. Though the EMC data is mainly confined in the region of $q^2 > 1$ Gev/c we assumed the result to be valid in the whole q^2 region. The result b^2_N would be modified in future when further data for heavy nucleus like Al would be available in $q^2 < 1$ (Gev/c) region.

If it is found that R(x) does not differ from that in the low q^2 region then b_N^1 will represent the muon energy loss which is still higher than that estimated by Dau et al.

Conclusion Assuming EMC results for R(x) to be valid in the low q^2 region, b_N value calculated using the structure function for deep inelastic muon scattering off a nucleon bound in a nucleus found to be higher than that obtained using the structure function for deep inelastic muon scattering off a free nucleon. Also both b_N^1 and b_N^2 rise with energy.

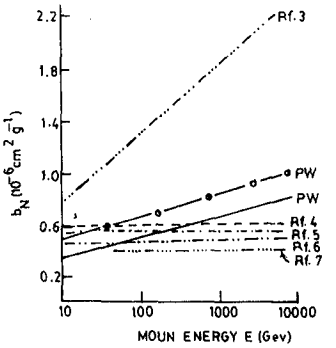

Fig.2: The energy loss parameter b_N plotted as a function of muon energy E —— present calculation for $F_2^p(x)$ -o-o-o- Present calculation for $F_2^{Fe}(x)$ and others taken from the references (3-7).

References

1. J. Aubert et al., Phys. Rev. Lett. 123 B 275 (1983).
2. A. Bodek et al., Phys. Rev. Lett. 50 1431, 51 534 (1983).
3. D. Kessler et al., Nuovo Cimento 17 809 (1960).
4. W. D. Dau, W. Constandt and H. Jokisch, J. Phys. G 9 391 (1983).
5. I. B. Bezrukov et al., Sov. J. Nucl. Phys. 15, 176 (1972).
6. K. Kobayakawa, Proc. 13th ICRC, Denver, 5, 3156 (1973).
7. Y. Minorikawa et al., Proc. 16th ICRC, Kyoto 10 240 (1979).
8. R. G. Arnold, SLAC, PUB-3434 (1984).
9. L. A. Kondratyuk et al., JETP Letters 39 324 (1984).
10. H. Georgi and H. P. Politzer, Phys. Rev. D 14 1829 (1976).
11. R. K. Roychoudhury et al., Proc. 18th ICRC 7 86 (1983).
12. S. D. Drell and Walecka, Ann. Phys. 28 18 (1964).

ON METHOD OF MUON SPECTRUM MEASUREMENTS BY THE SCINTILLATION DETECTORS OF A LARGE THICKNESS $T > 4t_o$.

O.G.Ryazhskaya

Institute for Nuclear Research, the USSR Academy of Sciences, 60th October Anniversary prospect,7a, Moscow 117312, USSR

The various methods are known for the study of muon spectrum. The direct ones include the muon energy measurements by magnetic spectrometers. The indirect ones deal with the reconstruction of the muon spectrum from the spectrum of secondary particles (γ-quanta, knock-on electrons and e^+e^--pairs) obtained by burst or calorimeter technique. The burst technique is based on the measurement of the number of cascade particles, mainly in the cascade maximum, by the detectors of small thickness $T \leq t_o$ (t_o - radiation unit). The calorimeter method consist in determination of the cascade energy with help of the cascade curve shape. For this purpose the multylayer detectors can be used. They are usually comprised of proportional counters, X-ray emulsion chambers or scintillation counters with the target material placed between them.

Using the scintillation detectors of a large thickness one can measure the total cascade energy directly. In this case the detector works as a true calorimeter. But when the total energy is detected, the cascade spectrum differs from the muon one.

Let us consider the spectrum of cascades generated by muons in the target of infinite thickness with Z=12. The spectrum is measured by the scintillation detector of thickness $T > 4t_o$. The cascades with energy $\nu > 200$ GeV are mainly generated by bremsstrahlung γ-quanta. The contribution of knock-on electrons decreases with energy. The value of $R_{\delta_b} = \frac{F_\delta(\nu)\, d\nu}{F_b(\nu)\, d\nu}$ (where $F_\delta(\nu)d\nu$, $F_b(\nu)d\nu$ are the spectra of knock-on electrons and γ-quanta, is the particle energy) depends on the muon spectrum index very weakly. The values of R_{δ_b} for Z=12 and $\gamma_\mu = 1.0$, 1.5 and 2.7 are presented in Table 1. One can calculate R_{δ_b} with the accuracy better than 5% according to the formula:

$$R_{\delta_b} \approx 409 \cdot \frac{1}{(Z+1)\nu} \qquad (1),$$

where ν is in GeV.

Table 1

ν, GeV		100	200	300	400	500	1000
R_{δ_b}	γ_μ=1.0	0.315	0.160	0.106	0.079	0.063	0.0306
	γ_μ=1.5	0.314	0.161	0.107	0.079	0.063	0.0303
	γ_μ=2.7	0.307	0.161	0.107	0.070	0.063	0.0299

The contribution of the cascades from e^+e^--pairs is about (3÷4)% for all energies /1,3,4/. Therefore, the spectra of the cascades generated only by muons through bremsstrahlung and inelastic scattering should be considered.

The bremsstrahlung cross section /1,2/ for Z=12 proves to be approximated with accuracy better than 1% by following functions:

$$d\sigma_b(v,\nu) = C_b \cdot f_b(v,\nu,Z) \cdot d \ln v \qquad (2),$$

where $C_b = 4\alpha\left(r_e \frac{m}{m_\mu}\right)^2 \cdot \frac{N_0}{A} \cdot Z(Z+1)$,

$f_b(v,\nu,12) = C_1 = 11.45$ for $v < 0.03$

$f_b(v,\nu,12) = A_1(B_1 + \ln\frac{1}{v})$; A_1=0.939, B_1=8.75 for $0.03 < v < 0.178$

$f_b(v,\nu,12) = D\cdot\ln\nu + (K - B\ln\nu)\cdot\ln\frac{1}{v}$, D=0.824, K=5.7, B=0.48 for $0.178 < v < 0.9$,

where $v = \frac{\nu}{E_\mu}$, ν, E_μ are in GeV.

For all other values of Z, $f_b(v,\nu,Z)$ is

$$f_b(v,\nu,Z) = f_b(v,\nu,12) - \frac{2}{3}\left(\frac{4}{3} - \frac{4}{3}v + v^2\right)\cdot\ln\frac{Z}{12} \qquad (3).$$

The approximations (2) and (3) are convenient for calculations of bremsstrahlung energy losses and of the γ-quanta spectrum, $F_b(\nu)\,d\nu$. The functions (2) and (3) as well as these functions multiplied by v^{γ_μ} can be integrated analytically. Calculated according to (2) the energy losses differ by less than 0.1% from the precise values. For power-law muon spectrum one gets the following expression for $F_b(\nu)\,d\nu$:

$$F_b(\nu)\,d\nu = \frac{d\nu}{\nu^{\gamma_\mu+1}} \frac{C_b}{\gamma_\mu}\left[L'(\gamma_\mu) + \left(D'(\gamma_\mu) - B'(\gamma_\mu)\frac{1}{\gamma_\mu}\right)\ln\nu + \frac{K'(\gamma_\mu)}{\gamma_\mu}\right] = \frac{d\nu}{\nu^{\gamma_\mu+1}}\frac{C}{\gamma_\mu}\cdot m(\gamma_\mu, \ln\nu) \qquad (4),$$

where in $L'(\gamma_\mu)$ the integration over v up to v_1=0.178 is performed,

$D'(\gamma_\mu) = D(1 - v_1^{\gamma_\mu})$, $K'(\gamma_\mu) = K\left[1 - v_1^{\gamma_\mu}(1 - \ln v_1^{\gamma_\mu})\right]$,

v_1=0.178, $B'(\gamma_\mu) = B\left[1 - v_1^{\gamma_\mu}(1 - \ln v_1^{\gamma_\mu})\right]$.

For γ_μ=1 the ratio $\frac{L'(\gamma_\mu)}{m(\gamma_\mu, \ln\nu)}$ is 27% and 23% for

ν = 200 and 2000 GeV respectively. For $\gamma_\mu > 2.5$ the ratio $\frac{L'(\gamma_\mu)}{m(\gamma_\mu, \ln\nu)}$ is less than 2%. According to (4) the bremsstrahlung spectrum can't be approximated by power law: for $\gamma_\mu = 2.5$ when ν is increased by the factor of 10, the value of $m(\gamma_\mu, \ln\nu)$ increases by 29% demonstrating thus the deviation from the power-law spectrum. The photon spectrum is flatter than the muon one. In the more rough approach when the bremsstrahlung spectrum is taken as power-law one, the difference between γ_μ and γ_b is equal to $\Delta\gamma = 0.11$ ($\gamma_\mu = 2.5$). Thus, when the total cascade energy is measured, the spectrum $F_b(\nu)d\nu$ is flatter than the spectrum of the parent muons.

If energy $\varepsilon = \nu \cdot q(\nu)$, where $q(\nu) < 1$, is deposited in the detector, the variation of q with energy can lead to the deformation of the energy release spectrum as compared with the photon one. The value of q is a function of the detector thickness, T, the distance between the point of the cascade generation and the position of the detector, X_b, and of energy, ν. With the detector thickness being constant and with the generator thickness being infinite, the energy release spectrum (in $cm^{-2} \cdot sec^{-1}$) can be calculated as:

$$F_b(\varepsilon)d\varepsilon = d\varepsilon \int_{\varepsilon/q_{max}}^{\infty} \frac{d\nu}{\nu^{\gamma_\mu+1}} \frac{dX_b(\nu)}{d\varepsilon} \frac{C_b}{\gamma_\mu} \left[L'(\gamma_\mu) + (D'(\gamma_\mu) - \frac{B'(\gamma_\mu)}{\gamma_\mu}) \ln\nu + \frac{K'(\gamma_\mu)}{\gamma_\mu} \right] \quad (5),$$

where $\frac{dX_b(\nu)}{d\varepsilon}$ is the variation of the thickness of the generation layer at which the cascade with energy ν releases energy in the range $[\varepsilon, \varepsilon + d\varepsilon]$ in the detector. For the steep spectrum it is convenient to use $d\ln\varepsilon$ instead of $d\varepsilon$. Taking into account the cascade curves /5/, which give the dependence q(x) for the detector of thickness T, one can obtain the dependence $\frac{dX_b}{d\ln\varepsilon} = X_b(T)\left[C_2 + \left(\frac{\nu_o}{\nu}\right)^{\gamma_1}\right]$, where $\nu_o = \varepsilon / q_{max}$ is the minimal energy of the cascade producing the energy release ε, q_{max} is the maximal fraction of released energy, $X_b(T)$ is the function weakly dependent on T, $C_2 \approx 0.23$, $\gamma_1 = 4.5$. The expression (5) can be integrated analytically. For $\varepsilon / q_{max} \geq 100$ GeV it is equal to

$$F_b(\varepsilon)\, d\ln\varepsilon = \frac{C_b X_b(T)}{\gamma_\mu} q_{max}^{\gamma_\mu}(T, \varepsilon) \frac{d\ln\varepsilon}{\varepsilon^{\gamma_\mu}} \left(\frac{C_2}{\gamma_\mu} + \frac{1}{\gamma_\mu + \gamma_1}\right) *$$

$$* \left[L'(\gamma_\mu) + (D'(\gamma_\mu) - \frac{B'(\gamma_\mu)}{\gamma_\mu}) \ln\frac{\varepsilon}{q_{max}(\varepsilon)} + \frac{K'(\gamma_\mu)}{\gamma_\mu} \right] \quad (6).$$

The accuracy of (6) is better than 4%. The energy release spectrum is seen from (6) to be of the same shape as the bremsstrahlung spectrum for the very thick detectors and for q_{max}=const. Generally for $\varepsilon > 100$ GeV and $T > 4t_o$ one has

$$q_{max}(T, \varepsilon) = q_{max}(T_o)\left(\frac{T}{T_o}\right)^{\alpha_b} + H_b - M_b \ln\varepsilon \quad (7),$$

$H_b = M_b \ln 100$, $\alpha_b = \alpha_b(T)$, $M_b = 2.93 \cdot 10^{-2}, 3.26 \cdot 10^{-2}, 3.48 \cdot 10^{-2}, 3.48 \cdot 10^{-2}, 3.46 \cdot 10^{-2}$ for $T = 12t_o, 10t_o, 8t_o, 6t_o, 4t_o$ respectively. For $4t_o \leqslant T \leqslant 6t_o$ one must take $T_o = 4t_o$, $\alpha_b = 0.83$, while for $6t_o \leqslant T \leqslant 13^o t_o$ - - $T_o = 6t_o$, $\alpha_b = 0.56$. For $T \geqslant 13t_o$ and for the large range of $\ln\varepsilon$ $q_{max}(T, \varepsilon) = 1$. The value of $q_{max}^{\gamma_\mu}$ can be written as:

$$q_{max}^{\gamma_\mu}(T, \varepsilon) = q_{max}^{\gamma_\mu}(T_o)\left(\frac{T}{T_o}\right)^{\alpha_b \cdot \gamma_\mu}\left[1 - \frac{\gamma_\mu \cdot (M_b \ln \varepsilon - H_b)}{q_{max}(T_o)\left(\frac{T}{T_o}\right)^{\alpha_b}}\right] \quad (8).$$

Then the energy release spectrum $F_b(\varepsilon)$ can be given as:

$$F_b(\varepsilon)d\ln\varepsilon = \frac{C_b X_b(T)}{\gamma_\mu} q_{max}^{\gamma_\mu}(T_o)\left(\frac{T}{T_o}\right)^{\alpha_b \cdot \gamma_\mu}\left(\frac{C}{\gamma_\mu} + \frac{1}{\gamma_\mu + \gamma_1}\right)\frac{d\ln\varepsilon}{\varepsilon^{\gamma_\mu}}\left[L'(\gamma_\mu) + \right.$$

$$\left. + (D'(\gamma_\mu) - \frac{B'(\gamma_\mu)}{\gamma_\mu})\ln\frac{\varepsilon}{q_{max}(\varepsilon)} + \frac{K'(\gamma_\mu)}{\gamma_\mu}\right] \cdot \left[1 - \frac{\gamma_\mu \cdot (M_b \ln \varepsilon - H_b)}{q_{max}(T_o)\left(\frac{T}{T_o}\right)^{\alpha_b}}\right] \quad (9).$$

The deviation of the spectrum $F_b(\varepsilon)d\ln\varepsilon$ from the power-law function $d\ln\varepsilon/\varepsilon^{\gamma_\mu}$ is connected with two terms depending logarithmically on ε:

$m' = L'(\gamma_\mu) + (D'(\gamma_\mu) - \frac{B'(\gamma_\mu)}{\gamma_\mu})\ln\frac{\varepsilon}{q_{max}(\varepsilon)} + \frac{K'(\gamma_\mu)}{\gamma_\mu}$ and $\lambda = 1 - \frac{\gamma_\mu(M_b \ln\varepsilon - H_b)}{q_{max}(T_o)\left(\frac{T}{T_o}\right)^{\alpha_b}}$

If the spectrum (9) is approximated by the power law, the spectral index for $T < 6t_o$ is somewhat greater than γ_μ and for $T \geqslant 8t_o$ is hardly less than γ_μ. The values of $\Delta\gamma = \Delta\gamma(T, \gamma_\mu)$ are presented in Table 2:

	T	4	6	8	10	12
$\Delta\gamma$	$\gamma_\mu = 1$	0.038	0.013	0.004	-0.0013	-0.0013
	$\gamma_\mu = 2.5$	0.12	0.036	0.004	-0.009	-0.021

Measuring the energy release spectrum by the detector with $T \approx 8t_o$, the energy dependence of the cascade energy deficit compencates for the increasing of the bremsstrahlung cross section. q_{max} varies from 82% to 66% for $\varepsilon = 100$ and 10000 GeV respectively. In real measurements cascades come from different directions where the detector has the various thickness. The total energy release spectrum in this case must be found as a sum over various thicknesses T_i involved in the measurements, i.e. $F_b(\varepsilon)d\varepsilon = \sum_i F_b(\varepsilon, T_i)d\varepsilon$. If the detector thickness varies from $6t_o$ to $12t_o$ and $\langle T \rangle = 8t_o$, the spectral index of $F_b(\varepsilon)d\varepsilon$ is almost equal to the muon spectrum index for $1 \leqslant \gamma_\mu \leqslant 3$. It is the Artyomovsk 100-ton scintillation counter that operates in this way /6/.

References

1. E.V.Bugaev, Yu.D.Kotov, I.L.Rozental. Kosmicheskie muony i neutrino, Atomizdat, Moscow (1970)
2. L.B.Bezrukov and E.V.Bugaev, 17th ICRC, 7, 102 (1981)
3. R.P.Kokoulin and A.A.Petrukhin, 12th ICRC, 6, 2436 (1971)
4. O.G.Ryazhskaya. Thesis, FIAN (1970)
5. T.A.Chuykova, 18th ICRC, 5, 316 (1983)
6. R.I.Enikeev et al. 18th ICRC, 7, 36 (1983)

HE 5.2-19

RANGE FLUCTUATIONS OF HIGH ENERGY MUONS PASSING THROUGH MATTER

Y.Minorikawa
Department of Physics, Kinki University, Osaka 577, Japan

K.Mitsui
Institute for Cosmic Ray Research, University of Tokyo, Tokyo 188, Japan

1. Introduction. The information about energy spectrum of sea level muons at high energies beyond magnetic spectrographs can be obtained from the underground intensity measurements if the fluctuation problems are solved. In the present paper we recalculate the correction factor R for the range fluctuations of high energy muons by analytical method of Zatsepin et. al[1], where most probable energy loss parameter are used. It is shown that by using the R at great depth together with the slope, Λ, of the vertical depth-intensity(D-I) curve in the form of $\exp(-t/\Lambda)$, the spectral index, γ, in the power law energy spectrum of muons at sea level can be easily obtained.

2. Formulation of the correction factor R. The R is defined as $R = I_0(t)/I(t)$, $I_0(t)$ is the intensity without fluctuations and $I(t)$ is the intensity, taking fluctuations into account. In order to find $I(t)$ the following diffusion equation has to be solved:

$$\partial I/\partial t - \beta(E_\mu)\,\partial I/\partial E_\mu = \int_0^1 W(E_\mu,v)\,[I(E_\mu/1-v,t)-I(E_\mu,t)]\,dv \quad (1)$$

$$W(E_\mu,v) = (N/A)\,\Phi_B + N\Phi_N$$

(N: Avogadro's number, A: atomic mass number), where Φ_B and Φ_N are the differential cross section of bremsstrahlung and nuclear interactions, respectively. To get the solution of eq.(1), we make two assumptions and introduce three dimensionless variables as follows:

$$\text{(i)}\ \beta(E_\mu) = a + b_p E_\mu, \quad \text{(ii)}\ f(v)/v = W/(b_B+b_N)$$

$$x = b_p t, \quad \varepsilon = b_p E_\mu/a, \quad b = (b_B+b_N)/b_p.$$

, where a is ionization loss and b_p, b_B and b_N are energy loss

parameters due to pair creation, bremsstrahlung and nuclear interaction, respectively. Then eq.(1) becomes

$$\partial I/\partial x - (\varepsilon + 1)\partial I/\partial \varepsilon = b\int_0^1 f(v)/v[I(\varepsilon/1-v,x)-I(\varepsilon,x)]dv \qquad (2)$$

In this notation the average energy loss may be written as

$$-d\varepsilon/dx = 1 + (1 + b)\varepsilon \qquad (3)$$

$I_0(\varepsilon,x)$ is given by combining eq.(3) with the boundary condition $I(\varepsilon,0) = B\varepsilon^{-\gamma}$ as

$$I_0(\varepsilon,x)= B\cdot\exp[-\gamma(1+b)x][\varepsilon+(1-\exp(-(1+b)x))/(1+b)]^{-\gamma} \qquad (4)$$

By analogy of eq.(4)we take the solution of eq.(2) in the form

$$I(\varepsilon,x)=B\cdot\exp[-\gamma(1+\chi b)x][\varepsilon+(1-\exp(-(1+\kappa b)x))/(1+\kappa b)]^{-\gamma} \times \exp[\phi(\varepsilon,x)] \qquad (5)$$

From eqs.(4) and (5) we get R for $\varepsilon = 0$ in the following way

$$R(0,x)=[\exp(b(\chi-\kappa)x)\cdot(1+b)/(1+\kappa b)\cdot[\exp((1+\kappa b)x)-1]/[\exp((1+b)x)-1]]^{+\gamma}\exp[-\phi(0,x)] \qquad (6)$$

At a great depth($t > 4000$ hg/cm^2) and under the assumption $\phi(0,t\to\infty)=0$, we get such a simple form as

$$R \approx [(b_p + b_f)/(b_p + \kappa b_f)]^{\gamma}\exp[-\gamma b_f(1-\chi)t] \qquad (7)$$

,where $b_f = b_B + b_N$.

3. Derivation of spectral index γ. It is assumed that the D-I curves are expressed by a unique exponential law of the type $I(t) = C\cdot\exp(-t/\Lambda)$ (8). Then combining eqs.(4),(7) and (8) we can obtain a relationship between γ and Λ :

$$\gamma = [\Lambda(b_p + \chi b_f)]^{-1} \qquad (9)$$

Here the constant χ is determined in such a way that $\phi(\varepsilon,x)$ approaches zero as $\varepsilon\to\infty$. By substituting eq.(5) into eq.(2) χ is given as

$$\chi = (1/\gamma)\int_0^1 f(v)/v[1-(1-v)^{\gamma}]dv \qquad (10)$$

For Φ_B, Φ_N we take the following formulae

$$\Phi_B=0.95\alpha(2r_0m_e/m_\mu)^2Z(Z+\xi)(4/3+v^2-(4/3)v)(1/v)\ln(P/Q) \qquad (11)$$

$$P=(2/3)k(m_\mu/m_e)Z^{-2/3},$$

$$Q=(k\sqrt{e}/2)(m_\mu^2/m_eE_\mu)(v/(1-v))Z^{-1/3}+1^{2)}$$

$$\Phi_N=\frac{\alpha}{\pi}\cdot\sigma_{\gamma N}\cdot\frac{1}{v}\left\{(v-1)+\left[1-v+\frac{v^2}{2}\left(1+\frac{2m_\mu^2}{\Lambda^2}\right)\right]\right. \qquad (12)$$

$$\left.\times\ln\frac{\frac{E^2(1-v)}{m_\mu^2}\left[1+\frac{m_K^2v^2}{\Lambda^2(1-v)}\right]}{\frac{Ev}{\Lambda}\left(\frac{Ev}{\Lambda}+\frac{\Lambda}{2M}\right)}\right\}^{3)}$$

($\sigma_{\gamma N}$ = 125 μb and Λ^2 = 0.4 Gev^2)

We calculated the values of χ as a function of γ for standard(Z=11,A=22) and K.G.F(Z=12.93,A=26.12) rocks at E_μ=1, 10,100 TeV. The results are shown in Fig.1. We find from this figure that the χ and γ has nearly a linear relation such that

$$\chi = m_1\gamma + m_2 \qquad (13)$$

In the case of E_μ=10 TeV we have m_1=-0.1085, m_2=0.9943 for S rock and m_1=-0.1092, m_2=0.9935 for K.G.F rock. Substituting eq.(13) into eq.(9) we get the equation for γ.

$$m_1b_f\gamma^2 + (b_p + m_2b_f)\gamma - 100/\Lambda = 0 \qquad (14)$$

(b_p,b_f are measured in units of 10^{-6} cm^{-2}g and Λ in units of 10^4 gcm^{-2})

For b_p, we use the expression taken from Bugaev's book[4]:

$$b_p=6.01\cdot10^{-8}Z(Z+1)/A[0.97\ln(p_1/Q_1)+2.15](g^{-1}cm^2) \qquad (15)$$

$$P_1=183Z^{-1/3}\ ,\quad Q_1=183Z^{-1/3}m_\mu^2/(2E_\mu m_e)+1$$

In the following we apply this equation together with the Λ of D-I curves for S rock and K.G.F rock to get γ. If we take $\Lambda=9.868\cdot10^4$gcm^{-2} ($8000\lesssim t\lesssim9000$ hgcm^{-2}) for S rock, which is derived from eq.(2) in ref.(5), and $\Lambda=9.00\cdot10^4$ gcm^{-2} ($t=10^4$ hgcm^{-2}) for K.G.F rock.[6]

The values of γ thus obtained is as follows:

$\gamma_1 = 2.70$ ($E \approx 30$ TeV) for S rock and

$\gamma = 2.62$ ($E \approx 50$ TeV) for K.G.F rock.

The former is consistent with the value of 2.71 by Bergamasco et al.[5] and the latter is also consistent with that of 2.6 by Miyake et al.[7], where fluctuations are treated by Monte Carlo Method.

4. Conclusions. By using the approximate R at great depth, γ can be easily obtained if the D-I curve has the form $I(t) = C \cdot \exp(-t/\Lambda)$. It is found that there is a discrepancy of γ between S rock and K.G.F rock in the same energy region.

References.

1) V.I.Gurentsov et al.,Sov.J. Nucl.Phys.,23,527,1976.

2) I.L.Rosental,Soviet Physics Uspekhi,11,49(eq.1.9),1968.

3) Y.Minorikawa,Uchusenkenkyu, (mimeograph in ICRR),22,376, 1978.

4) E.V.Bugaev et al.,Cosmic muons and neutrinos(in Russian),(Atomizdat),P78, 1970.

5) L.Bergamasco et al.,Nuovo Cimento,6C,569,1983.

6) Physics Data Cosmic Rays on Earth,(Eds.O.C.Allkoffer and P.K.F.Grieder),P322,1984.

7) M.R.Krishnaswamy et al., 15 th ICRC(Plovdiv),6,85, 1977.

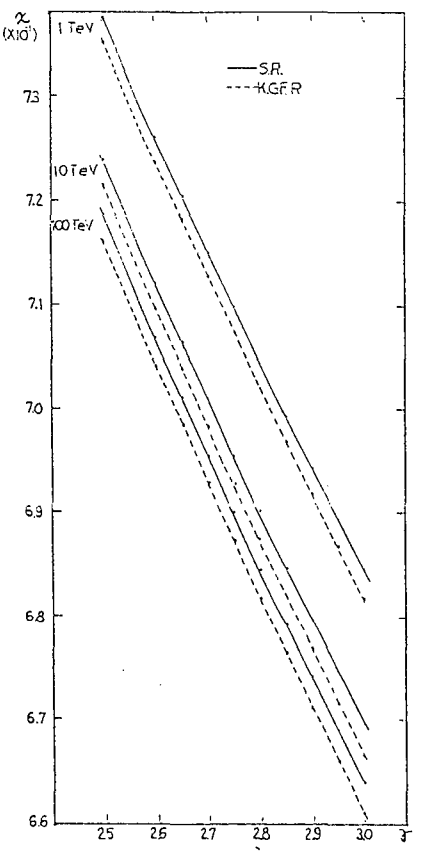

Fig.1 Dependence of χ on γ.

THE SPECTRUM OF NEUTRONS AT 60 hg m^{-2}

J.C. Barton,
The Polytechnic of North London, London, N7 8DB, U.K.

ABSTRACT

The rate of neutron interactions has been measured in the Holborn underground laboratory for the energy range 7.5-60 MeV, using a 3.85 kg cell of liquid scintillator. The neutrons are selected by pulse shape discrimination, with anticoincidence counters used to reduce interference from muons transversing the scintillator. The observed flux is interpreted in terms of neutrons produced from environmental uranium and thorium, those resulting from the capture of negative muons in nuclei and those from fast muon interactions.

1. Introduction. This paper describes the results obtained with an improved version of the experiment reported at the last conference (Barton, 1983). A preliminary attempt is made to estimate both the source spectrum of neutrons at this depth and the proportion of these neutrons which would be detected by the present system.

2. Apparatus. The counters are arranged as shown in Figure 1. The neutron counter is a cylinder of 175 mm diameter and length, containing 3.85 kg of NE213. The two anticoincidence counters are always operated in parallel; some results have been taken with them used in coincidence with the neutron counter. The 5 cm lead screen was removed for part of the observations.

The data from the pulse shape discrimination circuits were recorded as 2-dimensional histograms. Using an Am/Be neutron source, the discrimination was found to be very satisfactory up to its maximum energy ($\sim$ 12 MeV). Of course the discrimination becomes less at higher energies but is adequate to beyond 50 MeV. The present arrangement was less satisfactory at energies below 8 MeV because the photo-electron statistics were poor; a larger diameter photomultiplier might, in principle, improve the performance at low energies, but a tube with sufficiently uniform time response was not available.

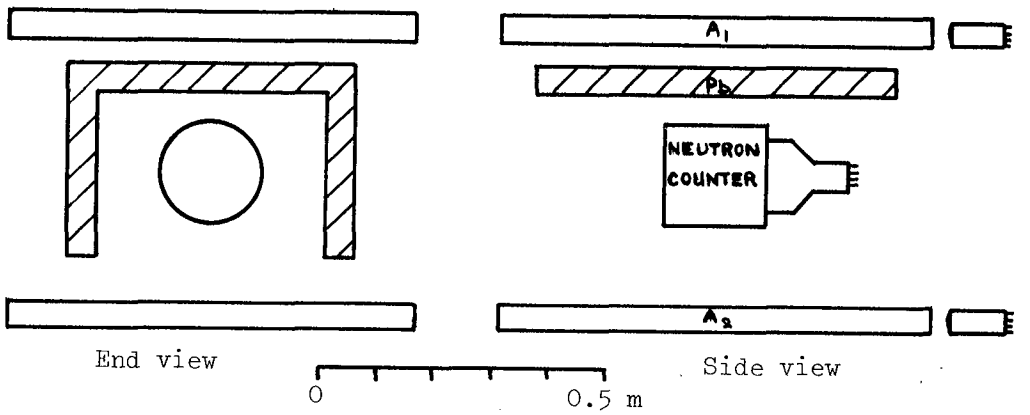

Fig. 1: Arrangement of apparatus

The discriminating properties of organic scintillators are associated with their non-linear response to more heavily ionizing particles. The position of the cosmic ray peak provides a direct calibration for minimum ionizing particles, but the energy scale for protons is not so easily established. There are no convenient calibration sources so the energy scale had to be taken from reports of calibrations made on other large NE213 counters used for accelerator experiments. The published data are not in good agreement so the neutron energy scale adopted here has an uncertainty of ± 15%.

The results have to be corrected for two types of spurious event. The trigger level for the leading-edge timing must be set low to avoid time-slewing which means that accidentals cause spurious zero-crossing times. Secondly, muons which stop in the counter may decay before the zero-crossing time (1.5 μs was used) and give distorted events. Both effects have been analysed theoretically and compared with the background events in the pulse-height/pulse-shape histograms in regions away from the muon or proton ridges. At worst the correction for the proton region was 15% and the additional uncertainty is generally less than the statistical one.

When operating the main counter in coincidence with the others, a well-resolved proton ridge was not observed. This is understandable, as the signal would be due to both muon and proton in proportions varying from event to event. These events would fall in the valley region between the two main ridges. Similarly, events with indications of particles ionizing more strongly than protons are ascribed to nuclear disintegrations in the scintillator. For the anticoincidence events both effects were sufficiently small that the true proton events could be separated with less difficulty.

3. Results. There was no clear difference between the anticoincidence results with or without the lead in position. The combined results are therefore used for Figure 2. The coincidence rates are also shown but, as explained above, there is much greater uncertainty about these.

4. Predicted source spectrum of neutrons. All rocks contain a small proportion of uranium, typically from 1-5 μg g^{-1}, about three times as much thorium and a few per cent of potassium. Neutrons can therefore result from spontaneous fission of ^{238}U, from (α,n) reactions and (γ,n) reactions. For a rock in the middle of the range indicated above, these processes give, respectively, about 5×10^{-8} g^{-1} s^{-1}, 1.2×10^{-7} g^{-1} s^{-1} and $< 10^{-9}$ g^{-1} s^{-1}. These values depend on the other constituents of the rock but not very strongly, except in particular ores. The spectra of neutrons from fission and (α,n) processes in thick targets are known to fall off rapidly above 2 MeV.

The stopping rate of all muons at this depth is $(21\pm2) \times 10^{-3}$ g^{-1} d^{-1} and for "standard" rock with $Z = 11$ about 0.5 x 0.5 will be captured and produce, on average, 1.2 neutrons each (Mukhopadhyay, 1977) giving a total yield 6×10^{-3} g^{-1} d^{-1}. The spectra given by Sundelin (1973) show that about a fifth of the neutrons have energy greater than 10 MeV and decreasing $\sim e^{-E/7}$.

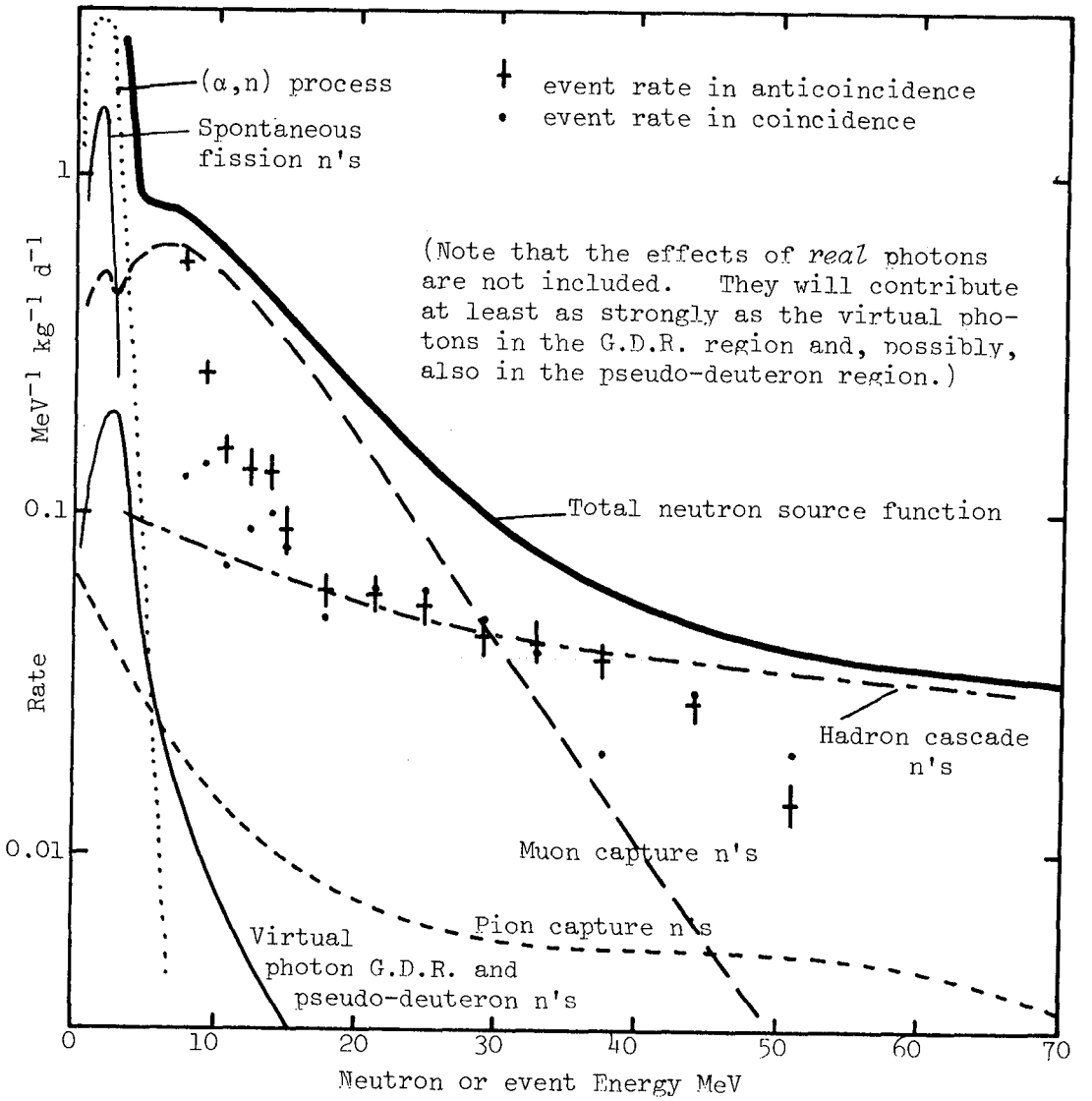

Fig. 2: Observed event rate compared to neutron source spectra

The fast muons traversing the rock produce neutrons through both real and virtual photo-nuclear interactions. For energies below 100 MeV most of the real photons result from bremmstrahlung of knock-on electrons and have a spectrum of the form $\sim E^{-2}$. In the same energy region the virtual photons have a spectrum $\sim E^{-1}$ so, at sufficiently high energies, will always be more important than the real photons. Although the various electromagnetic interaction processes producing real photons are well understood, the detailed Monte Carlo calculations required to estimate the absolute intensity of photons with energy comparable to the critical energy do not seem to have been carried out. For the spectrum of virtual photons, the plane wave Born approximation has been shown to be valid at low energies (Orth et al, 1981), whilst at energies above the pion production threshold the refined calculations of Bezrukov and Bugaev (1981) are available.

Photo-nuclear reactions are usually considered in three energy regions. Below 30 MeV the giant dipole resonance provides the mechanism and the resulting neutrons have a spectrum similar to those from the evaporation process. Between 30 and 150 MeV the pseudo-deuteron model of Levinger has recently received more precise experimental support for light and medium nuclei (Homma et al, 1983). The neutron usually receives half the energy of the photon, less the binding energy. Above the pion production threshold neutrons are produced both directly in the hadron cascade and from the capture of negative pions by nuclei. The spectrum of the neutrons in the cascade falls off as $\sim E^{-2}$ between 10 and 50 MeV but more rapidly at higher energies (Metropolis et al, 1958), with the absolute values estimated from the total amount of energy transferred via muon nuclear processes. Negative pions produced by the same mechanism are captured by pseudo-deuterons in nuclei and produce one or two neutrons with a rather flat spectrum up to $\sim$ 100 MeV (Madey et al, 1982); the number of pions stopping at 60 m.w.e. has been determined experimentally (Slade, 1966). Figure 3 includes estimates of the main contributions to the neutron source spectrum.

In the present experiment, as was pointed out earlier, only the anticoincident results enable the neutron events to be separated unambiguously. Those neutron sources in which the originating muon is closely collimated with the neutron will therefore be excluded. A further complication is that the neutrons may be scattered and lose energy before reaching the detector. Overall, it must therefore be expected that the observed anticoincidence spectrum will be softer than the source spectrum and substantially lower in magnitude. Examination of Figure 2 shows this to be true but it is not yet possible to say whether the difference can be accounted for quantitatively.

5. Conclusions.

1. The observed spectrum of neutron events at 60 hg cm^{-2} falls sharply up to 15 MeV and then decreases rather slowly.
2. The observed intensity of neutron interactions, not closely accompanied by muons, above 15 MeV at this depth is 1.8 ± 0.3 kg^{-1} d^{-1}.
3. The total intensity is at least double this value and is not in disagreement with what can be predicted from known processes.

References

Barton, J.C., (1983), Proc. of 18th Int. Cosmic Ray Conf., Bangalore, 11,462-5

Bezrukov, L.B. and Bugaev, E.V., (1981), Proc. 17th Int. Cosmic Ray Conf., Paris, 8, 90-3

Homma, S., Kanazawa, M., Maruyama, K., Murata, Y., Okuno, H., Sasaki, A. and Taniguchi, T., (1982), Phys. Rev. C., 27, 31-45

Madey, R., Vilaithong, T., Anderson, B.D., Knudson, J.N., Witten, T.R., Baldwin, A.R. and Waterman, F.M. (1982), Phys.Rev.C., 25, 3050-67

Metropolis, N., Bivins, R., Storm, M., Miller, J.M., Friedlander, G. and Turkevich, A., (1958), Phys. Rev., 110, 204-219

Mukhopadhyay, N.C., (1977), Phys. Rep., Phys. Lett. 30C, 1-144

Orth, C.J., Knight, J.D., Wolfsberg, K. and Johnson, M.W., (1980), Phys. Rev. C., 21, 1967-73

Sundelin, R.M. and Edelstein, R.M., (1973), Phys. Rev. C., 7, 1037-60

Slade, M., (1966), Ph.D. thesis, University of London

A Transient Digitiser for Fast Air Shower Events

N.R. Wild and R.W. Clay

Physics Department, University of Adelaide, South Australia, 5001.

1. Introduction Measurements of air shower structure often have to be made on time scales of a few nanoseconds. Longitudinal disk structure near the core is of the order of metres in dimension, air Cerenkov pulses have full widths at half maximum of the order of tens of nanoseconds, and fast timing over typical arrays is usually measured to nanosecond accuracy. Measurements over these time scales are neither easy nor cheap. Oscilloscopes can be used but have very limited dynamic range (see eg. Liebing et al, 1984) and can be expensive if measurements down to a few nanoseconds are to be made. For our fast Cerenkov work, we needed an instrument with better dynamic range than an oscilloscope and with a time resolution sufficient to enable us to make measurements limited only by our system risetime of a few nanoseconds. We have built a 16/32 channel, 8 bit, fast transient digitiser which can be run at sample intervals down to ~ 1 nanosecond per channel. The system cost for 16 channels was less than US$ 2000.

2. System Description The digitiser is based on a series of sample and holds which are gated almost at the same time by a trigger pulse and which sample a progressively delayed signal. The signal delay medium is coaxial cable and the time between samples can be as low as ~ 1 nanosecond. We investigated a number of possible fast sample circuits, such as a gated double balanced mixer, but were generally unable to obtain our required 100:1 or better dynamic range. We finally found a system described by Baldis and Aazani-Zangareh (1973) which uses sampling gates based on a matched Schottky diode bridge (see fig 1). The bridges are gated by the application of both a positive and a negative sub-nanosecond pulse which are applied along striplines on the circuit board as indicated. The gated sample of the signal is then amplified and applied to a slow sample and hold/8-bit digitiser. The sub-nanosecond sampling gate signals are produced by an fast impulse generator and power splitter (Avtech Electrosystems, Ottawa, Canada). These represent the major part of the gating system expense and were the parts we found most difficult to produce ourselves. The digitiser output is transferred to a Commodore 64 microcomputer for storage and handling.

The system has a bandwidth ($\gtrsim$ 300 MHz) determined by the total of the successive gate capacaitances. For 16 channels this is sufficient to place an impulse completely (>10% amplitude) within a single one nanosecond sample interval. One bit corresponds to a few millivolts in amplitude but, more importantly perhaps, the system dynamic range is close to being a true 8-bit range with long term drift and noise being of the order of the one bit level.

The digitiser can be run as a triggered oscilloscope with an event rate of up to ~ 3 Hz into the Commodore 64 microcomputer or as a logic gated device with a possible reset whilst an analog sample is held in a

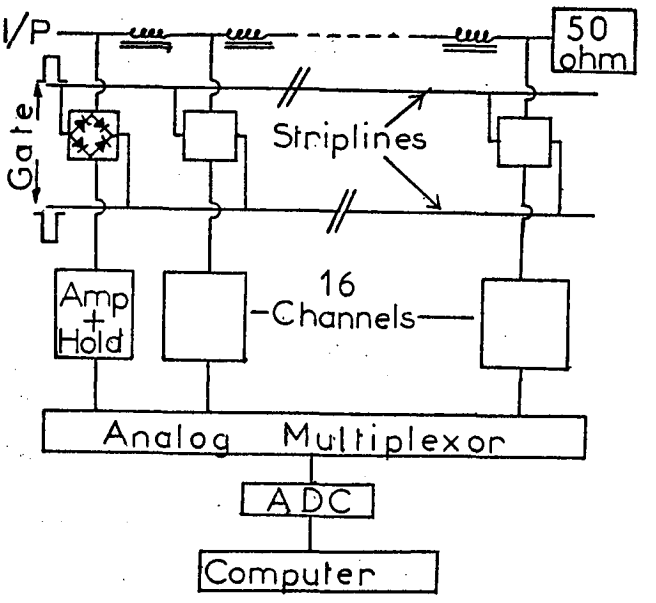

Fig. 1 Schematic of the transient digitiser. The signal is delayed by external cable between the sample gates.

sample and hold before digitisation. In this case a 30 kHz trigger rate is possible with selection of the events which we require to digitise by the input of an appropriate external gate. The latter mode is of particular interest for air shower work where a photomultiplier output can be sampled and one can then wait up to 5 μs to determine whether or not an air shower of interest has also been detected. These rates should be compared to an oscilloscope previously used by us for similar purposes, the Tektronix 7834 storage oscilloscope. This device has a maximum useful trigger rate for photographic recording of poorer than 1Hz and has a dynamic range of much less than 50:1 for high speed operation.

In conclusion, we have built a fast transient digitiser which can digitise 16 channels at intervals down to 1ns with a dynamic range of ~ 200:1. The device is particularly useful for air shower transient studies at a cost which is affordable on a quite modest budget.

Acknowledgement

This work was supported by a grant from the University of Adelaide.

References

Baldis, H.A. and Aazam-Zanganeh, J. (1973) Rev. Sci. Inst. 44, 712

Liebing, D.F., Clay, R.W., Gregory, A.G. and Patterson, J.R. (1984) J. Phys. G., 10, 1283

LIMITS ON DEEPLY PENETRATING PARTICLES IN THE $>10^{17}$ EV COSMIC RAY FLUX

Baltrusaitis, R.M., Cassiday, G.L., Cooper, R., Elbert, J.W., Gerhardy, P.R., Loh, E.C., Mizumoto, Y., Sokolsky, P., Sommers, P. and Steck, D.

Physics Department, University of Utah, Salt Lake City, UT 84112

ABSTRACT

We report on a search for deeply penetrating particles in the $>10^{17}$ eV cosmic ray flux. No such events have been found in 8.2×10^6 sec of running time. We consequently set limits on the following: quark-matter in the primary cosmic ray flux; long-lived, weakly interacting particles produced in p-air collisions; the astrophysical neutrino flux. In particular, the neutrino flux limit at 10^{17} eV implies that $\bar{z}$, the red shift of maximum activity is <10 in the model of Hill and Schramm[6].

1. Introduction. We report on a search for deeply penetrating particles in the $>10^{17}$ eV cosmic ray flux. The search was performed using the University of Utah Fly's Eye detector[1], as part of its normal operation. No unusual deeply penetrating events have been found in 8.2×10^6 sec of running time.

We consider the following as candidate sources for such events (2): a. metastable quark matter as part of the primary cosmic ray flux; b. taus and other long-lived particles produced in the interaction of the primary cosmic ray flux with the atmosphere; c. weakly interacting particles of astrophysical origin such as neutrinos.

2. Search Philosophy. We search for deeply penetrating particles in two ways. EAS's observed in the Fly's Eye fiducial volume with $80 < \theta_z < 90$ typically must traverse >3000 g/cm^2 of atmosphere before interacting. We expect to see no such events from normal hadronic interactions in our exposure time. Upward EAS's must originate in the Earth and hence must be produced by weakly interacting particles. Figures 1 and 2 show the observed zenith angle and depth of first observed interaction (Xo) distributions in our data. Note that the Xo distribution extends beyond the expected distribution of the actual point of first

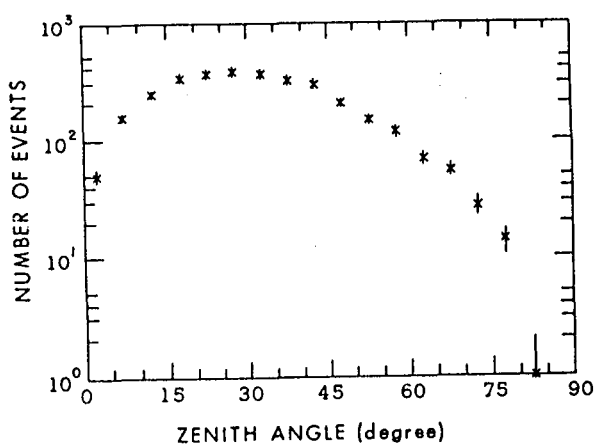

Figure 1

Zenith Angle Distribution

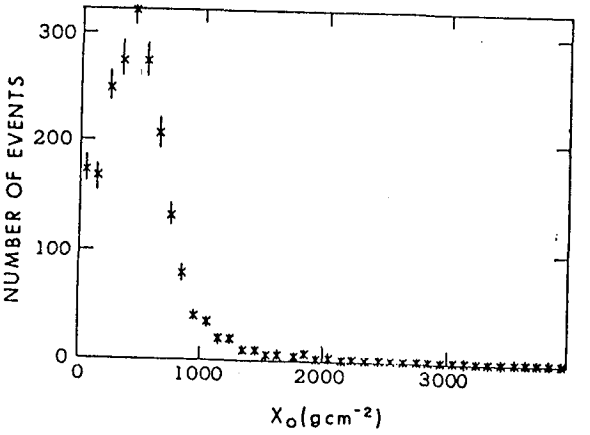

Figure 2

Depth of First Observed Interaction X_o

interaction since Xo is always an upper limit on the actual interaction length.

3. Quark Matter Limits. We search for metastable quark matter globs exploding deep in the atmosphere via the mechanism proposed by Bjorkien and McLerran[3]. In that picture, quark matter globs of a given baryon number No will explode at a given atmospheric depth, independent of initial energy (assuming they have not ranged out before exploding). We detect such events by searching for downward EAS with Xo between 3000 and 10000 g/cm^2. Table 1 gives resultant quark matter flux limits in (cm^{2}sec sr)$^{-1}$ as a function of explosion depth and explosion energy. The 10^{15} eV data point is derived by assuming that the Mt. Chacaltaya Centauro events[4] are quark-matter explosions.

TABLE 1
Limits on quark-matter flux in the primary cosmic-ray spectrum in units of (cm^{2}sec sr)$^{-1}$

Explosion depth g/cm^2	Explosion energy (eV) 10^{15}	10^{18}	10^{19}
500	3×10^{-14}		
3000		1.0×10^{-18}	3.7×10^{-19}
6000		8.8×10^{-19}	1.4×10^{-19}
9000		1.3×10^{-18}	2.1×10^{-19}

4. Limits on Long-Lived Weakly Interacting Particle Production. Hadronic decays of $>10^{17}$ eV taus and tau like particles produced in the interactions of the primary cosmic-ray flux with the atmosphere are possible sources of deeply penetrating downward EAS. Very distant cosmic ray interactions, not themselves detectable by the Fly's Eye, could produce taus which penetrate into the Eye's fiducial volume and decay into observable EAS's. We set limits on tau production cross sections by using the known cosmic ray flux intensity for $10^{17} < E < 10^{19}$ eV and the known tau lifetime and branching ratios. Our sensitivity for such decays is maximized for $1.0 < X < .1$ and $10^{18} < E < 10^{19}$ where $X = E\tau/Ep$ and Ep is the energy of the primary particle. In this interval, we set a limit on $(\sigma_\tau/\sigma_{tot})\cdot n(X)$ where σ_τ/σ_{tot} is the probability of producing a tau in a cosmic ray interaction and n(X) is the normalized tau distribution function for such interactions. We find $\sigma_\tau/\sigma_{tot}\cdot n(X)$ is less than 4.0×10^{-2} and 1.3×10^{-1} for X=1.0 and

X=0.5 respectively. If the cosmic ray flux at these energies is primarily composed of protons, we find, using our measured p-air cross section of 520 mb[5], that $\sigma_\tau \cdot n(X) < 20$ mb for X=1.0 and <69 mb for X=.5.

We also set limits as a function of the decay length on production cross sections for hypothetical weakly interacting particles produced in cosmic ray interactions with decay lengths $20 < c\gamma\tau < 500$ km (see Table 2). These are assumed to decay into hadron and/or electrons with a branching ratio of 0.5.

TABLE 2
Limits on $(\sigma/\sigma_{tot})n(x)$ for weakly interacting particles in cosmic-ray-air interactions as a function of $c\gamma t$ and X.

E_p(eV)	$c\gamma\tau$(km) 50	100	200	500	1000
			X=1		
1.0×10^{17}	5.9×10^{-3}	2.2×10^{-3}	1.3×10^{-3}	1.2×10^{-3}	1.3×10^{-3}
1.0×10^{18}	8.8×10^{-2}	3.6×10^{-2}	2.2×10^{-2}	1.9×10^{-2}	2.2×10^{-2}
1.0×10^{19}	6.1×10^{-1}	2.5×10^{-1}	1.5×10^{-1}	1.2×10^{-1}	1.3×10^{-1}
			X=0.5		
4.10^{17}	4.4×10^{-2}	1.8×10^{-2}	1.1×10^{-2}	8.8×10^{-3}	1.0×10^{-2}
1.0×10^{18}	1.3×10^{-1}	5.4×10^{-2}	3.4×10^{-2}	2.8×10^{-2}	2.8×10^{-2}
1.0×10^{19}		4.4×10^{-1}	2.6×10^{-1}	2.2×10^{-1}	2.7×10^{-1}
			X=0.1		
1.0×10^{18}		2.2×10^{-1}	1.5×10^{-1}	1.5×10^{-1}	1.9×10^{-1}

5. Limits on the Ultra-high energy Neutrino Flux. We have recently reported limits on astrophysical electron neutrino fluxes at energies of $>10^{18}$ eV[2]. Here we update the flux limits and extend them down to 10^{17} eV.

If the neutrino interaction cross section for $E>10^{17}$ eV is 10^{-33}cm^2 as predicted by the standard model, we maximize our sensitivity to such a neutrino flux by searching for upward EAS's. Electron neutrino interactions in the earth's crust will be detectable at depths of hundreds of meters below the surface because the LPM effect slows down the rate of shower development for the high energy electron produced in the interaction. This allows the electron shower to emerge into the atmosphere and be detected. Figure 3 shows the electron shower size at shower maximum as a function of electron energy and depth of interaction in the crust. Table 3 gives limits on the neutrino flux as a function of energy. Calculations by Hill and Schramm[6] indicate that if the neutrino flux is produced by interaction of UHE protons with the 2.7 deg black body radiation, then the flux at 10^{17} eV is sensitive to $\bar{z}$, the red-shift of maximum activity. Their calculation indicates that with our flux limit of $2.0\times10^{-12}\nu$/cm^{2}sec str at 10^{17} eV, $\bar{z}$ must be less than or equal to 10.

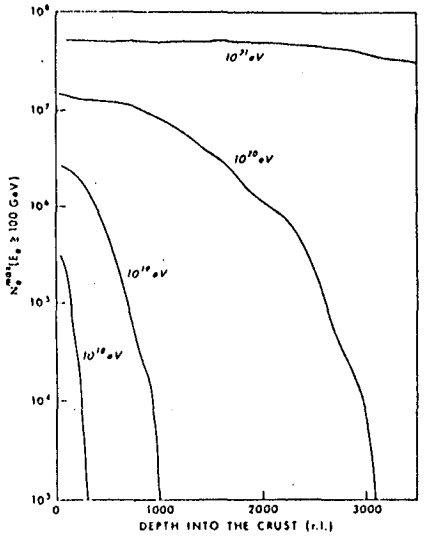

Figure 3. Electron Shower Size at Shower Maximum as a Function of Electron Energy and Depth of Interaction in the Crust.

Figure 3

TABLE 3
Limits on ν_e flux based on upward events ($\nu/cm^2 sec$ str.) and $\sigma_\nu = 10^{-33} cm^2$.

E_ν(eV)	10^{17}	10^{18}	10^{19}	10^{20}	10^{21}
	1.3×10^{-12}	5.3×10^{-14}	6.6×10^{-15}	2.8×10^{-16}	3.6×10^{-17}

6. Acknowledgements. The authors are grateful to Dr. Larry McLerran and Dr. Chris Hill for useful discussions. We gratefully acknowledge the National Science Foundation for providing funds for this research.

References.

1. Baltrusaitis, R.M., et al, Nuclear Instrum. Methods (to be published).
2. Baltrusaitis, R.M., et al, Phys. Rev. D 31, 2192 (1985).
   Baltrusaitis, R.M., et al, Astrophys. J. 281, Lg (1984).
3. Bjorken, J.D., and McLerran, L.D., Phys. Rev. D20, 2353 (1979).
4. Kazanas, D., Balasubrahamanyan, V.K., and Streitmatter, R.E., Phys. Lett. 142, 23(1984).
5. Baltrusaitis, R.M., et al, Phys. Rev. Lett. 52, 1380 (1984).
6. Hill, C.T., and Schramm, D.N., Phys. Rev. D31, 564(1985).

HE 5.3-5

RESULTS OF LOW ENERGY BACKGROUND MEASUREMENTS WITH THE LIQUID SCINTILLATION DETECTOR (LSD) OF THE MONT BLANC LABORATORY

M.Aglietta, G.Badino, G.F.Bologna, C.Castagnoli, W.Fulgione,
P.Galeotti, O.Saavedra, G.C.Trinchero, S.Vernetto
Istituto di Cosmogeofisica del CNR, Torino, Italy
Istituto di Fisica Generale dell'Università di Torino, Italy

V.L.Dadykin, V.B.Korchagin, P.V.Korchagin, A.S.Malgin, F.G.Ryassny,
O.G.Ryazhskaya, V.P.Talochkin, G.T.Zatsepin, V.F.Yakushev
Institute of Nuclear Research of the Academy of Sciences, Moscow, USSR

ABSTRACT

The 90 tons Liquid Scintillation Detector (LSD) is fully running since october 1984 in the Mont Blanc Laboratory, at a depth of 5,200 hg/cm^2 of standard rock underground. Even if the detector is a multi-purposes experiment, the main goal is to search for neutrino burst from collapsing stars. The experiment is very sensitive to detect low energy particles (at a threshold of 0.8 MeV), and thus has a very good signature to gamma-rays from (n,p) reaction which follows the $\bar{\nu}_e + p \rightarrow n + e^+$ neutrino capture. We present here the analysis of data, and discuss the preliminary results on low energy measurements.

1.Introduction. The analysis of low energy pulses in a massive detector deep underground is of primary importance to understand the background in experimental neutrino astronomy at low energies, when the signal is to be extracted from the background. Hence, a well defined analysis on the energy distribution of background pulses can be used as a calibration method for the existing underground stations of low energy neutrino astronomy. In addition, it provides an experimental basis to evaluate the feasability to detect low energy neutrinos, for example from solar origin, in future and more massive detectors.
The low energy background in a detector located very deep underground, is mainly due to gamma-rays from Compton scattering, either from the rock surrounding the laboratory or from small contaminating impurities in the material which the detector itself has been constructed with. Since it is necessary to reduce such a background to the lowest level, we have carried out a systematic study of the background spectrum in the energy region $\geqslant$ 0.8 MeV, in our 90 tons Liquid Scintillation Detector, located inside the Mont Blanc tunnel and fully running since

October 1984. The results of such an analysis are here reported and discussed.

2. The LSD experiment. The aims and performances of our apparatus are described elsewhere (ref.1 and these proceedings, HE 5.3-6). Briefly, it consists of 72 scintillation counters, 1.5 m^3 each shielded with Fe slabs 4 cm thick (see fig.1 of HE 5.3-6).

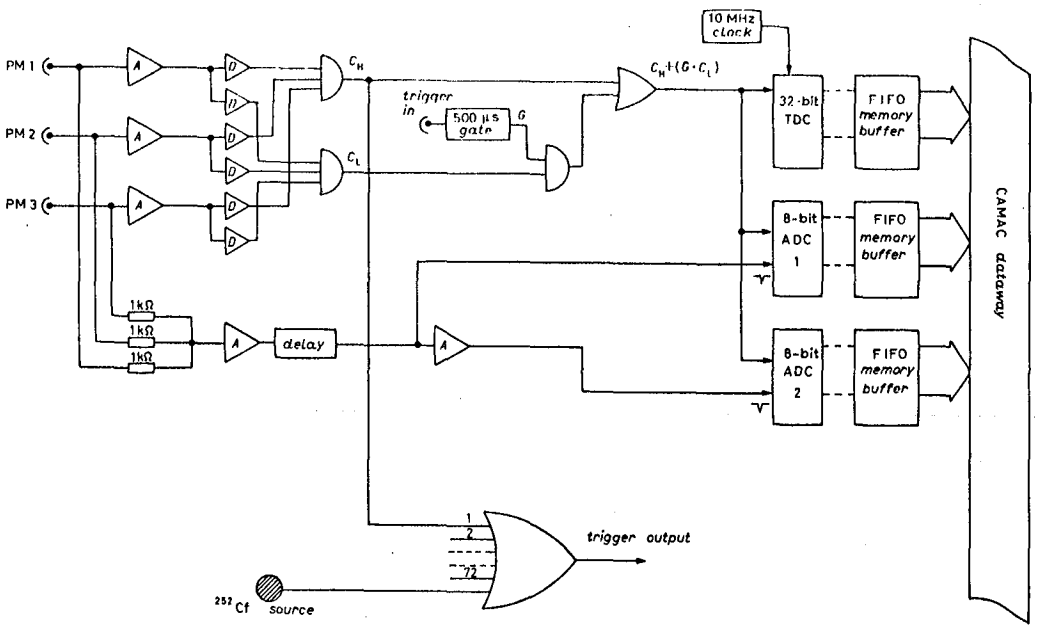

– Electronic block diagram for one counter channel.

Fig.1

Our recording system is triggered whenever one, out of the 72 counters, gives a pulse with energy threshold 7 MeV. The electronic method allows us to record the following parameters which could follow the main trigger: a) pulse height (at the energy threshold 0.8 MeV) in any of the 72 scintillation counters, during a 500 μs gate duration, b) time delays among pulses in the gate with an accuracy of 100 ns, up to the gate duration, c) multiplicity of pulses for each counter and each event, up to 16 pulses. Fig.1 shows our electronic system for one scintillation counter.

3. The calibration method. To calibrate our counters, we used, as a neutron source, neutrons from the spontaneous fission of ^{252}Cf; the source, enclosed in a semiconductor silicon surface barrier counter (SBC) in a stainless steel box, was placed inside a scintillation counter (ref.1). During several calibration runs, we used two different triggers following the spontaneous fission of the ^{252}Cf source, namely: either pulses given by the SBC, or direct detection of pulses from high energy prompt gamma rays ($E > 7$ MeV) in the counter; the rate of the former is 0.12 s^{-1}, and that of the latter is 0.017 s^{-1}.

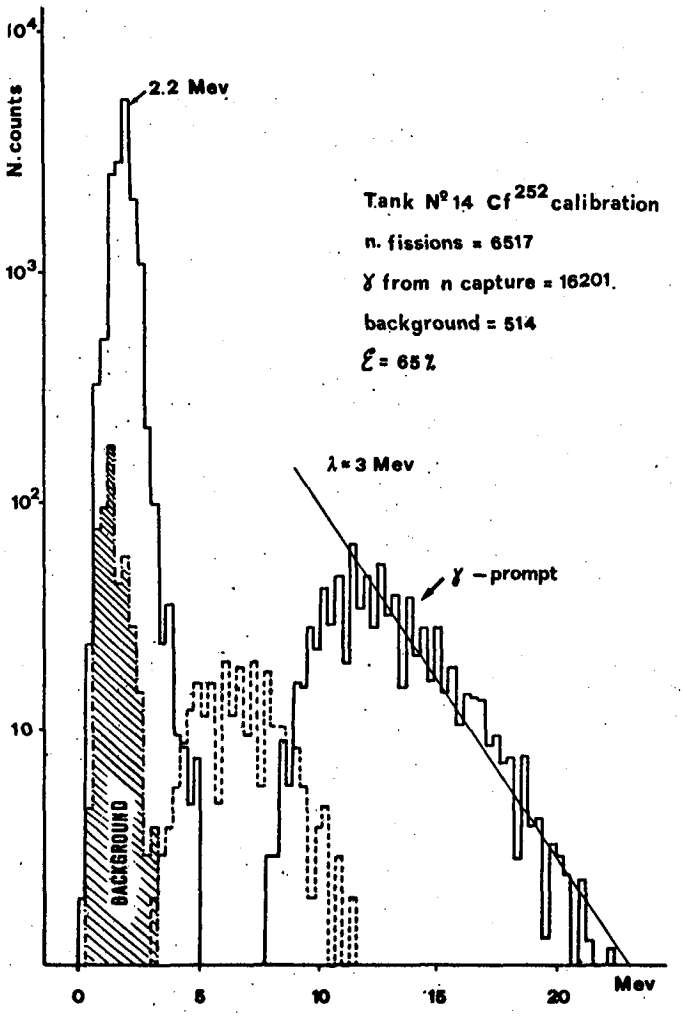

Fig.2

Fig.2 shows the results of our measurements on the inner counter n.14. The measured gamma spectrum (peaked at 2.2 MeV) is compared with the background distribution (shaded area) and with the spectrum of prompt high energy gamma rays, which extends up to 20 MeV. By subtracting the distributions of prompt and 2.2 MeV gamma events, one obtains a spectrum peaked at ~ 6 MeV (dashed line, fig.1). The high sensitivity of our apparatus is shown by the ratio of the resulting counting rate to that of the 2.2 MeV gammas from (n,p) capture, which is only 0.015. The origin of these pulses is now under an accurate analysis.

Moreover, our data show that the efficiency of neutron detection is of order or better than 0.65. This efficiency is nearly the same for all the other counters tested so far with this calibration method.

4. Analysis of background pulses. Since all the 216 photomultipliers of our detector have been chosen with a very low noise, with a single counting rate in the range 10^3 to $5\ 10^3$ per s, the 3-fold coincidences in one counter are less than $3\ 10^{-7}$ during the gate duration (500 μs), when our detector is sensitive at the low level discrimination ($\geqslant$0.8 MeV). The background in this energy range is mainly due to the local radioactivity of the rock in the laboratory. For the high level discrimination at E $\geqslant$ 7 MeV, besides this source of background, one should also take into account the soft component of muons crossing the rock near the apparatus; this effect is much more evident in the counters at the edge of the detector.

For background analysis we exclude all the muon-like events, and only

single events on any out of the 72 counters are considered. In this way, the background analysis has been made, within the 500 μs gate duration, for the remaining 71 scintillation counters.

5. Conclusions. An example of the measured energy distribution of the events analysed according to the previuos criteria is given in fig.3 for the scintillation counters n.10 (inner one) and n.22 (at the edge).

Fig.3

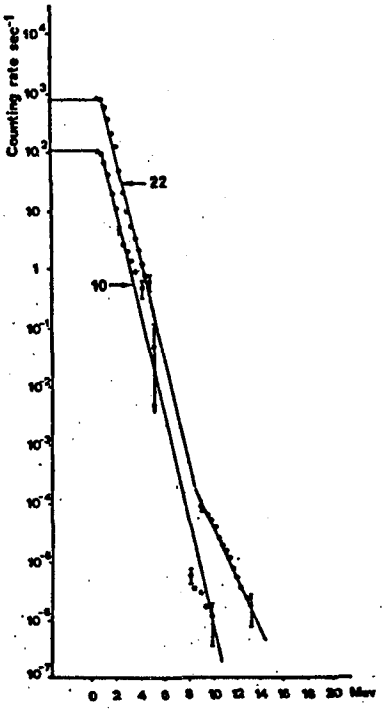

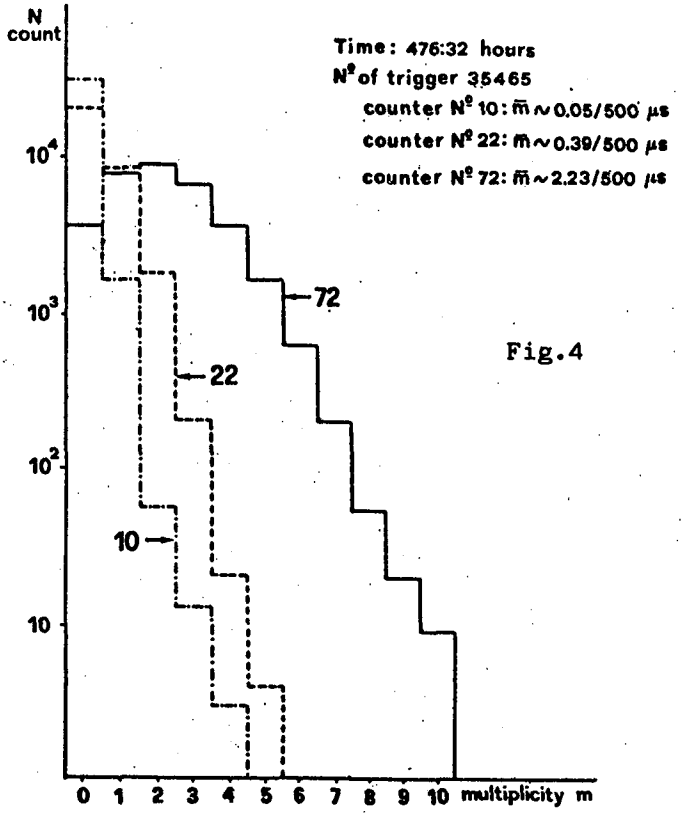

Fig.4

During 476 hours lifetime, out of 35465 triggers, the average value is 0.052 and 0.39 pulses/trigger for counters n.10 and n.22 respectively. In addition, the measured multiplicity of events in the same counters during the gate duration is shown in fig.4 together with that of the top layer counter n.72, for which an average value of 2.2 pulses/trigger has been obtained.

Similar distributions were also obtained for the other counters, thus showing a rather good uniformity in the counting rates. Finally, the ratio of background counting rates between inner counters to the top ones is on the average better than 0.05, and between the inner counters to those at the edge of the detector is of order of 0.1. This result clearly confirms the feasability of our detector in performing neutrino astronomy with a very high sensitivity.

References

1) G.Badino et al., Nuovo Cimento C, 7, 573, 1984

THE RESEARCH PROGRAM OF THE LIQUID SCINTILLATION DETECTOR (LSD) IN THE MONT BLANC LABORATORY

V.L.Dadykin, V.F.Yakushev, P.V.Korchagin, V.B.Korchagin, A.S.Malgin, F.G.Ryassny, O.G.Ryazhskaya, V.P.Talochkin, G.T.Zatsepin
Insitute for Nuclear Research of the Academy of Sciences, Moscow, USSR

G.Badino, G.F.Bologna, C.Castagnoli, B.D'Ettorre Piazzoli, W.Fulgione, P.Galeotti, G.P.Mannocchi, P.Picchi, O.Saavedra, S.Vernetto
Istituto di Cosmogeofisica del CNR, Torino, Italy
Istituto di Fisica Generale dell'Università di Torino, Italy

ABSTRACT

A massive (90 tons) Liquid Scintillation Detector (LSD) is running since October 1984 in the Mont Blanc Laboratory at a depth of 5,200 hg/cm^2 of standard rock. The research program of the experiment covers a variety of topics in particle physics and astrophysics. We present here the performances of our detector, the main fields of research, and we discuss the preliminary results.

1.Introduction. Since October 1984 a massive (90 tons) Liquid Scintillation Detector (LSD), is fully running in the Mont Blanc Laboratory, in a cavity inside the road tunnel linking Italy and France, at a depth of 5,200 hg/cm^2 of standard rock. LSD has been designed as a multipurposes experiment, with a large mass of sensitive material deep underground, to perform researches in several fields of particle physics and astrophysics (ref.1). In particular: a) search for $\bar{\nu}_e$ bursts from collapsing stars, b) direct measurements of atmospheric ν_e and $\bar{\nu}_e$ spectrum at energies $\geqslant$10 MeV, c) possible detection of solar neutrinos at the energy threshold 5 MeV, d) search for nucleon instability, n-$\bar{n}$ oscillations and magnetic monopoles, e) researches in cosmic ray physics: muons, muon-bundles, μ-stop, electromagnetic and hadronic cascades, prompt muon production at high energies.
The experiment has been designed with the combination of four excellent conditions, namely: a) large depth underground of the Laboratory, b) good shielding against the local radioactivity background, c) high performances in the electronic system, and d) good quality and efficiency in the detection system (scintillator and streamer tubes).

2. The LSD experiment. The detector is made of 72 scintillation counters (1.0x1.5x1.0 m^3 each) on 3 layers as shown in fig.1. To reduce the low energy local radioactivity background from the rock, each counter

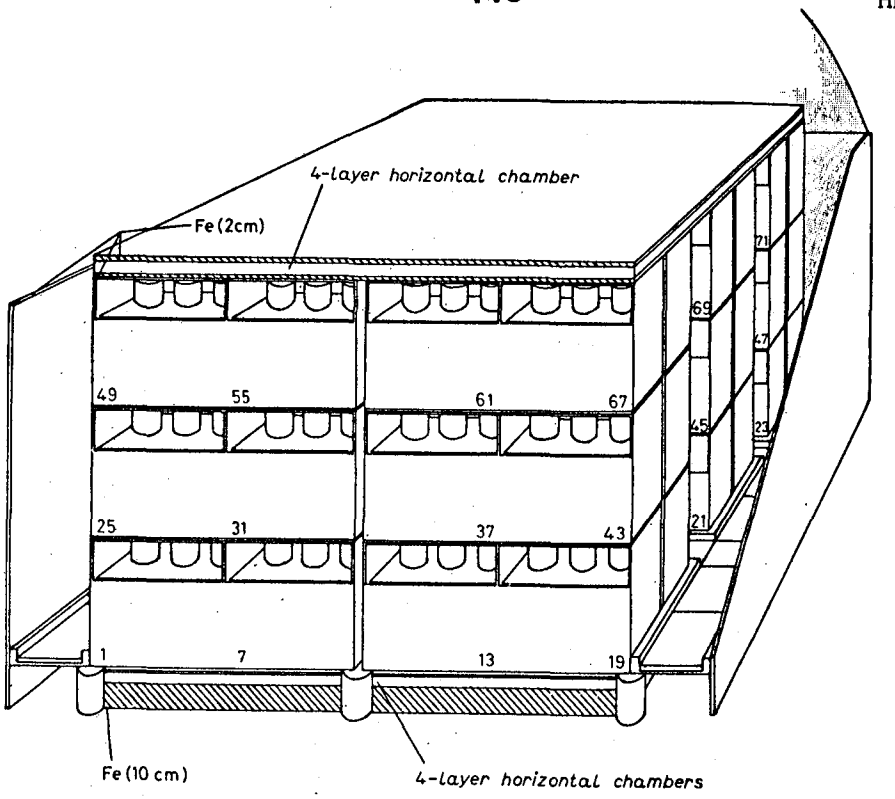

Fig. 1. – The 90 ton liquid scintillation detector in the Mont Blanc Laboratory (dimensions $(7 \times 8 \times 5)$ m^3).

and the whole detector (8x7 m^2 area, 5 m height) are shielded with Fe slabs. The total mass of Fe in the shield is 200 tons, and the 100 tons internal can be considered also as a target and active material. In the scintillator we have 8.5 10^{30} free protons, and 5.1 10^{31} bound protons and 6.0 10^{31} electrons in the scintillator and inner Fe.

A 4π anticoincidence system, made of limited streamer resistive tubes of the NUSEX type (ref.2), is now under construction. The system allows to reconstruct tracks of charged particles, mainly muons at our depth, with an accuracy of ~ 1 cm in spatial resolution and with an angular resolution better than 0.2° for particles crossing the apparatus.

The electronic system, monitored by a PDP 11/24 computer, consists of (ref.3) two level discriminators for each scintillation counter: a high level discriminator (for pulses with energy threshold 7 MeV), which is OR-ed for main trigger functions, and a low level discriminator (with an energy threshold 0.8 MeV) active only during a 500 μs gate, opened by the main trigger. Two ADC's measure the energy deposition of charged particles in the scintillation counters in two overlapping energy ranges: 0-70 MeV and 0-700 MeV respectively.

A 200 ns resolution time provided by a coincidence system for every pulse is recorded by a TDC, 32 bits of dynamic range. The absolute time of each event is recorded with an accuracy better than 1 ms, to

correlate our detector with the neutrino network. A FIFO memory buffer system is used for each channel to accumulate up to 16 events/channel before the read out.

Background measurements and results on the efficiency to detect low energy pulses are reported elsewhere (ref.3 and these proceedings HE 5.3-5). In particular we have measured the efficiency in detecting low energy neutrons, which give a very good signature to $\bar{\nu}_e$ from collapsing stars in a delayed coincidence with positron pulses.

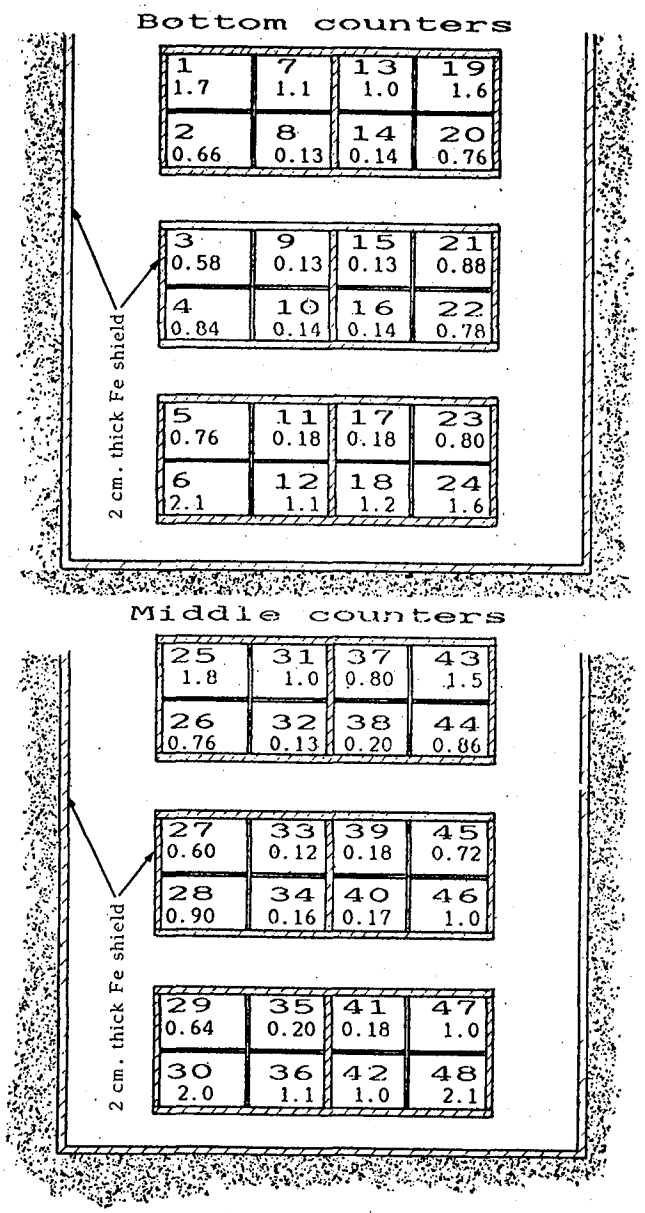

Fig.2

3. Data analysis. We report here the results from a preliminary analysis made after 76 days lifetime. In order to estimate the counting rates in our apparatus, we performed a separate analysis of events in any of the 72 scintillation counters, both at the energy threshold 7 MeV and 0.8 MeV. Fig.2 shows the counting rates above the low level discrimination for bottom and middle counters; the top layer of counters is not desplayed because of the lack of the Fe shield, which will be set up in the near future. From fig.2 we conclude that the uniformity and homogeneity of the counting rates are within 90% for counters in similar positions; this represents a good check on the consistency of our apparatus.

In HE 5.3-5 we present the analysis of the low energy pulse distribution; here we discuss the data analysis above the 7 Mev energy threshold. At this discrimination level the counting rate (which represents the total trigger frequency in our apparatus) is 1.2 events min^{-1}.

For muons in single counters the pulse amplitude distribution has been cut at ∿ 20 MeV in software analysis. Fig.3 shows the events pulse-height distribution for vertical through going muons, crossing a vertical telescope of 3 scintillation counters. From this distribution, and from that of the pulse-height in single counters, the ADCs scale has been calibrated, giving a sensitivity of 3.0 MeV/channel, and covering an energy range up to 700 MeV for each scintillation counter.

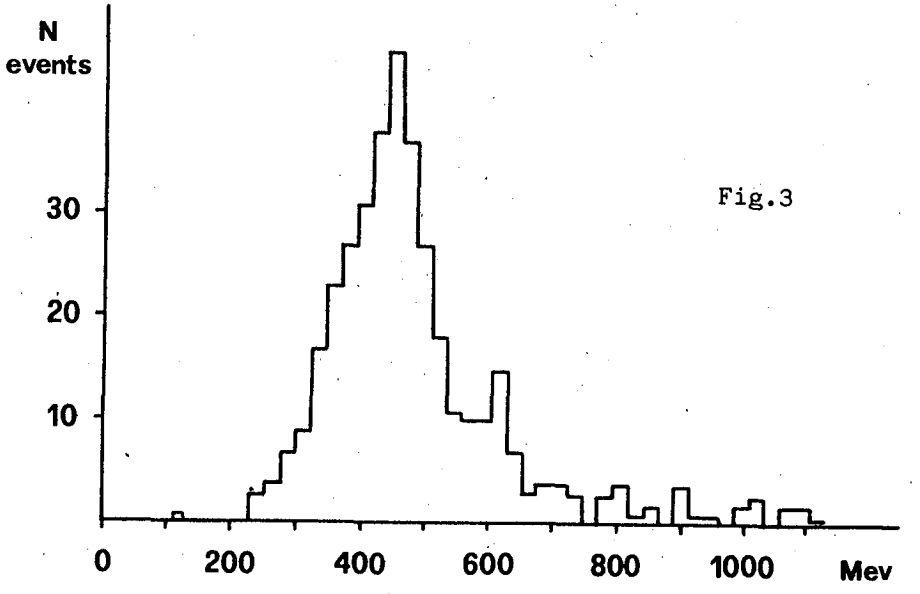

Fig.3

4. Conclusions. From the analysis of our data, we obtained the multiplicity m of counters fired per event (see table I). From the 5291 muons involving at least 2 counters, a rate of 2.9 muons/hour has been obtained for the whole our detector; this value agrees with the expected one at our depth, obtained with previous experiments in the Mont Blanc Laboratory.

The analysis on muon-bundles, muon-interactions, confined events, neutrinos from collapsing star, etc. is now in progress.

m	1	2	3	4	5	6	7	8	9	10	11	12	13
n. of events	11173	2399	2009	657	130	57	14	11	4	4	3	2	1

Table I

References

1) G.Badino et al.,Proc.Int.Conf.Neutrino'84,Dortmund,Germany,1984,p.556
2) G.Battistoni et al., Phys.Lett.B,133,454,1984
3) G.Badino et al., Nuovo Cimento C,7,573,1984

A STUDY OF ATMOSPHERIC NEUTRINOS WITH THE IMB DETECTOR

J. M. LoSecco,[4] R. M. Bionta,[2] G. Blewitt,[4] C. B. Bratton,[5] D. Casper,[2] P. Chrysicopoulou,[2] R. Claus,[2] B. G. Cortez,[4] S. Errede,[2] G. W. Foster,[2] W. Gajewski,[1] K. S. Ganezer,[1] M. Goldhaber,[3] T. J. Haines,[1] T. W. Jones,[7] D. Kielczewska,[1,8] W. R. Kropp,[1] J. G. Learned,[6] E. Lehmann,[4] H. S. Park,[2] F. Reines,[1] J. Schultz,[1] S. Seidel,[2], E. Shumard,[2] D. Sinclair,[2] H. W. Sobel,[1] J. L. Stone,[2] L. Sulak,[2] R. Svoboda,[6] J. C. van der Velde,[2] and C. Wuest[1]

[1]University of California, Irvine, CA 92717
[2]University of Michigan, Ann Arbor, MI 48109
[3]Brookhaven National Laboratory, Upton, New York 11973
[4]California Institute of Technology, Pasadena, CA 91125
[5]Cleveland State University, Cleveland, Ohio 44115
[6]University of Hawaii, Honolulu, Hawaii 96822
[7]University College, London WC1E 8BT, United Kingdom
[8]Warsaw University, Warsaw PL-00-681, Poland

ABSTRACT

A sample of 401 contained neutrino interactions collected in the 3300 metric ton fiducial mass IMB detector is used to study neutrino oscillations, geomagnetic modulation of the flux and to search for point sources.

1. Introduction. The IMB detector is an 8000 metric ton imaging water Cherenkov detector (1). The device has been used to search for nucleon decay. The active dimensions are 22.5 m × 17 m × 18 m. The detector is shielded at a depth of 1570 m.w.e. and has a fiducial mass of 3300 metric tons. In a 417 day exposure, 401 contained events have been recorded. The majority (>95%) of these events are attributable to neutrino interactions. For the most part, these neutrinos are believed to originate as tertiary products of cosmic ray interactions in the atmosphere. The neutrinos are a mixture of ν_e and ν_μ. They may be used to study some fundamental problems in particle physics, cosmic rays and astronomy.

2. Neutrino Oscillations. Neutrinos are incident on the detector from all directions. According to theory, neutrino oscillations should manifest themselves as an Energy (E)/Distance (L) dependence of the neutrino rate. The detector measures the visible energy E_{vis} deposited by a track. This is the energy of a photon with the equivalent light output. The visible energy may be converted to an energy and momentum if a particle mass is assumed (π, μ, e, γ). The direction of tracks is also measured. The event direction can be projected back to determine the point the neutrino entered the Earth. So the distance traveled is also measured. The distance varies from a few kilometers for nearly vertical neutrinos to 13,000 kilometers for those going upward. The mean energy is about 950 MeV.

A neutrino oscillation disappearance experiment has been carried out (2) (on a 135 event subset of these data) by comparing the energy spectrum of the downward neutrinos ($\theta_z < 53°$) to that of upward neutrinos ($\theta_z > 127°$). The comparison was done using the Smirnov-Cramer-Von Mises test. This yields an excluded region in $\sin^2 2\eta$ and Δm^2 seen in Figure 1. We can exclude masses as low as 2.2×10^{-5} eV^2 at maximum mixing.

This result can be extended. Electron neutrino and muon neutrino interactions may be distinguished by the presence of a muon in the final state. The detector has an efficiency of about 50% to observe the muon decay following the initial interaction. Muons coming from pions produced in electron neutrino interactions can be suppressed by using only single track events in the

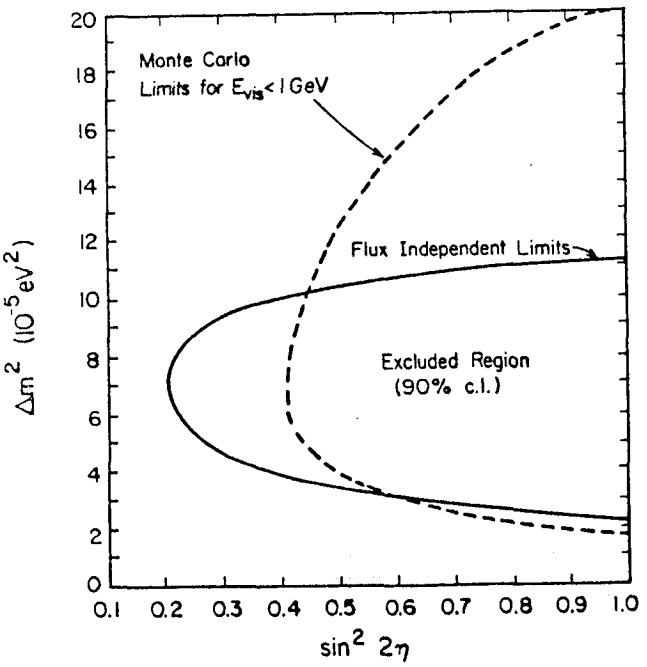

Figure 1. The excluded region for a test of oscillations into sterile neutrinos.The dashed curve is the result of a Monte Carlo test. The solid curve is from a comparison of the shapes of the energy distributions.

analysis (quasi-elastic charged current events). We select events that have a definite muon decay signature. There are 15 in the upward 1/5 solid angle sample and 21 in the downward 1/5 solid angle sample. By comparing the energy spectrum of these two samples we can get limits on the oscillation of muon neutrinos. This gives the excluded region seen in Figure 2. It may be possible to identify and distinguish showering tracks from muons and so a similar analysis can be performed on a purely ν_e sample.

3. Geomagnetic Effects. In the preceding work we assumed that neutrino spectrum (shape) was independent of distance. The Earth's magnetic field tends to deflect the lower energy primaries incident near the equator. For our detector (52° N geomagnetic latitude) this implies a lower flux of neutrinos coming upward, since the mean magnetic field is greater than the local field that affects the downward going, locally produced neutrinos. Notice this effect is similar to the effect of neutrino oscillations. The lowest energy upward going neutrinos appear to be attenuated. Our previous results could be strengthened and extended if the geomagnetic effects were well understood. For the present, we will just compare our data to predictions (3). In Figure 3, we plot log E/L for our data and compare with expectations. An isotropic distribution would reverse the height of the two peaks. The geomagnetic modulation is a better fit to the data. The neutrino energy spectrum and zenith angular distribution also agree well. The double peaks in Figure 3 reflect the solid angle subtended. Most of the solid angle is either nearby or on the other side of the Earth.

The χ^2 comparison of the two curves gives $\chi^2 = 29$ with 14 degrees of freedom. But almost half of this comes from the bin centered at $\log(E/L) = -2.23$. This corresponds to $E/L = 5.8 \times 10^{-3}$ MeV/meter. Removing this bin yields a χ^2 of 17 for 13 degrees of freedom. Only statistical errors have been included in these calculations.

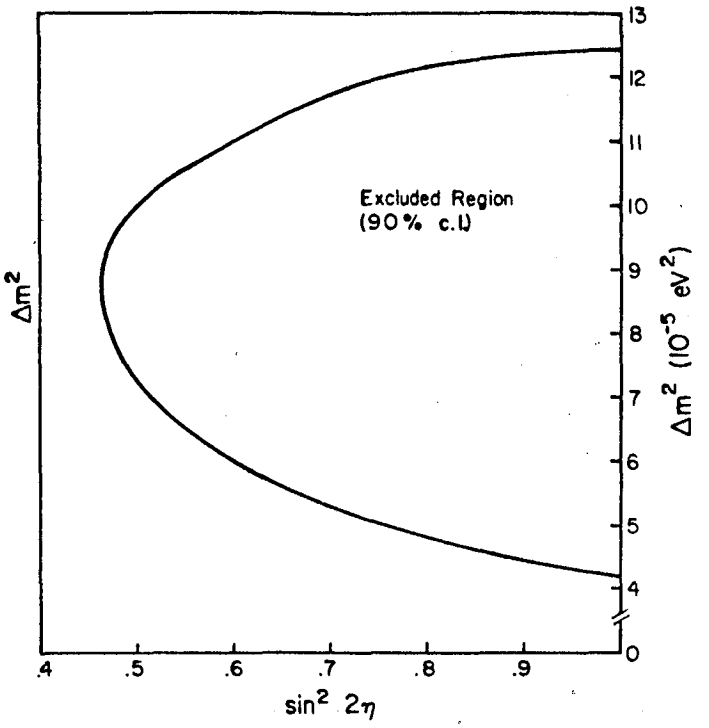

Figure 2. The excluded region for a test of ν_μ oscillations. This comes from a comparison of the energy distribution for muon containing single prong events in the upward and downward 1/5 of the solid angle.

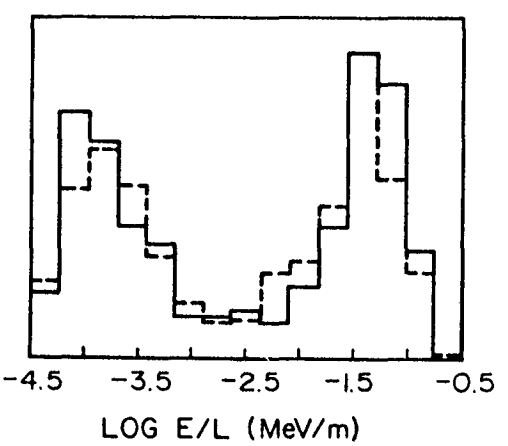

Figure 3. A comparison of the log (E/L) distribution with that predicted by theory (dashed curve). The good agreement supports the theory which includes geomagnetic modulation of the flux.

4. Point Sources. Our data rate corresponds to a neutrino flux of about 4.1 ± .6 ν/(min cm^2 str.) with an energy above ~400 MeV. These data may be used to search for point sources of neutrinos. All terrestrial point sources (reactors, accelerators, etc.) are normally too small to be seen. A search may be made for extraterrestrial neutrino sources. The events have been plotted in right

ascension and declination and various cuts have been imposed to enhance any signal. Topological cuts to retain only single prong events have been tried. At the present time, no statistically significant evidence for a point source is known to be present in the data.

Acknowledgements. This work was supported by the U.S. Department of Energy. We are grateful to the Morton-Thiokol Company for their hospitality at the Fairport mine. One of us (JML) was supported by a DOE Outstanding Junior Investigator grant. We would like to thank J. McGowan for help with the ν_μ analysis.

References

1. H. S. Park, G. Blewitt *et al., Phys. Rev. Lett.* **54**, 22 (1985), and references quoted therein.
2. J. M. LoSecco *et al., Phys. Rev. Lett.* **54**, 2299 (1985), May 27, 1985.
3. T. K. Gaisser, T. Stanev, S. A. Bludman and H. Lee, *Phys. Rev. Lett.* **51**, 223 (1983). Our comparison is with a distribution supplied by Gaisser and Stanev in early 1985.

Atmospheric Neutrinos Observed in Underground Detectors

T.K. Gaisser and Todor Stanev[+]

Bartol Research Foundation of the Franklin Institute, University of Delaware, Newark, DE 19716, U.S.A.

1. Introduction

Atmospheric neutrinos are produced when the primary cosmic ray beam hits the atmosphere and initiates atmospheric cascades. Secondary mesons decay and give rise to neutrinos. We have calculated the neutrino production and compare our predictions with the neutrino fluxes detected in underground detectors. Such a comparison will provide knowledge about the neutrino background for nucleon decay and for extraterrestrial neutrinos.

There are two ways to detect neutrinos in underground detectors: direct neutrino interaction within the volume of the detector (contained neutrino events) and detection of muons produced in a neutrino interaction in the rock surrounding the detector (neutrino induced muon).

Contained neutrino events are characterized by observation of an interaction within the fiducial volume of the detector when the incoming particle is not observed. The reconstruction of the event gives the energy and in some cases the flavor of the interacting neutrino. Because of the large angle between the neutrino and the produced lepton in quasielastic collisions at low energy the determination of the angle of the incoming neutrino is restricted in principle. Both the neutrino flux and the containment requirement restrict the energy of the neutrinos observed in contained interactions to less than several GeV. Our detailed calculations of neutrino fluxes emphasize this low energy region, though we have calculated fluxes up to 1000 GeV at specific angles to compare with earlier calculations.

Neutrinos interact with the rock surrounding the detector but only muon neutrino interactions can be observed, as the electron energy is dissipated too fast in the rock. The direction of the neutrino is preserved quite well in the interaction and at energies above 1 TeV the angular resolution is restricted mainly by the scattering of the muon in the rock. An energy measurement is, however, impossible and the muon rate reflects the neutrino spectrum above some threshold energy, determined by the detector efficiency for muons.

Contained Neutrino Events

All primary nucleons with energy above the production threshold contribute to the flux of neutrinos, which produce contained events. The low energy primary flux is subject to modulation while penetrating both the solar and terrestrial magnetospheres. Thus the intensity and the energy spectrum of the primary beam is different for each direction at each location at each epoch of the solar cycle.

We have calculated the flux of atmospheric neutrinos as

$$\frac{dN_\nu}{dE_\nu} = \int_{E_\nu}^{\infty} dE_o \, Y(E_\nu, E_o, \theta) \Omega(E_o, \theta, \phi) \frac{dN}{dE_o} \qquad (1)$$

where $Y(E_\nu, E_o, \theta)$ is the yield of neutrinos in an atmospheric cascade generated by a primary cosmic ray of energy E_o incident at zenith angle θ. Ω is the geomagnetic cut-off and dN/dE_o is the flux of primary nucleons. For each primary energy and zenith angle we made a Monte Carlo simulation of atmospheric cascades and recorded the energy distribution of the four types of

neutrinos. The program follows the secondary particles and their interactions down to the neutrino threshold energy in a realistic atmospheric model, accounting in detail for the decay kinematics and the energy loss of the charged particles. The major approximation of the calculation is its linearity, which does not affect significantly the neutrino fluxes above 50 MeV and the angular distribution above 200 MeV.

The interaction model is based on a parametrization of hadron-nucleus collisions and is tuned to fit the available data in both the GeV and TeV regions. The main features of the interaction model include: (a). Leading hadron elasticity skewed toward small values; (b). Energy dependent hadronic cross-sections, both around the production threshold and at high energy; (c). Energy dependent K/π ratio. Details of the model as well as comparison with data are discussed in Ref. 1.

The event rate due to the neutrino flux is

$$Rate = \sum_i \int_{E_i} \int_{E_\nu} dE_i\, dE_\nu \frac{dN_\nu}{dE_\nu} \frac{d\sigma_i}{dE_i} \epsilon_i(E_i) \qquad (2)$$

where $d\sigma_i/dE_i$ is the cross-section for $\nu_i + N \rightarrow l_i + X$ with visible energy E_i in the detector and ϵ_i is the corresponding efficiency.

A correct calculation of the neutrino rates thus requires a proper knowledge not only of the neutrino cross-section, but also of the energy threshold and the efficiency of each detector, which are obtainable only through an extensive Monte Carlo study of the detector properties. Such studies have been performed for the detectors with significant neutrino statistics.[2,3]

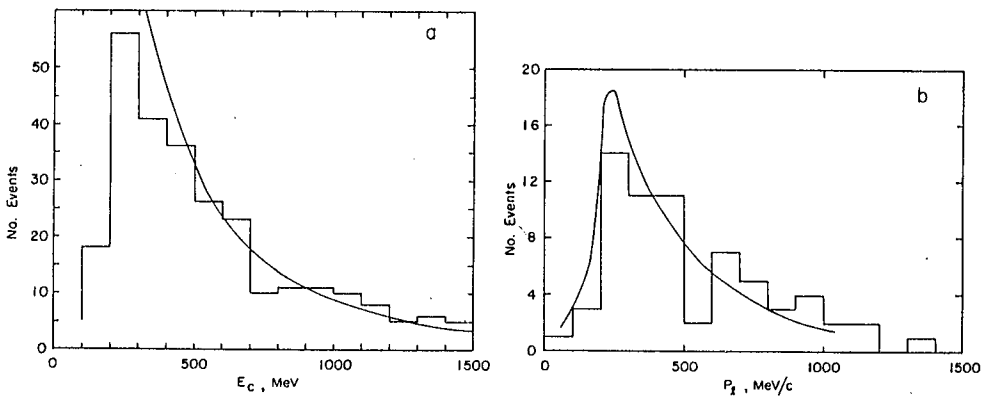

Fig. 1. Comparison of the calculated lepton energy spectrum in quasielastic neutrino interactions with data. In the case of IMB (a) the histogram shows Cherenkov energy distribution ($E_c = E_e$ for electrons and $E_c = E_\mu$ - 200 MeV for muons) for neutrino interactions with assymetry > 0.6. The Kamioka data[3] show the lepton energy distribution in single ring events.

Even without a detector Monte Carlo, however, we can compare the detected lepton energy spectrum to our prediction for quasielastic neutrino interactions for lepton energies above 100 MeV, where neutrino cross-sections on bound nucleons are not drasticly different from the free nucleon cross sections. The comparison for the IMB and Kamiokande detectors is shown in Fig.

1[a,b]. A more detailed comparison would require accounting for the detector efficiency, which is estimated to be 80 per cent for IMB[4]. There appears to be a lack of leptons at Kamioka at energies below 300 MeV, which comes from the low number of electrons detected in this region.

Neutrino Induced Muons.

The flux of muons produced by interactions of ν_μ with energy E_ν in the surrounding rock is

$$\frac{dN_\mu}{dE_\mu dE_\nu} = N_A \int_0^\infty dX \int_{E_\mu}^{E_\nu} dE'_\mu g(X,E_\mu,E'_\mu) \frac{d\sigma}{dE'_\mu} \frac{dN_\nu}{dE_\nu} \qquad (3)$$

where $g(X,E_\mu,E'_\mu)$ is the probability that a muon starts with energy E'_μ and ends up with energy E_μ after propagating a distance X in rock. Because the muon production cross-section and range both increase in proportion to the energy up to a several TeV, muons are produced by neutrinos with a large range of energies. On average the correlation between the neutrino and lepton direction is quite good. The dependence of the flux of neutrino induced muons on the detection energy threshold is remarkably small.

At high energies our neutrino fluxes are in very good agreement with previous work, which use the kinematic relations between production of muons and neutrinos and the measured muon flux as a normalization. The most detailed of these is the one by Volkova [5], who gives the angular dependence of the neutrino fluxes up to very high energy. We have used Volkova's high energy neutrino fluxes to calculate the rates of neutrino induced muons as a function of the muon energy and angle. The comparison with experimental results is shown on Fig. 2.

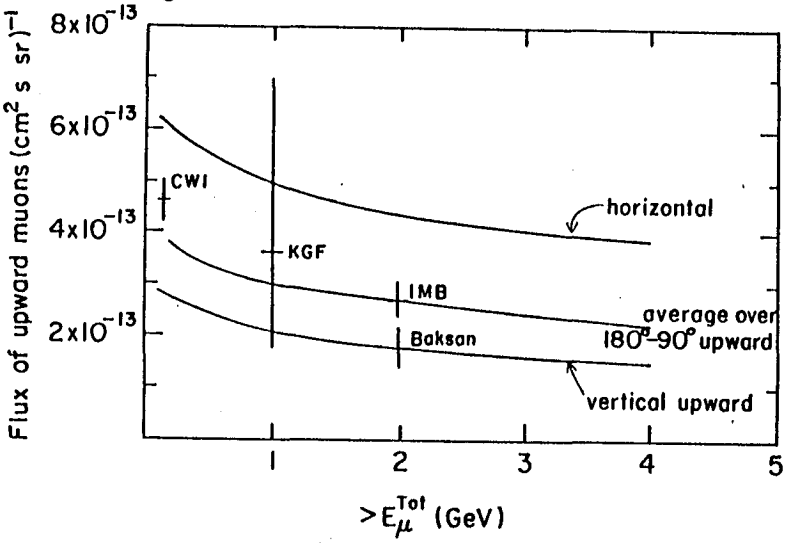

Fig. 2. Comparison to data on upward muons. CWI[6] and KGF[7] data are horizontal, Baksan[8] - vertical and IMB[9] is averaged over all $\theta > 90°$.

Discussion and Conclusions

The absolute and relative rates and the energy distribution of the contained neutrino events, as well as the fluxes of neutrino induced muons, are fully consistent with the predicted neutrino fluxes of atmospheric origin. The

uncertainty of the absolute normalization of our calculation is 10 to 20 per cent. On the basis of the observed rates alone one cannot exclude the possibility that a similar fraction of events has a more exciting origin - nucleon decay candidates or extraterrestrial neutrinos.

The agreement between the predicted and observed angular and energy distributions, however, suggests that the majority of detected neutrinos are of atmospheric origin and leaves little room for point neutrino sources. The identification of nucleon decay candidates requires a better knowledge of the neutrino-nucleus cross-sections and interaction properties.

Acknowledgments

The authors are grateful to J. van der Velde for numerous helpful discussions of the IMB data.

This work is supported in part by the U.S. Department of Energy under contract DE-AC02-76ER05007 and by the National Science Foundation under Grant PHY-8410989.

References

(*) On leave of absence from the Insttitute for Nuclear Research and Nuclear Energy, Sofia 1184, Bulgaria.

(1) T.K.Gaisser and Todor Stanev, in preparation. For a short description of the calculation see T.K. Gaisser *et al.*, Phys. Rev. Lett. 51 , 223 (1983).

(2) See, e.g. R. M. Bionta *et al., Talk presented by Hye-Sook Park at the 20th Rencontre de Moriond, 1985.*

(3) M. Koshiba, *Talk at the Sixth Workshop on Grand Unification,* Minneapolis, USA, April 1985.

(4) J. C. van der Velde, *private communication,* 1985.

(5) L. V. Volkova, Yad. Fiz. 31 , 1510 (1980) [Sov. J. Nucl. Phys. 31 , 784 (1980)]

(6) M. F. Crouch *et al.*, Phys. Rev. D 18 , 2239 (1978).

(7) M. R. Krishnaswamy *et al.*, Pramana 19 , 525 (1982).

(8) M. M. Boliev *et al., Proc. 17th International Cosmic Ray Conference,* Paris, 7 , 106 (1981).

(9) R. M. Bionta *et. al., Talk presented by D. W. Caspar at the Santa Fe meeting of the Particles and Fields division of APS,* 1984.

GEOPHYSICAL SEARCHES FOR THREE-NEUTRINO OSCILLATIONS

J. R. Cudell
Physics Department
University of Wisconsin
Madison, WI 53706

T. K. Gaisser
Bartol Research Institute
University of Delaware
Newark, DE 19716

Introduction. The possibility of using cosmic ray induced neutrinos to detect oscillations in deep underground experiments has been considered by many authors.[1-5,12] Most of the estimates are made neglecting matter effects, or in the two neutrino case. The matter effects, however, are non-negligible:[3,4] in the two neutrino case, they reduce a mixing angle of 45° to 7.5° for 1 GeV neutrinos of squared mass difference 10^{-4} eV^2 going through the earth (average density = 5.52 g/cm^3) making the oscillation totally unobservable. Also, they produce a natural oscillation length of about 6000 km in the case of massless neutrinos, invalidating all estimates based on wavelength arguments. Adding a third neutrino flavor considerably modifies the oscillation pattern and suggests that scales down to 5×10^{-5} eV^2 could be observable even when we take into account matter effects and the electron contribution to the incoming flux.

In this paper, after defining the model of the earth used in the calculation, we will show the effect of matter on the probability curves for different cases, varying the masses and the mixing matrix. We will then give the prediction for the ratio upward $\nu + \bar{\nu}$/downward $\nu + \bar{\nu}$ as a function of the zenith angle at Cleveland, neglecting angular smearing and energy threshold effects.

1. Simple Model for the Earth: The 3 neutrino oscillation formalism has no analytic solution in the case of a continuous medium with varying density.[7] We therefore approximated the real density profile of the earth by a 3 layers model. The earth's density, especially in the core, is rather poorly known.[8] The only firm constraint, i.e. - that the average density is 5.52 g/cm^3 and the diameter 12756 km, has been included in our model: the three layers have respective densities of 3.5 g/cm^3, 5.5 g/cm^3 and 10.17 g/cm^3 and respective radial thicknesses of 928 km, 1950 km and 3500 km. These densities and thicknesses come from a crude estimate made on one of the models quoted in Reference 6.

2. Probabilities. We now study oscillations through a diameter of the earth using the notations of Reference 7.

The main problem is the choice of a mixing matrix: in the case of Dirac neutrinos, the mixing matrix depends on 3 angles and one phase. We do not know of any model predicting a 3 neutrino mixing matrix with mixing angles large enough to be observed.

Accordingly, we consider the following matrices, with $U_{\alpha i}$ the amplitude to go from a charged-current eigenstate $|\nu_\alpha>$ to a mass eigenstate $|\nu_i>$ of mass m_i:

Case 1: 2 neutrino mixing matrix "Cabibbo like":

$$U_2 = \begin{pmatrix} \cos\alpha & -\sin\alpha & . \\ \sin\alpha & \cos\alpha & . \\ . & . & 1 \end{pmatrix} \quad \text{with } \alpha = 45° \text{ (maximal vacuum mixing)} \quad 22.5° \text{ (lifting the } \delta m^2 \text{ sign degeneracy}^7\text{)} \qquad (1)$$

Case 2: 3 neutrino mixing matrix with maximal muon mixing:

$$U_2 = \begin{pmatrix} \frac{1}{2} & 1/\sqrt{2} & -\frac{1}{2} \\ 1/\sqrt{2} & 0 & 1/\sqrt{2} \\ -\frac{1}{2} & 1/\sqrt{2} & \frac{1}{2} \end{pmatrix} \quad \text{This reduces the outgoing } \nu_\mu \text{ flux most.} \qquad (2)$$

Case 3: Big 3-neutrino mixing with a phase. To study the phase-dependence we use the Kobayashi-Maskawa matrix with a phase δ and all angles 45°:

$$U_3 = \begin{pmatrix} 1/\sqrt{2} & . & . \\ . & 1/\sqrt{8} - \frac{1}{2}e^{i\delta} & 1/\sqrt{8} + \frac{1}{2}e^{i\delta} \\ . & 1/\sqrt{8} + \frac{1}{2}e^{i\delta} & 1/\sqrt{8} - \frac{1}{2}e^{i\delta} \end{pmatrix} \qquad (3)$$

We study the probability P_α to get flavor α from a beam of νe or ν_μ when we let it evolve through matter and assume one of the previous mixings. The results are shown in Fig. 1 for 1 GeV neutrinos.

We see that a squared mass difference of 10^{-4} eV^2 in the 2 neutrino case is unobservable due to matter effects.[3,4] However, this estimate is violated in the 3 neutrino case: for an appropriate mixing matrix, δm^2 scales of order 10^{-4} eV^2 are attainable. Furthermore, graphs (b) and (c) clearly show that the oscillation pattern is totally modified by matter effects. Notice that the probabilities do not go back to their original value in the course of the oscillation. This is a matter effect which one always encounters in the presence of more than two uniform media. Also, we see that 3 neutrino oscillations are very sensitive to the phase of the mixing matrix and that matter effects can, in principle, distinguish between $\delta m^2 > 0$ and $\delta m^2 < 0$ as has already been pointed out.[7]

3. Upward to Downward Ratios at Cleveland. We now present results for the upward to downward ratio of contained events at Cleveland, corresponding to incoming fluxes partitioned into zenith angle bins such that $.1 \times n < \cos\theta \leq .1 \times (n+1)$ where θ is the zenith angle and $n \in [0,9]$. The energy is integrated for each bin from .2 GeV to 3 GeV. We neglect the effect of the layer above the detector and define the geometry assuming the detector at the surface of the earth. The zenith angle dependent fluxes that we use have been described elsewhere.[2,9,10] The calculation is made at solar minimum and we assume a ratio $\nu/\bar{\nu}$ of 1.3. We take a fiducial volume of 2×10^{33} nucleons[11] and the inclusive cross sections[2]: $\sigma_\nu = .737 \times E \times 10^{-38}$ cm^2 and $\sigma_{\bar{\nu}} = E \times .31 \times 10^{-38}$ cm^2 with E the neutrino energy in GeV. We show in Fig. 2 the results of our calculations in the form of ratios upward $\nu + \bar{\nu}$ /downward $\nu + \bar{\nu}$. We first exhibit the effect of matter on 2 neutrino oscillations at the scale $\delta m^2 = 10^{-4}$ eV^2. Although one would expect a big depletion (Fig. 2d) of the ν_μ flux from a naive argument based on vacuum oscillations, we see in Fig. 2c that matter effects completely modify the picture and make the phenomenon unobservable in this case. We also show results in the 3ν case which suggest that it is possible to observe δm^2 scales of order 10^{-4} eV^2.

4. Conclusions: We have shown in this work that matter effects totally modify the expectations for neutrino oscillations through the earth, making the accessible range for the squared mass difference of the order of 10^{-2} eV^2 to 10^{-3} eV^2 in the 2 neutrino case and of the order of 10^{-4} eV^2 to 10^{-5} eV^2 in the 3 neutrino case. In both cases, the mixing needed to reach this precision must be unrealistically big.

In the energy averaging of § 3, we have taken the same electron and muon thresholds. An interesting possibility exists for the case where the electron threshold is lower than the muon threshold, as for the example of contained interactions shown in Fig. 2. One can then imagine a situation in which the upward ν_e interaction rate is increased without a significant decrease in the corresponding rate of ν_μ interactions. (This is possible because, at a given neutrino energy, $\nu_\mu/\nu_e \approx 2$). An oscillation effect maximum around 500 MeV could therefore increase the ν_e interaction rate via $\nu_\mu \to \nu_e$ more than it would be depleted via $\nu_e \to \nu_\mu$ without affecting the ν_μ interaction rate significantly since the latter is due primarily to neutrinos of energy $E \gtrsim 1$ GeV.

REFERENCES

1. P. H. Frampton and S. L. Glashow, Phys. Rev. D 25, 1982 (1982).
2. T. K. Gaisser and T. Stanev, Phys. Rev. D 30, 985 (1984).
3. P. V. Ramana Murthy, Proceedings of 18th International Cosmic Ray Conference, Vol. 7, p. 125 (1983).
4. G. V. Dass and K. V. L. Sarma, Phys. Rev. D 30, 80 (1984).
5. D. S. Ayres, B. Cortez, T. K. Gaisser, A. K. Mann, R. E. Shrock and and L. R. Sulak, Phys. Rev. D 29, 902 (1984).
6. L. Wolfenstein, Phys. Rev. D 17, 2369 (1978).
7. V. Barger, K. Whisnant, S. Pakvasa and R. J. N. Phillips, Phys. Rev. D 22, 2718 (1980).
8. A. De Rujula, S. L. Glashow, R. R. Wilson and G. Charpak, Phys. Rep. 99, 341 (1983).
9. T. K. Gaisser and T. Stanev, talk presented at ICOBAN '84, p.61(1984).
10. T. K. Gaisser, talk presented at Fourth Moriond Astrophysics Meeting, La Plagne, France (1984).
11. D. Sinclair, et al., talk presented at the "Science Underground" meeting, Los Alamos (1982), A.I.P. Conference Proceedings, no. 96.
12. T. K. Gaisser, talk given at Telemark III Miniconference (1984), Madison preprint MAD/PH/241 (1985).

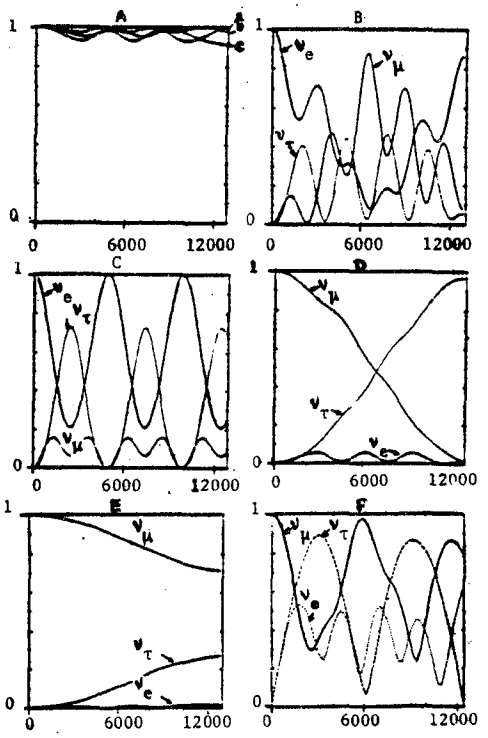

FIGURE 1.

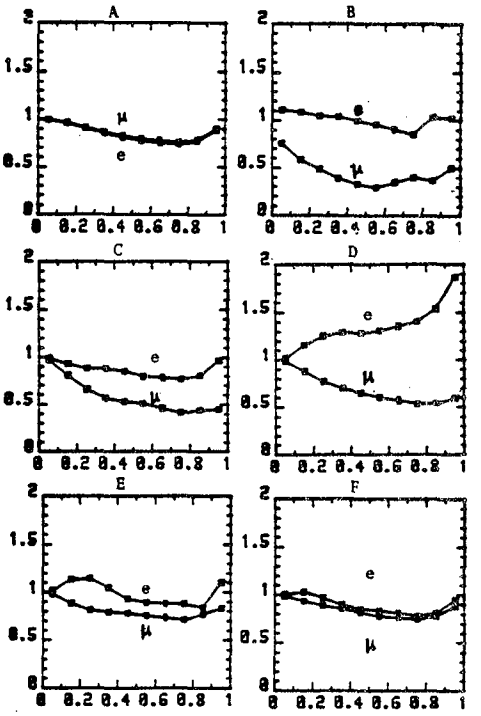

FIGURE 2.

FIGURE 1. Neutrino oscillations through a diameter of the earth. Horizontal axis: distance traveled through the earth; Vertical axis: probability P_α.

(a) Case 1 with $|\delta m^2| = 10^{-4}$ eV^2. The three curves give P_e for a pure ν_μ incoming beam, for $\alpha = 45°$ (curve a), $\alpha = 22.5°$ and $\delta m^2 < 0$ (curve b), $\alpha = 22.5°$ and $\delta m^2 > 0$ (curve c).

(b) Case 3 with $\delta = 0°$, $m_1^2 = m_2^2 = 10^{-8}$ eV^2, $m_3^2 = 10^{-3}$ eV^2.

(c) Same as (b) considering the earth as a vacuum.

(d) Case 3 with $\delta = 270°$, $m_1^2 = 0$, $m_2^2 = 1.5 \times 10^{-4}$ eV^2, $m_3^2 = 5 \times 10^{-5}$ eV^2.

(e) Same as (d) but with $\delta = 0°$.

(f) Case 2 with $m_1^2 = 0$, $m_2^2 = 10^{-4}$ eV^2, $m_3^2 = 5 \times 10^{-4}$ eV^2.

FIGURE 2. Ratios $\frac{(\nu+\bar{\nu})\text{up}}{(\nu+\bar{\nu})\text{down}}$ for 10 even bins in cos θ.
Horizontal axis: cos θ; vertical axis: ratio $\frac{\text{up}}{\text{down}}$.

(a) Without oscillations.

(b) Case 2 with $m_1^2 = 0$, $m_2^2 = 10^{-4}$ eV^2, $m_3^2 = 5 \times 10^{-4}$ eV^2.

(c) Case 3 with $\delta = 270°$, $m_1^2 = 0$, $m_2^2 = 1.5 \times 10^{-4}$ eV^2, $m_3^2 = 5 \times 10^{-5}$ eV^2.

(d) Case 1 with $\alpha = 45°$, $\delta m^2 = 10^{-4}$ eV^2, neglecting matter effects.

(e) Same as (d) but with matter effects.

(f) Same as (e) but with $\alpha = 22.5°$.

MEASUREMENT OF NEUTRINO OSCILLATIONS IN MACRO EXPERIMENT

The MACRO Collaboration

Paper presented by J. Musser

ABSTRACT: We consider the possibility of investigating neutrino oscillations in the proposed MACRO experiment. We calculate its sensitivity taking into account the theoretical uncertainties coming from flux calculations, geomagnetic effects and propagation through matter, as well as the experimental limitations.

1. The use of atmospheric cosmic ray neutrinos in underground experiments for investigating neutrino oscillations could in principle allow to explore a region of parameter space beyond that accessible in reactor or accelerator experiments.

Unfortunately, many limitations prevent to reach the nominal high sensitivity deriving from the long oscillation path (i.e. the Earth diameter $D \sim 10^4 Km.$)

First, the low statistics ineherent in this kind of experiments makes small mixing angles not accessible. Furthermore, an average over the neutrino energy spectrum and neutrino directions, i.e. over oscillation lengths, is unavoidable: in particular, the effect of averaging over directions is much larger than the averaging over source dimensions.

The last limitation arises because of the matter. The different indices of refraction in matter for ν_μ and ν_e, generated by the charged current contributions to elastic $\nu_e - e$ scattering, lead to a decoherence of the ν_μ and ν_e components after a characteristic length of $\sim 9000\ Km$ in the earth.

2. Considering only two neutrino flavours, namely ν_μ and ν_e, an underground experiment can record the disappearence of ν_μ or the variation of the ratio ν_μ/ν_e. The disappearence method needs the knowledge of the expected flux and hence is affected by uncertainties of the order of $10 - 20\%$, as confirmed also from results of large nucleon decay experiments.

The influence of the Earth magnetic field, as well as that of solar wind, adds further uncertainties to the calculation of the low energy part of the spectrum.

The angular distribution of the muons produced by ν in the surrounding rock and the ratio ν_μ/ν_e are however less sensitive to systematic uncertainties. In fact, the energy of parent neutrino for muons traversing an underground apparatus is high enough ($E_\nu \geq 10\,GeV$) to allow neglecting geomagnetic effects, and the comparison between different path lengths makes unnecessary an absolute monitor on the flux, provided the angular distribution is known with sufficient accuracy.

The ratio ν_μ/ν_e is obviously less dependent on theoretical uncertainties.

Two final remarks on experimental possibilities are in order.

A direct comparison of the downward and upward neutrino fluxes using muons produced in the rock is difficult, since, at the deepness of the existing and proposed large underground detectors the cosmic muon background is too high even near the horizontal direction.

In addition, the energy of neutrinos that produce muonic events contained in a detector of reasonable size is very low, so the angle between the produced muon and the parent neutrino is large, making less efficient the distinction between up and down directed neutrinos.

3. We evaluated the sensitivity of MACRO [1] using a complete Montecarlo computation, including generation, transport and tracking of leptons. The ν_μ flux is taken from ref. [2], assuming equal contribution for ν_μ and $\overline{\nu}_\mu$ and $\Phi(\nu_e) = 0.2 \times \Phi(\nu_\mu)$. The interaction cross section includes quasielastic, Δ and inelastic channels. The survival probability for ν_μ is :

$$P(\nu_\mu \rightarrow \nu_\mu) = 1 - (1-\rho) sin^2(2\theta) sin^2(\pi L/l_v) \qquad (1)$$

in vacuum, and

$$P(\nu_\mu \rightarrow \nu_\mu) = 1 - (1-\rho) sin^2(2\theta)(l_m/l_v)^2 sin^2(\pi L/l_m) \qquad (2)$$

in matter.

In the above formulas, θ is the vacuum mixing angle, ρ the ratio ν_e/ν_μ, $l_v = 2.5E/(m_1^2 - m_2^2)$ (oscillation length in vacuum), $l_0 = 2\pi/GN_e = 9 \times 10^3\ Km$ and

$$l_m = l_v(1 + (l_v/l_0)^2 \mp 2l_v/l_0 cos2\theta)^{-1/2} \qquad (3)$$

is the oscillation length in matter [3]. The signs refer to neutrino and antineutrino respectively.

A μ produced inside the detector must be fully contained to cut the background of the entering stopping muons, and its verse of motion cannot be identified. Thus we consider only the total number of contained events.

The maximum flux reduction for oscillations in such case is 20% requiring a knowledge of the expected flux better than the present.

A μ produced in the rock must traverse the detector with a minimum track length to allow the determination of the verse of motion by time-of- flight measurement. The median energy of parent neutrinos is, in this case, $\sim 60GeV$ and the mean $\nu - \mu$ angle is $\sim 3.5^o$.

The modulation factor, defined as the ratio between the measured and the expected angular distribution of the detected muons, is shown, for various Δm^2 and at maximum mixing, in Fig.1 and 2.

Matter effects reduce the sensitivity in Δm^2 by about an order of magnitude.

The error bars indicated in Fig.2 correspond to about 3 years of exposure and show that a $3\,\sigma$ lower limit of $\Delta m^2 = 5 \times 10^{-3}$ is achievable. For $\Delta m^2 > 5 \times 10^{-2}$ the modulation factor becomes again nearly flat, giving the upper limit for this experiment.

REFERENCES

[1] See paper HE 6.1 - 4 in these proceedings.
[2] L.V. Volkova, Sov.J.Nucl.Phys. **31**, 784 (1980)
[3] L. Wolfenstein, Phys. Rev. **D17**, 2369, (1978)

Figure Captions

1) Modulation factor at MACRO, only vacuum oscillations.

2) Modulation factor with matter effects taken into account. Error bars refer to 3 years of data taking.

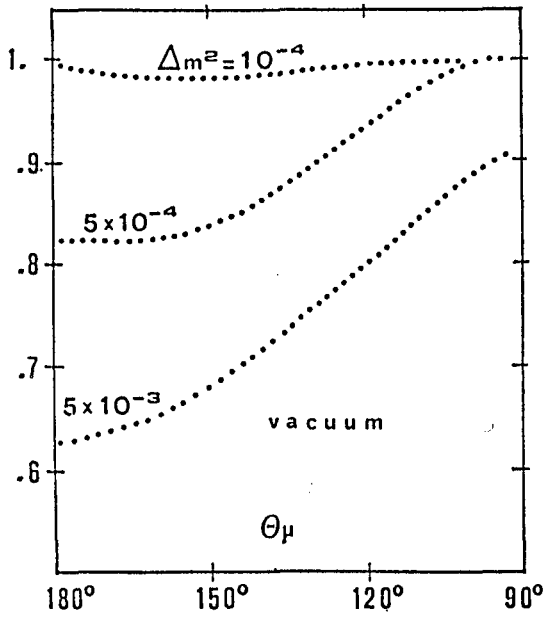

fig. 1

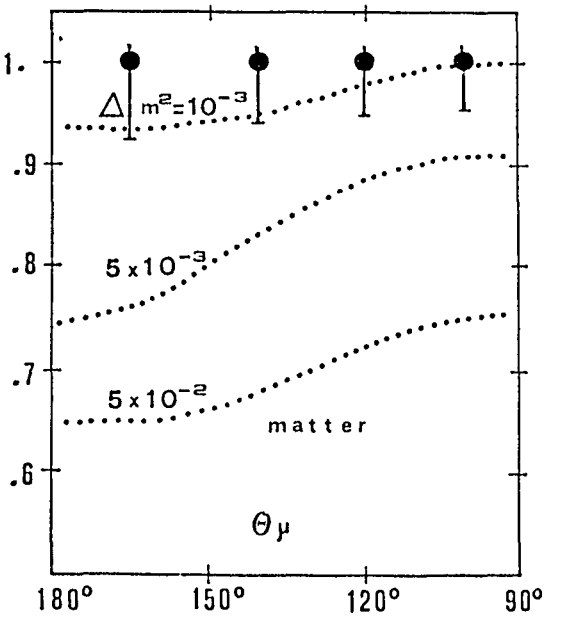

fig. 2

SEARCH FOR STELLAR COLLAPSE WITH THE MACRO DETECTOR AT GRAN SASSO

The MACRO Collaboration
presented by
R. Steinberg, Physics Department
Drexel University, Philadelphia, PA 19104

The generally accepted modern view of stellar evolution[1] holds that stars in the range of 8 to 12 solar masses evolve gradually as increasingly heavier nuclei are produced and then consumed in a series of exothermic thermonuclear processes ultimately leading to the formation of a core composed almost entirely of nickel and iron. When the mass of this hot iron-nickel core reaches the critical value of approximately 1.4 solar masses, electron degeneracy pressure is no longer able to support the outer layers of the star and a collapse process begins. Since the core has exhausted its thermonuclear fuel, further stages of thermonuclear burning cannot prevent a runaway collapse.

As the density reaches 10^{10} gm/cm^3 at a temperature near 10^{10} K, most of the heavy nuclei are dissociated into free nucleons and electron capture on free protons leads to a decrease in the degeneracy pressure and further acceleration of the collapse process. This implosion of the stellar core takes place on a time scale only slightly longer than the free fall time (tens of ms) and leads to the formation of a neutron star or black hole and to the sudden release of a large fraction of the star's gravitational potential energy, much of which is ultimately emitted as a huge burst of neutrinos and antineutrinos of various species.

Although this general picture has received substantial confirmation over the past two decades with the discovery of radio pulsars (neutron stars), X-ray pulsars (accreting binary neutron stars) and Cyg X-1 (probably an accreting black hole), an actual neutrino burst has not yet been convincingly detected.

The **MACRO** detector[2] will employ 700 tons of liquid scintillator contained in 572 individual scintillation elements located in the favorable deep-underground, low-radioactivity environment of Hall B of the Gran Sasso Laboratory. The large mass and high sensitivity ($\leq$10 MeV visible energy threshold) of the detector will allow an extremely sensitive search for neutrino burst events.

The total energy released during a collapse event will be the gravitational binding energy of the residual neutron star, *viz.*

$$E = 3 \times 10^{53} (M/M_\odot)^2 (10 \text{ km}/R) \text{ ergs.}$$

Inserting typical values for neutron star masses and radii gives an energy release of about 3×10^{53} ergs. Since only

a small fraction of this energy goes into the exploding envelope of the star, most of the energy is emitted in the form of neutrinos and (possibly) gravitational waves.[3]

Detailed computations of the time evolution of the collapse distinguish three phases:

a) **Neutronization**, lasting a few milliseconds, in which most of the protons in the core capture an electron to produce a neutron and a neutrino; only electron neutrinos are emitted in this phase.

b) **Deleptonization**, which can last up to 1 second, in which the remaining lepton (and hence proton) excess is radiated through the same process as above, although a sizeable antineutrino flux can also occur.

c) **Cooling**, lasting from 1 to 10 seconds. In this period, neutrinos of all flavors are emitted with a Fermi-Dirac thermal spectrum, modified by absorption in the source. The bulk of the neutrino radiation is in this phase; furthermore, the emission of electron antineutrinos, which are the most easily detected, is essentially limited to this phase.

We have performed Monte-Carlo calculations of the detection efficiency of the **MACRO** liquid scintillation detector to evaluate the sensitivity of a stellar collapse search with this instrument. The effective mass for neutrino burst detection is 600 tons of liquid scintillator with a chemical composition of C_nH_{2n}.

The main detection channel for antineutrinos is the charged current interaction with free protons; neutrino detection is mainly via elastic scattering on electrons. In the Monte-Carlo code we included the effects of module geometry and the appropriate neutrino cross sections and energy loss rates for electrons and positrons. The neutrino energy distribution for the burst was assumed to be a thermal Fermi-Dirac distribution, modified by absorption in the collapsing star[4]. We considered two sets of collapse parameters taken from the literature[5,6]. See Table I.

TABLE I. STELLAR COLLAPSE MODEL PARAMETERS

Parameters	Model I[4]	Model II[5]
Flux($\bar{\nu}_e$) at Earth	6×10^{11} cm^{-2}	1.7×10^{11} cm^{-2}
Flux(ν_e) at Earth	6×10^{11} cm^{-2}	2.4×10^{11} cm^{-2}
$<E_{\bar{\nu}_e}>$	12 MeV	10 MeV
$<E_{\nu_e}>$	10 MeV	10 MeV
Δt	20 s	10 s
E_{tot}	6×10^{53} ergs	2×10^{53} ergs
Number of Positrons:		
D = 1 kpc	3×10^4	4×10^3
D = 10 kpc	300	40

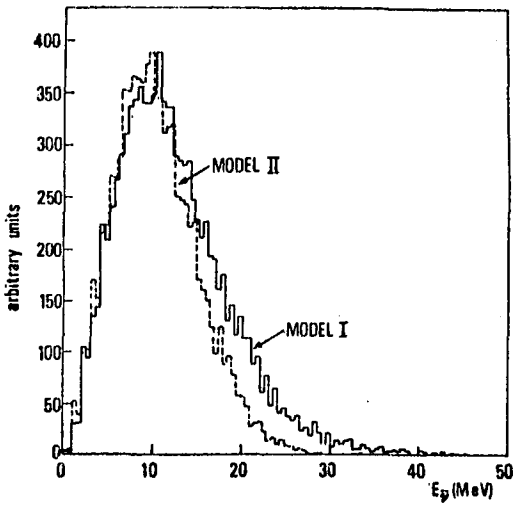

Fig. 1. Two theoretical models for the energy distribution of the neutrinos emitted during stellar collapse. Model I is from Ref. 5, while Model II is from Ref. 6.

Fig. 1 shows the neutrino energy distributions for the two models. Fig. 2 summarizes the results of our Monte Carlo calculations for the single module visible energy distributions of the positrons produced by electron antineutrinos. Note that, since the cross-section for antineutrino absorption increases as E_ν^2, the average positron energy of about 15 MeV is higher than that of the antineutrinos which produce them. Fig. 3 shows our result for the energy distribution of the electrons resulting from elastic scattering of electron neutrinos.

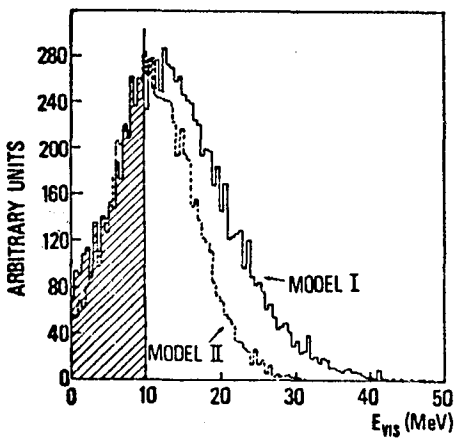

Fig. 2. Results of the Monte Carlo calculation for the energy distribution of positrons produced by electron antineutrinos.

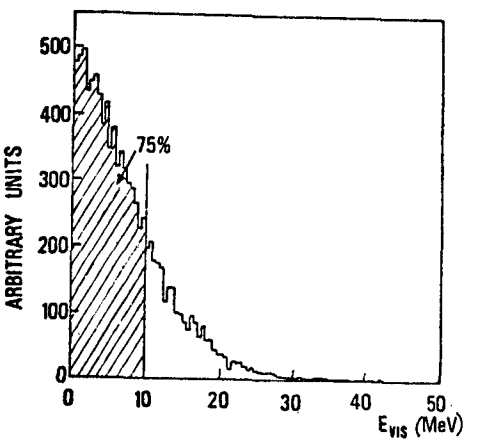

Fig. 3. Results of the Monte Carlo calculation for the energy distribution of electrons produced by electron neutrinos.

From Fig. 2 we conclude that, for the anticipated detection threshold of 10 MeV, positron detection efficiencies are 75% and 60%, respectively, for the two models. From Fig. 3, the electron detection efficiency is 25%, since the elastic scattering cross section grows only linearly with E_ν and the average electron energy is only $\sim .5\ E_\nu$.

The last two lines of Table I show the expected numbers of detected positrons for the two models, assuming a visible energy threshold of 10 MeV, for distances of 1 and 10 kpc. Even in the more pessimistic Model II, 40 counts are obtained for a collapse at the Galactic center.

Statistical fluctuation of the radioactive background counting rate in the detector can mimic a neutrino burst. For a 5 year run, 90% confidence level detection of a neutrino burst requires the frequency of spurious bursts to be kept below 1 per 12 years. Allowing this rate for spurious bursts, Fig. 4 shows the minimum detectable neutrino flux as a function of the background counting rate of the scintillator system for several values of the burst duration.

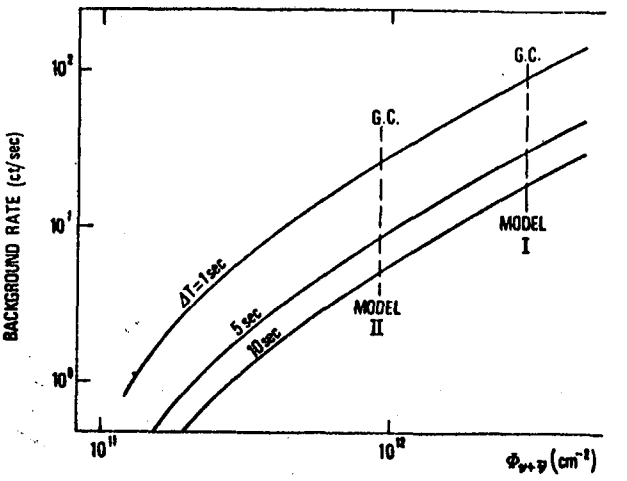

Fig. 4. Minimum detectable neutrino flux vs. detector background rate.

With an estimated maximum background rate of 1 Hz and a typical burst duration of 5 sec, the minimum detectable neutrino flux is $2 \times 10^{11}/cm^2$. Thus, in Model I, the maximum range for burst detection would be 40 kpc, while Model II predicts a maximum detection range of about 15 kpc. The **MACRO** detector therefore will be sensitive to stellar collapses occurring anywhere within the Galaxy.

REFERENCES

1. See, for example, J.M. Lattimer, *Ann. Rev. Nucl. Part. Sci.* 31, 337 (1983).

2. The **MACRO** collaboration, paper HE 6.1-4, these proceedings.

3. Only a small fraction of the total energy released by collapse can be radiated in gravitational waves. See S.L. Shapiro, *Ap. J.* 214, 566 (1977).

4. P.V. Korchagin, *et al.*, Proc. 17th Intl. Cosmic Ray Conf., Bangalore, 7, 110 (1981).

5. D.K. Nadyozhin and I.V. Otroshchenko, *Sov. Astron.* 24, 47 (1980).

6. A. Burrows and T.L. Mazurek, *Nature* 301, 315 (1983).

HE 5.3-12

HIGH ENERGY NEUTRINO ASTRONOMY WITH MACRO

The MACRO Collaboration

Paper presented by G. Auriemma*

ABSTRACT

A large area underground detector with accurate muon tracking and directionality can be used for the search of extraterrestrial sources of high energy neutrinos. The sensitivity of the MACRO detector to possible sources of neutrinos was evaluated with a Monte-Carlo simulation of the neutrino interaction in the rock and of the detection in the real apparatus.

Two categories of possible neutrino sources are discussed in comparison with the detector sensitivity. Promising candidate objects for this search appear to be the two binary X-ray sources in the southern sky Vela X1 and LMC X4, which are known to emit γ-rays up to the $10^4\ TeV$ region .

A large flat underground muon detector can be used as a neutrino telescope because the horizontal and upward going muons are generated only by neutrino interactions in the rock [1,2]. The MACRO apparatus [3] in the Gran Sasso Laboratory is particularly well suited to this application due to its intrinsically very high tracking accuracy ($\Delta\theta \leq 1°$), its large area ($\sim 1000\ m^2$) and its time-of-flight resolution ($\sim 1\ nsec$). The depth of the Laboratory ($\sim 4000\ m.w.e.$) assures a good filtering of the downward muons generated by the cosmic ray interactions above the Gran Sasso mountain. The omnidirectional measured muon flux in the Laboratory [4] is $\sim 1\ \mu\ m^{-2}\ hour^{-1}$. Therefore the time of flight measurement given by the scintillator counters can distinguish the upward-going component of the muon flux with negligible contamination. Under this circumstances the background to the detection of extraterrestrial neutrino sources is given by the conversion of atmospheric neutrinos. The estimated rate of this background [5] is $\sim 1\ \mu\ day^{-1}$ over the entire MACRO apparatus.

An analytical computation of the response of underground detectors to extraterrestrial neutrinos was reported by Gaisser & Stanev [6]. This computation has shown that the detection efficiency for neutrinos is a fast rising function of the neutrino energy. Therefore the detectability of extraterrestrial neutrinos is related to the hardness of the spectrum of the source.

We have computed the response of MACRO to extraterrestrial neutrino sources with a Monte-Carlo program in order to derive that parameters , such as detection efficiency and the angular spread of the muons respect to the neutrinos direction, which cannot be easily deduced from analitycal computations.

The rate of muons in the MACRO apparatus can be factorized as follows :

$$N_\mu = A(\alpha,\delta) \times \epsilon \times \int_{E_T}^{\infty} F_\nu \times P_\nu \quad dE_\nu \tag{1}$$

where $A(\alpha,\delta)$ is the time averaged exposed area for the point in the sky with equatorial coordinates α,δ, ϵ the detection efficiency in the apparatus, E_T the minimum energy of the muon which can be detected in the apparatus, P_ν the probability that a neutrino produces an upward muon at the

* I.N.F.N. Sezione di Roma and Dipartimento di Fisica ,Università di Roma "La Sapienza", Rome, Italy

detector (see Gaisser & Stanev [6]) and F_ν is the spectral distribution of the neutrinos. Assuming , as costumary for astronomical high energy sources, a power-law spectral distribution for the neutrinos:

$$F_\nu = K_\nu \times E_\nu^{-\gamma} \tag{2}$$

we have estimated both the efficiency and the average neutrino conversion probability $\overline{P}_\nu$, defined :

$$\overline{P}_\nu = \frac{\int_{E_T}^{\infty} F_\nu \times P_\nu \, dE_\nu}{\int_{E_T}^{\infty} F_\nu \times dE_\nu} \tag{3}$$

and the average energy $\overline{E}_\nu$ of the neutrinos which have originated a muon detected in the apparatus:

$$\overline{E}_\nu = \frac{\int_{E_T}^{\infty} E_\nu \times F_\nu \times P_\nu \, dE_\nu}{\int_{E_T}^{\infty} F_\nu \times P_\nu \, dE_\nu} \tag{4}$$

In addition from the Montecarlo we have obtained also the angular point-spread function of the muons. Detailed description and results of the Montecarlo will be reported elsewhere [7]. We summarize in Table I the results obtained for spectral index from -2 to -3.8. We have included in the Monte-Carlo code the angular spread originated by the neutrino-nucleus interaction as well as the effect of transport in the rock. The differential cross-section of neutrino-nucleus scattering used takes into account both the effect of the mass of the W boson and the nucleon structure functions according to Duke & Owens parametrization [8]. In the transport section of the program we have included only the multiple Coulomb scattering of the muon . The distribution of the angle θ between the muon in the apparatus and the neutrino original direction shows a central dominating gaussian core and a tail corresponding to relatively rare large angle scatterings.We have therefore quoted two angular parameters in Table I. The one reported in column 6 is the r.m.s. angle wich is dominated by the Coulomb scattering and the one reported in column 5 is the angle wich includes 90 % of the total muons. Comparison between the two angular parameters shows that steeper spectra can be easily identified by the larger angular spread.

TABLE I. Summary of Montecarlo results

γ	$\overline{E}_\nu$ (TeV)	ϵ	$\overline{P}_\nu$ $E_T = 1GeV$	$\theta_{90\%}$	$\theta_{R.M.S}$	M.D.F. $(ergs\ cm^{-2}\ s^{-1})$
2.0	23.3	.75	$6. \times 10^{-9}$	$\leq 1°$	.47°	$2. \times 10^{-8}$
2.2	7.8	.68	$1. \times 10^{-9}$	1°	.61°	$1. \times 10^{-7}$
2.6	.86	.56	$7. \times 10^{-11}$	2°.25	1°.2	$1. \times 10^{-6}$
3.0	.095	.39	1.2×10^{-11}	6°.0	2°.0	$1. \times 10^{-5}$
3.8	.01	.14	3.2×10^{-12}	11°.5	4°.6	1.7×10^{-4}

The detection of extraterrestrial neutrino sources with MACRO is limited by the sensitivity of the experiment itself and not by the atmospheric background . Infact the resolution of the telescope for hard neutrino sources (*i.e.*sources with spectral index $\gamma \sim -2$) is better then 1 degree. Therefore

the expected atmospheric background is $\sim .05\ \mu\ year^{-1}$. The detection of neutrino emission from an identified celestial object can be unambiguously proved by the clustering of a small number of muons in a cone of aperture $\sim 1°$ around its direction. Therefore the minimum detectable flux (MDF) from a source, reported in Table I corresponds to the neutrino flux which gives 10 muons in a cone of 1° aperture in five years of exposure of the apparatus. The intrinsic neutrino luminosity of a source detectable with MACRO is :

$$L_\nu \geq (M.D.F.) \times 4\pi D^2 \tag{5}$$

where D is the distance of the source.

The localization of the Gran Sasso Laboratory at $38°N$ makes the MACRO experiment suitable for the survey of the southern celestial emisphere. Infact the time averaged exposure area in formula (1) is a function of the source celestial declination. We have reported in Fig. 1 a plot of the equal exposure contours in a galactic coordinates plot. The sensitivity given in table 1 corresponds to the maximum exposure in the direction of the celestial southern pole. For a given source the MDF reported in Table I must be scaled to the actual exposed area

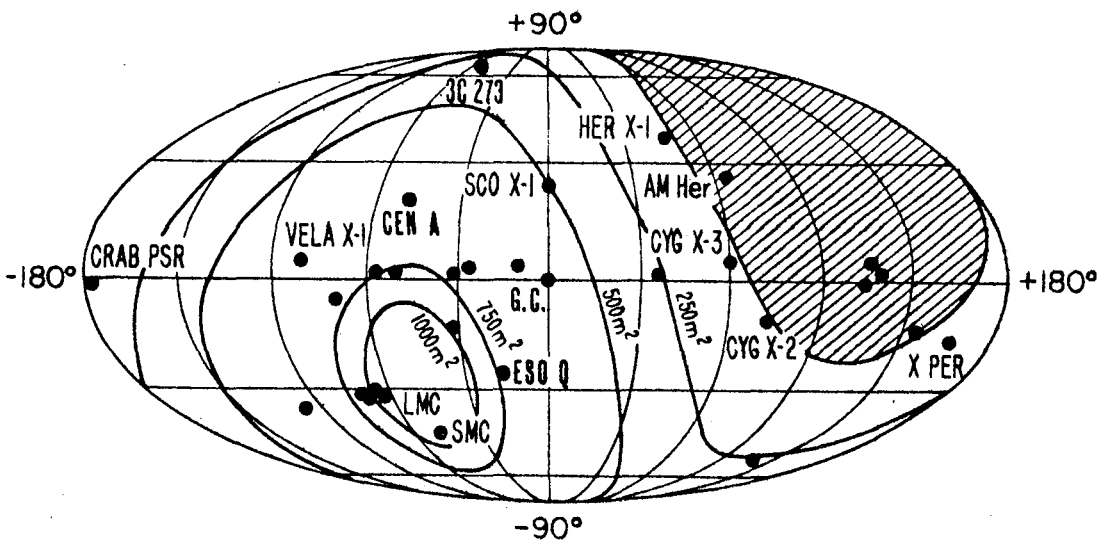

Fig. 1 MACRO field-of-view in Galactic coordinates.Contours represent equal time-averaged exposed area. The shaded region in the northern emisphere is inaccessible to MACRO survey.

It was shown that the MACRO survey will be sensitive mainly to high energy neutrinos. Several classes of objects were proposed as strong neutrino sources [9]. We will discuss briefly the detectability with MACRO of two interesting classes of objects.

a) U.H.E. binaries

Recently U.H.E. γ-rays ($E_\gamma \geq 10^4\ TeV$) emission was observed from the well known X-ray binaries Cyg X3,Vela X1 and LMC X4 [10,11,12,13]. Very reasonable models of this objects suggest that hard neutrino emission is expected [14] in the TeV region, if the U.H.E. γ emission is originated from hadronic interaction of accelerated protons (or nuclei) on the non-degenerate companion star. The spectral index of the neutrinos is predicted to be $\gamma \leq 2$ from the observed γ-ray spectrum. In

Fig. 1 we observe that two of this sources (*viz.* Vela X1 and LMC X4) are in a very good position for the MACRO apparatus.In particular the source in the Large Magellanic cloud is predicted to have a neutrino luminosity well above the detectability of MACRO.

b)Active Galactic Nuclei

Radio and X-ray observations of the compact nuclei of several peculiar galaxies (*viz.* Seyfert's type I galaxies, BL-Lac objects and Quasars) indicate that extreme non-thermal emission originate the huge luminosity of these objects. Neutrino emission could be associated to this non-thermal emission [15,16]. In particular the neutrino radiation could be extremely relevant in the case of continous re-acceleration of particles in the source. Recently high quality observations of the X-ray spectra have shown that the non-thermal emission of a large sample of objects can be fitted with an "universal" power law distribution[17]. This could be the evidence that in all these sources the particle spectrum has a spectral index $\gamma \sim 2.3$. In principle we can expect that the neutrino spectral index would be the same. To be detectable with MACRO a source with spectral index -2.3 should have an intrinsic neutrino luminosity of $L_\nu \geq 10^{45} \times D^2_{Gpc}$ *ergs* cm^{-2} s^{-1}. This neutrino luminosity is anyway too much high also for these type of objects, according to the current estimates.

We are gratefull to T. Gaisser, T. Stanev and V. Stenger for very helpfull discussions.

References

1. K. Lande *Ann. Rev. Nucl. Part. Scie.* **29**, 395–410,(1979)

2. J.C. van der Velde in J. Stone (edt) *"Monopole 83"*, Ann Arbor, Michigan, October 1983

3. B. Barish *Talk given to this Conference.*

4. A. Zichichi in G.Ciapetti,F.Massa & S.Stipcich (edts.) *"Physics and Astrophysics with Underground Track Detector"*, Rome, October 29-31,1981

5. A.F. Grillo & V.Valente *Talk given to this Conference.*

6. T. Gaisser & T. Stanev *Phys. Rev.* **D31**,June 1985 to be published

7. G.Auriemma,A.F. Grillo,J.Musser & G.Tarlé *in preparation.*

8. D.W. Duke & J.F. Owens *Phys. Rev.* **D30**,49,(1984)

9. V.J. Stenger *Astrophys. J.* **284**, 810,(1984)

10. M. Samorsky & W. Stamm *Astrophys. J. Lett.* **268**, L17–L22,(1983)

11. J. Lloyd-Evans *et al.Nature* **305**, 784–787, (1983)

12. R.J. Protheroe, R.W. Clay & P.R. Gerhardy *Astrophys. J. Lett.* **280**,L47–L50,(1984)

13. R.J. Protheroe & R.W. Clay *Nature* **315**, 205–207,(1985)

14. G. Auriemma, H. Bilokon & A.F. Grillo in *"Underground Physics 85"*, April 25-28, St. Vincent,Italy *in press.*

15. D. Eichler *Astrophys. J.* **232**,106–112,(1979)

16. V.S. Berezinsky & V.L. Ginzburg *Mon. Not. R. astr. Soc.* **294**,3–14,(1981)

17. R. Petre, R.F. Mushotzky, J.H. Krolik & S.S. Holt *Astrophys. J.* **280**,499–515,(1984)

HE 5.3–13

THE CAPABILITY OF THE EXISTING NETWORK OF INSTALLATIONS FOR DETECTING THE ANTINEUTRINO BURST FROM COLLAPSING STARS

Khalchukov F.F., Ryassny V.G., Ryazhskaya O.G., Zatsepin G.T.

Institute for Nuclear Research of the Academy of Sciences of the USSR, Moscow

1. Introduction. As the neutrino fluxes can bring information from the internal layers of the collapsing star, the problem of the neutrino burst detection is of importance for both the direct registering of the collapse itself and the investigation of its dynamics. The main characteristics of the neutrino fluxes have been obtained by simulations /1-7/. The total neutrino flux energy is estimated as $2.5 \div 10^{53} - 1.4 \cdot 10^{54}$ erg, the energy of $\tilde{\nu}_e$-flux being 10^{53} erg. Predictions on neutrino energy spectra are quite different. We will use two models of the collapse: the model by Bowers and Wilson /2/, hereafter "BW", and the model by Nadyozhin and Otroschenko ("NO"). The $\tilde{\nu}_e$-spectrum in the BW-model reaches the maximum at $E_{\tilde{\nu}}^{max} = 8$ MeV. Average energy of $\tilde{\nu}_e$ $\bar{E}_{\tilde{\nu}} = 10$ MeV. The NO-model /1/ gives $E_{\tilde{\nu}}^{max} = 10.5$ MeV and $\bar{E}_{\tilde{\nu}} = 12.6$ MeV. The $\tilde{\nu}_e$-burst duration is $\Delta\tau_\nu = 20$s for the NO-model. As the black hole formation is the result of the star collapse in the BW-model, $\Delta\tau_\nu$ is taken to be 5s according to /7/. In the NO-model the emission of $\nu_\tau\tilde{\nu}_\tau$ during star collapse is not taken into account. So in our estimates we correct the intensity of $\tilde{\nu}_e$-burst with the factor of 2/3, the latter resulting from the hypothesis about the equal energy release in various types of neutrinos.

2. $\tilde{\nu}_e$-burst detection efficiency of various scintillation installations

To detect the $\tilde{\nu}_e$-flux the reaction

$$\tilde{\nu}_e + p \rightarrow n + e^+ \qquad (1)$$

will be used. The neutrons will slow down during 5μs and then will be captures by scintillator protons ($\tau_{capt} = 170\mu$s);

$$n + p \rightarrow D + \gamma \; ; \; E_\gamma = 2.22 \text{ MeV} \qquad (2)$$

The $\tilde{\nu}_e$-burst detection has the following features /8/: 1) the counting rate increase in the energy range of 5--45 MeV during 5-20S; 2) the time correlation between the pulses due to reactions (1) and (2); 3) the homogeneous spatial distribution of the interactions (1) in a detector; 4) simultaneous events in various detectors.

We have considered /8/ the $\tilde{\nu}_e$ -burst detection capability of four installations : Artyomovsk scintillation detector (ASD), Baksan scintillation telescope (BST), the USSR-Italy liquid scintillation detector (LSD) and the scintillation telescope in the Homestake Gold Mine (HST). The main characteristics of the installations are presented in Table 1.

ASD /9,10/ is a steel cylinder (h =5.6 m, ⌀ = 5.6 m) containing 105 tons of C_nH_{2n+2}($\bar{n} \approx 10$) with a scintillator. The pulses in the energy ranges of 5-50 MeV (the 'positron' range) and of 1.5 - 4.5 MeV (the 'neutron' range) are analyzed. The 'neutron' channel is opened during 10- 510 μs after the 'positron' pulse arrival. The 97% of positrons and 80% neutrons from the reaction (1) can be detected. The background counting rates are 0.4 s^{-1} in the 'positron' range and $1.2 \cdot 10^3 s^{-1}$ in the 'neutron' one. The events are selected from background provided that at least 15 pulses in 20 appears in the 'positron' range, $\geqslant 10$ of them being accompanied by 'neutron' pulses. At the next step the events are selected if each of $\geqslant 13$ 'positron' pulses is accompanied by 1-3 'neutron' pulses. The same liquid scintillator is used for BST and LSD.

BST consists of 3136 standard modules 0.7 x 0.7 x 0.3 m^3 The pulses in the energy range of $E \geqslant 12.5$ MeV are analyzed. Three step criterion is used for the event selection. At the first step an event is selected provided that $\geqslant 5$ pulses in 20 S appear in the detection range. The spatial and time distributions are analyzed at the second and the third steps. The background counting rate is 0.034 S^{-1}/12, 13./

LSD /14/ consists of 72 modules 1.5 x 1.0 x 1.0 m^3. The neutrons from the reaction (1) can be detected. The threshold is adjusted to 6 MeV, resulting in the background counting rate less than 0.01 S^{-1}. The selection criterion: $\geqslant$ 4 pulses in 20 s in 6- 50 MeV energy range.

HST /15/ is under construction now. The telescope will employ 200 modules 8 x 0.3 x 0.3 m^3 filled with a liquid scintillator . The threshold is expected to be of 5-10 MeV. The background counting rate and the selection criteria have not been published.

We have calculated the energy spectra of e^+ produced by $\tilde{\nu}_e$ -burst in various detectors. The spectra are calculated assuming the distance to collapsing star to be R = =10 kpc and the scintillator mass M = 100 tons (Fig.1), The $\tilde{\nu}_e$ -spectra from /1,2/ were used for the calculations While simulating, the module design and light collection conditions for various detectors were taken into account.

We have used the e^+-spectra obtained for to determine the $\tilde{\nu}_e$ -burst detection efficiency. The e^+-spectra were not supposed to change with the time. When calculating, the positron and neutron pulses were generated at random and added to background pulses. Then the total pulse array was processed in search of $\tilde{\nu}_e$ -burst events and the depen-

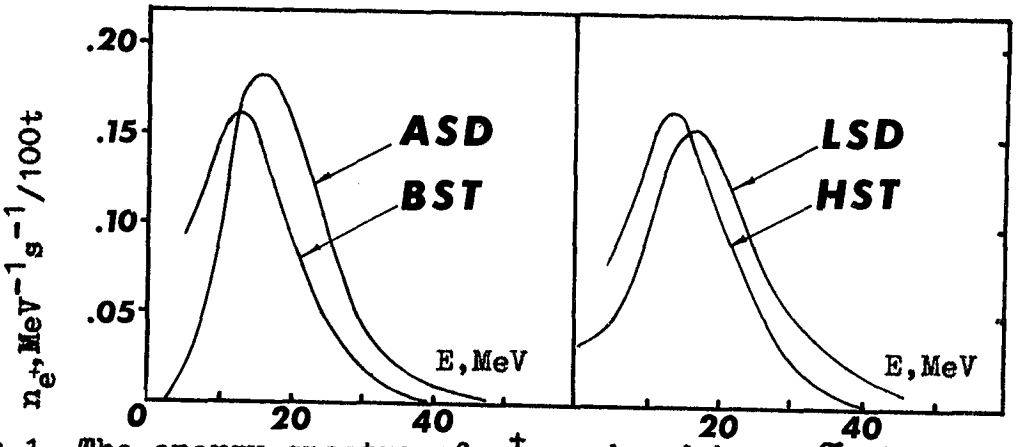

Fig.1. The energy spectra of e^+ produced by $\tilde{\nu}_e$-burst in various detectors (NO-model). The dashed lines -the electronic thresholds.

dence of the burst detection efficiency on the distance to collapsing star (W(R)) was determined for various installations.

The dependence W(R) and the Galaxy star distribution /16/, q(R), were used to calculate the probability of collapse $\tilde{\nu}_e$ -burst detection. The functions $W_c(R \leq R_o)$ are shown in Fig.2.

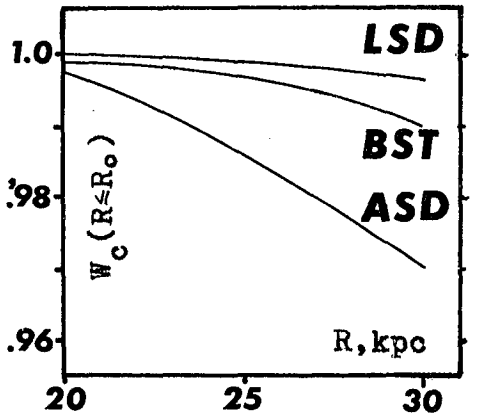

$$W_c(R \leq R_o) = \int_0^{R_o} W(R)\, q_l(R)\, dR \Big/ \int_0^{R_o} q_l(R)\, dR$$

Fig.2. The integral probability of collapse $\tilde{\nu}_e$ -burst detection.

3. The creation of the network of installations.

As one can see in Table 1 the $\tilde{\nu}_e$ -burst detection efficiency is rather great: $Q \equiv W_c(R<30$ kpc) 95% for every installation. It's to be noted, however, that the burst seems to be detected only by coincidence of signals from several installations. Let us estimate the possible imitation counting rate for every installation (n) supposing that coincidence counting rate has to be < 1/100 years. Provided the time resolution is $t \leq 10$ S, we'll obtain for two installations :

$$n_{2c} = 2tn^2 \leq 1/100 \text{ years} \Rightarrow n \leq 1/3 \text{ days};$$

and for three ones:

$$n_{3c} = 3t^2n^3 \leq 1/100 \text{ years} \Rightarrow n \leq 1/2.7 \text{ hours}.$$

Certainly the network of installations allows more 'soft' selection criteria to be used, which increases the $\tilde{\nu}_e$ -burst detection efficiency up to 99% for every installation. So the installation 'living' time (w_l) is of importance. If w_1 were 85% for every installation,

the detection efficiency of the network should be $\geqslant 90\%$.

It should be emphasized that the creation of the network requires the close cooperation between various research groups. The cooperation could start with the joint time planning of runs, as well as the prompt and continuous exchange of the information

Table 1. The main characteristics of installations k_{NO} - the average number of $\tilde{\nu}_e$ -interactions in a detector (NO-model); n_b -the background counting rate; Q -the Galaxy star part being observed by installation ($Q \equiv W_c (R \leq 30$ kpc)) ; $I^{min}_{\tilde{\nu}_e}$ - the minimum $\tilde{\nu}_e$ -flux which may be detected with probability $\omega \geqslant 0.9$.

Installation	Mass (t)	Depth (mwe.)	Threshold (MeV)	$\bar{k}_{NO}$	n_b (s^{-1})	Q		$I^{min}_{\tilde{\nu}_e}$, cm $\Delta\tau_\nu = 20s$
						NO	BW	
ASD	105	570	5	47	0.40 (0.18)*	0.97	0.94	$9 \cdot 10^{10}$
BST	130	850	12.5	27	0.034	0.99	0.95	$8 \cdot 10^{10}$
LSD	90	5200	6	35	$\leq$0.01 (0.001)*	1.00	1.00	$\leq 5 \cdot 10^{10}$
HST	140	4200	5-10	52-41	?	?	?	?

*) - the effective background counting rate with accounting the neutron detection.

References

1. D.K.Nadyozhin, I.V.Otroschenko. Preprint of IAM of the USSR Acad.Sci., N70, (1978).
2. R.Bowers, J.R.Wilson, Astroph.J., 263, 366(1982)
3. V.S.Imshennik, D.K.Nadyozhin, Preprints of IAM of the USSR Acad.of Sci. NN91,98 (1980)
4. A.Burrows , T.L.Mazurek, Nature, 301, 315(1983).
5. V.M.Chechetkin et al.Astr.Sp.Sci.,67,61 (1980)
6.D.K.Nadyozhin. Gravitational collapse, neutrino radiation and supernova bursts", thesis, Institute of Theor. and Exper.Physics, Moscow (1982).
7. D.K.Nadyozhin, Astroph.Sp.Sci.,53,131(1978)
8. G.T.Zatsepin,O.G.Ryazhskaya,V.G.Ryassny,F.F.Khalchukov. Preprint of INR of the USSR Acad.Sci.,NP-0388(1985).
9.V.I. Beresnev et al. Proc.of 16th ICRC,10, 293(1979)
10.F.F. Khalchukov,V.G.Ryassny,O.G.Ryazhskaya,G.T.Zatsepin Proc.18th ICRC, 7,112(1983)
11.A.E.Chudakov,O.G.Ryazhskaya, Proc.Int.Conf."Neutrino 77 "Nauka", Moscow, 1,115(1978)
12.E.N.Alexeev et al.Proc.16th ICRC,10,282(1979)
13.E.N.Alexeev et al., Proc.17th ICRC, 7,110(1981)
14. G.Badino et al.Proc.18th Workshop on Weak Interaction and Neutrino, Javea (Spain), 325 (1982)
15. M.L.Cherry Proc.1982 Summer Workshop on Proton Decay Exper., Argonne Nat.Lab.,ANL-HEP,Pr-82-24, 300;150 (1982)
16. J.N.Bahcall, Tsvi Piran, Astroph.J.Lett,267,L77 (1983)

Energy Spectra of High Energy Atmospheric Neutrinos

K. Mitsui
Institute for Cosmic Ray Research, University of Tokyo, Tokyo 188, Japan

Y. Minorikawa
Department of Physics, Kinki University, Osaka 577, Japan

1. Introduction

One of the important object of DUMAND is the measurement of high energy neutrinos. And also in the underground laboratories, such as Gran Sasso, neutrino physics will become more and more important subject. In such a case atmospheric neutrinos behave sometimes as guest and sometimes become an obstacle. In this paper focussing on high energy neutrinos ($\geq$ 1 TeV), we carried out a new calculation of atmospheric neutrino intensities taking into account EMC effects observed in P-A collisions by accelerator, recent measurement of primary cosmic ray spectrum and results of cosmic ray muon spectrum and charge ratio. Another features of the present calculation are a) taking into account kinematics of three body decays of kaons and charm particles in diffusion equations and b) taking into account energy dependence of kaon production.

2. Methods of the calculation

Energy moment Z_{hc}^{A} in which particle h collide with nucleus A and produce particle c is given as following;

$$Z_{hc}^{A} = \pi \int_0^1 X^{\gamma-1} f_{hA}(X,p_t)\, dp_t^2\, dX,$$

where $$f_{hA} = \frac{1}{\sigma_{hA}} E \frac{d^3\sigma_A}{dp^3} = f_{hp} \frac{\sigma_{hp}}{\sigma_h^o} \zeta_h^c A^{\alpha(x)}.$$

On the other hand in nucleus-nucleus collisions, we take A-A collision as sum of "nucleon"-A collision. Where "nucleon" is considered that a part of nucleon is quark-gluon(Q-G) state. So Z_{pc}^{A} is modified taking into account the primary cosmic ray composition as follows;

$$Z'^{A}_{pc} = \delta_p Z_{pc}^{A} + (1-\delta_p)[(1-\beta) Z_{pc}^{A} + \beta Z_{p\bar{c}}^{A}],$$

where δ_p is the proton excess at the top of the atmosphere and the value

is 0.79. β is the rate of Q-G state and 0.237 estimated from cosmic ray muon charge ratio. More details of the above formulas and the values of Z'^{A}_{hc} can be found in Minorikawa and Mitsui[1].

Next we consider prompt neutrino production. Prompt neutrinos are produced through decays of charm particles, such as $pp \to D\bar{D}X$ or $\Lambda_c^+\bar{D}X$. Inclusive distribution of D-meson is very similar to the distribution of mesons produced by h-A collision and the distribution of Λ_c^+ baryon is similar to that of proton without diffractive part. From the above points, energy moments of charm particles are presented as following;

$$Z'^{A}_{pD} = (Z'^{A}_{p\pi^+} + Z'^{A}_{p\pi^-}) \beta_D ,$$

$$Z'^{A}_{p\Lambda_c^+} = Z'^{A}_{pp} \beta_{\Lambda_c^+} ,$$

where $\beta_c = \sigma_c \langle n_c \rangle A^{\alpha} / \sigma_{pp}^{tot} \langle n_\pi \rangle A^{\alpha}$. As a cross section, decay mode and branching ratio of charm particles, we take those presented by Castagnoli et al[2] and the collision mean free path of charm particle with nucleon was taken 200 g/cm^2 for D-meson and 100 g/cm^2 for Λ_c^+ baryon at the energy of 1 TeV. For neutrino intensities produced by three body decays of kaon and charm particles we can calculate using diffusion equation taking into account kinematics by Hagedorn[3] and given as follows;

$$n_\nu(E_\nu,x,\theta^*) = \frac{\pi^2}{R_3} \int_{M_1}^{M_2} \frac{F(M)}{2M} dM \int_{E_1}^{E_2} \frac{B_i \sec\theta^*}{E_i \rho(x) p_i} P(E_i) n_i(E_i,x,\theta^*) dE_i ,$$

where B_i is decay constant and $B_{k^\pm} = 850$, $B_{k_L^\circ} = 201.8$, $B_{D^\circ} = 9.04 \times 10^7$, $B_{D^\pm} = 4.33 \times 10^7$ and $B_{\Lambda_c^+} = 2.12 \times 10^8$ in GeV. Focussing on the neutrino from the decay $D \to K\mu\nu$, we present as following;

$$R_3 = \frac{\pi^2}{4 m_D^2} \int_{M_1'}^{M_2'} dM^2 \frac{m_D^2 - M^2}{M^2} \sqrt{[M^2 - (m_k + m_\mu)^2][M^2 - (m_k - m_\mu)^2]} ,$$

where $M_1' = (m_k - m_\mu)^2$, $M_2' = m_D^2$, $M_1 = m_k + m_\mu$, $M_2 = m_D$,

$$F(M) = \sqrt{[M^2 - (m_k + m_\mu)^2][M^2 - (m_k - m_\mu)^2]},$$

$$E_1 = \frac{E_\nu}{1 - r_c^2} + \frac{m_D^2 - M^2}{4 E_\nu} , \quad E_2 = \frac{2 E_\nu}{1 - r_c^2} , \text{ and } r_c = M/m_D .$$

Primary spectrum was taken as $1.87 E_0^{-2.7}$ ($E_0 \leq 5 \times 10^6$ GeV/nucleon) and

$191\ E_0^{-3.0}$ ($E_0 > 5 \times 10^6$GeV/nucleon) in unit of $(cm^2 sec\ sr\ GeV)^{-1}$.

3. Results

Calculated differential neutrino spectra are presented in Fig.1 as solid lines. The calculations performed in the early, Volkova[4] and Inazawa and Kobayakawa[5], are shown in the figure, however latter intensity was raised by a factor π for kinematical correction. By integrating differential neutrino spectrum from 0° to 360° for azimuthal angle and from 0° to 90° for zenith angle, downward going integral neutrino intensities were estimated and presented in Fig.2.

4. Discussion

Rate of the intensity of electron neutrino to that of muon neutrino is 5.5% at 1 TeV and 2.6% over 10^6GeV. And also rate of the intensity of neutrino to that of anti-neutrino is 2.2 for muon neutrino and 1.7 for electron neutrino, independently of energy. The integral intensity of the prompt neutrino exceeds the conventional one at about 10 TeV for electron neutrino, and in the energy region of several hundreds TeV for muon neutrino. Because the above energy region will be covered by DUMAND, it seems to be able to detect the prompt effects.

This calculation was performed using the computer FACOM M180-II AD of the Institute for Nuclear Study, University of Tokyo.

References

1) Minorikawa Y and Mitsui K Lett. Nuovo Cimento 41 333 (1984)
2) Castagnoli C et al Nuovo Cimento 82A 78 (1984)
3) Hagedorn R Relativistic Kinematics (Benjamin Inc., New York, 1963)
4) Volkova L V Soviet J. Nucl. Phys. 31 784 (1980)
5) Inazawa H and Kobayakawa K Prog. Theor. Phys. 69 1195 (1983)

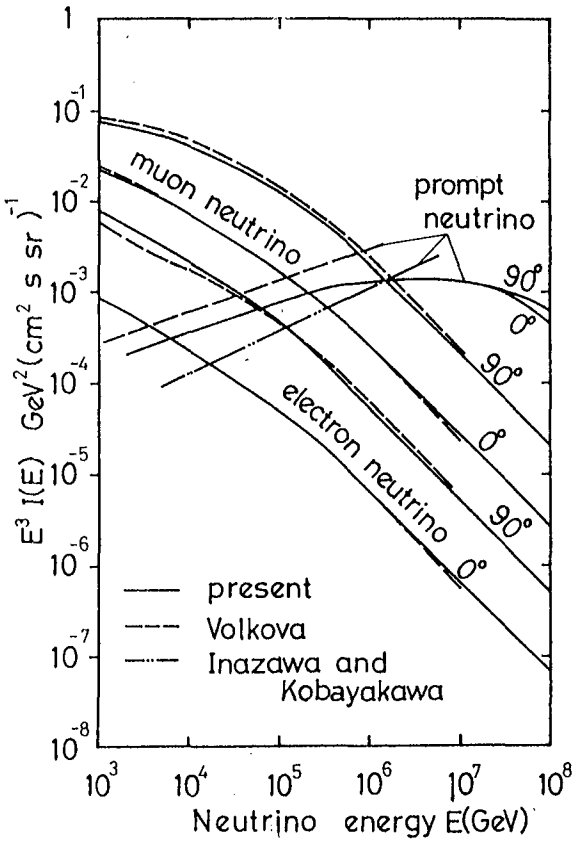

Fig. 1 :

Differential neutrino spectrum.
0° and 90° mean zenith angle.

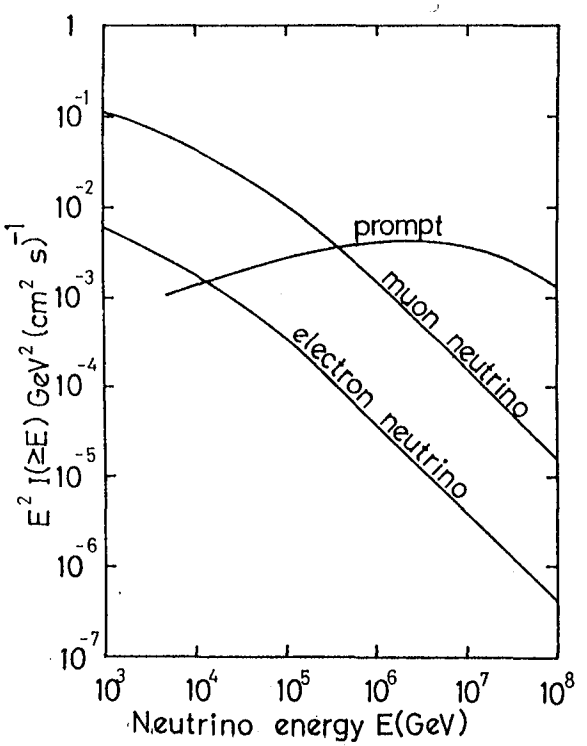

Fig. 2 :

Neutrino intensity I(≥E) obtained by integrating the differential spectrum from 0° to 360° for azimuthal angle and from 0° to 90° for zenith angle.

A STANDARD SOURCE FOR HIGH ENERGY NEUTRINO ASTRONOMY

V.S.Berezinsky[1], C.Castagnoli[2], P.Galeotti[2]

1) Institute of Nuclear Research
Academy of Sciences of USSR, Moscow, USSR
2) Istituto di Cosmogeofisica del CNR, Torino, Italy
Istituto di Fisica Generale dell'Università di Torino, Italy

ABSTRACT

We discuss here a standard source of high energy neutrinos composed of a source of accelerated particles imbedded in a cloud of low density gas. The main mechanism of neutrino production in the source is pp-collision, and the main process of detection is through muons produced underground by the neutrinos. The flux of neutrino-produced muons is computed for sources with different spectral index.

1. Introduction. High energy neutrinos ($E_\nu \geq 10$ GeV) can be generated in cosmic sources as a result of the interactions of accelerated protons with the ambient gas, through the chain of pions (kaons) decays, as well as charged mesons decay (prompt neutrinos). In the past, the possibility to detect high energy neutrinos was discussed mainly in connection with huge detectors, with an area of order 1 km^2, as the DUMAND project. The aim of this paper is to discuss high energy neutrino astronomy for relatively small (area $S \sim 100\ m^2$) underground detectors, and to consider a "standard source" of high energy cosmic neutrinos to which refer when considering (see Berezinsky et al., these proceedings) the real astrophysical sources.

The main process of neutrino production in the source is pp-collisions (which implies also p-nuclei collisions). In some cases prompt neutrinos can dominate, while usually $p\gamma$ neutrinos have too large energies and consequently too small fluxes to be detected in small detectors. The main reaction for neutrino detection is $\nu_\mu + N \rightarrow \mu + X$, for which at high energy muons retain the same direction of the parent neutrinos, so that the source is seen within the resolution angle of the detector. For a detector located deep underground, and for a source in antivertical direction, the atmospheric muon flux is negligible along the direction of the source, and the background is mainly due to the atmospheric neutrinos.

2. The standard source. Our standard neutrino source is a source of accelerated particles imbedded in a cloud of low density gas (1), in which neutrinos are produced through the chain of pions and kaons decays, which follows the pp-collisions. We assume that the column density of the cloud is $x \gg x_n \sim 70\ g/cm^2$, and at the same time transparent to neutrinos. In our calculations we used the follo-

wing spectrum of the accelerated particles:

$$\dot{N}_p(E)\,dE = (\gamma - 1)\,\gamma\,\left(\frac{E}{E_o} + 1\right)^{-(\gamma+1)} \frac{L_p}{E_o}\,\frac{dE}{E_o} \qquad (1)$$

where $\dot{N}_p(E)$ is the number of protons with kinetic energy E produced per second by the source, γ is the exponent of the integral spectrum, and L_p is the cosmic ray luminosity of the source: $L_p = \int_o^\infty E\,\dot{N}_p(E)\,dE$. In all our formulae the energy is given in GeV, $E_o = 1$ GeV, and L_p is given in GeV/s. For $E \gg E_o$ the neutrino flux at the Earth is given by(2):

$$j_\nu(E)\,dE = \frac{L_p}{4\pi r^2}\,\frac{(\gamma - 1)}{(1 - \alpha)}\,(\varphi_\nu + \varphi_{\tilde{\nu}})\,E^{-(\gamma+1)}\,dE \qquad (2)$$

where φ_ν and $\varphi_{\tilde{\nu}}$ are the neutrino yields, $\alpha \sim 0.5$ is the fraction of energy retained by a nucleon in a nuclear collision, and r is the distance to the source. This flux is accompanied by an equilibrium muon flux that can be calculated from the kinetic equilibrium $-\frac{d}{dE}\left[\beta(E_\mu)\,j_\mu(E_\mu)\right] = G(E)$, as:

$$j_\mu(E_\mu) = \frac{N_A}{\beta(E_\mu)} \int_{E_\mu}^{\infty} dE \int_{\bar{\varepsilon}}^{\infty} \frac{dE_\nu}{E_\nu}\,j_\nu(E_\nu) \int_0^1 dx \left[\eta\,\frac{d^2\sigma_\nu(E_\nu)}{dx\,dy} + \bar{\eta}\,\frac{d^2\sigma_{\tilde{\nu}}(E_{\tilde{\nu}})}{dx\,dy}\right] \qquad (3)$$

where $N_A = 6.02\,10^{23}$ is the Avogadro number, $\beta(E_\mu) = a + bE_\mu$ is the muon energy loss expressed in GeV cm^2/g with the values of a and b given by (3), $j_\nu(E_\nu)$ is the $\nu_\mu + \tilde{\nu}_\mu$ flux, $\eta = \varphi_\nu/(\varphi_\nu + \varphi_{\tilde{\nu}})$ and $\bar{\eta} = \varphi_{\tilde{\nu}}/(\varphi_\nu + \varphi_{\tilde{\nu}})$ are the fractions of ν_μ and $\tilde{\nu}_\mu$ neutrinos in the flux, $y = E_\mu/E_\nu$, and x is the scaling variable. The differential cross-sections can be written as:

$$\frac{d^2\sigma_\nu}{dx\,dy} = \frac{G_F^2\,(2\,E_\nu\,m_n + m_n^2)}{2\pi}\,\frac{A(x,Q^2) + \bar{B}(x,Q^2)\,y^2}{(1 + Q^2/m_w^2)^2}$$

$$\frac{d^2\sigma_{\tilde{\nu}}}{dx\,dy} = \frac{G_F^2\,(2\,E_\nu\,m_n + m_n^2)}{2\pi}\,\frac{\bar{A}(x,Q^2) + B(x,Q^2)\,y^2}{(1 + Q^2/m_w^2)^2} \qquad (4)$$

where $m_n = 0.94$ GeV is the nucleon mass, $m_w = 81$ GeV is the W boson mass, $G_F = 1.17\,10^{-5}$ GeV^{-2}, and the form factors can be expressed through the quark structure functions $x(u_v + d_v)$ and xS, with $S = 6\bar{u}$, as:

$$\begin{aligned}
\bar{A}(x,Q^2) &= 2\bar{B}(x,Q^2) = \frac{2}{3}\,x\,S(x,Q^2) \\
A(x,Q^2) &= x\left[u_v(x,Q^2) + d_v(x,Q^2)\right] + \frac{2}{3}\,x\,S(x,Q^2) \\
B(x,Q^2) &= x\left[u_v(x,Q^2) + d_v(x,Q^2)\right] + \frac{1}{3}\,x\,S(x,Q^2)
\end{aligned} \qquad (5)$$

In our calculations we used the structure functions given by[4]. Q^2 is defined as $2m_n E_\mu x(1-y)/y$ when larger than 4 GeV^2, and it is assumed $Q_o^2 = 4$ GeV^2 when smaller than Q_o^2. Inserting (4) and (5) into (3), one obtains, for a power law neutrino spectrum:

$$j_\mu(E_\mu) = j_\nu(E_\mu) \frac{\sigma_F N_A}{\beta(E_\mu)} \frac{G_F E_\mu^2 m_n}{\pi} i_\gamma(E_\mu) \qquad (6)$$

where $\sigma_F = 4.54\ 10^{-33}$ cm^2 is the Fermi constant and

$$i_\gamma(E_\mu) = \int_0^1 dz\, z^{\gamma-2} \int_0^1 dy\, y^{\gamma-1} \int_0^1 \frac{dx}{(1+Q^2/m_W^2)^2} \cdot \qquad (7)$$

$$\cdot \left[\eta A(x,Q^2) + \bar{\eta}\bar{A}(x,Q^2) + y^2\left\{\eta\bar{B}(x,Q^2) + \bar{\eta}B(x,Q^2)\right\}\right]$$

where $Q^2 = 2m_n E_\mu x(1-y)/yz$ if larger than 4 GeV^2, and $Q^2 = 4$ GeV^2 otherwise. The integral muon flux can thus be expressed by:

$$j_\mu(>E_\mu) = j_\nu(>E_\mu) \frac{\gamma \sigma_F N_A G_F E_\mu^2 m_n}{\pi} \int_0^1 du\, u^{\gamma-3} \frac{i_\gamma(E_\mu/u)}{\beta(E_\mu/u)} \qquad (8)$$

and the number of muons crossing an underground detector with area S during the time t is given by:

$$n_\mu(>E_\mu) = j_\mu(>E_\mu)\, S\, t \qquad (9)$$

We computed the values of $n_\mu(>E_\mu)$ for S = 100 m^2, t = 1 year, and our standard neutrino sourcewith a cosmic ray luminosity $L_p = 10^{43}$ erg/s at the distance r = 10 kpc, for different values of the exponent of the integral spectrum. Table 1 gives the results of our calculations.

3. Conclusions. From the values of $n_\mu(>E_\mu)$ reported in table 1, the following conclusions can be inferred:

i) to detect with a S = 100 m^2 area detector a galactic source at the distance of 10 kpc, a cosmic ray luminosity of order $L_p = 10^{43}$ erg/s is needed. Such a large luminosity can be provided only by supernovae explosions or young pulsars.

ii) to detect extragalactic neutrino sources, the scale of luminosity is $L_p \approx 10^{47}$ erg/s at the distance r = 1 Mpc, and $L_p \approx 10^{49}$ erg/s at r = 10 Mpc.

Integral spectral index γ	E_μ (GeV) 10	30	100	300	1000
1.1	$1.2\ 10^{3}$	$1.2\ 10^{3}$	$1.1\ 10^{3}$	$9.3\ 10^{2}$	$6.7\ 10^{2}$
1.2	$6.9\ 10^{2}$	$6.6\ 10^{2}$	$6.0\ 10^{2}$	$4.9\ 10^{2}$	$3.3\ 10^{2}$
1.3	$3.1\ 10^{2}$	$2.9\ 10^{2}$	$2.6\ 10^{2}$	$1.9\ 10^{2}$	$1.3\ 10^{2}$
1.4	$1.3\ 10^{2}$	$1.2\ 10^{2}$	$1.0\ 10^{2}$	$7.4\ 10^{1}$	$4.5\ 10^{1}$
1.5	$5.5\ 10^{1}$	$4.9\ 10^{1}$	$4.0\ 10^{1}$	$2.8\ 10^{1}$	$1.6\ 10^{1}$
1.6	$2.3\ 10^{1}$	$2.0\ 10^{1}$	$1.6\ 10^{1}$	$1.0\ 10^{1}$	5.3
1.7	$1.0\ 10^{1}$	8.6	6.2	3.9	1.8
1.8	4.7	3.7	2.5	1.5	$6.4\ 10^{-1}$
1.9	2.2	1.6	1.0	$5.7\ 10^{-1}$	$2.2\ 10^{-1}$
2.0	1.1	$7.4\ 10^{-1}$	$4.4\ 10^{-1}$	$2.2\ 10^{-1}$	$8.0\ 10^{-2}$
2.1	$5.3\ 10^{-1}$	$3.4\ 10^{-1}$	$1.9\ 10^{-1}$	$8.8\ 10^{-2}$	$2.9\ 10^{-2}$
2.2	$2.7\ 10^{-1}$	$1.6\ 10^{-1}$	$8.0\ 10^{-2}$	$3.5\ 10^{-2}$	$1.0\ 10^{-2}$

Table 1: number of muons with energy higher than E_μ crossing in 1 year an underground detector with area $S = 100\ m^2$, for our standard source with cosmic ray luminosity $L_p = 10^{43}$ erg/s at the distance $r = 10$ kpc.

References

1) Berezinsky, V.S., Castagnoli, C., Galeotti, P., (1985) Nuovo Cim.C,in press
2) Berezinsky, V.S., Volinsky, V.V., (1979), Proc.16th ICRC, Kyoto, vol.10, p.326, ibid., p.332, ibid., p.338
3) Bezrukov, L.B., Bugaev, E.B., (1981), Proc.17th ICRC, Paris, vol.7, p.102
4) Duke, D.W., Owens, J.F., (1984), Phys.Rev. D30, 49

A SEARCH FOR COSMIC SOURCES OF HIGH ENERGY NEUTRINOS WITH "SMALL" UNDERGROUND DETECTORS

V.S.Berezinsky[1], C.Castagnoli[2], P.Galeotti[2]

1) Institute of Nuclear Research
Academy of Sciences of USSR, Moscow, USSR
2) Istituto di Cosmogeofisica del CNR, Torino, Italy
Istituto di Fisica Generale dell'Università di Torino, Italy

ABSTRACT

On the basis of our standard source calculations (Berezinsky et al., these proceedings) of high energy neutrino fluxes, we discuss some models of astrophysical object (single stars and binary systems), from which a detectable muon flux is expected in small underground detectors.

1. Introduction. In connection with the discussions on the DUMAND project[1], high energy neutrino sources were extensively studied (2-6). In particular, the feature of such a discussion was on sources which can be detected with very large underwater detectors, with area of order 1 km^2. In recent years, with the aim to search for proton decay, relatively small underground detectors have been built, which are used for several other purposes. As regards high energy neutrino astronomy, their small area in comparison to the DUMAND project limits the number of sources which are possibly detectable.

High energy neutrinos can be produced in cosmic sources as a result of pp-collisions between accelerated protons and the ambient gas through the chain of pions and kaons decays, as well as charmed mesons decay (prompt neutrinos). The main reaction for detection is $\nu_\mu + N \to \mu + X$, being, at large depth underground, the main background mainly due to atmospheric neutrinos. Since the path-length of high energy muons in the rock is large, while the dimensions of the underground detectors relatively small, muons are produced mainly outside the detector; moreover, since high energy muons retain the same direction of the parent neutrinos, the source is seen within the resolution angle of the detector.

The low energy limit of the experimental neutrino astronomy is defined by the angle $\vartheta_{\nu\mu}$ between the parent neutrino and the muon produced in the νN-collision. Since this angle $\vartheta_{\nu\mu} \approx 2.6\ (100\ \mathrm{GeV}/E_\nu)^{1/2}$ degrees increases with decreesing neutrino energy, the background within the resolution angle of the detector increases at low energies; at the same time, also the νN cross-section and the range of muons decrease. All these factors reduce the muon flux and, consequently, the signal to noise ratio in the direction of the source at low energy ($E_\nu \lesssim 10$ GeV).

Our calculations of a "standard source" of high energy neutrino astronomy (paper I, these proceedings) show that the horizon for small detectors (area $S \approx 100$ m^2) is limited to our Galaxy. If the sources were transparent to gamma rays, then

there will be a connection between neutrino and gamma fluxes; in this case, the limits on the gamma ray flux ($f_\gamma < 10^{-6}$ cm^{-2}s^{-1} for the existing sources) show that in our Galaxy we cannot expect to observe stationary neutrino sources. Then we are left with the possibility to detect transient or hidden sources. The aim of this paper is to discuss such a sources of high energy neutrinos, and their detection with small underground detectors ;see(7) for a general discussion.

2. Detectable high energy neutrino sources.

2.1 It is well known that young supernova shells, filled with high energy particles, are a powerfull source of high energy neutrinos (8) during a period $\tau_\nu \approx 1.3\ 10^7$ s, (at time $t > \tau_\nu$ the high energy particles in the shell loose energy mainly due to the adiabatic expansion). Our standard source calculations are directly applicable to such a model, and, for a source located at the distance r = 10 kpc, with a cosmic ray luminosity $L_p = 10^{43}$ erg/s and an exponent $\gamma = 1.3$ of the integral spectrum (which is the commonly accepted value for the cosmic ray production), our results predict that of order 100 muons with energy $E_\mu \geqslant 1$ TeV cross an underground detector with an area S = 100 m^2 during 1 year. This is undoubtely a detectable neutrino source.

For a steep spectrum ($\gamma = 2.1$), a cosmic ray luminosity $L_p = 10^{44}$ erg/s is needed to detect 5 muons with energy $E_\mu \geqslant 10$ GeV in the same detector during the same time. In this case, a rather high luminosity of the source is required, and nevertheless the signature remains poor.

2.2 A neutrino source made by an active pulsar imbedded in a supergiant (9), a model previously (10) considered in detail, can be easily interpreted on the framework of our standard source. Both for a flat spectrum ($\gamma = 1.3$) and for a steep one ($\gamma = 2.1$), the results on the flux of neutrino-produced muons in an underground detector with area S = 100 m^2 are the same as for the previous case 2.1. This is, however, an example of a hidden source since, because of the large column density ($x \sim 10^5$ g/cm^2) along the supergiant radius, no gamma-rays are emitted from the surface of the system, and the source could be detected only through its neutrino emission.

2.3 A pulsar in a binary system yields neutrinos in the direction of the Earth during the eclipse of the pulsar by the companion, because neutrinos are produced in the atmosphere of the latter, opposite to the line of sight to the observer. Our standard source calculations are applicable for the total duration of the eclipse ($t_\nu \approx 2\ 10^6$ s, if the companion is a 5 $M_\odot$ giant); for r = 10 kpc, $L_p = 10^{43}$ erg/s and $\gamma = 1.3$, the number of recorded muons per orbital period is ~ 20 at the energy threshold $E_\mu = 10$ GeV. In this case, it would also be possible to discover the periodicity of the neutrino emission from the system.

If the companion is a main sequence star with M = 1 $M_\odot$, the numerical estimates are practically the same as for the previous model; however, in this case it is impossible to discover the periodicity of the neutrino pulsation.

2.4 As a result of accretion, a white dwarf in a binary system can undergo a supernova explosion with complete distruction. The energy emitted as cosmic

rays, accelerated by the shock wave in the outer layers of the star, can reach an energy of 10^{51} erg, and neutrinos are produced when the accelerated protons hit the giant companion. Our standard source calculations predict that more than 200 muons with energy $E_\mu \geq 100$ GeV cross the S = 100 m^2 underground detector during the short burst duration if the total energy emitted as cosmic rays is 3 10^{50} erg and the spectrum is flat ($\gamma = 1.3$).

3. High energy neutrinos from Cygnus X-3. We devoted[11] a special attention to Cyg X-3, which is currently interpreted in the framework of a binary system, proposed in 1979 (10) and further developed in 1982 (12), made by an active pulsar orbiting around a massive companion with orbital period of 4.8 hours. By connecting the neutrino and gamma-ray fluxes (assuming a target transparent to gamma rays) and by using the observed gamma radiation to fit the spectrum, one finds that the neutrino flux is:

$$j_\nu(>E) = \lambda\, 4.2\ 10^{-11}\ (E/1\ \text{TeV})^{-1.1} \qquad (1)$$

where λ is an enhancement factor that, for a gamma transparent target, is equal to the ratio of the durations of the neutrino and gamma pulses ($\lambda = \tau_\nu / \tau_\gamma$). By introducing this neutrino flux in our standard source calculations it is possible to estimate the number of muons crossing in 1 year an underground detector; for a 100 m^2 area detector, and for energy thresholds 10 GeV, 100 Gev, and 1 Tev one finds the values 6 $10^{-3}\ \lambda$, 5 $10^{-3}\ \lambda$, and 3 $10^{-3}\ \lambda$ respectively. Therefore, to detect high energy neutrinos from Cyg X-3 in a small detector, a large enhancement factor $\lambda \gtrsim 10^3$ is needed; however, this imposes serious constraints on the luminosity of the cosmic ray source in the binary system, that seem to be reasonable only for a young pulsar while any steady source should be ruled out.

The explanation of the excess of muons in the direction of Cyg X-3 observed in the Mont Blanc NUSEX experiment (13), as due to a flux of high energy neutrinos, requires the extreme choise of the parameters in the model; in particular it implies a very large cosmic ray luminosity of the source $L_p \approx 10^{42} - 10^{43}$ erg/s. With a neutrino flux compatible with the gamma ray observations, the interpretation of the muon excess as produced by neutrinos should be excluded. In addition the flux of muons produced by neutrinos is independent of the column density of rock above the detector, and this feature is in contraddiction with the NUSEX data. Thus we can conclude that the neutrino hypothesis to explain the excess of muons in the small detector seems to be unreasonable.

4. Conclusions. Neutrino astronomy with a small underground detector is characterized by the following considerations:

i) The low energy limit of neutrino astronomy is defined by the angle $\vartheta_{\nu\mu}$ between the parent neutrino and the muon produced in the inelastic νN collision; this limit is of order of $E_\mu \sim 10$ GeV.

ii) Only galactic sources can be detected with a small detector: at r = 10 kpc a cosmic ray luminosity $L_p = 10^{43}$ erg/s is needed. To detect extragalactic sources

the scale of luminosity is $L_p = 10^{47}$ erg/s at r = 1 Mpc, and $L_p = 10^{49}$ erg/s at r = 10 Mpc.

iii) A detectable neutrino flux is expected for several models of sources: young supernova shells, supergiant fed by an active pulsar in its debris, and several models of binary systems (pulsar and giant, supernova explosion in the system).

iv) Under reasonable assumption, the detection of the neutrino flux from Cyg X-3 in a small underground detector seems to be excluded.

v) Our standard source calculations exclude the possibility to detect neutrinos from flares in the opposite side of the Sun or from the decay of solar neutrons.

References

1) Proc.of the DUMAND 1976 Summer Workshop,Honululu 1976, A.Roberts Ed. Proc.of the DUMAND 1979 Summer Workshop,Kabarovsk and Baikal Lake, J.Learned Ed.,1980, Hawaii DUMAND Center
2) Silberberg R.,Shapiro M.M.,1977,Proc 15th ICRC (Plovdiv),vol.6,p.237
3) Berezinsky,V.S.,Zatsepin,G.T.,1977,Sov.Phys.Usp.,122,3
4) Eichler,D.,Schramm,D.N.,1978,Nature,275,704
5) Margolis,S.H.,Schramm,D.N.,Silberberg,R.,1978,Ap.J.,221,990
6) Berezinsky,V.S.,Ginzburg,V.L.,M.N.R.A.S.,1981,194,3
7) Berezinsky,V.S.,Castagnoli,C.,Galeotti,P.,1985,Nuovo Cimento C,in press
8) Berezinsky,V.S.,Prilutsky,O.F.,1978,Astron.Astrophys.,66,325
9) Thorne,K.S.,Zitkow,A.N.,1977,Ap.J.,212,832
10) Berezinsky,V.S.,1979,Proc.DUMAND Summer Workshop,J.Learned Ed.
11) Berezinsky,V.S.,Castagnoli,C.,Galeotti,P.,1985,Ap.J.Lett.,submitted
12) Vestrand,W.T.,Eichler,D.,1982,Ap.J.,261,251
13) Battistoni,G., et al. (Coll. NUSEX),1985, Phys.Lett.,in press

NEUTRINO ASTRONOMY AND THE ATMOSPHERIC BACKGROUND

T.K. Gaisser and Todor Stanev
Bartol Research Foundation of the Franklin Institute
Uiversity of Delaware
Newark, DE 19716
USA

ABSTRACT

We illustrate some aspects of neutrino astronomy by calculating the neutrino-induced muon flux from Cygnus X-3. The signal depends primarily on the power in cosmic rays at the source and on the distance to the source, and only relatively little on details of the matter distribution in the neighborhood of the source.

1.Introduction. Cygnus X-3 is a binary X-ray source in which the compact partner apparently accelerates particles to high enough energy to produce multi-TeV secondaries in the envelope or debris of the companion star.[1] The 10^{12}-10^{16} eV photon spectrum can be accounted for in this way if protons are accelerated to 10^{17} eV and then produce neutral pions which decay to photons.[2] Charged pions and kaons will also be produced, and these will be a source of neutrinos. Muon neutrinos and anti-neutrinos will interact in the Earth to produce a signal of muons, which might be visible above the background of atmospheric muons at sufficiently large angles. The general idea of neutrino astronomy is well-known.[3] Detailed models of Cygnus X-3, coupled with numerous observations of signals from this and other sources, motivated us to carry out a detailed calculation of the neutrino flux and of the neutrino-induced signal from it.[4]

2.Calculation of Neutrino Flux. Assuming that the compact partner accelerates protons which collide with material of the companion star, we calculate in detail the hadronic cascade induced by the proton beam[5], including interaction, energy loss and decay of charged pions and kaons. This is done for a grid of primary energies and phases of the period of the binary system. For the matter distribution of the companion we assume a 2.8 solar mass main sequence star. Since this is undoubtedly an oversimplification, we later compare the results obtained for a variety of densities and thicknesses. Fig. 1 shows the resulting neutrino flux averaged over a period, assuming an isotropic luminosity in cosmic rays at the source (10 kpc) of 10^{39} erg/sec. For comparison we also show the atmospheric neutrino flux. The signal/background ratio exceeds one above about 1 TeV.

We next attenuate the produced neutrinos in the companion. Stecker et al. [6] have pointed out that deposition by neutrinos of too much energy in the interior of the companion would disrupt the system. This can be used to place a limit on the luminosity of such a system in high energy cosmic rays.

FIG. 1. Neutrino flux from Cyg X-3 compared to atmospheric flux. Dashed line is an estimate of atmospheric background assuming detector resolution of 1°. For E_{ν} below about 1 TeV angular resolution is dominated by scattering angle in charged-current neutrino interaction rather than by detector resolution.

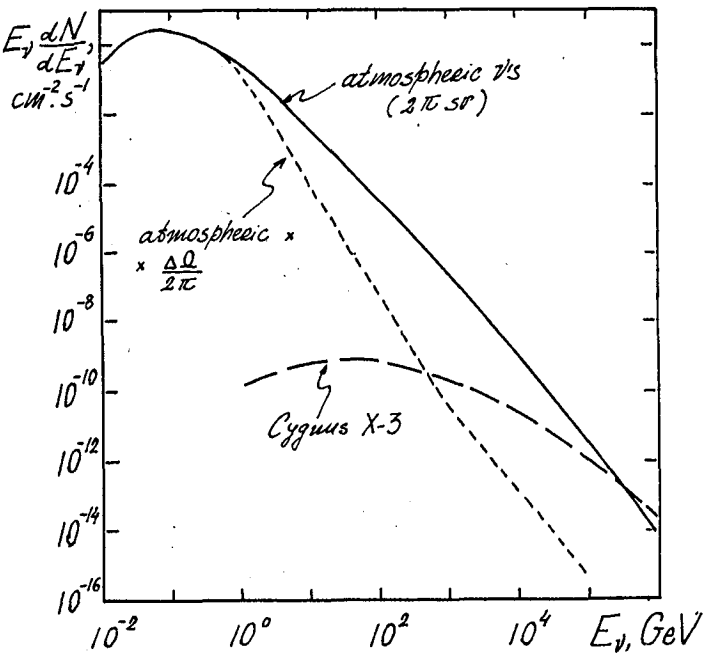

FIG. 2. Attenuation of neutrinos in the companion. Solid line shows neutrino flux before attenuation; dashed lines show transmitted flux at two angles relative to the surface of the companion.

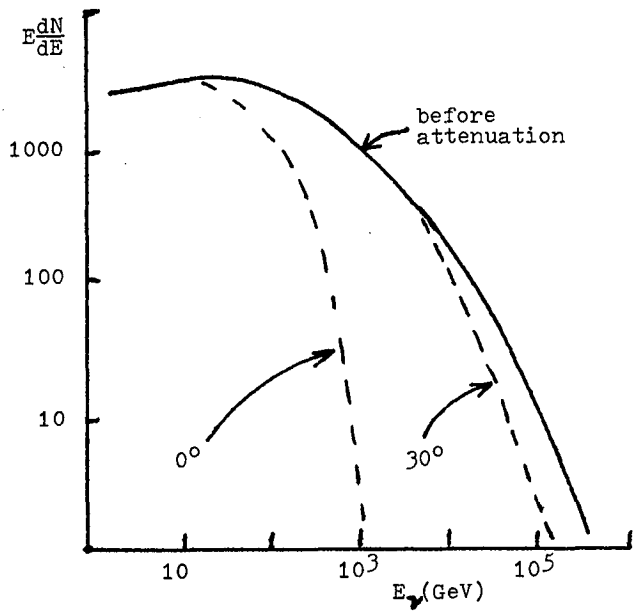

Fig. 2 shows the attenuation of the neutrino beam through the center of the companion (0°) and at 30°. For angles larger than 30° attenuation is negligible. For the case of spherically symmetric, 10^{17} eV monoenergetic protons, only about 0.5% of the total cosmic ray energy is deposited by high energy neutrinos in

the interior of the companion. (This is for a spherically symmetric matter distribution with $R=1.4*10^{11}$cm and a scale height of 8000 km for the companion star. The distance between the centers of the stars is assumed to be not much larger than R.) As pointed out by Stecker et al., this will be further reduced to some extent when compression of the companion by the intense cosmic ray flux is accounted for. This is becuase of increased cascading (rather than decay) of energetic charged pions in the denser medium.

3.Neutrino-induced upward muons. To calculate the induced muon signal at such high energies it is necessary to account for the effect of the W-propagator in the charged-current neutrino cross sections, as well as for the appropriate range-energy relation for the muons. We have done this with two different sets of nucleon structure functions and find [7] the result shown in Fig.3, independent of details of the structure functions. P_ν in Fig. 3 is the probability that a muon neutrino aimed at the detector produces a muon through the detector (assuming neutrino/antineutrino=1.2). This probability is folded with the neutrino spectrum to obtain the signal.

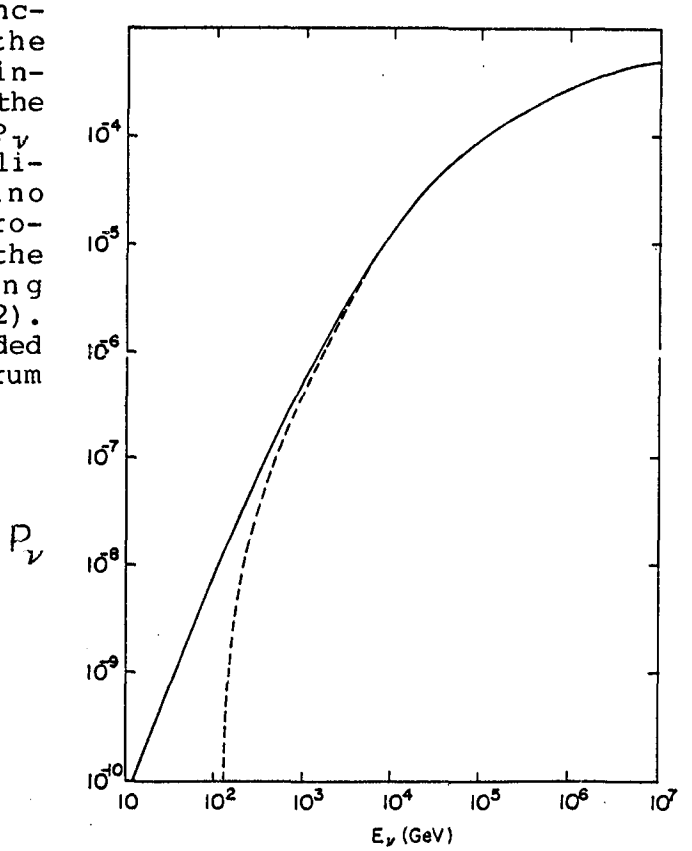

FIG. 3

Averaged over a period the result is

$$10^{-3} \text{ events} * \{L_{39}/(R_{10})^2\} m^{-2} yr^{-1}$$

where L_{39} is the luminosity of the source in units of 10^{39} ergs/sec and R_{10} is its distance in units of 10 kpc. Varying the density and thickness of target material in the region of the source changes this only by factors of two or three.

4.References

[1] David Eichler and W. Thomas Vestrand, Nature 307, 613 (1984).

[2] A.M. Hillas, Nature 312, 50 (1984).

[3] See e.g. David Eichler, Nature 275, 725 (1978); V.J. Stenger, Ap. J. 284, 810 (1984) and references therein.

[4] T.K. Gaisser and Todor Stanev, Phys. Rev. Letters 54, 2265 (1985).

[5] The calculation is similar to that for neutrino production by cosmic rays in the Earth's atmosphere. Only the incident spectrum and the stellar atmosphere are different. The atmospheric calculation is described by T.K. Gaisser, Todor Stanev, S.A. Bludman and H. Lee, Phys. Rev. Lett. 51, 223 (1983) and T.K. Gaisser and Todor Stanev in Proc. 11th Int. Conf. on Neutrinos and Astrophysics, ed. K. Kleinknecht and E.A. Paschos (World Press, Singapore, 1984), p.372.

[6] F.W. Stecker, A.K. Harding and J.J. Barnard, NASA/Goddard preprint, April 1985.

[7] T.K. Gaisser and Todor Stanev, Phys. Rev. D31, 2770 (1985).

HIGH-ENERGY NEUTRINOS FROM A LUNAR OBSERVATORY

Maurice M. Shapiro*
Max Planck Institut für Astrophysik
8046 Garching bei München, West Germany

and Rein Silberberg
Hulburt Center for Space Research
Naval Research Laboratory, Washington, DC 20375-5000 USA

The detection of high-energy (HE) cosmic and solar-flare neutrinos near the lunar surface would be feasible at energies much lower than for a terrestrial observatory. At these lower energies ($\gtrsim 10^9$ eV), the neutrino background is drastically reduced below that generated by cosmic rays in the earth's atmosphere. Because of the short mean free path (<1m) of the progenitor pi and K mesons against nuclear interactions in lunar rocks, the neutrino background would be quite low. At 1 GeV, less than 1% of the pions would decay; at 10 GeV, 0.1%. Thus, if the neutrino flux to be observed is intense enough, and its spectrum is steep enough, then the signal-to-noise ratio is very favorable. The observation of HE neutrinos from solar flares would be dramatically enhanced, especially at lower energies, since the flare spectra are very steep. Detection of these neutrinos on earth does not appear to be feasible. A remarkable feature of solar flares as viewed in HE neutrinos from a lunar base is that the entire surface of the sun would be "visible". Diffuse sources of HE neutrinos, such as the Galactic disc (especially from the Galactic center), would be detectable at energies between, say, 10^9 and 10^{11} eV. On earth, they are swamped by the overwhelming atmospheric background.

1. Introduction. The advantages of a lunar observatory for neutrino astronomy were discussed some years ago by F. Reines (1965). In the present paper we suggest that the investigation of neutrinos from astrophysical sites at energies between 1 and 10^3 GeV can be carried out better on the moon than on the earth. In the dense lunar materials, competition between nuclear interactions of pions and their decay suppresses the frequency of decay. In the tenuous upper atmosphere of the earth, on the other hand, the decay of pions (and their muon progeny) does generate neutrinos. Hence the flux of neutrinos near the surface of the moon is about 10^{-3} of that on the earth at energies between 1 and 10^2 GeV, and about 10^{-2} at 10^3 GeV. Only the background due to prompt neutrinos from the decay of charmed particles in the atmosphere is not suppressed.

At energies below 1 GeV, however, the path length of pions against decay diminishes as the Lorentz factor approaches unity, and pion decay

*Current Address: 205 Yoakum Pkwy. #2-1720
Alexandria, VA 22304, USA

is no longer suppressed, even on the moon. Furthermore, due to the absence of magnetic shielding on the moon, the flux of low-energy cosmic rays incident on the lunar surface is much higher than the average flux at the top of the earth's atmosphere. This further enhances the low-energy neutrino intensity (E>1 GeV) on the moon. (The suppression of neutrino background was quantitatively explored by Cherry and Lande (1985).

Accordingly, a lunar base is probably an unsuitable site for observing the low-energy neutrinos (~10 MeV) from stellar gravitational collapse. Moreover, it is not competitive for recording neutrinos at very high energies ($E>10^3$ GeV); this can be done more readily with Cerenkov light detectors in a large volume of sea water (some 10^8 m^3) near the bottom of the ocean. Such an array--DUMAND--a deep underwater muon and neutrino detector, will be emplaced in the waters near Hawaii in the near future (Peterson 1983).

2. Criteria for Candidate Neutrino Sources to be Explored on the Moon. What types of neutrino sources are likely to be observable between 1 and 10^3 GeV? This is the energy interval for optimum detection by a neutrino observatory under the lunar surface (say, about 100 m below). The sources should emit neutrinos much more copiously above 1 GeV than above 1 TeV, so as to permit the construction of a neutrino observatory significantly smaller than DUMAND. An important constraint is imposed by the interaction cross section of neutrinos, which increases linearly with energy between 1 and 10^3 GeV. As a result, the observation of lower-energy neutrinos becomes more difficult. This cross section is given by

$$\sigma_{\nu N} = (0.7 \text{ or } 0.8) \times 10^{-38} E_\nu \text{ cm}^2,$$

and

$$\sigma_{\bar{\nu} N} = 0.3 \times 10^{-38} E_{\bar{\nu}} \text{ cm}^2$$

for neutrinos and anti-neutrinos, respectively. Let the energy spectrum of the neutrinos be

$$\frac{dJ}{dE_\nu} = KE_\nu^{-\alpha}.$$

Then the event rate is proportional to

$$\int_{E_o}^{E_{max}} \sigma(E_o) KE_\nu^{-\alpha} \, dE_\nu;$$

i.e., it is proportional to

$$E_o^{-(\alpha-2)} - E_{max}^{-(\alpha-2)}.$$

Thus, one criterion for significant source strength in the energy interval between 1 and 10^3 GeV is a steep neutrino spectrum, with the exponent α appreciably greater than 2.

3. Some Promising Candidate-Sources. Solar flares generate particles having steep energy spectra, with α = 4 to 7 at proton energies above 1 GeV. Erofeeva, Lyutov, and Murzin (1983) explored the use of a deep underwater detector of 10^6 tons for observing neutrinos from solar flares. They did not investigate the neutrino background in their paper. We estimate that the background rate is about 10^3 per day. If the neutrinos are emitted in about 20 minutes, as are the gamma rays from a flare, then the background rate is down to 10 for the duration of the flare. If, moreover, an angular resolution of 1 steradian is obtained, then the background is down to ~1 event for the duration of the flare.

For observation of neutrinos from very large flares, such as occur about once per solar cycle, a terrestrial underwater observatory of 10^6 tons seems adequate. However, for larger observatories, $>10^6$ tons, the neutrino background on earth becomes prohibitive. Thus, for observing fine-time structure or neutrino energy spectra of very large flares, or for recording somewhat smaller flares, a lunar observatory of $>10^6$ tons provides an opportunity to carry out studies of flares that are not possible on the earth. Even flares on the remote side of the sun become observable, since neutrinos with energies $<10^{11}$ eV can traverse the solar diameter. In fact, for a given size of flare, neutrinos should reach the detector in greater numbers from the far side than from flares on the near side. This is due to the favorable rate of production of pions (hence of daughter neutrinos) that move toward the observer, when the progenitor protons or other energetic nuclei--on the far side--are directed toward the solar surface.

Another, more diffuse source of neutrinos with a fairly steep energy spectrum σ = 2.7, is that from the central annulus of the Galactic disk, $\pm 60^\circ$ in longitude and $\pm 5^\circ$ in latitude about the Galactic center. Stecker, Shapiro and Silberberg (1979) explored the detectability of these neutrinos at 10^3 GeV with a DUMAND array of 10^9 tons (having an effective detection volume of some 10^{10} tons). The estimated rate of neutrino events to be expected was 130 per year, swamped by 1.8×10^4 background events per year. At 1 GeV, the event rate is about 100 times higher, so that even in a smaller detector of ~10^7 tons, the event rate is about 10 per year, with the signal and background counts being nearly equal in a lunar observatory.

In addition, there are many interesting discrete candidate-sources of neutrinos: accreting neutron stars (including pulsars) in binary systems, active galactic nuclei with accretion disks from which matter drifts into ultra-massive black holes (Silberberg and Shapiro 1979), and the expanding shells around young pulsars (Berezinsky 1976, Shapiro and Silberberg 1979). However, the energy spectra of neutrinos from these sources are as yet unknown.

We present here the results of a sample calculation for SS433, which appears to be one of the most promising candidate sources in our Galaxy, at a distance of about 3 Kpc. This object is probably an accreting black hole in a binary system; it has two relativistic jets and other remarkable features. Its estimated power output is 3×10^{39} ergs/sec (Grindlay et al. 1984), but values that are higher by an order of magnitude have also been proposed (Eichler 1980). If we assume that a power input of 3×10^{39} ergs/sec yields

protons of energy ≥ 10 GeV, and that these protons suffer nuclear collisions, a detector of 10^6 tons would permit the observation of about 30 neutrino events per year. With 10^7 tons, several different sources of neutrinos become detectable.

4. Conclusions. We conclude that a neutrino detector of $\geq 10^6$ tons on the moon--i.e., one considerably more compact than the proposed DUMAND array--would open up a new window of neutrino astronomy, making possible the study of neutrinos at 1 to 10^3 GeV.* The effort must probably await the establishment of a substantial lunar colony. Because of its large size, the detector would probably have to be locally constructed (perhaps of glass fabricated from lunar materials.)

5. Acknowledgments. One of the authors (MMS) expresses his appreciation to Professors R. Kippenhahn and W. Hillebrandt for their hospitality at the Max Planck Institut für Astrophysik in Garching. He thanks Professor F. Reines for stimulating his interest in this problem.

*Even a smaller detector of 10^4 tons could detect a giant solar flare like that of Feb. 23, 1956. The pulse is likely to be of such short duration (<20 min) that the atmospheric background would not degrade terrestrial observation.

References

Berezinsky, V.S. (1976), Proc. of the 1976 DUMAND Workshop, Univ. of Hawaii, Honolulu, ed. A. Roberts, p. 229 ff.

Cherry, J.L. and Lande, K. (1985), Lunar Bases and Space Activities Symp.

Eichler, D. (1980) Proc. of 1980 DUMAND Symp. Hawaii DUMAND Center, 2, 266.

Erofeeva, I.N., Lyotov, S.I., Murzin, V.S., et al. (1983) Proc. 18th International Cosmic Ray Conf., Bangalore, India, 7, 104.

Grindlay, J.E., Band, D., Seward, F., Leahy, D., Weisskopf, M.C. and Marshall, F.E. (1984), Ap. J. 277, 286.

Peterson, V.Z. (1983), Deep Underwater Muon and Neutrino Detection, Composition and Origin of Cosmic Rays, ed. M.M. Shapiro, Reidel Publ. Co., Dordrecht, p. 261 ff., and references therein.

Reines, F. (1965), as reported by M.M. Shapiro in "Galactic Cosmic Rays," Proc. NASA 1965 Summer Conference on Lunar Exploration and Science, NASA SP-88, National Aeronautics and Space Administration, Washington, D.C., p. 317, ff.

Shapiro, M.M. and Silberberg, R. (1979), Proc. of the 16th International Cosmic Ray Conf., Kyoto, Japan, publ. by Univ. of Tokyo, 10, 363.

Silberberg, R. and Shapiro, M.M. (1979), Proc. of the 16th International Cosmic Ray Conf., Kyoto, Japan, publ. by Univ. of Tokyo, 10, 357.

Stecker, F.W., Shapiro, M.M. and Silberberg, R. (1979), Proc. of the 16th Internatinal Cosmic Ray Conf., Kyoto, Japan, publ. by Univ. of Tokyo, 10, 346.

HE 5.3-22

CHARACTERISTICS OF SLOW PARTICLES EMITTED IN THE CHARGED CURRENT INTERACTIONS OF NEUTRINOS WITH EMULSION NUCLEI

E-531 Collaboration

Spokesperson:N.W.Reay,Department of Physics,Ohio state university,174 West 18th Avenue,Columbus, Ohio 43210, USA.

To be presented by:A.EL-Naghy,Physics Department,Faculty of Science,Cairo University,Giza,EGYPT.

ABSTRACT

Multiplicity,angular and energy distributions of secondary particles, produced in the charged current inelastic interactions of high energy neutrinos with emulsion nuclei,were investigated.

1. Introduction.

In the charged current neutrino induced reactions on nuclei, a negative muon is emitted and a d-quark in a nuclear nucleon absorbing a W^+ boson, changes into a u-quark or a c- quark . This quark propagates inside the nucleus either singly or after immediate recombination into a meson, forming a leading particle system (LPS). The LPS may interact further with a nucleon inside the target nucleus with an effective cross section σ_0'. The value of σ_0' may depend on whether the LPS is a c-quark, u-quark, charmed meson or non-charmed meson . In each of these cases, the value of σ_0' may be reflected in grey track particle multiplicity distribution and its mean value observed in the final state. The aim of this paper is to test whether there is a difference in σ_0' for "charm" and "non-charm" events. Also, the study of the general characteristics of neutrino - emulsion charged current interactions . These characteristics are compared to the corresponding ones from proton - emulsion (P-Em) collisions.

2. Experiment.

The charged current interactions of neutrinos with emulsion nuclei were picked up from those observed in a hybrid emulsion spectrometer which was used in the Fermilab experiment E-531 to study charm particle lifetimes /1/ and their production cross sections /2/. The details of the performances of the apparatus and exposures were presented in /3/.

For the present study, the following selection criteria have been applied : (i) the event must be at least 20 mm apart from the stack edges. (ii) The event should include identified negative muon. The 260 events were selected, out of them 192 events with $N_h \geq 1$. These data were compared with events in which charmed particles were produced and a negative muon was identified without applying the geometrical cut mentioned in the criterion (i).These two sets are compared to each other and to proton - emulsion data /4/.

3. Multiplicities of Secondary Particles.

The table presents the average multiplicities of s,h,g and b particles emitted in "non-charm" and "charm" ν-Em charged current inelastic interactions. These values are compared to the corresponding ones from P - Em collisions at 22.5 GeV/4/.

Average multiplicity → / Class of events ↓	$\langle n_s \rangle$ * without $\bar{\mu}$	$\langle n_h \rangle$	$\langle n_g \rangle$	$\langle n_b \rangle$
"non-charm"	5.52±.15 * 4.52±.15	3.99±.30	1.35±.13	2.64±.25
"charm"	4.60±.26 * 3.60±.26	3.60±.60	1.23±.22	2.37±.37
P - Em at 22.5 GeV	5.61±.01	8.60±.25	3.38±.14	5.22±.29

The table shows that $\langle n_s \rangle$ for "charm" events is less than the corresponding one for "non charm" events by $0.85 \pm .30$ Such a difference could be explained by the copious D^0 meson production and generally by the fact that charmed particles are heavy ones which are usually produced with a relatively high momentum. The similarity of $\langle N_h \rangle, \langle n_g \rangle, \langle n_b \rangle$, observed in the table, between "charm" and "non-charm" events, indicates that there is no difference between a leading charmed or non-charmed particle. The table shows that for P-Em these values are about 1.5 times the corresponding ones from the ν-Em events. This observation can be explained by the known fact that hadrons tend to interact as soon as they enter the hit nucleus and after the first collision, there is still a considerable nuclear matter for the leading particle to propagate through it. Neutrino can interact at any point inside the target nucleus. Thus, the degree of intranuclear cascading in case of hadrons is more than the neutrino one.

The ratio of $n_g=0$ events, in ν-Em interactions , was calculated roughly from simple considerations of the quark theory and emulsion composition. Neglecting the cascading effects, the calculated value 0.4 agrees with the experimental value 0.5 ± 0.1 . This shows that the number of intranuclear cascading is very small in this case. The study of correlations between different multiplicities has shown that the excitation energy of the residual nucleus is independent on the number and nature of produced particles (pions or charm particles) i.e. these produced particles do not transfer any significant energy to the target nucleus.

4. Angular and energy distributions.

It is a remarkable feature that grey track particles from "charm" and "non-charm" events have the same angular distribution of the form $\frac{1}{N_{tot}} \frac{dn}{d\cos\theta_g} \simeq \exp(0.83 \pm 0.13) \cos\theta_g$ which agrees with the corresponding one in hadron - nucleus collisions $\frac{1}{N_{tot}} \frac{dn}{d\cos\theta_g} \simeq \exp(0.96) \cos\theta_g$

The forward peaked behaviour and the increase in the value of F/B ratio with the increase in particle track

range support the assumption that grey track particles are knock on receils. The energy distribution of grey track particles, assumed to be protons, from "non-charm" events has the form $N(E)\,dE \simeq E^{-(1.15 \pm 0.18)}\,dE$.

5. Conclusions.

The measured n_g- multiplicity is consistent with simple quark counting and the number of intranuclear cascading in the present interactions is very small, so the theoretically expected difference in the cross section of a leading charm or non-charm particle has not been observed. The angular distribution of grey track particles has the form

$$\frac{1}{N_{tot}} \frac{dn}{d\cos\theta_g} \simeq \exp(0.83 \pm 0.13) \cos\theta_g$$

and their energy distribution is of the form

$$N(E)\,dE \simeq E^{-(1.15 \pm 0.18)}\,dE$$

6. Acknowledgement.

A.EL-Naghy would like to express his thanks to the Japan Society for Promotion of Science for awarding him a one year fellowship and to Prof.K.Niu for various aspects.

7. References.

1. N.Ushida et al.,Nucl. Inst. 224 (1984) 50.

2.N.Ushida et al.,Phys. Lett. 121B (1983) 287;
Phys. Lett. 121B (1983) 292.

3. N.Ushida et al., Phys.Rev.Lett.45 (1980)1049;
Phys.Rev.Lett.45 (1980)1053;
Phys.Rev.Lett.47 (1981)1694;
Phys.Rev.Lett.48 (1982) 844.

4. H.Winzler , Nucl. Phys. B56 (1973) 333.

QCD ANALYSIS OF NEUTRINO CHARGED CURRENT STRUCTURE FUNCTION F_2 IN DEEP INELASTIC SCATTERING

Mohammad Saleem
Centre for High Energy Physics
University of the Punjab
Lahore-20, Pakistan

and

The Institute for Basic Research
96 Prescott Street, Cambridge
Massachusetts 02138
U.S.A.

AND

Fazal-e-Aleem
Centre for High Energy Physics
University of the Punjab
Lahore-20, Pakistan.

ABSTRACT

An analytic expression for the neutrino charged current structure function $F_2(x,Q^2)$ in deep inelastic scattering, consistent with quantum chromodynamics, is proposed. The calculated results are in good agreement with experiment.

1. Introduction. Recently, the CCFRR group[1] has measured the neutrino charged current structure functions. The data were obtained using the Fermilab narrow band beam and the Laboratory E neutrino detector[2-4]. The structure function $F_2(x,Q^2)$ extracted from the neutrino and antineutrino event samples is plotted versus Q^2 in Fig.1.

A number of attempts have been made to fit the data for lepton-nucleon deep inelastic scattering by using QCD. The analyses are based on fitting of Altarelli-Parisi (A-P) equations. For a fixed $Q^2=Q_o^2$, the structure function F_2 is assumed to be of a particular form, so as to give x dependence consistent with experimental data at Q_o^2. The A-P equations are then solved numerically to yield results which are consistent with experiment. The arbitrariness of Q_o^2 is, however, restricted to sufficiently large values of Q_o^2 for which perturbative calculations can be trusted. In this paper, an analytic expression for $F_2(x,Q^2)$, consistent with QCD, is proposed.

2. Calculations and Discussion. According to QCD, the singlet structure function $F_2(x,Q^2)$ and its momenta are related to each other[5] by the equation

$$\int_o^1 x^{n-2} F_2^s(x,Q^2)dx = \delta_s^2 A_n^s [\ln(Q^2/\Lambda^2)]^{-d_s^n} \qquad (1)$$

The function $F_2(x,Q^2)$ can not be expressed as a product of

two functions, one depending upon x only and the other depending upon Q^2 alone, because then the function of Q^2 alone as evaluated by using left hand side of equation(1) would be independent of n. This is not valid because right hand side of equation(1) depends upon n. To incorporate this n dependence, we assume that

$$F_2(x,Q^2) = A(1-x)e^{-ax}$$

where $$a = [\ln(Q^2/\Lambda^2)]^{0.747}$$

For large value of Q^2, this expression when substituted in equation(1) gives results which are consistent with QCD.

A very good agreement with experimental data for $Q^2>5$ $(GeV/c)^2$ is obtained by using A=2, Λ=0.5GeV/c.

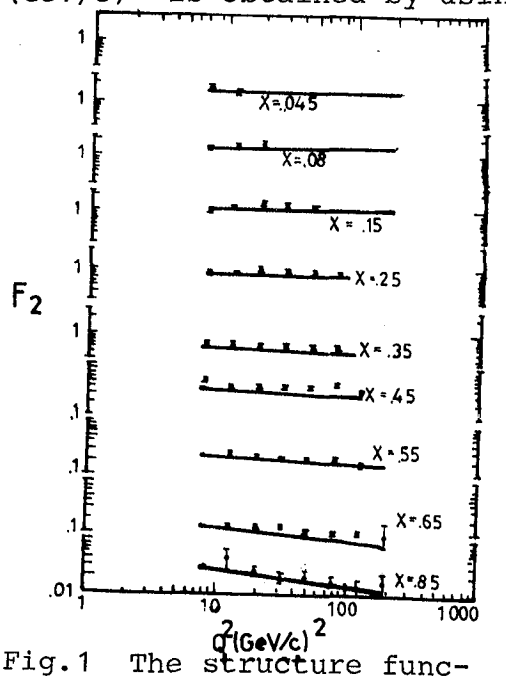

Fig.1 The structure function F_2 extracted from the CCFRR data versus Q^2 for fixed values of x. The solid curves represent the predictions of the model described in the text.

Fig.1 shows experimental data as well as theoretical predictions for $F_2(x,Q^2)$ plotted against Q^2 at fixed values of x. The agreement is quite satisfactory and confirms our assumption about the form of $F_2(x,Q^2)$.

3. Conclusion. Quantum chromodynamics is now believed to be the promising theory of strong interactions. The perturbative calculations of cross sections for deep inelastic scattering based on QCD are confirmed experimentally. However, numerical integration has to be performed to obtain various results. We have proposed a simple analytic expression for the structure function $F_2(x,Q^2)$. This expression yields results which are consistent with experiment.

4. Acknowledgement. The financial assistance from the Pakistan Science Foundation under contract No.P-PU/Phys(11/2) is gratefully acknowledged.

References

1. R.E.Blair et al., Preprint UR-831, COO-3065-339(1983).
2. P.Rapidis et al., Proceedings of the Summer Institute on Particle Physics, ed. A.Mosher, p.641, SLAC, Standford, California (1982).
3. R.Blair, Total Cross Section and -Distribution Measurements for Muon-Type Neutrinos and Antineutrinos in Iron, Ph.D. Thesis(1982), California Institute of Technology, Pasadena, California.
4. J.Lee, Measurements of υ_μN Charged Current Cross Sections from E_υ=25 GeV to E_υ=360 GeV, Ph.D. Thesis(1980), California Institute of Technology, Pasadena, California.
5. A.J.Buras, Rev.Mod.Phys.52, (1980)199.

ANGULAR DISTRIBUTION OF MUONS PRODUCED BY COSMIC RAY NEUTRINOS IN ROCK

Boliev M.M., Buckevich A.V., Chudakov A.E.,
Leonov-Vendrovsky A.V., Mikheyev S.P., Zakidyshev V.N.
Institute for Nuclear Research the USSR Academy of Science,
60th October Anniversary pr., 7a, 117312, Moscow, USSR

At present, measurement of the upgoing muons flux, produced by cosmic ray neutrinos is aiming at:
i) search for neutrino oscillation,
ii) search for extraterrestrial neutrinos from local sources,
iii) search for any hypothetical neutral penetrating radiation different from neutrinos.
In this paper we analyze experimental data of Baksan underground telescope on intensity of upward muons for three years of living time, having in mind mainly neutrino oscillation.

1.EXPERIMENTAL DATA. Baksan neutrino experiment[1,2] is in operation from December 1978. To distinguish upward particles from downward ones time-of-flight method is used. Fig.1 shows distribution of recorded muons as a function of c/v (v-measured velocity of particles and c-velocity of light). Value of ratio $c/v>0$ correspond to downgoing muons and $c/v<0$ to upgoing ones. It is seen that time resolution of Baksan underground telescope allows to select upward muons with high reliability.

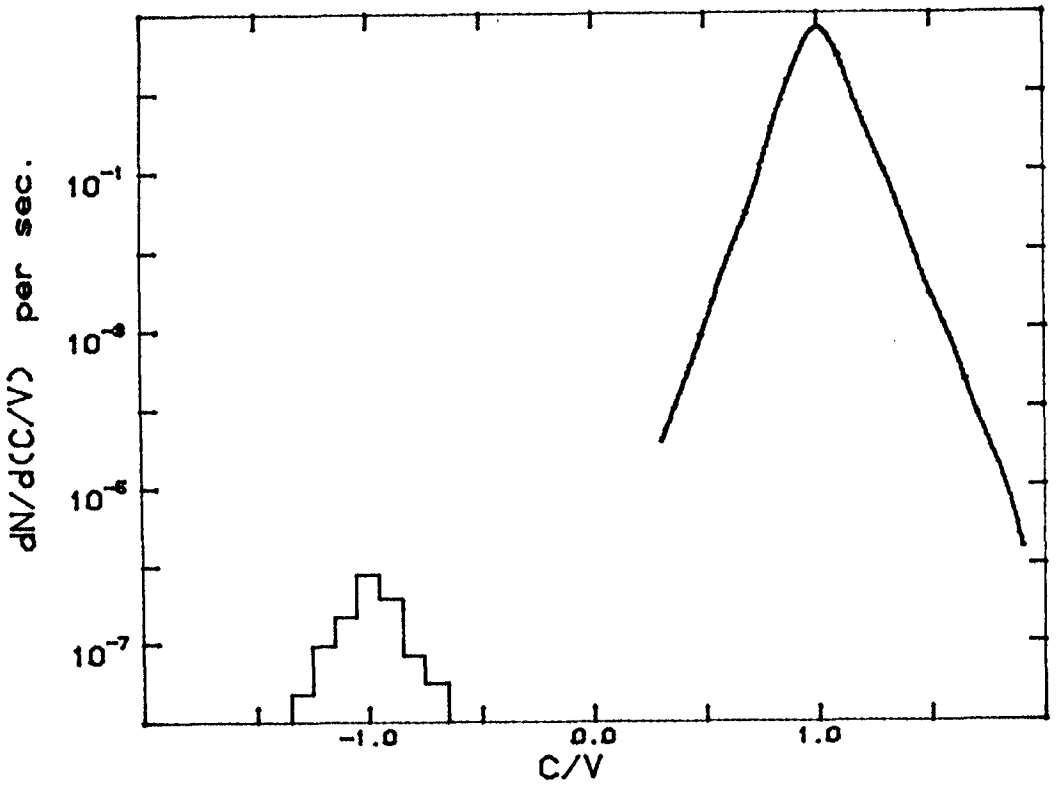

Fig.1 Separation of upgoing and downgoing muon trajectories.

371 events with zenith angles $\theta>90^{o}$ have been recorded. However significant part of them, generaly near horizontal direction, arised due to scattering at large angles of atmospheric muons in surrounding rock. Calculations show that intensity of scattered muons rapidly decreases while zenith angle increases and for $\theta>110^{o}$ is negligible. In zenith angle range $90^{o}<\theta<110^{o}$ effect from scattering is very large only for half of total azimuth angle 2π and is negligible for another half. Taking this into account, we selected 150 events as neutrino muons. In 139 events the trajectory of penetrating particle was seen, which crossed $>600 g/cm^2$ of matter. In 10 events muons stopped inside telescope and there is one cascade without penetrating particle (E 40GeV).

2.RESULTS AND DISCUSSION. Fig.2 shows the ratio of observed intensity to calculated one versus zenith angle. It is seen that there is no discrepancy between observation and prediction for zenith angle range $>130^{o}$, which is most sensitive to neutrino oscillations. Solid curves 1 and 2 were calculated for vacuum neutrino oscillations[3] with maximal mixing of two type of neutrinos ($Sin^2 2\theta=1$) and for difference of square masses 10^{-2} and 10^{-3} eV^2 correspondingly. Neutrino flux[4] and accelerator data on neutrino cross section was used for calculation. Upper limit $m^2<2\cdot10^{-3} eV^2$ (90% c. l.) follows from comparison of observed rate of neutrino events with predicted one for zenith angle $\theta>130^{o}$.

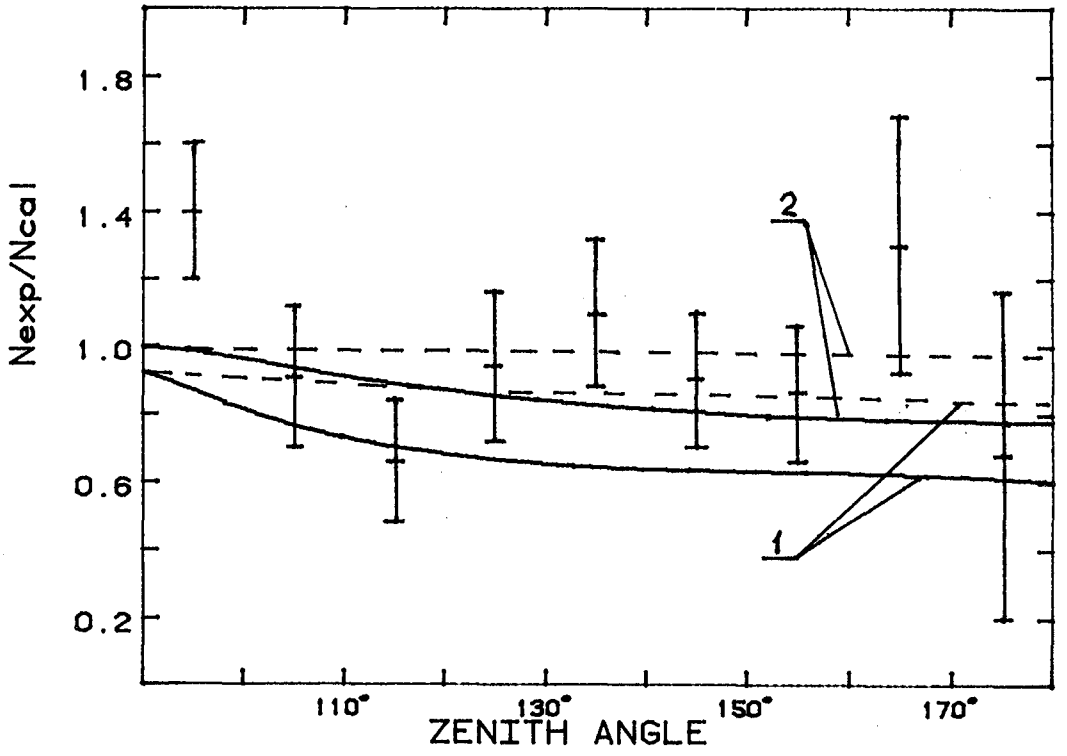

Fig.2 Angular distribution of neutrino induced events.

However, neutrinos pass through a large distance of terrestrial matter before interactions. It was shown[5] that matter can modify vacuum oscillation significantly at distance of the order of the size of the globe. The basis of this phenomena is that index of neutrino refraction in matter can produce an important change of phase. There are two possibilities to apply this idea: i) neutrinos are massive and vacuum oscillations exist; ii) neutrino are massless (vacuum oscillations are impossible).

First consider matter effect on vacuum oscillations[6]. The matter modifies vacuum oscillations because of difference in the amplitudes of elastic forvard scattering of ν_e and ν_μ which is due to charge current ν_e-scattering on electrons. In this case parameters of neutrino oscillations are:

$$\mathrm{Sin}^2 2\theta_m = \frac{\mathrm{Sin}^2 2\theta}{(1-2\cdot L_\nu/L_o\cdot \mathrm{Cos}2\theta+L_\nu^2/L_o^2)} \qquad (1)$$

$$L_m = \frac{L_\nu}{(1-2\cdot L_\nu/L_o\cdot \mathrm{Cos}2\theta+L_\nu^2/L_o^2)^{1/2}} \qquad (2)$$

Here $L_\nu=4\pi E/\Delta m^2$ is the oscilation length in vacuum and $L_o=1.77\cdot 10^7 m/\rho$ is characteristic length for 2π change of phase which depends on matter density (ρ) only. From (1) we see that for maximal mixing ($\mathrm{Sin}^2 2\theta=1$) of neutrinos in vacuum the parameter $\mathrm{Sin}^2 2\theta_m$ is less than 1 for any values of the oscillation length in vacuum. So, in this case matter effect results in suppression of vacuum oscillations. Dashed curves on Fig.2 were calculated for the same oscillation parameters as solid curves but matter effect was taken in account. One can see that impact of neutrino oscillations on the flux of neutrino induced muons is significantly less in this case. Therefore our limit on Δm^2 for ν_μ-ν_e oscillations changes to $2\cdot 10^{-2} eV^2$. Note that if oscillations ν_μ- ν_e occur and probability of transitions is suppressed then previous limit on Δm^2 holds.

Oscillations of massless neutrinos. In this case oscillations can arise due to nondiagonal neutral current interactions. In neutral current interactitions ν_μ states can change into ν_e or ν_τ. Probability to observe ν_μ after traversing distance x of constant density is given by

$$P=1-\mathrm{Sin}^2 2\theta\cdot \mathrm{Sin}^2(\pi\cdot\rho\cdot x/L)$$

where in case of ν_μ-ν_τ oscillation $\mathrm{Sin}^2 2\theta=1$, $L=1.77\cdot 10^7 m/(g_p+g_e+g_n)\mathrm{Sin}\alpha$; and for ν_μ-ν_e

$$\mathrm{Sin}^2 2\theta = \frac{4\cdot \mathrm{Sin}^2\alpha (g_p+g_e+g_n)^2}{1+4\cdot \mathrm{Sin}^2\alpha (g_p+g_e+g_n)^2}$$

and

$$L = \frac{1.77\cdot 10^7 m}{\sqrt{1+4\cdot \mathrm{Sin}^2\alpha (g_p+g_e+g_n)^2}}$$

$\mathrm{Sin}\alpha$ is the contribution of nondiagonal neutral current in interactions. In usual theories of neutral current interactions this parameter is zero. However it is impossible to exclude $\mathrm{Sin}\alpha\neq 0$ because of invisibility of final states of neutrinos. In standard model of electroweak interactions $|g_p+g_e+g_n|=0.5$. Con-

trary to the vacuum oscillations, this kind of oscillations do not depend on energy of neutrinos. These oscillations, if they occur, can change strongly angular dependence of cosmic ray neutrinos traversing the Earth. On Fig.3 curves calculated for $\sin\alpha$=0.1, 0.2 and 0.3 are shown. Comparison of observed angular distribution of neutrino events with calculated ones for this type of oscillations permits to set upper limit on $\sin\alpha$ as 0.2 (90%c.l.)

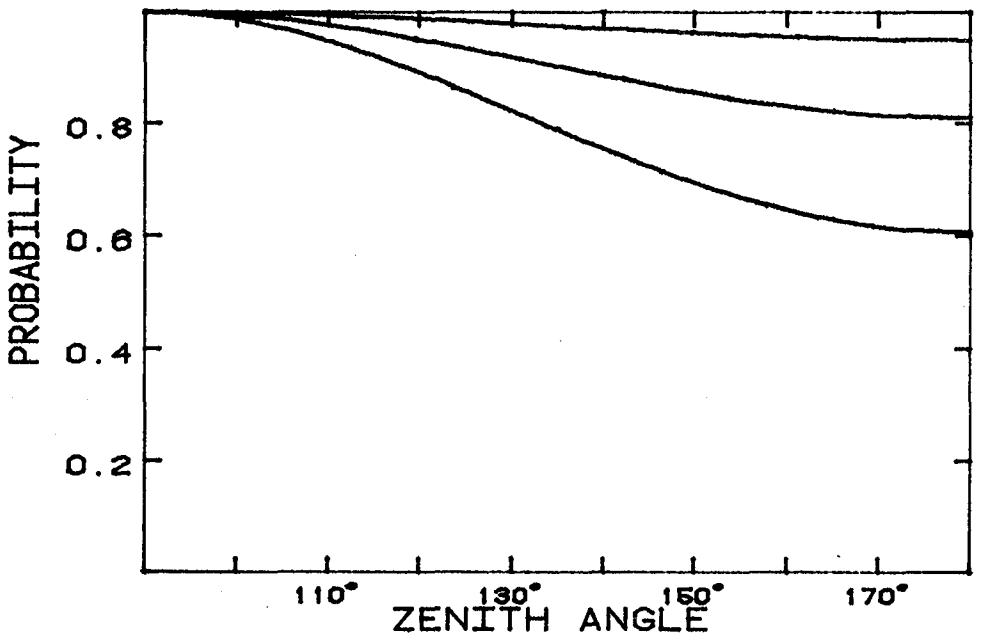

Fig 3. The probabilities of remaining muon neutrinos after traversing the Earth.

3.CONCLUSION. In this paper we assumed maximal mixing of two types of neutrinos. Obviously, if mixing decreases effect of neutrino oscillations decreases too. So there is no hope to see oscillations with small mixing using cosmic ray neutrinos. Moreover, matter effect reduces by an order of magnitude the sensitivity of underground neutrino experiments to vacuum neutrino oscillations. However, this kind of experiments is, apparently, a single possibility to search another type of oscillation arising due to nondiagonal neutral current.

REFERENCE

1.Chudakov A.E. et al Proc.16th ICRC v10,p.287 (1979) Kyoto
2.Boliev M.M. et al Proc. NEUTRINO-81 v1,p.283 (1982) Honolulu
3.Bilenky S.M.,Pontecorvo B. Phys.Rep. 41C, 225 (1978)
4.Volkova L.V. Sov. J. Nucl.Phys. 31, 1510 (1980)
5.Wolfenstein L. Phys. Rev. D17, 2369 (1978)
6.Ramana Murthy P.V. Proc.18th ICRC v7, p.125 (1981) Bangalore

HE 5.4-1

UNDERGROUND MEASUREMENTS ON SECONDARY COSMIC RAYS.

Wilson, C.W., Fenton, A.G., Fenton, K.B.
Physics Department, University of Tasmania, Australia.

INTRODUCTION. This report summarizes some recent measurements made at the Poatina cosmic ray station (41.8 S 149.9 E, 347 m.w.e.) from August 1983 July 1984. The cosmic ray primary particles responsible for events detected at the station have a median primary energy of 1.2 TeV. The motivation for part of this work has come from the reported detection of narrow angle anisotropies in the arrival direction of cosmic rays (e.g. 1,2,3).

EQUIPMENT. A new particle telescope composed of 2 metre long, 10 cm diameter proportional detectors was installed at the Poatina station early in 1983. The detectors are arranged in four layers, each layer contains 19 detectors situated side by side to form a flat plane of detectors. These layers of detectors are arranged as two upper and two lower sets with the detector axes at right angles for the layers within each set. The side elevation of the telescope is shown in figure 1.

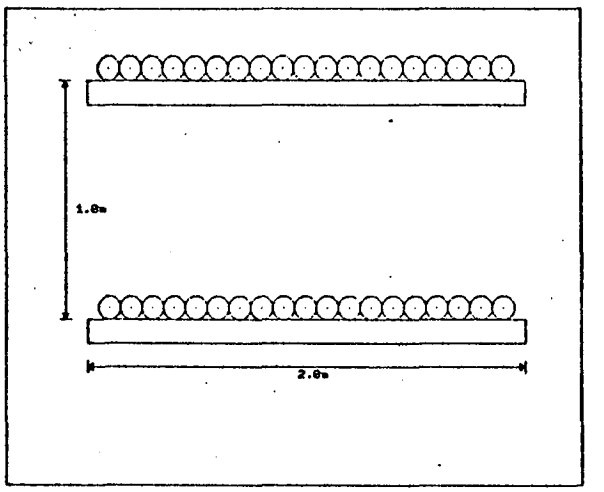

Figure 1. Side elevation of the telescope.

When a coincidence is detected between the four layers, the status of each detector is recorded by a small on-line computer. These events are accumulated for a period of 20 minutes, and are then stored as a record on magnetic recording tape. Additional information such as date, time and total count rate are also stored as part of each record. The telescope detects 2000 events per hour, and the quantity of data generated per week is 2 megabytes. The magnetic recording tapes used were good quality C90 audio tapes, and the recording principle was pulse width modulation at a data rate of 6600 bits per second on two tracks.

Due to the layout of the detectors, the arrival direction, the number of particles and the lateral spread of particles for each event can be estimated. The angular sensitivity pattern of the telescope is shown in figure 2 along one half of one axis of the telescope.

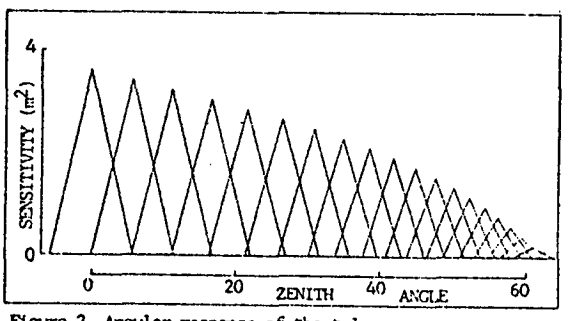

Figure 2. Angular response of the telescope.

ANALYSIS. The events containing more than one particle are analysed for arrival direction, particle muliplicity and particle spread by comparing the arrangement of triggered detectors in the upper and lower sets of detectors. The analysis scheme assumes events contain only high energy particles, and all particles in an event are travelling parallel to each other. Due to the relatively low spatial resolution for particle positions within the telescope, it is only possible to decode events which have particles travelling close to parallel with all particles passing through each layer of detectors. Multiple particle events that cannot be sensibly analysed are classified as complex, and by visual inspection appear to be mainly single particle events with one additional detector involved - possibly due to to a knock-on electron or random background coincidences. About 18% of the the total number of events contain more than one particle, and 25% of these events could be sensibly analysed.

The remaining events were consistent with only one particle traversing the telescope. The single particle events that were detected in the central 9 x 9 direction bins of the telescope were accumulated into local intensity maps - i.e. a map per 20 minute observation period (the 20 minute observation time was chosen so the angular movement of the telescope due to the Earth's rotation was similar to the 5 degree angular resolution of the telescope). For each 20 minute observation period, the count recorded for each of these 81 direction bins was normalized against the total count for all the 81 bins and the long term response of the telescope. This process removes wide angle variations such as atmospheric effects, and any variation in detector efficiency.

Celestial intensity maps are generated by averaging the intensities detected in telescope bins which have their central direction contained within common regions of 6 degrees in right ascension and 6 degrees in declination. These celestial maps are produced for each sidereal rotation of the Earth, and can then be combined as required.

RESULTS. The relative rate of detection of multiple particle events is shown in figure 3, and the spread of the particles in multiple events is shown in figure 4. Both rates have been adjusted for the loss of sensitivity caused by the finite size of the telescope. There are three contributions to figure 4: Below 0.2 metres there is a contribution from muons with an associated knock-on particle, below 0.8 metre separation there is a contribution apparently arising from rock showers, and outside this separation the events are assumed to result from multiple muons from atmospheric interactions.

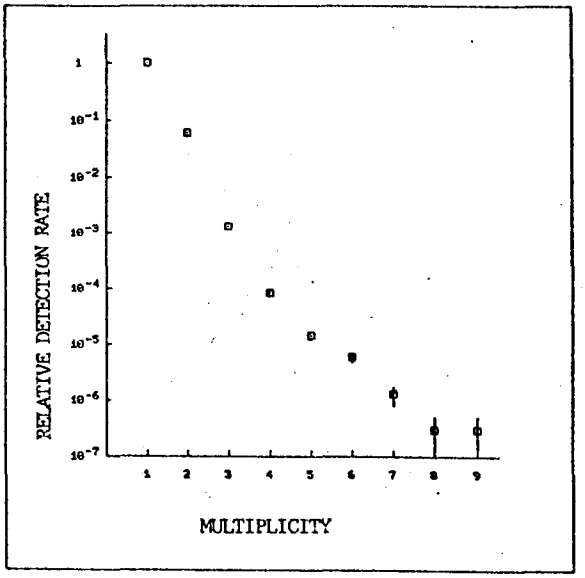

Figure 3. Relative detection rate versus particle multiplicity.

The roughness of intensity with respect to celestial coordinates has been considered by comparing the measured r.m.s. deviation of intensity to that expected from counting statistics. This comparison as a function of declination is shown in figure 5 (the errors are 1 s.d.), and it can be seen that apart from the -31 and -37 degree declination bands, the variation is explained completely by Poisson error. The declination band centred on -31 degrees contains a large positive excess at R.A. = 36 degrees, and this feature may be responsible for the excessive deviation in the -31 and -37 declination bands. It appears that this excess is due to a narrow angle flux of 1.3 +/- 0.3 x 10-8 particles/cm2/sec.

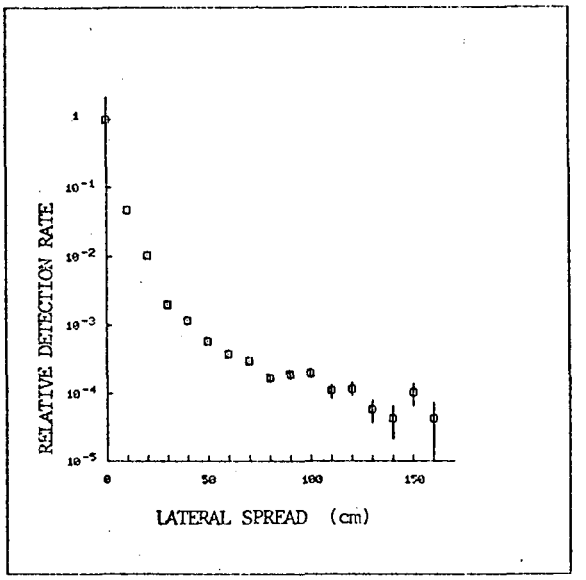

Figure 4. Relative detection rate versus lateral particle spread.

DISCUSSION. The right ascension of this excess (2.4 h) coincides with the phase of a previously detected sidereal anisotropy (4). The previous anisotropy was measured at Poatina with wide angle telescopes (semi-cubic geometry), and the amplitude is consistent with the anisotropy being produced by the narrow angle feature reported here. Measurements made in the northern hemisphere (e.g 5) have established the existence of a sidereal anisotropy with similar amplitude and phase to the wide angle measurements at Poatina, but it is unlikely that the narrow angle anisotropy at declination -37 degrees would have much effect on these measurements. This suggests that the sidereal anisotropy detected at Poatina is a narrow angle anisotropy, and may not have the same origin as northern hemisphere measurements. The consistency with the previous measurements which were reported for the period 1972 to 1974 suggests that the feature is stable with time.

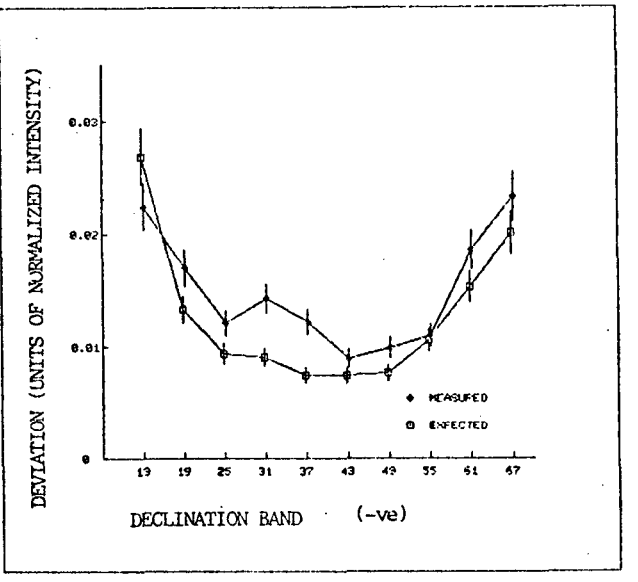

Figure 5. Standard deviation of normalized intensity for different declination bands.

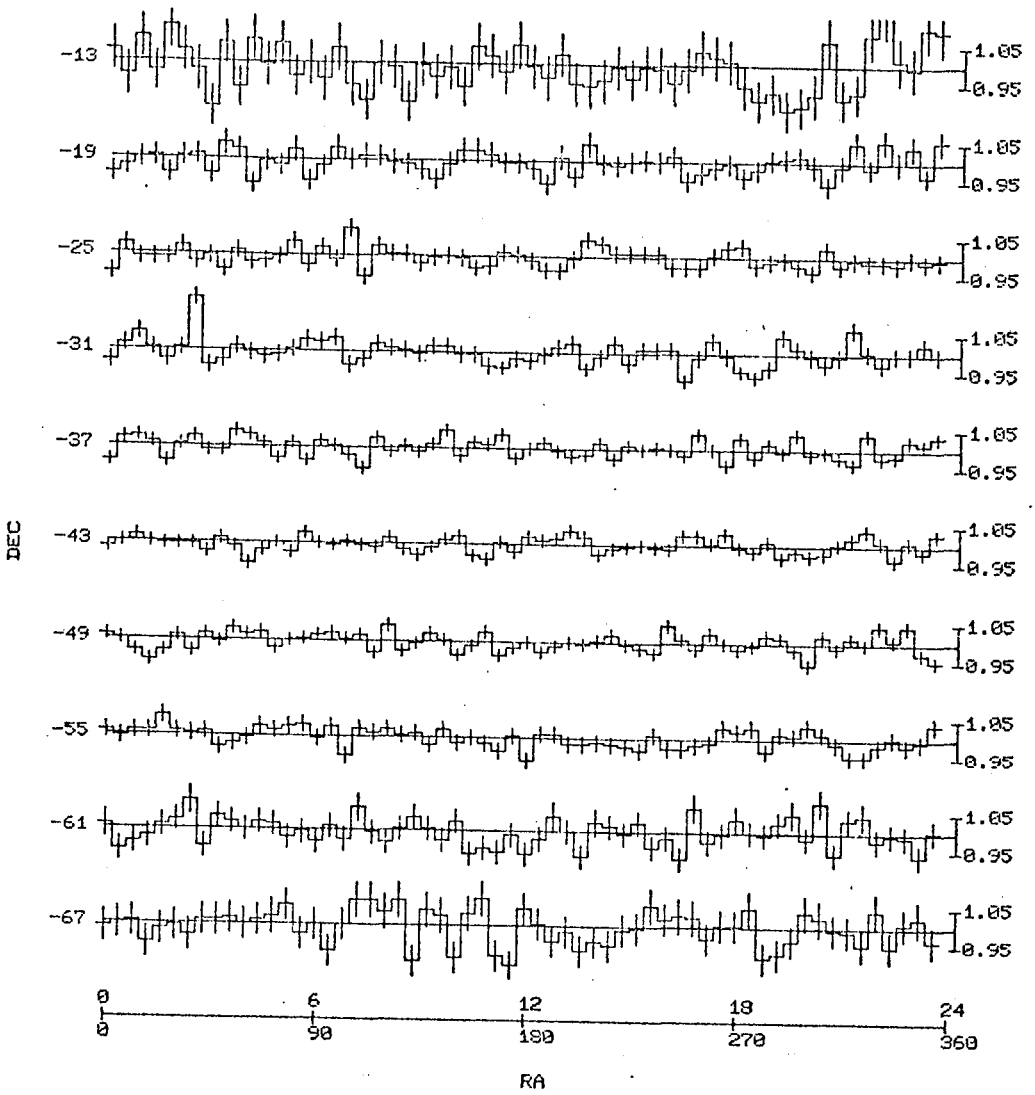

Figure 6. Celestial map of normalized intensity. This map has been produced by using data from every fifth day. The smearing due to sampling in solar time is minimised, and the amplitude of the anisotropy is slightly greater than for the total data set.

REFERENCES.

(1). Sekido, Y., Yoshida, S., Kamiya, Y., Phys. Rev. 113, p1108 (1959).
(2). Bukata, R.P., Standil, S., Can. J. Phys. 43, p883 (1965).
(3). Bazer-Bachi, A.R., Vedrenne, G., Sheldon, W.R., Benrook, J.R., 14th ICRC (Munich) 12, p4151 (1975).
(4). Fenton, A.G., Fenton, K.B., 14th ICRC (Munich) 4, p1482 (1975).
(5). Yasue, S., Mori, S., Sagisaka, S., Ichinose, M., 18th ICRC (Bangalore) 3, p387 (1983).

MULTIPLE MUONS OF CONVENTIONAL AND EXOTIC ORIGIN IN DUMAND

Peter K. F. Grieder
Physikalisches Institut
University of Bern
Switzerland

ABSTRACT

We present a first summary of results from a theoretical analysis, based on hadron - muon cascade calculations, that yield relative intensities of very high energy multiple muons originating from ultra high energy interactions initiated by primary protons and iron nuclei in the atmosphere, under consideration of normal as well as direct and exotic production channels. Lateral density distributions and target diagrams will be presented which show that only very large detectors, such as DUMAND, will be able to record multiple muons of conventional origin reliably. This, however, is a prerequisit for any primary mass determination based on multiple muon data.

On the other hand, detection of multiple muons originating from direct and particularly from exotic processes are likely to carry large transverse momenta. Such muons are partly intermixed with muons of conventional origin but tend to spread out in general to much larger distances from the axis of the event, which excludes their detection and identification with smaller installations.

Since all particles in our simulation calculations carry genetic information, such as the generation number of the interaction of their or, in the case of muons, their parent's origin with respect to the first interaction of the primary in the atmosphere, the height of the location of the respective interaction above sea level, and other relevant tags that identify their origin, we are able to carry out detailed studies on multiple muons and their likely origin.

Atmospheric Muons and Neutrinos, and the Neutrino-Induced Muon Flux Underground.

A. Liland
N-9785 Veidnesklubben
Norway

ABSTRACT

The diffusion equation for neutrino-induced cosmic ray muons underground has been solved. The neutrino-induced muon flux and charge ratio underground have been calculated. The calculated horizontal neutrino-induced muon flux in the energy range 0.1 - 10000 GeV is in agreement with the measured horizontal flux. The calculated vertical flux above 2 GeV is in agreement with the measured vertical flux. The average charge ratio of neutrino-induced muons underground was found to be $\mu^+/\mu^- = 0.40$.

1. Introduction

From the decay of charged mesons in the atmosphere ($\pi^\pm \rightarrow \mu^\pm + \nu$, $K^\pm \rightarrow \mu^\pm + \nu$) the intensity of cosmic ray muons at sea-level is obtained and compared with measured spectra (1). Then we consider neutrinos in stead of muons from the same decays and obtain the neutrino intensity and these neutrinos give neutrino-induced muons.

2. The neutrino Spectrum

We expect the neutrino spectrum to have the form

$$\mathcal{V}(E_\nu, \theta) = E_\nu^{-(\gamma+1)} f(E_\nu, \theta)$$

and approximate $f(E_\nu, \theta)$ by

$$f(E_\nu, \theta) = C(E_\nu)\left\{ \frac{G_{N\pi} R_{\nu\pi}^{\gamma}}{1 + \frac{E_\nu \cos\theta}{R_{\nu\pi} B_\pi(\theta)}} + C_K \frac{G_{NK} R_{\nu K}^{\gamma}}{1 + \frac{E_\nu \cos\theta}{R_{\nu K} B_K(\theta)}} \right\}$$

$R_{\nu\pi} = 0.25$ ($E_\nu = R_{\nu\pi} E_\pi$), $R_{\nu K} = 0.56$ ($E_\nu = R_{\nu K} E_K$)
$C_K = 0.635$ (Branching ratio for $K \rightarrow \mu + \nu$ decay) $G_{N\pi} \approx 0.07$
$G_{NK} \approx 0.009$ (1). $B_\pi(\theta)$ is the average decay constant for π's at zenith angle θ. $B_K(\theta)$ is the average decay constant for K's at zenith angle θ. $C(E_\nu)$ is only a little energy dependent and is obtained by comparing $\mathcal{V}(E_\nu, \theta)$ as given above with the calculated neutrino intensities.
$C(E_\nu) \approx 3.57$.

3. Neutrino-Induced Muons

The neutrino nucleon total cross section is given by
$\sigma_\nu = S_\nu \cdot 10^{-38} E_\nu$ cm^2, E in GeV
The neutrino intensity at depth h (g/cm^2) is then

$$\nu(E_\nu, h, \theta) = \nu(E_\nu, \theta)\, e^{-\frac{h E_\nu}{\Lambda_\nu}}, \qquad \frac{1}{\lambda_\nu} = \frac{E_\nu}{\Lambda_\nu}$$

$\lambda\nu$ is the interaction length for neutrinos. We introduce a maximum energy, E_{max}, for the validity of the cross sections given above and take $\nu(E_\nu, h, \theta) = 0$ for $E_\nu > E_{max}$ in calculation of muons induced by neutrinos. The diffusion equation for muons is

$$\frac{\partial \mu_\nu(E_\mu, h, \theta)}{\partial h} = \int_{E(E_\mu, h)}^{E_{max}} \nu(E', h, \theta) \frac{E'}{\Lambda_\nu} g_{\nu\mu}(E(E_\mu, h)/E') \frac{dE'}{E} e^{-bh}$$

$E = E(E_\mu, h)$ is muon energy at depth h. E_μ is muon energy at depth $h = 0$. We further have (4)

$$g_{\nu\mu^-}(u) = \frac{3}{16.75}(5.25 + u^2) \text{ from } \frac{d\sigma^\nu}{dy} = \frac{G^2 M E_\nu}{\pi}\{Q + (1-y)^2 \bar{Q}\}$$

$$g_{\bar{\nu}\mu^+}(u) = \frac{3}{8.25}(1 + 5.25\, u^2) \text{ from } \frac{d\sigma^{\bar{\nu}}}{dy} = \frac{G^2 M E_\nu}{\pi}\{\bar{Q} + (1-y)^2 Q\}$$

$$u = \frac{E(E_\mu, h)}{E'}. \qquad \text{with } \alpha \equiv \bar{Q}/(Q + \bar{Q});\ \alpha = 0.16$$

The energy loss of muons in standard rock was given by

$$-\frac{dE}{dh} = a + bE \qquad E(E_\mu, h) = e^{-bh}\left\{\frac{a}{b} + E_\mu\right\} - \frac{a}{b} \qquad a, b = \text{const.}$$

$$E_\mu = e^{bh}\left\{\frac{a}{b} + E\right\} - \frac{a}{b} \qquad dE_\mu = e^{bh} dE$$

$$\frac{\partial \mu_\nu(E_\mu, h, \theta)}{\partial h} = \int_{E/E_{max}}^{1} \nu(E/u, h, \theta) \frac{E}{u \Lambda_\nu} g_{\nu\mu}(u) \frac{du}{u} e^{-bh}$$

$$\mu_\nu(E_\nu, h, \theta) = \int_0^h \int_{E/E_{max}}^{1} \nu(E'/u, h', \theta) g_{\nu\mu}(u) \frac{du}{u} e^{-bh'} dh' \qquad \left(\frac{E'}{u\Lambda_\nu}\right)$$

$$E' = E'(E_\mu, h')$$

$$\mu_\nu(E, h, \theta) = \mu_\nu(E_\mu, h, \theta)\, e^{bh}$$

$$\mu_\nu(E, h, \theta) = \int_0^h \int_{\frac{E}{E_{max}}}^{1} \nu(E'/u, \theta) E'^{-\gamma} \frac{1}{\Lambda_\nu} u^{\gamma-1} e^{-\frac{h' E'}{u \Lambda_\nu}} g_{\nu\mu}(u)\, du\, e^{b(h-h')}\, dh'$$

$$h = \frac{1}{b}\{\ln(a+bE_\mu) - \ln(a+bE)\} \qquad E' = E'(E_\mu, h')$$

$$h' = \frac{1}{b}\{\ln(a+bE_\mu) - \ln(a+bE')\}$$

$$b(h-h') = \ln\frac{a+bE'}{a+bE} \qquad h' = h - \frac{1}{b}\ln\frac{a+bE'}{a+bE}$$

$$\mu_\nu(E,h,\theta) = \int_0^h \int_{E/E_{max}}^1 \phi(E'/u,\theta) E'^{-\gamma} \frac{1}{\Lambda_\nu} u^{\gamma-1} q_{\nu_\mu}(u) \left\{\frac{a+bE'}{a+bE}\right\}^{\frac{E'}{u\Lambda_\nu b}} e^{-\frac{hE'}{u\Lambda_\nu}} \cdot$$

$$\cdot \frac{a+bE'}{a+bE}\, du\, dh' . \qquad -\frac{dE'}{dh'} = a+bE' \qquad -dh' = \frac{dE'}{a+bE'}$$

$$\left.\begin{aligned} h'=0 &\Rightarrow E' = E_\mu \\ h'=h &\Rightarrow E' = E \end{aligned}\right\} \Rightarrow \int_0^h \dots dh' = \int_E^{E_\mu} \dots \frac{dE'}{a+bE'}$$

$$\mu_\nu(E,h,\theta) = \int_E^{E_\mu} \int_{\frac{E'}{E_{max}}}^1 \phi(E'/u) E'^{-\gamma} \frac{1}{\Lambda_\nu} u^{\gamma-1} q_{\nu_\mu}(u) \left\{\frac{a+bE'}{a+bE}\right\}^{\frac{E_\mu}{u\Lambda_\nu b}} \cdot$$

$$\cdot e^{-\frac{hE'}{u\Lambda_\nu}} du \frac{dE'}{a+bE} .$$

The solution of the diffusion equation for neutrino-induced muons under ground is now

$$\mu_\nu(E,h,\theta) = \frac{E^{1-\gamma}}{a+bE} \frac{1}{\Lambda_\nu} \int_{\frac{E}{E_\mu}}^1 \int_{\frac{E}{wE_{max}}}^1 \phi\left(\frac{E}{wu},\theta\right) w^{\gamma-2} u^{\gamma-1} q_{\nu_\mu}(u) \cdot$$

$$\cdot \left\{\frac{a+bE/w}{a+bE}\right\}^{\frac{E}{wu\Lambda_\nu}} e^{-\frac{hE}{wu\Lambda_\nu}} du\, dw, \qquad \frac{E}{w} < E_{max}$$

Deep underground we put $E_\mu = E_{max}$.

4. Discussion and Conclusion

The diffusion equation for neutrino-induced muons underground has been solved analytically, and the muon intensity is given in an integral form which we evaluate with a computer. We then obtain the calculated vertical muon flux for energies above 2 GeV: $2.02\ 10^{-13}\ sec^{-1}cm^{-2}sr^{-1}$ in agreement with the measured vertical flux above 2 GeV (2) which is $(1.92\pm0.44)\ 10^{-13}\ sec^{-1}cm^{-2}sr^{-1}$. For the horizontal muon flux in the energy range 0.1 GeV - 10000 GeV we obtain the calculated flux $4.62\ 10^{-13}\ sec^{-1}cm^{-2}sr^{-1}$ in agreement with the measured horizontal flux which is $(4.59\pm0.42)\ 10^{-13}\ sec^{-1}cm^{-2}sr^{-1}$ (3). We may conclude that there is no strong diffuse extraterrestrial neutrino source. The average muon charge ratio was found to be 0.40. The charge ratio varies between 0.34 at low energies and 0.47 at medium energies.

References

1. Klemke, G. et al.,The primary energy spectrum 0.1 - 50 TeV derived from high precision muon measurements 17'th ICRC, Paris 1981

2. M.M. Boliev et al., 17'th ICRC, Paris 1981. Vol.7, p.106.

3. M. F. Crouch et al., Phys. Rev. D 18, 2239 (1978)

4. B. C. Barish, Phys. Reports 39C (281) 1978

ANALYSIS OF THE ELECTRON AND MUON COMPONENTS OF E.A.S. AT OBSERVATION LEVEL 700 g.cm^{-2} WITH A SCALE BREAKING INTERACTION MODEL AND "GAMMAISATION" HYPOTHESIS.

J. Procureur
Laboratoire de Physique.Université de Bordeaux I
rue du Solarium
33170 Gradignan (France)

J.N. Stamenov,P.V. Stavrev,S.Z. Ushev
Institute of nuclear research and nuclear energy
Bld. Lenin 72
1184 Sofia (Bulgaria)

ABSTRACT

Scale breaking model and "gammaisation" processes for high energies give a correct description of the longitudinal development of E.A.S. From the analysis of phenomenological characteristics of E.A.S. at Tien-Shan experiment,it follows that for energies near 10^6GeV the secondary particle multiplicity increases with energy faster than is predicted by the accepted scale breaking model.

1. Introduction We simulate the muon and electron components of extensive air showers (E.A.S.) with fixed sizes in the region 10^4-10^6 at mountain altitude. In a previous work the same authors (1) used a scale breaking model (SBM) including parameters in accordance with the results from the SPS collider and in good agreement with KNO scaling model predictions.

The SBM gives a correct description of E.A.S. at Tien-Shan level but is not able to reproduce the longitudinal development of showers.

To obtain a correct position of the maximum of E.A.S. development,we include,as was first proposed by S.I. Nikolski (2),the "gammaisation" hypothesis i.e. a larger emission of γ rays than predicted by the traditional models.

It has been shown (3) that this model gives a correct description of the longitudinal development of E.A.S.

The aim of this work is to verify if the SBM including gammaisation is compatible with the experimental muon component for showers of fixed size.

2. Method Average values of the electronic and muonic sizes,N_e and N_μ,and lateral muonic densities $\rho_\mu(r)$ are simulated by a mixed simulation model including full Monte Carlo procedures for the first interactions of hadrons and analytic approximations for deeper interactions in the atmosphere.

More precisely, the main characteristics are the following :

- p-air cross section increases with energy E
  $\sigma_{p\text{-}air} = 269(1.+0.051\ln(E/100))$ (mb) for $E > 100$ GeV.
  fluctuations are determined by an exponential distribution.
- average charge multiplicity : $\langle n_s \rangle = 0.57+0.584\ln s+0.127(\ln s)^2$
  fluctuations around $\langle n_s \rangle$ satisfy to the KNO scaling.
  The structure function $\Psi(Z)$ is described by a gamma-k relation.
- average value of p_t increases with energy: $\langle p_t \rangle = 0.015\ln E + 0.23$
  distribution is defined by $f(p_t)dp_t = (p_t/p_o^2)\exp(-p_t/p_o)$
- the empirical rule $\langle n_\gamma \rangle = \langle n_s \rangle$ is contradicted by results from $p\text{-}\bar{p}$ collider where the estimation for $\langle a \rangle = \langle n_\gamma \rangle / \langle n_s \rangle$ is 1.4 for $\sqrt{s} = 540$ GeV. (4)

  Compilation of higher energy observations of cosmic rays jets and gamma-ray families is made in ref (2). In this publication the authors estimate that $\langle a \rangle$ could be near five for very high energy collisions.

  To take into account the "gammaisation" hypothesis we use an empirical parametrisation of the p-air interactions for E.A.S. simulations : $\langle a \rangle = 1. + 14\ln(E/10^5)$ for $E > 10^5$ GeV with the condition of saturation $\langle a \rangle \leq 3.$ which seems very reasonnable.
- results for showers with fixed sizes are obtained by :
  $$\chi(N_o) = \int_o^\infty \chi(E) P(E,N_o) \frac{dI(E)}{dE} dE$$, where $\chi(E)$ is the value of the observable χ for showers with fixed primary energy E. $P(E,N_o)$ is the probability for showers initiated by a given primary with energy E to obtain the fixed size N_o

To obtain a correct comparison with the experimental data we have taken into account the triggering conditions of the Tien-Shan array and the algorithm systems for the statistical data treatment.

All distorsions and statistical errors are included in a special algorithm which allows us to obtain from χ_{th} ,observable obtained from simulation using SBM, χ_p the corresponding pseudo-experimental characteristic (5).

3. Results

As shown in ref (2), gammaisation is a serious candidate to restore agreement between phenomenological predictions and experiment in E.A.S. about the absorption of showers. For exemple maximum's depth T_{max} as a function of the primary energy E is shown fig 1 for pure proton, pure iron primaries and mixed composition (60% p + 40% fe)

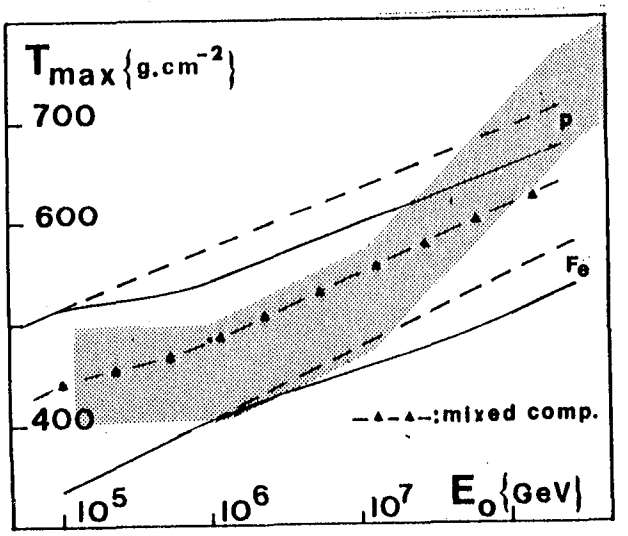

Dotted lines and full lines are respectively without and with gammaisation.

It can be noticed that the relatively large proportion of iron in the mixed composition

is a consequence of the small saturation value ($\langle a \rangle = 3.$) of the ratio $\langle n_\gamma \rangle / \langle n_s \rangle$

The comparison of the Tien-Shan dependence $N_\mu(N_e)$ with SBM calculation results shows some serious discrepancies (fig. 2) On this figure are drawn for fixed sizes N_e and mean zenith angle $\theta = 22^0$,the muon sizes N_μ for pure proton and iron primaries.

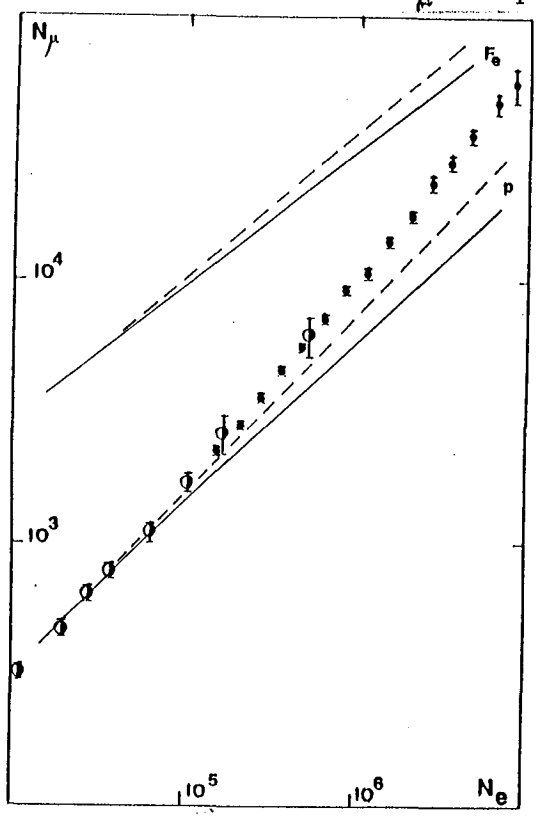

fig. 2

Dotted lines and full lines are respectively dependences without ($\langle a \rangle = 1.$) and with gammaisation.

As shown in ref. (1) the muon size dependence $N_\mu \sim N_e^\alpha$ simulated by the SBM model without gammaisation is defined in the size interval 10^5-10^7 by the parameter $\alpha = 0.67$

This value is different from the experimental one :

$$\alpha_{exp} = 0.800 \pm 0.008 \quad (6)$$

If we take into account the gammaisation this situation is worse for the largest values of N_e.

Indeed,the production of additional γ increases with energy,so imposes a flatter dependence of $N_\mu(N_e)$ i.e. $\alpha = 0.61$

It is possible to obtain results in better accordance with experimtal ones with a mixed primary composition.However the N_μ-N_e variation is never steep enough in comparison with the correspodant experimental results.

If we do not take into account the process of gammaisation (dotted lines fig.3),in the size interval 10^4-10^6 and in the range of distance 5-100 m,a good agreement is obtained for the lateral distributions of muons (the origin of the experimental points is given in ref. (1))

However,for large sizes and far from the axis of showers (R $>$ 100m),simulated densities become slightly smaller than the experimental ones. This gives,because the large number of muons far from the axis,the underestimation of $N_\mu(N_e)$ (see fig. 2)

As expected from results shown in fig. 2,with production of additional γ,the situation is the same for small showers and becomes less favorable for large sizes ($N_e \sim 10^6$) (full lines on fig. 3)

4. Discussion A consequence of the gammaisation hypothesis for high energies ($E > 10^5$ GeV.) is the decrease of the ratio N_μ/N_e for showers initiated by primaries with fixed energy. This imply for showers registered with fixed sizes a smoother variation of $N_\mu(N_e)$ than is obtained with the standard SBM model.

mixed primary composition.

However, because the agreement of the protonic showers for smallest sizes ($N_e \sim 10^4$) and the important decrease of the primary energy spectra, the effect of heavy primaries remains not large enough.

In any case, the N_μ-N_e dependence is never steep enough in comparison with the correspondant experimental results.

The agreement with experiment can be obtained with help of a stronger increase of multiplicity $\langle n_s \rangle$ with energy. This result is confirmed by the results of other authors (7) with calculations carried out under the assumption of SBM where $\langle n_s \rangle \alpha E^{0.25}$ Ours, coming from accelerators data is equivalent to $\langle n_s \rangle \alpha E^{0.13}$

However we have to notice that no experimental arguments from the accelerator region allow one to adopt such a strong dependence of secondary multiplicity on the energy of interactions.

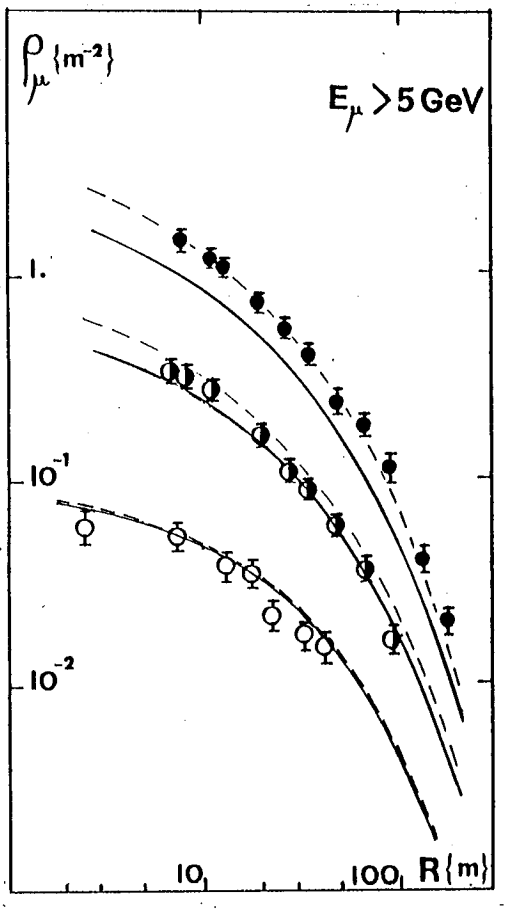

fig. 3

5. Conclusions

We have analysed E.A.S. electron and muon components in the Tien-Shan experiment on the basis of the SBM model including the "gammaisation" hypothesis. We have shown that with a correct description of the longitudinal development, a good agreement between experimental and calculated results is ontained if we use a mixed primary composition rich in proton and a stronger variation of multiplicity of secondaries with energy than the one given by accelerators results.

References :

(1) J. Procureur, J.N. Stamenov et al. to be published in J. Phys. G
(2) S.I. Nikolski (1970) Trudi FIAN 46, 100
(3) J.N. Capdevielle, J. Procureur J. Phys. G 10 (1984), 705
(4) N. Yamdagni (1982) proc. Workshop on Very High Energy Cosmic Ray Interaction, University of Pennsylvania, p 36
(5) S.I. Nikolski and J.N. Stamenov, Proc. 18th ICCR (1983) OG4-14
(6) I.N. Kirov, S.I. Nikolski et al., Proc. 7th ESCR (1980), 360
(7) A.D. Erlykin et al. Moscow (1984) FIAN n° 14

ANOMALIES IN COSMIC RAYS: NEW PARTICLES vs CHARM?

G.L.BALAYAN, A.YU.KHODJAMIRIAN, A.G.OGANESSIAN

Yerevan Physics Institute, Markarian st.2
375036, Yerevan, Armenia, USSR

For a long time two anomalies are observed in cosmic rays at energies $E \sim 100$ TeV: 1) the generation of "long-flying" cascades in the hadron calorimeter (the so-called Tien-Shan effect) /1/; 2) the enhancement of direct muon yield as compared with the accelerator energy region /2/. The aim of this paper is to discuss the possibility that both anomalies have common origin arising from production and decays of the same particles. The main conclusions are the following: 1) direct muons cannot be generated by any new particles with mass exceeding 10÷20 GeV; 2) if both effects are originated from the charmed hadrons, then the needed charm hadroproduction cross section is unexpectedly large as compared with the quark-gluon model predictions.

When energy grows from $E \sim 10$ TeV to $E \sim 100$ TeV, an increase of the hadron cascade mean penetration length is observed. This phenomenon is interpreted by the authors of Tien-Shan experiment /1/ as production (in the cosmic shower interactions with the calorimeter nuclei) of unstable particles which carry a substantial part ($\langle x \rangle \gtrsim 0.25$) of the incident energy and simultaneously have small inelasticity (or small cross section of the interactions with the calorimeter substance). When the incident energy becomes ~ 100 TeV, the mean decay path of these particles $\ell \sim \langle x \rangle E c\tau/m$ reaches the scale of the calorimeter vertical size ($\ell \sim 1$ m) so that the resulting hadron cascade is observed as "long-flying". The mass range of these particles is estimated /1/ as $2\ \text{GeV} \leq m \leq 450\ \text{GeV}$, their lifetime being respectively in the interval $10^{-12}\text{sec} \leq \tau \leq 10^{-10}\text{sec}$. The hadroproduction cross section of "long-flying" particles is $\sigma \sim 3 \div 5$ mb/nucleon at $E \sim 100$ TeV.

The direct muons produced in the primary pN-collisions with definite energy E_μ are characterized by the ratio of their yield to the number of pions produced with the same energy. We have obtained for this ratio R integrated over the primary spectrum with power $\gamma + 1 = 2.65$ the following estimate

$$R(E_\mu) \simeq 11.5 < n_\mu (E_\mu / < x_\mu >) > \int_0^1 \frac{dN}{dx_\mu} x_\mu^\gamma \, dx_\mu \qquad (1)$$

Here the familiar parametrization of pion inclusive cross section from /3/ was used and scaling for direct muons was assumed ($< n_\mu > = \sigma(\mu^+ + \mu^-)/\sigma_{tot}$ is the direct muon mean multiplicity, dN/dx_μ is the normalized spectrum over $x_\mu = E_\mu / E$; $< x_\mu >$ is the value at which the integrand in eq.(1) reaches its maximum). Due to the x_μ^γ factor the ratio R becomes a good analyzer of muons carrying a large part of the incident energy. Data from a few experiments /2/, although with large uncertainties, indicate that in the region $E_\mu = 1 \div 100$ TeV R may reach an order of 10^{-3} value.

Suppose that starting from 10÷100 TeV some new X-particles (of hadronic origin) are produced, which simultaneously are "long-flying" and have muonic decays. It turns out that already available SPS collider ($\sqrt{S} = 540$ GeV, i.e. $E \sim 150$ TeV) data sample allows us to reject too heavy X-particles generating large $p_\perp$ muons. To demonstrate this, we have calculated the ratio

$$\Delta(M_x) = \frac{\int dp_{\perp\mu}^2 \int dx_\mu \; \frac{d\sigma}{dx_\mu \, dp_{\perp\mu}^2} \left(p\bar{p} \to \underset{\hookrightarrow \mu}{X} + \ldots\right)}{p_{\perp\mu} > 5\,\text{GeV} \; |x_\mu| < 0{,}3} \Big/ \sigma\left(p\bar{p} \to \underset{\hookrightarrow \mu}{X} + \cdots\right) \qquad (2)$$

which determines that part of direct muons from X-particles to which the collider detectors are sensitive. In fact, $\Delta(M_x) > 10\%$ at $M_x > 10$ GeV (20 GeV), if the muon creates in $X \to \mu^\pm \nu$, $\mu^+\mu^-$ ($X \to \mu^\pm \nu + H, \mu^+\mu^- + H$) decays, where M_H may be $\leq \frac{1}{2} M_X$. The X-particle mean $p_\perp$ was chosen ~ 1 GeV/c (i.e. too low for real heavy particles) to decrease artificially the share of large $p_\perp$ muons. Nevertheless due to the large X-mass the substantial part of muons are produced with $p_{\perp\mu} \geq 5$ GeV. At

the same time, the value of Δ shows practically no change when the longitudinal X-spectrum is varied in wide limits (from $d\sigma/dx \sim (1-x)^5/x$ to $d\sigma/dx \sim x(1-x)$). From the UA1-data sample on the $W \to \mu\nu$ search /4/ we conclude that $\sigma(p\bar{p} \to \mu(p_{\perp\mu} > 5\,\mathrm{GeV}) + \cdots) \sim 0{,}2\,\mu b$ at $E \sim 150$ TeV. By means of coefficient (2) we immediately obtain the upper limit for the cross section of hypothetical X-particles:

$$\sigma(pN \to X + \cdots)\, B(X \to \mu) \leq 2\,\mu b \qquad (3)$$

which holds for all variants of X-production and decays mentioned above (we suppose that $\sigma(pN \to X + \cdots) \simeq \sigma(p\bar{p} \to X + \cdots)$ which is justified at such energies). It is easy to verify that the upper bound given by eq.(3) allows too few direct muons from X-particles ($R \ll 10^{-4}$). In addition, we think that: 1) more detailed scenarios of X-decays (involving a second muon and/or neutrino) will decrease the upper limit of the allowed X-masses up to the b-flavored hadrons; 2) the analogous consideration of jets from pure hadronic X-decays will allow also to reject too heavy X as "long-flying" cascade source. At the same time it is evident that the collider data obtained in the large $p_\perp$ region are not too sensitive to the muons from charm decays produced predominantly with $p_{\perp\mu} \lesssim 1$ GeV.

As it was noted earlier /1,5,6/, the charmed hadrons (Λ_c and $\mathcal{D}$) are really good candidates for "long-flying" particles. Particularly important is that their expected inelasticity is small as comaper with light hadrons due to the specific effect of c-quark leading inside Λ_c or $\mathcal{D}$ /6/. It is known also that the mean part of incident energy $\langle x \rangle$ carried by charmed hadrons may be really large. In particular, Λ_c -baryons were detected at ISR ($E \sim 2$ TeV) /7/ with spectrum

$$d\sigma/dx \simeq 3/2\,\sigma\sqrt{1-x} \qquad (4)$$

where $\sigma \leq 0.3$ mb, $\langle x \rangle \sim 0.4$. The whole effect of "long-flying" cascades may be understood in terms of charm if achieves ~ 3 mb at $E \sim 100$ TeV. Therefore, it is necess-

ary to postulate a rapid growth of charm yield in the fragmantation region ($X > 0.1$). We have chosen it as follows:

$$\sigma \simeq 0{,}3\,mb\left(1+\ell n\left(\frac{\sqrt{S}\ (GeV)}{60}\right)\right)^2 \qquad (5)$$

The muon spectrum from semileptonic decays of charm ($B(c\to\mu) = 10\%$) produced according to eqs.(4),(5) was calculated. This spectrum behaves like $(1-x_\mu)^6/x_\mu$ at $x_\mu > 0.05$ and gives $R\sim 1.3\cdot10^{-3}$ at $E_\mu \sim 10$ TeV.

Therefore, both effects: the "long-flying" cascades and direct muons are simultaneously explained if we suppose abundant charm production in the fragmentation region. Note that this phenomenon is rather unexpected in quark-gluon models of charm hadroproduction. Although the whole picture of heavy quark hadroproduction is yet far from understanding, it is clear that in the fragmentation region some non-perturbative mechanisms are essential. The models describing this region predict /8-10/ too slow rise ($\sim \ell n\, E$) of the cross section fragmentation part so that at $E\sim 100$ TeV in eq.(4) $\sigma \leq 0.5 \div 0.8$ mb.

We conclude that more detailed information about inclusive cross section of charmed hadroproduction at energies ~ 100 TeV would be of great interest from the viewpoint of the quark-gluon physics. New data on the cosmic ray anomalies at superhigh energies are therefore needed. Note that the proposed ANI installation /11/ will have a unique possibility to detect both "long-flying" cascades and direct muons.

REFERENCES

/1/ Yakovlev V.I. et al. Proc 18th ICRC,1983,v.5,p.102.
/2/ Kitamura T. ICR-Report-94/81/10,1981.
/3/ Hillas A.M. Proc.Paris Workshop on Cascade Simulations, 1981,39.
/4/ Arnison G. et al. Preprint CERN EP/83-196, 1983.
/5/ Cline D.B. Proc.16th ICRC,1979,v.14,p.271.
/6/ Khodjamirian A.Yu. VANT,1982,iss.3(12),p.14.
/7/ Basile M. et al. Lett.Nuovo Cim.,1981,v.30,p.481.
/8/ Brodsky S.J. et al. Phys.Lett.,1980,v.93B,p.451.
/9/ Boreskov K.G.,Kaidalov A.B. Yad.Fiz.,1983,v.37,p.174.
/10/ Khodjamirian A.Yu., Oganessian A.G. Proc.18th ICRC, 1983,v.5,p.48.
/11/ Danilova T.V. et al. Proc.18th ICRC,1983,v.5,p.520.

RELATIONSHIP OF SEA LEVEL MUON CHARGE RATIO TO PRIMARY COMPOSITION INCLUDING NUCLEAR TARGET EFFECTS

A. Goned, M. Shalaby, A.M. Salem, and M. Roushdy

Physics Department, Faculty of Science,
Ain Shams University, Cairo, EGYPT

ABSTRACT

The discrepancy between the muon charge ratio observed at low energies and that calculated using pp data is removed by including nuclear target effects. Calculations at high energies show that the primary iron spectrum is expected to change slope from 2-2.2 to 2.4-2.5 for energies $\gtrsim 4\times10^3$ GeV/nucleon if scaling features continue to the highest energies.

1. Introduction

It is well known that there is a discrepancy between the observed muon charge ratio at low energies ($E_\mu \lesssim 100$ GeV) and calculations based on p-p data (e.g. Thompson and Whalley, 1977). At these energies, the nuclear physics and primary composition are thought to be fairly well known. A common procedure is to normalize the charge ratio at some energy (e.g. E_μ = 10 GeV).

In the present paper, it is shown that the inclusion of nuclear target effects removes the above discrepancy. Observations at high energies can then be used to derive reliable information on the primary mass composition up to about 10^5 GeV/nucleon.

2. Calculations Neglecting Nuclear Target Effects

Detailed calculations of the muon spectrum and charge ratio have been made assuming the continuance of scaling features to the highest energies. Initially, nuclear target effects were assumed to be negligible, and recent pp data have been used in the calculations.

From a comparison between calculations and spectrograph measurements of the muon spectrum, the primary nucleon spectrum has been derived in the form $I(E)dE = AE^{-\gamma}$, with A = 2.139 and γ = 2.7 ($70 < E < 10^4$ GeV). At this value of γ, the fractional energy moments for proton and neutron production in pp collisions were found to be Z_{pp} = 0.2622 and Z_{pn} = 0.0711 respectively, yielding an effective isospin retaining probability β_{pp} = 0.7867. Our analysis of pp data also gives δ_π = 0.225 and δ_K = 0.517 for the pion and Kaon positive excesses, repsectively,

while for the primary proton excess, we take $\delta_o = 0.74$ (Erlykin et al, 1974).

In the charge ratio calculations, we take for π and K production in neutron interactions :

$$Z_{n\pi^{\pm}} = Z_{p\pi^{\mp}} \quad , \quad Z_{nK^+} = Z_{nK^-} = \tfrac{1}{2}\,(Z_{pK^+} + Z_{pK^-})$$

The results of calculations are shown in Fig. (1). At E_μ = 10 GeV, the calculated charge ratio is R_μ = 1.3489 which is about 5.5% higher than the observed one. The difference is significant compared to the experimental error.

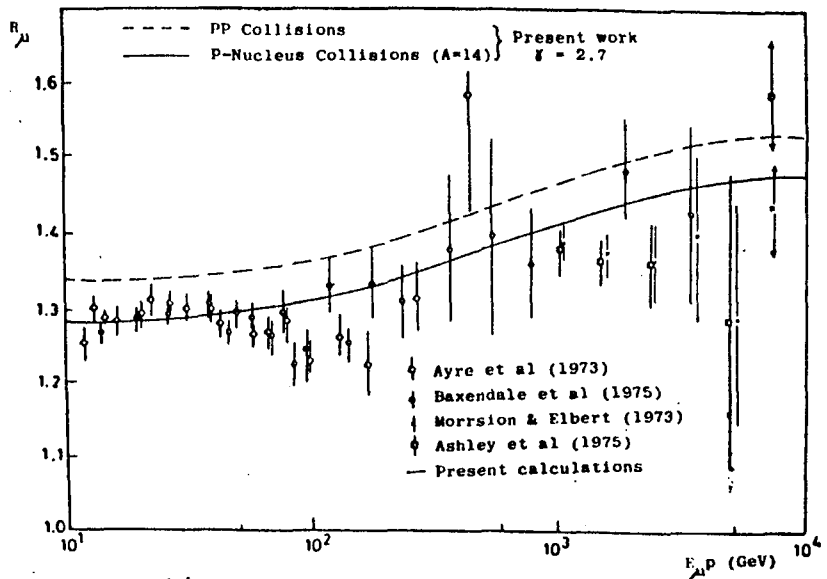

Fig. (1) Muon Charge Ratio at Sea level with and without Nuclear Target Effects (Scaling Model).

3. Calculations Including Nuclear Target Effects

The nuclear target effects have been included in the charge ratio calculations using a Glauber-Type model (Goned et al, 1985). For p-air we obtain Z_{pp} = 0.1094, Z_{pn} = 0.0347 and β_{pA} = 0.7591. We also take δ_π = 0.2025 and δ_K = 0.4653, which is 10% lower than the pp case. The results obtained for the charge ratio are also shown in Fig. (1). The calculated value at 10 GeV is R_μ=1.2794 which is in good agreement with the observed one (R_μ = 1.28).

4. Primary Mass Composition

Using charge ratio calculations with nuclear target effects, the neutron fraction in the primary beam (η)

has been derived from the data as shown in Fig. (2). The data below 100 GeV/nucleon correspond to direct measurements (Olejniczak et al, 1977). The curves correspond to the expected neutron fraction for different slopes γ_F of the primary iron component.

It can be seen that below about 4×10^3 GeV/nucleon, the charge ratio data are consistent with a slope γ_F = 2.0-2.2 compared to γ = 2.75 for protons and helium nuclei. If scaling continues above these energies then one should expect an increase to γ_F = 2.4-2.5. Other possibilities include significant scale breaking or a significant increase in the values of δ_π and δ_K in p-nucleus collisions.

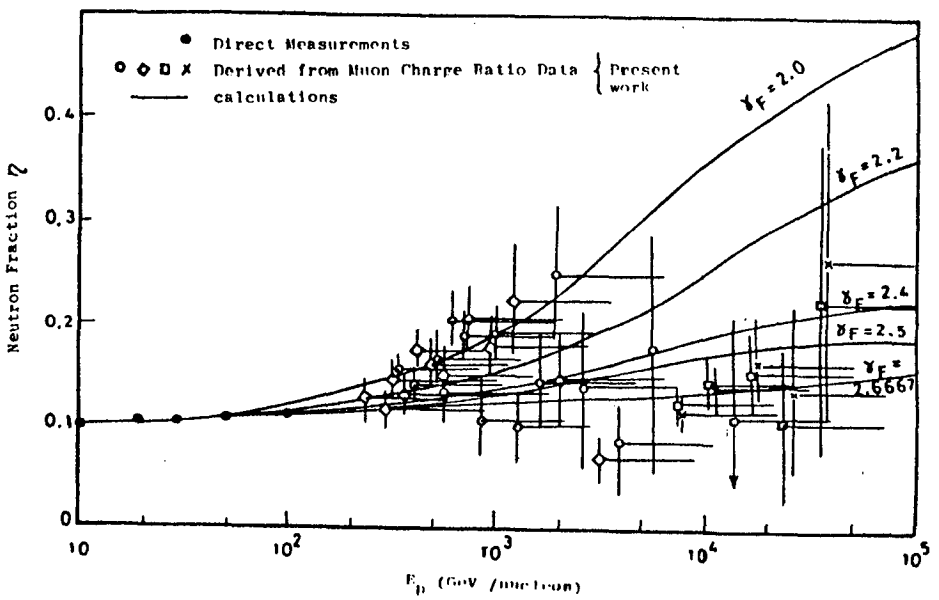

Fig. (2) The Neutron Fraction in the Primary Beam as a function of Primary Energy. γ_F is the differential exponent for the Fe group spectrum.

References

Erlykin, A.D., et al, 1974, J. Phys. A, 7, 2059
Goned, A., et al, 1985, J. Phys. G., 11, 613
Olejniczak, J., et al, 1977, J. Phys. G., 3, 847
Thompson, M.G., and Whalley, M.R., 1977, J. Phys. G., 3, 97.

STUDY OF PHOTONUCLEAR MUON INTERACTIONS AT BAKSAN UNDERGROUND SCINTILLATION TELESCOPE

Bakatanov V.N., Chudakov A.E., Dadykin V.L., Novosel'tsev Yu.F., Novosel'tseva M.V., Achkasov V.M., Semenov A.M., Sten'kin Yu.V.

Institute for Nuclear Research, the USSR Academy of Sciences, Moscow, USSR

ABSTRACT

The method of π-μ-e decays recording has been used to distinguish between purely electron-photon and hadronic cascades, induced by high energy muons underground. At energy ~1 Tev a ratio of the number of hadronic to electromagnetic cascades was found equal 0.11±.03 in agreement with expectation. But, at an energy ~4 Tev a sharp increase of this ratio was indicated though not statistically sound (0.52±.13).

1.Methods. The observation of high energy muon induced cascades at Baksan Underground Scintillation Telescope is described elswhere (1,2). Using π-μ-e decay's delayed signal recording an attempt has been made to distinguish the fraction of cascades induced by muons through inelastic μ-A interactions. The technique of μ-e decays recording is described in ref.(3). For every scintillators layer the summarized P.M.'s anode signal is put to 10-beam, 10 μs oscilloscope which is the main device to register μ-e decays. The recording efficiency ε depends on the position of the decay location relative to scintillator, also on the time window and on energy threshold, the mean value being $\langle\varepsilon\rangle = 0.05$. The energy threshold for delayed pulses recording was 7 Mev or about 300 photoelectrons from PM photocathode and it was high enough to exclude afterpulses. To check this we used high power pulsed X-ray sources.

2. Results and discussion. During a 11640 h run, 1302 cascades with an energy more than 700 Gev have been recorded and among them 556 cascades with π-μ-e decays. Unfortunately, a presence of decays is not a strong evidence for the cascade to be hadronic or not, because of nonzero probability to produce pions in purely electromagnetic cascade through photonuclear interactions of real photons. The mean number of stopping charged pions in electromagnetic cascade of energy E_c was calculated as:

$$\bar{n}_{\pi^\pm} = \frac{N_{Av}}{A^{0.1}} \cdot X_0 \cdot \int_{E_0}^{E_c} \sigma_{\gamma\rho}(E_\gamma) \cdot m_{\pi^\pm}(E_\gamma) \cdot \frac{d[N(E_\gamma)}{dE_\gamma} \cdot dE_\gamma$$

where A is the atomic weight of the target material, N_{Av} is Avogadro's number, X_0 is the radiation length (23 g/sm² in our case), $\sigma_{\gamma p}(E_\gamma)$ is the differential total photoproduction cross section taken from (4,5), $m_{\pi^\pm}(E_\gamma)$ is the yeild of stopping pions per one γ-A interaction, $E_0 \approx m_\pi$ is the threshold energy for photoproduction which is about pion rest mass, $dN(E_\gamma)/dE_\gamma$ is the differential photon spectrum in the cascade with energy E_c (6).

All stopping π^+ and only a fraction of π^- decaying in flight (35% in our case) should be taken into account. The total number of stopping pions in electromagnetic cascade of energy E_c was found to be $\bar{n}_{\pi^\pm} = 5.7 \cdot 10^{-3} \cdot E_c$.

Assuming stopping pions disribution along the cascade axis the same as for electrons, the mean number of π-μ-e decays recorded by the telescope has been calculated as a function of cascade energy. The results are shown in table 1 in the first two columns.

Assuming Poisson distribution for the number of π-μ-e decays in electromagnetic cascade criteria may be suggested to separate electromagnetic and hadronic cascades for each energy range. We chose as a criterion such number of μ-e decays n_t, that probability of $n < n_t$ is more than 99% for electromagnetic cascade. This "separation-number" is shown in 3th column of table 1 as a function of cascade energy. The total numbers of recorded (N_{rec}) cascades and that selected by the criterion as a purely electromagnetic ones (N_{em}) are plotted in 4th and 5th column. In the next columns there is a distribution of selected events in comparison with Poisson distribution (expected $\bar{n}_{\mu\text{-}e}$ are shown in the second column). An agreement is good enough and this is a reason to belive that the criterion is good.

Table 1

$\langle E_c \rangle$, Gev	$\bar{n}_{\mu\text{-}e}$	n_t	N_{rec}	N_{em}	0μ-e	1μ-e	2μ-e	3μ-e	4μ-e	5μ-e	6μ-e	
738	0.30	3	490	440	318	101	21					experim.
					326	97	15					Poisson
894	0.36	3	305	261	184	66	11					e
					183	65	12					P
1070	0.44	3	204	177	120	48	9					e
					114	50	11					P
1552	0.63	4	265	228	119	76	22	11				e
					121	78	24	5				P
3880	1.52	6	38	25	5	6	5	7	1	1	0	e
					5.5	8.3	6.3	3.2	1.2	0.4	0.1	P

The mean number of recorded μ-e decays in cascades distinguished as hadronic is shown in Table 2 as a function of the mean cascade energy $\langle E_c \rangle$. The expected values of $\langle n_{\mu\text{-}e} \rangle$ are shown in the last line of the table. The results from ref.(7) multiplied by our recording efficiency $\varepsilon = 0.05$ have been used:

$$\langle n_{\mu\text{-}e} \rangle \text{ (calculat.)} = \varepsilon \cdot 0.8 E_c^{3/4} .$$

Table 2

$\langle E_c \rangle$ in Gev	890	1060	1260	1790	4260
$\langle n_{\mu-e} \rangle$ (exper.)	10.2±.8	9.9±.7	12.3±1.3	15.4±1.4	28.7±4.8
$\langle n_{\mu-e} \rangle$ (cal.)	6.8	7.7	8.8	11.4	21.9

There is some excess in experimental data as compared with calculations. It should be emphasized that unlike to the case of electromagnetic cascades the fluctuations of $n_{\mu-e}$ in hadronic cascades in a given energy interval are certainly bigger, than Poissonian ones. But, there is nothing to make one suspicious of separation procedure as being not reliable.

The ratio of separated hadronic cascades to the electromagnetic ones is shown in fig.1 as a function of cascade energy. The expected ratio shown by the solid line is calculated suggesting muon energy spectrum at our depth as $\frac{dN}{dE} \sim (200+E)^{-3.8}$, E in Gev and using μ-A cross-section for hadronic and electromagnetic interactions from (8).

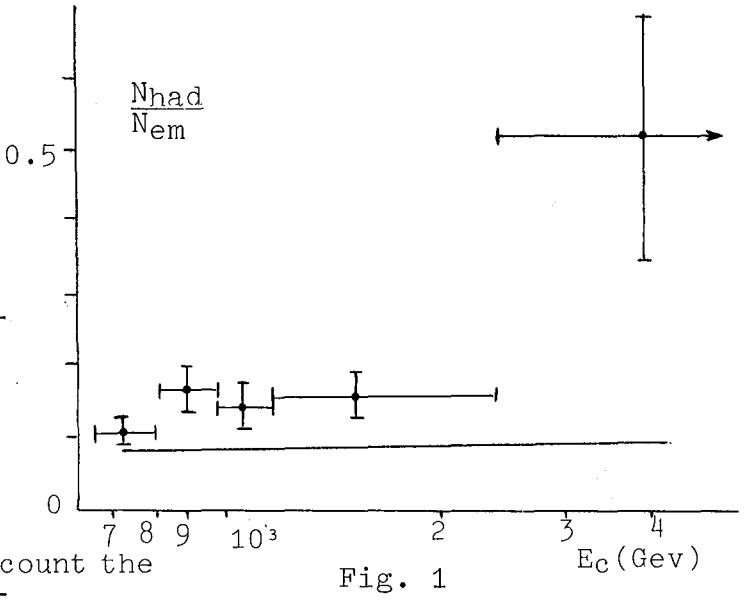

Fig. 1

In the energy range $E_c < 2500$ Gev the experimental data are in agreement with expectation if taken into account the statistical and possible systematic errors. For higher energies $E_c > 2500$ Gev there is an indication of a sharp increase of the fraction of hadronic cascades. This probably can not be taken too seriously as statistically it is only ~2σ effect.

References

1. Yu.M.Andreyev et al. Proc. of 17 ICRC, v.7, p.67, 1981.
2. V.N.Bakatanov et al. Proc. of 19 ICRC, HE 5.1-14.
3. V.N.Bakatanov et al. Proc. of 16 ICRC, v.10, p.179, 1979.
4. H.Meyer. DESY Preprint, 72/34.
5. R.Erbe et al. DESY Preprint 68/8.
6. S.Z.Belen'ky Avalanche processes in cosmic rays, Moscow, 1948
7. W.V.Jones et al. Phys. Rev., D7, p.2013, 1973.
8. E.V.Bugaev et al. Cosmic muons and neutrino, Moscow, Nauka, 1970.

HE 5.4-13

CALCULATION OF INTENSITY OF HIGH ENERGY MUON GROUPS OBSERVED DEEP UNDERGROUND

Vavilov Yu.N.
Lebedev Physical Institute
Moscow 117333
USSR

Dedenko L.G.
Moscow State University, Physical Department
Moscow 119899
USSR

ABSTRACT

The intensity of narrow muon groups observed in Kolar Gold Field (KGF) at the depth of 3375 m.w.e. has been calculated in terms of quark-gluon strings model for high energy hadron - air nuclei interactions by the method of direct modeling of nuclear cascade in the air and muon propagation in the ground for normal primary cosmic ray composition. The calculated intensity has been found to be $\sim 10^4$ times less than one observed experimentally.

1. Introduction. The observation of narrow muon groups at the depth of 3375 m.w.e. in KGF was reported in [1]. The radius of group was ~ 0.5 m for majority of muons and the number of muons in the group was ≥ 8. In the work[2] we have made an attempt to calculate the intensity of these groups in terms of simple model of hadron interactions. It was shown that in principle the narrow high energy muon groups (the thresold energy $\simeq 1.5$ TeV) can appear as a result of ordinary fluctuations. But quantitatively we must be careful in this estimation. At first, the simple model of hadron interactions does not take into account all possible fluctuations in these interactions. At the second, the Coulomb scattering of muons in the ground also was't taken into account. At last, it was considered that the group of muons had passed through the apparatus if in the limits of upper and lower plans of the apparatus there were the sections of the cylindre with radius 0.5 m and the axis, coinci-

dent with the EAS axis. In the present work we utilized the development of quark gluon strings model of interactions of hadrons with nuclei of the air /5/. Fluctuations in hadrons interactions, the muon scattering in the ground and their deflection in the Earth magnetic field have been taken into account also. The direct modeling of muon trajectories permits one to take into consideration the geometry factor of the apparatus correctly.

2. Model of interaction and the calculation method. The quark-gluon strings model describes the large number of experimental data about multiple production of hadrons in nucleon-nucleon interactions /3,4/. In the present paper we have used the development of this model in application to hadron-air nucleus interactions, developed in /5/. The mean lengths for nucleon, pion and kaons interactions were taken in accordance with /5/. The inelasticity coefficient for nucleons and incident pions and kaons were taken in accordance with inclusive spectra, calculated in /5/.

The ratio of kaon to total number of charged particle was 12%. The decays of pions and kaons were considered in the usual way. The transverse momenta distribution was taken in the form $f(p_\perp)dp_\perp \sim \exp(-\beta X_\perp)\, dp_\perp^2$, where $\beta = 2.85$; 7.15 and 6.9 for nucleons, pions and kaons correspondingly. For nucleons in the exponent $P_\perp$ was taken instead of $X_\perp$. The interactions of primary nucleus were taken into account in accordance with superposition hypothesys. The secondary particles energy spectrum was taken in accordance with /5/. The chemical composition and energy spectrum of primary cosmic radiation was taken as in /6/.

It was taken, that magnetic field of the Earth has the meridian direction component $H = 0.4$ G /7/.

The method of calculation consists of direct modeling of all processes. At first for some thresholds of the energy of the primary particles in accordance with the primary spectrum the real energy of primary particle was simula-

ted and then its atomic weight according to accepted chemical composition was sampled. Then in the limit of 30° to the vertical the zenith angle of primary particle and its azimuth and coordinates in the upper plan of the array were simulated. Then the points of interactions, the inelasticity coefficients, multiplicity and another parameters of all secondary particles were simulated. The acts of interaction of the hadrons were simulated in such a way that the conservation laws of energy, electric charge and transverse momentum and strangeness were conserved. The Coulomb scattering of muon in the ground was considered in accordance with the known Fermi formula which takes into account the correlation of the angle and the deflection in the fixed plane. The method of the calculation of the scattering was taken as in /8/. The energy losses for bremstrachlung and photonuclear interaction with ground nuclei were simulated with fluctuations taken into account. Ionization losses and losses for the e^+e^- pair creation were taken as continuous. We take into account not only Coulomb scattering of muon but also its scattering as a result of inelastic interactions with nuclei in the ground. The cross sections of muon energy losses were taken in accordance with /10-14/.

3. The result of calculation and conclusions. The tresholds of primary energy were chosen equal to $3.16 \cdot 10^{15}$, 10^{16} eV and so on. For each value of energy thresholds the simulated number of events in accordance with the primary spectrum /6/ were 500, 150, 70, 20 and 50 events correspondingly. The number of narrow muon groups, as it was determined above was 0, 0, 0, 0, 2 for threshold energies $3.16 \cdot 10^{15}$, 10^{16}, $3,16 \cdot 10^{16}$, 10^{17}, $3,16 \cdot 10^{17}$eV correspondingly. Comparing these data with the intensity of primary cosmic radiation and the intensity of groups /1/ it can be shown that the intensity of the calculated groups is approximately $\sim 10^4$ times less than experimental one. /1/ This conclusion implies the not trivial appearance of the narrow multiple muon groups.

4. Acknowledgements. The authors are indebted to Profs A.D. Erlykin, S.I. Nikolsky and Yu.M. Shabelsky for the discussion.

References

1. Krishnaswamy, M.R. et al., (1979), Proc. 16th ICRC, v. 13, p. 378, Kyoto.
2. Vavilov, Yu.N., Dedenko, L.G., (1981), Proc. 17th ICRC, v. 7, p. 38, Paris.
3. Kaidalov, A.B., (1982), Phys. Lett., v. 116 B, p. 459.
4. Kaidalov, A.B., Ter-Martirosyan, (1982), Phys. Lett., v. 117 B, p. 247.
5. Kaidalov, A.B., Ter-Martirosyan, K.A., Shabelsky, Yu.M., (1985), Preprint ITEP, in press.
6. Nikolsky, S.I., (1982), Workshops on cosmic ray interactions and high energy results, La Paz-Rio de Janeiro, p. 336.
7. Kaye, G.W.C., Laby, T.H. (1941), Tables of physical and chemical constants and some mathematical functions, London.
8. Albrecht, K.F., et al., (1973), Preprint JINJ I-7549, Dubna.
9. Borog, V.V. et al., (1977), Soviet J. Nucl. Phys., v. 25, p. 46.
10. Minorikawa, Y., Kutamura, T., Kobayakawa., K., (1981)., N. Cim., v. 4 C, p. 471.
11. Petrukhin, A.A., Shestakov, V.V., (1968), Canad. J. Phys., v. 46, p. 337.
12. Okada, A. et al., (1984), Fort. Phys., v. 32, p. 135.
13. Gruppen C., (1976), Fort. Phys., v. 23, p. 127.

HE-5.4-14

COLLIMATED GROUPS OF PARTICLES AS POSSIBLE MANIFESTATION OF HEAVY MESON PRODUCTION

Yu.A.Smorodin
P.N.Lebedev Physical Institute,
Academy of Sciences USSR, Moscow

ABSTRACT

The interpretation of miniclusters containing hadrons as well as γ-quanta by the cascade decays of heavy mesons, in the first turn, of charmed D^*-mesons is discussed.

1. Introduction.

Narrow groups of particles (NGP) - miniclusters - innovated by the Japan-Brazil collaboration /1/ have been intensively investigated in recent years with big scale X-ray film chambers.

We omit here for brevity the papers on chirons, where NGP have been considered as a new sort of produced particles, and confine ourselves to those examining the characteristic features of miniclusters themselves.

Investigated in the paper /2/ among the hadrons in chamber hadron blocks have been NGH. The paper /3/ considers NGG among the γ-e particles in G-block that failed to be accounted for without assuming availability of hadrons in the groups. The paper /4/ is concerned with distances from hadron to nearest cascades in family, indicating that hadrons fall into the narrow groups together with γ-e particles.

The conventional interpretation of NGG is electron-photon cascade being some cascade units of atmosphere above the chamber. Local nuclear interactions in the chamber target /5/ seem to be a trivial source of NGH. However NGP registered in the G- and H-blocks containing both hadrons and γ-e particles apparently cannot be interpreted by the known interaction processes that stimulate search for the new phenomena.

The purpose of the present paper is to show that the nontrivial NGP seem to be interpreted by the generation and subsequent decay of heavy mesons, in the first turn, by the charmed D^*-mesons now sufficiently well known /6/.

This possibility caused serious difficulties earlier due to the fact that the theoretical estimation on the charm production even at superhigh energies was small. Having suddenly revealed a high yield of D^*-mesons (up to 20%) in the jet particles, due to hard scattering of gluons, the experiment carried out with the SPS collider made it clear that earlier estimates disregarding some essential features (glueballs?) of the charm production are much lower. It is possible to treat nontrivial NGP as the manifestation of heavy mesons generation; high cross section of their production has been indicated in cosmic rays earlier /8,9/.

NGP could appear due to the strong interactions in the last tens meters of the atmosphere above a chamber. However the layer thickness less than 1/100 nuclear path is too small to explain the NGP flux, and the overhead floor is too low ($\sim$ 1 m) to account for the dimensions of NGP by the interactions in the floor substance.

2. Main characteristic features revealed by experiments.

Let us summarize the main characteristic peculiarities of NGP as they are established in the mutually consistent experiments.

1) The nature of NGP particles. As noted above, nontrivial NGP comprise γ-e particles and hadrons.

The penetrating ability of miniclusters due to hadrons has been pointed to in all the papers on chirons, from /1/. The most convincing and essential for estimates of NGP flux are the results of /3,4/.

In /3/, 30 γ-families each including more than two hadrons, necessary to sew accurately together cascades in the G- and H-blocks, have been selected among 54 γ-families with $\sum E_\gamma > 100$ TeV. Out of 1700 cascades in the G-block 156 were chosen (at threshold 2 TeV) and 130 (at threshold 4 TeV) penetrating into the H-block. One third of them had the spot optical density in the H-block exceeding that in the G-block. The simulations show that these very 3% of all γ-e particles are the penetrating nontrivial NGG. Seven of 30 such events in the G-block manifest a clearly revealed structure. Four events with 2-4 particles each in both blocks are presented in /3/ as a typical example of NGP.

In /4/ for 15 γ-families with $\sum E_\gamma > 100$ TeV, containing at least one hadron, distances R_{min} from a hadron to the nearest family cascade have been determined. The distribution over R_{min} (Fig.2) shows that 1/3 of the hadrons has a narrow, within 1 mm, accompaniment, i.e. belongs to an NGP.

2) Intensity of NGP flux. According to the data of /3,4/ the NGP flux can be estimated as 3% of the γ-e multiplicity of the γ-families and as 1/3 of the hadron number, with respect to the rate of γ-families with $\sum E_\gamma > 100$ TeV being 0.35 m^{-2} $year^{-1}$ (Pamir's data /10/). Using the data of /10/ on the mean family multiplicities one can obtain the general estimate consistent with the both results, i.e. there is on average about 1 NGP in a family with $\sum E_\gamma > 100$ TeV. This value seems to be strongly fluctuate.

3) Multiplicity of hadrons and γ-e particles in NGP. Experiment fails to give detailed information on the multiplicity of hadrons and γ-e particles and their correlation in NGP. Fig.1 shows the data available: the multiplicity of γ-e particles and hadrons in all NGH and NGG /2/, only 1/3 of them being nontrivial, and the total multiplicity of miniclusters observed in the two-layer chamber /1/. The distribution sharply falls so that the contribution of n = 5 decreases to several per cent.

For NGG $\langle n \rangle = 2.2$, for NGH $\langle n \rangle = 2.0$, and the total registered multiplicity in miniclusters with $n \geq 2$ seems to be about 4 ± 2. Note that these data can be treated as preliminary ones since the identification of hadrons and estimation of their registration efficiency for the decay cascades are very complicated.

4) Distribution over distances R. The summary of data on distances between the particles in NGP is shown in Fig.2, i.e. the distributions for NGH /2/ and those over R_{min} /4/. The former is distorted by the selection of events with $R < 0.5$ mm, the latter maximizes at 0.2 mm and extends to ~ 1 mm, where turns to usual distribution for family particles.

5) ER distribution. Fig.3 represents data /1/ on $\langle ER \rangle$ of miniclusters penetrating into lower chamber. The mean value is $\langle\langle ER \rangle\rangle = 2.0 \pm 2.2$ TeV m. The estimate of ER for NGH /2/ is close to that. The experiments don't show any differences in ER values for hadrons and γ-e particles,

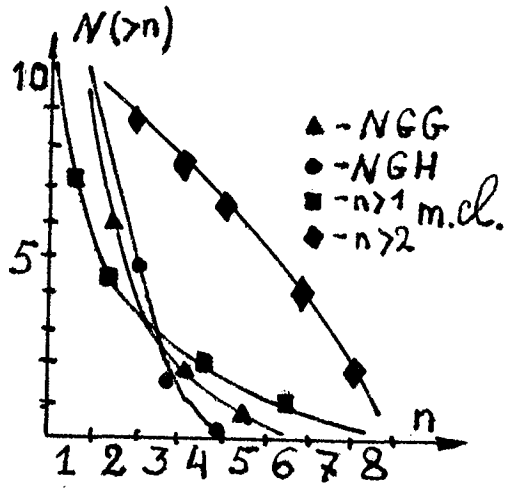

Fig.1. Data on n-distribution.

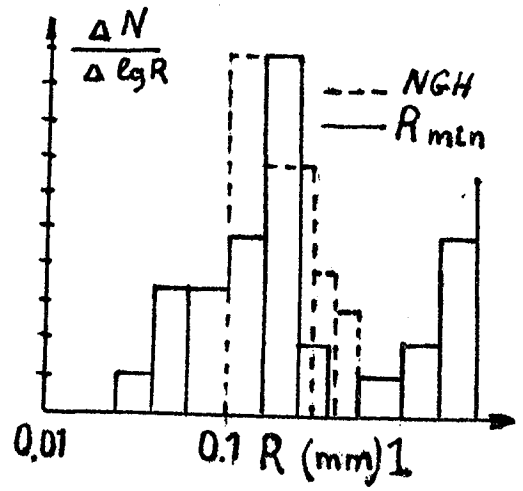

Fig.2. Data on R-distribution.

and seem to estimate the P_t value about 10 MeV/c.

It should be noted that small sizes of miniclusters are emphasized by the selection rules. The family target diagrams in /1/ show that in a number of events a minicluster is surrounded by particles with $R \sim 10$ mm. The partial separation of the narrow peak in Fig.2 shows that this is really the case.

We think it premature to discuss the large cross section of strong interaction of miniclusters reported in /1/ since narrow beams of particles are observed. In /2/ the authors noted a weak absorption of NGH in chamber target, which is also natural for the beams.

3. Charmed and heavy mesons.

The experiment /7/ reveals the production of charmed mesons in excited D^*-state, which decay momentarily into D and π-mesons and quanta. Assuming the production of D^{+-} and D^0-mesons to be symmetric one can obtain from /8/ the main signatures of the decays and their probabilities:

1) 2h - 32% 2) h+2γ - 42%

3) h+γ - 28% .

These modes occur with small decay momenta, providing particle transversal momenta $\lesssim 10$ MeV/c.

The subsequent decays of D-mesons occur at ct value about 0.03 cm leading to paths ~ 10 m at particle energies of tens TeV. The lepton modes with signatures including e^{+-} and μ^{+-} are about 20%.

Among a bulk of hadron decays producing K and π-mesons one can single out the following signatures with possibilities:

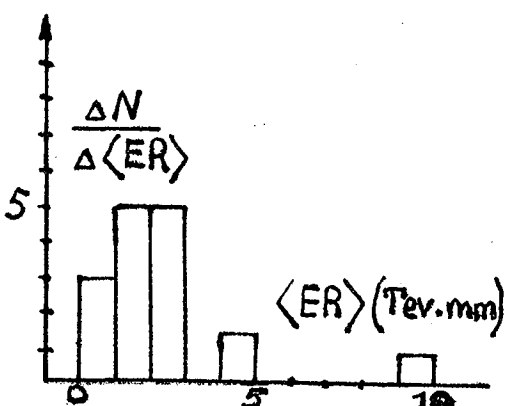

Fig.3. Data on ER-distribution.

1) 5h - 6% 2) 4h - 10% 3) 3h - 11% 4) 2h - 3%
5) 3h+2γ - 2% 6) 2h+2γ - 11% 7) 2h+4γ - 1% 8) h+nγ - 4%

The total decay momenta of these modes are hundreds MeV/c, but at a great number of particles after decay their transverse momenta are usually equal to tens MeV/c. For energies per particle 10 TeV NGP with $R < 1$ mm should be observed at paths ~ 100 m, the observation efficiency being estimated as 1/5 - 1/2.

Considering the meson systematics one can infer difference between the energies of the excited, $^3S_1$, and ground, $^1S_0$, states of mesons with quark mass increase. Thus, we should expect that the heavy mesons would generate NGP if value of their cross-section production is essential.

4. Discussion and results.

1) In the present half-qualitative analysis of the experimental data on NGP characteristics, i.e. multiplicity data, spatial-R and momentum-P distributions of NGP are consistent with the interpretation of NGP as cascade decays of charmed mesons.

2) Experimental estimations of the rate of NGP registration, namely about 1 observed NGP per γ -family with $\sum E_\gamma > 100$ TeV (nuclear-electron cascade initiated by primary proton at energies $\gtrsim 3 \cdot 10^{15}$ eV in the atmosphere) at observation efficiency 1/2 - 1/5, don't contradict the extrapolation of the latest SPS data on the superhigh energies and the data by K.Niu /8/ in cosmic rays.

3) Verification of the results seems to be possible when selecting and processing systematically by scanning X-ray films of hadron chambers with NGP. To compare experimental data with theory it is necessary to simulate decay cascades including the real efficiency of the particle registration.

4) The search for decays of heavy mesons which do not lead to NGP production, electron decays, etc. is also necessary.

The author expresses his gratitude to prof. Yu.L.Dokshitser and V.A.Hoze for the stimulating discussion.

R e f e r e n c e s

/1/ Brazil-Japan Collab., Proc. of Workshops on CR and HE, 42, 1982.
/2/ L.A.Khizanishvili et al., Proc. of the 18th ICRC, 11, 133, Bangalore, 1983.
/3/ H.Bielawska et al., Proc. of Int. Symp. on CR and Particle Physics, 374, Tokyo, 1984.
/4/ M.Tamada, Proc. of Int. Symp. on CR and Particle Physics, 352, Tokyo, 1984.
/5/ G.G.Leptukh et al., Proc. of Int. Symp. on CR and Particle Physics, 394, Tokyo, 1984.
/6/ A.H.Rozenfeld et al., Review of particle properties, CERN, Geneva, 1984.
/7/ UA 1 Collab. Preprint CERN-EP/84-86, 1984.
/8/ K.Niu, Proc. of the 14th ICRC, 7, 2442, Munich, 1975.
/9/ V.I.Jakovlev et al., Proc. of the 18th ICRC, 5, 102, Bangalore, 1983.
/10/ Pamir Collab., Annalen FIAN, v.154, Moscow, 1984.

MODULAR DETECTOR FOR DEEP UNDERWATER REGISTRATION OF MUONS AND MUON GROUPS

A.I.Demianov, L.I.Sarycheva, N.B.Sinyov, I.N.Vardanyan, A.A.Yershov

Institute of Nuclear Physics, Moscow State University, Moscow II9899, USSR

Abstract. Registration and identification of muons and muon groups penetrating into the ocean depth, can be performed using a modular multilayer detector with high resolution bidimensional readout - deep underwater calorimeter (project NADIR). Laboratory testing of a prototype sensor cell with liquid scintillator in light-tight casing, testifies to the practicability of the full-scale experiment within reasonable expences.

Introduction

The most popular conception of DUMAND, in its optical version, is a spatial lattice with numerous PMTs in sites, serving as immediate receptors of Cherenkov radiation, produced by high energy particles in the sea water. On the experimental plane, any practical approach to such a design makes one ponder upon many an implicit circumstances, e.g. persumably unsteady operational conditions during a long-running period.

The intricate combination of natural factors - as deep-sea currents, plankton migrations, bioluminiscence, etc. - would very likely result in sporadic variations of water transparency, light background, and other substantial parameters. Besides, unsufficient rigidity of the whole immense construction does not exclude some accidental and intractable changes in the preset sensor geometry or inter-orientation. All these problematic issues should not be ignored as a source of possible ambiguity in data interpretation.

Modular Underwater Calorimeter

We have proposed /I/ a more compact apparatus, in which the sensor cells have closed sensitive volume and hence their parameters unaffected by the minute changes in outer medium. In the structural respect, these cells are metal tubes 30-50 cm in diameter and I5 m long, filled with liquid scintillator and viewed from both butt-ends by two groups of PMTs. The tubes are assembled in planes I5xI5 m^2 fixed on rigid support frames; 6 such planes spaced 2m apart one above another with alternating tube orientation, form a calorimeter module, which contains I80-300 sensor cells with independent analogue readout.

The operation of electronics - data acquisition, processing and transient recording, autotrimming and system testing - are monitored by a local computer, which is housed in a sealed case close by the sensor array and communicates with the central control station on shore via a low-speed cable line.

The fiducial volume of such a module is 2.10^3 m^3 of water, angular track resolution 30-50 mrad, energy resolution for electromagnetic bremsstrahlung showers 5-6%. A full-scale experiment should include some 100 modules, placed firm side by side on the bottom at 3 km below the ocean surface (project NADIR).

As a stand-alone experimental installation, it will allow investigation of the features of high-energy muon flux and associated characteristics of primary cosmic rays and nuclear-cascade process in Earth's atmosphere. In particular, single muon spectrum can be measured up to 100 TeV, while the data on muon groups must yield information about the chemical composition of cosmic ray radiation at energies of primary nuclei ~ 10 TeV/nucleon /2/.

Prototype Scintillation Sensor

At this stage, we have built and tested in laboratory a prototype sensor cell for the deep underwater calorimeter, its architecture and functions being the same as those of the practical one, except for size.

Fig. 1 presents a sketch of the cell construction. A light-tight casing (1) poured with liquid scintillator (whitespirit) is manufactured of thin-wall alluminium tube Ø 15 cm, closed from butt-ends with plexiglass windows (2). Electronic equipment (3) is sealed in two identical alluminium containers (4) rated at high external pressure and attachable to the flanges at the opposite ends of the tube. When immersed in the water, the excess of the tube buoyancy-originating from lower density of whitespirit relative to water - is expected to compensate the effective weight of massive containers.

From each container, 3 PMTs (5) view the scintillator through a conic 5 cm thick plexiglass illuminator (6) glued into an alluminium hoop, which is adjusted to the container mouth and equipped with rubber packing rings for hermetization.

A double-conductor waterproof cable (7) connects the containers with each other, and with minicomputer "Electronica-60" serving for an "executive controller" monitored from a remote terminal. The intercommunication is carried

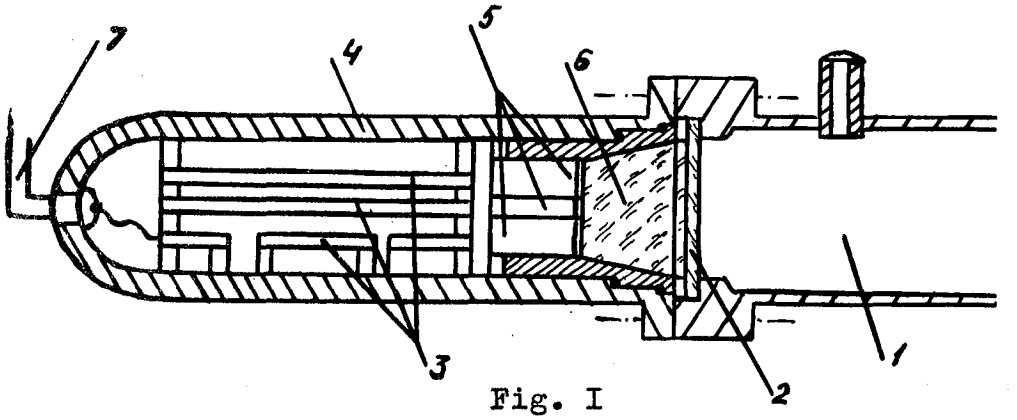

Fig. 1

out at a frequency 20 kc (10^4 bit/sec transmission rate). The same cable is used to supply power voltage +12 V feeding the electronic equipment.

Electronics

The basic elements of the front-end control/data acquisition electronics are diagrammed in fig.2. It is subdivided in two twin modules, each occupying one of the two containers.

The general purpose elements available in both modules are: a power supply block (1) transforming +12 V from the supply main into stabilized +9 V, +5 V and -10 V DC; a module controller (2); an interface (3) performing data and command exchange between the modules and with the "executive controller"; a first-level majority coincidence circuit (4) firing on coincidences of at least 2 (any) of 3 PMTs; and a LED driver (5) intended for calibration of PMTs on the opposite end of the sensor cell.

Three identical PMT channels include: high-voltage converters for PMT feeding (6) with 8-bit output potential setting by means of a computer-monitored DAC (7); 12-bit PMT noise counters (8); pulse shapers (9); and 7-bit log ADCs for pulse-height digirization (10).

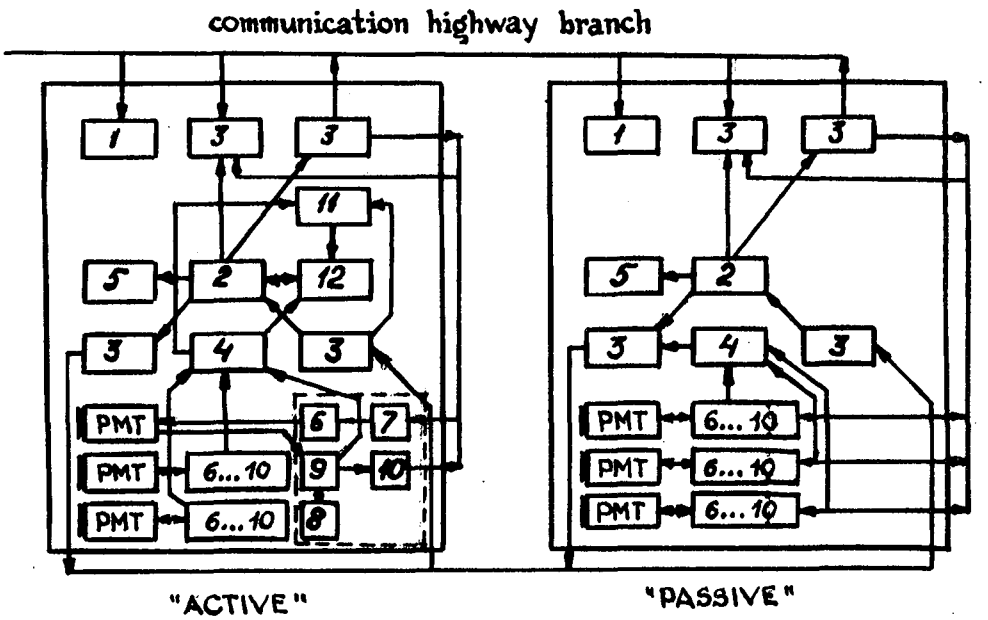

Fig. 2.

In addition, one of the modules contains a second-level (intermodular) coincidence circuit (II), and a "mask register" (I2) fitting an actual pattern of trigger bits to the computer-defined trigger-enable mask. This module (named "active") initiates a regular intercommunication cycle, addressing its counterpart (named "passive") and the "executive controller" on detecting of an "event" or routinely once every I0 sec on receipt of a timer signal.

Laboratory Test Data

The emphasis of the laboratory testing programme was focused on the following subjects:

Technological solutions conditioned by the specificity of sensor cell operation deep in the sea water;

Realistic parameters and optimum operational rates;

Stability and reliability of electronic equipment; and

Actual money and labour consumption, in view of the prospects for serial production of like sensor cells for the full-scale experiment.

The general conclusions are that rather not elaborate a device, as that described in the preceeding sections, may be running for a long period of time without logic malfunctions and significant drift of parameters. Of particular importance for this type of detector is the efficiency of light collection onto PMT's photocathode from a relatively short and distant particle track, since the optical contact between the liquid scintillator and metal cistern eliminates total internal reflection. The laboratory test data indicate that due to high transparency of whitespirit (attenuation length estimated to exceed I0 m), the reliable registration can be anticipated of a minimum ionizing particle traversing somewhere a I5m long sensor cell, with sufficient pulse-height resolution, unless the inner surface of alluminium casing is too much tarnished (reflection coefficient below 0.6) - a restriction that would hardly cause any technological problem.

On the whole, judging from the experience obtained with the prototype sensor cell, the full-scale experiment seems to be realizable within reasonable expences.

References

I. G.L.Bashindzhagyan et al. Deep Underwater Measurements with Ionization Calorometer. - I7th ICRC, v.7, p.I4I-I44 (Paris, I98I).

2. I.N.Vardanyan et al. Experiment "NADIR": Single Muon Spectra and Muon Groups in the Ocean Depth. - All-Union Cosmic Ray Conf. (Yakutsk, I984) - in Russian.

RESULTS OF INVESTIGATION OF MUON FLUXES OF SUPERHIGH ENERGY COSMIC RAYS WITH X-RAY EMULSION CHAMBERS

Ivanenko I.P., Ivanova M.A., Kuzmichev L.A., Ilyina N.P., Mandritskaya K.V., Osipova E.A., Rakobolskaya I.V.
Institute of Nuclear Physics, Moscow State University, Moscow 119899, USSR

Zatsepin G.T., Institute of Nuclear Investigation, Academy of Sciences of the USSR, Moscow

The paper presents the overall data of investigation of the cosmic ray muon flux in the range of zenith angles (0-90)° within the energy range (3.0-5 0) TeV. The exposure of large X-ray emulsion chambers underground was 1200 tonn. year.

The data were processe using the method which has been applied in the experiment "Pamir" and differred from the earlier applied one. The obtained value of a slope power index of the differential energy spectrum of the global muon flux is =3.7 that corresponds to the slope of the pion generation differential spectrum, $\gamma_\pi = 2.75 \pm .04$.

The analysis of the muon zenith-angular distribution showed that the contribution of rapid generation muons in the total muon flux agree the best with the value .2% and less with .7% at a 90% reliability level.

In Moscow State University a large array of 140 X-ray emulsion chambers comprising the total of 250 tonn of lead and 5000 m^2 of X-ray film was esposed during 10 years from 1970. The goal of the exposure was to determine the energy and zenith-angular distributions of high-energy cosmic ray muons. The array was located at 5-6 meters underground, the chamber planes forming angles of 45° and 60° with the horizon and providing a similar registration of the vertical and horizontal fluxes.

During the exposure the results on 400 chambers that is equal to 1200 tonn-year were obtained. The total efficiency of the array is $2.4 \cdot 10^{17}$ g·s·ster.

The methodical aspects of the experiment and the result of processing the data have been reported at several International Cosmic Ray Conferences /1,2,3/.

At the Conference in Paris/3/, we reported on the spectra and zenith-angular distribution obtained using a bulk of statistical material.

A power index of the differential energy spectrum of the global muon flux in the energy range (3-30) TeV was equal to 2.92±.07. The processes of rapid generation of muons with energy (3-13) TeV in the nuclear interaction was estimated as (.1-.2)%.

Lately we investigated experimental fluctuations in the electron-photon cascade development in a chamber and

calibrated the methods of cascade energy determination/4/. Errors in the energy determination were shown to be somewhat larger than expected ones and the mass of π^0-meson determined by a calibration installation at the Pamirs used in earlier muon papers was shown to be underestimated. Comparison of the methods applied when processing the Pamirs and muon chambers, indicated that different approaches to allowance for the diffuse light in photometering and somewhat different optical density curves may lead to a change in the energy spectrum slopes by $\Delta\gamma = .10-.15$.

In connection with the above consideration, the total bank of experimental data from the muon chambers was processed using the procedure of going over from optical density to energy accepted in the Pamir Collaboration. The bank was simultaneously processed by the earlier method allowing more correct regarding of experimental bais and installation apparatus.*

The total of 7000 electron-photon cascades with energy higher than 2 TeV were detected. Thus, we measured the energy spectrum of bremsstrahlung gamma-rays in the range of zenith angles 0°-90° and, proceeding from this spectrum and regarding chamber efficiency, measurement fluctuations and muon zenith-angular distribution, we found the vertical muon flux spectrum in the energy range 3.0-50 TeV(In the last interval from 32 to 50 TeV 9 muons and one muon with energy $\sim$ 130 TeV were registered).

The slope power index of a differential spectrum of the global flux of electron-photon cascades proved to be $3.72\pm .04$. Its value corrected for electromagnetic and experimental fluctuations was $\gamma_{EPC}=3.61\pm.04$. The errors shown are statistical ones.

For the global flux of cosmic ray muons a power index was found to be $\gamma=3.7$, and after going over to the vertical it was obtained to be $\gamma=3.75\pm.04$. The latter value corresponds to the power index of the pion generation differential spectrum, $\gamma_\pi=2.75\pm.04$.

After processing the data bank by the earlier used method proved to be $2.86\pm.05$ that is by a factor of .15 less than the value in /3/.

Fig.1 shows the data of various papers on investigation of the energy spectra of cosmic ray muons in various energy ranges. Our latest data are in good agreement with conclusion made by the authors of "Mutron"/5/ and conclusions of the authors of /6/(the underground array in Artemovsk).

Thus, at high energies the muon spectrum is steeper by some 3.65-3.75, if steepening is observed at all, that may be caused by a small variation of a power index of the primary nucleon spectrum or by a weak scaling violation

---

* The bank was processed by N.Ilyina using the Pamirs method, and by E.Osipova using the earlier used method

in the fragmentation region(in the nucleon energy range from 16 TeV to 200-300 TeV).

The contribution of rapid generation muons into the total muon flux was also analysed. Fig.2 presents the ratios of the number of cascades from the horizontal muon flux($\theta > 66°$) to that from the vertical flux ($\theta < 66°$) as a function of muon energy. Analysed were all cascades with energy higher than 3.0 TeV(muon energy ~ 4 TeV).

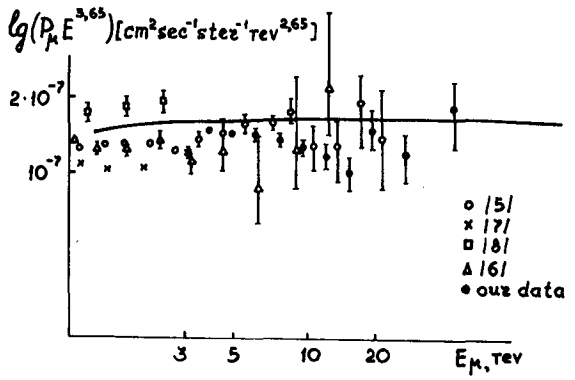

Fig.1. Intensities of the muon vertical flux obtained in various papers. The solid line is for calculations of the muon flux intensity from /10/.

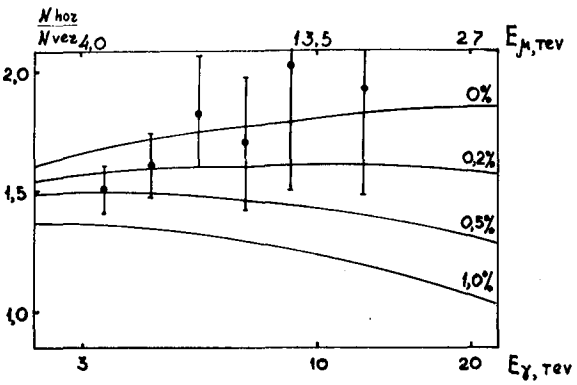

Fig.2.The ratio of the number of cascades from the vertical muon flux versus cascade energy

The solid curves show the expected flux ratios at various values of fast muon fractions, R(R denotes the ratio of inclusive cross sections of production of fast muons to that of pions averaged with respect to the primary cosmic ray spectrum), the kaon content being assumed of 15%. The χ^2-test performed to estimate R showed the best agreement of experimental data at R = .2%. R = .7% with a 90% reliability. The results obtained are consistent with our earlier conclusions /3/ and show R to be unsensitive to methodical corrections of our experiment. The data also agree with contemporary theoretical estimates of cross sections of charmed particle production.

We are grateful to Sokolskaya N.V. for enthusiastic discussion and for criticism.

References

1. Amineva T.P. et al. Proc. 14th ICRC, HE-6-9, 1975.
2. Amineva T.P. et al. Proc. 15th ICRC, v.11, p.358-362, 1977.

3. Ivanova M.A. et al. Proc. 17th ICRC, v.7, p.23, 1981.
4. Osipova E.A. et al. Proc. 18th ICRC, v.8, p.100-103,1983.
5. Matsuno S et al. Phys. Rev. D, v.29, No29, p.28-33, 1984.
6. Khalchukov et al. Proc. 19th ICRC, 1985, La Jolla.
7. Alkofer O.C. et al. Proc. 8th Europian Cosmic Ray Symp., p.79.
8. Thompson M.G. et al. Proc. 15th ICRC, v.6, p.21-25, 1977.
9. Castognoli C. Nuovo Cim. 82A, p.278, 1984.
10. Erlikin A.D. Questions of Atomic Science and Technique, vyp. 2/8/, p.34, 1981.

SEARCH FOR MAGNETIC MONOPOLES USING PROPORTIONAL COUNTERS FILLED WITH HELIUM GAS

C. Cho, S. Higashi, N. Hiraoka, A. Maruyama, S. Ozaki
T. Sato, T. Suwada, T. Takahashi and H. Umeda

Physics Department, Osaka City University
Sugimoto, Sumiyoshi-ku, Osaka, Japan

K. Tsuji

Physics Department, Kinki University
Kowakae, Higashi-Osaka, Osaka, Japan

ABSTRACT

Slow magnetic monopoles in cosmic rays have been searched at sea level with the detector which consists of seven layers of proportional counters filled with a mixture of He + 20% CH_4. The velocities and the energy losses of the incident particles are measured. The upper limit of flux for the monopoles in the velocity range of $1\times10^{-3}<\beta<4\times10^{-3}$ is $2.78\times10^{-12}/cm^2$ sr sec of 90% confidence level.

1. INTRODUCTION

The prediction of the primordial production of super massive magnetic monopoles ($MC^2\sim10^{16}$GeV) by Grand Unification Theories (1), and of the subsequent acceleration of these monopoles to the velocities of $v=\beta c$ with $\beta\sim1\times10^{-3}\sim1\times10^{-2}$, have caused interest in experimental search for slowly moving magnetic monopoles in the cosmic rays (2). Many methods to detect the monopoles have been used, but all experimental results except Cabrera (3) are negative. First, we have searched the monopoles with five layers of proportional counters filled with a mixture of 90% Ar + 10% CH_4, to measure velocity by time-of-flight method and track positions for incident particles (4). The upper limits of the flux for the monopoles in the velocity range of $1\times10^{-3}>\beta>4\times10^{-3}$ at 90% confidence level is $1.5\times10^{-12}/cm^2$ sr sec, which is slightly higher than the value reported in (4), because of the increase in running time. Second, mixed gas of 80% He + 20% CH_4 is used for the counters, since a CH_4 molecule is ionized through the Penning effect by a He metastable state excited by the monopole. More two layers of proportional counters are added to measure energy losses and track position along the

wire. Experimental results at second stage are described in this paper.

2. EXPERIMENTAL APPARATUS

The apparatus consists of seven layers of proportional counters, the aperture of $2.24 m^2 sr$, 3m height as shown in Fig. 1. Each of 2 and 6-layer has an area of 120cmx500cm, the others 120cmx450cm. Each layer consists of 12 counters; each of which is made of a rectangular alminium tube with a cross section of 5cmx10cm. Two kinds of counters are used; a T-counter which has two anode wires of 50μφ gold plated tungsten and a ground wire at the center of the tube, and a Z-counter which has a 50μφ nichrom wire at the center. 1,3,4,5 and 7-layer which consist of T-counters measure the velocities by time-of-flight method and position of incident particles, but 2 and 6-layer which consist of Z-counters measure the energy losses and the position along the wire using a charge division method. A mixed gas of 80% He + 20% CH_4 which is chosen on the basis of the measurements of the velocity and stability for different ratio of mixture, flows through all counters at a rate of 200cc/min. The high voltage is 2.3KV, and the discriminator level for trigger signals is 7 times of minimum ionization of cosmic rays.

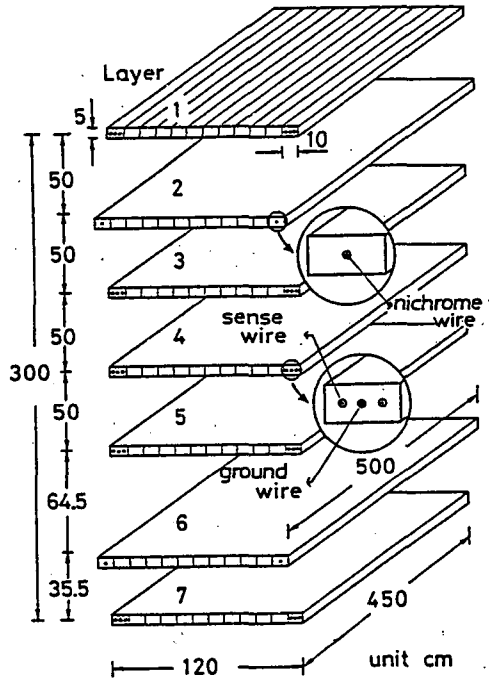

Fig. 1 The apparatus

Each signal from 1,3,4,5 and 7-layer, 24 signals in a layer, a total of 120 goes through a amplifier/discriminator on the counter, and delayed by 10μsec. Any signals from the each layer are used to make trigger pulse using a sort of succesive delayed coincidence method. The time between trigger and delayed signal from each wire is measured by 20MHz clock, 8 bit scaler and 8 bit shift resister (TDC) for all 120 wires. Each of 2 and 6-layer has 12 anode wires, and the adjacent two wires are connected at one ends of the both wires. Pulse heights from both ends of the wire with length of 10m are measured with 11 bit analog to digital

converter (CAMAC ADC), the ratio and the sum of two heights gives the position along the wire with the accuracy of about 20cm and the energy losses, respectively for a incident particle. Data are taken by a on-line micro-computer and recorded on floppy diskets.

The drift velocity of electrons in the gas used in this experiment are about 100ns/mm which is very slow compared with that of 90% Ar + 10% CH_4, 20ns/mm. So this time jitter of the pulses is at most 2.5μs for drift space of 25mm. A veto pulse, which prevent cosmic ray muons and reduce trigger rate, is generated by the 4 fold coincidence among 1,3,5 and 7-layers with the time resolution of 2.5μsec. With this data taking system, the velocity range to be observed is between $3m/2.5\mu sec;\beta=4\times10^{-3}$ and $3m/10\mu sec;\beta=1\times10^{-3}$ for the virtical incidence of the particle to the apparatus.

3. ANALYSIS AND RESULTS

Each event has data on positions and, times from 120 wires of T-counters and on pulse heights from 24 wires of Z-counters. The following requirements are applied to select the monopole candidate. First, the total number of hit-wire of T-counters in a event is less than 10. Second, the wires hitted have to draw a straight line, and the least square method is applied to positions of the anode wires fired to measure the straightness. The resultant root mean square deviation of the wire positions from the straight line; σ(L) is calculated. Third, the arrival times of the pulses from the wires have a linear relation to the virtical position of the player. The gradient of the straight line gives the the velocity for the monopole candidates, the distribution of D(L) and $D(1/\beta)$ for cosmic ray muons are obtained and

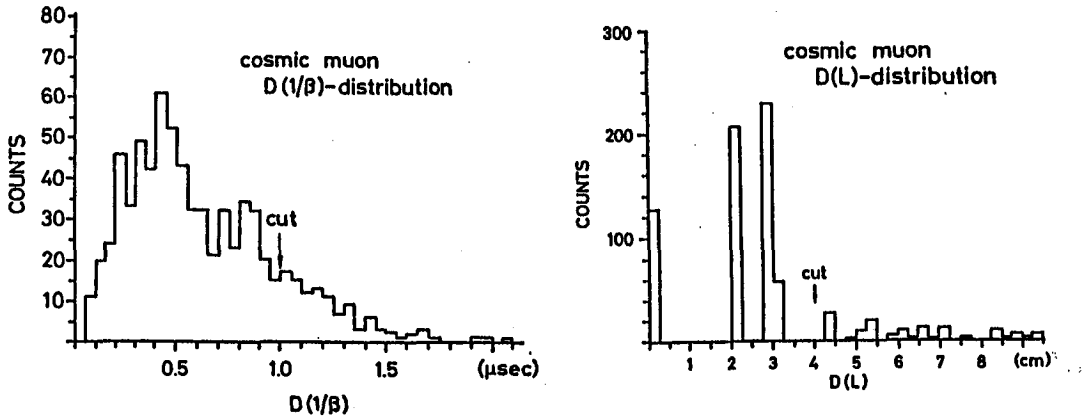

Fig. 2 $D(1/\beta)$ and D(L) distribution for cosmic ray muons.

shown in Fig. 2, where $D^2(L)$ and $D^2(1/\beta)$ is the sum of squares of the deviations from the straight line for position and time data respectively. From these results, selection criteria for the monopole candidates are $D(L)<4cm$; $\sigma(L)<2.31cm$; and $D(1/\beta)<1\mu s$; $\sigma(1/\beta)<577ns$, which gives selection efficiency of 85%. After observation from January 1, 1984 to May 28, 1985; the running time of 2.17×10^7sec, 95,000 events are recorded, on which selection criteria mentioned above are applied. Until December 12, pulse heights are not measured, then monopoles are searched only by the velocity. No track has been found to have velocity range of $1\times10^{-3}<\beta<4\times10^{-3}$ for the running time of 1.82×10^7sec. Fig. 3 shows ionization losses as a function of the velocities for monopole runs after the selections are carried out. The energy loss calculated by Drell at el (5) is also shown. No track has been found to have energy loss corresponding to the velocity. Combining two results, the upper limit of the monopole flux in cosmic ray at sea level is $2.78\times10^{-12}/cm^2sr$ sec at 90% confidence level in the velocity range of $1\times10^{-3}<\beta<4\times10^{-3}$.

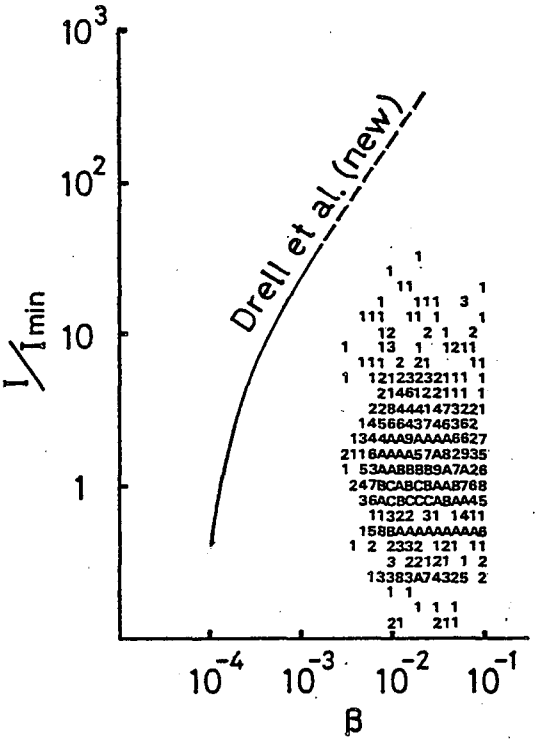

Fig. 3 The energy loss and β correlation for monopole candidates, where the number increases as 1,2,..,9,A,B,C,...,Z.

REFERENCES

1. Georgi, H. et al, (1974) Phys.Rev.Lett., 32, 438
2. Kajino, F. et al, (1984) Phys.Rev.Lett., 52, 1373
3. Cabrela, b. , (1982) Phys.Rev.Lett., 43, 1378
4. Higashi, S. et al, (1983) 18th I.C.R.C., 5, 69
5. Drell, S.D. et al, (1983) Phys.Rev.Lett., 50, 644

ACKNOWLEDGEMENTS

We wish to thank Prof. T. Kitamura for his help and encouragement.

Magnetic Monopole search by 130 m^2sr He Gas Proportional Counter

T.Hara, N.Hayashida, M.Honda, K.Kamata, M.Kobayashi*, T.Kondo*, Y.Matsubara**, M.Mori**, Y.Ohno, G.Tanahashi, M.Teshima** and Y.Totsuka***

Institute for Cosmic Ray Research, University of Tokyo, Tanashi, Tokyo, 188 Japan
* National Laboratory for High Energy Physics, Oho-machi, Tsukuba, Ibaraki, 305 Japan
** Department of Physics, Kyoto University, Sakyo-ku, Kyoto, 606 Japan
*** LICEPP, Faculty of Science, University of Tokyo, Bunkyo-ku, Tokyo, 133 Japan

A search experiment for cosmic ray magnetic monopoles has been performed by means of atomic induction mechanism by using He mixture gas proportional counters of the calorimeter(130 m^2sr) at the center of Akeno AS array. In 3,482 hours operation no monopole candidate is observed. The upper limit of the monopole flux is 1.44×10^{-13} cm^{-2} sec^{-1} sr^{-1} (90% C.L.) for the velocity faster than 7×10^{-4}c.

1. Introduction.

The magnetic monopole has been one of the most charming objects not only in experimental but also theoretical physics. There has been so many monopole search experiments using many kinds of detectors. However, mass of monopole which grand unification theory suggests is too heavy to accelerate a monopole up to relativistic speed with the Galactic magnetic field. In this case the monopole is expected to have a velocity about 10^{-3}c(where c is the light velocity) or less. For such slow monopoles, the availability of usual detectors except super conducting coil is not clear for monopole detection because the energy loss of such slow monopole is expected to be extremely small in the matter. However, Drell et al. suggested that the atomic induction mechanism in Helium or Hydrogen gas is effective for monopole detection down to 10^{-4}c of monopole velocity(1). In this paper we report a result of slow monopole search experiment with He mixture gas proportional counters using the above mechanism.

2. Apparatus and experiment.

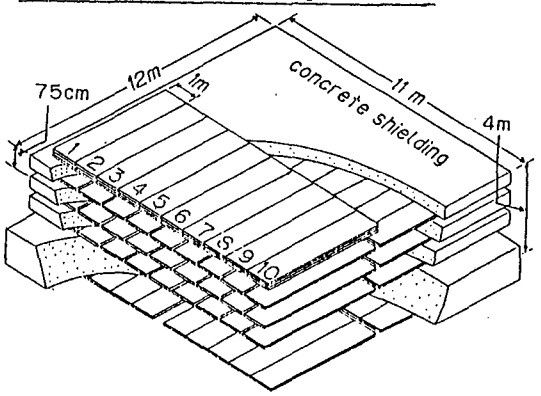

Fig.1 Apparatus for monopole detection.

For monopole search experiment, we use the proportional counters of the calorimeter at Akeno air shower array(2). The proportional counters, each unit size is 10cm x 10cm x 500cm, are set in four layers among the concrete shieldings and arranged to lie in the same direction. For monopole search experiment, we changed the proportional gas to He mixture gas(He85% + $CH_4$15%) and provided two more layers of the same proportional counters on the top of the calorimeter. The rough sketch is shown in fig.1. Though the monopole

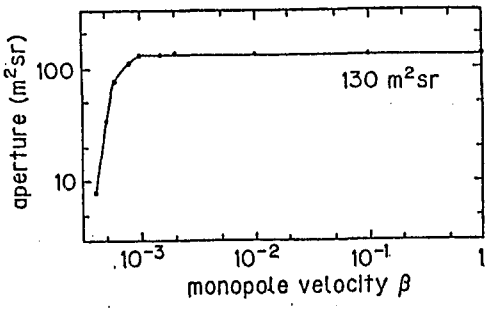

Fig.2 Aperture of the detector.

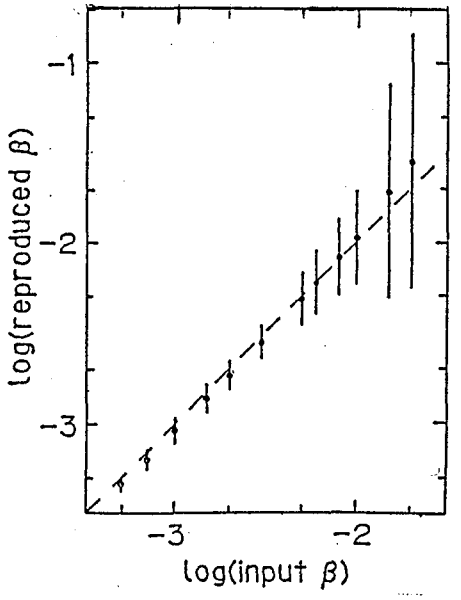

fig.3 Availability for the determination of monopole velocity.

excites only He-atoms by the atomic induction mechanism, added inner methane molecules produce free electrons in the proportional counter when they collide with the excited He-atoms through Penning effect. With the process, we can observe the signal of the monopole from the proportional counter.

The experiment has been continued since the beginning of Nov. in 1984.
The apparatus is triggered when any counter in any trigger block unit, which is composed of adjacent 10 proportional counters in the same layer, produces a signal larger than 10 times of minimum ionization of single cosmic ray muons in each layer of the counters. In order to decrease shower events, the trigger pulse is killed whenever more than 2 trigger block units in any layers satisfy the trigger condition('shower veto'). With the threshold of 10 times of the minimum ionization, monopoles with the velocity faster than 4.1×10^{-4}c are expected to be detected by our He mixture proportional counters from the comparison of electron pairs produced by relativistic cosmic ray muons with that by monopoles which is estimated by the revised calculation of Drell et al.(3) assuming 83% of Penning effect(4).

The aperture of the apparatus for both upward and downward monopoles, which varies with monopole's velocity, is calculated by Monte Carlo simulation assuming the arrangement of the apparatus, the trigger condition and the trigger gate time(46μs), and found to be 130m^2sr for monopoles of the velocity larger than 7×10^{-4}c. The detectable minimum velocity of the monopole is 5×10^{-4}c as shown in fig.2.

We record the pulse height of each proportional counter and the time difference(resolution time is 0.5μs) between the signal from each trigger block and the main trigger signal, with which we can estimate the velocity of the monopole, in magnetic tapes by using the registration system of Akeno air shower array. The time response of our proportional counter is slow because of the drift velocity of electron in He gas(about 1μs/cm). We measured the time response of our counter in the same condition as that of the experiment by using pion beam(2 GeV) from the KEK PS accelerator as a function of the impact parameter to the anode wire. Using the data, a Monte Carlo simulation was made on the availability of our apparatus for the determination of monopole velocity.

In our apparatus we can determine monopole velocity only projected to the vertical plane perpendicular to the long axis of proportional

counters. Therefore, the velocity thus determined is always less than the true velocity. The simulation results are shown in fig.3 which indicates that we can determine the velocity within the error of 50% for the monopole passing through with the velocity less than $2\times10^{-2}c$, but for faster monopole, the systematic error is too big to determine the velocity. Undeterminable region of the velocity for the apparatus was also checked experimentally by using the data triggered by relativistic cosmic ray muons. Both data are consistent with each other.

3. Analysis and results.

Almost all the triggered events are accidental ones caused by radio isotopes contained in the concrete or the wall of our counters or small air shower events escaped from 'shower veto'.

First of all, we reduce these events by off line computer analysis by checking that the 'on' counters make a straight line within the allowance of 20cm displacement and the number of 'on' counters in any layer does not exceed more than three.

Secondly the events survived the computer reduction are checked with more severe criterion for making a straight line(10cm allowance) by visual scan on graphic display and then are carefully studied for both the energy loss along the line and the timing data. If the monopole passes through the apparatus, the energy loss in each counter, which depend on the velocity of the monopole, is almost same to the others because the fluctuation of the energy loss by atomic induction mechanism is considered to be small. On the other hand if the apparatus is triggered by small showers or surrounding backgrounds, the signal from each counter is expected to be different in the magnitude from the others.

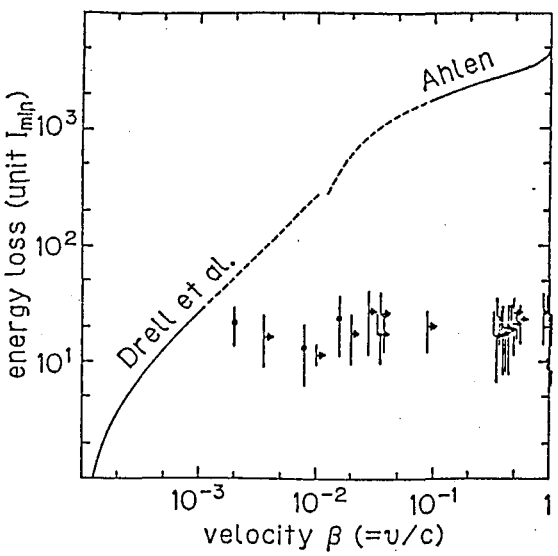

Fig.4 Events survived to the final analysis.

In fig.4 are shown the event survived the visual scan. The velocity of each event is determined by χ^2 -fitting using the timing data which are sometimes lacking in one or two counter layers because of unresponse of timing circuit and is plotted the plausible lowest value even if the χ^2-minimum can not be found. Accordingly we cannot rule out that all these events have faster velocity up to light velocity. The vertical bar of each event in the figure shows the one standard deviation of energy losses in 6 layers of the counters. Except two events these are considered to be produced by small cascades developed in the concrete from the signal transition in successive counters. The exceptions in which the signals of all layers are almost the same to one another may be caused by successive cascades by high energy muons. In any case their energy losses are still too small comparing with the calculation by Drell et al.. We can see that there is no monopole event in our data.

4. Conclusion.

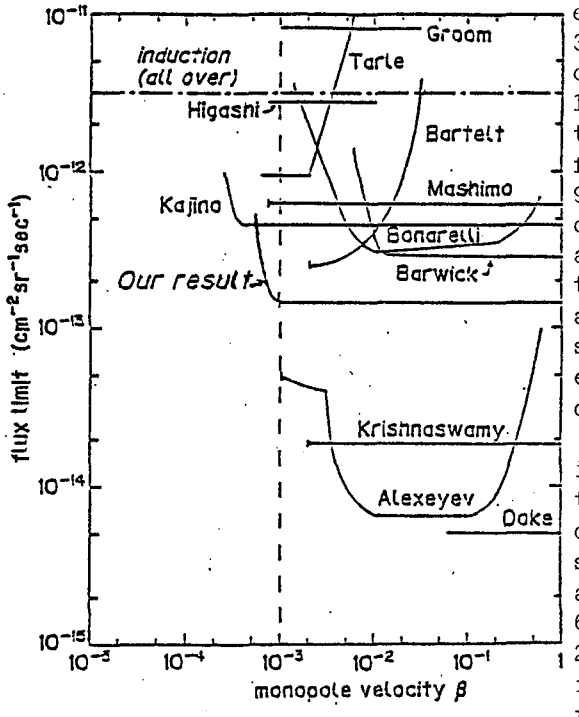

Fig.5 Upper limit of monopole flux.

Up to now we have no monopole event in the observation time of 3,482 hours. Since the aperture of our monopole detector is about 130m^{2}sr, we have the upper limit of the flux 1.44 x10^{-13} cm^{-2}sec^{-1}sr^{-1} for monopoles faster than 7x10^{-4}c in 90% confidence level. We show more detailed flux upper bound in fig. 5 as a function of monopole velocity taking into account the aperture(fig.2). In fig.5 we also show the results of other experimental groups(5) for the comparison.

Recently, Ahlen et al. investigated the availability of these detection methods for monopole detection(6). They conclude that scintillation detectors can not be applied to monopoles slower than 6x10^{-4}c and Argon counters to 2x10^{-3}c. For other experiments in fig.5, we show the results only for the applicable velocity regions in accordance with the discussion by Ahlen et al.. It is seen that our upper bound shows the lowest value in the velocity region slower than 10^{-3}c by counter experiment.

5. Acknowledgments.

The authors would like to thank the member of Akeno AS group for their help. We also thank the member of accelerator division of National Laboratory for High Energy Physics for the use of the accelerator beam. Analysis and calculation were done by FACOM M380 at the computer room of Institute for Nuclear Study, University of Tokyo.

References

1. Drell,S.D. et al. Phys. Rev. Lett. 50 644(1983)
2. T.Hara et al. 17th ICRC 11 373(1981)
3. Kroll,N.M. et al. 'Monopole 83' ed. Stone,J.L. Plenum.(1984)
4. Jesse,W.P. J. Chem. Phys. 41 2060(1964)
5. Groom,D.E. et al. Phys. Rev. Lett. 50 573(1983), Higashi,S. et al. private communication(1985), Tarle,G. et al. Phys. Rev. Lett. 52 90(1984), Bartelt,J. et al. Phys. Rev. Lett. 50 655(1983), Mashimo,T. et al. Phys. Lett. 128B 327(1983), Bonarelli,R. et al. Phys. Lett. 126B 137(1983), Krishnaswamy,M.R. et al. Phys. Lett. 142B 99(1984), Alexeyev,E.N. et al. 18th ICRC 5 52(1983), Doke,T. Phys. Lett. 129B 370(1983), Kajino,F. et al. private communication(1985), Barwick,S.M. et al. Phys. Rev. D28 2338(1983)
6. Ahlen,S.P. and Tarle,G. Phys. Rev. D27 688(1983), Liss,T.M. et al. Phys. Rev. D30 884(1984)

RESULTS OF A SEARCH FOR MONOPOLES AND TACHYONS IN HORIZONTAL COSMIC RAY FLUX

Ashitkov V.D., Kirina T.M., Klimakov A.P.,
Kokoulin R.P., Petrukhin A.A.

Moscow Physical Engineering Institute, Moscow 115409, USSR

Abstract. A search for monopoles and tachyons at ground level has been carried out using an arrangement consisting of an ionization calorimeter and two hodoscope detectors. No clear evidence for these particles has been obtained. The flux of monopoles with velocities $\beta \geq 10^{-2}$ is found to be less than 5.1×10^{-13} cm^{-2}s^{-1}sr^{-1}(95% c. l.). The upper limit on the tachyon flux density is set as 6×10^{-9} particle/cm^{2}event.

1. Introduction. In spite of the fact that monopoles and tachyons are absolutely different objects the search for these particles has been conducted using the same experimental arrangement. A detailed description of the detector used in the experiment, the motivation and first results have been published elsewhere [1-3]. The arrangement consisted of a six-layer ionization calorimeter and two G.-M. counter hodoscope detectors, and

i) events in the calorimeter with approximately equal ionization of more than 100 cascade particles observed in all six layers have been selected as monopole candidates;

ii) muon induced cascade showers in the calorimeter were used as reference events to search for preceding particles (tachyons) produced in high energy collisions in the upper atmosphere.

Present paper sums up results obtained during five experimental runs in 1980 - 1984. The total observation time exceeded 2.2×10^4 hours so available statistics have been doubled in comparison with the publications at the previous conference [2,3].

2. Monopole. If the massive monopole would traverse the calorimeter the ionization in all six layers would be approximately equal. In our experiment trigger signals were generated when ionization in any three layers of the calorimeter exceeded a threshold level 80 cascade particles (c.p.) within the time gate of 40 μs. The events with the measured ionization $\geq$ 40 c.p. in all layers of the calorimeter and with the angle between the particle trajectory and calorimeter axis less than 55° have been selected for the analysis.

The ratio of the maximum measured ionization to the average one was used as a quantitative criterion of equal ionization:

(1) $R = I_{max}/(\sum_{j=1}^{6} I_j/6)$, where j is the layer number.

In a real experiment even in the case of equal ionization R may appreciably deviate from the unit due to measurement errors. We estimate the upper limit of r.m.s. ionization measurement error as 20%. Assuming that errors followed to the log normal distribution we calculated the distribution of events as a function of R for the case of uniform ionization along calorimeter depth (dashed curve in Fig.1).

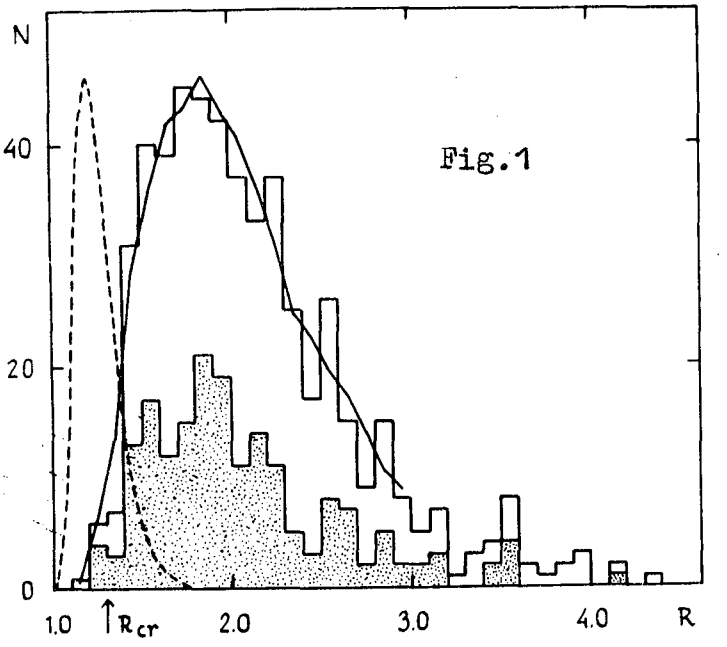

Fig.1

The observed distribution for six-layer events with average ionization of more than 100 c.p. (solid histogram in the figure) drastically differs from that for uniform ionization. We suppose that all these events are cascade showers. To estimate the background from the showers the Monte Carlo simulation of six-layer events was performed (broken line). A good agreement of this calculation with experimental data gives the evidence that all six-layer events represent a background.

The ionization from a single heavily ionizing particle must be localized in one or two adjacent chambers in every layer. This fact permits to cut the shower events due to their wide transversal ionization distribution. The events selected in accordance with this additional restriction are presented by the shaded histogram in the figure. Finally, hodoscope information was used to reject shower events which are often accompanied by plural fired counters in the exit detector.

In the previous paper [2] we used $R_{cr} = 1.5$ to separate possible monopole events from shower ones. However, calculations showed that the optimal value of R_{cr} is equal to 1.3 which corresponded to monopole selection efficiency $\geq 65\%$.

With the above criteria no monopole candidates were found. Taking into account the geometric acceptance (11.3 $m^2 sr$), available operation time (8×10^7 s) and selection efficiency (0.65) we have estimated the upper limit of monopole flux from the top hemisphere as $5.1 \times 10^{-15} cm^{-2} s^{-1} sr^{-1}$ (95% c.l.). According to theoretical calculation for monopole energy loss [4] the ionization range $\gtrsim 100$ c.p. corresponds to monopole velocities $\beta \gtrsim 10^{-2}$.

3. Tachyon. The situation around the tachyon hunt is rather complicated. There are almost no theoretical predictions concerning the interactions of these superluminal particles, therefore it seems reasonable to use every possible means to found tachyons. Our experiment is based on the assumption that tachyons are very common particles: i) tachyons may be produced in high energy collisions of primary nucleons in the atmosphere or in the decays of any secondaries; ii) they can arrive to and be detected on the Earth surface; and iii) the efficiency of their registration by G.-M. counters is not equal to zero.

Tachyons may be identified as particles which arrive the observation point earlier than other particles produced in the same interaction. High energy cascade showers initiated by muons in the ionization calorimeter were used as triggers while potential tachyons were detected by hodoscope only. The number of triggering muons was $\sim 8\times10^4$ for the minimal cascade shower energy ~20 GeV. The effective energies of muons and those of primary nucleons corresponding to this threshold were ~100 GeV and ~1 TeV, respectively.

The time and arrival direction information from hodoscope detectors was recorded in the time interval $T \simeq 26$ ms before the trigger, but the delaying events were also analysed for the comparison. Only preceding and delaying particles with trajectories parallel to those of triggering muons have been selected. The observed events are presented by points in the (ΔT - cos θ) diagram (Fig.2). There is no apparent difference between the preceding ($\Delta T < 0$) and delaying ($\Delta T > 0$) particles.

The fly-off time between the relativistic muon and preceding or delaying particle depends on the particle velocity v and the distance from the primary nucleon interaction altitude to the observation point L, which in its turn depends on the zenith angle θ and the interaction depth in the atmosphere x: $\Delta T = (1/v - 1/c)L(\theta,x)$. (2)

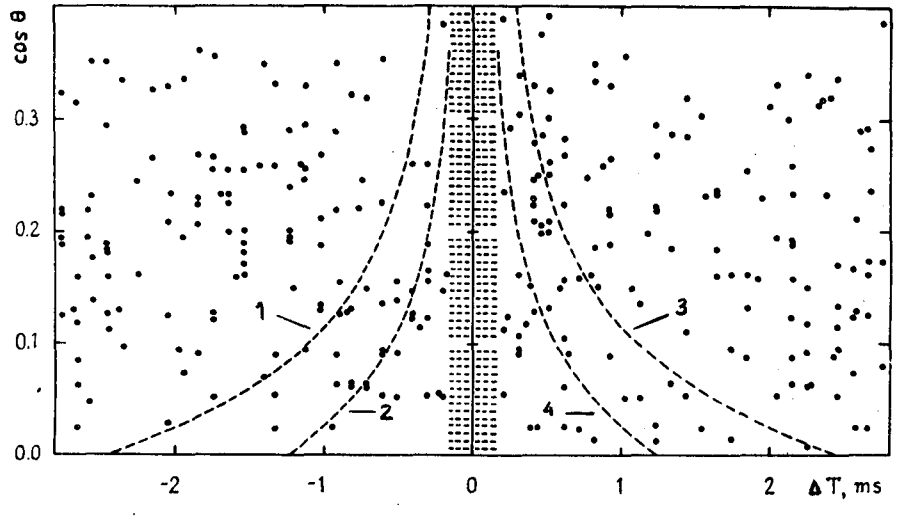

Fig.2

Since in our experiment the large zenith angles ($\theta \geq 60°$) are accessible, values of L were calculated for x = 12.6 g/cm^2 depth along the particle trajectory. Assuming a 120 g/cm^2 nucleon absorption length, this value corresponds to 10% attenuation of primaries so 90% of tachyons would be produced at such or shorter distances. The curves 1 and 2 in the figure give the angular dependence of ΔT for preceding particles with velocities $v = \infty$ and $v = 2c$ correspondingly. Since there are no predictions about the definite tachyon velocity we considered the case of arbitrary velocities, i.e. all events under the curve 1. The observed number of these events was 39. The curves 3 and 4 are drawn symmetrically for the comparison. The number of delaying particles under the curve 3 was 47. The expected value of the background was calculated considering: i) area under the curve 1, ii) angular distribution of muons, and iii) the total number of events in 26 ms interval, and was equal to 37.0 + 1.7. The sumed collecting area of the hodoscope detectors constituted 3.0×10^9 cm^2. Taking into account the hodoscope efficiency (of about 0.8) the upper limit of the density of tachyons associated with high energy muons was estimated as 6×10^{-9} particle/cm^2 event.

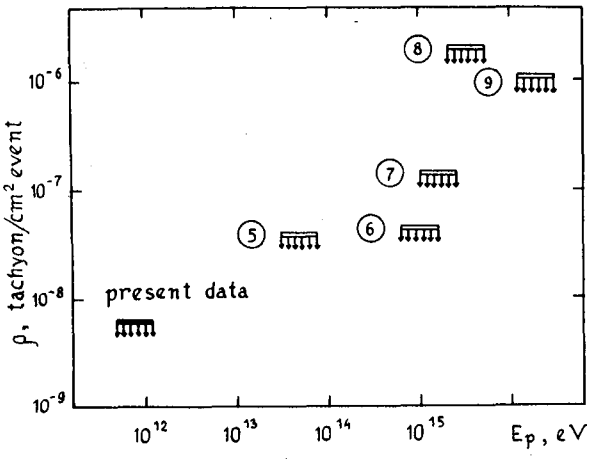

Fig.3

The direct comparison of our results with other searches for tachyons is complicated since only few authors give quantitative limits. Therefore we estimated upper limits of tachyon densities using the published experimental data[5-9] as follows:

$$(3) \qquad \rho \leq 3\sqrt{n \cdot \Delta T \cdot N}\,/\,S \cdot N,$$

where n is a background rate; S is the area of the tachyon detector; N is the number of triggers; ΔT = 100 ms is the preceding time interval for the vertical direction ($v = \infty$, x = 12.6 g/cm^2). Results of these calculations are presented in Fig.3. Ciphers near the bars correspond to the reference numbers.

1. V.D.Ashitkov et al.Izv.AN SSSR,Ser.Fiz.,45, 1319 (1981)
2. V.D.Ashitkov et al. Proc.18th ICRC, 5, 65 (1983)
3. V.D.Ashitkov et al. Proc.18th ICRC, 7,129 (1983)
4. S.P.Ahlen,K.Kinoshita.Phys.Rev.D, 26, 2347 (1982)
5. P.V.Ramana Murthy. Lett.Nuovo Cim.,1, 908 (1971)
6. G.R.Smith, S.Standil. Can.J.Phys., 55,1280 (1977)
7. M.V.Emery et al. Proc.14th ICRC, 7, 2486 (1975)
8. D.J.Fegan et al. Proc.14th ICRC, 7, 2480 (1975)
9. G.C.MacNeill, D.J.Fegan. Proc.18th ICRC, 5, 110 (1983)

MONOPOLE, ASTROPHYSICS AND COSMIC RAY OBSERVATORY AT GRAN SASSO

The MACRO Collaboration[1]
Presented by J. Stone, Department of Physics
The University of Michigan, Ann Arbor, MI 48109

ABSTRACT

A new large area detector, MACRO, has been approved for installation at the Gran Sasso Laboratory in Italy. The detector will be dedicated to the study of naturally penetrating radiation deep underground. It is designed with the general philosophy of covering the largest possible area with a detector having both sufficient built-in redundancy and use of complementary techniques to study very rare phenomena. The detector capabilities will include Monopole investigations significantly below the "Parker" bound; Astrophysics studies of very high energy gamma ray and neutrino point sources; Cosmic Ray measurements of single and multimuons; and the general observation of rare new forms of matter in the cosmic rays.

1. Introduction. The Gran Sasso Laboratory, which is being constructed in Italy, is a unique facility in the world allowing a new generation of very sophisticated underground facilities. Unique features of the laboratory include impressively large halls with easy access and basic facilities typically available only at accelerator laboratories. The MACRO detector, described here, has recently been approved for installation at the laboratory.

MACRO is a large area detector optimized for the study of rare phenomena in the naturally penetrating radiation. The detector size will have a planar surface of $\sim$1400 m^2 with an acceptance for an isotropic particle flux $\sim$12,000 m^2sr.

The primary physics objective is to perform a definitive search for magnetic monopoles using excitation-ionization methods. The response of excitation-ionization detectors to monopoles is now well understood and represents the most practical means for reaching the very large areas required to address astrophysics limits. The importance to physics of the actual discovery of monopoles is obvious. In addition, it is worth noting that MACRO will be the first detector capable of setting a significant limit on the contribution of monopoles to the dark matter in the Universe, in the event of a negative result.

Another major objective of MACRO is to search for astrophysical point-like sources through the detection of muons induced by neutrino interactions. It is well established that some peculiar cosmic objects produce powerful mechanisms of particle acceleration. It is expected that some of these objects (e.g., Cygnus X-3, Vela X-1, LMC X-4, etc.), through secondary processes, are prolific emitters of high energy neutrinos and MACRO is large enough and has sufficient resolution to have the capability to open this observational window. In addition, the neutrino astronomy capability of the detector will allow a sensitive search for gravitational stellar collapse.

In a more general sense, the MACRO detector will perform systematic investigations of the penetrating component of the cosmic radiation yielding quantitative distributions and studies of possible anomalies in the cosmic rays. The abilities of the detector for accurate timing and directional measurements coupled with measurements of the dE/dx and β of particles crossing the detector will open an observational window to a wide variety of possible exotic effects.

2. Detector Description. The MACRO detector has been designed to be installed in Hall B of the Gran Sasso Laboratory. The initial design is shown in Figure 1. Although some modifications in the arrangement of modules are present under consideration, the final detector is

expected to have similar acceptance to the design described here. The active dimensions of the detector are 111.4 m along the hall; 12 m across, and 4.6 m high. The general mechanical design of the detector provides a concrete floor at a height of 5.7 m from the original floor which could be used for other experiments. The acceptance of this closed structure for an isotropic particle flux (e.g., monopoles) is $\sim$12,000 m^{2}sr.

The main part of the detector is a horizontal structure consisting of two layers of liquid scintillator counters, ten layers of plastic streamer tubes and a sandwich of plastic track-etch detectors. These sensitive elements are distributed throughout a thick concrete structure as shown in Figures 2 and 3. The liquid scintillator counter system consists of 25 cm thick liquid scintillator counters providing accurate dE/dx and timing information, while the 10 layers of streamer tubes will provide tracking and ionization information.

The scintillator counters (572 total) consist of PVC boxes (12 m × 50 cm × 25 cm). A safe, stable, and highly transparent mineral oil based liquid scintillator fills the module, which utilizes total reflecting optics by lining each box with low index of refraction (n = 1.35) FEP TEFLON. A data acquisition system provides wide dynamic range pulse height information from each phototube.

The plastic streamer tubes consist of single cells of 3 × 3 cm^2, having a wire of diameter 60μm. They are arranged in 8-tube units and have both x and d pickup for two dimensional localization. The units are 12 m long and 25 cm wide, so that two units cover one scintillator counter.

The combined detector will give a spatial accuracy in the streamer tubes of

$$\Delta x \sim \Delta y \sim \Delta z \sim 1 \text{ cm} .$$

The ten track points of through-going particles yield an angular accuracy

$$\Delta\theta \sim 0.2^\circ .$$

The scintillator counters in a single layer using phototubes at each end have spatial and timing accuracy

$$\Delta x \sim 15 \text{ cm} \quad \text{and} \quad \Delta t \sim 1 \text{ ns} ,$$

while the streamer tubes give

$$\Delta t \sim 50 \text{ ns} .$$

The ionization loss for minimum ionizing particles crossing both scintillators is measured with an accuracy

$$\frac{\Delta(\Delta E/\Delta x)}{(\Delta E/\Delta x)} \sim 5\% .$$

The ionization threshold for fully efficient detector triggering by the streamer tubes is

$$(\Delta E/\Delta x)_{\text{min}} \sim 10^{-2} \, (\Delta E/\Delta x)_{\text{min. ion. part.}} ,$$

while for scintillators the corresponding threshold is $\sim 10^{-1} \, (\Delta E/\Delta x)_{\text{min. ion. part.}}$.

The threshold for an individual scintillator counter to detect electrons with good background rejection is

$$E_e \sim 10 \text{ MeV} .$$

The average minimum energy for muons to cross the whole detector is

$$E_\mu \sim 3 \text{ GeV} .$$

3. Conclusion. The MACRO detector to be installed in the Gran Sasso Laboratory is a multipurpose device with impressive capabilities for monopoles, astrophysics, and cosmic ray investigations. The device is modular in construction with a proposed schedule of having the first module (about 12% of the total detector) operational in 1986 and the full detector completed in 1988.

Reference

1. MACRO is an acronym for Monopole, Astrophysics and Cosmic Ray Observatory. The collaboration is an international collaboration between Italy-U.S.-CERN groups with B. Barish and E. Iarocci serving as co-spokesmen.

The present collaboration:

Bari*: C. DeMarzo, O. Enriquez, N. Giglietto, F. Posa

Bologna*: M. Attolini, F. Baldetti, G. Giacomelli, F. Grianti, A. Margiotta, P. Serra

Caltech: B. Barish, C. Lane, G. Liu

CERN: P. Musset, G. Poulard, H. Sletten

Drexel: R. Steinberg

Laboratori Nazionali di Frascati dell'INFN: G. Battistoni, H. Bilokon, C. Bloise, P. Campana, V. Chiarella, A. Ciocio, A. Grillo, E. Iarocci, A. Marini, A. Rindi, F. Ronga, L. Satta, M. Spinetti, L. Trasatti, V. Valente

Indiana: S. Ahlen, B. Brabson, R. Heinz, S. Mufson, H. Ogren, P. Smith

Michigan: J. Musser, J. Stone, L. Sulak, G. Tarlé

Pisa*: C. Angelini, A. Baldini, C. Bemporad, A. Cnops, V. Flaminio, G. Giannini, R. Pazzi, B. Saitta

Roma*: G. Auriemma, M. De Vincenzi, E. Lamanna, G. Martellotti, S. Petrera, L. Petrillo, P. Pistilli, G. Rosa, A. Sciubba, M. Severi

Texas A&M: R. Webb

Torino*: M. Arneodo, G. Borreani, P. Giubellino, F. Marchetto, A. Marzari, S. Palestini, L. Ramello

Virginia Tech: S. Torres, P. Trower

*Sezione INFN e Dipartimento di Fisica dell'Universitá.

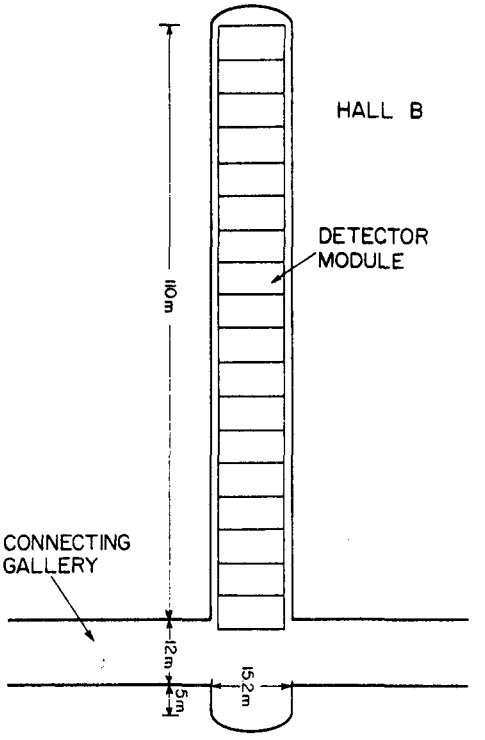

Fig. 1. Layout of the detector modules in Hall B of the Gran Sasso Laboratory.

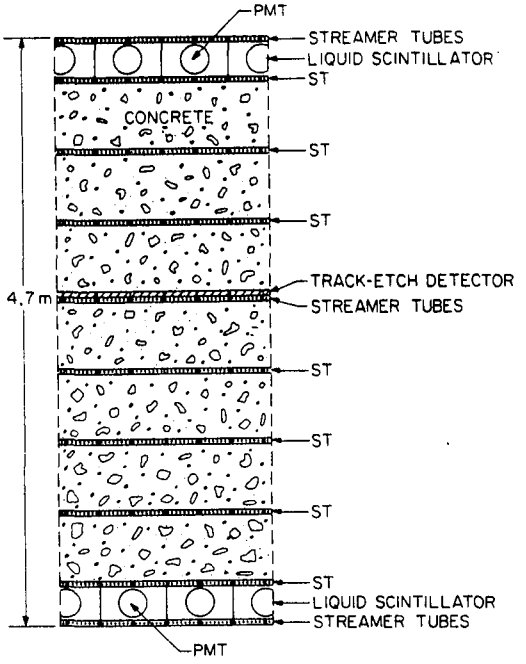

Fig. 2. Cross sectional sketch of the detector showing the relative position of the various components.

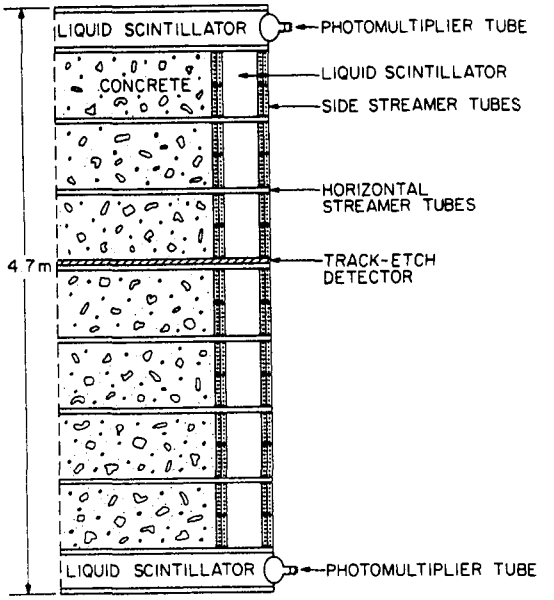

Fig. 3. Cross sectional sketch showing the active components which close the sides of the detector.

MONOPOLE SEARCH BELOW THE PARKER LIMIT WITH THE MACRO DETECTOR AT GRAN SASSO

The MACRO Collaboration
Presented by G. Tarle , Department of Physics
The University of Michigan, Ann Arbor, MI 48109

ABSTRACT

The MACRO detector approved for the Gran Sasso Underground Laboratory in Italy will be the first capable of performing a definitive search for super-massive GUT monopoles at a level significantly below the "Parker" flux limit of 10^{-15} $cm^{-2}sr^{-1}s^{-1}$. GUT monopoles will move at very low velocities ($V \sim 10^{-3}c$) relative to the Earth and a multifaceted detection technique is required to assure their unambiguous identification. Calculations of scintillator response to slow monopoles and measurements of scintillation efficiency for low energy protons have shown that bare monopoles and electrically charged monopoles moving at velocities as low as $5\times10^{-4}c$ will produce detectable scintillation signals. The time-of-flight between two thick (25cm) liquid scintillation layers separated by 4.3m will be used in conjunction with waveform digitization of signals of extended duration in each thick scintillator to provide a redundant signature for slow penetrating particles. Limited streamer tubes filled with He and n-pentane will detect bare monopoles with velocities as low as $1\times10^{-4}c$ by exploiting monopole induced level mixing and the Penning effect. A layer of solid state nuclear track detectors located in the center of the detector will be processed in the event that the active detectors record a monopole candidate. With an acceptance of $\sim12000 m^2sr$, MACRO will reach a sensitivity to monopole fluxes $F < 10^{-16} cm^{-2}sr^{-1}s^{-1}$ in a few years. For a monopole mass of 10^{16} GeV/c^2 this flux corresponds to 10% of the "Parker" limit. If no events are detected, monopoles would be ruled out as contributing no more than 4% to the "missing" mass of the universe.

1. Introduction

The existence of supermassive ($M>10^{16} GeV/c^2$) magnetic monopoles is a natural consequence of Grand Unified Theories (GUTs) that are characterized by a single coupling constant. Such monopoles should have been copiously produced in a standard early universe and the failure to detect them has created a problem for GUTs. New inflationary universes have been proposed that alleviate this problem by delaying the symmetry breaking phase transition to a later epoch. At the present time cosmology offers little guidance in prediction of monopole fluxes. Astrophysical constraints on monopole flux can be obtained from the continued existence of the Galactic Magnetic Field (GMF) and the closure density of the universe. The so-called "Parker" limit[1] ($10^{-15} cm^{-2}sr^{-1}s^{-1}$) is derived by demanding that monopoles do not extract energy from the GMF at a rate faster than it can be replenished by a Galactic dynamo. Mechanisms have been proposed that circumvent the Parker limit by permitting monopoles to interact with the GMF in a resonant fashion. For a nominal velocity of $10^{-3}c$ and a mass of 10^{16} GeV/c^2 an isotropic flux of monopoles of $10^{-15} cm^{-2}sr^{-1}s^{-1}$ would constitute 40% of the critical density $\rho_c = 2\times10^{-29} g/cm^3$ needed to close the universe. It is both a peculiar and intriguing coincidence that these two completely independent astrophysical limits are so close to one another. It would indeed be interesting to find monopoles at the Parker limit resonantly interacting

with the GMF in some way that regulates its magnitude. Today an "interesting" search for monopoles is one that goes well beyond the Parker and closure limits with detection techniques that are convincing regardless of whether the search is positive or negative.

2. Slow Monopole Detection

A variety of techniques have been applied to the detection of slow monopoles. Superconducting detection and certain detection methods based on ionization or excitation can be considered as direct in that they rely solely on the electromagnetic interaction of monopoles. Although superconducting detectors respond to monopoles of arbitrary velocity it is difficult to build them large enough to perform an "interesting" search. Any detector based on ionization and/or excitation will likely have a minimum threshold velocity determined by kinematic limitations on energy transfers to atomic electrons and the need to provide a minimum excitation energy to the system. Ahlen and Tarle[2] have shown that scintillators make ideal monopole detectors both because their velocity threshold $V \sim 5\times10^{-4}c$ is well below the astrophysically important region and because they can be fabricated in large areas at relatively low cost. By scaling monopole-electron and proton-electron cross sections and by using available data on scintillation by low energy recoil protons they were able to calculate the response of scintillators to slow monopoles. Empirical verification that electromagnetically interacting particles moving as slowly as $9\times10^{-4}c$ can produce scintillation light has recently been obtained by Ahlen et al[3]. By exposing scintillators to a neutron beam at the Brookhaven High Flux Beam Reactor, low energy recoil protons were produced within the volume of the scintillator and a response curve (see figure 1) was obtained. Two different models of proton stopping power were used to convert the measured light output per unit energy, dL/dE, to light output per unit length, dL/dx. The measured points lie somewhat below the predicted curve of Ahlen and Tarle but are within the quoted uncertainties of the calculation. An interesting technique to extend the response of ionization detectors to bare monopoles as slow as $1\times10^{-4}c$ has been suggested by Drell et al[4]. This method takes advantage of monopole induced level mixing in He atoms and employs the Penning effect to transfer this excitation to a gas of low ionization potential.

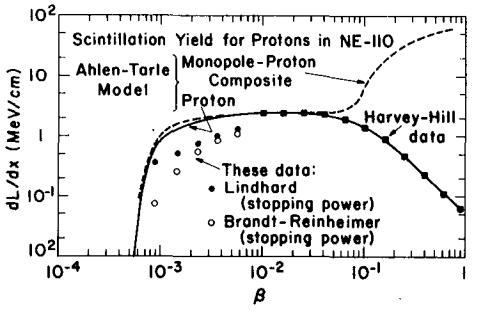

Fig. 1. Light output of organic scintillator for low velocity particles (see text).

Several novel yet indirect techniques have been used to search for monopoles with special properties at levels below the Parker limit. For example Price et al[5] has searched for monopole-Al induced tracks in ancient muscovite mica. This technique requires monopoles to pick up a nucleus at least as heavy as Al in the Earth's crust prior to penetrating the mica buried at an average depth of 5km. If monopoles are produced as positive dyons or pick up protons in the early universe or the interstellar medium as suggested by Bracci and Fiorentini[6] then Coulomb repulsion would prevent the capture of Al nuclei and no tracks would be formed in the mica. It has been argued[7] that cross sections are large

for monopole induced baryon nonconserving reactions (the so-called Rubakov effect). If so, then it has been suggested that neutron stars could be used as monopole detectors. From observational limits on ultraviolet and x-ray backgrounds, very stringent flux limits have been placed on GUT monopoles[8] ($\lesssim 10^{-22}$cm^{-2}sr^{-1}s^{-1}). A less stringent limit (10^{-14}cm^{-2}sr^{-1}s^{-1}) has been placed[9] by looking directly for monopole induced baryon decays with the IMB proton decay detector. Caution is required when interpreting limits requiring the Rubakov effect. For example, it has not yet been established that baryon number is not strictly conserved. The problem with indirect techniques is that if no monopoles are found, a long list of experimentally unverifiable assumptions must be satisfied before a negative observation can be interpreted as a limit.

3. The MACRO Detector

The MACRO detector now approved for the Gran Sasso underground laboratory in Italy (for a complete decription see ref. 10) will be the first capable of extending a direct search for monopoles to flux levels significantly below the Parker limit. The principal detection scheme for monopoles (figure 2) will involve the use of two thick (d=25cm) liquid scintillator layers separated by a large distance (D ~ 4m). A slow monopole will produce a characteristic signal of extended duration in each of the thick layers. Waveform digitizers will record these signals and continuity of pulse height and timing information will provide redundancy for slow particle identification. In addition we will require that the ratios of pulse durations in the two scintillators and time-of-flight between layers $\Delta t_1 : \Delta t_2 : T$ are in the same ratio as the layer thicknesses and separation d:d:D. the scintillation detectors will respond to monopoles of arbitrary electric and magnetic charge and having any velocity in excess of ~5×10^{-4}c. In addition to the scintillation system there will be 10 layers of limited streamer tubes filled with a 3:1 mixture of He and n-pentane and having a separate trigger. The Drell mechanism will allow detection of bare monopoles down to a velocity of 1×10^{-4}c. For monopoles with positive electric charge the Drell mechanism will not be operative[11] and the threshold velocity will exceed 2×10^{-3}c as a result of kinematics. In the event a monopole candidate is observed by either the scintillator or limited streamer tube system, two types of solid state nuclear track detectors (Lexan and CR-39) located in the center of the MACRO detector will be etched and scanned for tracks. The CR-39 threshold for bare monopoles is ~5×10^{-3}c although diamagnetic effects may reduce this threshold[12] to as low as 5×10^{-5}c. The Lexan detectors with a threshold of 0.3c will only be sensitive to events having large signals in the electronic detectors. The MACRO detector is in the form of a box 12m x 5m x 111m with detectors covering all sides. The total acceptance for monopoles will be ~12000m^{2}sr corresponding to four events/year at the Parker bound.

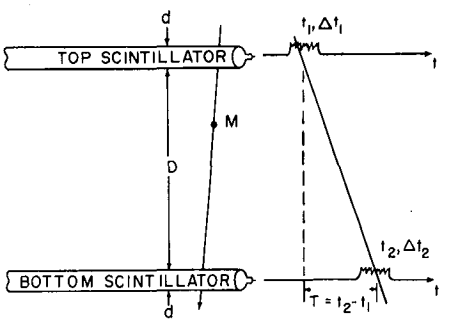

Fig. 2. Simplified monopole detection scheme for MACRO.

4. Conclusions

The current status of searches for GUT monopoles is shown in

figure 3. Experiments involving indirect techniques or those for which the response to monopoles is uncertain have been shown with dashed lines. The Baksan scintillation detector[13] is the only detector using direct techniques that has approached the Parker bound. Because the effective integration time of the Baksan trigger electronics is only 50ns, slow particles will have a higher effective velocity threshold than the excitation threshold of scintillators. According to the model of Ahlen and Tarle the effective threshold for monopoles in the Baksan detector is $1x10^{-3}c$. The new results of Ahlen et al[2] suggest that this threshold should be even higher. The MACRO detector will have seven times the acceptance of Baksan and will have an integrated trigger that will

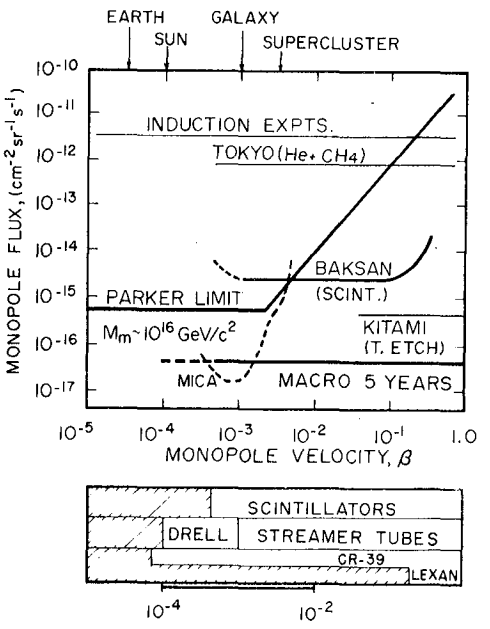

Fig. 3. Current status of GUT monopole searches and expected sensitivity of MACRO. Escape velocities for various astrophysical objects are indicated.

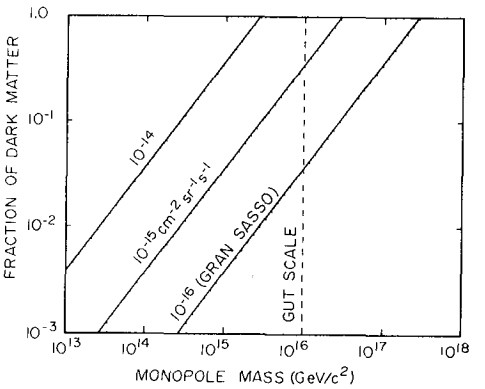

Fig. 4. Sensitivity of monopole search experiments to dark matter.

respond to monopoles having velocities only slightly in excess of the excitation threshold for scintillators. After five years of operation the MACRO detector will reach a sensitivity of better than $10^{-16}cm^{-2}sr^{-1}s^{-1}$. Figure 4 shows that at this level, the sensitivity of MACRO to dark matter composed of monopoles is a few percent of ρ_c for monopole mass and velocity having nominal values of $10^{16}GeV/c^2$ and $V=10^{-3}c$ respectively.

References

1. Turner, M.S., Parker, E.N. and Bogdan, Phys. Rev. 26D, 1296 (1982).
2. Ahlen, S.P. and Tarle , G., Phys. Rev. 27D, 688 (1983).
3. Ahlen, S.P. et al, submitted to Phys. Rev. Lett. (1985).
4. Drell, S.D. et al., Phys. Rev. Lett. 50, 644 (1983).
5. Price, P.B. et al., Phys. Rev. Lett. 52, 1265 (1984).
6. Bracci, L. and Fiorentini,G., Phys. Lett. 143B, 357 (1984).
7. Rubakov, V., JETP Lett. 33, 644 (1981).
8. Kolb, E.W. et al., Phys. Rev. Lett. 49, 1373 (1982).
9. Errede, S. et al., Phys. Rev. Lett. 51, 245 (1983).
10. The MACRO Collaboration, HE6.1-4, these proceedings.
11. Kroll, N. et al., Monopole '83, ed. J.L. Stone (Plenum, NY, 1984), pp. 295-315.
12. Price, P.B., CERN EP/84-28, submitted to Phys. Lett. (1984).
13. Chudakov, A.V., Proceedings of UP'85, St. Vincent. (1985).

LIMITS ON MONOPOLE FLUXES FROM KGF EXPERIMENT

M.R. Krishnaswamy, M.G.K. Menon, N.K. Mondal,
V.S. Narasimham and B.V. Sreekantan

Tata Institute of Fundamental Research,
Bombay - 400 005, India

Y. Hayashi, N. Ito and S. Kawakami

Osaka City University, Osaka, Japan

S. Miyake

Institute for Cosmic Ray Research,
University of Tokyo, Tokyo, Japan

1. Introduction

The nucleon decay experiment at KGF at a depth of 2.3 Km is eminently suited for the search of GUT monopoles, whose velocities at the present epoch are predicted to be around 10^{-3}C. At this depth the cosmic ray background is at a level 2/day in the detector of size 4m x 6m x 3.7m and one can look for monopoles traversing the detector in all directions, using three methods[1] i.e., i)dE/dx (ionisation), ii)time of flight and iii)catalysis of nucleon decay. The detector is composed of 34 layers of proportional counters arranged in horizontal planes one above the other in an orthogonal matrix. Each of the 1594 counters are instrumented to measure ionisation in the gas (90% Argon + 10% Methane) as well as the time of arrival of particles.

2. Method and Results

(i) dE/dx

The ionisation deposited in each counter is converted to an equivalent number of minimum ionising muons(Neq), whose distribution is approximately Gaussian with $\sigma=0.4/\sqrt{Neq}$ upto Neq=100 particles. With a threshold of 1/4 I_{min}, the counters are sensitive for monopole

velocities > 5 x 10^{-4}c(whereas the trigger needs a path length > 45 cm corresponding to 7.5 x 10^{-4}c). In this method we look for uniform ionisation all along the track, a hall mark of monopole signals. To make the search sensitive, only tracks with lengths > 1.5m are considered so that a minimum of 12 sampling points are available for analysis. Moreover, we impose a restriction Neq > 2.5 to avoid closely spaced muons as well as the tail of resolution function of single muons. This corresponds to a lower limit on velocity of 1.3 x 10^{-3}c.

A total of 1900 events were recorded in a period of 952 days since March 1982. Since none of them have survived the statistical tests on uniformity in ionisation along the track, we set an upper limit on the monopole flux as $F < 2.3/(S\Omega)T = 1.2 \times 10^{-14} cm^{-2} sec^{-1} st^{-1}$ (90% C.L) for the velocity range 1.3 x 10^{-3}c -- c.

(ii) Time of flight method

The pulses in the proportional counters have a mean rise time of 0.6μsec and consequently the timing resolution achieved is~0.4μsec. The arrival times are measured in a window of 0.5μsec -- 7μsec for all tracks with lengths > 1.5 m but without any restriction on ionisation. These cuts correspond to a sensitive velocity region of 7 x 10^{-4}c--4 x 10^{-3}c providing a good overlap with method(1). In a period of 623 days a total of 1200 events were recorded with the timing data. No event has shown the expected progressive delay and hence we obtain the following upper limit of

$$F < 1.7 \times 10^{-14} cm^{-2} sec^{-1} st^{-1} \quad (90\% \text{ C.L}).$$

(iii) Monopole catalysis of nucleon decay

The methods (i) and (ii) are crucially dependent on the monopole ionisation as a function of velocity. If the monopoles catalyse nucleon decay, one can extend this

search to low velocities provided the cross section is close to that of strong interactions. One would then record either a chain of decays or isolated decay event depending on the mean free path λ.

(a) Chain decay In this detector a chain of decays can be recorded only if the second decay event occurs within 7μsec of the first one and if the chain length is in the range 0.4m - 4.5m. During a period of 3.6years of operation of the detector, no event was recorded with characteristic chain decay. Fig 1a shows the flux limit as a function of the monopole velocity for 2 representative values of the cross section. For example, with σ = 10mb, the flux $F < 1.8 \times 10^{-14} cm^{-2} sec^{-1} st^{-1}$ for all $\beta > 10^{-3}$, where β is the reduced velocity.

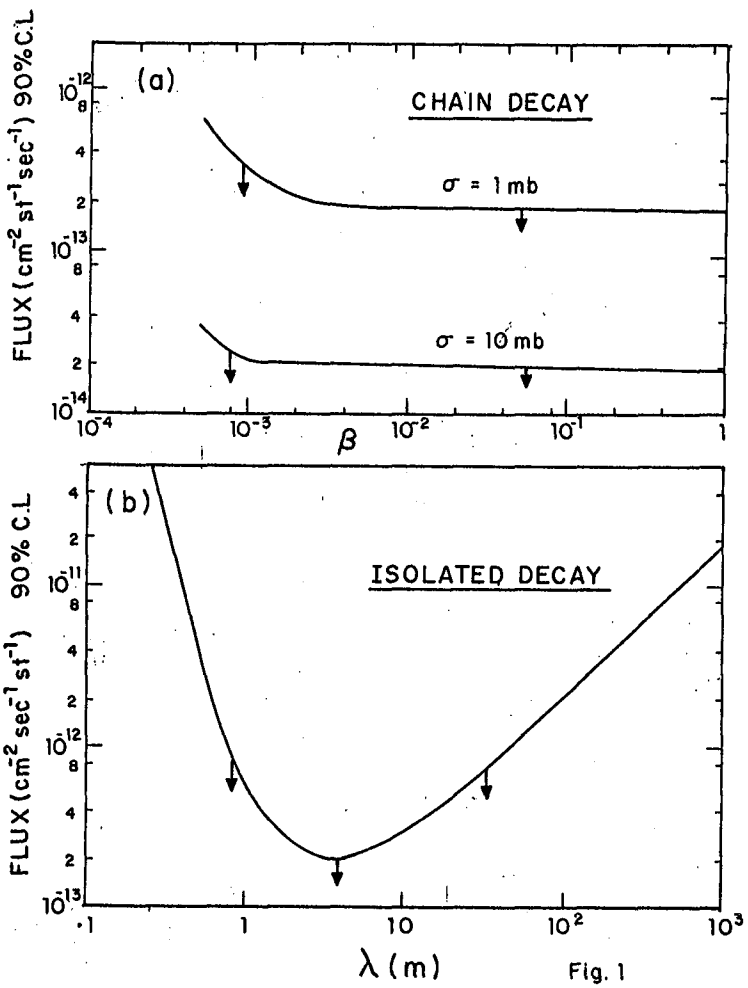

Fig. 1

(b) Isolated decay

If the monopole catalysis results in a momentum imbalance of less than Fermi momentum in iron nucleus it will be indistinguishable from the spontaneous nucleon decay; for larger momentum transfers, it mimics low energy ν-collisions. Thus we consider all the low energy ($\lesssim$ 1 GeV) confined events as possible candidates for catalysis and set upper limit as shown in Fig 1b without background subtraction.

3. Conclusions

There is no evidence for a monopole signal in the present experiment and the best limit is

$$F < 1.2 \times 10^{-14} cm^{-2} sec^{-1} st^{-1} \quad \text{for } \beta > 10^{-3}.$$

While this is 2 times higher than the Baxan limit, it spans a larger range of velocities and is based on large number of samplings (average number is 25) along the track resulting in an unambiguous search for monopoles.

4. Acknowledgements

We are grateful to the Officers and other staff of Bharat Gold Mines Ltd., for their cooperation in the operation of the detector. The Ministry of Education, Japan is thanked for their financial assistance. We are deeply indebted to Messers. B. Satyanarayana, R.P.Mittal, S.D. Kalmani, P.S. Murty, T. Ravindran and J.D. Kulkarni for their technical help in the successful operation of the detector.

References

1. M.R. Krishnaswamy et al., Phys.Lett. 142B (1984) 99
2. M.R. Krishnaswamy et al., Phys.Lett. 115B (1982) 349

AN EXPERIMENT TO DETECT GUT MONOPOLES

G. MacNeill and D.J. Fegan
Physics Department
University College
Dublin 4, Ireland

1. INTRODUCTION

Recent advances in the development of Grand Unification Theories have led to several interesting predictions. One of these states that Grand Unification Monopoles (GUMs) exist as solutions in many non-abelian gauge theories. Another consequence of Unification is the possibility of baryon decay. In fact it has been postulated[1,2] that GUMs may catalyse proton decay in a reaction of the type

$$p + m \longrightarrow m + e^{+} + \text{mesons}$$

Although it is still unclear with what cross section this interaction would proceed, it has been suggested that it would be comparable to that of a strong interaction ($\sigma \sim 10^{-26}$ cm^2). If this is indeed so then the detection of magnetic monopoles may be feasible by observing successive proton decays.

Another experimental technique used to detect monopoles depends on the possible ionization loss by GUMs in their passage through ordinary matter. Although the processes involved in such interactions are well understood for relativistic particles, the exact mechanism by which GUMs of various velocities might lose energy is still uncertain.

For velocities in the range $10^{-4} < \beta < 10^{-3}$ (where $\beta = v/c$), energy losses are mainly due to adiabatic excitation of the atoms, arising from the interaction of atomic electrons with the monopoles magnetic field. The monopole leaves the atoms in an excited state, an effect known as the Drell[3] effect. This may be detected by observation of the de-excitation photons or by observing ionization caused by energy transfer from excited atoms to complex molecules with small ionization potentials.

The Drell mechanism is effective when the monopole-atom collision energy exceeds the spacing of atomic levels. However, for smaller values of β, energy loss is due to elastic monopole-atom collisions arising from the long range magnetic charge - magnetic dipole interaction. The energy is eventually dissipated into heat.

Detailed estimates of the stopping power and scintillation light yield for the passage of a GUM through NE110 plastic scintillator have been made by Ahlen et al.[5] They have shown that while there is an effective velocity threshold for observable energy loss by a GUM in this material of $\beta \sim 6 \times 10^{-4}$, for values of $\beta \geq 7 \times 10^{-4}$ a considerable enhancement in energy loss is expected as compared to that of a relativistic muon.

Based on these predictions of how a monopole would interact with matter, a detection system has been constructed, in which monopole catalysis of baryon decay may be observed while simultaneously monitoring ionization loss of slowly moving particles.

OUTLINE OF EXPERIMENT

The main component of the experimental system is a cylindrical tank containing .88 tons of water. The passage of relativistic charged particles through this tank will be marked by the production of Cerenkov radiation. It has been suggested that a monopole passing through a tank such as this would catalyse successive baryon decays, thus giving a unique signature in a detector of this type, observable through the ensuing decay products. The aim of the experiment therefore is to monitor the water for a number of events which are statistically unlikely to have arisen from the cosmic ray background.

The number of 'Rubakov' type decays that might occur during the passage of a monopole through the water tank can be estimated using the formula for the interaction length given by

$$\lambda = \frac{4300\,\beta}{\sigma_0 \rho} \quad \text{(cm)}$$

where σ_0 is the interaction cross section of the order of unity for strong interactions and ρ is the density of the medium in which the interaction takes place.

The path length will be uncertain by several orders of magnitude because of the considerable uncertainly in σ_0. However, for monopoles with $10^{-5} \leqslant \beta \leqslant 10^{-3}$, λ could be in the range between .4 mm and 40 m. Thus for a detector such as ours, where the average track length is of the order of 1 metre, the passage of GUMs, with values of σ_0 and β that combine to give values of λ in excess of .25 m, is unlikely to be registered.

In addition to this 'Rubakov' type experiment, one which detects an ionization loss by a slowly moving particle has also been incorporated into the system. Based on the assumption that a detectable signal would be observed when a GUM encounters a scintillation counter, six plastic scintillators have been placed around the water detector in an attempt to register the passage, through the water, of a slowly moving ionizing particle.

In this set up an event would be deemed to have occurred when an ionization loss is observed in any two of the six scintillators accompanied by at least one interaction in the water tank.

The resolving time between successive scintillator pulses will determine the range of β for which the experiment is sensitive. For $10^{-5} \leqslant \beta \leqslant 10^{-3}$ a resolving time of 1 ms should be suitable. By excluding pulses occurring within a few micro seconds of one another, events due to the cosmic ray background can be considerably reduced.

3. DESCRIPTION OF EXPERIMENTAL SYSTEM

The water tank (diameter = .92 m, height = 1.35 m) is viewed from above and below the water by 2 RCA 4525 photomultiplier tubes. The signals from these tubes are fed directly to individual Le Croy MVL100 amplifier-discriminators. Logic level outputs from these amplifiers are fed to a pair of pre-set counters, which generate a master trigger pulse when the number of applied output pulses exceeds a previously stored value in either a 400 ns or a 2 μs interval. Having selected pre-set values of 3 events in 400 ns and 4 in 2 μs, the expected

accidental rates from the cosmic ray background are 2.5 x 10^{-4} d^{-1} and 3.7 x 10^{-7} d^{-1} respectively.

The analog outputs from the MVL100s are fed to a Transient Data Analyser (TDA), which samples and digitizes the waveform every 50 ns. The resultant 8 bit words are stored in 4096 bytes of memory. Upon receipt of a master trigger pulse, further sampling is disabled and the contents of the memory are transferred to a VAX11/780 for subsequent analysis.

The six plastic scintillators, surrounding the water, are each viewed by 2 RCA 4518 photomultiplier tubes, which are then coupled to six individual MVL100 amplifiers. These are followed by several Le Croy modules, which are used for the purposes of level transformation and coincidence forming. The resultant logic levels are then applied to some additional circuitry which generates a master trigger pulse if signals from any two scintillators occur, separated in time by an interval of between 10 μs and 1 ms.

At the same time a second TDA samples the analog outputs from the water tank every 1 μs and stores the resultant 8 bit words in 1024 bytes of memory. This gives a total sweep time of 1.024 ms. When a master trigger pulse is generated, the contents of the TDA memory are 'frozen' and transferred to an on-line micro-computer, where they are examined, in real time, to determine whether or not any observable interactions occurred in the water detector. A positive conclusion to this examination results in a further interrogation of some associated latches in order to determine in which scintillators the interactions occurred and the length of the interval that separated them in time.

Both this information and the contents of the TDA memory are recorded and the system is then re-armed, ready for the next event. If however no interactions were observed in the water tank then the system is re-armed immediately, thereby reducing the dead time considerably.

4. RESULTS

The efficiency of the water tank detector in registering a 'Rubakov' type decay will vary with both the interaction length and the GUM's velocity, expressed in terms of β. The efficiency decreases at large values of β (> 10^{-2}) because of the limited resolving time of the detector (~50 ns). At lower values of β the time between interactions is such that the criterion of 4 events in 2 μs can no longer be satisfied.

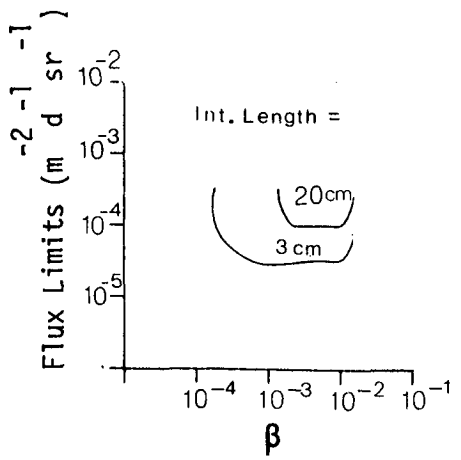

Fig. 1 plots the estimated flux as a function of β for 2 different interaction length, both within the sensitive range of the detector.

The 'Rubakov' experiment has now been in operation for almost 2 years with an estimated live time of 80%. During this time no candidate events have been observed leading to an estimated upper limit on the flux of

$$7.82 \times 10^{-5} \ m^{-2} \ d^{-1} \ sr^{-1}$$

The ionization loss detection system has only recently come on line and as yet no results are available from this experiment.

5. REFERENCES

1. Rubakov, V., Nucl. Phys. B203, p311 (1982).
2. Callan, C., Nucl. Phys. B212, p391 (1983).
3. Drell, S.D. et al., Phys Rev. Lett., V50, No. 9 p644 (1983).
4. Bosetti, P.C. et al., Phys. Lett. 133B No. 3,4, p265 (1983).
5. Ahlen, S. et al., Phys. Rev. D 27, 688 (1983).

SEARCH FOR SUPERMASSIVE MAGNETIC MONOPOLES USING MICA CRYSTALS

P.B. Price and M.H. Salamon
Physics Department, University of California, Berkeley, CA

1. Introduction. The survival of the Galactic magnetic field almost certainly sets an astrophysical upper bound of $\sim 10^{-15}$ cm^{-2} sr^{-1} s^{-1} on the flux of monopoles. To improve significantly upon this Parker limit with direct, real-time searches would require a detector area $\sim 10^4$ m^2 and a collection time of years. Several such searches are being contemplated. We have pursued a novel alternative scheme using large mica crystals capable of recording and storing tracks of slow monopoles over a time scale of $\sim 10^9$ years.

2. Mica as a Detector of GUT Monopoles. At $v > 10^{-2}c$ heavy ions deposit energy mainly by electonic excitation and ionization at a rate S_e; some fraction of this energy is converted into displaced atoms. If the linear density of displaced atoms in a solid is sufficiently high, a track can be revealed by chemical etching. At $v < 10^{-2}c$ the energy lost by ions goes directly into displacing atoms. This "nuclear" component of energy loss, S_n, has its peak value for ion velocities $\sim 10^{-3}c$, the region of interest for GUT monopole detection.

Muscovite mica, available in large, transparent, sheet-like crystals, is the most thoroughly studied of all track-recording solids [1,2]. Etchable tracks have been shown to be produced in mica which is irradiated with very low-energy ions ($5 \times 10^{-4}c < v < 0.0025c$) having $8 \leq Z \leq 90$ [2]. In this regime, where S_e is negligible, the rate of etching along a particle track is given by $v_T = 0.012(\mu m/hr) \cdot S_n(GeV\ cm^2/g)$, for muscovite etched in 40% HF at 25° C. As Fig. 1 shows, in evaluating visibility of an etched track, one must consider not only v_T but also $v_\perp$, the rate of etching perpendicular to the cleavage surface in the absence of a track, and $v_\parallel$, the etch rate parallel to the cleavage plane. For the above etching conditions, $v_\perp = 0.027$ μm/hr and $v_\parallel = 1.36$ μm/hr. In order for a penetrating particle at zenith angle θ to leave a track detectable after an etch time t, it is necessary that $v_T t \cos\theta - v_\perp t > H_{crit}$, where H_{crit}, the minimum detectable depth of the etched track under normal scanning conditions, has been determined by us, using Tolansky multiple beam interferometry, to be ~ 0.1 μm. For t = 48 hr (used by us) it follows that $S_n \cos\theta$ must exceed ~ 2.42 GeV cm^2/g to produce a detectable track. S_n for a slow, bare monopole is far too small to form a track [3]. However, many authors have concluded that monopoles will form bound states with nuclei through magnetic dipole-magnetic monopole interactions [see refs. in 4]. An estimate of S_n of such a composite system in mica is given by evaluating S_n for the nucleus, replacing its mass with the huge mass

of the monopole, using an expression for S_n which has a sound theoretical basis and has been well fit to experimental data [5]. One finds that for a monopole bound to ^{27}Al (the most abundant nucleus in the earth's crust with a large nuclear moment), $S_n > 2.42$ GeV cm^2/g for velocities from 2×10^{-4}c to 0.002c. Thus, if monopoles capture nuclei in the earth's crust, they will record tracks in mica located beneath the capture point. Estimates of radiative capture cross sections [4] and of nuclear abundances in the crust yield capture mean free paths of ~10 km. The mean burial depth over the lifetime of mica crystals now in collections is ~3 km. Thus, a substantial fraction of monopoles penetrating a mica detector would be detected.

3. Status of the Search. Price et al. [4] searched for monopole tracks in a 13.5 cm^2 sample of mica with a fission-track-retention age of 4.5×10^8 yr. To eliminate backgrounds due to the accidental alignment of spontaneous fission tracks and other etchable defects, they demanded the linear alignment of etch pits on four cleavage surfaces separated by ~200 μm, about 20 times the range of a single fission track. The curve labeled "old mica limit" in Fig. 2 shows the flux upper limit resulting from that search, in which they found no quadruply aligned etch pits.

We report here the status of a new search which, when complete, will have an area X time factor ~100 times greater than that of the previous mica search. We collected micas from Museum d'Histoire Naturelle (Paris), the British Museum (London), the Smithsonian, and the Stanford collection. Application of four criteria eliminated all but three crystals with total area ~1200 cm^2: (i) absence of any mechanical deformation; (ii) <100/cm^2 background tracks (due to spontaneous fission of random ^{238}U atoms); (iii) fission track retention age $>5 \times 10^8$ yr; (iv) >3000 alpha recoil tracks from U + Th atoms per ^{238}U fission track. The last criterion assures that, on the assumption that its radiation damage distribution is similar to that of the recoiling daughter of a U or Th α-decay, any track of a monopole-nucleus bound state would survive for the full fission-track retention age.

We laser-cut three crystals with track-retention ages of 0.9, 0.6, and 0.6 billion years into ~150 cm^2 squares, cleaved them into several ~100 μm-thick sheets, etched them for 48 hours in HF, reassembled a pair of sheets at a time and scanned them in transmitted light at ~100 X with the microscope focussed on the common surfaces. Each fission track that crossed the common surface produced a pair of superimposed etch pits. In a total of 470 cm^2 scanned to date, we found three cases that satisfied our criterion for approximate quadruple alignment. Superimposing a third sheet in its correct position on the two others (as in Fig. 1), we found that all three events failed the requirement of sextuple coincidence.

Based on this null result we calculated the curve labeled "new mica limit" on Fig. 2, taking into account the mean free capture paths of ^{27}Al and

^{55}Mn, the most abundance nuclides with large magnetic moments, and assuming that monopoles are not bound to protons when they hit the earth. The reduction of sensitivity at large velocities is due primarily to the decrease in S_n. The cutoff velocity at $3 \times 10^{-4}c$ is due to a threshold associated with overcoming the diamagnetic repulsion of inner-shell electrons [6].

4. Critique of the Mica Limit

a) Reduction of nucleus capture cross section? Arafune and Fukugita [6] showed that the long-range force between a monopole and a nucleus due to extra angular momentum carried by a monopole-electric charge system would result in an enhanced or a reduced capture cross section, depending on the sign of the anomalous magnetic moment of the nucleus. For the cases of ^{27}Al and ^{55}Mn, which have a positive anomalous moment, the cross section would be enhanced, so that the limit of Fig. 2 would be even lower if this effect were taken into account.

b) Monopole already bound to a proton. Bracci et al. [7] calculated the fraction of monopoles bound to protons that they captured in the early universe. For all reasonable values of the monopole-proton binding energy (40 to 200 keV) and of the baryon to photon ratio (4 to 7×10^{-10}), they concluded that essentially all monopoles are now bound to protons, and therefore, because of Coulomb repulsion, cannot become bound to an Al nucleus. However, they overlooked a factor 2π in the exponent of their expressions for formation and dissociation. When the correct expressions are used, the fraction, f, of monopoles bound to protons drops to values in the range $f = 0.15$ to 0.98, which raises the mica limit by the rather small factor $1/f$.

c) Catalysis of baryon decay. Rubakov [8] and Callan [9] argue that for GUTs that predict proton decay, GUT monopoles strongly catalyze baryon decay, making it likely that monopole-nucleus bound states would be short-lived. However, there is no proof yet that baryon-number violating processes occur. Moreover, it has been argued that SU(5) GUT monopoles might not catalyze baryon decay [10,11], that monopoles in some other GUTs would not catalyze baryon decay [11,12], and that in some GUTs baryon number violating proton decay does not occur. The mica result places a very stringent limit on the flux of monopoles that do not strongly catalyze nucleon decay. Direct searches sensitive to bare monopoles or to monopole-catalyzed proton decays are an essential complement to the mica search, even though they probably can never be as sensitive as the mica nor are they as sensitive as indirect limits based on the assumption of catalyzed decays inside neutron stars or white dwarfs [13]. The indirect limits may, however, have loopholes.

Final results of the mica search, including data on etching and thermal stability of very low-energy heavy-ion tracks, will be reported elsewhere. This work was supported by NSF Grant PHY-8403710. We thank A.M. Clark (British Museum) for supplying mica samples B.M. 1982, 274a, b, and c.

References

1. R.L. Fleischer et al., Nuclear Tracks in Solids, (U.C. Press, Berkeley, 1975).
2. J. Borg et al., Rad. Effects 65, 133 (1982); J. Borg, Ph.D. Thesis, Paris, 1980.
3. S.P. Ahlen and K. Kinoshita, Phys. Rev. D26, 2347 (1982).
4. P.B. Price et al., Phys. Rev. Lett. 52, 1265 (1984).
5. W.D. Wilson et al., Phys. Rev. B15, 2458 (1977).
6. J. Arafune and M. Fukugita, Phys. Rev. Lett. 50, 1901 (1983).
7. L. Bracci et al., Phys. Lett. 143B, 357 (1984).
8. V. Rubakov, JETP Lett. 33, 644 (1981).
9. C. Callan, Phys. Rev. D26, 205B (1982).
10. T.F. Walsh et al., Nucl. Phys. B232, 349 (1984); M Hortacsu et al., Phys. Lett. 145B, 411 (1984).
11. D.P. Bennett, Phys. Rev., in press.
12. S. Dawson and A.N. Schellekens, Phys. Rev. D27, 2119 (1983); E. Weinberg et al., Nucl. Phys. B236, 90 (1984).
13. See, e.g., E.W. Kolb and M.S. Turner, Ap. J. 286, 702 (1984); K. Freese, Ap. J. 286, 216 (1984).

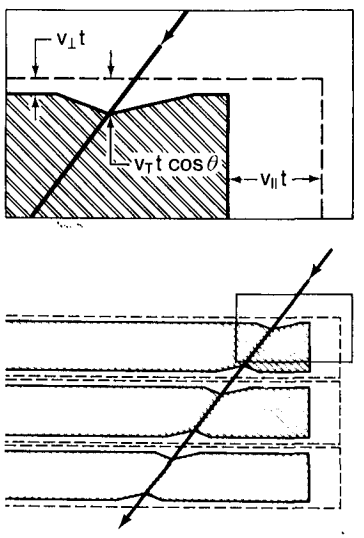

Fig. 1. Collinear etch pits along the trajectory of a hypothetical monopole-nucleus bound state in three sheets of mica that had been cleaved, etched, and superimposed again.

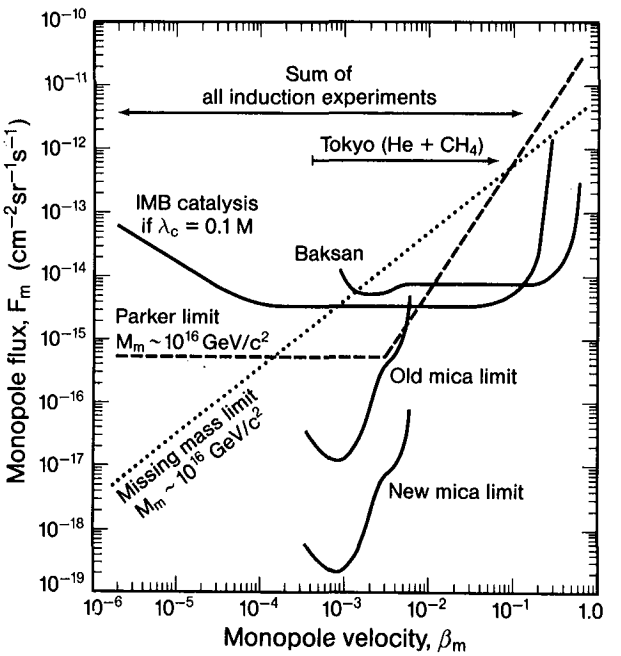

Fig. 2. Monopole flux limits vs monopole velocity for several direct searches (solid curves) and indirect astrophysical arguments (dashed curves).

THE HOMESTAKE SURFACE-UNDERGROUND SCINTILLATORS -- DESCRIPTION

M.L. Cherry*, S. Corbato*, T. Daily*, E.J. Fenyves+, D. Kieda*, K. Lande*, and C.K. Lee*

* Depts. of Physics and Astronomy, Univ. of Penna., Philadelphia, PA 19104
+ Dept. of Physics, Univ. of Texas, Dallas, TX 75080

Two new detectors are currently under construction at the Homestake Gold Mine -- a 140-ton Large Area Scintillation Detector with an upper surface area of 130 m^2, a geometry factor (for an isotropic flux) of 1200 m^2 sr, and a depth of 4200 m.w.e.; and a surface air shower array consisting of 100 scintillator elements, each 3 m^2, spanning an area of approximately 0.8 km^2. Underground, half of the LASD is currently running and collecting muon data; on the surface, the first section of the air shower array will begin operation in the spring of 1985. We describe the detectors and their capabilities.

I. Introduction

Underground, the Large Area Scintillation Detector will be used to 1) search for slow, massive magnetic monopoles with a combination of large area, low dE/dx, low background, and electronic sensitivity to the entire velocity range $10^{-4}<\beta< 1$; 2) study the zenith angle distribution of neutrino-induced and penetrating muons; 3) search for neutrino bursts from stellar collapse events in the Galaxy; and 4) serve as a prototype for a solid, large volume scintillation detector used to search for nucleon decay and ^8B solar neutrinos. The combined surface-underground telescope will be used to 5) measure the multiplicity and transverse momentum distributions of high-energy cosmic ray muons; 6) study the primary cosmic ray nuclear composition near 10^{15} eV; and 7) search for cosmic point sources of neutrinos, gamma rays, and high-energy cosmic rays (for example, Cygnus X-3) with very good angular resolution (3-10 mrad with the combined surface and underground detectors). We describe the design of the detectors here; in an accompanying paper[1], we discuss the initial performance of the LASD.

II. The Underground Large Area Scintillation Detector

The Large Area Scintillation Detector is located at a depth of 4850 ft. (4200 m.w.e.) in the Homestake Mine (Fig. 1). It consists of a hollow 8m x 8m x 16m box composed of 200 30cm x 30cm x 8m liquid scintillation detectors surrounding the existing ^{37}Cl solar neutrino tank of Davis et al.[2]. The detector is sufficiently large to mount a search for magnetic monopoles at the Parker limit (10^{-15} cm^{-2} sec^{-1} sr^{-1}) in 3 years. Each of the 200 scintillator elements is a PVC box lined with teflon (for total internal reflection) containing a low-cost mineral oil-based liquid scin-

tillator developed to have excellent light collection and transmission characteristics, a light attenuation length of approximately 7 m, long-term stability, a high flash point, and low toxicity. In addition, since the same scintillator oil is used in the surface array, the oil maintains its clarity down to very low temperatures. Each detector element is viewed by two 5-inch photomultiplier tubes in coincidence, one at each end. Fast muons passing through the middle of one of the modules produce an average of 350 photoelectrons at each photomultiplier. A particle ionizing even at 0.01 times minimum would thus produce 3-4 photoelectrons at each photomultiplier and still be visible. The low energy threshold is therefore set not by the scintillator light yield, but rather by the background produced by the ambient radioactivity (primarily MeV gamma rays) from the rock walls. We have initially set our thresholds at 1/10 minimum ionizing, or 5 MeV.

The individual detector elements have $\pm$ 1.3 ns time resolution, spatial resolution of $\pm$ 15 cm, and a very low muon background flux. Cosmic ray muons and neutrino-induced muons will typically produce two pairs of coincident photomultiplier tube pulses, one pair as the muon enters the detector and one delayed pair as the muon leaves the detector. The delay between the entering and exiting pulses will be about 25 ns. We can recognize multiple muons passing through a given module by the large pulse height and the mismatch between time differences and pulse height ratios. From the location of the entering and exiting points, the muon direction can be determined to $\pm$ 3°.

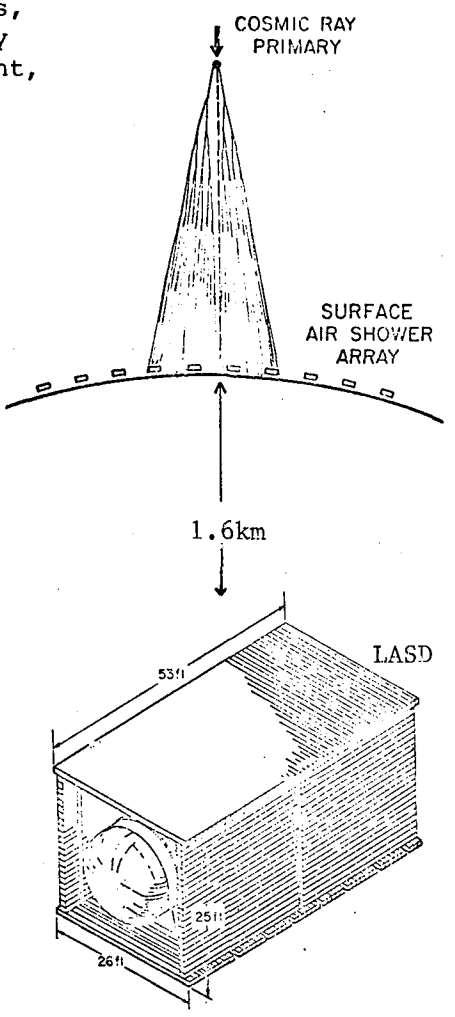

Fig. 1. Surface and underground Homestake detectors.

For a monopole, we expect a pair of slow pulses with width 1 ns/β as the monopole enters the detector and, after a delay of 25 ns/β , a second pair of slow pulses as the monopole leaves. For slow monopoles with $10^{-4} \lesssim \beta \lesssim 10^{-3}$, the delay time between the two entering and exiting pulses will be 25-250 μs. Such long delays can only be correlated in a very low background environment such as that available in a deep mine. The monopole position in each box will be determined from the ratio of pulse heights at each end of the box; the individual pulse heights are then corrected for the position, and the monopole pulse height is deter-

mined.

The electronics are designed to permit us to look at both fast muons and slow monopoles. The muon circuitry is currently running on the southern half of the detector. The range of interesting times is from 1 ns to 250 μs. The system is therefore equipped with a fast clock (2.5 ns resolution) which covers the first 500 ns and a slow UTC clock (0.2 μs resolution) to cover the time span thereafter. A 16-pulse (or event) deep memory buffer is associated with each photomultiplier so that multiple pulses for each event can be recorded.

The monopole circuitry is presently being built. It provides the functions of a transient recorder for each photomultiplier, using fast flash ADC's (7 bits, 20 MHz) associated with 2048-byte memories. Five parallel ADC-memory channels are associated with each tube, displaced in time by 10 ns each. When a trigger is seen, the memories are read out for every phototube which fires, giving a record of pulse heights in intervals of 10 ns over a duration of up to 100 μs for a single wall. Individual walls of the detector are triggered independently, so that the total length of the event can be 300 μs, sufficiently long to see slow monopoles ($\beta \geq 10^{-4}$) or low-energy neutrons. A fast (10 ns) muon pulse can then be clearly distinguished from a slowly rising ($1/\beta$ ns) monopole pulse; in addition, we measure the flight time across the room, and the individual pulse heights.

The mechanical work on the underground detector is essentially finished. The southern half of the detector has been filled with liquid and turned on. Since Jan. 1985, we have collected 2×10^4 muon events which are currently being analyzed. We are now installing the north-side electronics and filling the remaining detector modules with oil. The detector is expected to be fully operational (including the monopole electronics) in the fall of 1985.

III. The Surface-Underground Telescope -- Composition and Point Sources of Cosmic Rays

The surface array will consist of approximately 100 scintillation detectors, spaced by 15 - 200 m and deployed over an area of about 0.8 km^2 over the underground chamber. The individual detector elements consist of reinforced concrete boxes 4 ft x 8 ft x 2 ft high with 3" thick side walls, covered on top by a 24 gauge galvanized tin cover plate. The inside of the box is lined with styrofoam insulation and an aluminum light reflector. The active detector is 4" of liquid scintillator, designed to have a high flash point and to remain clear at low temperatures. The scintillator is viewed by two 5" photomultiplier tubes operating in coincidence. Twenty-seven detector elements are presently in position and ready to begin operation.

The telescope can operate either in a "prompt" mode in which only the surface elements fire, or in a "delayed" mode in which a trigger pulse from the underground detector arrives approximately 14 μs after the surface array signals. The 14μ s delay is the result of the 5 μs muon flight time from the surface to the underground detector plus the 9 μs signal propagation time along the cable connecting the underground

detector and the surface array.

The location of the shower core will be calculated from the locations, pulse heights, and arrival times seen by those detectors firing in the shower. We expect to locate shower cores to within 4 m in the central section of the array and 10 - 20 m in the outer part. Underground, the liquid scintillator elements make it possible to resolve tracks separated by 1 ft; however, the final underground position uncertainty of 2.5 m is determined primarily by scattering in the rock. The angular resolution of the combined surface-underground telescope is then 3 - 10 mrad. The expected surface-underground coincidence rate will be a few hundred per year.

By combining the large air shower array on the surface with the underground detector, we can measure the cosmic ray composition between 10^{14} and 10^{16} eV. Measuring the total electron number N_e on the surface (i.e., the total energy/nucleus) and the multiplicity of high energy ($E_\mu \gtrsim 2.7$ TeV) muons underground (i.e., the energy/nucleon) permits discrimination between primary species in a way that depends essentially on energetics. In order to reach our depth, muons must have roughly 2.7 TeV at the surface of the earth. Such muons can be produced by proton primaries with energies in excess of 10^{13} eV or, for example, by iron primaries with energies above a few times 10^{14} eV. A proton generally gives rise to a single high energy muon while an iron, consisting of a superposition of 56 separate nucleons, has a large probability of multiple muon production, particularly above 10^{15} eV. Our data will thus consist of muon multiplicity and separations underground, and shower size at the surface. For small showers ($E \lesssim 10^{15}$ eV) we expect to observe single muons primarily from cosmic ray protons, while for large showers ($E > 10^{15}$ eV) we expect a mix of single and multiple muons from protons and heavy (nominally iron) primaries.

The combined surface-underground detectors can also be used as a high angular resolution telescope to look for intense point sources of cosmic gamma rays or neutrinos [1].

Funding for the Homestake scintillator experiments is provided by the U.S. Department of Energy. The assistance and generous cooperation of the Homestake Mining Company are deeply appreciated. We are especially indebted to A. Gilles and J. Dunn. In addition, we appreciate the advice, assistance, and participation of T. Ashworth, K. Brown, B. Cleveland, R. Davis, I. Davidson, J. Lloyd-Evans, R. Reid, E. Marshall, R. Steinberg, and A. Watson.

References

1) M.L. Cherry, S. Corbato, T. Daily, D. Kieda, K. Lande, and C.K. Lee, 19th Intl. Cosmic Ray Conf., La Jolla, paper HE 5.1-3 (1985).
2) J.K. Rowley, B.T. Cleveland, and R. Davis, Jr., Solar Neutrinos and Neutrino Astronomy, ed. by M.L. Cherry, K. Lande, and W.A. Fowler, AIP Conf. Proceedings No. 126, AIP, New York (1985).

HE 6.1-11

UPPER LIMIT ON MAGNETIC MONOPOLE FLUX FROM BAKSAN EXPERIMENT

Alexeyev E.N., Boliev M.M., Chudakov A.E., Mikheyev S.P.
Institute for Nuclear Research the USSR Academy of Science,
60th October Anniversary pr., 7a, 117312, Moscow, USSR

No indication of slowly moving penetrating particles in cosmic radiation unerground was found during two years observation. Particle velocity and pulse shape are main criteria for search. Probability of the imitation of slow particles ($\beta<0.1$) by atmospheric muons is negligible. Our upper limit on superheavy magnetic monopole flux is now $1.86\cdot10^{-15}cm^{-2}sr^{-1}s^{-1}$ (90% c.l.) for velocity range $2\cdot10^{-4}<\beta<0.1$.

Resent years activity in the search for magnetic monopole has been increasing[1] in spite of negative results of all performed experiments. However, limit on monopole flux achieved so far is still larger than bound set from astrophysical consideretion. At present Baksan underground telescope[2-4], having the largest acceptance for monopole (1850 m^2sr), accumulates data for more than two years live time. In this paper we represent new limit on flux of superheavy magnetic monopoles set from Baksan experiment.

1.EXPERIMENTAL DETAILS. Following characteristic features of Baksan telescope make it most suitable detector for monopole searches: i) big size (16m×16m×11m); ii) 3200 scintillators arranged in 8 layers separeted by concrete absorber; iii) timing registers to measure particles velocity; iv) recording of pulse shape for each layer.

In order to select slowly moving particles special trigger is used. Its logic can be understood from time diagram presented in Fig.1. Signal (a) arises when only one from six external layers is hitted. This signal opens time gate (b) of 50μs duration with 50ns delay for delayed signal from any two internal layers(c). Initial signal triggers the memory for 1.5μs to record co-ordinates of hitted scintillators(d). Delayed coincidence signal triggers memory again now for 50μs and also triggers oscilloscope to record pulse shape. The delays of the signals from all layers relative to initial one are measured up to 50μs. All the signal thresholds for trigger logic, detector co-ordinates and timing cor-

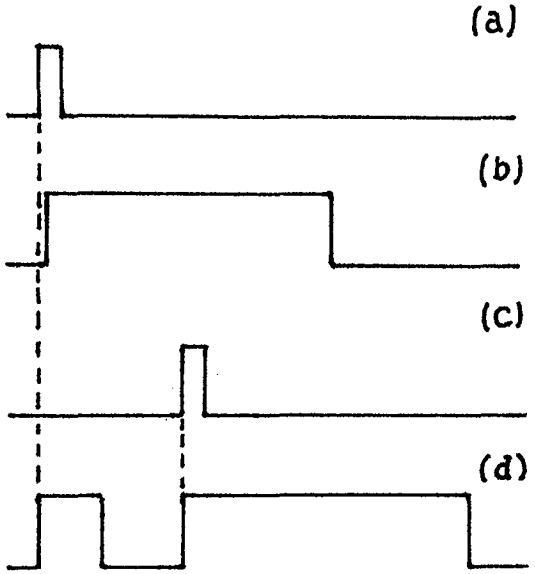

Fig.1 Time diagram of trigger logic.

respond to 0.25 of amplitude of minimal ionizing particle. The trigger rate is 237 per day.

2.RESULTS AND DISCUSSION. Two types of events are selected by the trigger. The first is when there are signals from two scintillator layers one external and one internal and second is when there are signals from more than two layers. The rate of events of the first type 82.6/day is due to chance coincidences with a single internal pulse, secondaries from muon interactions outside of telescope and stopping muons. In the last case muons are stopped in absorber between scintillator layers so that decay electrons produce a signal in internal layer. Second type of events is due to chance hit of fast muon in time gate 50μs (152.1/day) and muons with time of flight between external and internal layers bigger than 50ns(2.3/day)

Two criterions are chosen to select candidates for further analysis of time of flight, amplitudes and pulse shape. In order to exclude firs type of events we required signals from at least three layers. Second type of events was excluded by requirement of time intervals no less than 0.1us between successive layers. During live time 18,546 hours analazed so far no candidates has been recorded.

The trigger and criterions of selection make acceptance dependent on velocity. The calculations show that for velocity range $2\cdot10^{-4}<\beta<0.1$ acceptance is nearly constant 1850m^2sr. So we can set upper limit on monopole flux as:

$$1.86\cdot10^{-15}m^{-2}sr^{-1}s^{-1}$$

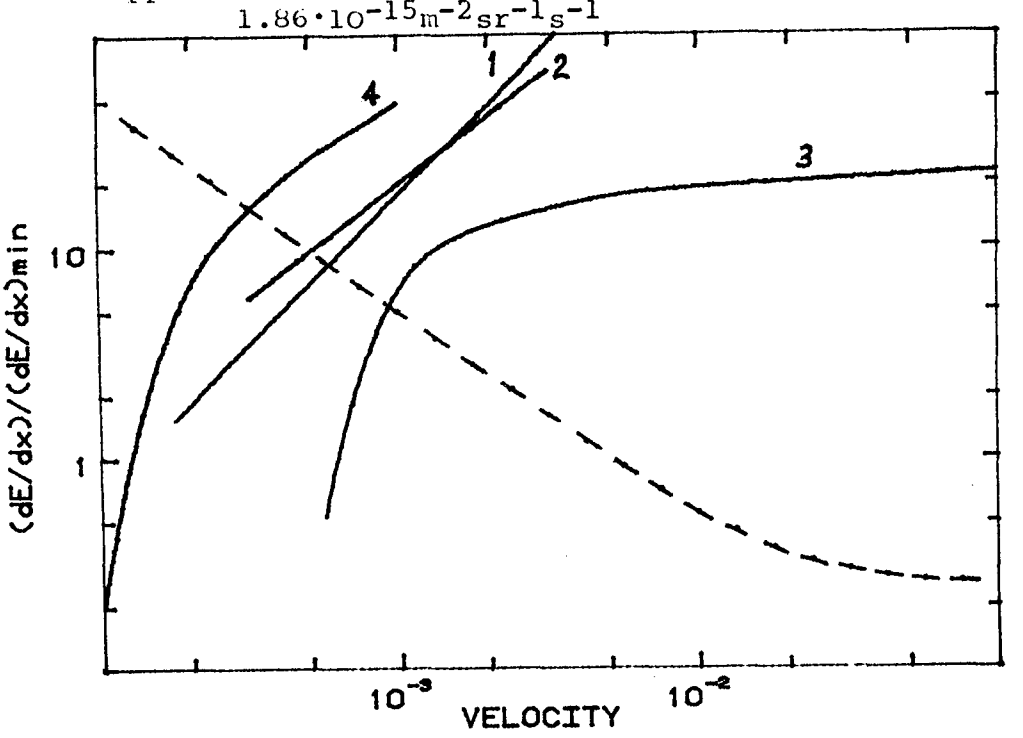

Fig. Ionization losses of monopole as function of velocity; curves 1-[3], 2-[5], 3-[6], 4-[7]

However, there is problem of ionization losses of energy by slowly moving monopoles. Number of estimates and calculations has been made. They are shown on Fig.2. Curve 1 is estimate of ionization losses[3] made from ionization power of slowly moving protons taking into account peculiarities of interactions of moving magnetic charge with electrons. Curve 2 was calculated for magnetic monopoles in a degenerated Fermi gas[5]. Curve 3 is calculation of light emitted of organic scintillator with the energy gap 5 eV[6]. In calculation of curve 4 it has been taken into consideration possible excitation of atoms due to shift of atomic levels by magnetic field of monopoles[7]. These calculations are made for atoms of helium and it is not clear if there is contribution of this effect to excitation of scintillator. It is seen from Fig.2 that for $\beta > 10^{-3}$ there is no problem in sensitivity of usual ionization detectors to magnetic monopoles. For velocity range 10^{-3}-10^{-4} the possibilities of such kind of detectors are quite uncertain and for $\beta < 10^{-4}$ there is no hope to detect monopoles using ionization technique. Besides amplitude of monopole signal can be reduced due to stretch of pulse if time of traversing through detector is bigger than integrating time of the circuit. Really this effect results in increase of threshold. On Fig.2 dashed curve shows dependence of real threshold of recording of slowly moving particle on velocity for Baksan telescope. So, ionization power of monopoles limit velocity range of our experiment to $\beta \sim 10^{-3}$.

However we can use hypothesis[8] on catalysis of proton decay by monopoles to set limit on monopole flux for $\beta < 10^{-3}$. For proton decay taking place inside the concrete absorber or scintillator the mean detection efficiency is 0.56. If the catalysis cross section is 50mb then the efficiency of Baksan telescope to record monopoles trough catalysis process is more than 0.9.

Therefore, our limit is model independed for monopole velocity $\beta > 10^{-3}$ and is valid for $\beta > 2 \cdot 10^{-4}$ if catalysis cross section is >50mb.

REFERENCE

1.See, for example, Proc. of the Conf. 'MONOPOLE-83'
Ann Arbor, Michigan, USA, 1984, edited by J.Stone
2.Alexeyev E.N. et al Proc.16th ICRC v10,p.276, (1979) Kyoto
3.Alexeyev E.N. et al Lett. Nuovo Cimento 35, 413 (1982)
4.Alexeyev E.N. et al Proc.18th ICRC v5,p.52 (1983) Bangalore
5.Ahlen S.P., Kinoshita K., Phys. Rev. D26, 2347 (1982)
6.Ahlen S.P., Tarle G. Phys. Rev. D27, 688 (1983)
7.Drell S.D. et al Phys. Rev. Lett. 50, 644 (1983)
8.Rubakov V.A. Pis'ma Zh. Eksp. Teor. Fiz. 33, 658 (1981)

HE 6.1-12

RESULTS FROM THE UCSD MAGNETIC MONOPOLE SEARCH

Masek, G.E., Knapp, L.M., Miller, E.
Stronski, J.P., Vernon, W. and White, J.T.

Department of Physics, B-019
University of California, San Diego
La Jolla, CA 92093 USA

1. Introduction. The energy loss mechanism for slowly moving magnetic monopoles in helium calculated by DKMPR[1] provides a means of extending the search for such particles by ionization techniques to velocities down to $\sim 3\times10^{6}$cm/sec ($\beta \cong 10^{-4}$). Other gases (e.g. CH_2 or CO_2) mixed with helium will be ionized with high efficiency[2] by collisions with excited helium atoms, thus allowing the use of large proportional chamber systems for the detection of the monopoles. The first reported results utilizing this mechanism was the experiment of Kajino et al.[3] using a detector with an area-solid angle product ($A\cdot\Delta\Omega$) of 24.7 m^2sr. They set a limit on the flux of monopoles of $< 7.2\times10^{-13}cm^{-2}sr^{-1}sec^{-1}$ at a 90% confidence level for $\beta > 3\times10^{-4}$. Here we report on the results of a He:CH_2 proportional tube array designed to extend the velocity limit down to $\beta \sim 10^{-4}$, and push the flux limits closer to theoretical bounds.[4] The detector which has been operating at the University of California, San Diego (UCSD) since last summer, is a prototype for a larger array currently under construction at UCSD. The data presented here is from 200 days of live time with the prototype detector.

To attain limits on the flux approaching current theoretical bounds, detectors with $A\cdot\Delta\Omega$ the order of 1000 m^2sr to 10000 m^2sr are needed. Given fiscal constraints and the desire to achieve large $A\cdot\Delta\Omega$, the basic design philosophy for the UCSD detector is to require only the simplest criteria for monopole detection. Thus the detector employs an array of proportional chamber tubes arranged to observe only a projected track and a projected velocity window. In addition, the array is operated at sea level with no earth overburden, and uses electronic rejection to eliminate the fast muon cosmic ray background. If indeed any signal were observed with this minimum criteria, this would be ample justification for construction of a more expensive, sophisticated detector.

2. Detector Description. The layout of the prototype detector shown in figure 1, consist of 225 individual aluminum proportional tubes, each approximately 2.5 cm x 2.5 cm in cross section, and each $\sim$ 7.2 m. in length. They are strung with .002" diameter gold plated tungston wire, and arranged in an array of six layers as shown in the figure. The gas mixture used was 15% CH_2 and 85% He. An ionizing particle passing through the array leaves an electronic signature of which tubes were traversed and the relative time of transit for each tube.

A simplified flow diagram of the electronics trigger and data acquisition system is shown in figure 2. Outputs from each of the 225 channels is first amplified (gain $\sim$ 300, integrating time, $\sim$ .5 μs) and then individual comparators select a minimum signal threshold. These signals are then split, half forming sums of all signals in individual

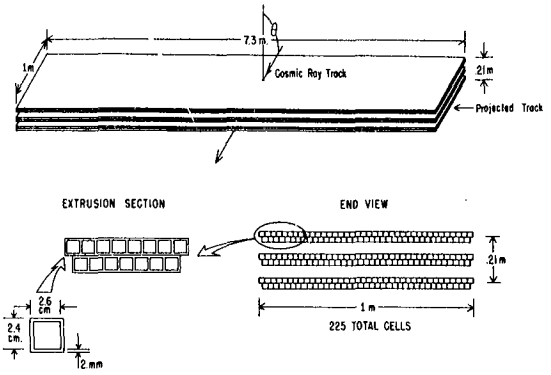

Fig. 1 - Magnetic Monopole Detector Layout.

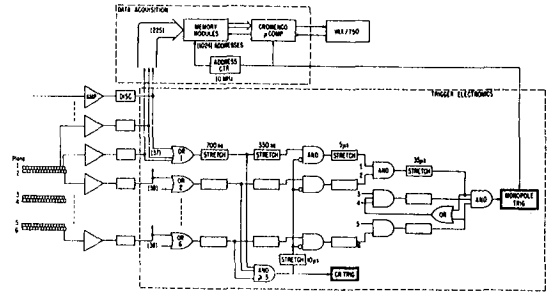

Fig. 2 - Simplified flow diagram of Electronics.

planes to be used in the trigger electronics, and the other half feeding directly to memory modules for data acquisition. In the memory modules, the separate channels are recorded on 1025 x 8 RAMS (AMD AM9128-70) whose addresses are continuously cycled at 10 Mhz. The information stored in the RAMS is read out when an appropriate signal from the trigger electronics is received.

In the trigger electronics shown in figure 2, the logic imposes the following criteria on an event to be read out:

i. All six planes must have recorded a hit within 35 μs (the maximum sensitive time for the detector corresponding to a $\beta = 10^{-4}$ particle traversing with an aximuth of $\sim 80°$).

ii. If any three planes have hits within .7 μs, the event is rejected. This is the main criteria for rejecting cosmic ray muons, and also sets the minimum transit time (1.4 μs) accepted in the trigger. (As mentioned above, final analysis cuts set a limit of 1.5 μs on accepted events, just outside the 1.4 μs trigger limit.)

iii. In addition, events are rejected unless times from the two planes in each of the three pairs (1-2,3-4,5-6) are within 5 μs, and the time of the middle pair must come after either of the outer pairs. These are broad conditions that must hold for a real track within the velocity window.

3. Detector Operation and Results. The energy loss vs β for slow monopoles in helium is calculated in reference 1. The ionization threshold for the detector determines the lower limit on the β which can be detected. In the array described here, the ionization threshold (determined by the high voltage operating point and discriminator threshold) was $I_{thres}/I_o \cong 1/3$ giving $\beta_{min} \simeq 1.1 \times 10^{-4}$.

As described above, the data is first stored in the memory modules, and when the appropriate conditions are met in the hardware trigger electronics, the data is read out through a Cromenco microprocessor to a VAX 750 computer for off-line analysis. In addition, the microprocessor also permits a software trigger condition to be imposed. We require that in each of the three pairs of planes (1-2,3-4,5-6), there be at least one set of adjacent hits (called a cluster) in the two planes making up the pairs. The trigger conditions and subsequent rates are

summarized in Table 1. Thus, of the initial rate of 520 Hz of cosmic ray muons traversing the detector, only the order of one per hour are recorded by the VAX computer.

TABLE 1

Rates at Various Stages in the Data Acquisition and Analysis

Stage	Rate	Rate (Normalized to CR)
Cosmic Ray Rate thru six planes	520/sec.	1
Hardware Trigger Electronics (see text)	14.4/hr	7.7×10^{-6}
Software Trigger in μ-Processor (see text)	1.35/hr	7.2×10^{-7}
Offline Analysis Cuts (see text)	0.5/dy	1.1×10^{-8}

In the off-line analysis, summary files of the data are made by imposing rather broad cuts on the data to select out monopole candidates. These cuts are:

i. Track candidates are selected by requiring a projected linear fit to clusters in each of the three pairs of planes.

ii. For selected track candidates, the mean time of each of the three clusters making up a track, must be increasing or decreasing from top to bottom in the array. This selects the correct time sequence for slowly moving particles passing down through the array or up through the array.

iii. At least one of the hits associated with a track candidate has to be identified with the original hardware trigger timing sequence.

iv. The time difference between the outer planes must be greater than 1.5 μs.

v. A track is rejected if 3 planes have hit times within .7 μs.

Additionally, for the track candidate, two Chi-Squared relations are calculated. A linear fit to the mean projected position ($XMEAN_i$) of each cluster, gives a fit position ($XFIT_i$) then $XSQ = \sum_{i=1}^{3} (XMEAN_i - XFIT_i)^2$. Also a linear fit to the mean times of hits vs distance along the track on each of the six planes ($TMEAN_j$) gives a fit time ($TFIT_j$), then $TXSQ = \sum_{j=1}^{6} (TMEAN_j - TFIT_j)^2$. (The units of the two quantities are cm^2 and .1 μsec^2, respectively). The effect of the cuts described above on the rates is also given in Table 1, thus only an effective rate of 1/2 event per day survives for further consideration. The final step in the analysis consists of making an event display of each event in the summary file, and individually scanning these events. A typical event display is shown in figure 4. In the top, the projected view of the end of the array is shown, along with an indication as to which cells were hit in the event. For each hit, the time of the hit (in units of .1 μs) and the duration of the pulse (also in units of .1 μs) are given beside each cell hit. The solid line gives the fit to the track clusters and the XSQ is displayed in the upper left. In the lower left corner of the display is a plot ot time vs distance along the track. The solid

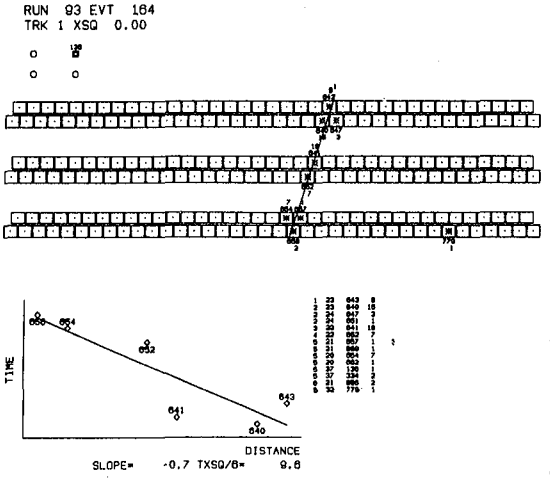

Fig. 3 - Event Display. Event shown is a μ-e event (see text).

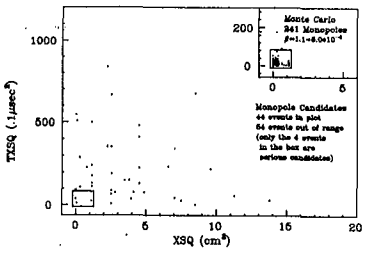

Fig. 4 - TXSQ vs XSQ for Candidate Events. The inset is the plot for Monte Carlo Monopole events.

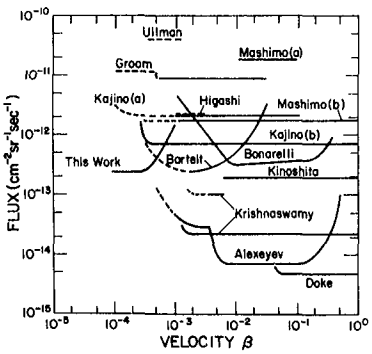

Fig. 5 - Compilation of flux limits on magnetic monopole vs β at 90% confidence level. Taken from ref. 3, but including this work.

line here gives the fit to the six mean times, and the TXSQ is displayed beneath the plots. The scanning of the 98 surviving monopole candidates on the summary files gave no events which could be interpreted as a slowly moving particle in the time window between 1.5 μs and 35 μs. The numbers scanned can be substantially reduced by employing the Chi-squared cuts. Figure 4 gives a scatter plot of XSQ vs TXSQ for all of the data in the summary files. Imposing cuts of XSQ < 1.5, and TXSQ < 84 accepts 99% of the Monte Carlo monopole events and leaves only 4 events for further consideration. Of interest is the characteristics of the summary candidates. The majority of these events can be interpreted as cosmic ray muons that stop in the walls of the detector, and subsequently decay into an electron that then passes through the remaining planes of the array (a μ-e event). A measure of the energy deposition of a particle passing through a cell is given by the width of the pulse, which is also recorded with each event. For these μ-e events the pulse width near the end of the muon range should increase. This is clearly observed with these events, and the frequence and magnitude agree with what would be expected for stopping muons. Thus these events afford a very nice check on the overall performance of the system. Moreover, the pulse width (height) information can be used as an additional requirement on the monopole candidate, although in fact it was not necessary for rejecting the candidates in this data sample.

4. Conclusion. The $A\cdot\Delta\Omega$ for this prototype apparatus is 54.6 m^2sr for particles with $\beta = 1.1\times10^{-4}$ within the time window acceptance 1.5 μs to 35 μs. For a live time of 200 days, this gives an upper limit on the monopole flux (at the 90% confidence level) of $2.4\times10^{-13}cm^{-2}sr^{-1}sec^{-1}$. As discussed above, the detector was optimized for the lowest detectable velocities, and the effective $A\cdot\Delta\Omega$ decreases with increasing velocity. The limits set for this experiment from $\beta = 1.1\times10^{-4}$ to $\beta = 10^{-3}$ are shown in figure 5 along with recent limits from other ionization experiments.

References

1) S.D. Drell, N.M. Kroll, M.T. Mueller, S.J. Paske, and M.A. Ruderman, PRL 50, 644 (1983).
2) W.P. Jesse, J. Chem. Phys. 41, 2060 (1964).
3) F. Kajino, S. Matsumo, Y.K. Yuan, and T. Kitamura, PRL 52, 1373 (1984).
4) D. Groom, UU HEP 83/19, revised 19 Jan. 1984.

HE 6.2-2

SEARCH FOR PROTON DECAY IN THE FREJUS EXPERIMENT

AACHEN[1], ORSAY[2], PALAISEAU[3], SACLAY[4], WUPPERTAL[5], Collaboration

ABSTRACT

We will report, in this paper, the present status of the Frejus experiment and the preliminary results obtained in the search for nucleon decay.

1. Frejus laboratory and detector. A modular, fine grain tracking calorimeter has been installed in the Frejus laboratory in the period extending from October 1983 to May 1985. The 3300 m^3 underground laboratory, located in the center of the Frejus tunnel in the Alps is covered in the vertical direction by 1600 m of rocks (4400 m w.e). The average number of atmospheric muons in the lab. is 4.2/m^2. day. Fig. 1 shows a sketch of the Frejus laboratory with the detector.

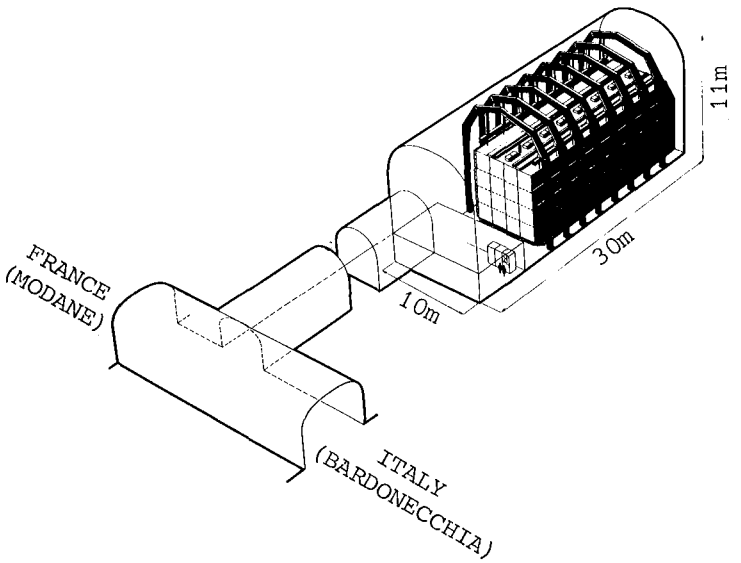

The 912 ton detector is made of 114 modules, each one including eight flash chamber and one Geiger vertical planes of (6 × 6) m^2 dimensions. The flash chamber (and Geiger) planes are alternatively crossed to provide a 90° stereo reconstruction.

Figure 1 : General picture of the Frejus laboratory

[1] *Ch. Berger, A. Hoffmann, F. Raupach, J. Tutas, G. Schmitz*
I. Phys. Inst. der Techn. Hochschule, Aachen (Germany)
[2] *B. Dudelzak, P. Eschstruth, G. Deuzet, S. Jullian, D. Lalanne, F. Laplanche, C. Longuemare, C. Paulot, Ph. Roy, G. Szklarz*
Laboratoire de l'Accélérateur Linéaire, Orsay (France)
[3] *L. Behr, R. Bland, B. Degrange, U. Nguyen-Khac, P. Serri, S. Tisserant*
Laboratoire PNHE, Ecole Polytechnique, Palaiseau (France)
[4] *P. Bareyre, R. Barloutaud, G. Chardin, L. Di Ciaccio, J. Ernwein, G. Berbier, M.A. Jabiol, W. Kolton, L. Mosca, L. Moscoso*
DPhPE, CEN Saclay (France)
[5] *K.H. Becker, H.J. Daum, S. Demski, R. Hinners, W. Kohrs, B. Kuznik, R. Mayer, H. Meyer, D. Ortmann, J. Peters, M. Schubnell, J. Thierjung*
Universitaet - Gesamthochschule Wuppertal (Germany)

they are separated by 3 mm iron plates as illustred in Fig. 2.

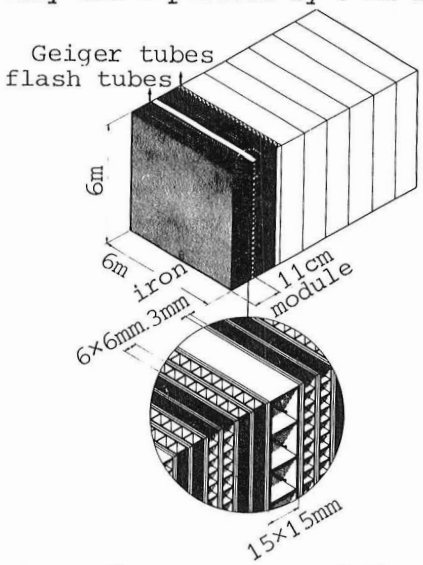

Figure 2 : Structure of the Frejus detector

The 934.000 (5 × 5) mm^2 section polypiopylene flash tubes are filled with a neon-helium gas mixture in which a plasma is produced when an electrical field of 8 KV/cm is applied. The plasma detected at the end of each tube by a capacitive read-out method allows the localization of a charged particle in the detector with an accuracy of the order of 2 mm.

The 40.000 (15 × 15) mm^2 section, aluminium Geiger tubes filled with an argon-ethanol gas mixture provide the trigger of the flash chambers when a charged particle is produced inside or crosses the detector. They also give a spatial and time information on the event.

2. Status of the experiment. The detector performances are summarized in Table 1. The space resolution, the amount of background and the separation

- efficiency per cell :	flash 80 %, Geiger 85 %
- background per cell per trigger :	flash 8.10^{-5}, Geiger 5.10^{-4}
- space resolution :	2 mm
- energy resolution :	electron $\sigma(E)/E = 12\ \% \sqrt{E}$
	muon $\sigma(p) \simeq 10$ MeV/c at 500 MeV/c
- particle identification	$e-\mu(\pi)$ separation : less than 10 % above 200 MeV/c
- $\mu^+ \rightarrow e^+$ decays :	$\sim$ 60 % efficiency

Table 1

between showering and non showering particles may be illustrated in Fig. 3

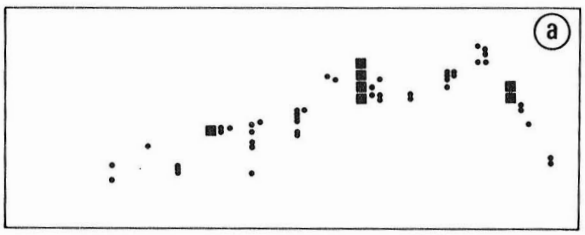

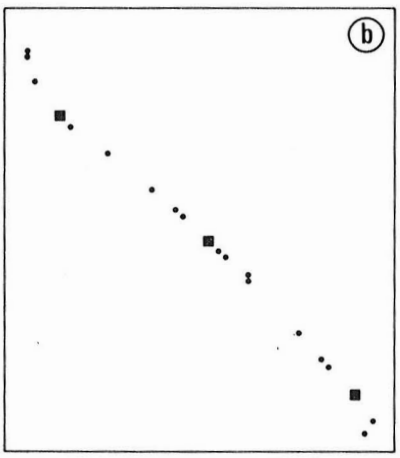

Figure 3 : Contained event :
ⓐ electron-like track
ⓑ muon-like track

when two contained events with electron (a) and muon (b) are displaid. The trigger logic consists on the coincidence (within 300 ns resolution time) between five Geiger tubes belonging to five adjacent planes with a maximum contribution of three tubes per plane. In these conditions the trigger rate amount to about 40 per hour, half of them being random coincidences due to radioactivity while the other half is essentially due to atmospheric muons.

Although the complete detector (912 tons) is in operation since June 1985, data have been taken during the installation since March 1984 when its total mass amounted to 240 tons.

3. Data analysis and preliminary results on contained events. The on-line scanning of the events and the monitoring of the detector is assured by a physicist controlling the experiments outside the underground laboratory. Off-line analysis consisting of a systematic check of the on-line scanning and the measurement of the important events, has recently started.

Only events originating at more than 50 cm of the external faces of the detector are considered as produced in the detector. Strict containment conditions are equally defined to assure that the charged particles stop in the detector. The preliminary results presented thereafter are based on a sensitivity of 194 TON(FID).YEARS. Table 2 summarizes the raw data obtained

Raw data : on line scanning	
- single muons	71 400
- stopping muons	520
- muon bundle	2 010
- exotic	470
- events inside the detector	30
Data reduction of events inside the detector from the 30 scanned events	
13	have their vertex outside fiducial volume
1	is a vertical crossing muon
2	are vertical downward stopping muons
1	is an upward stopping muon
13	are contained vertex events
9	with tracks fully contained
4	with tracks partly contained

Table 2

after the on-line scanning and the final number of events produced in the detector fully or partly contained. The nature of the (eventual) charged lepton found in each event is defined and its zenithal angle determined ; this is presented in Fig. 4a. Assuming first that all these events are atmospheric neutrino interactions, one deduces after trigger efficiency correction a number of 90 ± 30 and neutrino interactions for kiloton-year, and a ratio $\frac{(\bar{\nu})_e \text{ interactions}}{(\bar{\nu})_\mu \text{ interactions}} = 0.7 \pm 0.4$. These numbers agree within the statistical error with the previous results found in other large underground detectors and with the Monte Carlo predictions.

For each event the visible energy has been evaluated. The distribution of this quantity as a function of the number of prong of the events is shown in Fig. 4b, for the fully and partly contained events. From this figure we consider that the only candidates for nucleon decay into charged lepton are the fully contained events with at least 2 prongs and a visible energy less than 2 GeV. For the two events fullfilling these conditions the asymmetry parameter $|\Sigma\vec{P}|/E$ has been determined and is shown in Fig. 4c. These events are clearly incompatible with a nucleon decay for which the asymmetry parameter should be close to zero.

Therefore no candidate for the nucleon decay into charged lepton is found in this first sample of events. This leads after correction for trigger efficiency to a lower limit for the partial lifetime $\tau_{N \to \ell^{\pm} + X} > 4.10^{31}$ years with 90 % C.L.

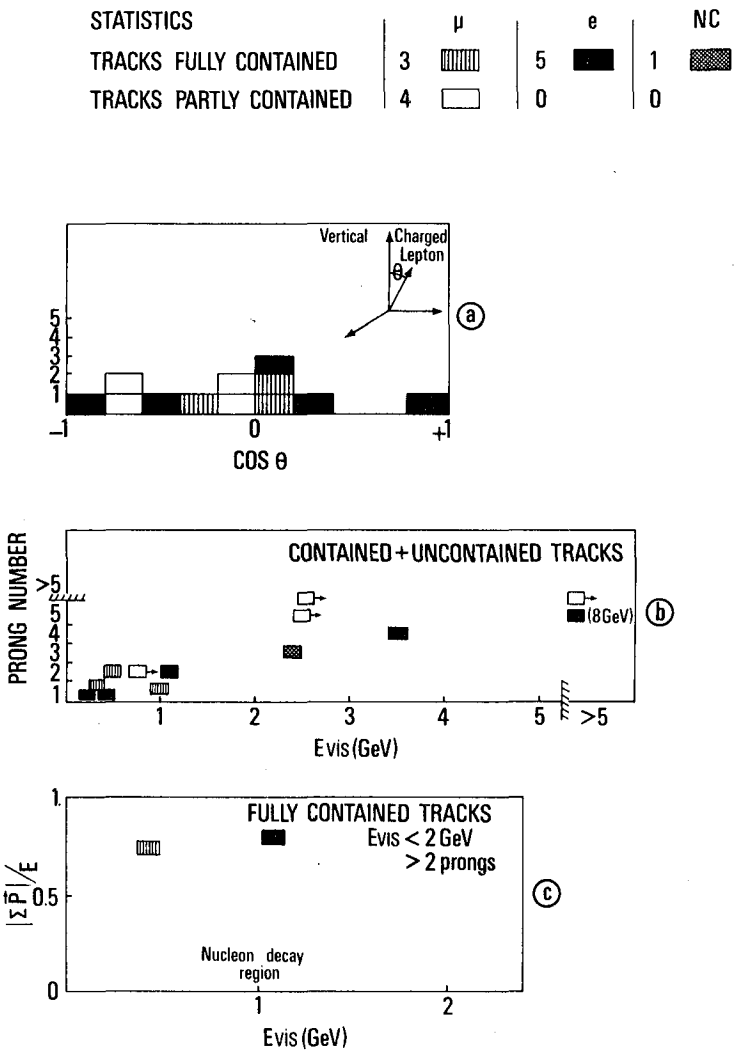

Figure 4 : ⓐ angular distribution
ⓑ topology versus visible energy
ⓒ asymmetry versus visible energy

HE - 6.2 - 3

RESULTS ON NUCLEON LIFE-TIME FROM THE KOLAR GOLD FIELD EXPERIMENT

M.R. Krishnaswamy, M.G.K. Menon, N.K. Mondal*, V.S. Narasimham and B.V. Sreekantan

Tata Institute of Fundamental Research, Bombay - 400 005, India

Y. Hayashi, N. Ito and S. Kawakami

Osaka City University, Osaka, Japan

S. Miyake

Institute for Cosmic Ray Research, University of Tokyo, Tokyo, Japan

1. Introduction

The KGF nucleon decay experiment has been in operation since October 1980 with a 140 ton calorimetric detector at a depth of 2.3 Km underground. The detector comprises 34 layers of proportional counters arranged in an orthogonal geometry with 12 mm thick iron plates in between successive layers. The proportional counters are made up of square (10 x 10 cm^2) iron plates of wall thickness 2.3 mm. Each of the 1600 counters is instrumented to provide data on (i) ionisation, dE/dx and (ii) arrival time.

The visible energy of a particle is determined to an accuracy of ~20% from the ionisation and range of its track. The end point ionisation of a stopping track provides the direction of motion as well as the nature of the particle (μ/π, k, p). Decay of μ^+ is recorded with an overall efficiency of only 20% in view of the thickness of 13 g/cm^2 between successive layers.

2. Method and analysis

The great depth of the installation has resulted in suppression of the intensity of cosmic ray muons and their associated background to about 2 events/day. The neutrino background, at energies < 2 GeV is less (~70%) compared to the other detectors operating around the world in view of the location of the detector at ~ 3^oN (Geomagnetic).

About 2600 events were recorded in a live time of

---

* now at Argonne National Laboratory, U S A

3.6 years and 96% of them are due to atmospheric muons and are easily identified as such. From the remainder, only 40 events have a vertex inside the detector and are mostly due to the cosmic ray γ-collisions. For nucleon decay search, we consider only 19 events whose tracks are fully confined to the detector volume, from this sample of 40 events. The energy distribution of these events is shown in Fig 1 and compared with the predictions (solid curve) on the γ-induced events. It is clear that there is no clustering of events around the nucleon mass, implying that an event by event analysis is necessary to isolate decay signals, if any. These 19 events could be broadly classified as (i) single-prong (9) and (ii) multi-prong events (10) in which a large fraction are γ-induced.

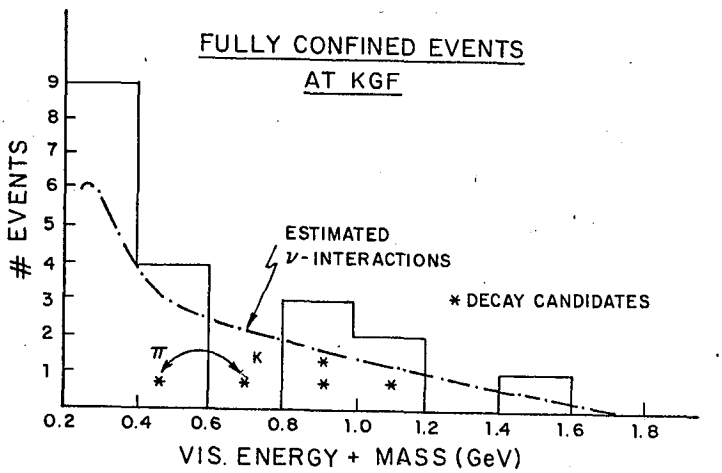

Fig 1: Energy spectrum of confined events. The solid curve is predicted for γ-induced events. The 4 candidate events are shown in the appropriate energy bins.

Candidates for nucleon decay

Four confined, multi-prong events were identified as plausible examples of nucleon decay on the basis of the total energy, momentum balance and track configurations.

(i) Event 587 is composed of showers of electromagnetic nature with total energy 980±200 MeV and momentum imbalance < 250 MeV/c and is interpreted as $p \rightarrow e^+ + \pi^o$. The background from γ-interactions is estimated as < 0.5 events at 90% C.L.

(ii) Event 867 appears at first glance as a single track with a kink around the middle of its range of 167 g/cm^2 with an angle of 40°. A closer examination based on the end point ionisation indicates that it is a good candidate for $p \rightarrow \bar{\nu} k^+$ with $k^+ \rightarrow \mu^+ \bar{\nu}\mu$. The total energy of the kaon is ~700 MeV and of the decay muon ~270 MeV. It could have been produced in a N.C interaction of neutrinos with a very low probability. A conservative estimate of ν-background is 0.2 events at 90% C.L.

(iii) Event 877 has 3 clear tracks in a back-back configuration. A down moving track with large angle scatter is interpreted as a muon of energy 340 MeV. The two upmoving particles with a large opening angle have effective mass consistent with that of k^0_S, if they are interpreted as pions. Thus the overall interpretation of the event is $p \rightarrow \mu^+ k^0_S$ with $k^0_S \rightarrow \pi^+\pi^-$; the total energy being 900 ± 150 MeV. In this event the end point ionisation of 2 tracks (μ and π) clearly establishes their opposing directions of motion, a necessary condition for proton decay. The ν-background for this event is < 0.2 events at 90% C.L.

(iv) Event 1766 is a semi-isotropic event with a total visible kinetic energy of 650 MeV and is unusual of a ν-interaction. The event comprises a shower and well seperated penetrating tracksapparently in the opposite hemisphere. It could be interpreted as $n \rightarrow \bar{\nu}\eta^0$, $e^+\rho^-$ or $p \rightarrow e^+k^0$ but the data are insufficient to pin down the preferred decay scheme.

A majority of the single prong events are due to low energy muons produced in elastic ν_μ, $\bar{\nu}_\mu$ collisions. However, Event 2099 has kinetic energy 340 MeV and if interpreted as due to a pion, the total energy of 480±50 MeV is consistent with that to be expected in the decay $p \rightarrow \bar{\nu} + \pi^+$. This event is used to set a limit on the life time, τ, of the proton decaying through this specific mode.

3. Results and discussion

The 4 multi track candidate events discussed above form a special category and cannot be simply dismissed as ν-interactions as can be seen from the estimated backgrounds. From the presently available fluxes and cross-section of cosmic ray neutrinos we expect to record only 15±3 confined events from this source with half of them of multi-prong nature. Among them, events having back-back topology with opening angle > 140° are estimated to be < 10% i.e., less than 0.8 events during the entire operation of the detector. Energy cuts around

the nucleon mass will reduce this to about 0.3 events or less. We thus consider our data as compatible with nucleon decay even though the statistical significance needs to be improved.

For life time estimate, we consider only the fiducial weight of 60 - 70 tons in the interior of the detector. The partial lifetimes, τ/BR as well as 90% C.L. limits for several decay modes are listed in Table 1. In this calculation we include the detector efficiency as well the probability of hadron absorption inside the iron nucleus.

Table 1

Proton Years : 6.05×10^{31}

Neutron Years : 6.98×10^{31}

Decay mode	Events	τ/BR(Years)	90% C.L
1. $p \dashrightarrow e^{+}\pi^{o}$	1	3×10^{31}	7.7×10^{30}
2. $p \dashrightarrow \mu^{+}k^{o}_{s}$ (└--> $\pi^{+}\pi^{-}$)	1	2.1×10^{31}	5.4×10^{30}
3. $p \dashrightarrow \bar{\gamma}\ k^{+}$	1	3.8×10^{31}	9.8×10^{30}
4. $p \dashrightarrow \bar{\gamma}\ \pi^{+}$	1	4.2×10^{31}	1.1×10^{31}
5. $n \dashrightarrow \bar{\gamma}\ \eta^{o}$	1^{a}	1.1×10^{31}	2.9×10^{30}
6. $n \dashrightarrow e^{+}\ \ ^{o}$	1^{a}	3.5×10^{31}	8.9×10^{30}

a: corresponds to the same event no. 1766

4. Acknowledgements

We are deeply indebted to Messers. B. Satyanarayana, R.P. Mittal, S.D. Kalmani, P.S. Murty, T. Ravindran and J.D. Kulkarni for their technical help in the successful operation of the detector. We are grateful to the Officers and other staff of Bharat Gold Mines Ltd., for their cooperation in the operation of the detector. The Ministry of Education, Japan is thanked for their financial assistance.

HE 6.2-4

DATA ACQUISITION SYSTEM FOR PHASE-2 KGF PROTON DECAY EXPERIMENT

M.R. Krishnaswamy, M.G.K. Menon, N.K. Mondal,
V.S. Narashimham and B.V. Sreekantan
Tata Institute of Fundamental Research
Bombay-400 005, India

Y. Hayashi, N. Ito and Kawakami
Osaka City University
Osaka, Japan

S. Miyake
Institute for Cosmic Ray Research
University of Tokyo
Tokyo, Japan

Abstract

Phase-2 of KGF proton decay experiment using 4000 proportional counters will start operating from middle of 1985. The detection system in addition to measuring the time information to an accuracy of 200 n see also records ionization in the hit counters. It also monitors different characteristics of the counters like pulse height spectrum, pulse width spectrum and counting rate. In this paper we discuss this data acquisition system.

The detector comes under the category of fine-grain calorimeters, in which measurements are made on the ionization of charged particles as they traverse through the detector. This has a total of 375 tons of iron distributed uniformly over an area of 6m X 6m and height 6m. The detector comprises 60 layers of horizontally arranged iron plates (6mm thick) and proportional counters (of cross section 10cm X 10cm and 6m long). The alternate layers of proportional counters are arranged in an orthogonal pattern in order to get both the X and the Y coordinates of the tracks. The main detector is surrounded by a veto shield of proportional counters. This shield is located very close to the rock wall and consist of two layers of proportional counters with 2.54cm of iron in between. In addition to increasing the fiducial mass of the detector, this shield will be very useful to look for other interesting events like Kolar events.

The front end electronics consist of individual amplifier-discriminator chain for data read out and analog multiplexers for monitoring the pulse height. Analog pulses from individual counters are shaped to have uniform decay time constant using a R-C network and are fed to an amplifier of gain 80. The amplified pulses are then passed on

to a discriminator and also to an analog multiplexer. The width of the discriminator output is related logarithmically to the input pulse height and is a measure of ionization in the proportional counter.

The discriminator output pulses are then carried to a data acquisition card (DAC) using flat ribbon cable. There are a total of 60 DAC each one accepting discriminator signals from one complete layer (60 channel). In DAC, the width pulses are provided to the following circuits.

(1) A CMOS static RAM for temporary storage of the width information. These RAMs are being operated as a circular buffer and always contain the history of a channel of the previous 200microsec.

(2) A monoshot to generate fast pulses for trigger.

(3) A priority encoder and a digital multiplexer for monitoring the width pulses.

The fast trigger pulses from individual monoshot are passed on to a set of preprogrammed EPROMs. These EPROMs accept fast trigger pulses from individual channels as their address inputs and produce a set of outputs whenever a layer trigger logic is satisfied. At present three different trigger outputs are available from each layer (i.e. each DAC). These are layer 1-fold (an OR of all the channels in a layer), a layer 2-fold (a 2-fold coincidence among 6 adjacent channels in a layer) and a layer 3-fold (need coincidence of 3 or more adjacent channels). Using these layer trigger pulses a final trigger will be generated in a central trigger processor.

Read out of the stored width data is being done in parallel using eight Z-80 based microprocessors. Each of these microprocessors supervises data acquisition from 8 layers. After receiving a trigger interrupt from the trigger processor, the microprocessors will allow the DACs to continue writing data for a further 187.5 μsec before switching the RAMs to read mode. Since the cycle time of the RAMs is 200 μsec, by this technique 12.5 μsec of pretrigger history will also be available in addition to 187.5 μsec of post trigger history of a channel. Once the readout cycle begins, the microprocessors will transfer the stored width data from the individual RAMs to a central buffer memory. A host computer will finally transfer these data to a mass storage device in a proper format.

HE 6.2-5

CONSTRUCTION OF THE SOUDAN 2 DETECTOR

D. S. Ayres, W. L. Barrett, J. W. Dawson,
T. H. Fields, M. C. Goodman, J. Hoftiezer, E. N. May,
N. K. Mondal, L. E. Price, J. L. Schlereth, J. L. Thron
Argonne National Laboratory, Argonne, IL. 60439

T. Kafka, W. A. Mann, R. Milburn, A. Napier, W. Oliver, J. Schneps
Tufts University, Medford MA. 02155

H. Courant, K. Heller, S. Heppelmann,
T. Joyce, M. Marshak, E. Peterson, K. Ruddick, M. Shupe
University of Minnesota, Minneapolis MN 55455

W. W. M. Allison, G. Barr, C. B. Brooks,
J. H. Cobb, D. H. Perkins, P. Shield
University of Oxford, Oxford OX1 3RH, England

D. Cockerill, P. J. Litchfield, G. F. Pearce, E. W. G. Wallis
Rutherford Appleton Laboratory, Didcot, OX11, England

paper presented by M. C. Goodman

We report here on the progress in construction of the Soudan 2 nucleon decay detector which is being built at the Soudan iron mine in Minnesota. We also report the expected event rate and characteristics of low energy neutrino events, muon events, multiple muon events, and other cosmic ray phenomena which we might be sensitive to.

1. Description of the Detector.

The detector is an iron calorimeter with high density (2 g/cm^3) which emphasizes dE/dx measurement and excellent tracking. It consists of 256 identical modules with a total mass of 1.1 kilotons (Fig. 1.) Each module consists of formed steel sheets in a honeycomb pattern, with 0.5 meter drift cells read out by 2.5 m by 1.0 m proportional wires and cathode strips (Fig. 2.). Each drift cell is 14 mm in diameter and layers are separated by 1.6 mm of iron. A gas mixture of 85% Argon with 15% CO_2 will be used, and a drift field of 200 V/cm, which will give a drift velocity of 0.92 cm per microsecond. For each wire and cathode strip, the pulse height will be recorded in each of 256 time bins which are 200 ns long. Vertical and horizontal positions of hits will be determined by matching anode and cathode pulse heights. Positions along the electron drift direction will be measured in 2 mm bins using timing information. Sampling every 0.2 radiation lengths coupled with ionization information will give good event reconstruction often including particle identification. The direction from stopping tracks will be determined by the rise in pulse height at the end of a track. This will greatly aid in vertex identification, which is important in distinguishing proton decay events from neutrino interactions.

The modularity of the detector will allow calibration in a neutrino beam. We believe previous proton decay experiments indicate that this will be an important ingredient in separating proton decay candidates from neutrino induced backgrounds, as well.

To reduce the number of electronics channels required, the cathodes and anodes will be separately multiplexed by a factor of 8. Associating a module with a given hit will require demultiplexing of both anode and cathode signals, but for the simple topologies of events expected (small volume clusters of hits and tracks along straight lines) this will not be difficult.

The experiment will be located at a depth of 2200 m of water equivalent. This will shield the detector from the hadronic and electromagnetic component of cosmic ray showers, and from muons with an initial momentum of less than 700 Gev. Triggers will be caused by high energy muons, neutrino events, and radioactivity in the mine. A muon rate of 0.3 Hz is expected. Some of the muons may interact outside of the detector and give hadrons and electrons which enter the detector. Therefore a two-layer shield is being constructed around the entire detector, made out of 23 ft long aluminum proportional wire planes.

2. Trigger.

The trigger will consist of some multiplicity of hits in a local region, probably around 4 out of 16 wires. We will have the ability to finely tune the trigger in each area of the detector, which will minimize effects of radioactivity from the cavity walls while maximizing acceptance to more difficult proton decay modes, such as $p \rightarrow K^{+}\nu$.

3. Current Progress.

The first 5-ton module has been constructed and is being tested with cosmic rays. By the time of the meeting, several more will have been built and tested, so that considerable experience will have been gained on the construction and performance of the modules. The testing program will reconstruct large numbers of straight-through cosmic ray muons. We will use spatial reconstructions of the tracks to identify the individual tubes struck by each cosmic ray. We will evaluate the performance of each tube in a module to obtain statistics on efficiency, attenuation, pulse-height resolution, and position resolution. Such an analysis has already been performed on data from a 1-ton prototype of the detector and shows excellent performance, with position resolution along the drift direction limited by the flash ADC clock. A sample of stopping muon data demonstrates the direction-tagging ability of the detector. We expect to begin installing modules in the mine in November 1985 and complete installation of all 256 modules in December of 1987.

4. Cosmic Ray Capabilities.

The excellent tracking capabilities will enable this detector to do certain studies of cosmic ray physics as a byproduct to searching for nucleon decay. In particular it is desirable to try to confirm the time correlations of multiple muon events seen in the Soudan 1 detector, as well as single muons which may be coming from Cygnus X-3 and other astrophysical sources[1,2]. For single muon events, the Soudan 2 detector will have 15 times the acceptance that the Soudan 1 detector had. The multimuon acceptance should increase by more than this, the actual rate depending on the lateral spread of the muons when they reach the level of the detector. It will certainly be possible to look for Cygnus X-3 and other possible astrophysical cosmic ray sources as well. It is also possible that the multimuon event distributions will give some information about the elemental composition of cosmic rays in the 10^{14} eV energy range.

Neutrino events are expected at a rate of about 100 per year. It is possible to calculate the ν_μ/ν_e ratio, charged current to neutral current ratio, and flux as a function of energy and angle that are expected from cosmic ray neutrinos produced in the earth's atmosphere. Neutrino oscillations could change the ν_μ/ν_e ratio as a function of angle. Any new weakly interacting neutral particle might manifest itself as an excess in the apparent neutral current to charged current ratio. Any astrophysical sources of neutrinos, such as high energy particles produced in solar flares, would give neutrinos associated with a particular direction in the sky.

The detector would be sensitive to a monopole flux of 1.0×10^{-14} $cm^{-2}s^{-1}sr^{-1}$ in one year. The memory time for each event is 50 μsec, so it will be possible to see monopoles (if they ionize) with a velocity down to 2×10^{-4} c.

5. Conclusion.

A 1.1 kiloton tracking calorimeter is being constructed for use in the Soudan mine in Minnesota. As well as a tool in the search for nucleon decay, it will be possible to study cosmic ray muons and neutrinos and look for other cosmic ray phenomena.

1. J. Bartelt et al., submitted to Phys. Rev. D.
2. M. Marshak et al., Phys. Rev. Lett. 54, 2079 (1985).

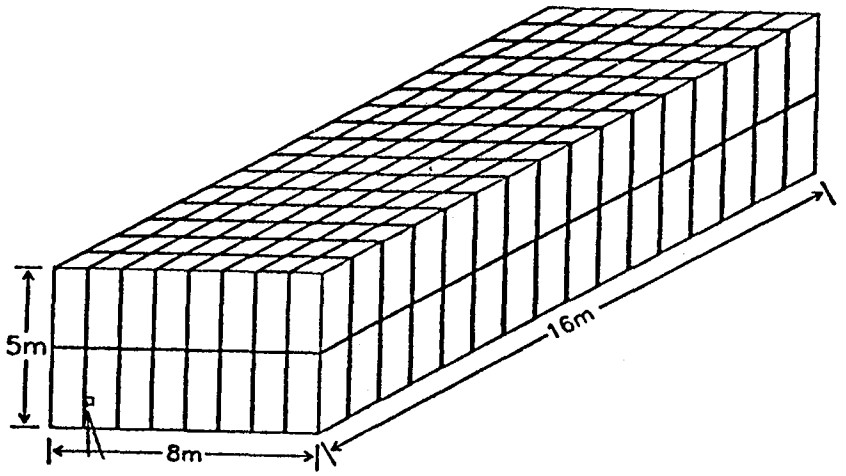

Fig. 1. Soudan 2 Nucleon Decay Detector

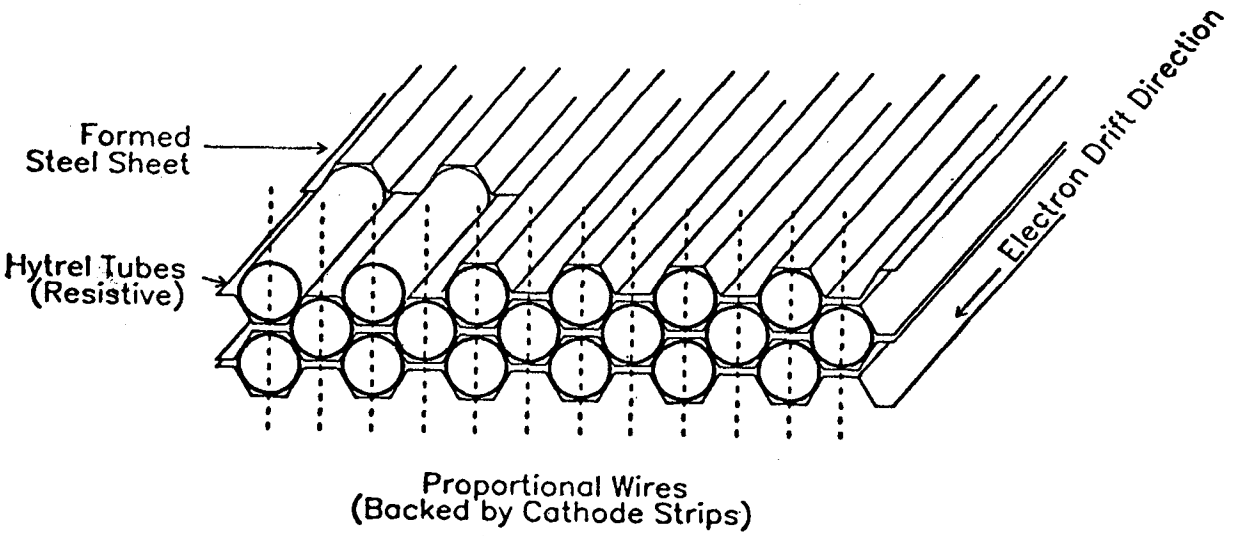

Fig. 2. Closeup of Honeycomb Pattern in Drift Chamber

Nucleon Decay and Atmospheric Neutrinos in the Mont Blanc Experiment

G. Battistoni[1], E. Bellotti[2], G. Bologna[3], P. Campana[1], C. Castagnoli[3], V.Chiarella[1], A.Ciocio[3], D. C. Cundy[4], B. D' Ettorre Piazzoli[3], E. Fiorini[2], P. Galeotti[3], E. Iarocci[1], C. Liguori[2], G. Mannocchi[3], G. P. Murtas[1], P. Negri[2], G. Nicoletti[1], P. Picchi[3], M. J. Price[4], A. Pullia[2], S. Ragazzi[2], M. Rollier[2], O. Saavedra[3], L. Satta[1], L. Trasatti[1], L. Zanotti[2]

[1]Laboratori Nazionali dell' INFN, Frascati, Italy
[2]Dipartimento di Fisica dell' Universita' and Sezione dell' INFN, Milan, Italy
[3]Istituto di Cosmogeofisica del CNR and Istituto di Fisica Generale, Turin, Italy
[4]CERN, European Organization for Nuclear Research, Geneva, Switzerland.

Abstract

In NUSEX experiment, during 2.8 years of operation, 31 fully contained events have been collected; 3 among them are nucleon decay candidates, while the others have been attributed to υ interactions. Limits on nucleon lifetime and determinations of υ interaction rates are presented.

The Detector.

NUSEX detector is a digital tracking calorimeter, planned to study the stability of nucleon.

It has been running since June 1st, 1982 in a cave aside the Mont Blanc Tunnel, covered by a minimum overburden of $\approx$ 5000 hg cm^{-2} S. R., with a live time of 2.5 years, that is about 86% of solar operation time.

The detector is a sandwich of 136 iron plates 1cm x 3.5 x 3.5m^2, interleaved by layers of plastic streamer tubes of the resistive cathode type.

Each plane of tubes is formed by an array of 320 tubes, 3.5m long and 1 cm^2 cross-section, aligned with the tunnel axis.

Tubes are made of extruded PVC; a high resistivity varnish covers the cathode walls; anodes are ø100 µm wires, and tubes are operated at 3.9 kV with an Ar-CO_2-Penthane (1+2+1) gas mixture.

Position of each hit in the detector is recorded through two sets of Al strips (each set has a 1 cm pitch),mounted externally to the tubes, which are respectively parallel (320 strips) and orthogonal (288 strips) to the wires.

Total mass is 150 tons; a detailed description of the detector will be shortly published[1].

Data are collected via CAMAC serial readout by a PDP 11/60 computer on magnetic tape.

Minimum trigger patterns are: either 4 contiguous planes hit or 3+2 contiguous planes hit or 2+2+2 contiguous planes hit, plus any combination of higher plane multiplicity.

Data set for each event consists of the coordinates of each tube fired together with time of firing relative to trigger start, recorded by 100 ns TDC' s.

Time information allows identification of μ decays (μ stopping inside the detector) in 17% of the cases.

A trigger to detect magnetic monopoles has also been implemented and is described in [1].

Data concerning nucleon decay and atmospheric neutrinos.

An extimate of rate and topologies of υ interactions in our detector has been obtained through an exposure of a test module to a $\upsilon_\mu(\bar{\upsilon}_\mu)$ beam in CERN, designed to simulate atmospheric υ spectra in the energy region around 1 Gev[4].

Data thus collected have been used to compute backgrounds to nucleon decay that will be quoted further, considering also the presence of υ_e' s in atmospheric υ flux.

Data from NUSEX experiment have been selected according to the foollowing characteristics:

1-. Vertex of the event must be inside the volume of the detector;

2-. Tracks coming from vertex must stop inside volume of the detector;

3-. No incoming visible track pointing to the vertex is required.

We guarantee thus to collect only events due to υ interactions in the detector, and possibly due to nucleon decay.

31 events satisfy the above quoted features; they are uniformly distributed in the detector volume and cannot be ascribed to neutron interactions ($\Phi_n < 10^{-6}$ cm^{-2} s^{-1} sr^{-1}); the first 10 among them have already been discussed in detail elsewhere [2,3].

Neutrino rates.

Trigger requirements put an effective threshold both for μ and e at 250 MeV total energy. At this energy trigger efficiency is 40% and rapidly falls below that value.

Supposing that all 31 events are υ interactions, we can identify 21 events

as ν_μ interactions, 9 as ν_e interactions, while 1 is ambiguous ($\nu_\mu - \nu_e$). Correcting for detection efficiency (trigger x containment efficiency) event by event, we get the total ν interaction rate in our detector, above the threshold of $E_{visible}$ = 200 MeV:

$$R_\nu = 152 \pm 20\ \nu/(\mathrm{Kton\ x\ yr})$$

and the ratio of ν_e and ν_μ interactions:

$$R(\nu_e/\nu_\mu) = 0.28 \pm 0.09 \pm 0.02$$

where the first term in the error is due to statistics and the second to ν_e ν_μ ambiguity. A plot of visible energy distribution of data uncorrected for detection efficiency is reported in fig. 1.

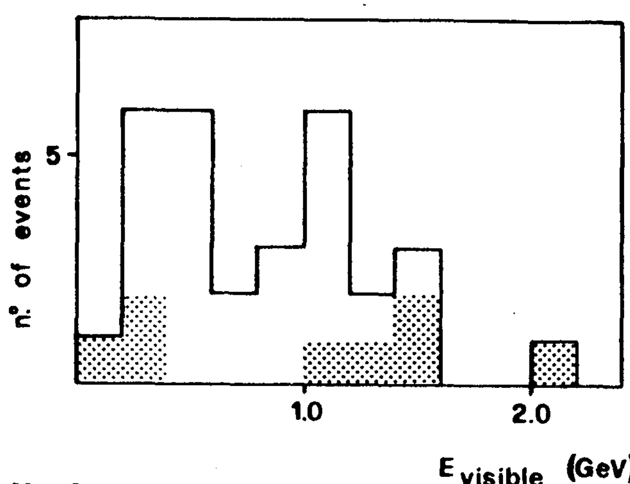

Fig. 1. Visible energy distribution of events, not corrected for detection efficiencies.
Shaded areas are ν_e events.
White areas are ν_μ events.
1 ν_e event of 3.7 GeV is out of scale.

Nucleon stability.

At present we have 3 events that can be considered nucleon decay candidates.

Event n. 1, that has been widely discussed elsewhere(2), is a proton decay candidate, fitting well the hypothesis:

$$p \dashrightarrow \mu^+ + K^0, \quad K^0 \dashrightarrow \pi^+\pi^-$$

with E = 1.0 ± 0.2 GeV, P = 0.4 ± 0.2 GeV/c, p_μ = 0.38 ± 0.15 GeV/c, $M_{\pi\pi}$ = 0.55 ± 0.08 GeV/c^2, p_K = 0.3 ± 0.1 GeV/c. Errors on total energy and momentum are mainly due to candidate μ track going almost parallel to iron plates. Other decay modes also fitted(2) are $p \dashrightarrow \nu + K^*$ and $p \dashrightarrow 3\mu$.

Background computed from test run is 2 events in 403 ν interactions (corresponding to ≈35 years of data taking with NUSEX), leading to the expected background rate:

$$B = 0.1 \pm 0.07$$

Second candidate is event n. 22, which is a $\geq$ 2 back to back showers event; best fit is given by a 3 showers hypothesis with:

$E_1 = 370 \pm 110$ MeV $\theta_{12} = 160^\circ$; $E_2 = 550 \pm 140$ MeV $\theta_{13} = 140^\circ$

$E_3 = 140 \pm 80$ MeV $\theta_{23} = 50^\circ$; $E_{tot} = 1060 \pm 200$ MeV; $P = 250$ MeV

consistent with a $p \rightarrow e^+ + \pi^0$ decay mode. Expected background from analysis of $\mu\pi$ events in υ test run and electrons of 1.5 GeV from e beam test simulating the topology of our event gives a rate:

$$B = 0.25 \pm 0.07$$

Event n. 30 is a candidate for $n \rightarrow \mu^+\pi^-$ decay; kinematical fit is very good, both for total energy (.85 GeV) and for missing momentum (.35 GeV/c). However in this channel from our test we expect 0.6 background events.

Among other channels we have events compatible with nucleon decay only in $p \rightarrow \upsilon + \pi^+$; 7 events have been collected, but the expected background from quasi-elastic υ_μ is 6. Limit reported in Table 1 has been computed by background subtraction.

Table 1

Decay mode	N. of candidates	Background	Lifetime/branching ratio (yr x 10^{31}) 90% C. L.
$p \rightarrow e^+ \pi^0$	$\leq$ 1	0.25	> 0.6
$n \rightarrow e^+ \pi^-$	0		> 0.8
$N \rightarrow e \pi$			> 1.0
$p \rightarrow \mu^+ \pi^0$	0		> 0.7
$n \rightarrow \mu^+ \pi^-$	1	0.6	> 0.3
$N \rightarrow \mu \pi$			> 0.8
$p \rightarrow \bar{\upsilon} \pi^+$	$\leq$ 7	6	> 0.2
$n \rightarrow \bar{\upsilon} \pi^0$	0		> 1.1
$p \rightarrow \bar{\upsilon} K^+$	0		> 0.8
$n \rightarrow \bar{\upsilon} K^0$	0		> 0.9
$p \rightarrow \mu^+ K^0$	1	0.1	> 0.7

References

1-. G. Battistoni et al. " The NUSEX Detector " to be submitted to N. I. M.

2-. G. Battistoni et al. Phys. Lett. **118B** (1982) 461

3-. G. Battistoni et al. Phys. Lett. **133B** (1983) 454

4-. G. Battistoni et al. Nucl. Instr. & Methods **219** (1984) 300

A SEARCH FOR HEAVY LONG LIVED PARTICLES IN HIGH ENERGY COSMIC RAYS

A. Mincer, H. Freudenreich, J.A. Goodman
S. C. Tonwar and G. B. Yodh
Department of Physics and Astronomy
University of Maryland, College Park, MD 20742

R. W. Ellsworth
Department of Physics
George Mason University, Fairfax, VA 22003

D. Berley
Physics Division, National Science Foundation
Washington, DC 20550

ABSTRACT

We present the results of an experimental search for energetic particles which arrive at sea level delayed with respect to the shower front, with an order of magnitude greater exposure than previous experiments. The experiment was sensitive to showers from cosmic rays between 10^5 and 10^7 GeV per nucleus. No evidence for the existence of heavy long lived particles in air showers was found. We set an upper limit to the flux of these particles at the 90% confidence level of 1.4×10^{-12} $cm^{-2}sr^{-1}s^{-1}$.

1. Introduction. The experimental search for heavy long lived particles such as heavy leptons, heavy quark matter, super-symmetric particles and magnetic monopoles is of great current interest. The cosmic ray beam may provide particles with sufficiently high energy to produce such objects by their interactions in the atmosphere. It is also possible that the cosmic ray beam may contain heavy stable particles of very large mass ($\geq 10^3$ GeV) as a minor component. Heavy cosmic rays, such as these would have escaped detection in searches for ultra heavy nuclei if they had a small net charge.

Several cosmic ray experiments have been carried out to search for such particles. The technique used is to detect energetic hadrons delayed with respect to the fast electrons ($\beta = 1$) in the air shower.[1-3] In the delayed particle experiments a search is made for the presence of a substantial signal in scintillation counters placed inside a calorimeter which is delayed with respect to the shower front by a time interval in the range 20 ns $< \tau <$ 200 ns. We have carried out a new experiment at sea level to search for delayed large calorimeter signals with a total exposure factor $\sim$20 times greater than previous experiments.

2. Experimental Technique and Data Sample. (A) The arrangement: A set of 12 unshielded counters was used to sample shower particles and determine the times of arrival of the shower front. Eight of the shower counters were of 0.36 m^2 each and had a thickness of 7 cms of liquid scintillant. The counters are labelled S_1 through S_8 in figure 1 which shows a plan view of the experimental layout.[5,6] The remaining four counters, labelled A_1 through A_4 were placed directly over four calorimeters which sampled the hadrons in the shower. These counters were 0.64 m^2 in area and had 1.25 cm thickness of NE(102) scintillators. The apparatus was located in College Park, MD, at sea level. Counters were placed in the calorimeter at several depths to sample hadronic cascades. The longitudinal depth in radiation lengths of the counters for the two configurations is given in Table 1. We note three features of the design: (1) The top absorber consisting of 2" of Pb and 6" of Fe has sufficient number

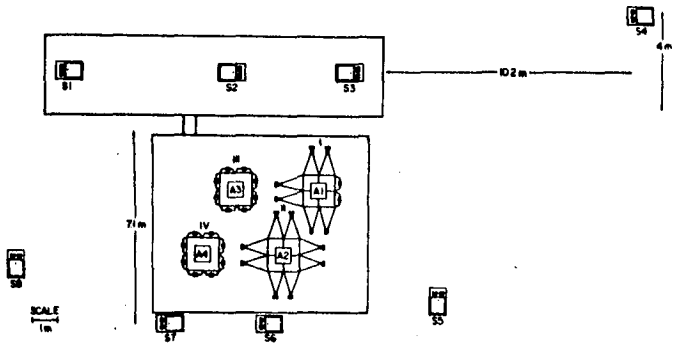

Figure 1: Experimental layout

Table 1

Calorimeter Profiles

Counter	Material	Size	Depth(in radaition lengths) Calorimeters I,II,III	IV
A	Ne 114	22" x 44" x 1/2"	0	0
T	Ne 102	24" x 24" x 1/2"	-	17.7
B	Ne 114	24" x 24" x 1/2"	17.7	17.7
C	Ne 114	24" x 24" x 1/2"	19.9	17.9
E	Ne 114	22" x 44" x 1/2"	37.2	35.1
D	Liquid Scintillator	24" x 24" x 1/2"	37.2	35.1

of radiation lengths to absorb the electromagnetic component of the air shower so that the B counters will not be triggered by the shower front. (2) The absorber in the first layer extends 25.4 cm beyond the B and C counters in all lateral directions so that EM component from side showers won't trigger them and (3) that each detector layer is divided into four quadrants in order to allow a measurement of the lateral spread of the hadronic cascades. (B) The trigger: The experiment was triggered when two conditions were satisfied: (1) The sum of the signals from the B and C counters in at least one of the calorimeters exceeded 70 equivalent particle levels and (2) there was a signal in two A counters in "coincidence" with the B + C pulse. In order to study delayed hadrons near cores of air showers further off line cuts were made. These required that the average signal in the A counters corresponded to eight particles or a density of 13.6 ptls/m^2 and a signal in B + C counters of one calorimeter was greater than 75 particles. At least two A's were required to have this density. (C) The data: In 9266 hours, 179,102 events triggered the array. Of these events, 29,182 passed the off line cuts. For each event we calculated the time difference between the arrival times of B and/or C counters from that of the A counter immediately above the calorimeter associated with the B and/or C counter. Most of the hadrons arrive in time with the shower. Two percent of the events have at least one counter delayed by greater than 20 ns. The majority of these events have $S \leq 20$ equivalent particles.

The 72 large signal, large delay (called LSLD) events can be divided into three classes: (1) Single Counter Delays (SCD): large signal in a single counter with little or no energy deposited in neighboring counters separated by as little as 1gm/cm^2. (2) Single Quadrant Delays (SQD): large signal in one B or C counter with delay, with other B or C counters also delayed in the same quadrant. (3) Multiple Quadrant Delays (MQD): a large signal delayed counter and at least one counter in another quadrant delayed. Among these events, the most promising candidates for the presence of an energetic delayed hadron are those where some penetration by the cascade is evident. There were 27 events of this type.

3. Simulation of the Experiment and Analysis. In order to determine the significance of these 27 events (whether they might indicate the presence of an unusual particle as discussed in the introduction), a four dimensional Monte-Carlo simulation of the atmospheric cascades was carried out. These calculations used a particle production model which was based upon Fermilab, CERN.ISR and SPS-$\bar{P}P$ collider data, an increasing cross section for hadron-air inelastic processes and a superposition model for primary nuclei other than protons. The program records the energy, position and arrival time for those hadrons which cross the detector altitude. Each π^0 is decayed into 2γs and the electromagnetic cascade of each γ-ray is calculated in approximation B and its contribution to shower density at the location of each hadron is obtained using a modified Nishumara-Kamata-Greisen lateral distribution.[6]

In simulating the actual trigger, the response of the calorimeter counters to hadrons, muons and electrons incident upon the calorimeter was simulated.

To determine response at low energies we exposed a prototype calorimeter to low energy (1 to 10 GeV/c π and p) hadron beams at the AGS test beam in order to study fluctuations in cascade development. We were able to measure fluctuations in the observed pulse height in the calorimeter counters at different depths to 10^{-4} to 10^{-5} level.[7] At higher energies we used data obtained at Fermilab[8] in a calorimeter with counters at depths similar to our B and C counters. A detailed Monte-Carlo simulation of hadronic cascades was done using the Oak Ridge code of T. Gabriel[9] to understand the observed fluctuations and to provide "Monte Carlo data" to use in our simulations at energies where no actual experimental data was available.

These measurements and calculations show that low energy hadrons which can arrive delayed, occasionally give a much larger than average energy deposit in the detector counters giving rise to abnormally large signals. Our calibration and subsequent calculations showed that 7 percent of 3.5 GeV hadrons give a signal greater than 20 equivalent particles while 0.2 percent give a signal greater than 50 equivalent particles.[7,9]

The Monte Carlo program was run on a set of incoming primaries of different nuclear species and picked according to energy spectra (typically $E^{-2.6}$) based upon different models.[10]

4. Discussion and Conclusions. We have carried out simulations for the distribution of pulse heights for delayed events generated by proton and iron primaries. The predicted distributions are shown in figure 2. We note that the distribution shape is essentially the same for the two species. Therefore the flux limit derived below is independent of the nature of the primary.

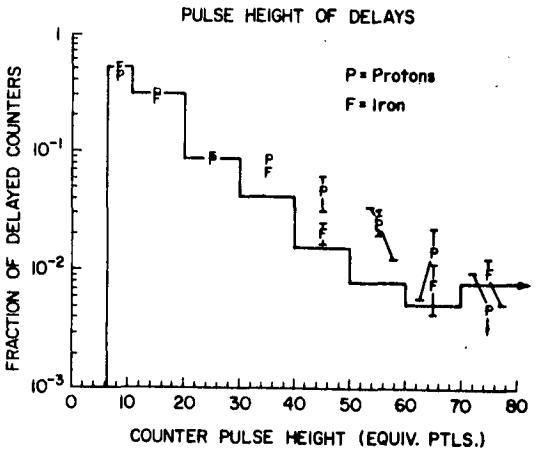

Figure 2: Predicted and measured (solid line) signal distributions for delayed events

We have compared the data with the signals predicted for a composition obtained from a rigidity confinement model of cosmic ray propagation.[11,16] The observed distribution can be accounted for both qualitatively and quantitively without the need for the presence of either new particles or processes. In Table 2 is shown the relative fraction of large signal events in each of the three categories. Good agreement is seen.

Table 2

Comparison of Observed and Simulated Delayed Events

Event Type	Fraction(%) Data	Simulated
Single Counter (SCD)	56 ± 9	41 ± 9
Single Quadrant (SQD)	24 ± 6	31 ± 8
Multiple Counter (MCD)	20 ± 5	28 ± 8

We calculate the upper limit to the flux of "Massive Long Lived" particles, ϕ, from the observation in Section 2 that no events of the SQD or MQD type were seen to penetrate into the D counters giving a pulse height larger than one particle (see Table 2). From our Monte Carlo we can estimate that 54 percent of all signals generated by 20 GeV incident hadrons should give $\geq$ 2 particle signal in D if they generate 20 particle signal in B + C. Therefore since none were observed we estimate at the 90 percent confidence level that we have a flux of less than 2.3/0.54 particles in 9266 hours with an area solid angle factor of 9.4 m^2sr, $\phi < 1.4 \times 10^{-12} cm^{-2} sr^{-1} s^{-1}$.

We remark that the large signal delayed events seen in a recent experiment reported by a Japanese group[11] and all other previous experiments can be explained in terms of fluctuations in cascades from low energy delayed hadrons in air showers.

This work was supported in part by a grant from the National Science Foundation. The support of the Computer Science Center of the University of MD and of the Tata Inst. of Fundamental Research is gragefully acknowledged.

5. References

1. For a review of particle searches in cosmic rays see L. W. Jones, Rev. Mod. Phys. 49, 717 (1979).
2. J. A. Goodman et al., Phys. Rev. D19, 2572 (1979).
3. A. Mincer et al., Proceedings of the 18th ICRC, Bangalore, India, Vol. 11, 20 (1983)
4. A. Mincer, Ph. D. Thesis, Univ. of MD (1984) (unpublished). Further details about the experiment can be found here.
5. J. A. Goodman et al., Phys. Rev. D26, 1043 (1982).
6. A. M. Hillas and J. Lapikens, Proceedings of the 15th ICRC, Plovdiv, 1977, Vol. 8, p. 460.
7. A. Mincer et al., Nucl. Inst. and Methods (1984) to be published.
8. We want to thank J. Ritchie and A. Bodek for making their data at GEV available to us.
9. A. Mincer et al., Nucl. Inst. and Methods (1984) to be published.
10. R. Cowsik et al., In Proceedings of the 17th ICRC, Paris, France, 1983, Vol. 2, page 120.
11. M. Yoshida, Y. Toyoda et al., J. of Physical Society of Japan 43, 1983 (1984).

HE 6.2-8

DELAYED PARTICLES IN EAS AT AKENO

H. Sakuyama, N. Suzuki and K. Watanabe

Department of Physics, Meisei University, Hino, Tokyo 191

K. Mizushima

Kobe Women's Junior College, Ikuta, Kobe 650

ABSTRACT

Using two 2.25 m^2 fast scintillation detectors, delayed particles in EAS have been observed at Akeno Observatory. These are set under 1 m concrete and 2.5 cm lead plates respectively. About 2500 EAS are analyzed. The lateral distribution of delayed particles for the EAS size $>10^7$ is flatter than that for $<10^7$. The lateral density of delayed particles is almost constant for the size range $2.2\times10^5 \sim 10^7$ and increases rapidly above 10^7.
These facts may suggest change of nuclear interaction at 10^7 and substantially the existence of heavy particles with long life.

Above 10^{15} eV delayed particles in EAS were observed near to the core, by using two 1 m^2 fast scintillation detectors telescoped.(1)(2)
These results are as follows.
Lateral distribution of delayed particles becomes flat for various EAS size ranges and lateral density for the size $<10^7$ is almost constant, while it increases rapidly $>10^7$.(3)
Relation between the frequency and the delay time for the EAS size $>10^5$ may be approximated by an exponential function. From these facts nuclear interaction for the EAS size 10^5 and 10^7 seems to change and two kinds of heavy particles with long life are claimed. The possibility of a massive particle has also been reported by measuring the arrival time distribution of electron.(4)

From the end of 1983, two 2.25 m^2 fast scintillation detectors are set at Akeno Observatory and in August, 1984 two more fast detectors(1 m^2, 2.25 m^2, respectively) are set. These are enclosed in a black housing and constructed Hamamatsu P.N. R-1250 fast photomultiplier; rise time and size of them are 3.4 ns(2000V) and 127 mm diameter. Output from them is connected with 100 MHz stragescope using a coaxial cable (11D-4AF). The recorder consists of 35 mm automatic camera. These are set under 1 m concrete and 2.5 cm lead respectively.

The experimental apparatus is shown in Fig. 1.

About 2500 EAS of the present experiment have been analyzed. The lateral distribution of delayed particles with a delay time larger than 20 ns and burst sizes more than 10 particles is shown for the EAS size range $10^5 \sim 2\times10^8$, in Fig. 2. Relation between lateral density at some distance range (10-20 m) from the core axis and EAS size is shown in Fig. 3. Lateral density seems to be constant for the EAS size range $2.2\times10^5 \sim 10^7$ and this is also seen in the other distance range from the core axis.

If the observed delayed particles are fluctuations of ordinary hadrons in EAS, their lateral density should increase with EAS size. Nevertheless it is almost constant for the EAS size range $2.2\times10^5 \sim 10^7$ and increases rapidly above 10^7. From this, in $10^5 \sim 10^7$ and above 10^7 nuclear interaction seems to change and two kinds of heavy particles with long life seem to contribute for every new interaction.

An example is shown in Fig. 4 for which two detectors have two same delay signals in EAS with size 10^8 at a distance of 42 m from the core axis.

References

(1) H. Sakuyama et al: 18th ICRC at Bangalore, EA 1.1-52, EA 1.2-21 (1983). Nuovo Cimento 6C, 371 (1983). Nuovo Cimento 78A, 147 (1983)

(2) H. Sakuyama and K. Watanabe : Lett. Nuovo Cimento 36, 389 (1983)

(3) H. Sakuyama and N. Suzuki : Lett. Nuovo Cimento 37, 17 (1983)

(4) M. Yoshida et al : J. Phys. Soc. Japan 53, 1983 (1984)

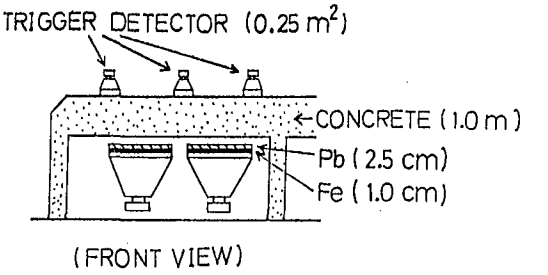

Fig. 1 Two 2.25 m^2 fast scintillation detectors

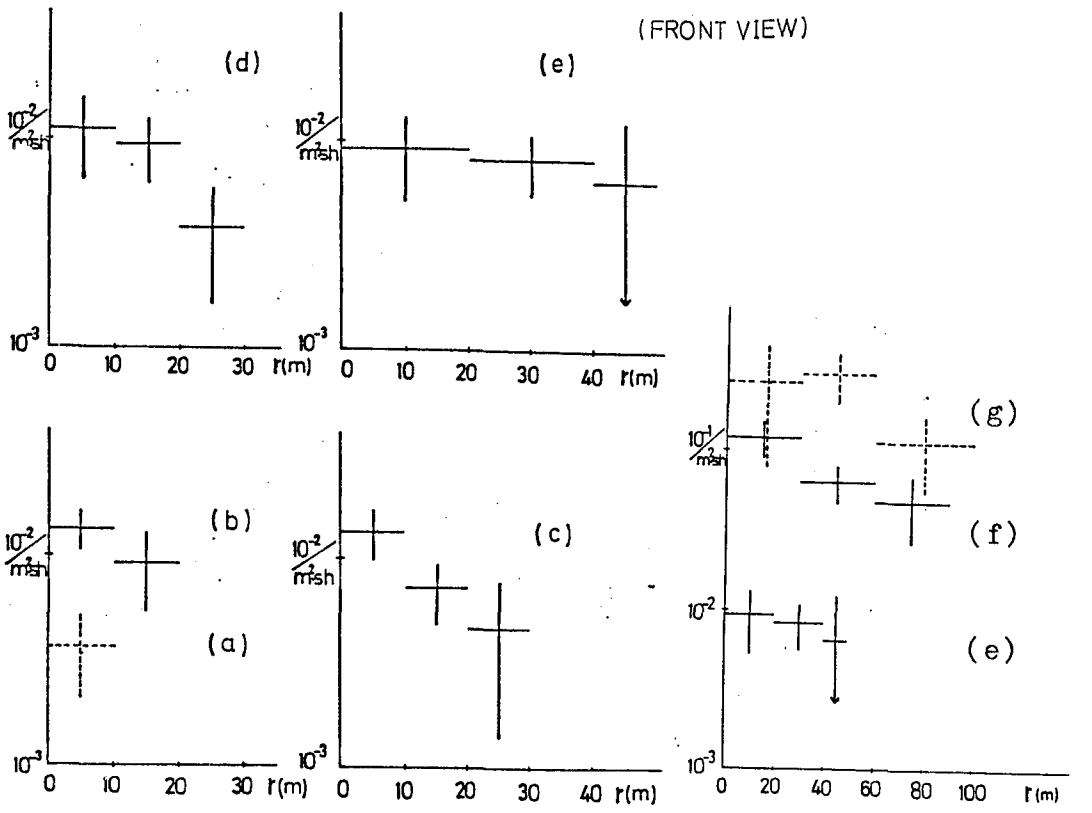

Fig. 2 Lateral distribution of delayed particles with a delay time larger than 20 ns and burst sizes more than 10 particles.

(a) $10^5 < Ne \leq 2.2\times10^5$, (b) $2.2\times10^5 < Ne \leq 4.8\times10^5$,
(c) $4.8\times10^5 < Ne \leq 10^6$, (d) $10^6 < Ne \leq 2.2\times10^6$,
(e) $2.2\times10^6 < Ne \leq 10^7$, (f) $10^7 < Ne \leq 4.8\times10^7$,
(g) $4.8\times10^7 < Ne \leq 2\times10^8$

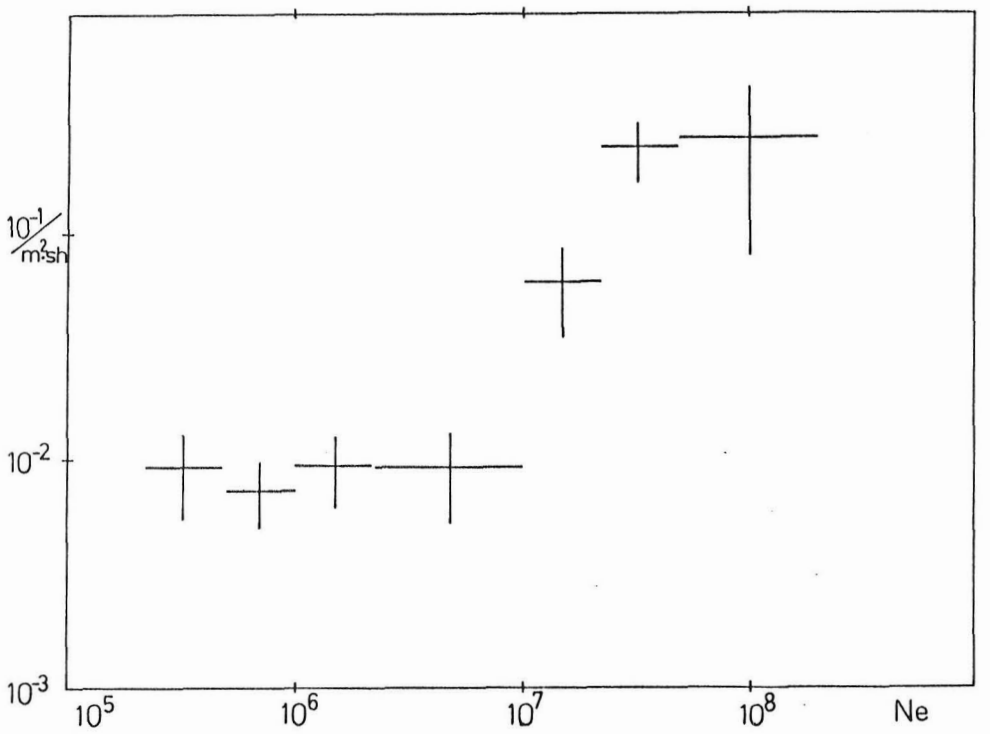

Fig. 3 Relation between EAS size and lateral density at 10-20 m from the core axis

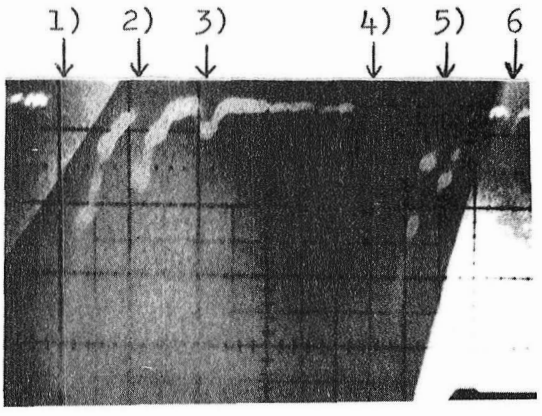

Fig. 4
An examle; two fast detectors have two same delay signals in EAS with size 10^8 at a distance of 42 m from the core axis.

1) No delay signal of fast detector.
2) Delayed signal with the time of 62 ns from signal 1) with the burst size of 43 particles. 3) Delayed signal with 107ns from 1) with 16 particles. 4) No delay signal of another fast detector. 5) Delayed signal with 62 ns from signal 4) with 12-16 particles. 6) Delayed signal with 109 ns from signal 4) with 4 particles.

HE 6.2-9

Energetic delayed hadrons in large air showers observed at 5200m above sea level

Kaneko, T.
Department of Physics, Okayama University, Okayama 700, Japan
Hagiwara, K.
The Institute of Physical and Chemical Research, Wako, Saitama 351, Japan
Yoshii, H.
Faculty of General Education, Ehime University, Matsuyama 790, Japan
Martinic, N., Siles, L. and Miranda, P.
Instituto de Investigaciones Fisicas, Universidad Mayor de San Andres, LaPaz, Bolivia
Kakimoto, F., Tsuchimoto, I., Inoue, N. and Suga, K.*
Department of Physics, Tokyo Institute of Technology, Meguro, Tokyo 152, Japan

ABSTRACT

Energetic delayed hadrons in air showers with electron sizes in the range $10^{6\cdot0}$ to $10^{9\cdot0}$ have been studied by observing the delayed bursts produced in the shield of nine $4m^2$ scintillation detectors in the Chacaltaya air-shower array. The frequency of such delayed bursts is presented as a function of electron size, core distance and $\sec\theta$.

1. Introduction

The Bolivian Air Shower Joint Experiment (BASJE) group carried out a series of measurements of the arrival time distributions both of muons in air showers with primary energies above 10^{17}eV and of atmospheric Cerenkov light from air showers with primary energies from 5×10^{15}eV to 2×10^{17}eV in the Chacaltaya air-shower array ($550gcm^{-2}$ atmospheric depth, 5200m above sea level). On the basis of these measurements, we concluded that the longitudinal developments both of muons and of electrons at the early stages are consistent with those expected from very high multiplicity models of particle interactions(1)(2). This conclusion is supported by measurements of the arrival time distributions of muons and of atmospheric Cerenkov light in the Akeno air-shower array ($930gcm^{-2}$ atmospheric depth, 900m above sea level) by the Tokyo Institute of Technology group using the almost same apparatus as used in the Chacaltaya array(3)(4).

Furthermore, high-energy delayed hadrons in air showers have been studied in the Chacaltaya array to examine whether the character of the multiple production of nucleons and anti-nucleons in high-energy interactions is also consistent with this conclusion, and to obtain an information on unknown heavy particles which may be produced in high-energy interactions. These delayed hadrons were observed as delayed bursts produced in the shield of nine $4m^2$ scintillation detectors in the Chacaltaya array.

In this report frequencies and delay time spectra of these delayed bursts are presented for air showers with electron sizes in the range $10^{6\cdot0}$ to $10^{9\cdot0}$.

---

*Present addres: Department of Physics, Meisei University, Hodokubo 337, Hino-shi, Tokyo 191, Japan

2. Experimental

The observation started in May 1982. The shield of detector is composed of 231gcm^{-2} of galena (PbS ore), 132gcm^{-2} of concrete and 23gcm^{-2} of lead. The signal from a 5in fast photomultiplier (Philips XP2040) in each detector was fed to an adding circuit. This combined signal was stored in a 100MHz storage oscilloscope (Tektronix 466) by local trigger signal generated when at least 7.0 particles passed through an unshielded 0.83m^2 detector just above the central 4m^2 shielded detector (this trigger level was changed to 3.0 particles from October 1982) and at least 3.5 particles passed through five shielded detectors out of nine. When this local trigger signal coincided with a master signal from the array, which observed an air shower with electron size above $10^{6.0}$, the stored signal was photographed. The time response of the whole system was 4.5ns in rise time between 10% and 90% of the signal and 12ns in full width at half maximum (FWHM).

3. Analysis

About 12,400 showers with electron sizes (N_e) above $10^{6.0}$ and secθ (θ: zenith angle) from 1.0 to 1.8 were observed until October 1983.

The delayed burst produced by a high energy hadron was picked up primarily when the burst was recognized as a separate delayed peak in the signal. Moreover, in order to avoid a contamination of apparent delayed signals due to fluctuation in the arrival times of muons, following criteria were requested for further screening:

(1) The burst size (n_b) is larger than 15 particles.
(2) The value of FWHM of the delayed signal is shorter than 20ns.

Since the number of particles was measured simultaneously using a 16in photomultiplier (DuMont K1328) in each 4m^2 scintillation detectors, the signal was accepted as the delayed burst finally when the number of particles contained in the separate delayed peak was equal to the number of particles of burst recognized from the pattern of the numbers of particles measured in nine detectors within the uncertainty. The delay time of the burst was measured from the particle front in the photograph.

The distribution of sizes of bursts produced by hadrons with energies E (GeV) were already calculated for the BASJE shielded detector[5][6]. And the average n_b is given by E/1.0GeV.

The delayed bursts were classified by N_e, secθ and core distance (R) into bins whose ranges were 0.5 in $\lg N_e$, 0.2 in secθ and 50m in R, respectively.

4. Results

Since the frequency of bursts is almost independent of secθ from 1.0 to 1.8, the results are presented by combining all of data in each bins of secθ. Figure 1 shows an example of delay time spectra of the bursts. The frequency decreases monotonously with delay time. In figure 2 the frequencies of delayed bursts are presented against electron sizes in three bins of core distances. As is seen in the figure, the frequency increases monotonously with electron size except for bursts with n_b larger than 15 in air showers with N_e larger than 10^8 in figure 2(a) and 2(b), where the first peak in the signal arising from muons is high and the tail obscured the delayed peak arising from the burst. The frequencies shown in the figure were compared with those estimated from the calculations on delayed nucleons and anti-nucleons made by Grieder[7] with a rising cross section of hadrons and an increasing multiplicity of nucle-

ons and anti-nucleons. In the present estimation, the fluctuation in sizes of bursts from hadrons with a given energy was taken into account by referring to the calculation made by Rappaport(5). The frequencies of delayed bursts observed in the present experiment are higher than those estimated at electron sizes larger than 10^7, and the dependence on N_e is steeper than that estimated. At present, the dependence of multiplicity of nucleons and anti-nucleons on energy is being examined to explain the frequencies of observed delayed bursts.

Figure 3 shows a diplot of the burst sizes and the delay times of all delayed bursts in the present observation. Seven delayed bursts with n_b larger than fifty particles and the delay times longer than 50ns were found. Whether these bursts with large sizes and delay times are reasonably explained as arising from nucleons and anti-nucleons is an important problem and is being carefully examined.

References

(1) F. Kakimoto et al: J. Phys. G; Nucl.Phys. 5(1983)339.
(2) N. Inoue et al: J. Phys. G; Nucl. Phys. 11(1985)669.
(3) F. Kakimoto et al: HE 4.7-4 in this Conference
(4) N. Inoue et al: J. Phys. G; Nucl. Phys. 11(1985)657.
(5) S. A. Rappaport: PhD Thesis, M.I.T. (1968)
(6) H. V. Bradt and S. A. Rappaport: Phys. Rev. 164(1967)1567
(7) P. K. F. Grieder: Riv. Nuovo Cimento 7(1977)1 and private communication on the calculations at altitude of 3000m and 5000m.

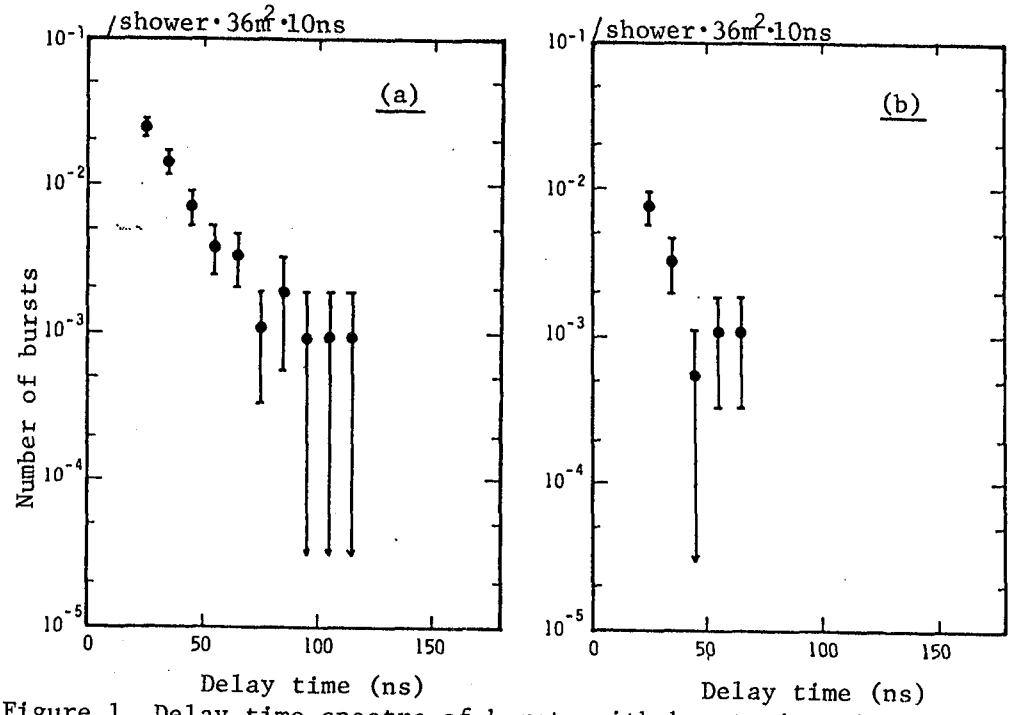

Figure 1. Delay time spectra of bursts with burst sizes larger than 15 in (a) and larger than 30 in (b) for air showers with electron sizes from $10^{7.0}$ to $10^{7.5}$ and core distances from 50m to 100m.

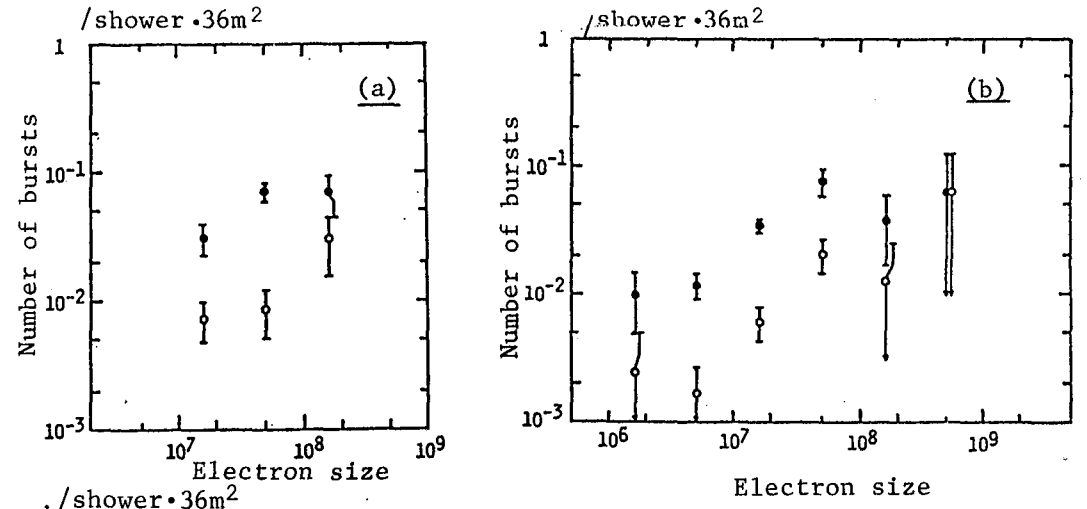

Figure 2. Frequencies of bursts with delay times longer than 30ns and with burst sizes larger than 15(●) and larger than 30(○) against electron sizes at core distances of 50-100m(a), 100-150m(b) and 150-200m(c).

Figure 3. Diplot of the burst sizes and the delay times for air showers with N_e larger than $10^{6.0}$, sec θ of 1.0 -1.8 and core distances smaller than 200m.

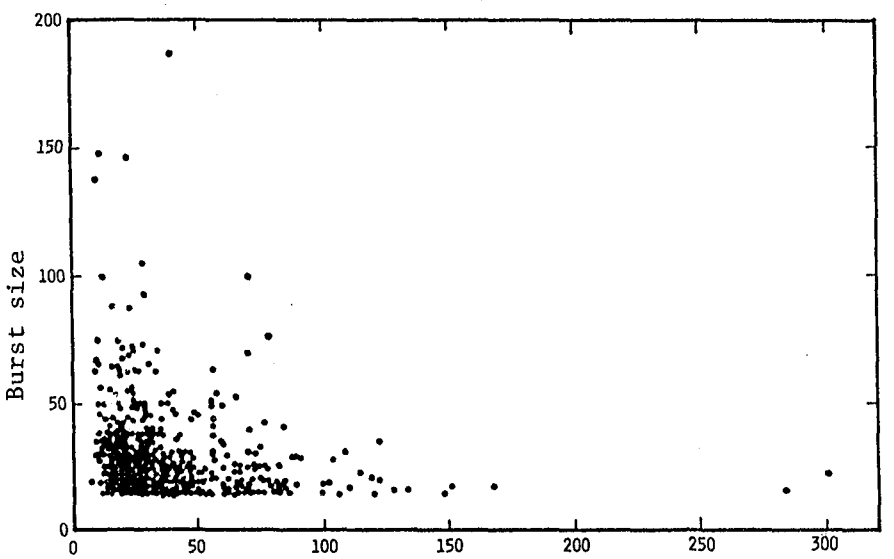

Figure 3. Delay time (ns)

SEARCH FOR LONG-LIVED MASSIVE PARTICLES IN EXTENSIVE AIR SHOWERS

M. Kawamoto and N. Inoue

The Graduate School of Science and Technology, Kobe University, Kobe 657, Japan

Y. Misaki, O. Manabe, T. Takeuchi and Y. Toyoda

Department of Physics, Kobe University, Kobe 657, Japan

Abstract

Air showers containing delayed sub-showers which may be produced by a long-lived massive particle have been investigated by using twelve detectors. Ten events have been selected out as the candidates. However, a definite conclusion cannot be got at the present time.

1. Introduction

In our previous experiment, some effort to seek long-lived massive particles which may be produced in extensive air showers (EAS) was attempted (1) (2). Double-peaked coincidence pulses from plural detectors set at separate places in EAS array were investigated to observe these particles. This method is based on the following idea. If a long-lived massive particle is produced by a high-energy interaction in the upper atmosphere and it decays to some particles after long flight, the secondary products from them will arrive at ground as delayed sub-showers relative to main EAS particles. Four events were reported as candidates for the massive particles, and furthermore, three events were added by an observation after that time. This observation, however, was carried out by using a few detectors, and accordingly the information on the size of delayed sub-showers could not be obtained. A new extended experiment has been carried out by using twelve detectors in the Akeno EAS array to get more information. Some preliminary results are reported in this paper.

2. Experimental

Twelve scintillation counters for measuring the arrival-time distribution of EAS particles were set in the Akeno array (S2 station). The arrangement of detectors is shown in Fig. 1. In the figure, D1 and D2 detectors were piled up inserting iron sheets with total thickness of 10 cm between them. The signals from detectors A1∿A3 were transmitted to a storage oscilloscope (100 MHz, Iwatsu TS-8123) through co-axial cables with different length, respectively, and accordingly three signals were displayed on the same sweep of the oscilloscope. Detectors B1∿B3 and C1∿C3 were also operated by the same system. Signals displayed on each oscilloscope were send to a micro-computer (NEC PC-9801) through A/D converters and the pulse profiles were stored in a floppy disk. The pulses from detectors D1∿D3 were displayed on a normal storage oscilloscope (100 MHz, Tektronix 466), and recorded by an autocamera. Each oscilloscope was triggered by the coincidence pulses from the three detectors shown in the figure, and events accompanied by air shower master pulses from the Akeno array were recorded.

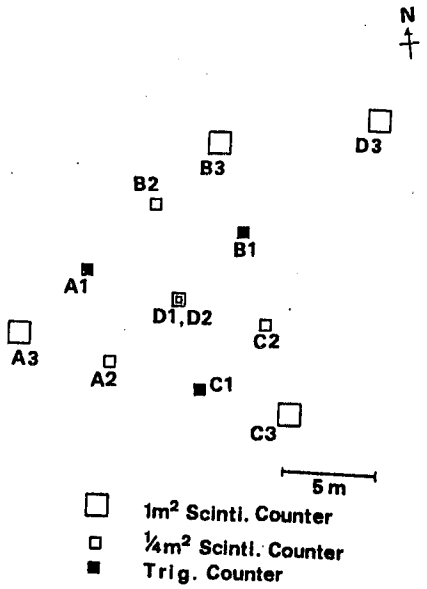

Fig. 1 Arrangement of detectors

However, 32 of these events show the second pulses with the same time delay (the time interval between the first peak and the second peak), considering the difference of the time response of each detector (4 ns). Further, only ten of these events show the double pulses from adjacent three detectors arranged in a regular triangular form. An example of these showers is given in Fig. 2. In most of these cases, delayed pulses do not distribute over these triangular areas. We have selected out these ten events as candidates containing the delayed sub-showers, and investigated various characters of these showers : shower age, incident angle and muon size et al. These showers show normal character in various points.

3. Results

Pulses of 6300 showers were analyzed in detail. The core distances of 95% of analyzed showers are less than 75 m. In these showers, we found about 70 events whose pulses from three or more detectors showed double peaks and one or more of these delayed second pulses contained at least five particles.

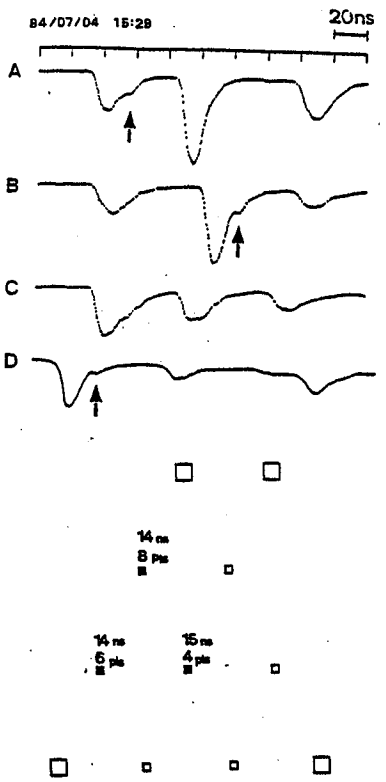

Fig. 2 An example of candidates containing delayed sub-showers

The EAS size is 3.0×10^6 and the core distance of the sub-shower is 35 m. The closed squares show the detectors with the second pulses and the figuers are the delay times and particle numbers of the second pulses.

4. Discussion

When the number of incident particles to a detector is small, spurious double pulses are produced due to the statistical fluctuation of the arrival-time distribution of main EAS particles. Using the average arrival-time distribution (HE 4, 7-2)(3) and the density distribution obtained by our experiment for various core distances, this effect was investigated by Monte Carlo simulation. An example of the results is given in Fig. 3. In the figure, observed integral numbers of double-peaked pulses, curve (a), are shown as a function of the time delay, and curve (b) is a result of the simulation. As seen in the figure, the observed numbers are much more than the calculated value. The origin of the difference is not clear. Any useful calculation about the fluctuation of the arrival-time distribution of electromagnetic shower particles or nuclear cascade particles is not obtained at the present time.

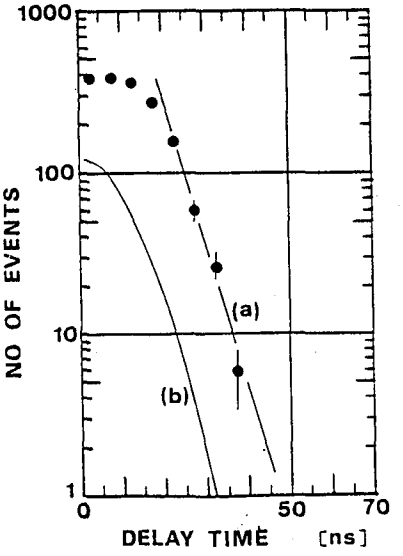

Fig. 3 Integral number spectrum of double-peaked pulses

The spreads of detectable delayed particles are of the order of 5 m from the present experiment, and then we could not get the detailed information about the structure of delayed sub-shower from our arrangement of detectors. A preliminary observation has been carried out by the compact arrangement which consists of 9 detectors within a regular triangle of 10 m sides. We have found three events which contain five or more pulses showing double peaked structure with the same time delay. Finally, to arrive at the conclusion about the long-lived massive particle, a more elaborate experiment is necessary.

references

(1) Yoshida, M. et al. : 18th ICRC at Bangalore, 11, 371, (1983)
(2) Yoshida, M., Toyoda, Y. and Maeda, T. : J. Phy. Soc. Japan, 53, 1983, (1984)
(3) Inoue, N. et al. : HE 4. 7-2 of this conference

HIGH ENERGY COSMIC RAY SIGNATURE OF QUARK NUGGETS

J.AUDOUZE[1,2], R. SCHAEFFER[3] AND J. SILK[4]

1 Institut d'Astrophysique du CNRS, 98 bis, boulevard Arago 75014 Paris, FRANCE

2 Laboratoire René Bernas, 91405 Orsay, FRANCE

3 Service de Physique Théorique, CEN-Saclay 91191 GIF S/Yvette, FRANCE

4 Astronomy Department, Univ. of California, BERKELEY CA 94720, USA

It has been recently proposed (Witten, 1984) that dark matter in the Universe might consist of nuggets of quarks which could populate the "nuclear desert" between nucleons and neutron star matter. Witten further suggested that the "Centauro" events which could be the signature of particles with atomic mass A~100 and energy $E \sim 10^{15}$ eV (Bjorken and McLerran, 1979) might also be related to debris produced in the encounter of two neutron stars. In this paper, we examine a further consequence of Witten's proposal and show that the production of relativistic quark nuggets is accompanied by a substantial flux of potentially observable high energy neutrinos.

Witten (1984) noted that quark matter can exist in the form of droplets of finite size, "quark nuggets", and be more stable than nuclear matter, or at least metastable. If the hypothesis that quark matter is more stable than nuclear matter is correct, then the end-point of the evolution of a massive star will consist of core collapse following exhaustion of nuclear fuel and formation of a ~1 Mo quark star. When quark stars are disrupted by collisions or by tidal interactions, as would happen in the vicinity of a massive black hole, one might expect to find prolific production of quark nuggets. Even if the quark phase is only metastable then passage of a shock through a neutron star involved in a collision should also trigger formation of quark nuggets.

A plausible astrophysical scenario for the production of quark nuggets may readily be constructed. Strong evidence exists that there is a black hole of $\sim 3\ 10^6$ M⊙ at the center of our galaxy devouring matter at a rapid rate (Lo et al., 1985). This black hole most likely formed, as did other supermassive black holes in the nuclei of active galaxies and in quasars, by stellar collisions in dense galactic cores. Studies of the evolution of such cores suggest that dynamical relaxation occurs within a few 10^9 years to form exceedingly compact nuclei of stars surrounded by more diffuse halos. Within these nuclei, stars collide with one another. Collisions between ordinary stars will trigger the formation of neutron stars and one ends up

with a compact central cluster of neutron stars. This cluster continues to evolve dynamically until the neutron stars collide and the debris aggregate to form a central black hole. This process is greatly accelerated by gravitational radiation towards the final stages (Shapiro and Teukolsky, 1985).

Once the massive black hole forms, neutron stars in eccentric orbits will occasionaly plunge within the Roche limit and be tidally disrupted. Occasional collisions will also occur, guaranteeing a continuing supply of fuel for the central black hole.

All of this falls within the more or less conventional scenarios for the evolution of a massive or supermassive black hole in the nucleus of a galaxy. According to computations of neutron star collisions (Gilden and Shapiro, 1984) approximately 30% of the neutron star mass may be heated and disrupted. In the case of collisions between two quark stars, we anticipate that the typical fragment size will have baryon number $A = 10^2$-10^3 or larger. We shall proceed on the hypothesis that the baryon number of surviving quark nuggets is of this order. In the case of tidal disruption, we expect a similar outcome.

We note first that the binding energy of quark matter is ~100 MeV per unit baryon number. Hence a shock in excess of this energy should suffice to cause disruption. This is precisely the energy that one would expect for shocks induced within a few gravitational radii of the central black hole. Post-shock heating will cause the temperature to exceed 100 MeV, and there will be prolific emission of $\nu\bar{\nu}$ pairs. We expect that the neutrino emission will amount to $E_\nu \sim 10^{53}$ erg per quark star disruption and that the spectrum of neutrino produced will peak near 100 MeV.

Now let us consider the fate of the quark nuggets, we shall assume that quark stars have many properties in common with pulsars, in particular a magnetic field $B_{12} = B/10^{12}$ g ~ 1, radius R_6 (in 10^6 cm units)~1 and a rotation period p (in sec)~1. Newly formed quark stars should have millisecond periods but quark stars that survive for more than a few 10^6 years before disruption will have a longer period.

We shall use the model of Goldreich and Julian (1969) to estimate the electrostatic acceleration of quark nuggets as they are disrupted from the rapidly spinning magnetic quark stars. In this simple model which assumes that the magnetic dipole moment is aligned with the rotation axis, charged particles escape along magnetic field lines that extend outside the light cylinder where they are electrostatically accelerated up to energies of $3\ 10^{12}\ Z\ R_6^2\ B_{12}/p^2$ eV. The typical charge of a quark nugget is $Z \approx 5\ A^{1/3}$ (Farhi and Jaffe, 1984) and we infer that the typical energy to which quark nuggets can be accelerated is $\varepsilon = 10^5\ A_{100}^{1/3}\ p^{-2}$ GeV .

How many of these relativistic nuggets would one expect ? Let us assume that we can tap the entire rotation energy $E_R \sim 10^{47}\ p^{-2}$ erg of the quark stars. Then we expect that $N \sim 10^{42}\ A_{100}^{-1/3}$ relativistic quark nuggets of energy ε will be produced per quark star disruption. Note that this only amounts to a small fraction of ($\sim 10^{-11}$) of the quark star mass. Hence the acceleration process should be complete and the rotational energy reservoir depleted long before final disruption of the quark star occurs. A similar estimate could also apply to acceleration of Fe nuclei if they could survive neutron star disruption.

If the putative $3\ 10^6$ M⊙ black hole at the galactic center formed over the past 10^9 years, it must have grown on the average by 1 M⊙ per 300 years. Let us suppose that it grew by quark star swallowing, involving either collisions or tidal disruption. The Larmor radius of a quark nugget exceeds that of a proton of the same energy by a factor $0.2\ A^{2/3} \sim 5\ A_{100}^{2/3}$. Hence its Larmor radius will not exceed a few pc and we infer that relativistic quark nuggets will be well coupled to the galactic magnetic field. Hence they will accumulate throughout the cosmic ray confinement region usually taken to be the galactic halo, over a typical containment time of $\sim 10^8$ years. Assuming N nuggets per solar mass captured are emitted and retained in the galaxy for $\sim 10^8$ years we estimate the mean flux of relativistic quark nuggets of energy ε to be $\sim 10^{-10}\ (N/10^{42})\ cm^{-2}\ sec^{-1}$. We also predict a flux of 100 MeV neutrinos amounting to $\sim 10\ cm^{-2}\ sec^{-1}$.

The observed anomalous high energy cosmic rays events (Jones, 1984) correspond to a flux of $\sim 10^{-9}\ cm^{-2}\ s^{-1}$ at an energy per event of $\sim 10^6$ GeV which agrees rather well with our estimates. Our calculated 100 MeV neutrino flux is also close to the cosmic flux of energetic neutrinos (>100 MeV)$\sim 11\ cm^{-2}\ s^{-1}$ obtained from the 17 events/kiloton/year reported by the Kamiokande experimenters (Totusa, 1984) to be in excess of the atmospheric background events. Conservatively, we should regard this experiment as setting an upper limit on the background flux of 100 MeV neutrinos. Therefore the black hole in the center of our galaxy may generate both the Centauro events, interpreted as relativistic quark nuggets, and the high energy neutrino background flux that is consistent with current observations in proton-decay detectors.

References

1. Bjorken J.D., and Mc Lerran L., 1979, Phys. Rev. D 20, 2353
2. Farhi E., Jaffe R.L., 1984, Phys. Rev. D 30, 2379
3. Gilden D.L., and Shapiro S.L., 1984, Ap.J., 287, 728
4. Goldreich P., and Julian W.H., 1969, Ap.J., 157, 869
5. Jones W.V., 1984, in High Energy Astrophysics, Ed J. Audouze and J. Tran Thanh Van, p.59

6. Lo K.Y., et al., 1985, Nature, 315, 124
7. Shapiro S.L., and Teukolvsky S., 1985, preprint
8. Totusa Y., 1984, Proc. XIX Rencontres de Moriond, Ed. J.Tran Thanh Van, 1, 625
9. Witten E., 1984, Phys. Rev., D 30, 272.

Search for Anomalons Using Plastic Nuclear Track Detectors

W.Heinrich, H.Drechsel, C.Brechtmann, J.Dreute
Physics Department, University of Siegen, D5900 Siegen, W.Germany

ABSTRACT

We exposed a stack of CR39 track detectors containing Ag foils to a 1.7 GeV/nucleon ^{56}Fe-beam and investigated the anomalous mean free path effect. Neither the whole set of 7517 nor a subset of 2542 interacting fragments produced probably in the Ag target show an effect. By combining the data of this and an earlier experiment we can also exclude an effect for 3219 interacting fragments produced in $\Delta Z=1$ collisions.

INTRODUCTION

The situation of mean-free-path (mfp) measurements for relativistic projectile fragments (PF's) under different experimental conditions is still not clear. The results of emulsion experiments /1-3,11/ showing an anomalously large interaction cross section of PF's within the first few centimeters from their point of emission are contradicted by some other experiments using different techniques like Cherenkov detectors /4,5/, plastic nuclear track detectors /6,7/ or even by experiments using nuclear emulsions /8-10/. There are some indications that the effect is preferentially observed for fragments produced in collisions with heavy target nuclei and for fragments produced in extremely peripheral collisions:

In nuclear emulsion a large number of collisions occurs with silver target nuclei whereas the experiments using Cherenkov or plastic nuclear track detectors provide targets not heavier than oxygen. If anomalons would be produced only in collisions with heavy targets this would explain all the negative results in these experiments.

Furthermore some observations are supporting the idea, that anomalons are produced in extremely peripheral collisions. The most striking hint comes from a bubble chamber experiment /12/, where collision products of a 3.7 GeV/nucleon ^{12}C beam were analyzed. No anomalous behavior was observed for all types of analyzed interaction products except ^{12}C projectiles that had undergone a collision, but did not loose charge. If we follow the hypothesis, that anomalons are produced preferably in peripheral interactions, all experiments having a low sensitivity in detecting these interactions should see a reduced or no effect of anomalous mfp's. Experiments of this type are our first plastic track detector experiment /6/ and the nuclear emulsion experiment of the BCJJL collaboration /9/.

THE EXPERIMENTAL METHOD

We performed a new experiment which meets the requirements of both heavy target and high efficiency for the detection of $\Delta Z=1$ interactions. For this purpose 200µm thick silver foils were stacked between the CR39 foils ($C_{12}H_{18}O_7$) of 600µm thickness. A stack of each 150 silver and plastic foils with a size of 10cm * 8cm was exposed at the Bevalac to a 1.7 GeV/nucleon Fe beam with 10^3 particles per cm^2. The beam nuclei were

slowed down in the stack to 0.8 GeV/nucleon. Due to the high sensitivity of the detector material tracks of fragments with charges $Z \geq 7$ were recorded.

After etching of the detectors the tracks of all particles were measured using our automatic measuring system /13/. After a calibration the particle charges were determined from the measured areas of the tracks. The reconstruction of particle trajectories through the stack was performed in a similar way as described earlier /7,14/. By measuring the particle tracks on both sides of the detectors it was in principle possible to separate the interactions that took place in the plastic from those that occured in the silver foils. In the following analysis only tracks with a length >4mm containing at least 10 etch cones are included.

RESULTS

The interaction mean free paths $\lambda_Z(x)$ were determined for intervals of distance x from the point of emission of the fragments as described earlier /7/. These $\lambda_Z(x)$ were normalized to a value λ_Z^c which was calculated considering the relative yield of the different isotopes as described in /6/. No statistically significant deviations between the measured interaction mean free paths and the calculated values can be observed. A comparison of the data by a χ^2-test gives a $\chi^2=46.3$ for 37 degrees of freedom.

To improve the statistical significance the normalized interaction mean free paths for all individual fragment charges were compiled to one data set of $\lambda^*(x)$ shown in figure 1. The horizontal bars indicate the intervals of distance from the interaction point. This result based on 7517 interactions of fragments with charges $7 \leq Z \leq 25$ shows no significant deviation from a constant mean free path.

To investigate a dependence of the result on the mass of the target nucleus we analyzed separately $\lambda^*(x)$ for those fragments produced in collisions with silver target nuclei. Because of some uncertainties of the separation the data set contains only a part of about 70% of fragments produced in silver which however is greater than the equivalent part in experiments with nuclear emulsion. Also this result shown in figure 2 which is based on 2542 interactions gives no indication on a dependence of the mean free path on x.

As described above the experimental data available until now indicate that anomalons may be produced more efficiently in peripheral collisions. Therefore we analyzed separately interactions of fragments produced in $\Delta Z=1$ collisions for this experiment including data of an earlier experiment exposed to an ^{40}Ar beam for which the analysis was extended to Z=16 and Z=17 fragments. From this stack data of tracks longer than 2mm are available. Our efficiency for the detection of a fragmentation with $\Delta Z=1$ decreases from unity to about 84% when the length of the track decreases from 20 to 10 foil layers. The efficiency was measured by artificial shortening of long fragment trajectories contained in our data. This reduced efficiency would equalize a small anomalous mfp effect. We corrected our data based on the measured efficiencies. Figure 3 shows the normalized $\lambda^*(x)$ of fragments produced in $\Delta Z=1$ collisions for which 3219 interactions were observed. No anomalous mfp effect is seen behind the first cm.

Figure 4 shows three curves of confidence in the plane of the parameters α and λ_A, where α is the admixture of the anomalons in the set of PF's and λ_A their mfp. Pairs of the parameters from the region above the curves can be rejected at a confidence level of 95%. One curve results from the fragments produced in $\Delta Z=1$ collisions, another one from those produced in the heavy silver target. Additionally we combined all our data available until now from experiments described in this paper, /6/ and /7/ without any restriction. These experiments with Ar and Fe beams at 1.7 and 1.8 GeV/nucleon, fragments in the range from Z=7 to Z=25 and CR39- or Ag-targets have contributed with altogether 16847 interactions. The resulting curve is drawn in figure 4.

CONCLUSION

In summary we have investigated two hypothesises about the anomalous mfp effect. In our high-statistic experiments using CR39 nuclear track detectors we found no evidence for the existence of anomalons. Neither the use of a heavy silver-target, nor the restriction on the data obtained from the fragments produced in $\Delta Z=1$ collisions are consistent with a strong anomalous mfp effect reported earlier /1-3/. Due to the possibility to measure the mfp at small distances from the interaction point our data provide a higher significance for the rejection of the anomalon-hypothesis than earlier experiments /4/ at interaction lengths below 0.5cm.

ACKNOWLEDGEMENT

This work was supported by the Bundesminister für Forschung und Technologie No. 06 SI 159 . We are grateful to the staff of the Bevalac for the exposure of the plastic stacks.

REFERENCES

1. E.M.Friedlander et al., Phys. Rev. Lett. 45, 1084 (1980)
2. P.L.Jain and G.Das, Phys. Rev. Lett. 48, 305 (1982)
3. H.Barber et al., Phys. Rev. Lett. 48, 856 (1982)
4. J.D.Stevenson et al., Phys. Rev. Lett. 52, 515 (1984)
5. T.J.M.Symons et al., Phys. Rev. Lett. 52, 982 (1984)
6. W.Heinrich et al., Phys. Rev. Lett. 52, 1401 (1984)
7. H.Drechsel et al., Phys. Rev. Lett. 54, 30 (1985)
8. R.Holynski et al., Proceedings 18th ICRC, Bangalore Vol.11, paper He 2.2-30, to be publ. in Zeit.f.Phys.
9. S.Beri et al., Phys.Rev.Lett. 54, 771 (1985)
10. G.Baroni et al., Nucl.Phys, A437 (1985) 3,4 p.729 at 7. High Energy Heavy Ion Study GSI/Darmstadt (1984)
11. E.A.Alekseeva et al., Pis'ma Zh.Eksp.Teor.Fiz. 38,no.8,411 (1983)
12. A.P.Gasparian, N.S.Grigalashvili, Zeit.f.Phys.A 320,459 (1985)
13. W.Trakowski et al., Nucl. Instrum. Methods 225, 92 (1984)
14. H.Drechsel et al., Nucl. Instrum. Methods 227,342 (1984)

Fig.1: Normalized interaction mfp as a function of distance x from the point of emission in the composed target CR39+Ag. The dashed line represents the mean value of 0.985±0.012 .

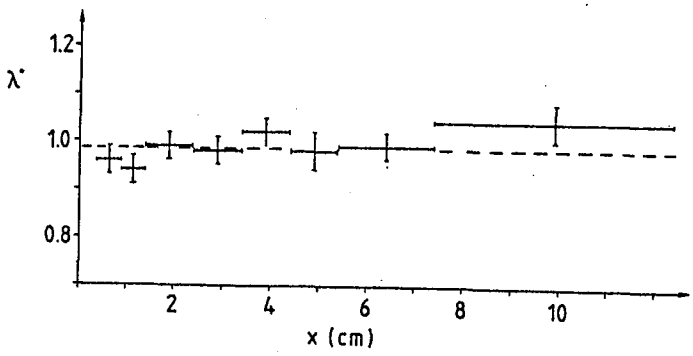

Fig.2: Normalized interaction mfp of fragments produced in the Ag-part of the target as a function of distance x from the point of emission. The mean value is 1.002±0.020 .

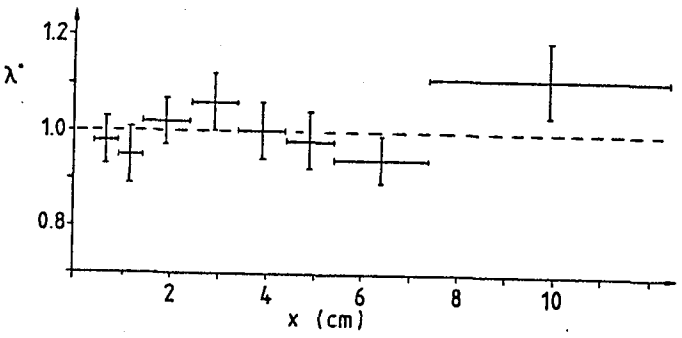

Fig.3: Normalized interaction mfp of fragments produced in ΔZ=1 collisions as a function of distance x from the point of emission. The mean value is 0.986±0.018 .

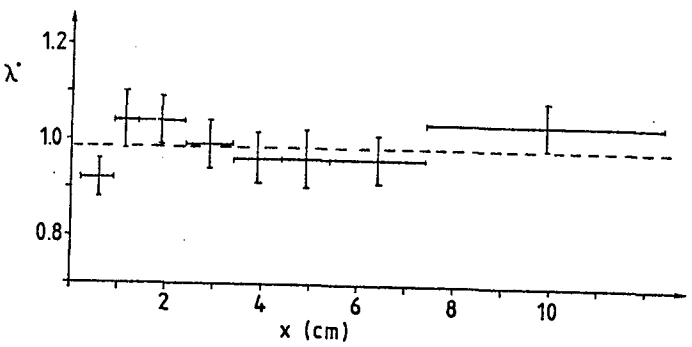

Fig.4: Curves of confidence in the plane of the abundance of anomalons and their assumed mfp obtained from two subsets and a combination of all our data. The regions above the curves are ruled out at a 95%-confidence-level.

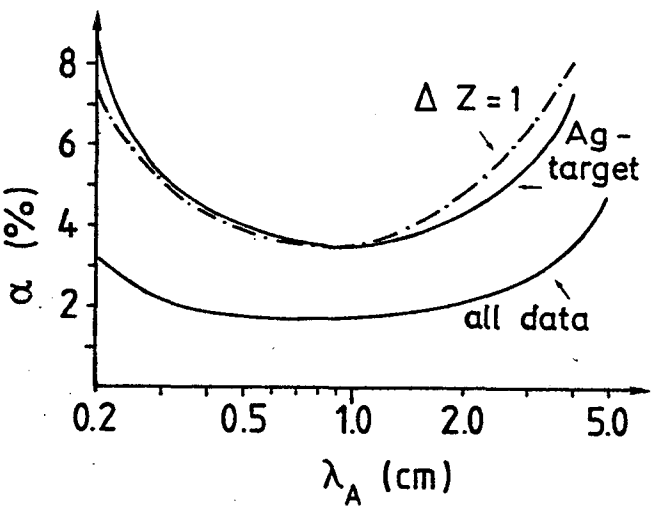

Search for tachyons associated with extensive air showers in the ground level cosmic radiation

H.F. Masjed and F. Ashton
Dept. of Physics, Durham University, Durham, England

Abstract

Events detected in a shielded plastic scintillation counter occurring in the 260μs preceding the arrival of an extensive air shower at ground level with local electron density $\geq 20 m^{-2}$ and the 240μs after its arrival have been studied. No significant excess of events (tachyons) arriving in the early time domain have been observed in a sample of 11,585 air shower triggers.

Introduction. According to the special theory of relativity a particle of rest mass m and moving with velocity $v=\beta c$ has total energy $E=\gamma mc^2$ where $\gamma=1/\sqrt{1-\beta^2}$ so that velocities greater than the velocity of light c are forbidden. To accommodate velocities >c in the formalism Recami and Mignami (1974, pg 263) suggest that for such objects (tachyons) $E=imc^2/\sqrt{\beta^2-1}$ where the complex number i is associated with the superluminal Lorentz transformation and not the 'rest mass' of the tachyon. For such objects their total energy would decrease as their velocity increases tending to zero as $\beta\rightarrow\infty$. Thus if tachyons are produced in the collision of high energy primary cosmic ray protons in the atmosphere via P+N→N+N+t+$\bar{t}$+pions etc. then one would expect that they are produced with high velocities ($\rightarrow\infty$) at their production energy threshold. If produced, tachyons would arrive at sea level before the air shower front (comprising mainly electrons moving with velocity $\simeq c$) and for a primary proton incident in the zenith direction and making its first interaction at 17.7km above sea level the relevant time for infinite velocity tachyons is 59μs. For showers incident at a zenith angle of 60° the relevant time is 150μs. To cover all possibilities ionising events occurring in a $1.05 m^2$ area plastic scintillator (shielded by 15cm of lead and 15cm of iron) occurring in the 260μs time domain preceding the arrival of air showers with local electron density $\geq 20 m^{-2}$ have been recorded. Events occurring in the 240μs after the arrival of showers have also been recorded for comparison purposes. Some details of the experimental arrangement were described by Darjazi et al (1983).

Results. The occurrence time distribution of events recorded in the tachyon detector relative to the arrival time of the extensive air shower are shown in figure 1. Events occurring in the tachyon detector were continuously injected into a 265μs delay line system and its out-out was recorded on a dual beam oscilloscope which was triggered by the arrival of an air shower at the detector. Particles and photons penetrating the shielding above the tachyon detector and interacting with it thus occur at the time of 265μs in figure 1. It is seen from figure 1 that there is no evidence for an excess of events occurring in the 150μs preceeding the arrival of an air shower as expected if there is a significant flux of tachyons associated with air showers at ground level.

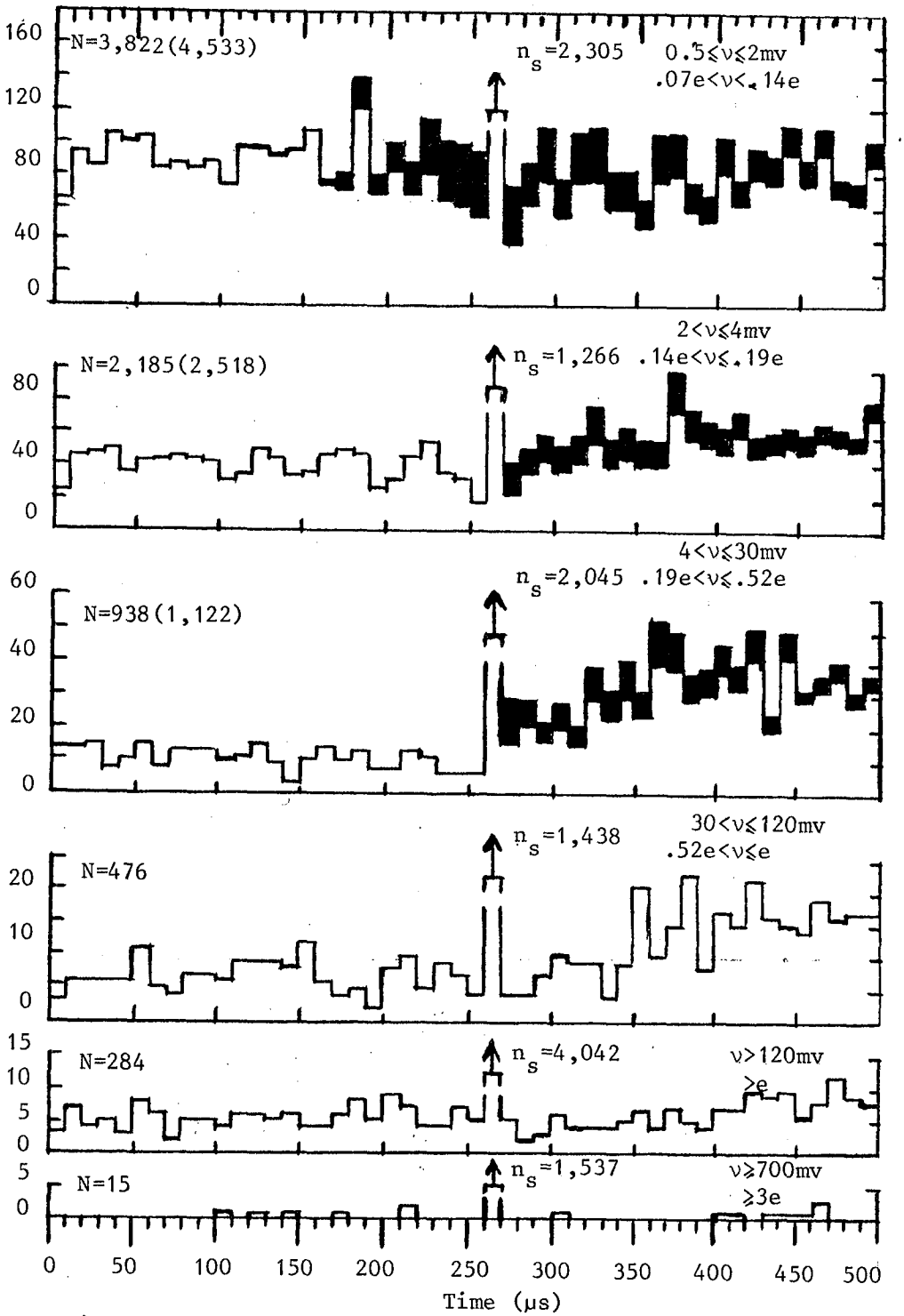

Figure 1. Time distribution of pulses occurring in different ranges of pulse height from a sample of 11,585 shower triggers. Time is measured from the start of the oscilloscope time base and the shower front occurs at the well defined time of 265 μs. The number of pulses in the 260-270μs time bin (which contains shower front pulses with

Caption to Figure 1 continued

pulse heights in the stated range of energy deposition) are too large to be plotted and are indicated by n_s. N is the total number of measured events in the 0-500μs time range but excluding the events in the 260-270us time bin and the figure in brackets is the number obtained after correction for experimental bias. The range of pulse height ν is as measured on the recording oscilloscope. Also shown is the corresponding range of energy deposition in the scintillator in terms of e where e is the energy loss (10MeV) produced by a relativistic muon traversing the scintillator at normal incidence. The amplifiers used in conjunction with the delay lines had a non linear response so the range of pulse height is not linearly related to the range of energy loss. The shaded portions of the histograms represent the effect of experimental bias produced by large shower front pulses that saturate the recording electronics and cause pulses occurring after the shower front pulse to be unmeasureable. Large shower front pulses are preceeded by an oscillation which causes a loss of measureable pulses at small pulse height (<2mv) before the occurrence of the shower front pulse.

It is apparent from figure 1 that there is evidence for more events being observed to occur in the tachyon detector at times after the arrival of the air shower than before it for energy deposits in the detector of .19e - .52e and .52e - e. e = 10MeV is the energy deposited in the detector when a relativistic muon traverses it at normal incidence. Table 1 gives quantitative data on this effect.

Conclusion. No evidence is found for a significant flux of tachyons in regions of showers with electron density $\geq 20m^{-2}$ in a sample of 11,585 air shower triggers. The excess of events found to trail the arrival of the air shower front could be due to either photons in the air shower electromagnetic cascade which have undergone diffusive scattering, to low energy evaporation neutrons from air nuclei produced in the air shower hadron cascade which subsequently interact in the detection scintillator or low energy nuons from π-μ decay.

Pulse height range	N(0-260μs)	N(270-500μs)	$\frac{N(0-260\mu s)}{N(270-500\mu s)}$
0.5≲ν≲2mv 0.07e≲ν≲0.14e	2,225 (2,459)	1,597 (2,074)	1.39±0.05 (1.19±0.04)
2 ≲ν≲4mv 0.14e<ν≲0.19e	1,048	1,137 (1,470)	0.92±0.04 (0.71±0.03)
4 <ν≲30mv 0.19e<ν≲0.52e	273	665 (849)	0.41±0.03 (0.32±0.02)
30 <ν≲120mv 0.52e<ν≲e	175	301	0.58±0.06
ν>120mv ν>e	138	146	0.95±0.11
ν≳700mv ν≳3e	6	9	0.67±0.35

Table 1. The ratio of the number of events $\frac{N(0-260\mu s)}{N(270-500\mu s)}$ occurring in the time regions 0-260μs and 270-500μs with times measured from the start of the oscilloscope time base. The shower front pulse occurs at 265μs from the start of the oscilloscope time base. The numbers in brackets are the results obtained after correcting the observed number of events for experimental bias. Assuming all pre shower front and post shower front pulses are random coincidences the expected value of the ratio $\frac{N(0-260\mu s)}{N(270-500\mu s)} = 1.13$.

References.

Darjazi, M.S., Masjed, H.F., and Ashton, F., 1983, Proc.Int. Cosmic Ray Conf. (Bangalore), 11, 268-271.

Recami, E., and Mignami, R., 1974, Rivista del Nuovo Cuinento, 4, 209-290.

HE 6.2-14

CHARGE 4/3 LEPTONS IN COSMIC RAYS

Tomonori Wada and Yoshihiko Yamashita
Okayama University, Japan
Kuninisuke Imaeda and Isao Yamamoto
Okayama University of Science, Japan

A cosmic ray counter telescope has been operated at zenith angles of 0°, 40°, 44° and 60° in order to look for charge 4/3 particles. A few million clean single cosmic rays of each zenith angle were analyzed.

For (4/3)e charged leptons, GUTs (Grand unified theories) propose some predictions[1,2,3]. Especially SU(5) proposed by H.Georgi and S.L.Glashow[1] predicts the existence of fractionally charged vector boson ($X_{4/3}$,$X_{1/3}$) and the proton decay, but these boson mass must be greater than 10^{15} GeV. It is hard to produce these particles by accelerators. So one must detect relic fractionally charged particles from the "big bang" by a cosmic ray telescope.

A cosmic ray counter telescope at sea level has been operated and analyzed[4,5] in order to look for charge (4/3)e particles. Four RUNs were performed at different zenith angles as the following table.

A: RUN name	I	II	III	IV
B: zenith angle (degree)	40°	0°	60°	44°
C: measuring time (days)	130	130	260	150
D: pre-triggers ($\times 10^6$)	8	16	8	8
E: pure (4/3)e zone events	15	16	22	31
F: single track in the column "E"	6	2	2	9

Results under adaptation of strict selection rules are shown in fig.1a, 1b, 1c and 1d. These figures show that data of zenith angles of about 40° are different from data of other zenith angles; single track events of (4/3)e zone are rich at 40° and 44°.

If a point source of fractionally charged leptons exists, that momentum must be larger than 10^{21} eV/c. The other side, our experimental trigger condition is $\beta\gamma > 4.8$ and if some of these (4/3)e zone events at 40° and

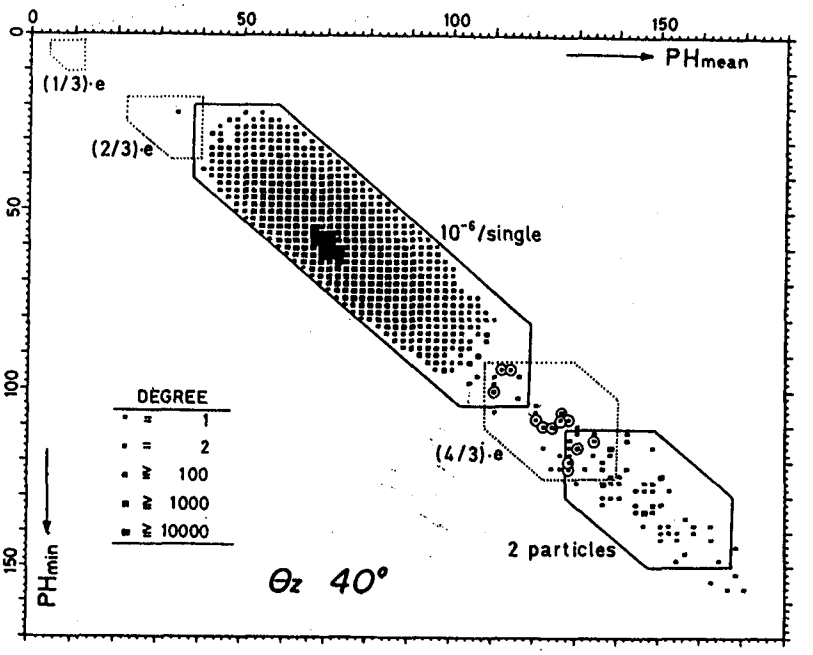

Fig. 1a. Final results of RUN I.

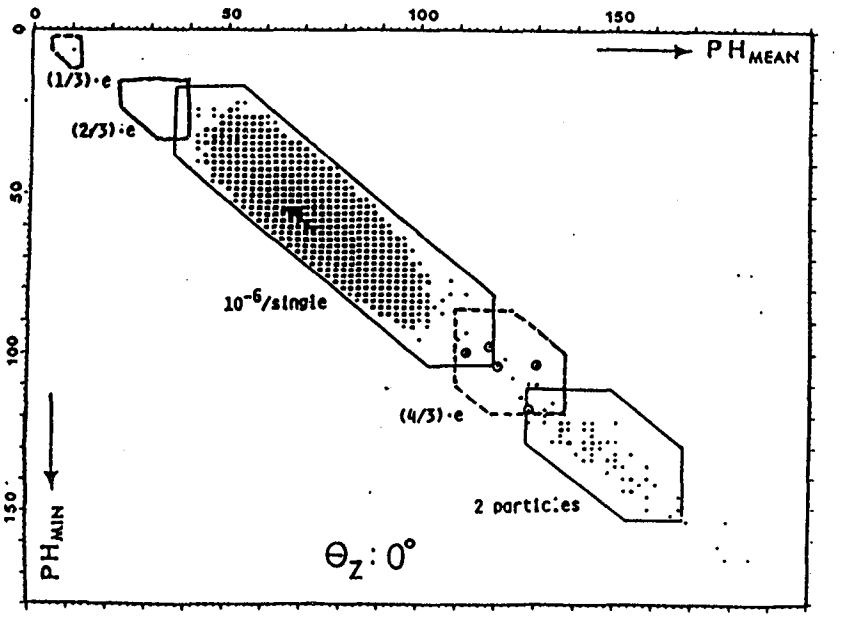

Fig. 1b. Final results of RUN II .

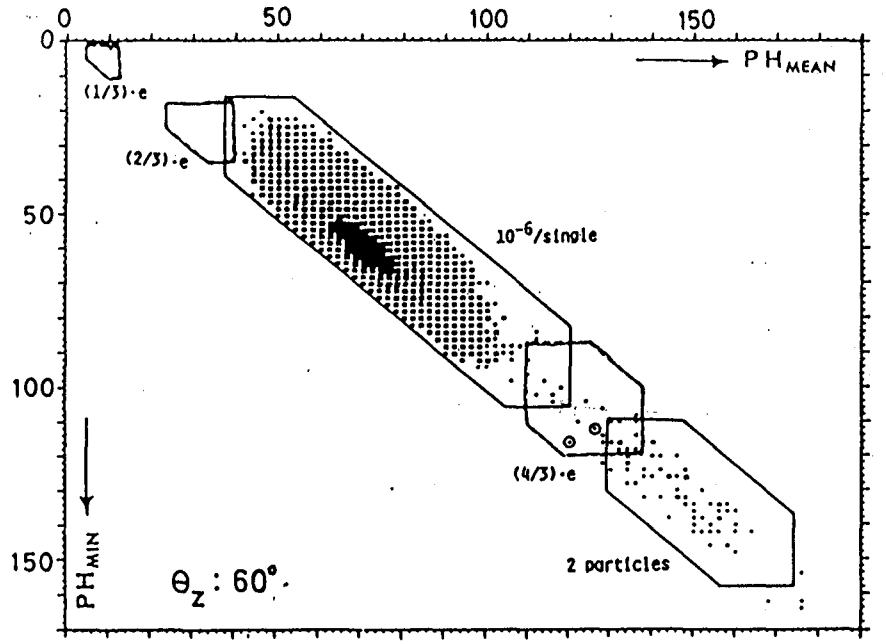

Fig. 1c. Final results of RUN III.

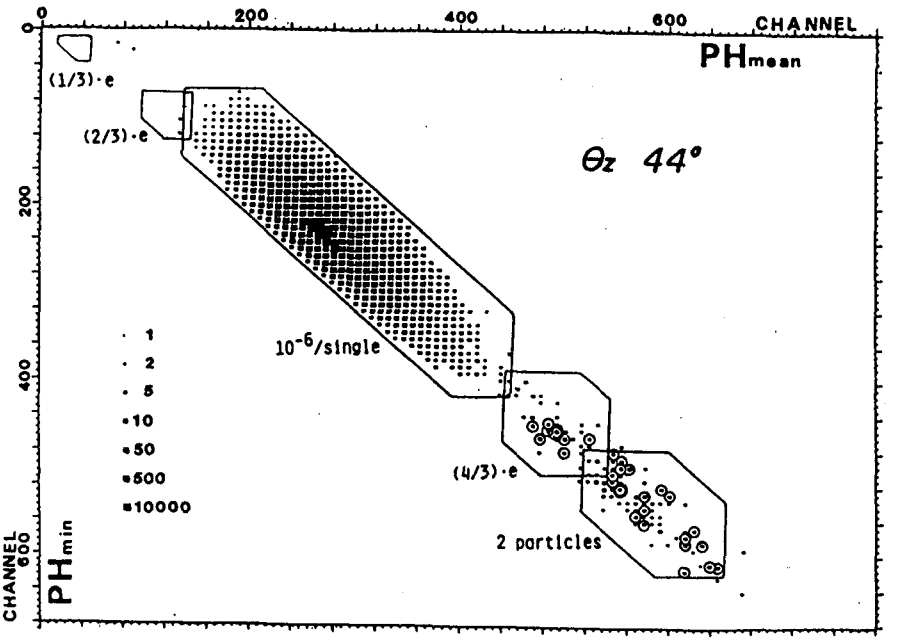

Fig. 1d. Final results of RUN IV.

44° are $X_{4/3}$ vector boson,

$$P = \beta\gamma M_{4/3} \simeq 5 \times 10^{15} \times 10^{9} = 5 \times 10^{24} \text{ (eV/c)}.$$

The momentum, 5×10^{24} eV/c is enough to pass through our Galaxy.

" Where did (4/3)e leptons come from ? "

Single track events of (4/3)e zone at 40° and 44° are plotted in the equatorial coordinates; fig. 2a and corresponding events of two particles zone at 44° are also plotted in the equatorial coordinates; fig. 2b. Points of fig. 2a. mostly separated into two groups, but those of fig. 2b. were spread all over the map.

In this stage, the map of fig. 2 is not clear, so our observation has continued.

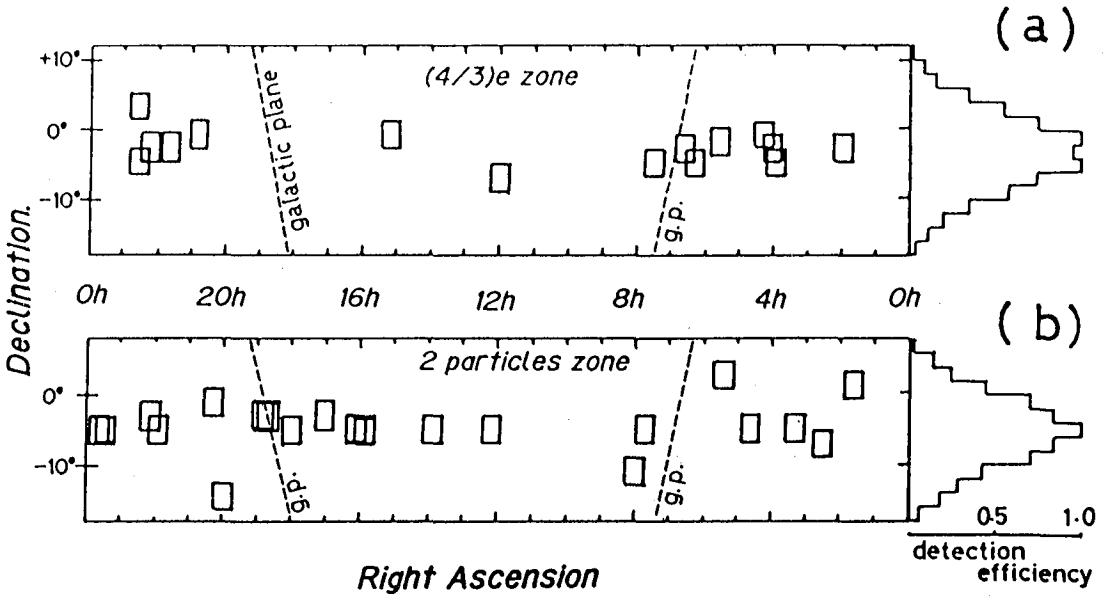

Fig. 2. Arrival directions of single track events for (4/3)e zone and two particles zone.

References

1. Georgi, H. and Glashow, S.L., (1974), Phys. Rev. Lett., 32, 438
2. Goldverg, H. et. al., (1981), Phys. Rev. Lett., 47, 1429
3. Li, L.-F. and Wilczek, F., (1981), Phys. Lett. B, 107, 64
4. Yamamoto, I. et. al., (1982), Nucl. Instrum. Methods, 201, 457
5. Wada, T. et. al., (1984), Lett. Nuovo Cimento 2, 40, 329

HE 6.2-15

PROGRESS REPORT ON A NEW SEARCH FOR FREE e/3 QUARKS IN THE CORES OF $10^{15} - 10^{16}$ eV AIR SHOWERS

A.L. Hodson*, R.M. Bull+, R.S. Taylor*, and C.H. Belford*

*Department of Physics, University of Leeds, Leeds, U.K.
+Department of Physics, University of Nottingham, Nottingham, U.K.

ABSTRACT

The Leeds 3 m^2 Wilson cloud chamber is being used in a new search for free e/3 quarks close to the axes of $10^{15} - 10^{16}$ eV air showers. A 'ratio trigger' circuit is used to detect the incidence of air shower cores; the position of the shower centre and the axis direction are determined from photographs of current-limited spark chambers. It is thus possible, for the first time, to know "where we have looked" for quarks in air showers and to select for scanning only those cloud chamber photographs where we have good evidence that the shower axis was close to the chamber. 250 g cm^{-2} of lead/concrete absorber above the cloud chamber serve to reduce particle densities and make a quark search possible very close to the shower axes. This paper gives the current status of the search.

1. Introduction. We report on a new search for free e/3 quarks in the core region of cosmic ray air showers. That is the very region where, if free quarks exist, they are most likely to be found but one which it has not been possible to explore properly in the past because of high particle densities and low rates of shower core 'hits'.

The 3 m^2 Leeds cloud chamber is ideally suited for such a search and this is now operating under absorber in conjunction with an array of discharge chambers which give information on the positions and directions of shower axes relative to the cloud.chamber. Since the stereo scanning of cloud-chamber photographs for lightly-ionizing e/3 quark tracks is very time-consuming and tedious we can now be much more selective regarding which photographs are scanned; currently we scan only those events in which a shower core fell on a 35 m^2 discharge chamber array above the cloud chamber so that we know that the shower axis either passed through the cloud chamber or was in the close vicinity

Many improvements in technique and in the experimental arrangement have been made since a previous quark search with this cloud chamber (Hazen et al., 1975; Kass, 1977).

2. Experimental arrangement. Information on the shower cores is derived from a 7 m × 5 m close-packed array of 1 m^2 (2 cm gap) discharge chambers with Georgian-wired glass faces. This is mounted directly on the underside of a thin sandwich-panel roof ($\sim$ 2·2 g cm^{-2}), some 6·5 m above the cloud chamber (Figure 1), and is photographed from below. The direction of incidence of the showers may be derived (within $\sim 1-2^{o}$) from the mean projected 'track' angles in two 1 m^2 (4 cm gap) orthogonal vertical discharge chambers and one 1 m^2 (8 cm gap) horizontal discharge chamber beneath the array.

Beneath the 'discharge chamber room' and under 15 cm of lead ($2 \cdot 10^4$ kg) and 25 cm of concrete ($1 \cdot 1 \cdot 10^4$ kg) is located the Leeds 3 m^2 (× 1 m deep) Wilson cloud chamber (Hodson et al., 1965) with its 'front' window

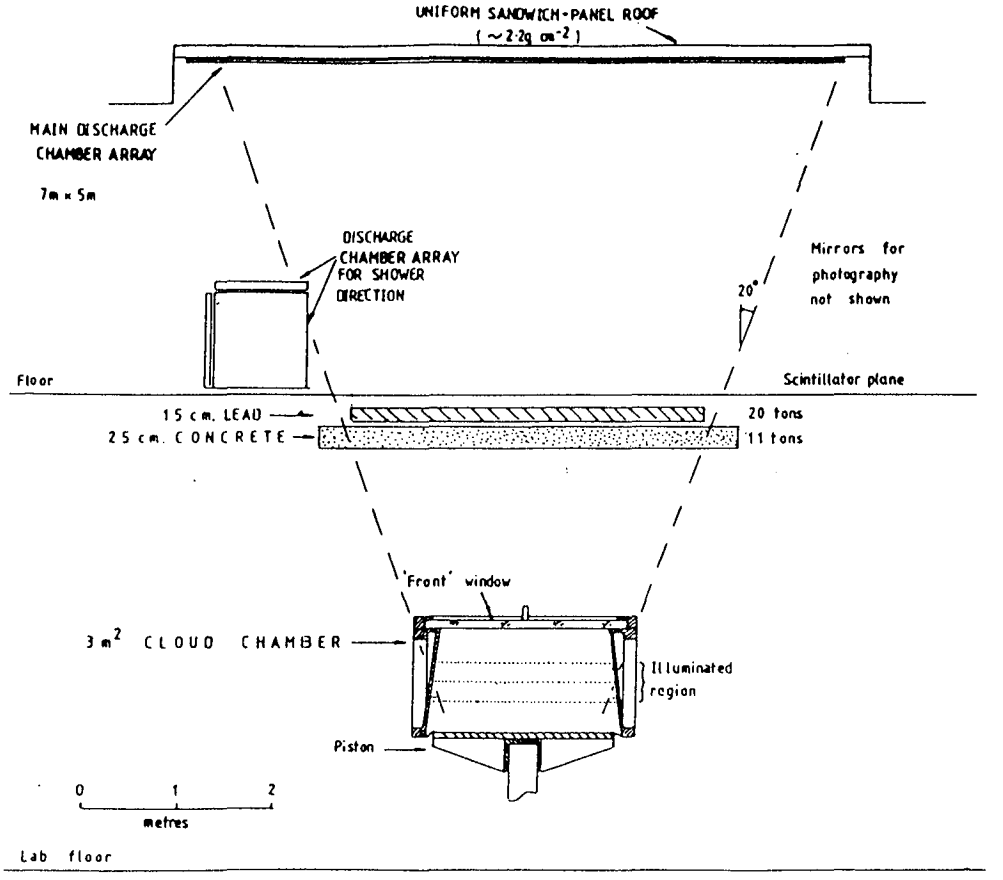

Figure 1: Elevation of Leeds Discharge Chamber/Cloud Chamber Installation

horizontal (and its original internal plates removed).

The discharge chambers and cloud chamber are triggered by pulses from an array of 7 plastic scintillators. A new trigger circuit, based on *ratios* of pulse heights following the work of Green and Hodson (1979), has recently been introduced to select showers whose cores fall within the 35 m^2 discharge chamber array and to exclude, as far as possible, those falling outside the array.

Four cameras are used to take stereo photographs of the cloud chamber, four views on 68 mm wide film and two on 200 mm wide film (Kodak Technical Pan 2415). A 40 cm deep section of the chamber is illuminated by four linear flash tubes (135,000 joules total flash energy). The photographs are taken effectively from above, via a mirror, so that the tracks appear foreshortened and a lightly-ionizing track (such as is expected from a relativistic e/3 quark) is more readily visible. Each track passes, at some point, through the region of best focus and good illumination; the photographic conditions are such that droplets on individual ions are recorded. The expansion time of the cloud chamber is

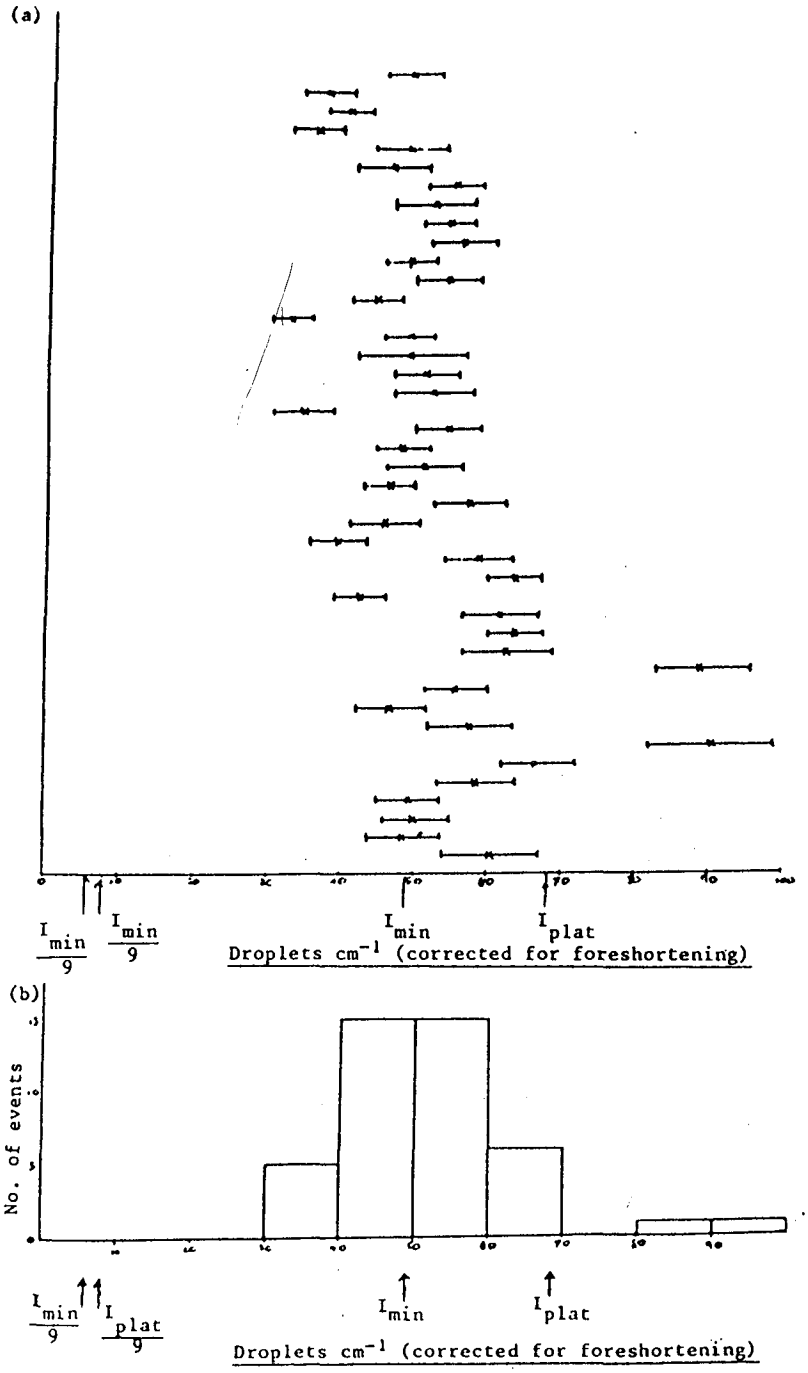

Figure 2: Individual drop count measurements (a), and preliminary distribution (b), for recent film.

The arrows indicate expected values for charge e particles and e/3 quarks at "minimum ionization" and at relativistic plateau ionization ($\approx 1{\cdot}4\ I_{min}$)

slowed to ∿200 ms to allow the ions to diffuse and give track widths in the chamber ∿3·5 mm wide suitable for the counting of resolved droplets.

The absorber above the cloud chamber removes the soft component of air showers and enables a search for free e/3 quarks to be made near the shower axes. After locating the position of the incident shower core at roof level in the discharge-chamber array it is then possible to trace the shower axis down through the absorber to the cloud chamber level using the directional information on the shower. The distance between the centre of the cloud chamber, in which the search is made, and the shower axis can then be found.

Voltages applied to horizontal planes of wires, 20 cm apart, within the cloud chamber serve to remove background ionization. By using electric fields of alternating directions between these planes and removing these fields promptly when a shower is detected, we are able to distinguish unambiguously between a genuine quark track and possible artefacts due to low condensation on separated negative ion columns still present in the chamber from pre-shower particles.

3. Current status of the search. The equipment is being run on as near as possible a continuous basis. Between January 1984 and May 1985 we photographed over 5400 events (∿ 1200 with cores) at trigger rates of ∿0·5 - 1 hr^{-1}. To date, ∿650 core-related events have been scanned in stereo; no e/3 quark 'candidates' have yet been found.

Droplet counts on charge e shower tracks show a preliminary distribution as expected and demonstrate good discrimination between charge e ionization and the one ninth levels expected from free e/3 quarks (Fig.2).

We are currently refining our technique for superimposing 'artificial quark tracks' on occasional photographs to check observability and scanning efficiency.

4. Acknowledgements. We wish to thank the Science and Engineering Research Council for financial support. We are also indebted to our film scanners, Mrs J.Barker and Mrs P.A.Young, and former scanner, Mrs J Wilson, for their invaluable assistance.

References

Green, B.R., and Hodson, A.L., 1979, Conference Papers, 16th International Cosmic Ray Conference (Kyoto), 13, 211

Hazen, W.E., Hodson, A.L., Winterstein, D.F., Green, B.R., Kass, J.R., and Keller, O.A., 1975, Nuclear Physics B 95, 189

Hodson, A.L., Bacon, T.C., and Pullan, B.R., 1965, Proceedings, 9th International Conference on Cosmic Rays (London), 2, 1082

Kass, J.R., 1977, Ph.D. thesis, University of Leeds

Observation of Genetic Relation Among New Phenomena Geminion, Chiron and Mini-Centauro

Brasil-Japan Collaboration of Chacaltaya Emulsion Chamber Experiment

Abstract

The threshold energy problem of exotic type interactions is discussed on the basis of available information from Chacaltaya emulsion chamber experiment. The genetic hypothesis is proposed as a working hypothesis to explain the discrepancy seen in cosmic-ray study and CERN $\bar{p}$-p collider experiments.

1. Introduction.

Brasil-Japan collaboration of Chacaltaya emulsion chamber experiment have reported in several occasions observation on exotic type interactions which could hardly be reconciled with the known processes of pion production. They are the multi-particle production without association of neutral pions emission, and called "Centauro" family with reference to the first event Centauro-I in 1972. They include variety of phenomenologically similar events with different particle multiplicity and p_t[1]. The recent progress of collider technique made the energy region of the accelerator experiments overlap over a part of the region of the cosmic-ray study. $\bar{p}$-p collider experiment at CERN, covering the energy region of E_0=155 TeV in the laboratory frame, however, found none of these exotic interactions. In 1985, there is an increase of the energy of machine at CERN to the region $E_0 \simeq$ 500 TeV and also the start of collider experiments at FNAL up to the region of $E_0 \simeq$ 2000 TeV. Thus it is important to make guess on the threshold energy for such exotic interactions from the available information. At the same time, the problem requires to solve a puzzle that cosmic-ray experiments are observing exotic interactions of energy smaller than the available energy at CERN collider. The present paper concerns to an attempt at such guess and a working hypothesis of genetic relation of exotic interactions is proposed and studied[2].

2. C-jets and Pb-jets-lower in Chacaltaya chamber no.19.

In order to make clear the problem which we are faced with, here we present brief summary of the most recent observation of exotic phenomena in C-jets and Pb-jets-lower study. It was made a systematic study on 198 C-jets and special Pb-jets-lower of visible energy greater than 5 TeV in one half of lower detector of Chacaltaya chamber no.19, 28.8 m^2year exposure[3]. Among those, there are found following exotic-type C-jets and Pb-jets-lower. Such exotic events are here triggered by studying non pi-naut emission events after asking whether the individual shower core is electromagnetic origin or hadronic in the lower detector. They are ;

i) 8 C-jets of Mini-Centauro type, ($n \geq 3$)

ii) 3 C-jets of n = 2 with very large invariant mass ($m(\gamma)(1\text{-}2) > 1.8$ GeV), consistently interpreted as Geminion-type interaction in target layer.

iii) 2 Pb-jets-lower with large $p_t(\gamma) > 1$ GeV/c, with n= 2, consistently interpreted to be Geminion and Chiron type interactions in the lead of lower detector. n means number of shower cores.

It shows several % of the whole observed C-jets is of exotic type. All those exotic events range from 5 TeV -25 TeV in their visible

energy, then the energy of incident hadron are estimated to be as much as an order of $\bar{p}$-p collider energy or less.

3. Genetic hypothesis of exotic interactions.

We will propose a working hypothesis to explain why the CERN collider did not see those exotic phenomena, despite the cosmic-ray observation shows the existence of exotic type event even in lower energy than collider. The working hypothesis assumes that the concerned exotic interaction is generated by the "exotic hadrons", but not a proton, a pion, nor any of the known hadrons. It also assumes that the "exotic hadrons" are produced out of the exotic interactions. Under the above hypothesis we have the following picture as shown in Fig.1. An exotic event seen at Chacaltaya is, then, the last one in a chain of exotic interactions connected by a passage of an exotic hadron in the atmosphere. Thus the origin of exotic hadrons can be located high up in the atmosphere to the first point in the chain of exotic interactions, probably made by primary cosmic-ray particles.

4. A possible candidate of exotic hadrons, the "B-particles".

It is remarkable that we found such genetic relation in the systematic study of C-jets and Pb-jets-lower in chamber no.19, just introduced above. Among 8 C-jets of Mini-Centauro type, three associates with atmospheric families, two with Chiron type and one with super-family M.A.III[4], one Pb-jet-lower with large $p_t(\gamma)$ nature associates with M.A.III.

It was already reported that the secondary particles in Chiron type family show several strange features not seen in a common type family, and we put the name "B-particle" for them[1].

Though the observation is still in preliminary stage and is being continued, we may try to see how it can be a candidate for exotic hadrons. First of all, its large pt at the momentum transfer, and it is outside the region of soft lnS physics. This can be considered as one of the necessary conditions to be a candidate for the exotic hadrons.

5. Example of cascade of exotic interactions ; Chiron families.

Under the genetic hypothesis as described above, experimental study was extended to every C-jet and Pb-jet-lower of $\Sigma E(\gamma) > 5$ TeV from 30 Chiron families, all the statistics in Chacaltaya chamber no.19 and a high energy Chiron type family from chamber no.18. Out of those 30 Chiron-type families, there are, in lower chamber, 20 showers with $\Sigma E(\gamma) > 5$ TeV which satisfy the criteria of the multi-core structure. The following gives a list of those observed showers.

- 9 showers of ordinary pion production in the target -- pi-nauts are found
- 5 showers of successive interactions in the chamber -- upper and target layers
- 1 shower of Chiron candidate -- Pb-jet-lower
- 3 showers of Mini-Centauro candidate from the target
- 2 showers of mini-cluster candidate in the target

It indicates about one third, 6/15, is of exotic type. Among them, the case of a Chiron candidate is most impressive, #507(47S-17I). It is a shower with three diverging cores, and the geometry measurement on the core position allows us to locate the point of vertex in the lower chamber itself as shown Fig.2. We obtain average p_t of three cores as

$\langle p_t(\gamma) \rangle = 1.7 \pm 0.4$ GeV/c, a quite high value. If we correspond each core to a quantum of gamma-ray, it will be hard to explain them by the ordinary pion production. Under the Chiron hypothesis, it is just what we expect. From the Chiron interaction in the lower chamber, a number of B-particles will be emitted with large pt. Because of the limited material thickness in the lower chamber, some or most of B-particles created will penetrate through the chamber, thus the three cores of the event will be mini-clusters.

During extending the study to chamber no.18, we found a special high energy Chiron type family, C18-154S-133I[5]. The family is of wide spread and hadron rich character. We found a strongly penetrative mini-cluster of the spread of 1 mm in radius in upper chamber, and in lower chamber one C-jet and one Pb-jet-lower are found inside the region of the shower continuation from the upper mini-cluster. What is remarkable is that the C-jet, consists of seven cores with $\Sigma E(\gamma) = 12.2$ TeV, is of the nature of Mini-Centauro candidate, having no-pi-naut coupling among constituent showers, and the Pb-jet-lower with diverging four cores is of the nature of Chiron type candidate. Fig.3a shows the target map and Fig.3b the divergence measurement among four cores and Table 1 gives some details of the Pb-jet-lower. We see similar characteristics of large $p_t(\gamma)$ nature in this Pb-jet-lower with the one of Chiron type, #507(C19-47S-17I). What is especially interesting in this example is that hadrons(plural) which make different types of exotic interactions are in the same mini-cluster.

6. Discussions.

We do not know yet much about primary cosmic-ray particles in very high energy region. If we extrapolate the knowledge of lower energy region, the primary particles will be more likely to be protons. At the level of Chacaltaya, the observed rate of exotic event is about 0.5 m^2 year . This value corresponds to the rate of a primary proton with $E_{inc} > 10^{16}$ eV. In this means, we may expect that the exotic interaction is produced by a primary proton with energy Einc as shown in Fig.1 because of the steep energy spectrum of primary protons and the sharp rise of cross section near the threshold.. Since the cosmic-ray experiment pick up only events of the type which occupies a substantial fraction in the nuclear collision, the real threshold value of the exotic interaction will be lower than 10^{16}eV. Thus we may think that there is a fair chance of seeing the exotic interactions produced artificially by the collider of FNAL with energy 2×10^{15}eV. Here, we should mention other possibilities, too. The one is the proposal of new phase of the hadronic matter, quark-gluon plasma formation, in nucleus-nucleus collision[6], different from $\bar{p}$-p collisions and the other is that the primary cosmic-ray contain exotic objects such as quark globs[7] besides known nuclei. It is an interesting hypothesis and if it is the case the observation of exotic type interactions will have a connection with the astrophysical problems.

Acknowledgement. The collaboration experiment is financially supported in part by Conselho Nacional para o Desenvolvimento Cientifico e Tecnologico, Fundacao de Amparo a Pesquisa do Estado de Sao Paulo, Financiadora de Estudos e Projetos, in Brasil, and Institute for Cosmic-ray Research, University of Tokyo and Grant-in-Aid from the Ministry of Education, in Japan.

References.
[1] C.M.G.Lattes et al. ; Physics Report Vol.65 no.3(1980) 151
Brasil-Japan Collaboration ; AIP Conf. Proceedings(1981) 500
[2] S.Hasegawa ; Proc. Int. Cosmic Ray Symp. Tokyo(1983) 718
[3] Brasil-Japan Collaboration ; HE 3.2-6
[4] S.Yamashita ; Jour. of Phy. Soc. of Japan Vol.54 no.2 (1985) 529
[5] M.Tamada and K.Yokoi ; private communications
[6] for instance, E.Shurak ; Physics Report. No.61 (1979) 71
[7] J.D.Bjorken and L.McLerran ; Phys. Rev. D20 (1979) 2353

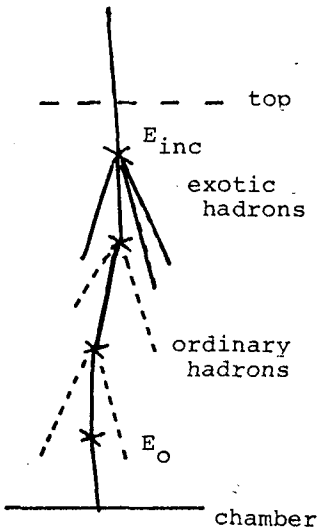

Fig.1 Explanation of genetic hypothesis.

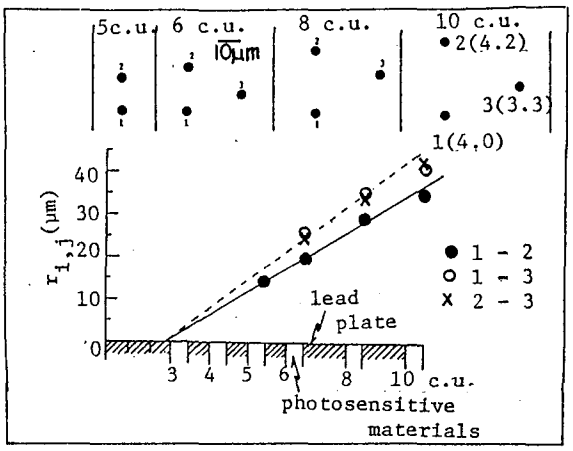

Fig.2 Target map and convergence measurement of #507 (47S-17I)

Table 1. Details of Pb-jet-lower in the event C18-154S-133I

#	$E^{(\gamma)}$(TeV)	θ ($\times 10^{-4}$)	$p_t^{(\gamma)}$ (GeV/c)
1	15.0	1.05	1.6
2	15.0	1.05	1.6
3	3.5	6.90	2.4
4	2.4	15.0	3.6

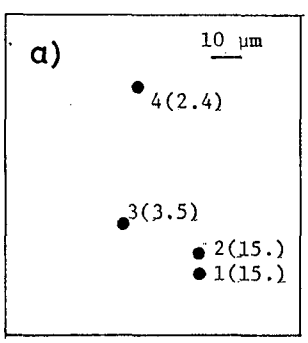

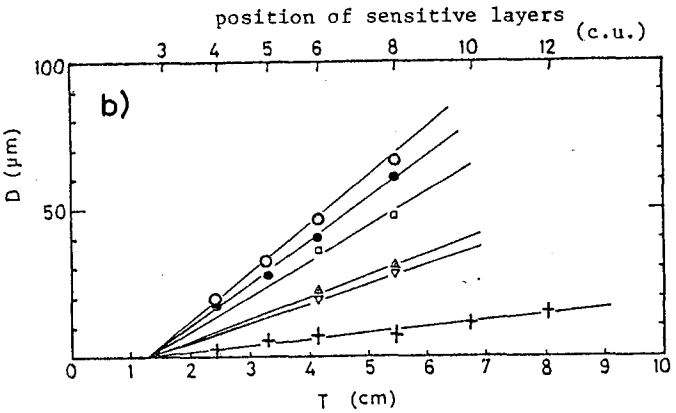

Fig.3 a) target map and b) convergence measurement of Pb-jet-lower in the event C18-154S-133I.

HE 6.2-17

TIEN-SHAN EFFECT AND CHARMED PARTICLES.

I.M.Dremin, D.T.Madigozhin, V.A.Saakjan, A.D.Serdukov, V.I.Yakovlev - P.N.Lebedev Physical Institute, Moscow 117924, Leninsky Prospect 53, USSR,
P.I.Golubnichy, L.A.Efimenko, R.T.Savchenko - Voroshilovgrad Mashinery Building Institute, USSR.

Abstract

It is shown that the Tien-Shan effect of long-flying component can be explained as a consequence of charmed particles production with high enough production cross-section (about 5 mb/nucleon at 100 TeV).

The investigation of attenuation peculiarities of EAS hadronic component energy flux in the calorimeter with lead absorber has shown /1,2/ that energy dependence of hadronic component energy attenuation length L(E) has a peak-type behaviour (see fig.1 in /1/). This phenomenon, named as "Tien-Shan effect", we ll account for as a consequence of generation and following decay of particles with charmed quarks. The most important conclusion from the comparison of theory and experiment is that charmed particles have to be produced in the fragmentational region and their production cross-section at energies about 100 TeV must be equal (5±2) mb/nucleon.

For a qualitative analisis of influence of particles with heavy quarks on the hadronic cascade we use as the first approach only one sort of particles called conventionally as charmed ones. It simplifies the system of kinetic equations for processes investigated:

$$\begin{cases} \frac{dS_c}{dz} = -\gamma S_c\,; \quad \frac{dS_N}{dz} = -\beta S_N + \delta S_c\,; \\ \frac{dS_{\pi^\pm}}{dz} = -\alpha S_{\pi^\pm} + \frac{2}{3}\beta S_N + \frac{2}{3}(\gamma-\delta) S_c \end{cases} \qquad (1)$$

with initial conditions

$$\begin{cases} S_c(0) = \langle X \rangle \sigma_c/\sigma_N\,; \quad S_N(0) = 1 - K_N\,; \\ S_{\pi^\pm}(0) = 2/3\,(K_N - \langle X_c \rangle \sigma_c/\sigma_N) \end{cases} \qquad (2)$$

Here S - are the fractions of primary energy transferred into charmed (C), nucleon (N) and pion ($\pi^\pm$) components;

Z is the coordinate along the axis of cascade developing; σ_c/σ_N -is a probability of charmed particle production. Eqs (1) show energy variation of charmed, nucleon and pion components because of their decay and interaction. Coefficients in (1) are :

$$\alpha=\frac{1}{3\lambda_\pi};\ \beta=\frac{K_N}{\lambda_N};\ \gamma=\frac{1}{\lambda_d}+\frac{K_c}{\lambda_c};\ \delta=\frac{1-B}{\lambda_d} \qquad (3)$$

where λ_i, K_i are mean free paths and inelasticities of i-th component. B is the energy fraction transferred into pions by the particle decay into nucleons and pions (kaons have interaction properties close to those of pions). The complete solution of the system of equations is given in /3/. In particular case B = 1; K = 1, the total energy of pions is written in the form :

$$\frac{2}{3}S_{\pi^\pm}=e^{-\alpha z}+\frac{\sigma_c}{\sigma_N}\frac{\langle X_c\rangle}{\gamma-\alpha}\left[\alpha e^{-\alpha z}-\gamma e^{-\gamma z}\right] \qquad (4)$$

It is seen that "the standard cascade" $\exp(-\alpha z)$ acquires additional contribution from the charmed component. At the small depths it is negative that corresponds to cascade damping because some energy is kept by charmed particles. After decay of those particles the energy is added to the cascade so that at the depth $Z_0=(\ln\gamma/\alpha)/(\gamma-\alpha)$ the transferred into pions energy becomes just the same as the energy in standard cascade. The maximum contribution from the charmed particles is achieved at the depth $Z_{max}=2Z_0$, after that the cascade decreases along the same exponent as a standard one, but with an enlarged coefficient. So the charmed particles in the beginning of cascade start to "eat up" the standard cascade, then supply the additional "bump" which transforms into the usual decrease at the tail of the cascade.

More comprehensive system of kinetic equations for distributions of particle multiplicity F_i (index i means the particle's sort) of energy E along depth Z :

$$\left(\frac{d}{dz}+\frac{1}{\lambda_i}+\frac{m_i}{E_i\tau_i c\rho}\right)F_i(E,z)=\sum_j\frac{1}{\lambda_j}\int_E^{E_0}F_j(E',z)W_{ij}(E,E')dE'+\sum_j R_{ij} \qquad (5)$$

The dump of particles i because of interaction (λ_i) and

decay (τ_i) is compensated by their production in the inelastic interactions (W_{ij}) and decays (R_{ij}) of particles j. The pion production spectrum has been chosen of CKP type, but for Λ_c it was admitted to be independent of X /4,5/ with $\overline{X}$ = 0,5. The D meson's spectrum is soft, but harder for primary pions to take into account the leading effect. Mean free paths have been taken as λ_N=192 g/cm^2; $\lambda_{\pi\pm}$ = 210 g/cm^2 /7/, and inelasticities are equal to K_N=0,63; $K_{\pi\pm}$ = 0,7 /7/; K_c=0,1 /8/. The hadronic mode of decay only has been taken into account. Charmed particles production cross-section is assumed to increase starting from FNAL energy, passing through ISR energy and achieving the constant value at an energy 100 TeV. Cascade curves in the depth's interval 374-924 g/cm^2 (as in experiment) were fitted by exponents, which determined attenuation lengths of cascades. The results are shown in fig.1. L(E) dependence for a standard cascade is shown by a dotted line. Numbers mark corresponding asympthotical cross-section values equal 1,2,5,10 mb at 100 TeV. One can see that 5 mb value corresponds to the best agreement with the experiment. The energy fraction carried out of the calorimeter by charmed particles grows with a primary energy (fig.2). It means that we use in the experiment another energy scale because we group all events according to the energy released in the calorimeter. Accounting this fact leads us to the unexpected effect i.e. narrowing of peaks and moving them to lower energies (fig.3).

For a detailed comparison with the experiment we are performing now the Monte-Carlo calculations.

Thus sufficiently effective charmed particles production in the fragmentational region leads to the energy dependence of cascade's attenuation lengths with clear maxima. It describes well qualitatively the main peculiarities of the Tien-Shan effect.

REFERENCES:

1. Yakovlev V.I. et.al., Proc 18 ICRC,Bangalor 1983,v.5,102

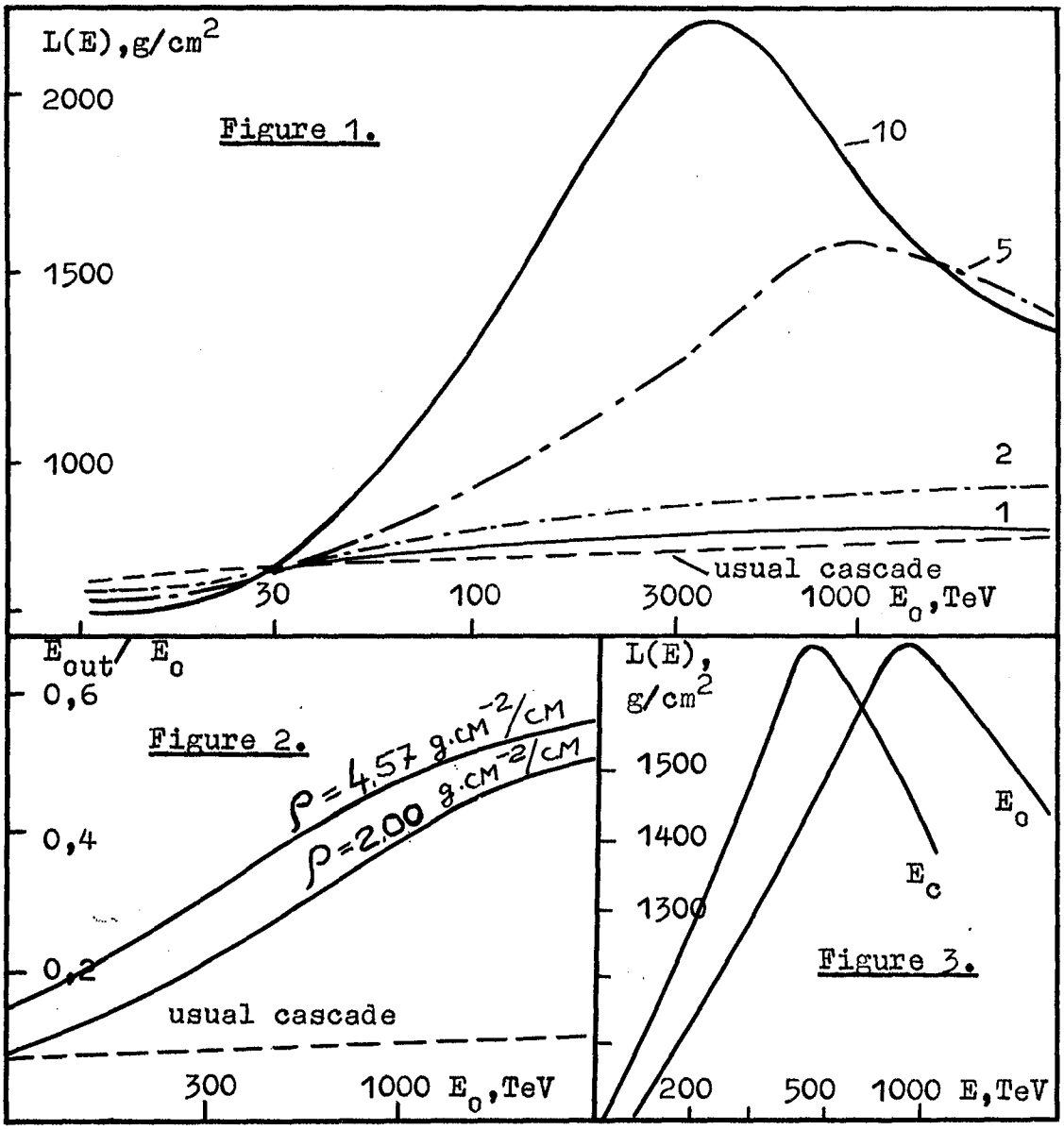

Figure 1.

Figure 2.

Figure 3.

2.Yakovlev V.I et.al.Proc.16 ICRC,Kyoto 1979,v.6,p.59.
3.Dremin I.M. et.al. Yadernaya Phisika,1985 in print.
4.Basile M.et.al.Let.Nuovo Chim.30,487,1981.
5.Hwa R.C. Phys.Rev. D27, 653, 1983.
6. Bodek A.et.al.Phys.Lett.126 b,499,1983.
7.Bazarov E.V. Prepr.FIAN,102, 1981.
8.Hodzhamirjan A.Yu. Voprosy Atomn.Nauki i Tehniki, seriya phys.experiment,3,/12/,14,1982.

HE 6.2-18

MUON AND NEUTRINO FLUXES

P.G. Edwards and R.J. Protheroe
Department of Physics, University of Adelaide
Adelaide, South Australia 5001

Abstract. We report the result of a new calculation of the atmospheric muon and neutrino fluxes and the energy spectrum of muon-neutrinos produced in individual extensive air showers (EAS) initiated by proton and γ-ray primaries. We also examine the possibility of detecting atmospheric ν_μ's due to γ-rays from sources.

1. *INTRODUCTION.* Interactions of ~1 GeV neutrinos can mimic nucleon decay events and it is therefore important to know the atmospheric neutrino flux in order to calculate the expected rate of background events in nucleon decay experiments. With the development of large nucleon decay detectors this topic has received much interest over the past few years (Gaisser *et al.*, 1983a,b; Dar 1983). These large detectors can also be used for other purposes, however. Their large masses make them good neutrino detectors allowing searches for neutrinos from bright extra-terrestrial sources. Here again an accurate knowledge of the atmospheric neutrino background due to cosmic rays is important.

The detection of UHE γ-rays from Cygnus X-3 (Samorski and Stamm, 1983; Lloyd-Evans *et al.*, 1983), Vela X-1 (Protheroe *et al.*, 1984) and LMC X-4 (Protheroe and Clay, 1985) has added further impetus to the neutrino observations as it is usually considered that a neutrino signal would almost certainly suggest a π^0-decay origin for the γ-rays. Gaisser and Stanev (1985a,b) have recently calculated the expected ν_μ flux and light curve for Cygnus X-3 on this basis together with the response of deep detectors to extraterrestrial neutrinos.

Here, we report the results of a new calculation of the sea level atmospheric muon and neutrino fluxes. We have also calculated the energy spectrum of ν_μ's in individual EAS initiated by primary protons and γ-rays to test whether atmospheric neutrinos from γ-ray initiated EAS could be detected with existing detectors.

2. *THE CALCULATION.* The simulation procedure was identical to that used in our earlier work (Edwards *et al.*, 1985) and consisted of numerical solution of the following coupled equations (see e.g. Gaisser *et al.*, 1978):

$$\frac{\partial N_i(E,x)}{\partial x} = -N_i(E,x)\left[\frac{1}{x_i(E)} + \frac{(dh/dx)}{(cE/m_i)\tau_i}\right] + \frac{\partial}{\partial E}\left[N_i(E,x)(dE/dx)_i\right] + \sum_j \int_E^\infty \left[\frac{F_{ji}(E,E')}{E}\,\frac{N_j(E',x)}{x_j(E')}\right]dE', \qquad (1)$$

where N_i is the energy distribution of particles of type i at depth x; x_i is the mean interaction length, m_i is the rest mass, τ_i is the mean decay time, and $(dE/dx)_i$ is the mean ionization energy loss rate of particles of

type i; and $F_{i,j}(E,E')dE/E$ is the probability of a particle of type j and energy E' producing a particle of type i and energy E to E+dE per interaction. The particles considered in the simulation were: nucleons, charged pions, charged and neutral kaons, muons and both muon and electron neutrinos (by "neutrinos" we include anti-neutrinos).

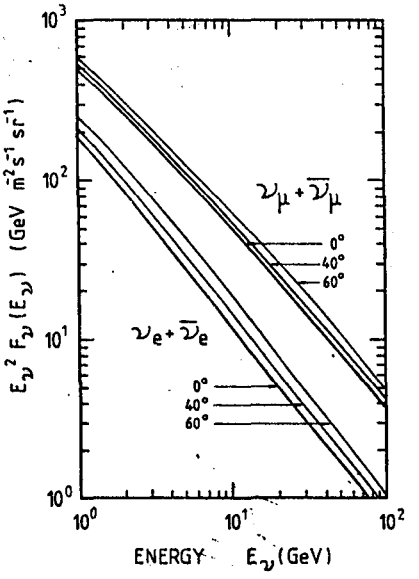

Fig. 1. Sea level atmospheric neutrino flux at 0°, 40° and 60° to the zenith.

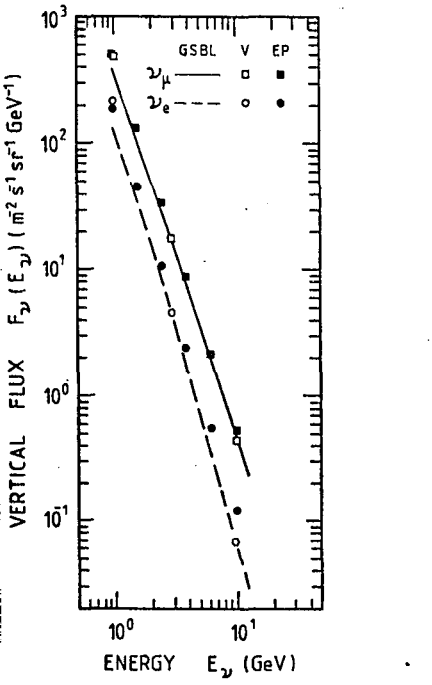

Fig. 2. Vertical neutrino flux from present work (EP) compared with the predictions of Volkova (1980) (V) and Gaisser *et al.* (1983a,b) (GSBL).

The model of inclusive particle production in proton-air nucleus interactions used in the simulations is that described by Gaisser, Protheroe and Stanev (1983). The nucleon-air nucleus interaction length used was that given by Ellsworth *et al.* (1982). The pion and kaon-air nucleus interaction lengths were suitably scaled from this (Hillas, 1979).

The primary cosmic ray nucleon flux used was based on the results of satellite and balloon-borne detectors (Simpson *et al.* 1983; Ryan *et al.* 1972; Gregory *et al.* 1981; Simon *et al.* 1980; Juliusson *et al.* 1983; Sood 1983) and the superposition model.

3. ***RESULTS.*** First we present our results on the flux of atmospheric muons and neutrinos. The calculated sea level neutrino flux is shown in Fig. 1 for a number of zenith angles and is seen to increase with increasing zenith angle (i.e. atmospheric thickness). We have compared our calculated neutrino fluxes with previous results. Fig. 2 shows the good agreement found with the vertical flux calculated by Gaisser *et al.* (1983a,b) and Volkova (1980). The results of Tam and Young (1969) (not plotted) are similarly in agreement.

The vertical muon flux we calculate is plotted in Fig. 3 where it is compared with the experimetal results obtained by Mitsui *et al.* (1983) and Allkofer *et al.* (1971) and found to

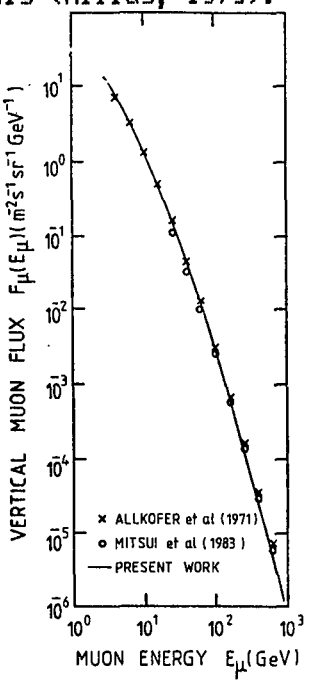

Fig. 3. Calculated vertical muon flux compared with recent observations.

be in good agreement.

We turn now to neutrinos produced in individual cosmic ray and γ-ray initiated EAS. In Fig. 4 we show the differential energy spectra of ν_μs produced in individual EAS divided by the primary energy. Over the 10^{15} - 10^{18} eV primary energy range, the ν_μ spectrum in γ-ray initiated EAS is ~10 to 100 times lower than in proton initiated EAS. Also, the number of neutrinos divided by primary energy decreases with increasing primary energy in cosmic ray EAS but is approximately independent of primary energy for γ-ray initiated EAS. This behaviour is similar to that of muons in cosmic ray and γ-ray initiated EAS (Edwards *et al.*, 1985).

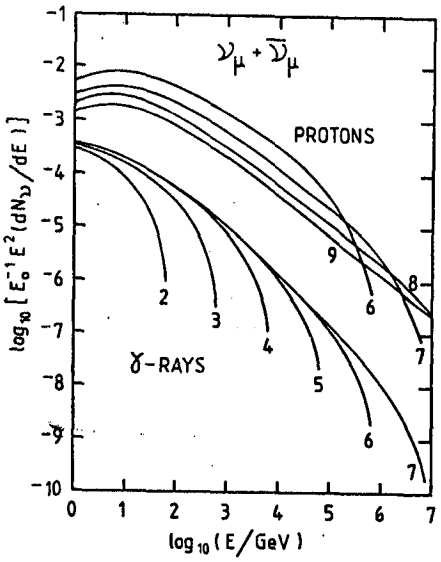

Fig. 4. Differential energy spectrum of muon neutrinos in proton and γ-ray initiated EAS divided by primary energy, E_0. (Numbers attached to the curves are $log_{10}[E_0/GeV]$).

4. *DISCUSSION.* Recently Gaisser and Stanev (1985a) have calculated the expected ν_μ flux and light curve of Cygnus X-3 assuming it is due to protons produced near the neutron star interacting in the atmosphere of its companion to produce a mini-EAS in in the star's atmosphere. Cocconi (1985) has also suggested that LMC X-4, being a bright Southern UHE γ-ray source, would be a good neutrino source candidate for study by Northern observers.

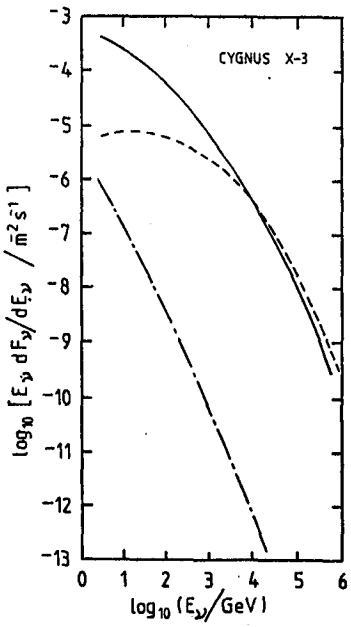

Fig. 5. Expected flux of atmospheric ν_μs due to γ-rays from Cygnus X-3 (dot-dash line) compared with the flux expected directly from the source (solid and dashed lines) under two different assumptions (Gaisser and Stanev, 1985a).

It is possible (although we consider it unlikely) that the γ-rays from Cygnus X-3 are due to interactions of electrons accelerated to extremely high energies. If this were the case, we would expect no neutrinos from the source. Observation of neutrinos from Cygnus X-3 would then indicate that the γ-rays were almost certainly due to interactions of high energy protons. Atmospheric neutrinos due to γ-rays from Cygnus X-3 might also be detectable, however. If this was so, then such a conclusion would be invalid although it may be possible to distinguish the two origins through the light curves which would be different in each case. Here, we calculate the differential ν_μ flux due to γ-rays from Cygnus X-3 by convolving the ν_μ spectra in γ-ray initiated

EAS of Fig. 4 with the γ-ray spectrum of the source:

$$N(E) = 4.5\times10^{-4}(E/GeV)^{-2} \text{ (photons m}^{-2}\text{ s}^{-1}\text{ GeV}^{-1}\text{)}. \quad (2)$$

This is based on the integral flux reported by Lloyd-Evans *et al.* (1983). The result is shown in Fig. 5 where it is compared with the expected ν_μ flux due directly to the source as calculated by Gaisser and Stanev under two different assumptions. At 1 TeV the atmospheric ν_μ flux is $\sim10^{3}$ lower than that due directly to the source and would be considerably below current detector sensitivities (Stenger 1985).

5. *CONCLUSIONS.* Our calculated atmospheric muon flux is in good agreement with observations. The calculated neutrino flux is in agreement with other recent predictions. We support the view that a neutrino observation of a UHE γ-ray source would be strong evidence that the UHE γ-rays and neutrinos result from high energy interactions of protons or nuclei.

Acknowledgments. P.G.E. is in receipt of a Commonwealth Postgraduate Research Award. This research has been supported by the provision of a Queen Elizabeth II Fellowship a grant from the A.R.G.S. to R.J.P.

REFERENCES

Allkofer OC, Carstensen K and Dau WD 1971 Phys. Lett. B 36, 425
Cocconi G 1985: CERN preprint
Dar A 1983 Phys. Rev. Lett., 51, 227
Edwards PG, Protheroe RJ and Rawinski E 1985 J. Phys. G: Nucl. Phys. (letter) in press. (See also these proceedings HE 4.5-7)
Ellsworth RW, Gaisser TK, Stanev T and Yodh GB 1982 Phys. Rev. D 26, 336
Gaisser TK *et al.* 1978 Rev. Mod. Phys. 50, 859
Gaisser TK, Protheroe RJ and Stanev T 1983 Proc. 18th Int. Conf. on Cosmic Rays (Bangalore) 5, 174
Gaisser TK, Stanev T, Bludman SA and Lee H 1983a Proc. 18th Int. Conf. on Cosmic Rays (Bangalore) 7, 91
Gaisser TK, Stanev T, Bludman SA and Lee H 1983b Phys. Rev. Lett. 51, 223
Gaisser TK and Stanev T 1985a Bartol preprint BA-85-12
Gaisser TK and Stanev T 1985b Bartol preprint BA-85-9
Gregory JG *et al.* 1981 Proc. 17th Int. Conf. on Cosmic Rays (Paris) 9, 154
Hillas AM 1979 Proc. 16th Int. Conf. on Cosmic Rays (Kyoto) 9, 13
Juliusson E *et al.* 1983 Proc. 18th Int. Conf. on Cosmic Rays (Bangalore) 2, 21
Lloyd-Evans J *et al.* 1983 Nature 305, 784
Mitsui K *et al* 1983 J. Phys. G: Nucl. Phys 9, 573
Protheroe RJ, Clay RW and Gerhardy PR 1984 Ap. J. (Lett.) 280, L47
Protheroe RJ and Clay RW 1985 Nature in press. (See also these proceedings paper OG 2.6-10)
Ryan MJ, Ormes JF and Balasubrahmanyan VK 1972 Phys. Rev. Lett. 28, 985
Samorski M and Stamm W 1983 Ap. J. (Lett.) 268, L17
Simon M *et al.* 1980 Ap. J. 239, 712
Simpson JA 1983 "Composition and Origin of Cosmic Rays" ed. MM Shapiro
Sood RK 1983 Nature 301, 44
Stenger VJ 1985 Hawaii DUMAND Center preprint HDC-4-85
Tam AC and Young ECM 1969 Proc. 11th Int. Conf on Cosmic Rays (Budapest) 307
Volkova LV 1980 Sov. J. Nucl. Phys. 31, 1510

SEARCH FOR ACOUSTIC SIGNALS FROM HIGH ENERGY CASCADES

Raymond Bell and Theodore Bowen
Department of Physics
University of Arizona, Tucson, AZ 85721, USA

Introduction. High energy cosmic ray secondaries can be detected by means of the cascades they produce when they pass through matter. When the charged particles of these cascades ionize the matter they are traveling through, the heat produced and resulting thermal expansion causes a thermoacoustic wave. These sound waves travel at about 10^{-5} the speed of light, and should allow an array of acoustic transducers to resolve structure in the cascade to about 1 cm without high speed electronics or segmentation of the detector.

Experimental System. The University of Arizona cosmic ray group operates an observatory at 747 g/cm^2 atop Mt. Lemmon, 72 km from the campus in Tucson, Arizona. The system, whose layout is shown in Fig. 1, consists of an experimental stack offset to the side of the building, and four airshower detectors located near the four corners of the building. The shower detectors are liquid scintillation tanks 1.8 m x 1.8 m in size. The experimental stack, shown in Fig. 2, consists of a cascade generator of Fe and Pb followed by a tank of trichloroethylene located at a depth corresponding to the maximum of a cascade generated by a 0.7 TeV gamma ray. This trichloroethylene tank acts as the acoustic detector and has four acoustic transducers located within the tank. The Pb above and Fe below the tank are in contact with the tank walls and provide an acoustic mirror. Beneath the acoustic detector is a hodoscope to provide some positioning information for the cascade core, and a three section calorimeter consisting of liquid scintillation detectors sandwiched between layers of Fe. The acoustic signals are continuously digitized by a multichannel waveform digitizer. When a large signal is found in the calorimeter, a trigger pulse is generated. The trigger pulse stops the digitizer after an appropriate delay to allow the acoustic wave to arrive at the transducers. Also, pulse heights from the shower detectors, calorimeter, and hodoscope are recorded, and the arrival times of the shower detector pulses are recorded to provide azimuth and zenith information.

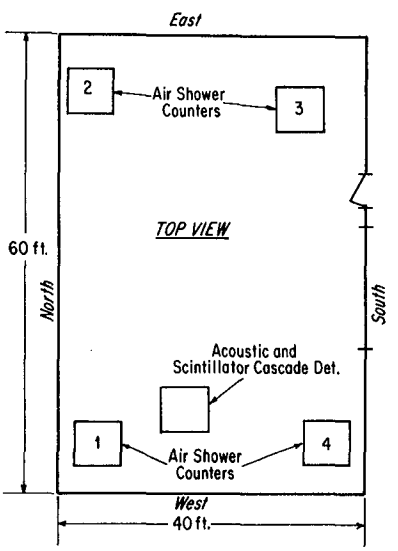

Fig. 1. Observatory layout, showing position of airshower counters and experimental stack.

Acoustic Detector. The acoustic detector first used in this experiment was a tank of mineral oil instead of the tricholoroethylene currently used. The expected signal-to-noise (S/N) ratio in the near field of a cascade-produced thermoacoustic wave in mixed units is given by[1]

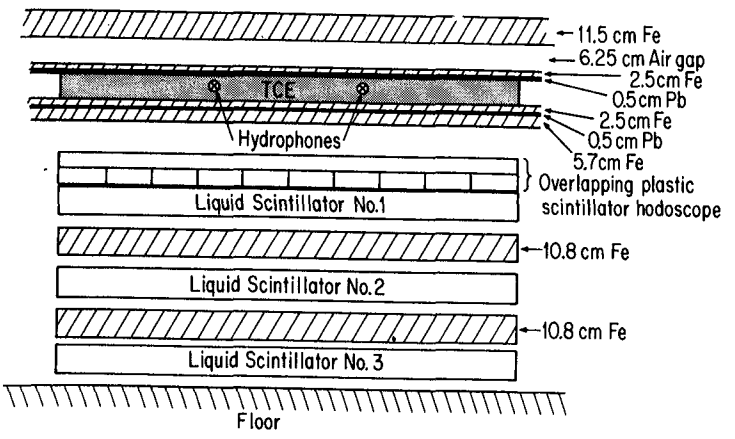

Fig. 2. Side view of acoustic and scintillator cascade detector.

$$\left(\frac{S}{N}\right)_{\text{near field}} = (2.2\times10^{-9})\, L\, n^2/R_0(m),$$

where

$$L \equiv [\beta(°C^{-1})c(m/s)/C_p(cal\text{-}g^{-1}\text{-}°C^{-1})]^2\, [dE/d\xi(MeV\text{-}g^{-1}\text{-}cm^2)]^2_{min}\, \rho(g\text{-}cm^{-3})/T(°K).$$

n is the number of charged particles in the cascade and $R_0(m)$ is the distance to the observation point. A gamma ray of 50 TeV with a Pb shower generator is expected to achieve a S/N ratio of 7, for which the thermoacoustic wave should be clearly visible relative to the thermal noise. With trichloroethylene, it is calculated that a gamma ray of 15 TeV is necessary to achieve a S/N ratio of 7. The transducer amplifier system used in the detector can be characterized by the constant k in the equation

$$\left(\frac{N}{S}\right)_f = k\left(\frac{N}{S}\right)_i ,$$

where $(N/S)_i$ is the acoustical noise-to-signal ratio, $(N/S)_f$ is the electrical noise-to-signal ratio at the amplifier output, and k is a degradation constant. For the system used, k has a value of 1.2, so that the expected S/N ratios in the recorded data are about 80% of those in the detector itself. In the fall of 1984, simulations of this process were conducted at the University of Arizona Health Sciences Center with an 18 MeV electron linac. One of the results indicates that a minimum density of 5×10^5 electrons/cm^2 is needed in mineral oil to produce a detectable acoustic wave. When this condition is applied to cosmic ray cascades, $\pi\lambda\!\!\!^{-2}$ gives the size of the cascade core over which n must exceed 5×10^5, where $\lambda\!\!\!^{-} = \lambda/2\pi$ and λ is the wavelength determined by the transducer center-frequency. For the 50 kHz center frequency of the transducers in this experiment, $\pi\lambda\!\!\!^{-2} = 0.35$ cm^2.

Present Results. At the time of writing of this paper, no strong candidates for acoustic signal events have been recorded by this experiment. The reason for this is intimately connected to the gamma ray family phenomena. The density of charged particles in the acoustic detector produced by a cascade depends on the lateral distribution of energy among the gamma rays when they enter the shower generator. For example, a 100 TeV gamma ray will produce a higher particle density than if that same 100 TeV is spread out laterally among many gamma rays.

Event rates for this detector were expected to be low. However, the gamma ray family phenomena has made the rate less than initially expected. The integral spectrum of individual gamma rays[2] observed at 650 g/cm^2 can be used to calculate the worst-case event rate. In this case, a rate of 1 event per 11,000 hours for mineral oil and 1 event per 1,100 hours for trichloroethylene is found. However, these individual gammas are members of families. If, instead, we employ the integral spectrum of gamma ray families[3] and assume the lateral spread of the members of the families is small, we obtain an optimisic rate of 1 event per 736 hours for mineral oil and 1 event per 110 hours for trichloroethylene.

The integral spectrum of events which occurred during 829.7 hours of exposure with the mineral oil detector has $\gamma=-2.2\pm0.3$, in agreement with gamma-family results for $\Sigma' E_\gamma$. During the mineral oil run, 4 events were observed with energy >50 TeV; it is believed that these events did not produce a sufficient particle density because each cascade did not result from a single gamma ray. The integral spectrum calculated from particle densities observed at the shower detectors gives a spectral index of -1.42 ± 0.1. The differential flux of events as a function of $\cos\theta$ can be expressed as

$$f(\cos\theta)d\Omega = f_0[\exp(-x/\Lambda\cos\theta)]d\Omega \quad ,$$

where x is the atmospheric depth and Λ is the mean-free path. We obtain a value of $\Lambda=78\pm8$ g/cm^2.

At this time, the trichloroethylene detector has been exposed for 155 hours, and one weak candidate for an acoustic signal has been seen. It is hoped that this detector will provide interesting results in the months to come.

References

1. T. Bowen, Proc. 16th ICRC, Tokyo, 11, 184 (1979).

2. M. Akashi et al., ibid, 7, 68 (1979).

3. M. Akashi et al., ibid, 13, 98 (1979).

HE 7.1-2

EXPERIMENTAL INVESTIGATION OF RADIATIVE-ACOUSTIC EFFECTS IN THE WATER BY THE THERMODYNAMICAL CONDITIONS OF DUMAND.

P.I.Golubnichy,S.D.Korchikov-Voroshilovgrad Mashinery Building Institute, USSR,
S.I.Nikolsky,V.I.Yakovlev - P.N.Lebedev Physical Institute 117924 Moscow,Leninsky Prospect 53, USSR.

Value of the sound pulse produced by high energy neutrino, if thermoacoustical mechanism of sound generation takes place, is proportional to the density of energy emerged so as Grunaisen parameter $\Gamma = kc^2/c_p$ of the substance. Here $k=k(t^0, P_0, S\text{ ‰})$; $c=c(t^0, P_0, S\text{ ‰})$; $c_p = c_p(t^0, P_0, S\text{ ‰})$ are coefficient of termal expansion, sound velosity and specific heat depended on temperature t^0, pressure P_0 and saltness S ‰ of sea water /1/.

The acoustical signal initiated by the beam of relativistic electrons was investigated in the distilled /2/ as so in the salt water with the concentration of NaCl varied frcm 0 to 35 ‰ /3/. It was shown that acoustical signal by the normal temperature has mainly thermoacoustical nature.

In this experiment thermodynamical conditions corresponding to the deep underwater (H=5000 m, P_0=500 atm, $t=2^0$ C; S=35 ‰) was realised by helping of high pressure chamber. The chamber has inputs for electron (E=50 MeV) and laser beams, experimental conditions were closed to those in /2,3/. Comprehensive analysis of acoustic signal by the varyation of pressure, temperature and saltness of water was performed using the laser beam. Using the electron beam measurements of acoustic signal was performed in the next conditions: P_0=1 atm, $t=16^0$C and P_0=500 atm, $t=1^0$C and $t=16^0$C. Fig.1 demonstrates experimental values of acoustical signals for laser and electron beams after correction on energy absorbed so as geometry of experiment.

At the same picture iterpolated dependences of Grunaisen coefficient Γ on t, P_0 and S are plotted (solid lines) using tabular data /4/; experimental data from /2,3/ also are shown here. It is seen from the figure that acoustic signal value J follows well Grunaisen coefficient.

Thus one can affirm in the thermodynamical conditions close to deep underwater acoustical signal from the beam of relativistic electrons has mainly thermoacoustical nature. The value of Grunaisen coefficient corresponding to conditions of DUMAND ($t=2^0$, $P_0=500$ atm, S=35 ‰) is equal to $\Gamma \approx 0{,}12$.

To model possible contribution of another acoustical mechanisms in the total signal the dependence of sound value initiated by vapour microbubles on hydrostatic pressure was investigated. Ensemble of vapour microbubles was initiated by laser beam striked the polydisperce mixture of grains in water (grain's sizes $\sim 10^{-5}$–10^{-3} cm, grain's number $\sim 10^4$ cm^{-3}, density of laser beam energy 10^{-2}–10^{-1} J/cm^2; full points in fig.2). Acoustical signal value from the single caverne initiated by laser break of water (~ 1 J/cm^2) in dependence on hydrostatical pressure was also investigated (■ in fig.2). It is seen from the figure that the value of soft (evaporating) heterocomponent of acoustical signal becames diminutive at depths greater than ~ 1000 m. The value of hard heterocomponent i.e. acoustical signal from laser break of water is practically independent on hydrostatical pressure. The Grunaisen parameter is shown in fig.2 by solid line taking into account the change of t^0, P_0 and S ‰ of water in dependence of water depth. The experimental data on acoustical signals initiated by laser (▽) and electron (o) beams also are shown in fig.2.

It is nessesary to point out that the sensitivity of hydrophones made of piezoceramic CTS-19 was changed not more than 10 % in the pressure range 1-500 atm.

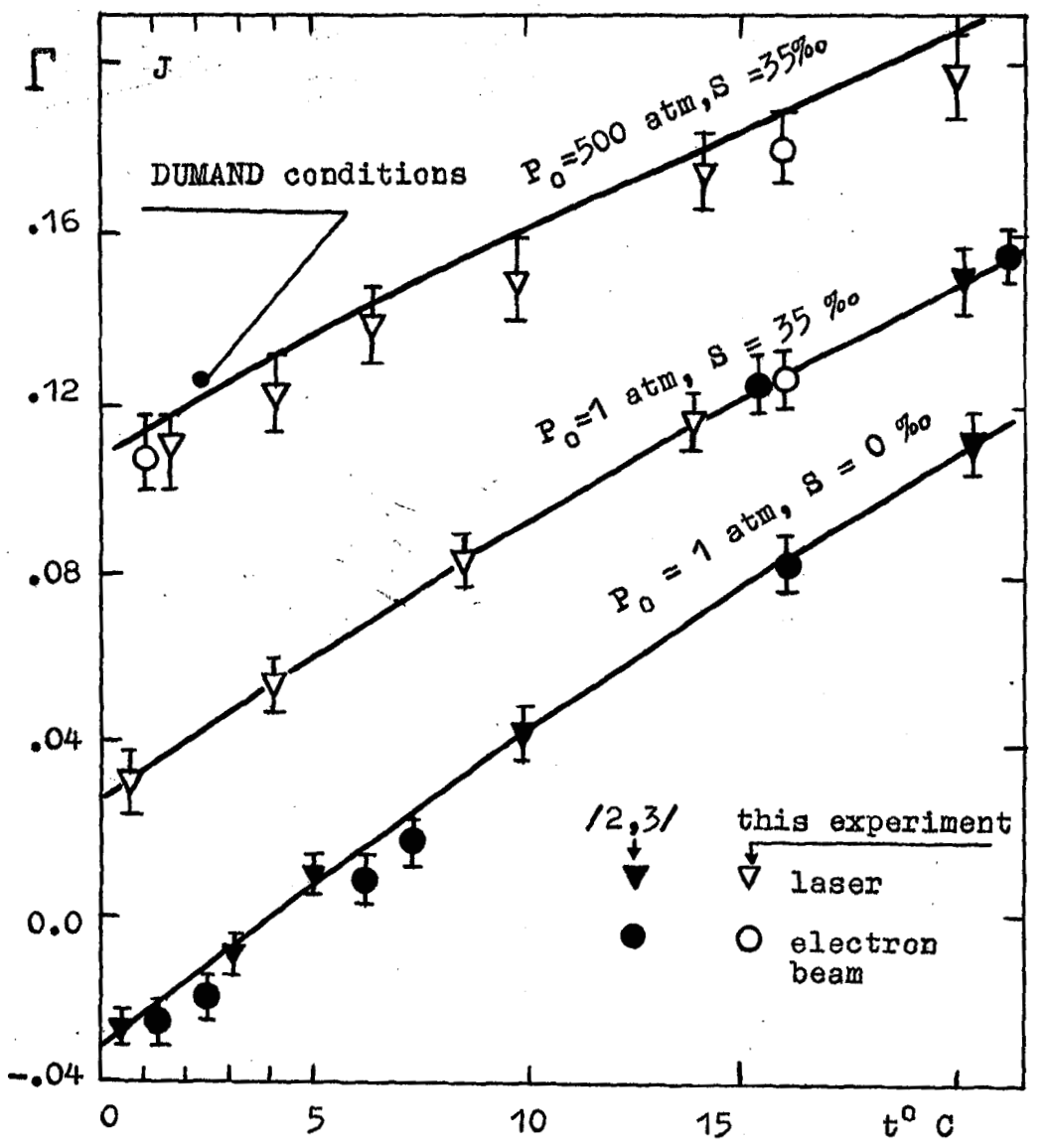

Fig.1 Temperature dependence of acoustical signal J by the different water saltness S ‰ and pressure P_0. Solid lines - tabular /4/ interpolation of Grunaisen coefficient.

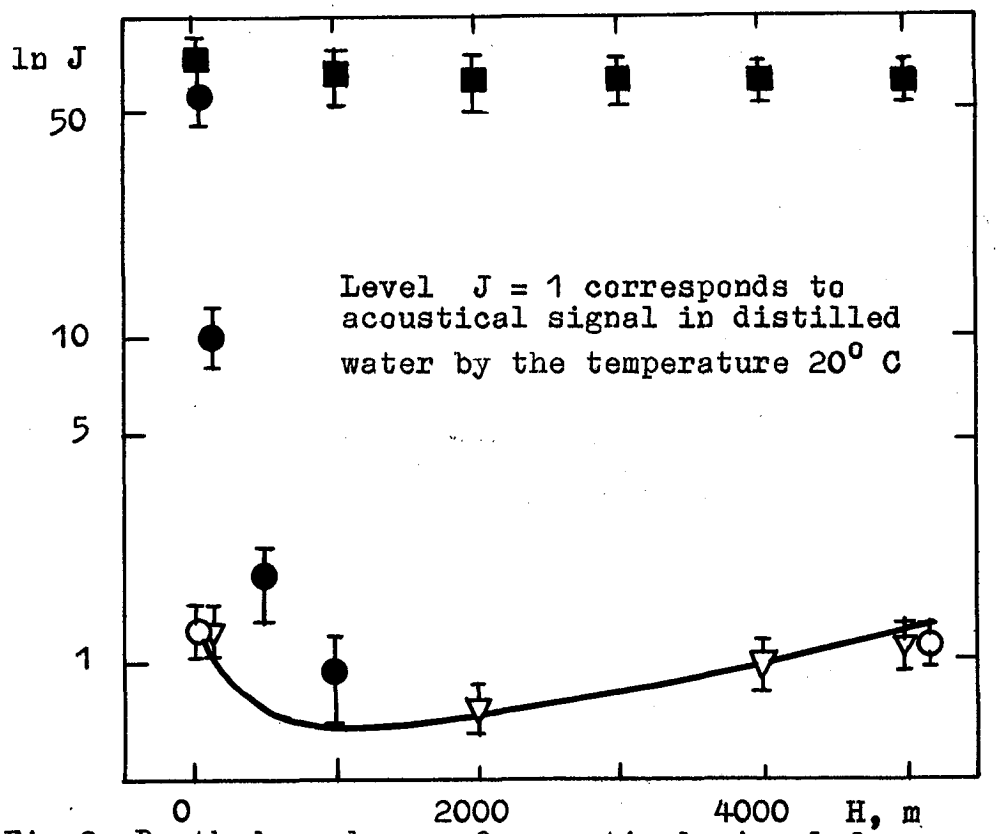

Fig.2 Depth dependence of acoustical signal for : electron O and laser ▽ beams by the thermo-acoustical mechanism (solid line - tabular data for Grunaisen coefficient); laser beam, vapour microbubbles ● ; single caverne by the laser break of water ■ .

REFERENCES :

1. Askarjan G.A.,Dolgoshein B.A., Prepr.FIAN, N°160, 1976.
2. Golubnichy P.I.,Kaluzhny G.S.,Korchikov S.D.,Petrenko V.N.,Ponomarjev V.V.,Yakovlev V.I., Sovjet JTP, Pisma, v.5,is.5,p.272, 1981
3. Golubnichy P.I.,Kaluzhny G.S.,Korchikov S.D.,Ponomarjev V.N.,Yakovlev V.I., Voprosy Atomnoi Nauki i Tekhniki, N° 1(13), p. 92, 1983.
4. Popov N.I., Fedorov K.N., Orlov V.A., Morskaya voda, Moskwa, Nauka, p. 327, 1979.

HE 7.1-3

EXPLORING RESULTS OF THE POSSIBILITY ON DETECTING COSMIC RAY PARTICLES BY ACOUSTIC WAY

Jiang Yin-lin, Yuan Yu-kui, Li Yan-guo,
Chen Duon-bao, Zheng Rong-ting.

Institute of High Energy Physics, Academia Sinica
P.O.Box 918, Peking, China

Song Jian-ning.

Institute of Acoustics, Academia Sinica

1 Introduction

The idea of detecting ultrahigh energy cosmic ray particles by acoustic way has been suggested for years. To date many theoretical and experimental researches have been completed(1-9). In order to pursue this possibility the acoustic background noise in ocean and large lake have been examined. Stenger et al first explored the ultrasonic signals in the sea off the Barking Sand coast of the Hawiian island Kauai in May 1977(10). Some waveforms of transient and ultrasonic signals were recorded. But there is no conclution on the sources and the properties of these signals.In the recent years Kaneko et al have examined the possibility on observation of super giant air showers above 10^{20}eV by aid of detecting the acoustic signals generated by the shower cores in a lake at mountain level(11). In the past we reported that there are some transient and puzzling ultrasonic signals in large reservoirs(12). In order to clarify the sources and the properties of these signals and to examine whether some signals among them are produced by ultrahigh energy cosmic ray particles a new experiment was carried out during the period from June to August in 1984 at Reservoir Miyuin.

2 Experimental status and apparatus

The experiment was carried out on a ship floating on Reservoir Miyuin(altitude:134m). The distance from the ship to the major dam is about 150m. Observation was conducted at night. The new apparatus consists of a hydrophone array, a small EAS array and electronic instruments. A schematic diagram of the experimental setup is shown in Fig. 1.

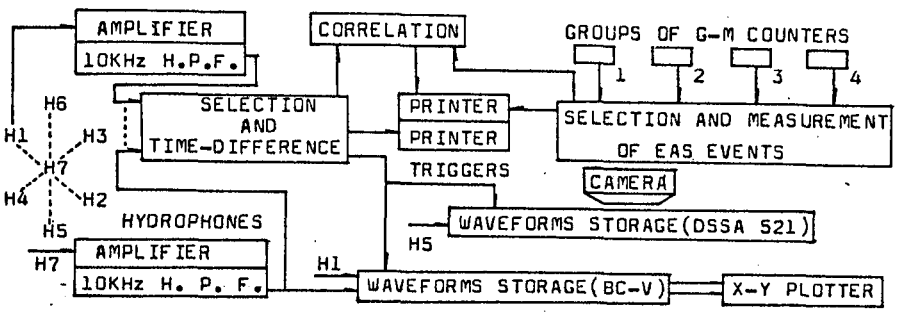

Fig. 1: Aschematic diagram of the experimental setup.

The construction of acoustic array is a rectangular coordinate system. Radial distance from central hydrophone to external one is 1m. The depth of the center of the array is 2.85m under water. The hydrophones with pre-amplifiers(gain: 20db) subject to three types. Frequency response is uniform in the range from 4KHz to 100KHz($\pm$3db). The sensitivity is from 150μv/μbar to 350μv/μbar. Self noise of all acoustic system is approximate to (0.2-0.5)μbar. Sevenfold coincidence with discrimination threshold of 2μbar was used for selecting transient ultrasonic signals. It provides a counting rate of 30 hour^{-1}. The occurence time, three waveforms recieved by three different hydrophones(H1,H5 and H7) and time-differences between central hydrophone signal and external ones were recorded for each selection event. The accuracy of positioning based on hypothesis of the point source is better than 20% within 10m.

The small EAS array consists of four groups of G-M counters(J109-γ). The efficient area of each group having two layers of G-M counters is 0.32m^2. They were placed on the top of the ship(area:~14x4m^2). A threefold coincidence between four groups provides a counting rate of 40 hour^{-1}. The threshold energy of EAS array is equal to 10^{14}eV in such a case. The occurence time and local particle densities were measured.

There is a correlation circuit between acoustic event and EAS one. If an acoustic event take places after the occurence of an EAS event within 1 s the delay time ΔT can be measured by the correlation circuit. If an equation, $C \times \Delta T = R$, is satisfied(where C is the velocity of sound in water, R the distance from the sound source to the center of acoustic array) the position of this signal source may be coincident with EAS core.

3 Results and analysis

The aim of this experimental was directed at trying to investigate the question whether the ultrasonic signals in water were relevant to high energy cosmic ray particles.

Correlation events: During an efficient observation term of about 329 hours 116 correlation events were recorded. The distribution of the delay time ΔT of these events consists with uniform distribution. In addition according to the counting rates of acoustic array and EAS array there must be 110 accident coincidence events. Therefore most of them belong to accident coincidences. We could not find any event which shows that the equation $C \times \Delta T = R$ is realized within the sensitive distance of 10m. The results imply that the threshold energy of detecting EAS core with this acoustic array is above 3×10^{16} eV and that the mechanism of sound generated by EAS core in water may be the thermo-acoustic mechanism(6,7). Unfortunately we can not answer an important question whether there were real correlation events at R above 10m. In future it is necessary for detecting acoustic signals created by EAS cores in water to develop new high sensitive and low noise hydrophones and

to extend the sensitive distance of acoustic array. If the sensitive distance of an acoustic array with a small EAS array is about 500m perhaps it is possible to detect acoustic signals generated by EAS cores of energies above 10^{18}eV.

Ultrasonic signals under water: It is very important to search for acoustic signal created by high energy nuclear cascade in water. This is one of the possible effects on the basis of which DUMAND project try to observe cosmic ray neutrinos in deep ocean. During our observation many transient ultrasonic signals under water were recorded. In order to explore whether some of them are relevant to the local cascades produced by high energy cosmic ray particles their caracteristics were examined. Two typical waveforms of these signals and basic data are shown in Fig. 2. Obvious properties

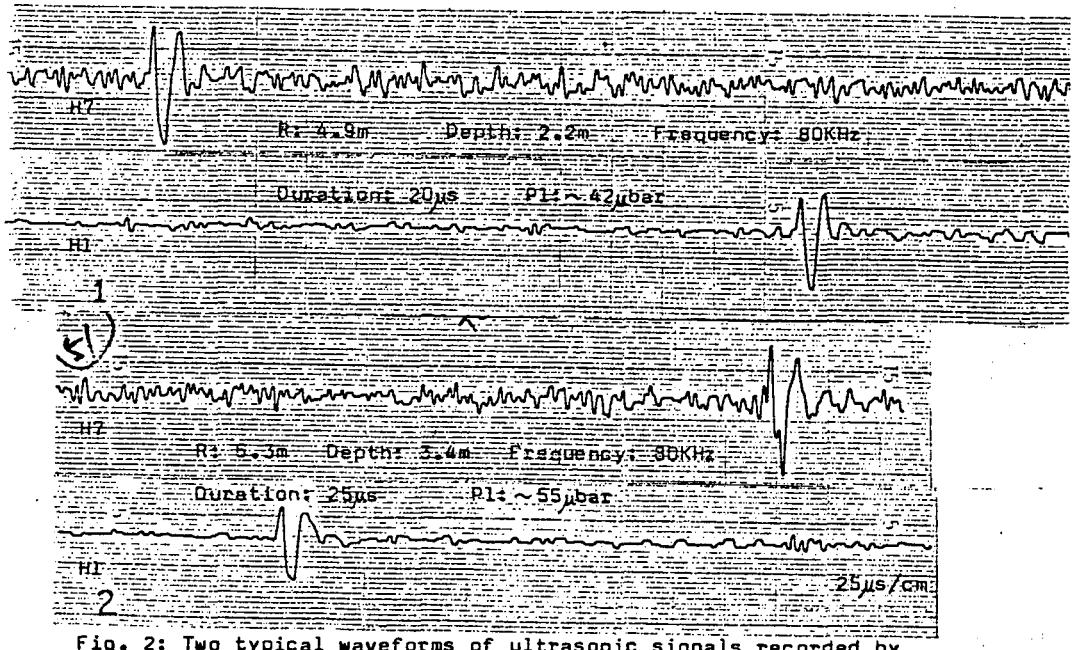

Fig. 2: Two typical waveforms of ultrasonic signals recorded by waveform storage(8C-V) under water.

of signals is as follows:transient and individual, multipole (most of them are tripolar pulses), short duration of from 25μs to 60μs, ultrasonic frequency of from 60KHz to 100KHz. An evaluation based on hypothesis of the point source shows that the peak sound pressure P1(normalization at 1m from the source) is approximate to several tens μbar and that the total energy radiated by a source is about several GeV. These properties are very similar to that of sound signals radiated by microbubbles with radii from 3×10^{-3}cm to 7×10^{-3}cm (13). These microbubbles have the potential energy in the range from 10^{11}eV to 10^{12}eV(14). Taking account of the radiation efficiency of about 1.5% they are capable of releasing the acoustic energy of several GeV(13). In addition it is impossible

that the total acoustic energy arises directly from local energy deposition produced by local nuclear cascade. Therefore a primary conclution is that the mechanism of generating there ultrasonic signals under water is sound radiation of micro-bubbles. It is well known that there are a lot of microbubbles in natural water(15). Many years since it has been investigated that cosmic ray particles can create bubble nuclei in water(16, 17). We suppose the local energy depositions produced by nuclear cascades in water may induce sound radiations of a part of microbubbles.

4 Conclutions

Although it has been demonstrated experimentally and theoretically that high energy particles produce detectable sound in water many years ago. However no one can find an acoustic signal generated by high energy cosmic ray particle in water as yet. Our results show that transient ultrasonic signals in a large lake or reservoir are fairly complex and that transient signals under water may arise mainly from sound radiation of microbubbles. This field is not explored in detail. Maybe the sounds created by cosmic ray particles hide in these ultrasonic signals. Thus in order to develop the technique of acoustic detection it is the most important to make a thorough investigation of these ultrasonic signals in water.

5 Acknowledgements

We wish to thank Prof. He Ze-hui and Prof. Huo An-xiang for the contributions to experimental work and beneficial discussions,and to specifically thank staffs of Institute of Acoustics who have made hydrophones and supported our experimental work.

References

1. V.D.Volovik et al. 14th ICRC Vol 8(1975)3096
2. Proceedings of the 1976 DUMAND Summer Workshop p523
   proceedings of the 1979 DUMAND Summer Workshop p128
3. V.D.Volovik and G.F.Popov. 15th ICRC Vol 9(1977)37
4. W.V.Jones. 15th ICRC Vol 6(1977) 271
5. A.Roberts. AD-A048601 December 1977
6. S.Hanish. AD-A050563 May 1978
7. W.L.Barrett. Science Vol 202(1978)749
8. G.A.Askariyan et al. NIM Vol 164(1979)267
9. V.J.Stenger et al. "Status Report on the Barking Sands Project" 1977
10. L.Sulak et al. NIM Vol 161(1979)203
11. T.Kaneko et al. 17th ICRC Vol 11(1981)426
    18th ICRC Vol 11(1983)428
12. Jiang Yin-lin et al.
    Proceedings of the 1980 DUMAND Symposium Vol 1 p109
13. D.Ross. "Mechanics of underwater noise" 1976 p62
14. W.Hentschel and W.Lauterborn. Applied Scientific Research Vol 38(1982)225
15. L.D.Rozenberg. "High-Intensity ultrasonic Fields" p279
16. D.Stette and F.Wangerlingh. Phys Rev Vol 125(1962)409
17. D.Stette and F.Wangerlingh. J.Acoust. Soc. Am. Vol 41(1967) 1074

ACOUSTIC DETECTION OF AIR SHOWER CORES

Gao Xiaoyu
Physics Dept. Yunnan University, Kunming, Yunnan, P.R.C.
Liu Yongyue
Institute of High Energy Physics, Beijing, P.R.C.
Du Songlin
Physics Dept. Yunnan University, Kunming, Yunnan, P.R.C.

ABSTRACT

At an altitude of 1890m, a pre-test with an As core selector and a small acoustic array set up in an anechoic pool with a volume of $20x7x7m^3$ was performed, beginning from Aug. 1984. In analysing the waveforms recorded during the effective working time of 186 hrs, three acoustic signals which can not be explained as from any sources other than AS cores were obtained and the estimation of connective parameters was made.

1. Introduction. Up to now, the only way of studying VH energy phenomena is by means of air shower. But, as the AS energy becomes higher and higher, the sensitive area needed to detect it becomes larger and larger. Limited finances make it difficult to perform the experiment. The suggested scheme of accoustic detection of AS cores (1) (2) will be not only less costly, but also able to determine the core energy and the accurate position at which the high transverse momentum may be shown. And furthermore, some topics associated with astrophysics can be studied by determining the directions along which AS's arrive. The experiments on acoustic signals caused by proton beams (3) have proved it is feasible to detect acoustic signals caused by high energy particles passing through water. Our preceding work (4), in which the influences of the duration of heating pulses and of the transient responses of hydrophones on the time structures and the amplitudes of acoustic pulses were studied in particular, indicated that the energy threshold of the acoustic detection calculated from the data of accelerator experiments, without taking into account the effect of spill time of the proton beam, was much too high. How-ever, the acoustic signals are still weak because of the very small energy transformation ratio (10^{-9}-10^{-10}). The low S/N ratio has been remaining the main difficulty in the application of the acoustic detection. Particularly, in a natural water body (such as an ocean or a lake) background noises from the surface conditions (wind, waves, boats) and from animal life will greatly reduce the S/N ratio. In order to accumulate experiences for designing a largescale acoustic detector, the pre-test was performed with an anechoic pool whose background noises were very low.

2. Methods. The experiment arrangement is schematically shown in Fig. 1. The AS core selector, which consisted of four counters with active area of $0.33m^2$ each set up on the corners of the pool, was arranged to select $E > 10^{15}$ ev events. When there was a fourfold coincidence pulse coming out of AS core selector, the fourstep staircase wave generator was triggered once and produced three simultaneous outputs. One of the outputs was used to trigger the double-beam oscilloscope and the other two were fed respectively to the two signal channels so as to increase the effective breadth of the screen by four times. The sweep speed of the oscilloscope was 0.2ms/cm, so that about two and a half timebase lines were enough to display the events happening at any spot in the pool, and the rest part of timebase lines which had no information relative to AS cores on it was used for comparison.

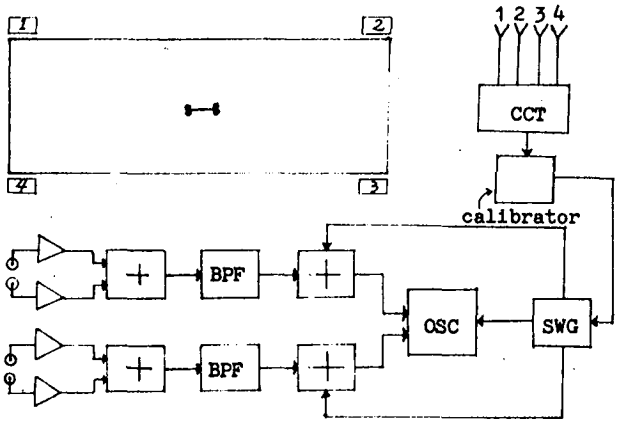

Fig. 1 Schematic of experimental arrangment and electronics.

The four PZT-5 spherical hydrophones used in the experiment are essentially the same, and their frequency response are flat up to 50 KHz. In each signal channel, acoustic signals with the same phase coming from the two hydrophones set up very closely together were amplified and then added together to improve the signal-to-electric-noise ratio. The output terminals of the two signal channels were connected respectively to the two input terminals of the oscilloscope.

According to the most propable spectrum distribution of signal and the influence of the response of hydrophones on the time structures of acoustic signal and the consideration on minimum BW with tolerable distortion, we employed filters with a pass-band of 3KHz to 30KHz to limit noises as much as possible. It was shown by our simulating experiment with Q-switch laser beams that these filters did not cause serious distortion. The anechoic pool used in the experiment had low background noises. Fig. 2 shows the noise spectrum for the whole detection system (including ambient noise, noises of hydrophones and amplifiers), the noise

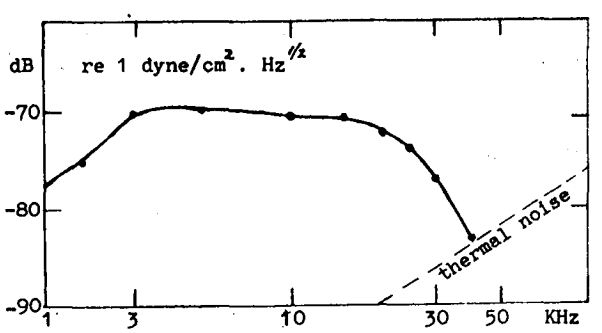

Fig.2 Noise spectrum for whole detection system.

lever is $1.5\times10^{-4}\mu b/Hz^{\frac{1}{2}}$ at a freqency of 30KHz. The water termperature was 18.5°C during the experiment.

3. Results and Discussion. In sweeping and analysing all of the traces recorded during the effective working time of 186 hr. The acoustic signals of three events which had the following characteristics in common were obtained.

1. The signals from the two channels are both bipolar pulses and have the same shape except the amplitudes.

The caculation (5) from thermoacoustic model and the experiments (3) (4) with proton beams and laser beams have shown that when a beam of charged particles passes through water, the acoustic signal caused by the sudden thermal expansion of water is a bipolar pulse. AS cores produce this type of event.

2. The positions at which the signal pulses appear on the timebase lines, which are determined by the propagation times of the sound wave from the source to the hydrophones in water, are accordant with the geometrical confiquration of the pool and the location of hydrophones in it.

3. The attenuation of the signals obeys the propagation law of the cylindrical wave, i.e. $p\propto 1/\sqrt{R}$.

Fig.3 Gives the copy of event acoustic signal No. KY 3.

The three characteristics mentioned above are only the necessary requirements that acoustic signals caused by AS cores must satisfy. On the other hand, the possibilities that the same results may be caused by other factors have to be considered and eliminated one by one.

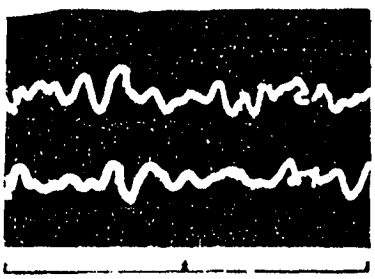

Fig.3 The copy of event acoustic signal No.KY 3. Scale is 200μs/cm.

(a) If any eletric interference was picked up, its waveforms from the two signal channels would appear at exactly the same position on the corresnonding timebase lines. We did saw these waveforms. But it was very easy to identify and ignore them. One kind of interference which must be considered is the noises from the electric equipment themselves. After they had worked continuously for 8hr., we short-circuited their inputs and observed the noise waveforms, it was seen that a large number of which were unipolar pulses emerging at random. No bipolar pulses were observed.

(b) If any acoustic disturbance was recieved by the hydrophones, its waveforms would be of damped oscillation form but bipolar pulses in general. Even if bibopar pulses had appeared, their amplitudes would not have varied as $1/\sqrt{R}$ as required in the near field configuration. We did not find any

possibility in the existance of a cylindrical source besides AS cores in the pool.

(c) If any other interferences were present, no matter at regular time or at random their waveforms would appear on every timebase line with the same probability, because the oscilloscope was triggered by the coincidence output of the AS core selector which occurred at random. In order to obtain sufficient record of the background noises, we triggered the oscilloscope manually at various intervals between different stages of the experiment and all of the timebase lines obtained had no information from AS cores on it, (we call them background lines). The number of all background lines (including the last one and a half lines obtained when the oscilloscope was triggered by the coincidence output of the AS core selector) were larger than that of the lines information on it. But no signals whose characteristics are the same as any one of the three event signals appear on the background lines. Therefore this kind of possibility can be eliminated.

From about, the three acoustic signals can not be explained as from any sources other than AS cores. The experiment date are listed in the following table in which the subscripts 1 and 2 indecate channels one and two respectively. From the table, it is can be seen that the values of the effective diameter of the cores causing acoustic effect are not inconsistant with the expected ones.

Event	t(μs)	P_1 (μb)	P_2 (μb)	d(cm)	f_c (KHz)	P_2/P_1	$\sqrt{R_1}/\sqrt{R_2}$
KY 1	50	0.23	0.37	7.5	20	1.66	1.64
KY 2	30	0.31	0.36	4.5	33	1.16	1.13
KY 3	40	0.24	0.25	6.0	25	1.06	1.02

Key: t— Duration of acoustic pressure pulse
P— Acoustic pressure
d— Effective diameter
f— mid-frequency
R— Distance from source to hydrophones

4. Acknowledgments. We would like to thank Prof. Yan Guigong (Yunnan University) for his encouragement and Engineer Jiang Weiluan, Gong Wending, Associate Engineer Huang Aiyong and Wong Liyan for their helps with this experiment.

References

1. Bowen, T. et. al.,"A lake Detection for High Energy Air Shower Near the Fly's Eye" Proc. of Air Shower Workshop, 1979.
2. Liu Yongyue, Gao Xiaoyu, (1981), Physics (Chinese), 10, p690.
3. Sulak, L., et. al., (1979), Nuci. Inst. & Meth. 161, p203.
4. Gao Xiaoyu, Liu Yongyue,(1983), 18th ICRC, 8, p166.
5. Boweb, T. (1977), 15th ICRC, p277.

DETECTION THRESHOLD ENERGY OF HIGH ENERGY CASCADE SHOWERS USING THERMOLUMINESCENCE PTFE-SHEET AND HOT-GAS READER

Kino,S.(1), Nakanishi,A.(1), Miono,S.(1), Kitajima,T.(2), Yanagita,T.(3), Nakatsuka,T.(4), Ohmori,N.(5) and Hazama,M.(6)

(1) Osaka City University, Osaka, Japan
(2) Ashikaga Institute of Technology, Ashikaga, Japan
(3) 5-4-301, Takakura-cho, Nishinomiya, Japan
(4) Department of Physics, Konan University, Kobe, Japan
(5) Department of Physics, Kochi University, Kochi, Japan
(6) Aichi Women's Junior College, Aichi, Japan

ABSTRACT

New thermoluminescence(TL) sheet was developed as a detector for high energy components in air showers. For the investigation of detection threshold energy for cascade shower, TL sheets were exposed at Mt.Fuji with X-ray films in emulsion chambers and were scanned by a hot-gas reader. From the result of this experiment, it is concluded that if a γ ray whose energy is more than 6 TeV enters vertically into lead chambers, the cascade shower caused by this γ ray is securely detectable at the maximum development.

1. INTRODUCTION

From the viewpoints that TL powder has wide dynamic range and can be used repeatedly, it can be said that it has more excellent properties than the emulsion plate and the X-ray film which are widely used at present (1). Particularly in experiments for very high energy phenomenon in cosmic rays, these features are very desirable.

We have been developing a new detector using TL material as a new device for the plan to observe high energy particles in air showers (2). For this purpose, we developed a new TL sheet using a glasscloth as the base and a fluorocarbon resin as the binder.

The detection threshold energy of cascade shower using this TL sheet and a hot-gas reader was investigated by the experiment exposed to cosmic rays at Mt. Fuji.

2. TL SHEET and HOT-GAS READER

TL sheets so far developed have some defects of the low sensitivity and the easy exfoliation from the base plate and so on (3)(4). Therefore, they are not suitable for the practical application as they are.

At this time, we produced new TL sheet by the manufacturing method as shown in Figure 1. $BaSO_4$:Eu powder was adopted as TL material (4) and it was controlled so as to have the grain size of about several μm and to have the glow peak at 180 ^{o}C.

TL powder was mixed with fluorocarbon resin dispersion (PTFE = polytetrafluoroethylene) with weight ratio 1:1 and churned well. After the glasscloth belt was impregnated with this mixed dispersion, it was dried and sintered in an electric oven and rolled up. This process was repeated ten and several times until the thickness of coating became to be a certain

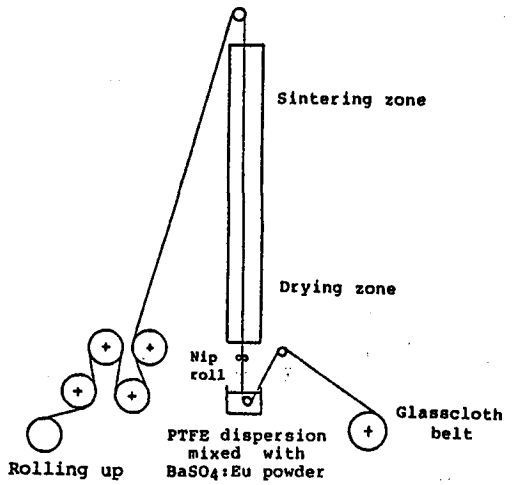

Fig.1. Schematic diagram of the manufacturing process of TL sheet.

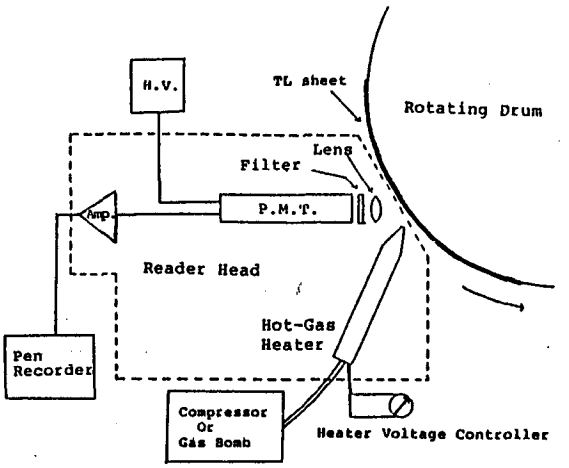

Fig.2. Basic scheme of scanning TL reader with hot-gas heating.

value.

Characteristics of this sheet are following.

1. High sensitivity. For example, 20 times higher than that of reference 3.
2. Flexibility. Free for bending and restoration.
3. TL coated layer is not cracked and does not come off by bending or hasty heating.

A readout system of this TL sheet is a scanning reader with hot-gas heating as shown in Figure 2. TL reader consists of a rotating drum on which TL sheet is fixed and a reader head at which thermoluminescence light is read out. The former is a cylinder made of steel and rotates with a constant velocity. The latter consists of a hot-gas heater and a photo-multiplier tube. As the drum makes one revolution, the reader head moves at a certain distance (3 mm) in the direction of axis of rotation of drum. The temperature of hot-gas stream is controlled by combination of the heater voltage and the rate of gas flow. In this experiment, to minimize the variation of flow rate, we used the nitrogen gas which is enclosed in high pressure gas bomb instead of air compressor.

The performance of new TL sheet was examined by means of this reader. Figure 3 shows the chart record of the reader soon after the irradiation by ^{90}Sr β source to TL sheet through 1 mm ϕ collimator. From this

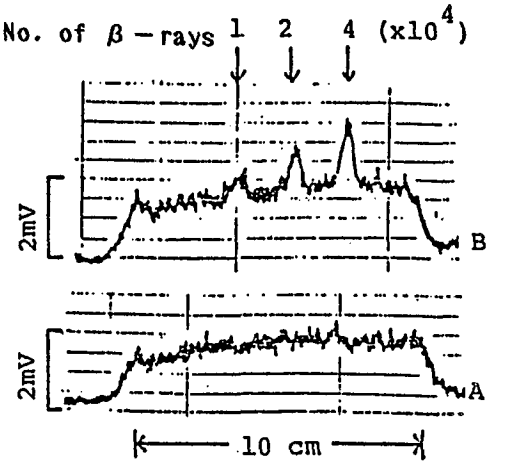

Fig.3. Scanning test of TL sheet.
(A):not irradiated.
(B):irradiated with ^{90}Sr.

result, the detection threshold seems to be about 1×10^4 β rays from ^{90}Sr source.

3. EXPRIMENTAL PROCEDURES AND RESULTS

For the investigation of the detection threshold energy of cascade shower using new TL sheet and hot-gas reader, we carried out an experiment by cosmic rays.

Chambers as shown in Figure 4 were constructed at Mt. Fuji (650 g/cm^2) in total area of 4 m^2 and exposed for a month. After development of X-ray films, cascade showers were picked up and each darkness was measured by photometry method. Figure 5 shows the energy spectrum of cascade showers induced by γ rays obtained from the transition of darkness. Since the present result agrees well with those obtained so far at Mt. Fuji (5), energy determination of cascade shower is appropriate.

On the other hand, TL sheets were scanned with hot-gas reader and it was examined whether TL signals appeared at the passing positions of cascade showers. The appearance frequency of TL signal is shown in Figure 6. The lower horizontal coordinate in the figure shows the darkness of X-ray film just above TL sheet, and the upper one shows the converted energy provided the darkness is the maximum darkness of a cascade shower which enters vertically. Figure 6(a) shows the appearance frequency of TL signal per sheet and Figure 6(b) shows the coincidence rate of TL signals between upper sheet and lower one at the same layer. The background noise in Figure 6 implys that the appearance frequency of TL signal at the position where cascade shower did not pass. This background noise is caused because the background level does not rise uniformly due to the ununiformity of sensitivity on TL sheet. The frequency of this background noise is therefore proportional to the period of exposure of TL sheet.

5. DISCUSSION

From the result of Figure 6, it is concluded that a cascade

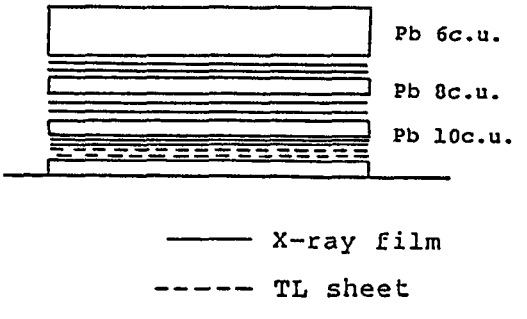

Fig.4. Design of the test chamber.

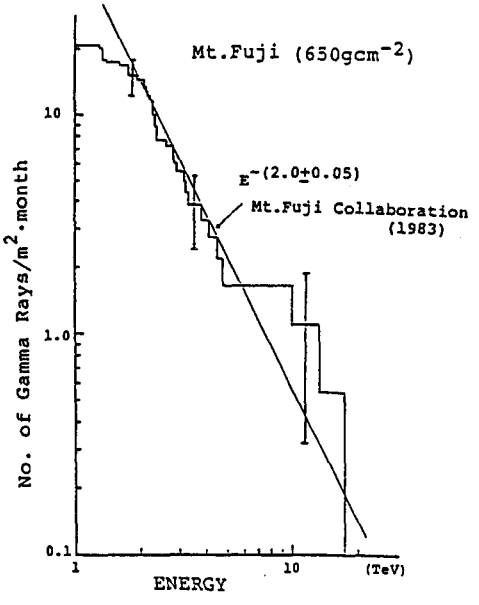

Fig.5. Integral energy spectrum of gamma rays.

shower of which energy is more than 6 TeV and incident angle is vertical is certainly detectable at its maximum development when we use new TL sheet and hot-gas reader. This threshold energy agrees with the evaluation from the comparison between the result of irradiation test by ^{90}Sr β source and the cascade calculation (6).

To lower the detection threshold energy, there are two methods. One is to use a more sensitive TL powder, and the other is to increase the sensitivity of TL sheet itself by increasing the proportion of TL powder or the thickness of coating. With regard to the latter, the present sheet is the best obtainable by the present manufacturing method. More sensitive TL powder of $BaSO_4$:Eu is available, but the ratio of sensitivity is limited to 1.5-2.0 at most. Another manufacturing method has to be developed to produce more sensitive sheet. One possible method is to compress the mixture of TL powder and fluorocarbon resin powder into a cylindrical form and to skive into a belt of a given thickness. The test sheet by this method is proved to have the sensitivity of about 3 times more than the present sheet.

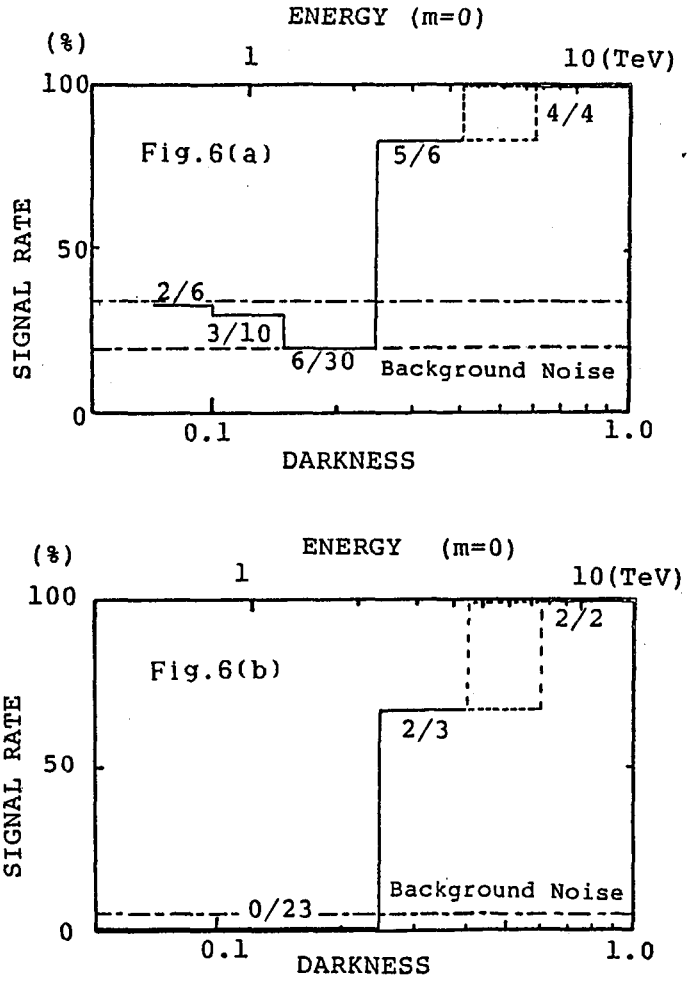

Fig.6. Appearance frequency of TL signal at the passing position of a cascade shower. (a):per sheet. (b): coincidence rate between two sheets.

References

(1) Miono, S., 1975, 14th ICRC (Munich), 6, 2072.
(2) Kino, S. et al., 1983, 18th ICRC (Bangalore), 11, 424.
(3) Miono, S., 1975, Nucl. Instr. and Meth., 128, 173.
(4) Okamoto, Y. et al., 1985, ICR-Report-120-85-1.
(5) Amenomori, M. et al., 1983, 18th ICRC (Bangalore), 11, 57.
(6) Shibata, T., private communication.

HE 7.1-6

Application of thermoluminescence for detection of cascade shower I
---- Hardware and software of reader system ----

M.Akashi, S.Kawaguchi and Z.Watanabe
Hirosaki University, Hirosaki, Japan

A.Misaki and M.Niwa
Saitama University, Saitama, Japan

Y.Okamoto
Science & Engineering Research Laboratory, Waseda University, Japan

T.Fujinaga, M.Ichimura and T.Shibata
Aoyama Gakuin University, Tokyo, Japan

S.Dake
Kobe University, Kobe, Japan

N.Takahashi
Okayama University of Science, Okayama, Japan

ABSTRACT

We developed a reader system for the detection of luminescence induced by heating sensitive material($BaSO_4$:Eu). The reader system is composed of following six instruments; i)Heater, ii)Light guide, iii)Image intensifier, iv)CCD camera, v)Image processor, vi)Micro computer. We report here the efficiencies of these apparatuses, and software utilities for image analysis.

I) Introduction

It has passed about 30 years since Nishimura*[1]* proposed emulsion chamber(EC) of today's type. Since then, it has played a pioneer-like role in the field of ultra high energy physics, where energy of accelerator could never reach. In the very near future, however, super machines, such as TEVATRON, LEP and DESERTRON, are surely to operate subsequently, which cover, or may exceed the energy region nowadays available for EC experiment at mountain station. So, most people think that the observation of air family by means of traditional EC *only* may be closed down soon. In fact, none of emulsion people expect that the current EC continues to work well in a coming decade further.

Under these situations, several groups, particularly those of air shower (AS) and EC*[2]*, are planning to start projects on new phase, combining active detectors(AS array) with passive ones(emulsion like), in order to build an unified picture of shower phenomena both in the atmosphere and the underground. Naturally, the scale of calorimeter thus combined is expected to be much larger, at least ten times or more, than today's.

From these points of view, we decided to develop reader system as well as a new kind of sensitive material*[3]*, thermoluminescence sheet(TLS), which is much more economical and efficient than X-ray film used now.

II) Reader system

Schematic view of reader system is illustrated in Fig. 1, where the use of image intensifier(I.I.) was at first proposed by Okayama group*[4]*.
i)Heater: We use infrared heater of 3 KW, providing uniform thermal beam on hot plate. Heating rate is of course adjustable by controller as we like within the range $\lesssim$ 10°C/sec. Both the heater and the stage attach-

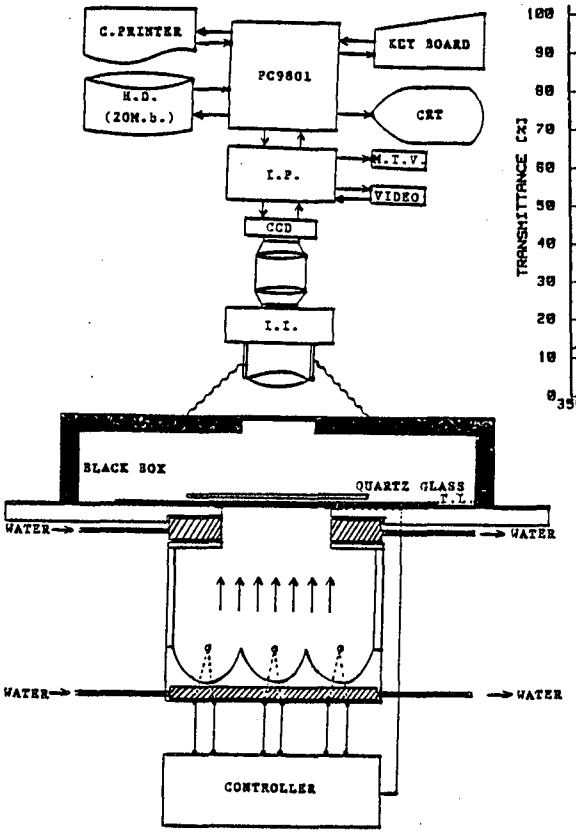

Fig. 1. Schematic view of TL-reader.

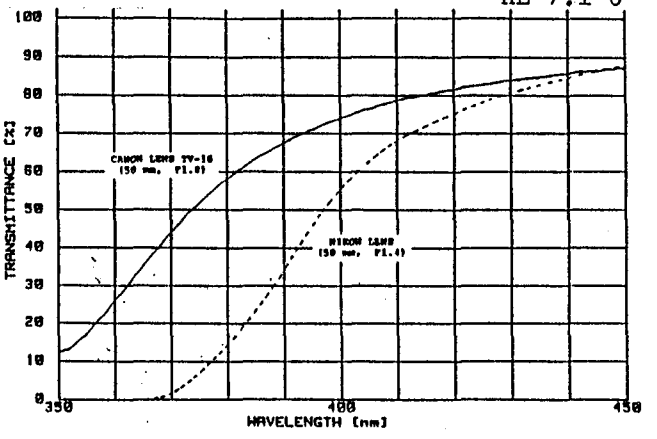

Fig. 2. Transmittance of commercial lens against wave length.

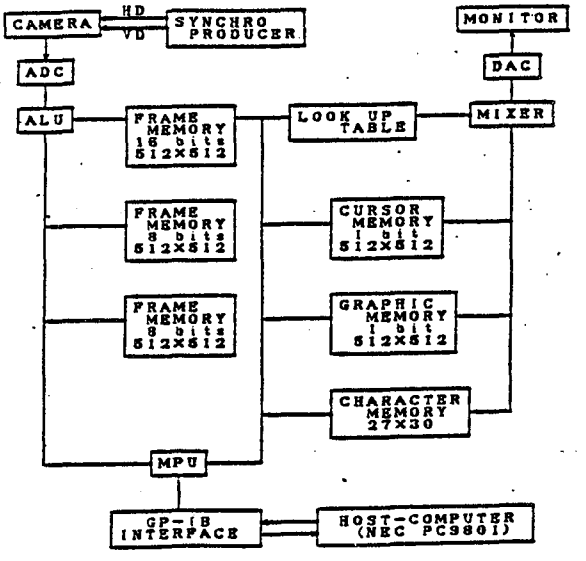

Fig. 3. Block diagram of I.P..

ed with hot plate are cooled by flowing water.

ii)Light guide: Wave length of thermoluminescence being $\sim$ 375 nm[5], we must use condenser lens transmitting well ultra violet light. We found CANON TV16 lens(50mm, F1.8) is the best among commercial ones. Its transmittance is demonstrated in Fig. 2, where the results of camera lens NIKON(50mm, F1.8) is also shown together. One finds the former is approximately ten times higher than the latter in the ultra violet region.

iii)I.I.(HAMAMATSU PHOTONICS,V2025): The imager incorporates a photocathode, a 2-stage micro-channel plate(MCP) and phosphor screen. The gain is variable within the range $10^2 \sim 10^6$. The effective area of the photocathode is 15mϕ, and the sensitivity for wave length of incident light lies around 350nm $\sim$ 650nm. THe best resolution of the phosphor screen is $\sim$ 15 lines/mm, high enough for our purpose.

iv)CCD camera(NEC): Effective number of picture elements is 489 × 384, and the size of effective photocathode area is 2/3 inch. The uniformities both in the geometry and individual photo-sensors are quite well.

v)I.P.(ADS CO.,LTD.): Block diagram of I.P. is shown in Fig. 3. Signals from each pixel of CCD are stored in the main frame memory(16bits × 512 × 512). In I.P., we have more frame memories as seen in Fig. 3, which are useful for image analysis. These data stored in frame memory are transmitted to RAM(640 Kb) in host computer PC9801, through GPIB interface.

III) Software system

In Fig. 4, we present the internal relation of software utilities for TL shower analysys. The system is composed of following four functions.
i)EDITOR: This function has mainly two utilities, the one for registration of numerical constants related to chamber structure(dilution factor D_f and position of sensitive material δ), and the other to convert the standard TL transition curves(D_f=1.2, δ=600μm) into those for the chamber just registered. The detail of these calculations will be reported elsewhere. In Fig. 5, we show an example of transition curves for the chamber TLC II *[6]* exposed at Mt. Fuji during one year from August of 1983.

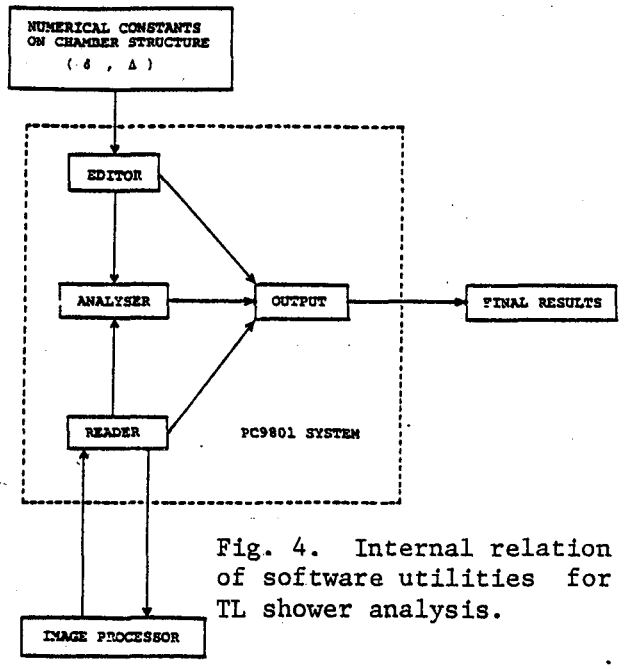

Fig. 4. Internal relation of software utilities for TL shower analysis.

Since the TL emission depends on experimental conditions, such as circumstance of exposure, gain of I.I. and so on, it must be calibrated for the amount of luminescence with use of nuclear emulsion plate, for every exposures, just in the same way as the calibration of X-ray film.
ii)ANALYSER: The function of ANALYSER is to find automatically the best fitting of theoretical ones mentioned above to experimental ones with use of least square method. Then, we get maximum TL luminescence I_{max}, which is approximately proportional to shower energy, and the penetration depth ΔT, familiar parameters in shower analysis.
iii)READER: As mentioned in II-v), the raw data storaged in frame memory of I.P. are transmitted to RAM memory in PC9801 through GPIB. These data are save in hard disk(20 Mb) and/or flopy disk(1 Mb). Utility of READER

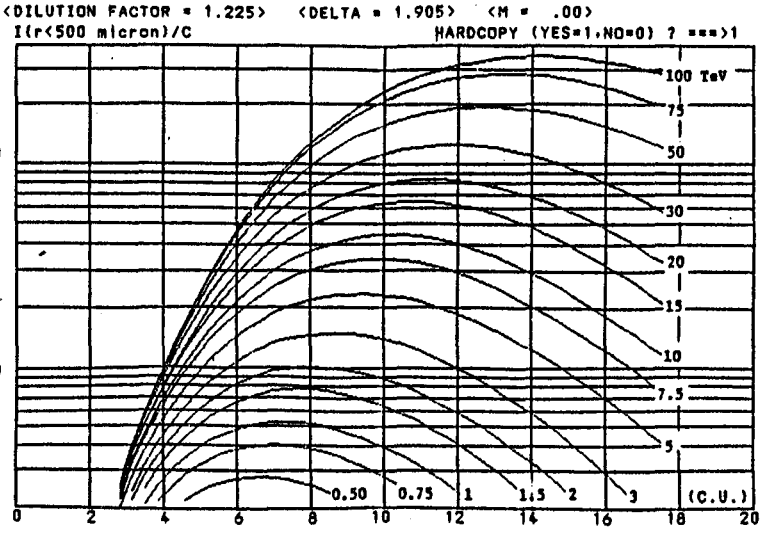

Fig. 5. Example of TL transition curves in the cases of tan θ= 0, initiated by electron-pair primary. Numerical value attached to each curve is shower energy. Conversion factor C denoted at vertical axis is to be determined by the calibration procedure with use of nuclear emulsion plate, as discussed in text.

is to provide following processes.
a)Drawing of glow curve on CRT in real time.
b)Background subtraction.
c)Two dimensional contour map.
d)Three dimensional contour map.
e)Lateral distribution of luminescence.

In Fig. 6, we demonstrate the three dimensional contour map of TL emission, which is obtained by 10 minutes irradiation of Sr^{90}.

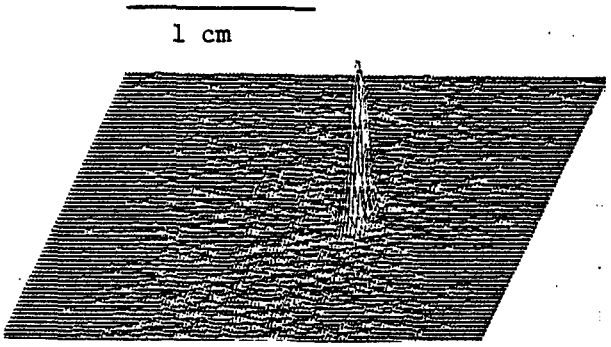

Fig. 6. Three dimensional contour map of TL emission, induced by Sr^{90} irradiation.

iv)OUTPUT: This is to provide utilities related to output processes for all physical quantities, stored in disk through the functions i), ii) and iii), on CRT and/or printer.

IV) Discussions

The reader system presented here is of course not enough for processing a big amount of TL sheets expected from future's super TL-calorimeter. In order to develop the present system further, we are now investigating to use optical fiber, instead of lens system, so as to collect TL light more efficiently, and to move TL-stage automatically to scan large area of TL sheet more quickly.

Results of TL measurements by means of the reader system here is reported in HE 7.1-7 in this volume.

Acknowledgements

The authors would like to express their sincere gratitude to the members of TL-Development Collaborative Group, particularly to Drs. T.Saito, T.Wada and I.Yamamoto, for valuable advices and discussions from the beginning of the present works.

We are also much indebted to Mr. M.Inoue(CANON Inc.) for providing us kindly various types of lenses and helpful works on transmittance measurements of those.

Numerical calculations on TL transition curves are performed by FACOM M180-II (Institute of Nuclear Study, University of Tokyo) and NEC ACOS750 (Aoyama Gakuin University).

References

[1] Original type of EC was at first proposed by Kaplon et al., Phys. Rev. 85(1952), p.900. The present type of EC was proposed by Nishimura in the meeting held at Research Institute for Fundamental Physics(1956), Kyoto University.
[2] For example, H.Sasaki, Talk at the symposium on future's air shower experiment held at ICR('85, Feb.). T.Shibata, Talk at the symposium on future's emulsion chamber experiment hetld at ICR('85, Feb.).
[3] S.Miono, N.I.M., 128(1975)173.
Y.Okamoto et al., ICR-Report-120-85-1(Univ. of Tokyo).
[4] I.Yamamoto et al., to be published to N.I.M..
[5] I.Yamamoto et al., N.I.M., 224(1984)573.
[6] M.Niwa et al., to be published to ICR-Report.

SPATIAL DISTRIBUTION READ-OUT SYSTEM FOR THERMOLUMINESCENCE SHEETS

I.Yamamoto, T.Tomiyama, K.Imaeda and K.Ninagawa
Okayama University of Science, Okayama Japan
T.Wada and Y.Yamashita
Okayama University, Japan
A.Misaki
Saitama University, Urawa Japan

ABSTRACT

A spatial distribution read-out system of thermoluminescence [TL] sheets is developed. This system consists of high gain image intensifier, a CCD-TV camera, a video image processor and a host computer. This system has been applied to artificial TL sheets ($BaSO_4$:Eu doped) for detecting high energy electromagnetic shower and heavy nuclei tracks.

Thermoluminescence [TL] sheet may be a very useful detector to observe high energy cosmic rays. To find a suitable TL sheet, several kind of sheets have been produced by the "Working group for development TLC"[1]. We have used Eu-doped $BaSO_4$ sheets. TL properties of $BaSO_4$:Eu for temperature and wave length are shown in Fig. 1. These properties (; Fig. 1) were measured by using TL spatial distribution read out system which was shown in Fig. 2.

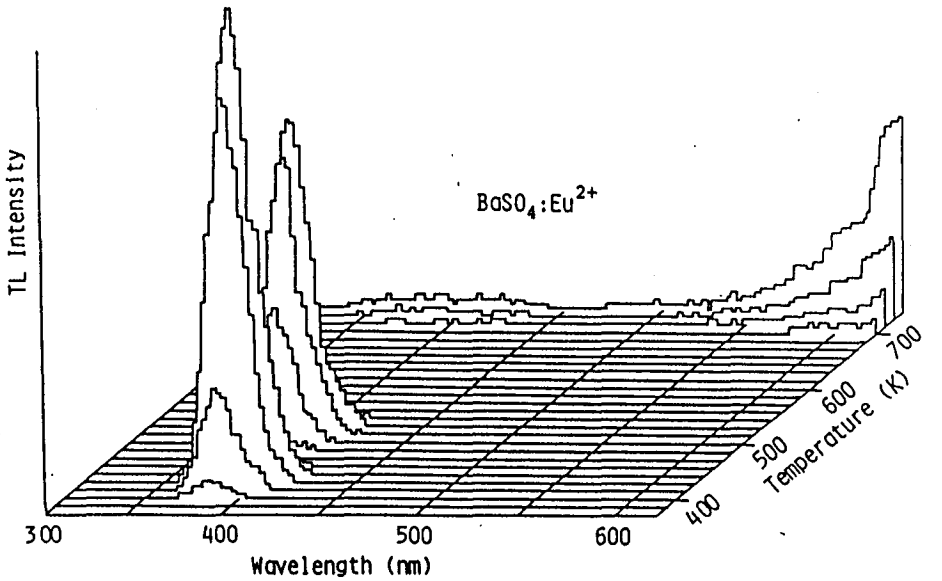

Fig. 1. TL spectra of $BaSO_4$:Eu at various temperatures after ^{90}Sr β-ray exposure to about 100 rad. The emission observed in the red region is due to the incandenscent radiation from the sample at high temperatures.

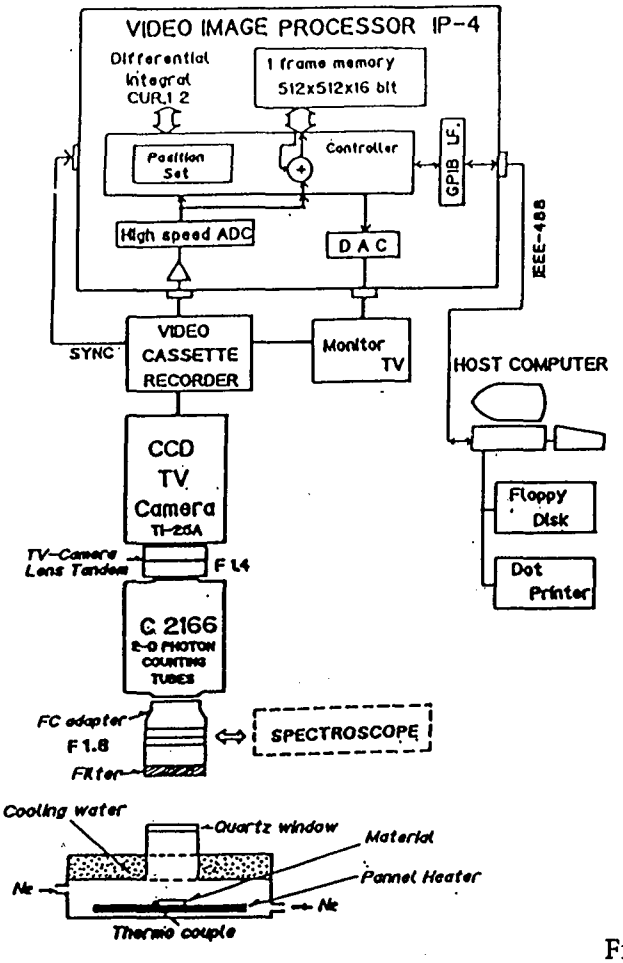

Fig. 2. The TL spatial distribution read out system.

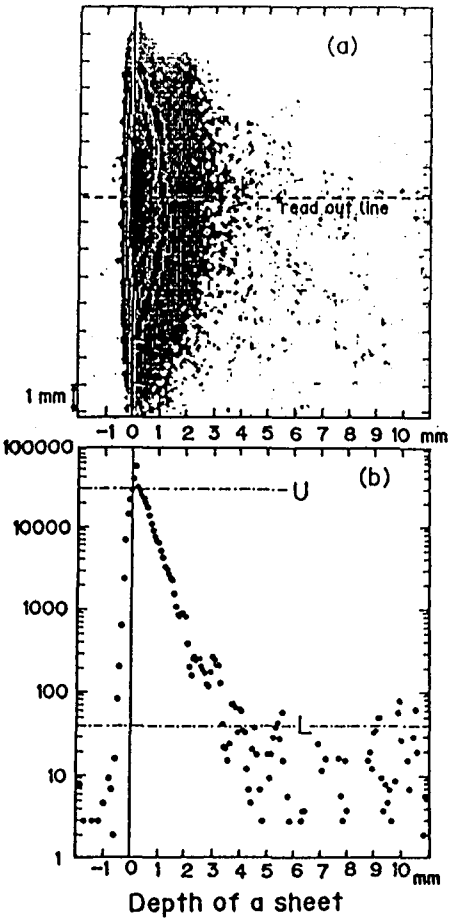

Fig. 3. TL read out example; a TL teflon -sheet was irradiated sideward with ^{90}Sr β-ray.

The equipment of Fig. 2 consists of a) a pannel heater, b) a bandpass filter, c) a photon imaging head, d) a CCD TV-camera, e) video cassette recorder, f) a video image processor and g) a host computer.

We show one example of an application in Fig. 3 —— the TL read out from a TL teflon-sheet ($BaSO_4$:Eu). The sheet was irradiated sideward with ^{90}Sr β-ray. The TL intensity of the "read out line" of Fig. 3a is plotted in Fig. 3b, and these points show the attenuation of β-radiation dose with depth in the teflon-sheet.

A TL calorimeter using these TL sheets had been set at Mt.Fuji (3776 m in altitude) for about one year. We have read out over an area (2 cm × 3 cm) of the TL sheet corresponding to a shower spot in an X-ray film. The results of read out 20 TeV shower are shown in Fig. 4.

We tried to read out a few TeV shower from the TL-sheet

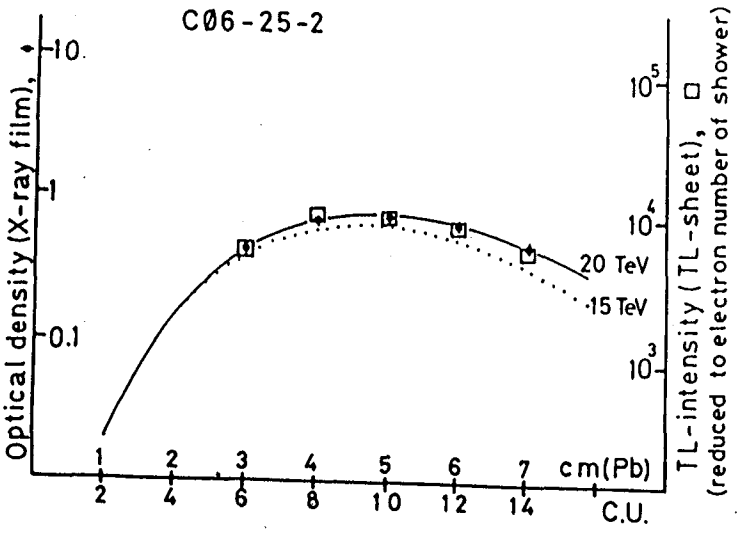

Fig. 4. The cascade shower curve of TL sheet and X-ray film. Solid curve: a typical 20 TeV cascade shower curve and dotted line: 15 TeV.

of Mt.Fuji TLC. For this purpose, a coincidence method (self-correlation on frame picture) has introduced. This method is using the TL property for temperature, that is glow curve shown in Fig. 5. Results of TL read out in each temperature region are shown in Fig. 6a and 6b. We used the TL sheet of Mt.Fuji-C03-14 C.U. Circled points A – I correspond to shower spots in the X-ray film [C03-14 C.U.]; following the corresponding table:

	shower name C03-	shower energy (TeV)	expected TL yeild at 14 C.U. by shower Max.
A	11.14	4.4	0.47
B	11.05	4.0	0.47
C	11.06	3.5	0.78
D	11.09	2.0	0.68
E	11.08 + 11.07	4.2 + 1.8	0.68
F	11.10	6.8	0.47
G	11.04	6.8	0.22
H	11.02	7.8	0.22
I	11.13	19.0	0.58

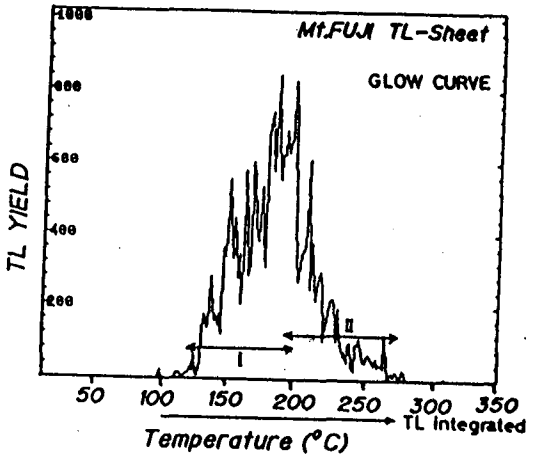

Fig. 5. The glow curve of β-ray irradiated Mt.Fuji TL-sheet. TL yeild of spatial distribution was integrated among increasing temperature.

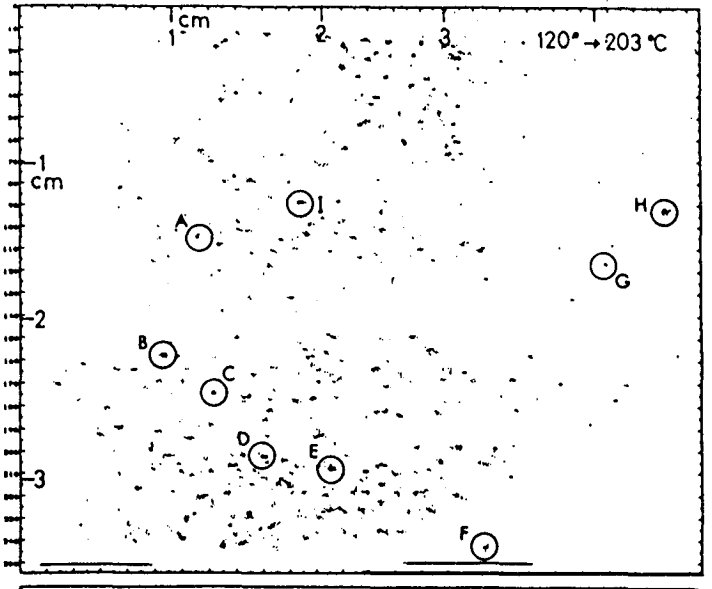

Fig. 6a. A integrated TL spatial distribution in temperature region I of Fig. 5 and the sample sheet is Mt.Fuji-C03-14 C.U.

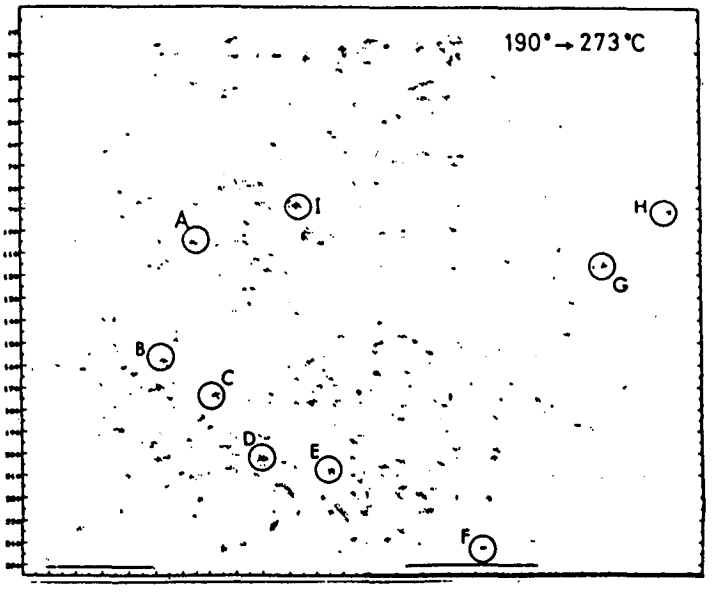

Fig. 6b. A integral TL spatial distribution in temperature region II of Fig. 5 and the same sample as Fig. 6a.

This system has been applied to detect other electromagnetic shower (~ 20 GeV) induced by muons[2] or to read out TL spatial distributions of natural materials[3].

References
1.Okamoto,Y. et. al., (1985),ICR-Report 120-85-1, Tokyo, Japan.
2.Wada, T. et. al., (1985), This conference paper, HE 5.2-10.
3.Ninagawa, K. et. al., (1985), This conference paper, SH 9.1-16.

HE 7.1-12

Application of thermoluminescence for detection of cascade shower II
---- Detection of cosmic ray cascade shower at Mt. Fuji ----

M.Akashi, S.Kawaguchi and Z.Watanabe
Hirosaki University, Hirosaki, Japan

A.Misaki and M.Niwa
Saitama University, Saitama, Japan

Y.Okamoto
Science & Engineering Research Laboratory, Waseda University, Japan

T.Fujinaga, M.Ichimura and T.Shibata
Aoyama Gakuin University, Tokyo, Japan

S.Dake
Kobe University, Kobe, Japan

N.Takahashi
Okayama University of Science, Okayama, Japan

ABSTRACT

We report here the results of thermoluminescence(TL) chamber exposed at Mt. Fuji during Aug. '83 ∿ Aug. '84. We succeeded to detect the TL signal induced by cosmic ray shower, and compared it with the spot darkness of X-ray film inserted together.

I) Introduction

Characteristics of various types of TL powder, LiF, $CaSO_4$:Tm, $BaSO_4$:Eu and Mg_2SiO_4:Tb, were reported in the last conference by TL-Developments Collaborative Group[1]. They concluded that $BaSO_4$:Eu powder is the best for practical purpose from various points of view, that is, it shows negligibly small fading damage, simple glow curve, wide dynamic range and so on.

On the basis of these systematic investigations, we started the use of TL sheet(TLS) composed of $BaSO_4$:Eu, which is coated on Aluminium base with the thickness of 150 μm.

During the time from Aug. '83 to Aug. '84, we exposed a test TL chamber(called TLC II), including both X-ray film and TLS. Therefore, we can calibrate TL intensity with use of spot darkness on X-ray film. The analyses of the latter are summarized in ref. 2, and we report here the preliminary ones of the TLS.

II) Linearity check of CCD and I.I.

Before going to the detail of TL measurements, we should check both linearities of CCD and image intensifier(I.I.), which are cores of our reader system(see Fig. 1 of ref. 3).

We exposed uniform light beam against CCD camera. In Fig. 1, we show the correlation between exposure time of the light and output signal (∝ electric charge storaged in CCD sensor), which is transmitted into frame memory of image processor(I.P.) through high speed ADC. One finds that the linearity is quite well.

Next, we set CCD camera on phosphor screen of I.I. through tandem lenses(NIKON COSMICAR, 50mm, F1.8), and exposed uniform weak

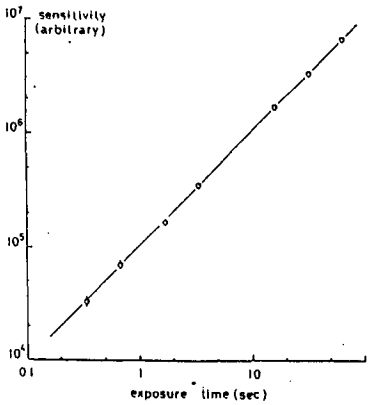

Fig. 1. Relation between exposure time of light and output signal from CCD.

light against photocathode of I.I.. In Fig. 2, we show the correlation between these two in the similar way as Fig. 1. Again we found the linearity is quite satisfactory.

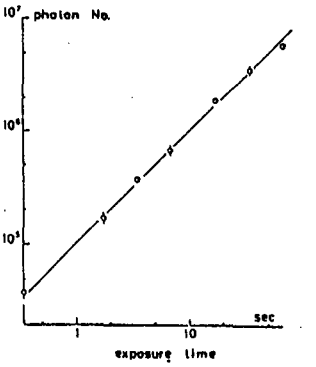

Fig. 2. Linearity check of I.I..

III) Characteristics of TL sheet $BaSO_4$:Eu

i) Glow curve

With use of the utility "READER" in PC9801 (see III-iii in ref. 3), we can draw the glow curve of TL emission on CRT in real time. In Fig. 3, we show an example thus obtained, where Sr^{90} is irradiated for 10 minutes against TLS used practically for TLC II. As the glow peak lies around 210°C, it is enough to integrate TL emission up to 250°C.

ii) Relation between RI intensity and TL emission.

In order to calculate TL transition curves, we need the correlation between electron density ρ ($\propto$ irradiation time of RI) and amount of TL emission I_{TL}. In Fig. 4, we present the relation $\rho - I_{TL}$ for two kinds of TLS; the one composed of Aluminium base coated with TL powder, and the other of the mixture of teflon and that.

Both are expressed by a simple relation,

$$I_{TL} \propto \rho^{1.22}$$

though the sensitivity of the latter gives one order higher than that of the former. The detail of the above supralinearity will be discussed elsewhere.

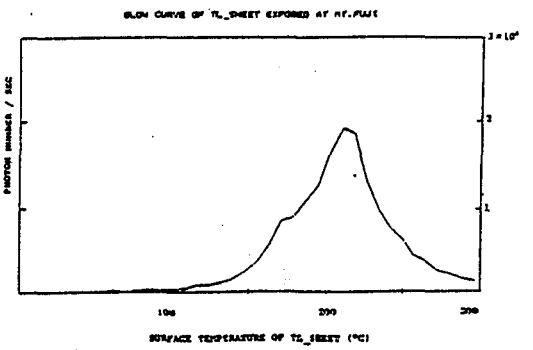

Fig. 3. Glow curve of TLS used for TLC II exposed at Mt. Fuji.

IV) Structure of TLC II

We constructed a TL chamber(TLC II) at Mt. Fuji in the August of 1983, and exposed for one year. The structure of TLC II is illustrated in Fig. 5, where CR39 is inserted at 10 c.u. by another Fuji Emulsion Collaborative Group in order to search monopole. We inserted there two sheets of TLS at every layers except 6 c.u., which enables us to confirm definitely whether light signal comes realy from TL emission, or due to background noise. That is, if we catch a TL signal in the upper sheet , the corresponding signal will be also detected near the same position in the lower one. In Fig. 6, we show an example of TL map, where two signals inside dotted circle correspond to those due to cosmic ray cascade shower. The transition curves of these TL signals will be discussed in the next section.

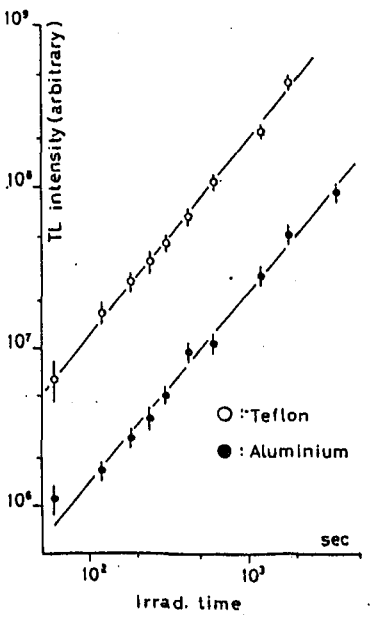

Fig. 4. Relation between RI intensity and TL yield.

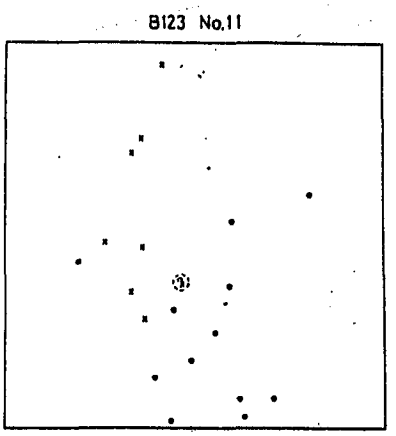

Fig. 6. Example of TL map.

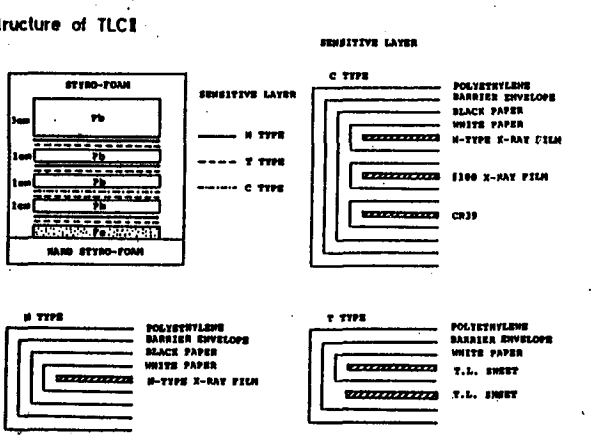

Fig. 5. Illustration of chamber structure TLC II, where three kinds of materials are inserted, X-ray film(Sakura N-type and Fuji #100-type), TL sheet and CR39. CR39 is inserted only at 10 c.u..

V) Transition of TL emission

As mentioned before, X-ray films are also inserted together with TLS. Since cascade shower is detected as dark spot on X-ray film by naked eyes, we can set the position of TL emission beforehand near the center of photocathode of I.I.. Setting error between these two is $\sim$ 2 cm, so that we can not find TL signal sometimes at the expected place.

In Fig. 7-a and 7-b, we give two transition curves; the former corresponding to those of spot darkness obtained by X-ray film, and the latter to those of TL emission. Here, the slit size is fixed $200 \times 200\ \mu m^2$ for the measurement of spot darkness, whereas TL emission is integrated within the radius of 500 μm.

In Fig. 8, we present the correlation between the spot darkness and the amount of TL emission. In this stage, it is difficult to conclude decisively the relation I_{TL} - D, because of poor statistics, particularly in the region $D \lesssim 1.0$.

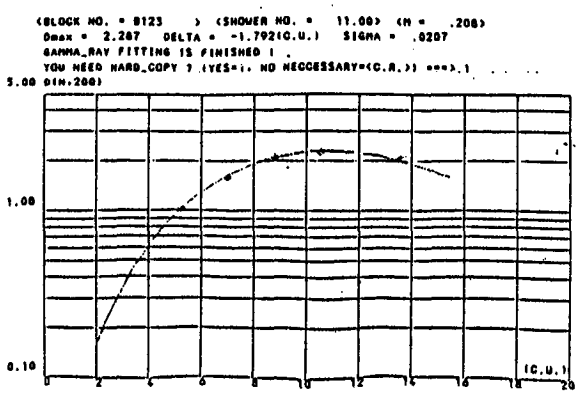

Fig. 7-a. Transition curve of spot darkness obtained by N-type X-ray film, where slit size is set 200 μm.

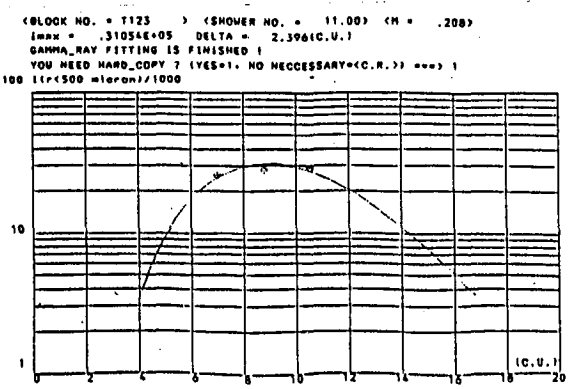

Fig. 7-b. Transition curve of TL emission, where vertical axis is integrated within the radius of 500 μm.

VI) Discussions

We succeeded to observe clearly TL signals induced by cosmic ray cascade showers. On the detection threshold of TL signal, we found, though preliminary, that those with $D \gtrsim 1.0$ are at least detectable, corresponding to 20 TeV. Of course, it depends strongly on the exposure time, and it needs more systematic studies to make this problem clear.

As was mentioned in ref. 3, we are now developing the present system so as to collect TL light more efficiently, and starting TL exposure at airplane. These observations will surely bring us to the realization of super TL calorimeter.

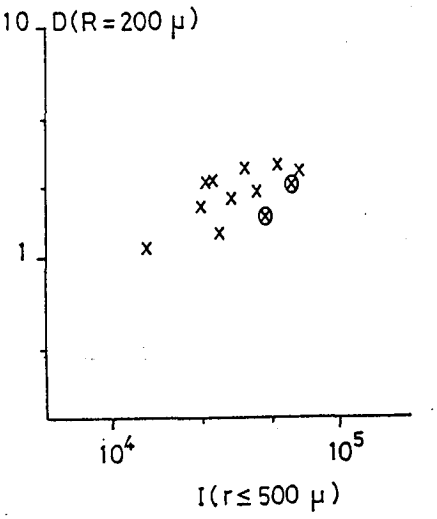

Fig. 8. Correlation between TL yield and spot darkness of X-ray film.

Acknowledgements

We are much indebted to the members of TL-Development Collaborative Group, in particular to Drs. T.Saito, T.Wada and I.Yamamoto, for continuous support and discussions for the present work.

The author are also grateful to Mr. K.Nishizawa(Nemoto Tokushu Kagaku Co. Ltd.) for his kind arrangements of various kinds of TL sheets.

References

[1] Y.Okamoto et al., 18th Cosmic-ray Conference(Bangalore, '83), Conf. Paper, Vol.8, T6-4, p.161.

[2] M.Niwa et al., To be published to ICR-Report(Japanese).

[3] M.Akashi et al., HE 7.1-6 in this volume.

AUTHOR INDEX

BIBLIOGRAPHIC DATA SHEET

1. Report No.	2. Government Accession No.	3. Recipient's Catalog No.
NASA CP-2376 Volume 8		

4. Title and Subtitle	5. Report Date
19th International Cosmic Ray Conference Conference Papers	August 1985
	6. Performing Organization Code

7. Author(s)	8. Performing Organization Report No.
Frank C. Jones, compiler	

9. Performing Organization Name and Address	10. Work Unit No.
Laboratory for High Energy Astrophysics Goddard Space Flight Center Greenbelt, MD 20771	11. Contract or Grant No.
	13. Type of Report and Period Covered
12. Sponsoring Agency Name and Address	Conference Publication
National Aeronautics and Space Administration Washington, D. C. 20546	14. Sponsoring Agency Code

15. Supplementary Notes

16. Abstract

These volumes contain papers submitted for presentation at the 19th International Cosmic Ray Conference, held on the campus of the University of California, San Diego in La Jolla, CA., August 11-23, 1985. The conference is held every other year. The present volume contains papers with Paper Codes HE 5.1 through HE 7.1 and deals with muons, neutrinos, magnetic monopoles, nucleon decay, searches for new particles and techniques employing acoustic and thermoluminescence detectors.

17. Key Words (Selected by Author(s))	18. Distribution Statement
muons, neutrinos, monopoles, nucleon decay, new particles, acoustic detectors, thermoluminescence detectors	Unclassified - Unlimited Subject Category - 93

19. Security Classif. (of this report)	20. Security Classif. (of this page)	21. No. of Pages	22. Price*
unclassified	unclassified		

*For sale by the National Technical Information Service, Springfield, Virginia

GSFC 25-44 (10/77)

National Aeronautics and
Space Administration

Goddard Space Flight Center
Greenbelt, Maryland 20771